Characterization of Wetland Vegetation Distribution Using Satellite Imagery

SM Chilufya

In fulfilment of the academic requirements for the degree of Doctor of Philosophy in the College of Agriculture, Engineering and Science

University of KwaZulu-Natal

Durban

July 2023

Supervisors: Dr M Akombelwa and Prof D. Stretch

Declarations

Supervisor(s) Declaration

As the candidate's Supervisor(s), I (We) agree/do not agree to the submission of this thesis.

Signed: [redacted] Dr M Akombelwa

…… ……

……

Declaration 1 - Plagiarism

I, Sexton Mwitwa Chilufya, declare that

1. The research reported in this thesis, except where otherwise indicated, is my original research.
2. This thesis has not been submitted for any degree or examination at any other university.
3. This thesis does not contain other persons' data, pictures, graphs or other information, unless specifically acknowledged as being sourced from other persons.
4. This thesis does not contain other persons' writing, unless specifically acknowledged as being sourced from other researchers. Where other written sources have been quoted, then:
   a. Their words have been re-written but the general information attributed to them has been referenced
   b. Where their exact words have been used, then their writing has been placed in italics and inside quotation marks, and referenced.
5. This thesis does not contain text, graphics or tables copied and pasted from the Internet, unless specifically acknowledged, and the source being detailed in the thesis and in the References sections.

Signed:

…… [redacted] ……

Declaration 2 - Publications

Chilufya M, Akombelwa M, and Stretch D, 2014. Identification of Optimal Field Spectral Measurements Wavebands for Discriminating among Spatial Features in support of Mapping Using Hyper-spectral Imagery., Whittal J and Motala S. (Eds) AfricaGEO 2014: Proceedings of the Second AfricaGEO Conference, 1-3 July, Cape Town, South Africa.

Signed:

……

Dedication

To Life's Hard Times!

Acknowledgements

Gratitude to my supervisors, Dr M Akombelwa and Prof D Stretch, for their unrelenting support and encouragement both academically and logistically. This research would not have been possible without you. To my wife, it has been a long and challenging journey. Thanks for putting up with my long hours of absence though present, week day or weekend. It would never have been possible to come this far had it not been for your sacrifice. To my children, thank you for realizing that this was crucial to Daddy.

My thanks are also extended to my employers, the University of KwaZulu-Natal, for funding this research through various sources that included staff tuition remission, competitive research fund, School scholarship, and University Capacity Development Programme. I would be failing in expressing my full gratitude if I do not mention the role Isimangaliso Wetland Park played in ensuring that field data was collected in a safe environment. Thank you for providing me with a Game Guard who ensured that I was protected against possible attacks from wild animals. Immense gratitude also goes to Dr Ricky Taylor for accompanying me to the site on my first day of field data collection and also for assisting with the naming of the wetland vegetation assemblages for which spectra measurements were taken in the field based on vegetation images captured during field data collection.

To Professor Mutanga, thank you for accepting and offering to link me up with your then PhD student Adelabu, whose advice served as a spark to what later developed into an approach used to undertake this research.

Lastly, but not least, I wish to thank the so many people too numerous to mention for the various roles they have played in supporting the accomplishment of this long journey.

Abstract

Distribution of wetland vegetation along an altitudinal gradient has been investigated using various ground, aerial and space-based techniques, yielding results with varying accuracies. The advent of space-based hyperspectral satellite imagery, however, provided an opportunity of adding to a pool of resources used by environmental managers in understanding wetland vegetation. This research investigates the use of Hyperion, a satellite hyperspectral imagery, to characterize wetland vegetation along an altitudinal gradient in terms of the hydrological regime determined indirectly by means of elevation change.

Hyperion imagery was captured over the Mfabeni wetland of the Isimangaliso World Heritage Wetland Park. A vegetation map of the Mfabeni wetland that served as a secondary source of ground truthing data, along with a topographic base map were then acquired. A 5m interval contour map and spot-heights for use to generate and assess the accuracy of a Digital Elevation Model (DEM) of the Mfabeni wetland were also acquired.

A vegetation map of the Mfabeni wetland was georeferenced to a topographic base map and transformed to the spatial reference of the Hyperion image. The georeferenced vegetation map was then superimposed over the Hyperion image and the vegetation assemblages' boundaries digitized into a shapefile. Vegetation assemblage classes were then defined. The Hyperion image was radiometrically calibrated to apparent surface reflectance values. Pixel based spectra were then randomly extracted from the Hyperion image for each of the vegetation assemblages and used to compute class spectra means and to identify optimal wavebands, using Random Forest and variable elimination. Class spectra means were used to create a spectral library with class spectra means as endmembers. Regions of Interest (ROIs) representing each of the vegetation assemblages were then extracted. Spectral Angle Mapper (SAM) algorithm was then used to classify the Hyperion image using the ROIs, class spectral means held in the spectral library and Hyperion image spectral subset corresponding to the identified optimal bands. The classified images were then assessed for accuracy. DEMs were also generated using various interpolation techniques and assessed for accuracy. The best classified image and best DEM were then overlain to create a composite image used for characterization of vegetation assemblages in terms of elevation.

The results showed that it is possible to characterize wetland vegetation assemblages in terms of elevation along an altitudinal gradient.

Table of Contents

List of Figures

List of Tables

List of Abbreviations

GPS – Global Positioning System

NASA - the National Aeronautics and Space Administration

NIR - Near Infra-Red

VNIR – Visible and Near Infra-Red

SWIR – Short Wave Infra-Red

VWR - Vegetation Water Ratio

DEM – Digital Elevation Model

SRTM – Shuttle Radar Topographic Mission

SI – International System of Units (abbreviated from French as Systeme Internationale)

MNF - Minimum Noise Fraction

ISDAS - Imaging Spectrometer Data Analysis Systems

ENVI - Environment for Visualizing Images

ACOR - Atmospheric CORrection

FLAASH - Fast Line-of-sight Atmospheric Analysis of Spectral Hypercubes

ATCOR - ATmospheric CORrection

MODTRAN - MODerate resolution atmospheric TRANsmission

LOWTRAN - LOW resolution atmospheric TRANsmission

ATREM - Atmospheric Removal

ACORN - Atmospheric Correction Now

DISORT - Discrete Ordinate Radiative Transfer

A/CHEAT - Auscover/Curtin Hyperion Enhancement and Atmospheric Correction Technique

SMARTS - Simple Model of the Radiative Transfer of Sunshine

DOS – Dark Object Subtraction

QUAC – Quick Atmospheric Correction

6S - Second Simulation of a Satellite Signal in the Solar Spectrum

MRF - Markov random field

RMSE - Root Mean Square Error

FWHM – Full Width at Half Maximum

nm - Nanometre

Chapter 1

Introduction

1.1 Background

The beautiful scenery provided by wetlands has for centuries rendered them vulnerable to human interference, oblivious of the damage caused to their biodiversity. It was not until recently that environmentalists realized the damage humans have done to wetlands (Owethu Pantshwa and Buschke, 2019). World over, therefore, measures to determine the extent, assess condition, restore and preserve wetlands have been put in place. The success of these measures, however, depends on among other things, monitoring changes in ecological zones that make up wetlands (Shen et al., 2019). In vegetation-dominated wetlands, such zones are vegetation communities and/or plant species adaptable to thriving under varying waterlogging conditions (LI et al., 2014). Monitoring spatial coverage and condition (state) of vegetation known to thrive under specific waterlogging conditions can therefore serve as a basis for characterizing wetland conditions.

The change in spatial coverage of vegetation communities and/or plant species in a wetland can be described in terms of the distribution of species along shoreline gradients, a concept known as 'shoreline zonation' (Chowdhury et al., 2019). The basis of shoreline zonation is that vegetation on the shorelines is closely connected with water levels. In turn, the distribution of animals is related to the zonation of wetland plants. Zonation patterns, therefore, summarize much of the spatial variation in wetlands and therefore can be used as models in the study of wetlands (Schoolmaster Jr and Stagg, 2018).

Four vegetation types and four plant growth forms on the basis of the water level may be identified using the shoreline zonation (Zhao et al., 2018) (figure 1.1);

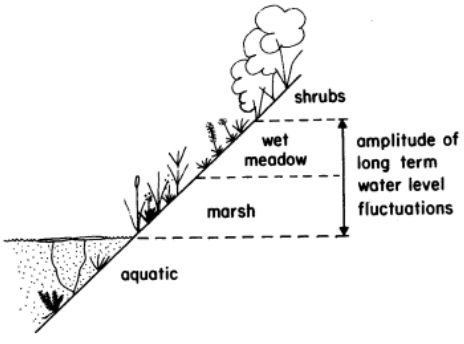

Figure 1. 1: Zonation of four vegetation types in relation to water level on shores with fluctuating water levels (Keddy, 2010)

- *Wooded wetland:* depicted as 'shrubs on figure 1.1 is found highest on the shores which are flooded for shorter periods of time each year and are dominated by trees and shrubs.
- *Wet meadows:* exist at lower elevations where there is more flooding. This vegetation stays uncovered from water for a few months in each growing season and so is occupied by plants that show minimum modification to cope with flooding.
- *Emergent marsh:* these are found at increased depth and duration of the flooded condition. Vegetation in emergent marshes may only be uncovered for a short time during drought periods, and as a result, show increased morphological adaptation to flooding. Linear leaves and parenchyma become conspicuous.
- *Aquatic plants:* These are truly aquatic plants, many of them with floating leaves, found in permanently flooded areas.

In a typical South African grassland-dominated wetland, where the study was conducted, the equivalent of these four zones includes; wet grassland, wet meadows, marsh, and open water vegetation (Kotze et al., 1994) (figure 1.2).

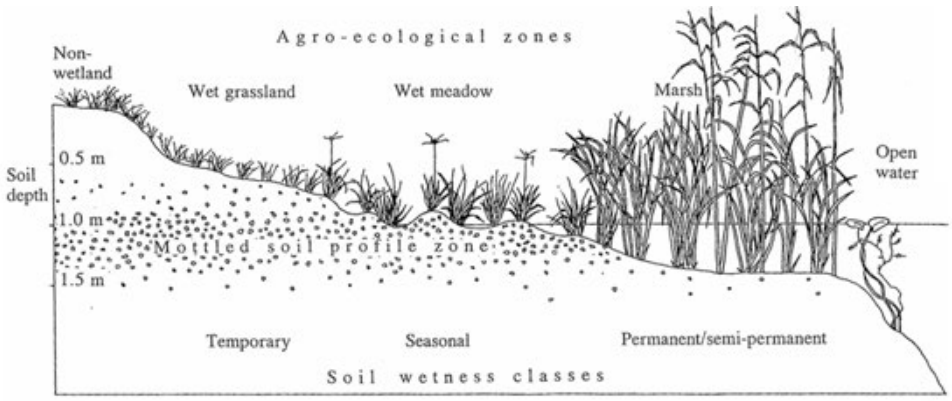

Figure 1. 2: Zonation of a typical South African grassland dominated wetland shoreline (Adopted from Kotze et al., 1994)

In this study, the concept of zonation was used in understanding the distribution of vegetation communities/plant species on wetland altitudinal gradients forming vegetation assemblages studied in characterizing wetland vegetation. The choice of this approach was motivated by the fact that previous studies have used the principle of zonation as a model for understanding biodiversity in wetlands among others (Stewart et al., 2021, Pimple et al., 2022). As vegetation present at a given elevation on the altitudinal gradient of the wetland is related to the water level, the presence or absence of a particular vegetation community/plant species can be attributed to the presence or absence of the water level required to sustain it (Ayyandurai and Venkateswaran, 2021). It can therefore be assumed that all other things being equal, the amount of water plants draw from the soil is inversely proportional to the elevation at which plants thrive relative to the

water table (Ayyandurai and Venkateswaran, 2021). Therefore, vegetation communities/plant species at a lower elevation are more capable of withstanding waterlogging conditions than those at high elevations. Characterizing vegetation assemblages in terms of elevation can, therefore, serve as an indirect way of characterizing vegetation in terms of its hydrological regime.

A hydrological regime of a wetland is a specific pattern of the extent, where and when water is present in a wetland and may be referred to as 'hydro-pattern' or 'water regime' (Department of Environment and Conservation, 2012). Components of a hydrological regime are the timing, frequency, duration, extent and depth, and variability of water presence (Rolls et al., 2018).

Vegetation characterization may be defined as a process of describing the characteristics of vegetation in relation to some other parameter. Applied to wetland vegetation, it implies the allocation of vegetation assemblages that thrive in a wetland in relation to soils, elevation, geology, water, or some other parameter. It is accomplished by means of vegetation mapping. Wetland vegetation characterization, therefore, calls for an effective mechanism for mapping vegetation community/plant species. One such mechanism is the use of satellite imagery.

1.2 Research Problem

Wetland vegetation studies have been undertaken using ground-based methods (Brand et al., 2013, Silva Mota et al., 2017, Prospere et al., 2014, Adelabu et al., 2014), aerial photographs (Varga et al., 2015, Klemas, 2014) and both aerial multispectral and hyperspectral (Bustamante et al., 2016, Atzberger et al., 2015, Mahdavi et al., 2018) imagery. While multispectral satellite imagery (Malinowski et al., 2015a, Whiteside and Bartolo, 2015, Tian et al., 2016) has been available and equally widely used in wetland vegetation studies. Satellite hyperspectral imagery did not exist before Hyperion imagery captured by the Earth-observing 1 (EO-1) satellite launched in November 2000 for exploratory purposes (USGS, 2017). From the launch of EO-1 to its decommission in February 2017 (USGS, 2017), the Hyperion imagery captured has been equally used in a number of vegetation related research, yielding a variety of results (Friedal et al., 2017). None of these researches, however, have focused on its use for the characterization of wetland vegetation on an altitudinal gradient in terms of the hydrological regime by indirectly relating spatial coverage of vegetation assemblages to change in elevation. Water level (water table) and the topography are always related, as water table lows occur at surface waters, which in turn occur in topographically low areas (O'Connor et al., 2019). This is especially true in areas with relatively low-permeable and/or anisotropic aquifers subjected to unusually high areal recharge rates and/or areas with shallow aquifers in flat or gently rolling terrain. This research was therefore born out of the need to investigate the effectiveness of satellite hyperspectral sensing in discriminating

among various wetland vegetation assemblages thriving along an altitudinal gradient using Hyperion imagery. Variation in vegetation assemblages in relation to elevation was used as a basis for the study of vegetation distribution and, thus, characterization of wetland vegetation. Random Forest machine learning ensemble and variable elimination techniques were employed as data dimension reduction techniques to identify wavebands most suitable for classifying the Hyperion image. The results obtained were then validated with the use of vegetation Moisture Stress Index (MSI) generated using the same Hyperion hyperspectral image. Mfabeni wetland, in the Isimangaliso Wetland Park, a World Heritage site situated on the eastern shores of South Africa, was used as a study area.

1.3 Research Question

How can satellite hyperspectral imagery be used to characterize wetland vegetation in terms of the hydrological regime by indirectly relating spatial coverage of vegetation assemblages to change in elevation? In attempting to answer this question, the following sub-questions were addressed:

1. Can wetland vegetation assemblages of the Mfabeni wetland be distinguished on the basis of spectra extracted from the Hyperion image pixels?
2. Is there a relationship between the classification accuracy obtained using random forest and the post-classification accuracy of the classified Hyperion image of the Mfabeni wetland?
3. Can the distribution of wetland vegetation along an altitudinal gradient be explained in terms of its hydrological regime by indirectly relating it to change in elevation?

1.4 Research Hypothesis

Wetland vegetation distribution along an altitudinal gradient can be characterized in terms of its hydrological regime by indirectly relating it to change in elevation using satellite hyperspectral imagery.

1.5 Research Aim and Objectives

The aim of this research is to characterize wetland vegetation distribution along an altitudinal gradient in terms of the hydrological regime determined indirectly from elevation change using satellite hyperspectral imagery.

In pursuance of this aim, the following objectives were set to be achieved;

1. *To establish whether vegetation assemblages in the Mfabeni wetland can be separated on the basis of the spectra extracted from the Hyperion image pixels*.

   This objective was intended to be achieved by developing a Random Forest predictive model with acceptable accuracy for selecting optimal wavebands in conjunction with variable elimination methods for discriminating among various spectra representing vegetation assemblages.

2. *To establish whether there is a relationship between the classification accuracy obtained using random forest and the post-classification accuracy obtained once the Hyperion image has been classified.*

   This objective was to be achieved by comparing the accuracy obtained from the use of Random Forest on image pixels extracted spectra against that obtained from the classification of the Hyperion image based on the most suitable (optimal) wavebands identified using a combination of Random Forest and variable elimination.

3. *To investigate the existence of a positive correlation between the distribution of wetland vegetation along an altitudinal gradient and the hydrological regime determined indirectly by means of the change in elevation.*

   This objective was envisaged to be achieved by establishing a relationship between the distribution of wetland vegetation assemblages' and elevation on an altitudinal gradient with elevation treated as an indirect measure of the water level.

1.6 Research Design

The methodology applied in this research was based on a holistic (system) approach to the landscape as theorised by (Ginzarly et al., 2019). According to this concept, a landscape is considered to be an integrated entity resulting from the mutual action and interaction of climate, rock, landform, soil, vegetation, fauna, water, and humans (Ginzarly et al., 2019). As the analysis was largely based on the changes in vegetation, this concept implied that the change in spectral reflectance was viewed as an indicator of the total complex of properties of the landscape in that area. Soil and water background, in this case, were taken as factors characteristic to a vegetation community, and therefore, no attempts were made to remove their background properties from the concerned vegetation spectra (Ginzarly et al., 2019).

Characterization of wetland vegetation in terms of the hydrological regime was based on the analysis of changes in spatial coverage of vegetation communities and/or plant species. In analyzing these changes, a basic underlying premise was that plant species are spectrally

separable and, indeed, so are the same plant species thriving under different moisture conditions. Accordingly, the vegetation assemblages these plant species give rise to are subsequently spectrally separable. Vegetation assemblages consisting of the same mix of plant species should therefore have the same spectral pattern unless they are growing under different hydrological conditions.

A Data Acquisition Request (DAR) specifying the latitude and longitude coordinates of the research site center was submitted to the United States Geological Surveys (USGS) for the capture of the Hyperion imagery of the research site once it had been identified. Following the capture of the Hyperion imagery, a field trip was undertaken to collect ground-truthing data within 15 days of the imagery capture in agreement with the requirements for vegetation mapping using satellite imagery and corresponding field spectra (Govender M et al., 2008) as no serious disturbance to the vegetation occurred from the date of image capture to the date(s) for field data collection.

Ground-truthing data were collected along a single transect across the Mfabeni wetland and at two other smaller wetlands within the Isimangaliso wetland park. A sampling scheme employed for the collection of ground-truthing data along each transect across the wetlands was different from that of the conventional approach used in vegetation mapping. Instead of diving up the transect into sampling cells of known dimensions in the field along one or more transects and subsequently estimating the percentage composition of vegetation communities/species in each cell (Silva Mota et al., 2017), samples were taken wherever the current vegetation assemblage noticeably differed from that taken just before it along a transect. The sampling cell size was subsequently defined during data processing to correspond with the spatial resolution of the imagery used. This approach was considered ideal for specifying sample cell size for medium spatial resolution imagery and hence viewed as a new contribution this research intended to make to the field of applied remote sensing.

The data collected using the above sampling approach was, however, considered insufficient due to reasons beyond the control of the researcher, rendering it unusable for meaningful and reliable results. A vegetation map of the Mfabeni wetland was therefore used as a source of reference data for the analysis to establish the relationship between vegetation and elevation, instead. The map was registered to the spatial reference of the Hyperion image and subsequently superimposed over image. Classes were then formulated for each of the vegetation assemblages constituting the vegetation map. Representative spectra were extracted for each of the classes representing vegetation assemblages using two approaches to serve as training data. The training data was subsequently used to create a spectral library of class spectra means and to identify optimal wavebands used for image classification.

A DEM was also generated from a 5m interval contour map, assessed for accuracy, and then combined with a classified image of vegetation assemblages of the Mfabeni wetland. The combined image was then used to characterize vegetation assemblages in terms of elevation on the Mfabeni wetland altitudinal gradient.

A vegetation Moisture Saturation Index (MSI) image was generated from the same Hyperion image of the Mfabeni wetland and then used to validate the elevation represented on a DEM and the distribution of vegetation assemblages in terms of the moisture content.

1.6 Research Scope

The concept of zonation, while considered ideal for the understanding of diversity in vegetation along an altitudinal gradient of wetlands, cannot be explained in terms of the hydrological regime only. Other factors, depending on the nature of the wetland, may account for some of the changes observed in plant distribution along an altitudinal gradient (Fu et al., 2019).

Originally, a relationship was intended to be established between soil moisture and elevation to confirm the theorized relationship between the two using field soil moisture measurement. The device for measuring the field moisture malfunctioned during field data collection, and due to its age, it could not be repaired to be used again during the same field campaign. A vegetation Moisture Saturation Index (MSI) was generated from the same Hyperion image of the Mfabeni wetland and used to establish a relationship between elevation and the moist conditions vegetation assemblages are able to thrive in.

1.7 Thesis Organization

This thesis comprises eight (8) chapters organized as follows:

Chapter 1 introduces the research in terms of the background, research problem, research question, research hypothesis, aim and objectives of the research, research design, and research scope.

Chapters 2, 3 and 4 are literature review chapters presenting an overview of wetlands concepts, hyperspectral remote sensing of wetlands vegetation and characteristics of the Mfabeni wetland used as a study area, respectively.

Chapter 5 is a methodology chapter providing a detailed account of the approach employed for data collection, pre-processing of satellite images, elevation data, and subsequent processing and analysis.

Chapter 6 provides a detailed description of the derived study results.

Chapter 7 provides a discussion of the results obtained/not obtained in relation to existing literature where possible.

Chapter 8 provides conclusions from the research and recommendations for related future studies.

Chapter 2

Wetlands Overview

2.1 Introduction

Wetlands have for centuries been exploited with no due consideration to the damage done to them. They were drained and converted to more obvious uses, such as agriculture (Brasher et al., 2019). Realizing the damage done to wetlands, environmentalists have established measures to help reverse the damage (Lewis, 2018). The success of these measures, however, depends on identifying observable field indicators of wetlands' health. The condition of these indicators subsequently serves as a means to gauge the health of the wetlands. The indicators, therefore, require monitoring to check their status. In vegetation-dominated wetlands, vegetation communities/species may serve as such observable indicators. Thus, the condition and/or spatial distribution of vegetation communities/species at any given instance may subsequently be used to establish the wetlands' health (Singh and Sinha, 2021, Yang et al., 2018). Establishing vegetation communities/species conditions or spatial distribution requires periodic mapping, which can be costly depending on the technique employed. This chapter presents an overview of wetlands and their characteristics.

2.2 Wetlands Definition

Wetlands are understood differently by different people (Xu et al., 2019, Rupasinghe and Chow-Fraser, 2019) . Wetlands are so-called because they predominantly contain water. Accordingly, the various definitions available for wetlands emphasize the presence of water, among other factors. (Keddy, 2010) defines a wetland as an ecosystem that occurs when water flooding creates anaerobic process-dominated soils forcing biota, especially rooted plants, to display adaptation to withstand flooding. A wetland is as an ecosystem that, at or near the substrate surface, relies on persistent or intermittent, shallow flooding or saturation with the minimum essential characteristics of wetlands being recurrent, prolonged flooding or saturation near the surface and physical, biological and chemical presence characteristics that represent recurrent, continuous flooding or saturation (Hemba et al., 2020, Mahdianpari et al., 2020, Prisley et al., 2020). Wetlands are commonly diagnosed in terms of hydrophytic vegetation and hydric soils, which should be present unless they have been removed or their development prevented by specific physiochemical, biotic, or anthropogenic factors. Wetlands as areas in transition between well-drained uplands, permanently flooded environments, areas, and deep water areas, which are important ecological systems of economic, biological, and benefits (Tollette et al., 2022, Maua et al., 2022).

The various definitions available for wetlands imply that no commonly accepted definition for wetlands exists (Herlihy et al., 2019). While the definitions for wetlands may differ depending on whether they have a scientific or legal connotation, (Mandlazi, 2017) lists three basic criteria as having been adopted for the characterization and identification of wetlands:

i). availability of wetland water (wetland hydrology),
ii). hydric soils, and
iii). hydrophytic plants (hydrophytes).

The presence of water is often considered the most significant of these criteria due to the dependence on water by both hydric soils and hydrophytic plants (Mitsch and Gosselink, 2015). Despite this acknowledgment, the presence of water alone has been shown not to be always enough for the accurate identification of wetlands boundaries, calling for the use of direct methods of soil morphology and vegetation (Mandlazi, 2017).

2.2.1 Wetland Hydrology

Wetland hydrology is the movement of water into, within, and out of a wetland (Zhang et al., 2019). It includes all hydrological functions of regularly flooded areas or has surface-saturated soils at some point in the growing season (Wetland Hydrology, ND). Hydrological processes, therefore, control the formation, function, persistence, and size of wetlands (Gao et al., 2018, Verry, 2018).

Wetland hydrology is characterized in terms of precipitation, ground-water, evapotranspiration, and surface water of the wetland's locality.

2.2.1.1 Precipitation

In the wetland water balance, precipitation is the primary and significant water source (Shen et al., 2022). Precipitation is the force that drives most wetlands' water budget (Rasmy et al., 2019). Precipitation serves as a direct water source for wetlands while providing surface water and ground water as secondary sources (MALTBY and BARKER, 2009). Depending on the wetland's location, the primary precipitation sources are rainfall or snow (Verry, 2018). Precipitation affects infiltration, interception, surface runoff, water level fluctuations, ground-water recharge, and inundation (Rasmy et al., 2019). The occurrence of these processes depends on rain or snow. Secondary precipitation sources contribute significantly to the quantity of water in wetlands. However, they get lost on the way to the wetland, leaving direct precipitation to serve as the main water source in some wetlands. The importance of direct precipitation in the water budget of the wetland changes among wetlands and is dependent on the size (area) of the wetland (Zhang et al.,

2021c). Most of the wetlands in South Africa do not cover large surface areas; hence direct precipitation makes minimal contribution to the overall wetland water budget (Maswanganye et al., 2022).

2.2.1.2 Evapotranspiration

In most wetlands, evapotranspiration is the main water flux by which water is lost. It affects water level fluctuations, water coverage area, and inundation period. Various evapotranspiration studies have been conducted, including those aimed at determining the overall consumptive usage by distinguishing between open water areas' evaporation demands and transpiration rates of specific wetland plants. (Xin et al., 2022, Getirana et al., 2021, Yeo et al., 2019).

Quantifying the rate of evapotranspiration in wetlands is difficult due to the variation in the nature of wetlands and the complexity of surface characteristics making up wetlands (Mandlazi, 2017). While various methods for estimating evapotranspiration in wetlands have been developed (Ramatsabana et al., 2019, Bao et al., 2021, Kadlec, 2020), most of them necessitate a significant amount of meteorological evidence, which is often unavailable for many wetlands. Methods determining evapotranspiration in wetlands using remote sensing have been found challenging due to the diversity in land cover types and high dynamic nature, which significantly change their radiation backscattering reflectance properties (Chomba et al., 2021, Carter and Liang, 2019).

The discussion of evapotranspiration also includes 'interception', a term that refers to the precipitation amount diverted by plant leaf surfaces and does not hit the soil surfaces. It is frequently regarded as a component of evaporation because the majority of water plants diverted ends up being evaporated (Yaseef et al., 2009). Interception is vital in the wetlands' water balance (Ciężkowski et al., 2018), particularly where vertical processes dominate. Interception is often restricted to the quantity of water diverted by the leaf surfaces as well as the soil and happens on the same day it rains (Baiamonte, 2021). The quantity of water plants intercept is dependent on the rainfall duration and intensity. Low-intensity rainfall over a short period of time yields great amounts of interception (Dunkerley, 2021). Vegetation type and height, leaf area index, wind energy, and wind speed all affect the quantity of water vegetation intercepts. Wetland interception studies have investigated various types of wetland vegetation (Ciężkowski et al., 2018).

2.2.1.3 Ground Water and Surface Water

The water balance of a wetland is influenced by both surface and ground water. Either can be a principal source of water in some wetlands, while other wetlands depend on both surface water

and ground-water. Surface water flow into wetlands happens via channel flow, base flow, and overland flow, while ground-water recharge and discharge, from and to wetlands, respectively, ground-water wetlands and flow all contribute to hydrological exchange between wetlands and ground-water (Nyarko, 2020).

There is an interdependence between ground-water and surface water (Preetha et al., 2021); hence they cannot be isolated (Sophocleous, 2002). Surface water and ground-water are frequently considered as one resource as they usually are often connected (Johnson, 2018). The manner in which ground-water interacts with wetlands, the part played, and the extent of interaction between ground-water and surface water in the wetlands are determined by various factors. These include the location of the wetland within the ground-water flow subsystem, aquifer characteristics, and soil settings of the wetland (Mandlazi, 2017), among others. Wetlands may form in high or low-lying areas where ground-water may recharge from or discharge into wetlands, respectively (Gibson et al., 2022).

2.2.2 Hydric soils

Wetland hydric soils are considered a vital component of wetlands because of their regulatory role in hydrological functions (Mandlazi, 2017). The soil separates precipitation into various components, including evaporation, infiltration, interflow, deep ground-water percolation, and surface runoff. These processes are significantly affected by the soil texture. Wetland soils may be organic, exhibiting a lower organic carbon content and higher clay content, and remain inundated with water over more extended periods (Faulkner and Richardson, 2020). They may also be mineral soils containing a low concentration of clay and a higher concentration of organic carbon (Singh et al., 2019). The presence of morphological features such as mottles and gleying of water within wetlands soil is indicative of the existence of water, while mottling signifies low levels of manganese and iron oxides in the soil and indicates patterns in annual water flow (Stanturf and Schoenholtz, 2019). Gleyed soils represent slow water movement downward to the unsaturated subsoil, where the occurrence of a deep water table is highly probable (Stanturf and Schoenholtz, 2019). Seasonal or temporary wetlands exhibit a higher presence of mottles than permanent wetlands with a lower concentration of mottles (Collins, 2005, Grenfell et al., 2019).

2.2.3 Wetland Vegetation

Vegetation happens to be the most visible aspect of a vegetation-dominated wetland environment (Grasel et al., 2021). Wetland plants have evolved to live under anaerobic environments that are influenced by altered soil chemistry for at least part of the year (Pretorious, 2016). Wetland plants may be submerged or floating, with the majority being emergent (majority of plant shoots appear

above the water level) (Grasel et al., 2021). Wetland ecosystems are unfriendly environments for plants to thrive in because of changes in water levels, flood duration and frequency, acidity, harmful elements mobilization, and exposure to vital resources that include water, light, nutrients, and oxygen (Zhang et al., 2021a). Plants surviving in wetlands have various adaptations in terms of their physiology and morphology, enabling them to withstand a saturated environment (Pretorious, 2016). Flexibility in germination, alternate pathways for metabolism, accelerated stem growth, and conservation of nutrients are among some plant physiology adaptations (Pretorious, 2016). Adaptations in plant morphology refer to the plant's ability to use lenticels, hollow stems, aerenchyma, pneumatophores, as well as shallow and adventitious roots (Grasel et al., 2021). Various processes and conditions affect the type, productivity, and distribution of wetland plants (Ye et al., 2019). Many conclusions, therefore, can be drawn about wetland ecological conditions by investigating the composition of wetland plant communities (Sieben et al., 2021).

Hydrophytic plant species are typically dominant in permanently wet wetland systems. Occurrences of plant species individuals do not have to be within waterlogged conditions to be regarded as hydrophytic. Some species have adapted to thriving on a wetness gradient due to the transitional nature of wetlands (Balwan and Kour, 2021) . Changes in environmental conditions are attributed to shifts in plant communities' composition, allowing for certain plant species to be used as indicators based on the differences in their tolerance to conditions in the environment (Sieben et al., 2014). Many publications, however, argue for the use of a group of species (vegetation community) to serve as indicators in preference to individual indicator species (Hussain et al., 2019). .

(Bothma, 1996), defines a plant (vegetation) community as an *"assemblage of plant species with a relatively uniform physiognomy or appearance, and occurs in a relatively consistent type of physical environment".* Certain species of plants have a strong similarity or relationship with one another and their ecosystem and may be assumed to coexist in some areas with greater certainty in comparison to other species (Mittelbach and McGill, 2019) . These vegetation communities may develop along a gentle, environmental gradient or be distinctly demarcated (Mittelbach and McGill, 2019). Vegetation communities have a tendency to colonize large areas and develop under the influence of various environmental factors that include light, slope, soil nutrients, temperature, and rainfall, which vary among different areas (Nyarobi, 2022).

In special ecological zones, like wetlands, the system ecology drivers function on a much narrower scale and usually are highly sensitive and very dynamic (Pretorious, 2016). In peatland wetlands, key environmental gradients described by (Charman, 2002) include:

- The water-table gradient,
- The acid/base (neurotrophic-ombrotrophic) gradient,
- The fertility gradient,
- Deep peat to mineral soil gradient.

Anaerobic conditions dominant in wetlands result in a reduction in nutrients required for average plant survival affecting vegetation composition (Cronk & Fennessy 2001). The drop and concentration of certain elements may alter the presence of vital plant nutrients, making them more available to plants (Pretorious, 2016). Wetlands with inadequate plant nutrients, like peatlands, are usually limited in certain essential elements. They hence tend to be acidic, with the result that many plant species get excluded with the availability of certain plant nutrients being affected.

2.3 Wetlands Distribution

Geographically, wetlands are distributed world-wide, differing slightly in type depending on the variation in climatic, hydrologic, and topographic influences (Laltaika, 2022). Natural wetlands occupy 8.6 million km2 (6.4 percent) of the Earth's ground surface, according to (Sonkamble et al., 2018), with around 4.8 million km2 in the tropics and subtropics. Around half of the world's wetlands have thus been destroyed in just a century, owing primarily to irrigation for agricultural purposes, urban development, and water resource control measures.

2.4 Classification and Wetland Types

Wetlands are so diverse that an essential first step in any scientific study is dividing and sorting them into similar types observed as particular association sets of animals and plants that recur. The recurrence is considered to be a result of the same causal factors and similar ecological relationships occurring within each type. Despite the observable similarities among various types of wetlands, there exists an abundance of names in use to describe wetlands (Shepard et al., 2019). These varying forms include marshes, swamps, bogs, floodplains, vleis, and pans (park Dams, 2019).

One other simple classification system of wetlands is based on hydrology. In this classification, three major water sources for wetlands are considered; precipitation, surface water, and ground water (Semeniuk and Semeniuk, 2018). Hydrology may further be used to distinguish between different classes of wetlands based on the capacity by plants to tolerate excess water arising from

the interaction between flooding duration and the depth of flooding. This phenomenon leads to wetlands being classified as peatland, aquatic, marsh, and swamp (Granger et al., 2021).

A system of wetland classification mostly accepted and widely used is the Cowardin system. The Cowardin system was developed for the Fish and Wildlife Service of the United States of America (Shepard et al., 2019). It has a hierarchical structure which at the general level, progresses from systems and subsystems to classes, subclasses, and dominance types (figure 2.1) (Veselka IV et al., 2021) . In this classification, subsystems, classes, and subclasses are modified by applying water regime modifiers and special modifiers.

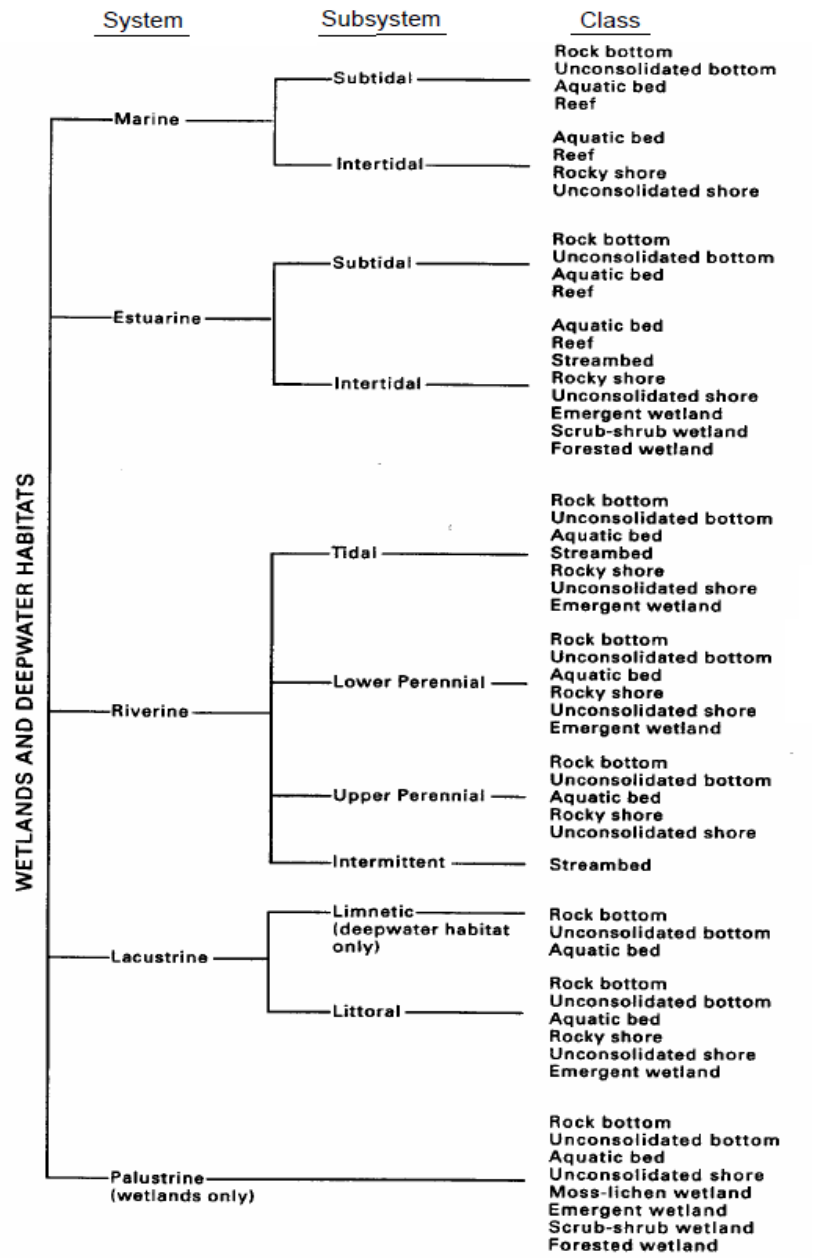

Figure 2. 1: Cowardin System of Wetland Classification (Cowardin et al., 1979)

2.5 Classification and Distribution of South African Wetlands

South Africa, situated within the tropics, tends to have wetlands with differences in type said to be a reflection of the different purposes for which the definitions are used, different perspectives of the individuals or organizations concerned as well as the different regions of the country Adame et al., 2019). A classification system for South Africa's wetlands was proposed based on a Cowardin system. The decision to adopt this system was based on the needs of the users, inventory expectations, and its desirable traits, such as its wide and open structure. These allowed for its application to local conditions with precision subject to just minor alteration (van der Valk, 2020).

The modifications proposed to the system were intended to cater to a full diversity in South African wetlands. They include the incorporating subsystems that are considered intermittent to the riverine system, division of the Palustrine system into four subsystems, and addition of the Endorheic system ((van der Valk, 2020). Figure 2.2 shows the changes made to the original Cowardin System classification template.

The proposed classification system presented in figure 2.2 was going to be subjected to field testing, a stage considered crucial to its adoption. This stage had not been done at the time of publication of the reference article (van der Valk, 2020). Field testing was planned to involve several targeted regions, each with a representative selection of wetland types, collectively constituting a mini-inventory exercise. The suitability of applying the classification in a full-scale national inventory was to be determined in terms of its effectiveness to accommodate a variety of wetland habitats encountered during the trial (van der Valk, 2020).

The application of the classification system to regions also needed to be explored. In its proposed form, a given taxon had no specific alliance to a region. It could represent any single or several parts of the country despite well-known variations in climate, soils, geology, and vegetation across regions considered relevant to the formation of varying wetland habitats. These regional variations also influence utilization and management practices. It was believed that several bioregional classification systems existing in South Africa could play a vital role in extending it or modifying it for regional use.

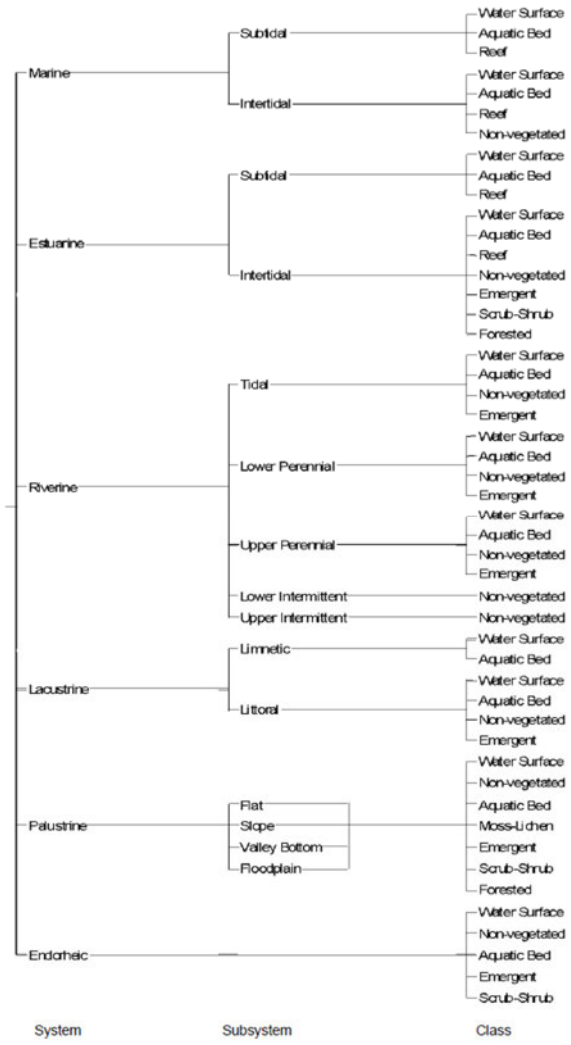

Figure 2. 2: Proposed South African Wetland System to Class Level (Dini, 8 -14 November 1998)

2.6 Wetland Ecology

Ecology is defined as a *"scientific study of the distribution and abundance of organisms"* (Keddy, 2010). Wetland ecology, therefore, can be described as the 'scientific study of the distribution and abundance of organisms' that constitute a wetland.

Though wetlands arise because of the presence of water, each specific wetland and the characteristics of its communities/species rely on other ecological considerations. The major properties characterizing wetlands include a high water table (hydrology indicator), hydric soils (pedological indicator), and hydrophytic vegetation (botanical indicator) (Kucera, 2021).

Various concepts are used to study the nature of wetland ecology. Accordingly, the ecology of a wetland can be understood by studying (i) the distribution of species along an altitudinal gradient and (ii) the relative abundance of species. The former is referred to as zonation, while the latter is known as diversity.

2.6.1 Zonation

Zonation in wetlands establishes a relationship between wetland vegetation distribution and water level. Sketching zonation patterns has served as a long-established practice of describing wetlands (figures 1.1 and 1.2). Zonation patterns sum up a lot of spatial differences in wetlands. Zonation, therefore, can be used as models in the study of wetlands. However, various environmental factors may be responsible for the zoning observed on the wetland shorelines (Shano et al., 2020) . According to (Keddy and Reznicek, 2018) , the close connection vegetation on the shorelines has with water levels constitutes a basis for shoreline zonation. The distribution of animals, in turn, is linked to wetland plants' zonation.

Mechanisms for zonation include ecological succession, biological interactions, and physical factors (Keddy and Reznicek, 2018) . According to ecological succession, vegetation communities appear to follow a temporal trend, the series of events that would develop as a wetland progressively filled with detritus and transformed into the land (Keddy and Reznicek, 2018) . Hence, zonation is regarded as a spatial approximation of succession series in time, even without clear evidence of transition (Keddy and Reznicek, 2018).

Zonation and succession may be closely linked on low-lying areas of peatlands and small pools, where organic matter builds up, but the linkage does not necessarily apply to steep shores. Therefore, the link between zonation and succession is said to be weak in cases other than those driven by the accumulation of peat, such as shores of large lakes and rivers, and confuses the sources of patterns observed in vegetation instead of clarifying them. Even on relatively flat slopes of peatlands where the link holds, it has been found that successional sequences may be delayed or even restarted by a variety of both natural and human-induced disturbances, inclusive of fires, floods, storms, and droughts (Keddy and Reznicek, 2018).

2.6.2 Diversity

Diversity relates to the number of species contained in an ecosystem or habitat. Diversity in species of a wetland is of prime importance to the understanding of wetland (Vanneste et al., 2020). The term diversity is often used synonymously with biodiversity (number of species in an entire community or larger geographic area) or species richness (number of distinct species in a collection), but precisely speaking, it includes the relative abundance of species (Reynolds et al., 2018)

Factors controlling the number of plant species in wetlands may vary but generally tend to include habitat size (area), elevation, exposure to waves, soil nutrients, disturbance by fire, amount of litter, precipitation, and many more (Barton et al., 2021). In this study, diversity in vegetation

communities/plant species is determined in terms of variation in water established indirectly using elevation change on an altitudinal gradient.

2.7 Relationship between Water Level and Topography

The water level in unconstrained aquifers, as depicted by the water table, is typically regarded as a subdued representation of an area's topography or ground surface (Mussa et al., 2020). This assumption, however, was proven wrong when it was applied to regional unconfined aquifers and, in some cases, was found to be in error (Mussa et al., 2020). Analysis undertaken to establish a rise in ground-water level in regional unconstrained aquifers, revealed conditions where the water table closely follows the topography and where it does not (Mussa et al., 2020). Based on their findings, a topography-controlled water table, most often exists in almost flat terrain or in anisotropic and comparatively low-permeable aquifers subjected to exceptionally high (due to the low permeability) areal recharge rates. Conversely, relatively permeable aquifers do not exhibit a direct correlation between water level and topography. It was also observed that the relationship between topography and water table is affected by the distance between surface water features as well as the aquifer thickness. Shallow aquifers existing in gently sloping or flat terrain may signify a water table that seems a subdued replica of the terrain surface. *".....in a very general sense, the water table and the topography are always related …… as water table lows occur at surface waters, which in turn occur in topographically low areas."* (Haitjema and Mitchell-Bruker, 2005)

2.8 Chapter Summary

This chapter discussed the definition of wetlands, their spatial distribution, and how they are classified, highlighting the fact that while different types of wetlands exist worldwide, they all have one underlying concept; the presence of water. Associated with the presence of water in wetland are hydric soils and hydrophytic vegetation.

Wetland vegetation being the focus of the study in relation to water (hydrology), the chapter also discussed the characteristics of wetland hydrology, namely precipitation, evapotranspiration, and ground and surface water. An overview of the wetland soils was also presented to highlight their role in the wetland hydrological functions. Wetland vegetation was also discussed, being the visible aspect of vegetation-dominated wetland that is crucial to the understanding of the wetland health.

The wetland ecology was presented with a focus on the concept of ‘zonation’. The research was born out of the need to investigate the principle of zonation in vegetation distribution on a wetland altitudinal gradient using satellite imagery. The chapter, therefore, discussed this principle as it

relates to different types of wetland vegetation. Diversity was discussed in terms of understanding the various factors that may affect the distribution of various wetland species, but more specifically, how the water available to plants would affect vegetation distribution in a wetland.

Lastly, the chapter presented a relationship between water and topography. The chapter highlighted the different conditions when the relationship between water and topography can be strong and when it can be weak. Knowledge of these conditions was crucial in establishing whether the wetland identified as a study area could serve as a suitable site for elevation to be used as a substitute for the water level (water table) when the latter's data is not available.

With the conceptual background set, the subsequent chapter discussed the techniques employed for data extraction from hyperspectral (Hyperion) imagery for mapping the spatial distribution of wetland vegetation on an altitudinal gradient so as to facilitate the investigation of the principle of zonation.

Chapter 3

Hyperspectral Remote Sensing of Wetland Vegetation

3.1 Introduction

Mapping wetland vegetation has been accomplished using a variety of techniques (Jin et al., 2022, Jeziorska, 2019, Durgan et al., 2020). This chapter presents an overview of such techniques with a review of prior research where vegetation communities and/or plant species extracted from satellite imagery have been employed as observable field indicators. The chapter also discussed how space hyperspectral imagery, with a focus on Hyperion imagery, is processed for vegetation mapping.

3.2 Techniques for Mapping Wetland Vegetation Spatial distribution

Mapping wetland ecological zones have been conventionally accomplished using ground-based survey techniques, including Global Positioning Systems (GPS) (Mishra, 2020, LaRocque et al., 2020). However, these techniques have been found to be laborious, and in some instances, less accurate in comparison to non-ground based techniques (Smith et al., 2021, Mahdavi et al., 2019). In a study to map stream microhabitats (Macus, 2001) confirmed the superiority of the airborne high spatial resolution hyperspectral imagery over ground-based techniques in many instances where the accuracy of the obtained results was compared, thus challenging classical mapping approaches.

Aerial based techniques using visible photographic images have been used as an alternative to ground-based techniques where and when large wetlands have had to be mapped (Mishra, 2020). They, however, have the shortcoming of not providing adequate means of distinguishing different plant species that make up vegetation communities (Jeziorska, 2019, Biswas et al., 2020). This shortcoming led to color infrared photography capable of distinguishing vegetation species based on their varying reflectance in the visible/infrared portion of the spectrum (Schmidt and Ahn, 2019). These techniques, however, had the disadvantage that acquired photographs needed converting to digital equivalents to develop digital inventories of wetlands ecological zones (Jeziorska, 2019).

The advent of digital multi-spectral imagery, therefore, saw a shift to the use of both airborne and satellite digital multi-spectral imagery capable of taking and recording earth surface images, inclusive of vegetation, in several bands (portions) of the electromagnetic spectrum, making

discriminating of certain vegetation assemblages/plant species inseparable using aerial photography, possible (Eid et al., 2020). Furthermore, this imagery made developing digital inventories of wetland ecological zones relatively easier (Westerfelt and Friberg, 2022). Airborne-based multi-spectral imagery, however, is prohibitively expensive for regular use to map extensive wetlands (Shafi et al., 2019), thus making wetlands monitoring difficult.

This shortcoming paved the way to explore satellite imagery which is comparatively cheaper and capable of providing higher temporal resolution, not obtainable from aerial imagery, making it highly suitable for mapping and hence monitoring extensive wetlands in a manner never possible before (Kim et al., 2019). However, effective usage of early satellite imagery for wetland mapping had limitations imposed by the spatial and spectral resolution. The limitations arose from the shortcoming by most satellite multi-spectral imagery to provide sufficient spatial detail (spatial resolution) to enable identification of earth surface features covering small areas, while the spectral bands (spectral resolution) used to capture features are too coarse to allow for discrimination of earth surface features having nominally similar characteristics (Li et al., 2019).

The limitation in spatial resolution made the economically affordable low and medium spatial resolution satellite imagery unsuitable for mapping wetland sub-ecological zones, leaving wetland managers no option but to use the expensive yet suitable high-resolution hyperspectral imagery (Peddinti et al., 2021; Kim et al., 2019).

(Na et al., 2021) proposed an adapted a sparse constrained least squares linear spectral mixture model (SCLS-LSMM) to map sophisticated scenes of wetlands. The performances of the proposed methods on wetland vegetation communities mapping were then compared with the traditional full constrained least squares linear spectral mixture model (FCLS-LSMM) using HJ-1A/B hyperspectral images. When compared with the traditional FCLS-LSMM, the accuracy assessment results of the proposed methods demonstrated significantly better performance with a systematic error (SE) of 0.004 and a RMSE of 0.059 for Weedy meadow and a SE of –0.014 and a root-mean-square error (RMSE) of 0.087 for Reed marsh. The proposed methods enhanced the unmixing accuracies of wetlands' vegetation communities and exhibited the potential to understand degradation process in wetlands induced by climate changes and degradation due permafrost.

By combining a machine learning method for detecting change with EO-1 Hyperion satellite hyperspectral imagery, (Ahangarha et al., 2019) proposed a new procedure for determining land surface changes within the semi-arid wetland and surrounding upland areas of Shadegan wetlands

in the south-west of Iran in Khuzestan province. The outcomes demonstrated the superiority of the adopted technique for extracting change maps with an overall accuracy margin of about 94%.

Using Landsat data to classify the bog, fen, marsh, swamp, and water classifications specified by the Canada Wetland Classification System (CWCS), (Pouliot et al., 2019) assessed the capability of deep-learning Convolution Neural Networks (CNNs). With region sampling, overall accuracies of 69% and 90% for the CWCS and reduced classes, respectively, were attained. The findings indicated that precise Landsat classification of wetland categories remained difficult, especially for tiny wetlands. Further research into deep learning techniques was advised in order to pinpoint CNN setups and sampling techniques that would work best for images with intermediate spatial resolution in a variety of situations.

(Hasanlou and Seydi, 2021) proposed a framework for hyperspectral change detection methods on wetland and water body areas using chrono chrome, Z-score analysis, Otsu algorithm, SImplex via Split Augmented Lagrangian (SISAL), Harsanyi-Farrand-Chang (HFC), Pearson correlation coefficient (PCC), and support vector machine (SVM). The proposed method's performance was then evaluated using multi-temporal hyperspectral Hyperion images of the Shadegan Wetland. The results showed that the proposed method methods had high accuracy and a low false alarm rate, with an overall accuracy of more than 96% and a kappa coefficient of more than 0.82. The proposed method could provide 'multiple changes' in addition to the magnitude of the extracted changes.

In this study, Hyperion satellite hyperspectral imagery was used while ‘Random Forest’ and ‘Variable Elimination’ statistical techniques were employed as data dimension reduction techniques to identify optimal bands for discriminating vegetation communities. Prior to this, a spectral library of the vegetation communities’ spectra extracted from the Hyperion image itself to serve as ground-truthing data was created.

3.3 Hyperion Hyperspectral Imagery Processing

Hyperspectral images are overdetermined spectrally. Hence, they contain excessive spectral data to allow for identification and discrimination between unique materials that otherwise are spectrally similar (but unique) and not distinguishable with multi-spectral imagery (Park et al., 2018). Consequently, hyperspectral imagery has the ability to offer more precise and comprehensive information retrieval than other forms of remotely sensed data.

Most hyperspectral images record reflected radiation as a collection of contiguous and narrow wavelength bands. On the contrary, multispectral sensors measure the reflectance using a few wavelength bands split by spectral sectors with no measurements (Park et al., 2018). A display (figure 3.1) of a single-pixel spectrum in hyperspectral imagery appears continuous. This kind of comprehensive pixel spectrum can provide far more details about a surface than is obtainable from a typical multispectral pixel spectrum. Hyperspectral imagery is determined by the narrowness and contiguous nature of the wavebands rather than the number of wavebands in the image. In general, phenomena on hyperspectral images are measured in bands of 10 to 20 nm intervals.

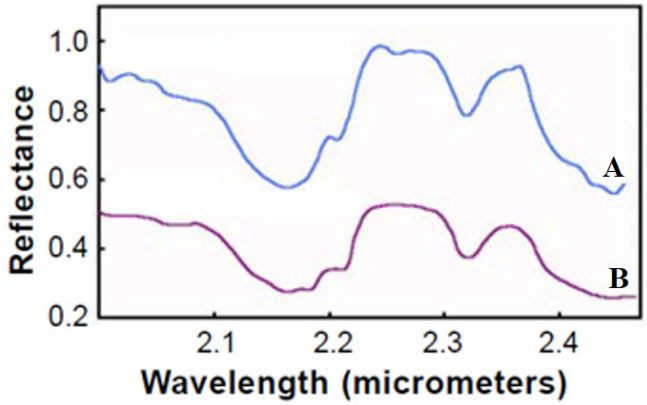

Figure 3.1: Pixel spectra of two different plant species (modified from (Smith, 2006))

Figure 3.1 illustrates the benefits of hyperspectral remote sensing. The figure shows spectra of two types of plant species measured by a hyperspectral sensor. Both plant species appear to exhibit similar absorption features across much of the spectrum. However, plant species depicted by spectrum B, displays a double-dip around 2.2μm (micrometres) of wavelength, while plant species represented by spectrum A shows only a single dip. The multispectral image, such as Landsat, records this entire spectral region around 2.2μm with one band and therefore does not provide sufficient detail to distinguish between these two plants species. The hyperspectral image records enough spectral detail to see the plant species double-dip depicted by spectrum B, thus using it to differentiate between the two very similar plant species. Related work has been undertaken using hyperspectral imagery to distinguish between plant species, construction materials, vegetation condition, forms of camouflage, and other spectrally similar materials.

Generally, there is a standard approach to processing hyperspectral imagery, like other types of imagery. Differences in the approach, however, only occur in terms of methods used for information extraction. Like all imagery, hyperspectral imagery depends on ancillary data, usually referred to as ground-truthing data, available in various forms that may include existing maps and

images or location and spectra of features obtained in the field. Once ancillary data has been acquired, hyperspectral satellite imagery is then subjected to a set of processing steps discussed below to obtain the desired results.

3.3.1 Sampling for Hyperspectral Imagery Processing

When collecting ground truthing data using existing maps, images or in the field, there is always a need to draw up a sampling scheme as data cannot be collected at every location. Sampling can be accomplished using a variety of approaches. The choice of the most suitable approach is dependent on various considerations.

3.3.2 Hyperion Hyperspectral Imagery Radiometric Pre-processing

Hyperspectral imagery used in this research was captured by the Hyperion sensor on-board NASA's Earth Observer-1 (EO-1) satellite launched in 2000 (Datt and Jupp, 2004, Barry, 2001). The pre-processing discussion presented here, therefore, focuses on the Hyperion hyperspectral imagery.

The Hyperion Sensor was NASA's first hyperspectral instrument in space under its New Millennium Program (NMP), covering the visible, near infra-red (VNIR), and short-wave infrared (SWIR) bands between 400 nm and 2500 nm. It operated for one year as an experimental mission. During this time, a team of scientists (NASA Science Validation Team (SVT)) assessed the technology and its applications (Datt and Jupp, 2004, Barry, 2001). The mission was then extended to provide hyperspectral data from space until 2017 when it was decommissioned. Data was made publicly available and distributed through the U.S. Geological Survey (USGS) by means of Data Acquisition Requests (DAR) during its post-experimental operation.

Hyperion was a narrowband push-broom imaging spectrometer that captured 242 spectral bands of data in strips of 7.7 km wide. It had a spectral range of 356-2577 nm of contiguous narrow bands of 10 nm nominal spectral range. The length of a Hyperion imagery scene is 42km or 185km with a pixel size of 30m x 30m. Hyperion flew at an altitude of 705km above the equator in a repetitive, circular, sun-synchronous, near-polar orbit. Hence, it could image virtually every point on the Earth's surface as it flew over all locations at about the same local time. It had a nominal revisit time of 16 days, with a potential of higher revisit frequency arising from possible sensor tilting (Eigemeier et al., 2012).

Several approaches to the pre-processing of Hyperion data exist (Barry, 2001; Dadon, 2010; Scheffler, 2014) with no established standard protocol (Scheffler, 2014). According to (Khurshid et al., 2006), pre-processing of a typical level 1 (format usually used by USGS to supply Hyperion

imagery) Hyperion image for retrieval of surface reflectance used in the analysis of ground surface-based features includes; spatial shift of the of the SWIR, destriping, angular shift correction, noise reduction, keystone detection and correction, smile detection and correction and atmospheric correction (figure 3.2).

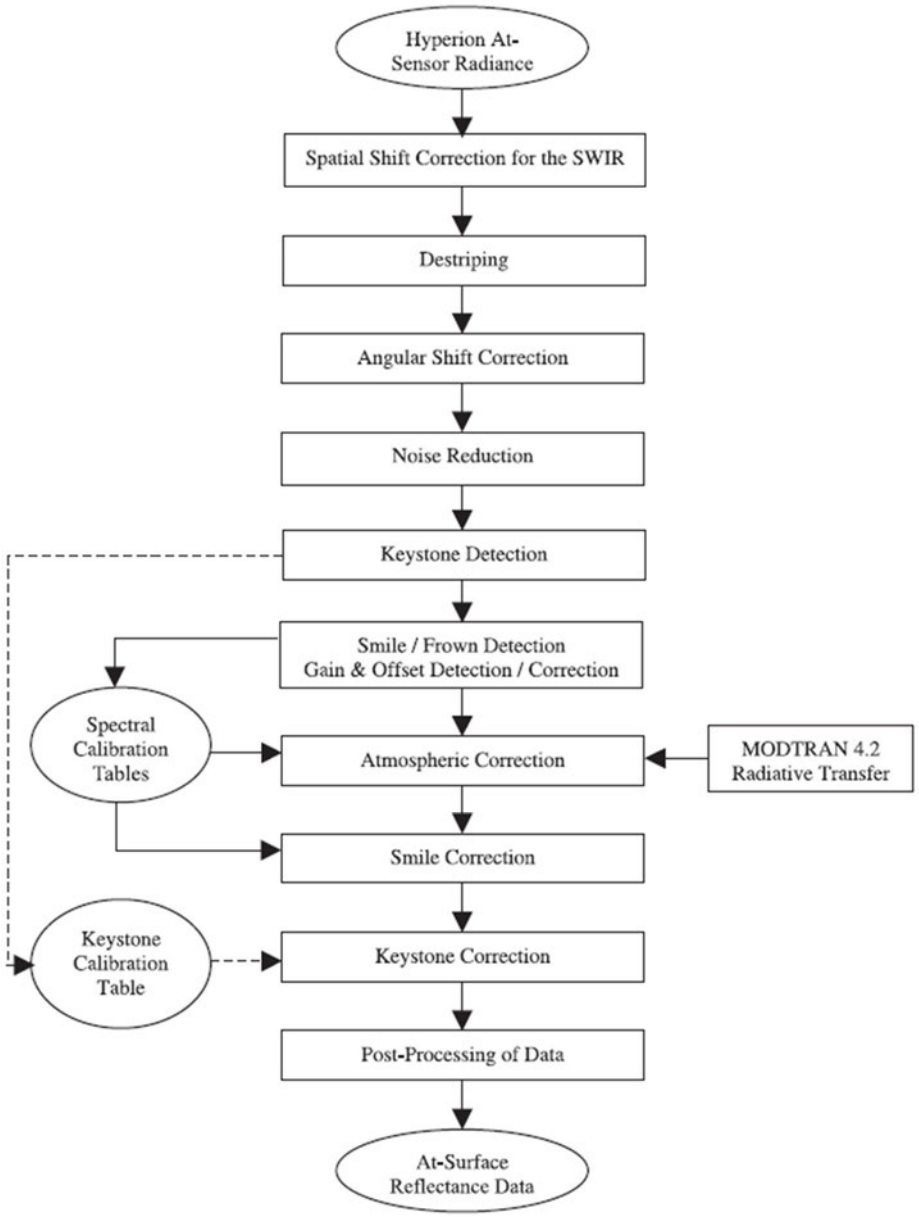

Figure 3.2: Hyperion Preprocessing Steps for Retrieval of Surface Reflectance (Khurshid et al., 2006)

However, (Datt et al., 2003) recommend pre-processing VNIR and SWIR separately, then combining them after pre-processing. Various researchers have included different steps in protocols (Farifteh, 2013). (Pervez et al., 2015), working on L1T processed Hyperion data, converted radiance from digital numbers first, then obtained reflectance from radiance, ending with atmospheric corrections/surface reflectance retrieval. (Aneece et al., 2019) propose a pre-

processing workflow that may include; (1) VNIR and SWIR separation, (2) Converting Digital Numbers to radiance, (3) Removing problematic bands, (4) Smile correction separately on VNIR and SWIR, (5) Merging VNIR and SWIR, (6) De-striping, (7) Atmospheric correction and (8) Cloud removal and spectral polishing/smoothing. Each of these processing steps is described below.

3.3.2.1 VNIR and SWIR Separation

Hyperion VNIR and SWIR data were captured by separate spectrometers with different calibration requirements. The VNIR data (bands 1-70) and SWIR (bands 71-242), therefore, should be separated to make subsequent steps easier, such as converting digital numbers to radiance that require different scaling factors, smile correction with different severity of smile effect and VNIR-SWIR alignment (Aneece et al., 2019).

3.3.2.2 Converting Digital Numbers (DN) to Radiance

Historically several Hyperion data processing levels have existed. Hyperion data were downlinked from EO-1, decoded, separated into files, and verified for data integrity and instrument performance. VNIR and SWIR datasets were then combined and converted into Hierarchical Data Format (HDF) to create Level 0 files. Level 0 processing did not remove SWIR smear, while echo artifacts correction was not performed. These corrections are required for all science applications (Barry, 2001).

Level 1 processed Hyperion data suitable for science applications was, therefore, obtained by removing SWIR smear and correcting for echo artifacts from level 0 processed data producing radiometrically calibrated Hyperion data (Barry, 2001). Level 1 data may be of the form L1R, L1G, and L1T (Kumar and Yarrakula, 2017), depending on subsequent processing performed on the data.

- **Level 1R (L1R)** data consists of images corrected for radiometric errors (watts/(sr-micron-m^2) x100) to compensate for variations due to detector sensitivity, formatted as HDF files and metadata added in binary and ASCII formats (USGS-EROS, ND). L1R data is pseudo geometrically corrected using scene corner points only.
- **Level 1Gst (L1Gst)** is radiometrically and geometrically corrected and supplied in 16-bit radiance values. It is also corrected for the effect of terrain using a DEM, thus correcting parallax error from variation in topography. Consequently, overall registration accuracy between bands is also greatly improved (Paolo, 2011). Elevation data used for correction is obtained from SRTM data sets and other elevation data sources as required (USGS-EROS, ND). L1Gst data is made available in Geographic Tagged Image-File Format (GeoTIFF).

- **Level 1T (L1T)** is corrected for radiometric, geometric, and terrain errors and scenes supplied in 16-bit radiance values. Unlike L1Gst data, L1T is geometrically corrected by the use of ground control points. Hence, they are only generated when there are adequate ground control points. L1T scenes are provided in GeoTIFF format images and are also available as Full Resolution Browse and GIS Ready Bundle products in JPEG format (NASA-EARTHDATA-CMR-Search, ND).

Given the above formats, the Hyperion data consisting of signed integers required converting to (SI) units of Wm-2 μm-1 sr-1 by multiplying by 40 in the VNIR and 80 in the SWIR to maintain both precision and avoid overflow of saturated pixels (Jupp et al., 2004). Converting Digital Numbers (DNs) to radiance entails dividing DNs in VNIR by 40 and those in the SWIR by 80 (Barry, 2001).

3.3.2.3 Removing Problematic Bands

Several of the Hyperion sensor's potential 242 spectral bands lack illumination (due to atmospheric absorption or a reduction in longer infrared wavelengths' incident solar spectral irradiance) or have a spectral response that is very low, while only 220 bands of these are unique. Several bands, therefore, are removed, leaving only 198 usable spectral bands covering wavelengths 436-926 nm in the VNIR (bands 8-57) and wavelengths 933-2406 nm in SWIR (bands 77-224) (Pearlman et al., 2003). Different researchers have retained slightly different sets of Hyperion bands, however. (Aneece et al., 2019) cited (Farifteh et al., 2013) as having retained bands 1-92 (426-1346 nm), 103-136 (1457-1790 nm), and 154-193 (1971-2365 nm) for a total of 166 bands, and (San and Suzen, 2010) as having used 141 bands that included 437-922, 925-1295, 1477-1739, 2012-2375 nm. Thus, the selection of which bands to retain is highly dependent on the application. However, three regions very commonly removed include bands around 925, 1385, and 1885 nm, which are mostly affected by water vapour absorption.

3.3.2.4 Smile correction separately on VNIR and SWIR

The spectral smile-frown, also referred to as *"spectral line curvature"* (Khurshid et al., 2006), is an effect of low frequency arising from the variation in full width at half maximum (FWHM) and central wavelength across a line of pixels (Yang et al., 2015). In push-broom sensors, such as Hyperion spectral smile is caused by lack of uniformity in spectral response across the detector arrays' elements in the VNIR and SWIR regions. In Hyperion data, the effect of spectral smile is less pronounced in the SWIR than in VNIR (Datt and Jupp, 2004).

The central wavelengths and FWHM's across the 256 pixels for all 242 Hyperion bands are available from the pre-launch calibration data. The central wavelengths and FWHM's of the central pixel (pixel 128) in the Hyperion level 1B1 data were provided in the image header files. In more recent level 1R data, average values of the central wavelengths and FWHM's across the 256 pixels are provided in the image header files (Datt and Jupp, 2004).

The effect of spectra smile on Hyperion images may vary considerably in different areas of the spectral range and among scenes. An indicator is usually required to detect spectral smile affected images as it is not apparent to the naked eye. (Mora, 2014), describes two methods of detecting spectral smile effect in the affected images; the first is to use O2 absorption features in specific spectra regions, and the second is the Minimum Noise Fraction (MNF) transformation. A technique developed by the Canada Centre for Remote Sensing (CCRS) employs atmospheric absorption features available at the sensor radiance spectra and common to all pixels in the scene for detection and subsequent adjustment of bandwidths and band center wavelengths (Neville, 2004).

Correction for spectral smile effect can be accomplished using various approaches. One approach would be to apply atmospheric corrections separately on each of the 256 individual columns of data, using central wavelengths and Full Width at Half Maximum (FWHM) for each column. This method, however, would be computationally intensive. An alternative would be to interpolate the image radiance data to the same set of central wavelengths and FWHM's across all 256 pixels of the image swath (Datt and Jupp, 2004). According to (Aneece et al., 2019), three among the various methods for smile effect removal outlined by (Goodenough et al., 2003) include *"moving a linear fitting and interpolation, column mean adjusted in radiance space and column mean adjusted in Minimum Noise Fraction (MNF)".*

During correction, the at-sensor Hyperion radiance in a specific absorption feature is compared to the modelled at-sensor radiance in the same feature measured with the radiative transfer (RT) code MODTRAN 4.2 to determine band center wavelengths and bandwidths. The smile–frown technique produces a new range of wavelength centers and bandwidths for each column along track as its final product (Khurshid et al., 2006).

Smile correction may be incorporated into the atmospheric correction such as by using FLAASH –IDL (Aneece et al., 2019)

Aligned with the concept of spectral smile is a term 'keystone', which refers to bad spatial registration between bands in imaging spectrometers (Neville et al., 2004). Keystone distortions may arise due to chromatic aberration or geometric errors, or a combination of both. These distortions result in a specific spatial pixel matching a particular detector element in the across-track alignment in one spectral band not being registered with the matching pixel in the other spectral bands on the ground. (Bannari et al., 2015). According to (Neville et al., 2004), the Hyperion sensor had minor keystone distortions for both VNIR and SWIR spectrometers and, therefore, not always included in Hyperion pre-processing chains.

3.3.2.5 Merging VNIR and SWIR

The Hyperion VNIR and SWIR data are spatially misregistered due to the misalignment of several detectors within the instrument used to provide broader spectral or spatial coverage (White et al., 2004). VNIR and SWIR images pre-processed separately in the previous steps, therefore require merging into a single image corrected for this misalignment.

This is accomplished in two steps; (1) spatial shift correction for the SWIR dataset (2) angular-shift correction.

Spatial shift correction entails correcting for a one-pixel shift which occurs between pixels 128 of the left half and 129 of the right half image of the SWIR data (figure 3.3).

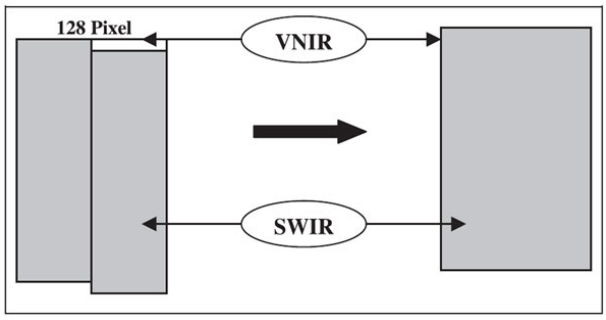

Figure 3.3: Spatial shift correction for SWIR data (Khurshid et al., 2006)

This vertical offset arises from the difference in the VNIR and SWIR spectrometers readout process. The correction allows VNIR and SWIR to look at the same pixel on the ground spectrally (Khurshid et al., 2006). (White et al., 2004) citing (Pearlman et al., 2003) states that Hyperion SWIR detector required shifting of columns 129-256 upward by one row to align with columns 1-128.

Following correction for vertical offset, the images need an angular shift to align pixels in the VNIR to that in SWIR images. The correction for angular shift matches two image planes from both detectors to determine the angular rotation required to align the detectors (White et al., 2004). (Khurshid et al., 2006) achieved this by a counter-clockwise rotation of VNIR by 0.22° using bicubic resampling applied to VNIR at-sensor radiance data, incorporated in the 'align detector' tool in Imaging Spectrometer Data Analysis Systems (ISDAS). Due to their lower radiometric fidelity, the VNIR data was matched to the SWIR data. Alternatively, the VNIR image's bands 56 and 57, which spectrally coincide with the SWIR image's bands 77 and 78, can be used to align the two images (Aneece et al., 2019).

3.3.2.6 De-striping

Image acquisition using scanning systems usually involves striping noise. Striping noise can be mitigated by means of radiometric calibration. However, the residual noise tends to affect the extraction of physical parameters and quantitative analysis of the images (Guzzi et al., 2019). Stripes may occur as a result of systematic noise such as from detector non-linearities, effects of temperature, or a single detector element's functional failure during image acquisition (White et al., 2004). Striping noise created by minor relative calibration errors in each detector caused by push-broom technology was visible in all Hyperion data and needed to be resolved in order to improve analysis and interpretation of Hyperion data (Hamadache and Smara, 2014).

Various methods exist for the removal (de-striping) of stripes from Hyperion imagery. When striping arises from a dead pixel, the pixels making up the stripe contain a zero value. The missing pixel value is replaced with a linearly interpolated value of the two nearest valid pixels (White et al., 2004). For all other stripes, de-striping is accomplished using a variety of approaches.

(Hamadache and Smara, 2014) evaluated three de-striping algorithms for Hyperion data; the local approach, the global approach, and the Discreet Wavelength Transform – Fast Fourier Transform (DWT-FFT) filtering approach, called the Combined Filter, to correct vertical stripes in Hyperion data without interfering with the spectral information. The results obtained were considered better using the global method because all stripes were removed than the two other methods. However, it caused considerable alteration of information resulting in poor image classification. The local approach provided more of a smoothed calibrated data based on smoothing filters, and though left some stripes, produced the best of the image classification results. A reduction of striping noise and an over smoothing on the results obtained by the combined filter approach was observed; however, the resultant image was badly classified (Hamadache and Smara, 2014).

(Aneece et al., 2019), tested several de-striping methods establishing the following based on the results obtained: (1) de-striping using the local approach is often used because it outperforms global de-striping (Datt et al., 2003); while local striping is found to decrease striping substantially, some stripes especially several adjacent to each other were not removed but could be removed using a wider filter kernel instead, (2) global de-striping, though not as good as local de-striping, can minimize the effect of spectral smile, (3) wavelet Fourier Adaptive Filtering techniques removed more stripes that did local de-striping, but with greater alteration of the original data.

When local de-striping is applied to an image on individual bands, the pixel masked out in one band may not be masked out in another adjacent band (Aneece et al., 2019). Hence the value of a pixel masked out in one band was often not different from the value of that pixel in adjacent bands where it was not masked out. Therefore, it was concluded that after bad bands have been removed from a Hyperion image, much of the striping issue is also resolved without further need for de-striping, thus making de-striping an unnecessary step to image processing and analysis of Hyperion data (Aneece et al., 2019).

3.3.2.7 Atmospheric Correction

Correction for atmospheric effects is a prerequisite if images have to be compared with site spectra and library spectra or application of models or when images captured at different times have to be compared. The process requires that Top of Atmosphere (ToA) reflectance is determined first. The reduction in energy due to the atmosphere that includes scattering, water vapor, ozone, and aerosols (Jupp et al., 2004), is then estimated to obtain surface reflectance. (Aneece et al., 2019) states that ToA can be calculated from equation 3.1, *"where L is at-satellite radiance in W m^{-2} sr^{-1} nm^{-1}, d is Earth-Sun distance in astronomical units, E_{sun} is solar irradiance in W m^{-2} sr^{-1} nm^{-1} and θ_z is zenith angle in radians."*

$$ToA = \frac{\pi * L * d^2}{E_{sun} * \cos(\theta_z)} \quad \text{..... 3.1}$$

(Aneece et al., 2019) further states that following removal of atmospheric effects, earth surface reflectance (SR) can be estimated from equation 3.2 assuming no presence of haze, *"where θ_v is viewing angle in radians, T is transmittance (unitless) affected by various atmospheric elements and E_{sun} is diffuse downwelling irradiance."*

$$SR = \frac{\pi * L}{\cos\theta_v * (E_{sun} * cos\theta_z * T + E_{down})} \quad \text{..... 3.2}$$

Transmittance, T, in equation 3.2 can be obtained from equation 3.3 *"where $T_{R\lambda}$ is Rayleigh transmittance (unitless) dependent on wavelength, λ, $T_{o\lambda}$ is ozone transmittance (unitless), $T_{n\lambda}$ is nitrogen dioxide transmittance (unitless), $T_{g\lambda}$ uniformly mixed gas transmittance (unitless), $T_{w\lambda}$ is water vapour transmittance (unitless) and $T_{a\lambda}$ is aerosol transmittance (unitless)."* (Aneece et al., 2019).

$$T = T_{R\lambda} * T_{o\lambda} * T_{n\lambda} * T_{g\lambda} * T_{w\lambda} * T_{a\lambda} \quad \text{..... 3.3}$$

E_{down} in equation 3.2 is calculated using equation 3.4, where τ_D is the dimensionless transmission coefficient for direct solar radiation (Aneece et al., 2019).

$$T_{down} = E_{sun} * \tau_D \quad \text{.....3.4}$$

(Aneece et al., 2019) cites (Gopinatha and Polokoana, 1960) as having provided details for calculating τ_D.

There are several algorithms available to compensate for the effects of the atmosphere on the measured signal. For the VNIR through to SWIR, they include statistical models that make use of empirical in-scene data and radiative transfer algorithms based on physics (Griffin and Burke, 2003).

Statistical or empirical models depend on pre-existing information present in the scene coupled with a regression algorithm sensor spectral observation. Models based on physics use atmospheric physical characteristics to derive contributions of aerosol, water vapor, and mixed gas to the atmospheric signal. Atmospheric compensation models' treatment of aerosols and characteristics of the scene, including atmospheric visibility, aerosol type, atmospheric temperature, and solar zenith angle, may vary considerably (Griffin and Burke, 2003).

According to (San and Suzen, 2010) several algorithms for atmospheric correction based on LOWTRAN or MODTRAN radiative transfer exist in literature and/or commercial use. Suitability of use of each of these algorithms is influenced by a variety of factors. In a study conducted by (San and Suzen, 2010) to evaluate the suitability of use of *"the Atmospheric CORrection (ACOR), the Fast Line-of-sight Atmospheric Analysis of Spectral Hypercubes (FLAASH), and ATmospheric CORrection (ATCOR 2-3)"* ACORN was found to be a slightly better corrector despite compromises in different wavelength regions.

According to (Aneece et al., 2019), several atmospheric models for solving radiative transfer equations to assess the influence of atmospheric components on incoming radiation have been discussed in many papers. Moderated Resolution Atmospheric Transmittance (MODTRAN),

Atmospheric Removal (ATREM), Atmospheric Correction Now (ACORN), Fast Line-of-Sight-Atmospheric Analysis of Hyper-cubes (FLAASH), Discrete Ordinate Radiative Transfer (DISORT), Auscover/Curtin Hyperion Enhancement and Atmospheric Correction Technique (A/CHEAT) and Simple Model of the Radiative Transfer of Sunshine (SMARTS) have been compared yielding varying results (Aneece et al., 2019).

A study involving five atmospheric correction algorithms (DOS, QUAC, FLAASH, ATCOR and 6S) undertaken by (Marcello et al., 2016) to identify the most appropriate technique(s) for vegetation cover discrimination using high-resolution Worldview-2 imagery and field spectroradiometer data collected simultaneously, revealed 6S as the best under the circumstances. The study provided a thorough review of the parameterization impact on the final results of the correction, with the aerosol model and its optical thickness being significant parameters that needed to be adjusted properly. (Marcello et al., 2016). (Seidel et al., 2010), however, had established that SMART model is 25 times faster than 6S with only 5% difference in spaceborne data processing results.

A comparative study involving the use of QUAC and FLAASH for atmospheric correction on hyperspectral imagery found FLAASH to be the better, thus recommending its use over QUAC to correct for atmospheric effects as well as correct identification and interpretation of any object or mineral composition (Rani et al., 2017, Somdatta and Chakrabarti, 2011). FLAASH is further considered suitable because it employs a full MODTRAN4 radiative-transfer code for atmospheric scattering and transmission properties modelling at the time of image capture (San and Suzen, 2010), including *"a full accounting for the adjacency effects (the scattering from adjacent pixels into the current pixel-sensor line of sight) associated with atmospheric scattering"* (Griffin and Burke, 2003). The use of FLAASH for atmospheric correction requires a visibility input value for estimating the levels of atmospheric aerosols as well as temporal and geographic scene details (San & Suzen, 2010).

FLAASH, can recalculate the visibility by using a ratio between dark pixels at 2100 nm (nanometres) and 600 nm.

However, a more precise estimation of visibility can be obtained by using a weather station ground-based optical measurements in the vicinity of the study location, if one exists. FLAASH was considered ideal for use in this research.

3.3.2.8 Cloud removal and Spectral Polishing/smoothing

It is often quite challenging to obtain satellite imagery that is free of clouds. Clouds and cloud shadows can affect spectral values and spectral profile shapes, and consequently, affected pixels need to be corrected for these artifacts (Aneece et al., 2019).

Threshold reflectance in the blue band and a sum of reflectance in the red, green, and blue bands can be used to detect the presence of clouds in the image (Aneece et al., 2019) since clouds usually have very high reflectance in the visible portion of the electro-magnetic spectrum. The sum of bands in the NIR and SWIR regions can be used to detect cloud shadows as shadows often have much lower reflectance in these regions. The thresholds and degree to which the user wants to mask out clouds and shadows may vary from image to image. It is worth noting that the mask used to remove cloud shadows also masks water bodies, thus requiring a more complex mask if the project involves water study (Aneece et al., 2019).

(Chandran and Jojy, 2015) propose adaptive Markov random field (MRF) approach for detecting and removal of clouds in hyperspectral imagery. MRF is a widely used method that integrates both spatial and spectral information for improved classification, including spatial temporal methods to address the problem of cloud-masking complicated by the non-rigid nature of the cloud masses (Chandran and Jojy, 2015). Conventional MRF methods only account for spatial dependency relations, ignoring the temporal information that is frequently present in image sequences. Therefore, the method was adapted to apply a spatio-temporal MRF method to the cloud masking problem complicated by the nonrigid nature of the cloud masses. A method uses two mass tracking techniques;

(1) *"an effective and efficient implementation of the probability hypothesis density (PHD) filter, which is based on Gaussian mixtures (GMs) and relies on finite set statistics (FISST)",*

(2) *"region matching procedure based on a maximum cross-correlation (MCC) characterized by low computational load"* (Chandran and Jojy, 2015).

The approach proved particularly useful in addressing the issue of cloud edge misclassification, which is usually caused by low contrast against a sea or land backdrop, by using cloud motion as an additional discriminant function against a static background. According to this research, cloud identification using the MAP-MRF technique is a more robust and effective tool than other cloud classification algorithms (Chandran and Jojy, 2015).

3.3.3 Geometric Correction of Hyperion Imagery

Whenever satellite imagery is to be used in conjunction with surface reflectance, there is always a need for georeferencing to establish a relationship between the image and its corresponding location on the ground location. Georeferencing, however, leads to resampling of the image that may or may not be accurate in terms of location or resulting re-sampled spectra (Beck, 2003). Therefore, it is important to decide at what stage in the processing chain georeferencing should be undertaken, and consequently, it may not constitute part of the pre-processing stage. It is usually recommended that georeferencing be undertaken after retrieval of reflectance to exclude the effects of resampling from the atmospheric correction (Rogass et al., 2014, Milewski et al., 2017).

Depending on the format Hyperion image is provided in (L1R, L1Gst or L1T), it may or may not require georeferencing or refinement of its georeference. If georeferencing has to be carried out, nevertheless, it can then be accomplished by the process of geocoding applied using either image-to-map or image-to-image registration.

During image to map registration, an existing map, usually, a topographic map is used as a spatial reference frame for georeferencing. Features not easily disturbed and easy to locate on both map and image such railway lines, bridges, road crossings, reservoirs, etc. are used as Ground Control Points (GCP) (Dobhal, 2008). First-order (affine or bi-linear) transformation with a minimum of 4 GCPs is considered appropriate for georeferencing Hyperion imagery because of the simplicity of its data geometry (Thulin, 2008, Thulin et al., 2014).

When image to image registration is undertaken, one of the images usually already registered to a spatial reference frame serves as a base for georeferencing. Image to image registration involves co-registration of matching pixels in the two images (Dobhal, 2008), and usually, a substantially large number of pixels representing features identifiable in both images are used.

The RMSE serves as a measure of georeferencing accuracy for both methods and is required to be no more than half the pixel spatial resolution. During georeferencing the appropriate datum is also specified to provide details of the associated geodetic projection and coordinate system of reference frame (Dobhal, 2008).

3.3.4 Spectral Library Development

Effective application of hyperspectral imagery, like all imagery, depends on the availability of spectra or spectral signatures of features being studied. Such spectra are best provided as part of

a digital database usually referred to as a spectral library. While hyperspectral imagery provides opportunities to map vegetation community types and plant species, their success depends on the availability of spectral libraries of the species being mapped (Zomer et al., 2009). The spectral library development process involves several stages: collecting spectra measurements, processing measured spectra, and compiling a database of processed spectra.

Spectra of target features (endmembers) for the development of a spectral library can be captured using various sources inclusive of in-situ field measurement, laboratory measurements, aerial and satellite imagery (Aneece et al., 2019, Nasarudin and Shafri, 2011, Beltran-Abunza, 2009, Rama Rao and Bernd, 2011, Manjunath et al., 2014, Rama Rao, 2008). Various conditions may have to be considered when collecting spectra. Requirements for in-situ field spectra measurements, for example, would include the position of the sensor (spectroradiometer) above the target (leaf or canopy level), choice of appropriate Field of View (FOV), calibration of the spectroradiometer before taking the target readings, and environmental conditions such as wind, as this affects reflectance recorded from the leaves (Manjunath et al., 2014).

Processing of collected spectra and associated data may vary widely depending on the source type and collection method and may require pre-processing. This may include data format conversion among various software packages to be used for processing (Nasarudin and Shafri, 2011). (Manjunath et al., 2014) pre-processed field measured spectra to remove erroneous readings arising from the difference in position of the spectroradiometer above the target features or abrupt change in sunlight conditions before determining spectra average for discriminant analysis. Additional pre-processing may include resampling of 1nm spectra to spectra with coarse wavebands. Resampling, however, is better undertaken as a precursor of the spectral matching process once the spectral resolution of the target spectra has been identified to make simple comparisons of wavelengths and reflectance values possible. Based on previous research which had established that wavebands in close proximity to one another produced similar information (Brogea and Leblancb, 2000, Thenkabail et al., 2002), (Manjunath et al., 2014) averaged 1nm spectral data to that in excess of 10nm, which reduces the number of data points for further processing. (Manjunath et al., 2014) citing (SAC, 2007), states that spectra range not more than 10 nm may be prone to noise while those in excess of 10 nm have a smoothening effect of many absorption peaks. There are several techniques for data resampling from 1 nm to 10 nm. (Zomer et al., 2009) assessed and inspected field spectra visually for data quality before grouping them into vegetation groups. Spectra means were then determined for the various subsets of vegetation categories, separately for both averages of monospecific and multiple mixtures of plant species abundances. These were then exported into ENVI software as data cubes for use as training data in subsequent image data analyses and the creation of an ENVI spectral library. The original un-

averaged spectra were also exported into ENVI following screening for quality and errors where they were organized into Regions of Interest (ROI) corresponding to the field measured vegetation abundance categories for subsequent use as training data in further analyses (Zomer et al., 2009).

Further processing in ENVI allowed for the separation of spectra along numerous axes and clusters of data points, revealing natural groupings corresponding to abundance categories of species/vegetation, thus confirming the use of spectral signatures to identify species and/or vegetation types (Zomer et al., 2009). *"Results from this analysis were used with a vegetation community analysis to classify and identify vegetation communities"* (Zomer et al., 2009).

The development of a database for storing spectra may follow any of the various existing approaches for creating a database. Though spectra constitute a spectral library's main content, various other data may be incorporated depending on the original purpose for which the spectral library is developed. Figure 3.4 illustrates a data model of the multiple aspects of featured crops making up a spectral library designed for the Chinese province of Guangdong (Chen et al., 2005).

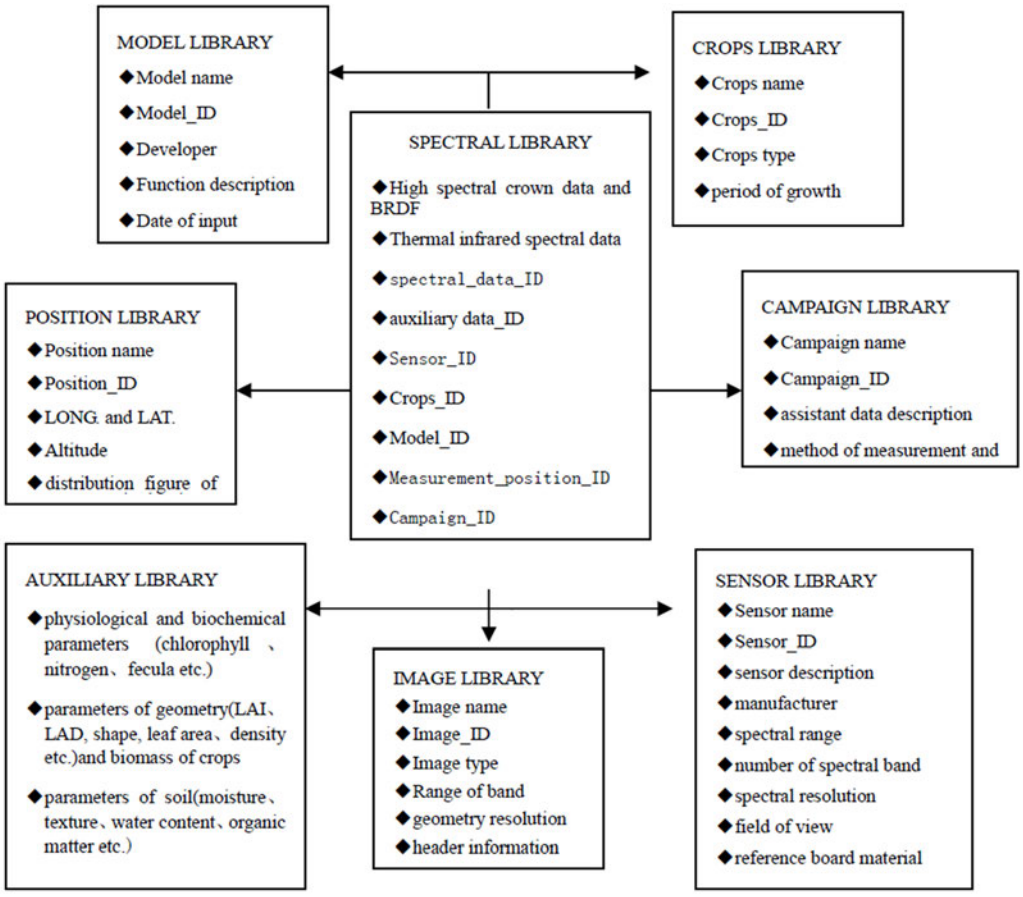

Figure 3.4: Spectral Library Data Model for featured crops of Guangdong Province (Chen et al., 2005)

Using MS-Access as a backend database, (Manjunath et al., 2014) organized species, spectral, and lab observations into plant details, observation details, biochemical details, indices, and spectra (Figure 3.5).

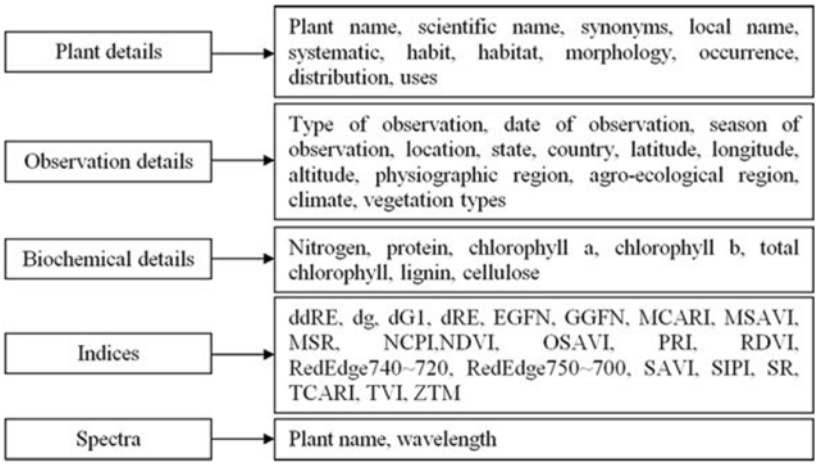

Figure 3.5: Spectral Library Data structure of Major Plant Species of Western Himalayas based on Ground Observations (Manjunath et al., 2014)

The tables created on the basis of data provided in figure 3.5 were joined through a common field (primary key) using one-to-many and many-to-one relationships. Figure 3.6 shows a display of the Graphical User Interface and query modules developed for the data structure depicted in figure 3.5.

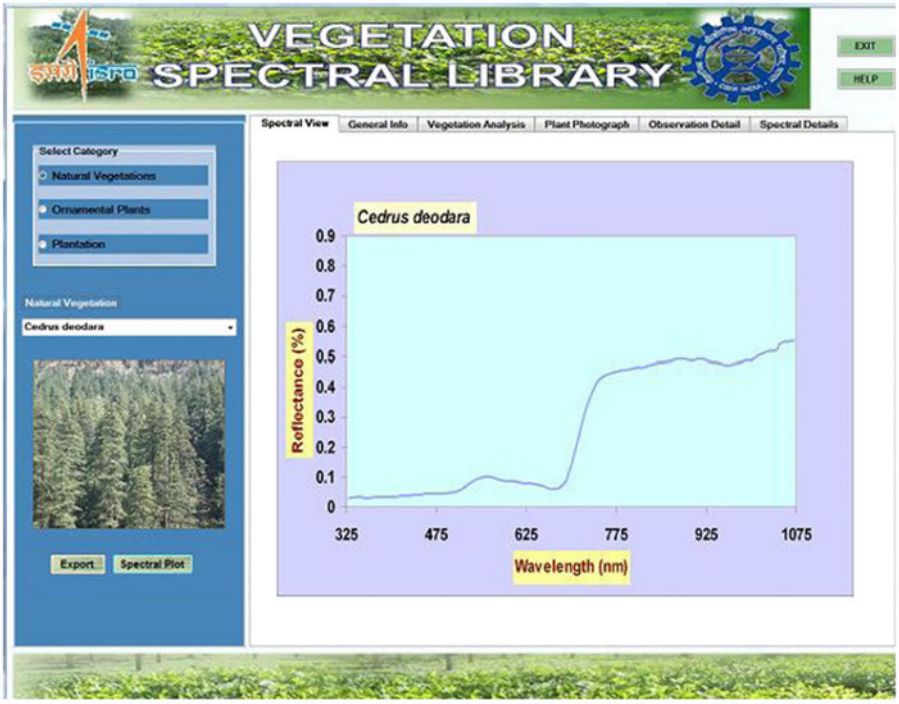

Figure 3.6: Spectral library Graphic User Interface (GUI) and query modules of the Major Plant Species of Western Himalayas based on Ground Observations (Manjunath et al., 2014)

Databases of spectra may be restricted to organizational use or be open to the entire remote sensing community and accessible using the Web. Formats used may vary accordingly, ranging from very simple forms such as a web-listing to more advanced forms that allow searches, query and download of specific spectra records (ibid). Simple websites, allowing listing, download and viewing of spectra datasets are used by the Unites States Geological Survey (USGS), ASTER, Arizona State University and Santa Barbara Urban Spectral Library (ibid).

During the development of a spectral library, (Chen et al., 2005) concentrated on a variety of factors, including the design of data organization, the nature of data organization, information security, shortcuts, powerful features, cutting-edge technologies, user-friendliness of the interface, sustainable updating, and data exchange information safety. With an internet-based visual interface, users could input and query any number of spectral curves inclusive of associated metadata to provide a convenient share of spectral information (Chen et al., 2005).

Metadata completeness and quality for spectral libraries intended for the exchange and sharing of spectra datasets are of vital importance in developing a spectral library (Rasaiah et al., 2015). Metadata serves to inform potential users of the suitability of use of the spectra datasets in the concerned spectral libraries to their applications, thus requiring standardization. Metadata was proposed as part of the spectra metadata standardization process by an international advisory panel of 90 experts representing a diverse community specialized in collecting spectroscopy data from a wide variety of disciplines. The metadata elements included viewing geometry, general target and sampling properties, location, instrument properties, illumination, reference standards, hyperspectral signal properties, calibration, atmospheric conditions, among other details (Rasaiah et al., 2014).

3.3.5 Selection of Optimal Wavebands for Spectral Matching

Spectral wavebands in the immediate neighborhood of hyperspectral data have been established to be highly correlated and thus found to contain similar and, in most cases, redundant information (Brogea and Leblancb, 2000, Thenkabail et al., 2002). Effective deployment of hyperspectral data for material identification calls for specialized techniques to facilitate the extraction of non-redundant details from reference spectra collected at higher spectral resolution before being applied to target spectra. This is usually the case with field and laboratory collected spectra where spectroradiometer with 1nm sampling interval are usually employed. Therefore, optimal waveband selection allows for the identification of the electromagnetic spectrum regions that can best be used in discriminating among various target materials based on certain characteristics (Adam and Mutanga, 2009). This is achievable by the use of data reduction techniques. The

optimal wavebands, once identified, are then subsequently used to cluster hyperspectral imagery pixels into categories of similar spectra for image classification purposes.

Identifying suitable wavebands for this reason without losing any critical information is a requirement in hyperspectral remote sensing applications. Techniques for the selection of optimal bands for the analysis of imagery data for a particular application abound. *"Discriminant analysis, canonical variate analysis, classification trees, support vector machines, and principal component analysis,"* among others (Adam and Mutanga, 2009, Mutanga and Skidmore, 2004) cited in (Mansour et al., 2012), have been used to identify suitable wavelengths for distinguishing plant species and vegetation assemblages as part of the data reduction process with varying degrees of success. (Kalacska et al., 2007) used principal component analysis, wavelet energy feature vectors and forward feature selection as well as pattern recognition classifiers to distinguish lianas and trees spectral signatures using a dataset of leaf-level and crown level (airborne hyperspectral image) spectra. The forward waveband selection approach produced the best results for the leaf level spectra, followed by the wavelet energy feature vectors, then a type of principal component analysis. Pattern recognition classifiers faired poorly across all reduction techniques. None of the techniques used provided optimal data reduction for the crown level spectra. Furthermore, different significant wavebands were identified between the leaf and crown levels. At the leaf level, the visible area was found to be the most important for distinguishing lianas and plants, while at the crown level, the shortwave infrared was discovered to be important in addition to the visible and near-infrared (Kalacska et al., 2007).

Among the various data reduction techniques explored by researchers, and thus for optimal waveband selection, Random Forest (RF) algorithm has been found to perform better in most instances (Prospere, 2014). RF is widely used for prediction and interpretation purposes in many research fields. Its popularity stems from a number of appealing features, including the ability to deal with high-dimensional data, variable correlations, and complex interactions (Hapfelmeier et al., 2014). It is well suited to handling a diversity of data sets and often only requires little pre-processing (Williams, 2011). Another important feature for the use of RFs is the provision of variable importance measures that can be used to identify the predictor variables most important for a given data set (Williams, 2011). (Mansour et al., 2012) acknowledge the robustness and accuracy of RF, both for variable selection and classification.

While RF ranks variables according to their importance, it does not automatically eliminate redundant bands (Poona and Ismail, 2013) or choose the optimum number of variables for the best classification accuracy (Adam et al., 2009, Mansour et al., 2012). It is therefore recommended to use variable importance measurement produced by use random forest to

determine the optimal subset of wavelengths. A commensurate number of wavelengths for classification is required to avoid the 'curse of dimensionality' (Merentitis et al., 2014), where too many wavebands for very few features (endmembers) would lead to poor classification. The 'curse of dimensionality' frequently results in reduced classification accuracies arising from the number of features being many times more than the number of samples.

3.2.5.1 Random Forest Algorithm

Random Forest is a tree-based machine learning ensemble algorithm that employs bootstrap aggregation (bagging) to construct multiple individual decision trees considered to be diverse due to the use of random samples drawn from the training data set (Mansour et al., 2012). A machine learning ensemble is a technique for making more accurate predictions by combining predictions from multiple machine learning algorithms. (Brownlee, 2016). (Williams, 2011) compares the performance of an ensemble of trees to bringing together panels of experts from various institutions such as government, industry, and universities to ponder over an issue to come up with a consensus decision which none of these panels working in isolation can achieve. *RF "uses bagging as the ensemble method and a decision tree as the individual model"* (Zhang et al., 2021). Bagging entails training a number of individual models in parallel, with each model being trained using a random subset of the data (Chen, N.D.). Bagging is unlike 'boosting', which involves training a number of individual models sequentially, with each subsequent individual model learning from the previous model's mistakes (Chen, N.D.). The actual model builder for RF *"could be a decision tree algorithm, a regression algorithm, or any one of many other kinds of model building algorithms"* (Williams, 2011). The RF algorithm builds hundreds of decision trees to their maximum depth without pruning and then creates a single model from them. The resultant combined model reduces the instability observable when single decision trees are built (Williams, 2011). The decision of majority constituent trees and the average of regression for trees for classification and regression respectively is taken as the ensemble's final decision.

According to (Williams, 2011) the deployment of Random forest involves (1) random selection of different subsets of training data (known as a 'bag') used to train each tree making up the ensemble, (2) train each tree using two-thirds of the training data with the remaining one-third (known as 'Out Of Bag' [OOB] being used to estimate error and variable importance, and (3) assigning the number of votes from all the trees to classes for classification to identify the most popular class or the average of the results for regression.

Applied to classification, (Breiman, 2001) describes an RF algorithm as consisting of a collection of decision tree classifiers (figure 3.7), each of which casts a unit vote for the most popular class, while for regression, the equivalent of the most popular class is the average.

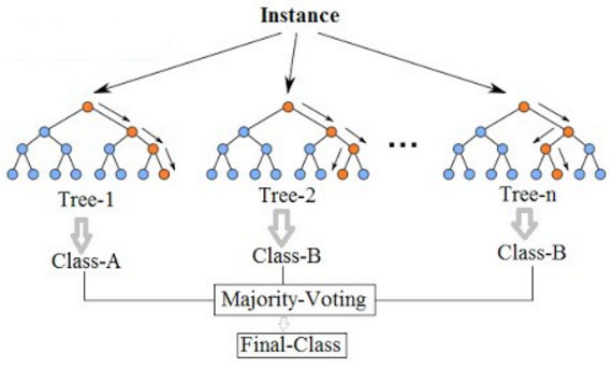

Figure 3.7: Simplified representation of RF ensemble decision making process for classification (Koehrsen, 2017)

According to (Mansour et al., 2012), each decision tree in the forest is constructed using the following steps;

1). Selection of the number of trees (T) to be grown.

2). Choosing the number of variables (f) to split each node with the requirement that f < F, where F is the input data variables (features) and (f) is a feature subset that remains constant during the forest formation.

3) Growing the number of trees (T = nTree) according to the following criteria:

a) Drawing a sample of size 'n' with replacement from which a sample of 'Sn' is selected to grow a tree.

b) Randomly selecting 'm' features and using them to find the best split to grow a tree at each node.

c) Growing each tree to maximum size without pruning.

(Chen, N.D.) lists the following as the steps involved in training each decision tree using a RF algorithm.

1). Random subsets n (e.g., 1000) are selected from the training set

2). n decision trees (e.g., 1000) are trained such that:

- one decision tree is trained using one random subset
- each decision tree's optimal splits are based on a random subset of features (e.g., 5 is randomly selected out of 10 features to split from a total of 10 features)

3). Each tree independently predicts the records/candidates in the test set.

4). The final prediction is determined from the majority vote for classification or average for regression.

The number of features searchable at each split point (m) must be specified as an algorithm parameter. While use of the square root (m = sqrt (p)) and one-third (m = p/3) of the total number of variables, for classification and regression, respectively, have been recommended as reasonable defaults, it is advisable to try different values and tune them using cross-validation in order to obtained optimized results with the lowest OOB (Brownlee, 2016). This is confirmed by (Mansour et al., 2012) who stated that RF is sensitive to the number of trees (nTree) and splits (mTry). In (Mansour et al., 2012) study, the high nTree and recommended mTry (mtry = sqrt (p)) setting yielded the lowest OOB error rate in agreement with earlier studies conducted by (Adam et al., 2009, Ismail, 2010, Breiman, 2001).

In terms of bagging, a 33% estimate of the dataset is excluded from every bootstrap sample drawn in RF, leaving the remaining data to be replicated to bring the dataset to full size. The 33% (one-third) estimate excluded from the samples is referred to as the out-of-bag (OOB) samples, while the dataset that is replicated is known as the in-bag samples (Ismail and Mutanga, 2009). RF, unlike bagging, can only select a random candidate features' subset to establish the split at each tree node (Ismail and Mutanga, 2009). Each decision tree makes predictions based on the OOB sample for the particular tree as it grows to its maximum. The prediction error then provides an unbiased assessment of the predictive accuracy as the training process does not use the OOB samples and hence can be used for performance assessment of the model (Ismail and Mutanga, 2009).

RF uses the OOB samples to provide an internal measure of variable importance, which can be used to evaluate the model's performance. These measures include permutation accuracy importance measure, number of times each variable is selected and Gini importance (Breiman, 2001). Permutation accuracy importance measure, also known as **'**mean decrease in accuracy' is considered best of these measures due to its ability to evaluate the variable importance based on mean accuracy decreases measured by the use of OOB samples (Breiman, 2001). Each OOB observation is placed down the corresponding classification tree from which it was excluded to calculate the OOB error. The misclassified proportion of that OOB observation is then used to calculate the error estimate. The OOB error yields a measure of the variables' importance by comparing how much the OOB error of estimate increases when a variable is permuted while all other variables remain constant (Mansour et al., 2012).

3.2.5.2 Variable Elimination

Variable elimination is used as a means to overcome the shortcoming of the RF algorithm, which automatically selects the optimal number of variables for the best classification by ranking them according to their importance (Adam et al., 2009). The modelling process is simplified by using

a smaller number of spectral parameters that provide the best predictive power and aid in interpreting the final model (Ismail and Mutanga, 2009).

Various techniques for variable elimination exist, inclusive of statistical techniques such as classification trees, discriminant analysis, support vector machines, canonical variate analysis, principal component analysis, backward feature elimination (Adelabu et al., 2014), forward feature elimination (Adam et al., 2009, Mansour et al., 2012) as well as wrappers and filters (Poona and Ismail, 2013). (Adam et al., 2009, Mansour et al., 2012, Ismail, 2010) used forward variable selection (FVS) algorithm to select an optimal subset of wavebands from the RF variable importance ranked bands.

(Adam and Mutanga, 2009; Mansour et al., 2012) used forward variable elimination to determine the optimal number of wave-lengths based on variables importance measurement obtained from random forest, adding respectively, five and two ranked wavelengths repetitively at each iteration until no more explanatory variables could be included into the final model. The optimal subsets of wavelengths with the lowest error rate, as determined by the OOB method, were then used for classification (Adam et al., 2009).

(Poona and Ismail, 2013) compared three wrappers; Regularized random forest, Recursive feature elimination and Boruta algorithm, all embedded within RF algorithm, in terms of their capacity to select an optimal wavelength subset that best differentiates between healthy and stressed three month old Pinus radiata seedlings.

To identify the smallest number of spectral parameters offering the best predictive power and assist in the final model interpretation, (Ismail and Mutanga, 2009) used a wrapper that employs regression tree ensembles to search for the best subset of spectral parameters. They implemented a greedy search function based on backward elimination commencing with all nine spectral parameters in their study. The least promising spectral parameters were then progressively eliminated, resulting in a nested spectral parameters subset offering the lowest root mean square error (RMSE). The resulting subset of spectral parameters was then evaluated on an independent test set not used during the variable selection process for comparative purposes. The test used (i) hold out test dataset (n = 20), (ii) 10 fold cross validation (CV) and (iii) out of bag (OOB) samples (Ismail and Mutanga, 2009).

3.2.5.3 Evaluation and Deployment of a Model of Identified Optimal Wavebands

Evaluation is an essential step in the data mining process that is frequently overlooked. (Williams, 2011). Once optimal bands have been identified, their effectiveness in discriminating among various features of interest, therefore, requires evaluation.

RF provides an internal mechanism of evaluating the accuracy of a model of optimal bands identified by means of the out-of-bag (OOB) error performed on one-third of the data used to build a model. This one-third of data may be split further into a 'validation dataset' and a 'testing dataset'. The default percentage split dataset when the RF algorithm is run using 'R Analytical Tool To Learn Easily' (Rattle), used in this study, is 70/15/15 for training dataset (used to build the model) / validation data/testing data respectively (Williams, 2011). The percentage between validation and testing data may be adjusted, however, as the user sees fit. For example, the entire 30% of data not used for model building may be used as a testing dataset only.

The validation dataset is used to test various parameter settings or different variable choices. It should not be used to provide error estimates of the final outcomes as it is used to build the model (Williams, 2011). On the other hand, the testing dataset should only be used to predict the final results' unbiased error. In no way should it be used to build or fine-tune the built models so as not to provide an unbiased model performance estimate. The testing dataset and, whilst the model is being built, the validation dataset, are used to test the model's performance by calculating the model error rate. Rattle also allows the model to be tested against the entire dataset from which the model is built.

Once the model has been evaluated, it can then be deployed on an independent dataset similar to that used to build the model. A confusion matrix can then be used to establish the model performance level of accuracy on a new, previously unseen dataset by comparing the decisions made by the model with those based on the actual data (Williams, 2011).

3.3.6 Spectral Matching

Spectral matching compares spectral reflectance patterns of one dataset against the other, such as observed spectra (e.g., from the image) against reference spectra available in a spectral library (figure 3.8). It employs spectral signatures, which define objects' characteristics based on their reflectance, absorbance, and transmittance of electromagnetic radiation (Shanmugam and Srinivasaperumal, 2014). Spectral matching is used in numerous applications, inclusive of target detection and spectra classification. Hence the spectral matching results in this research produced classified images used for further analysis.

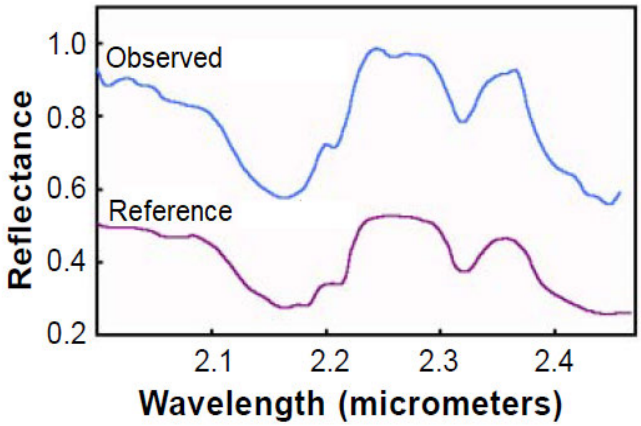

Figure 3.8: Observed spectrum and reference matched spectrum available from a spectral library (modified from (Smith, 2006))

The success of spectral matching depends on accurate image spectra-to-reflectance conversion. It performs best when the image contains large areas of pure materials with corresponding reflectance spectra in the reference spectral library (Smith, 2006). Spectral matching of hyperspectral images compounded by the presence of mixed pixels representing spatial mixtures of different features. These mixed spectra may match multiple pure reference spectra to varying degrees, possibly even including the spectra of features not present in the image. The matching reference spectra are ranked using some goodness of fit measure. The reference spectrum that matches best with the image pixel spectrum is considered dominant in the mixture and, therefore, the concerned pixel is assigned to this feature (Smith, 2006). In the absence of a reference spectrum with sufficient match, no available endmember (feature) is identified as dominant, and the pixel is left unassigned. The result of this process is a features map of the image portraying the dominant material in each of the image pixels (figure 3.9).

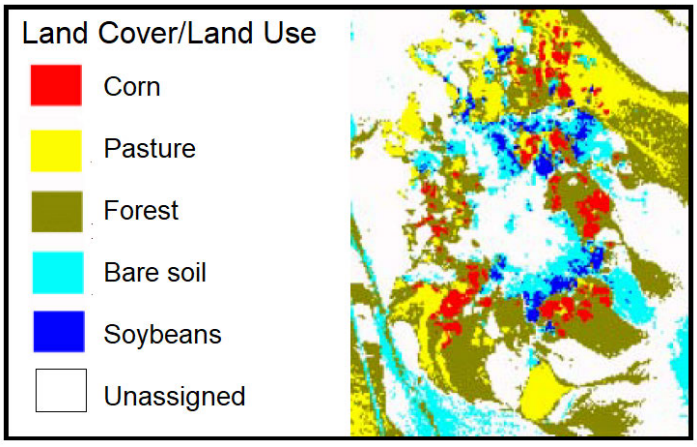

Figure 3.9: Feature map depicting land cover/land use created by matching image spectra to land cover/land use spectra in the spectral library. White areas produced no sufficient match to any of the selected reflectance spectra hence depict pixels left unassigned (modified from Smith, 2006)

Mixed spectra can be used to develop a spectral library or be included as part of the library of pure spectra to improve features identification for mapping. However, it is not always possible to include all conceivable mixtures (and all mixture proportions) in the reference library.

Spectral matching can be performed using various algorithms, including traditional clustering techniques and more recent automated matching models (Shanmugam and Srinivasaperumal, 2014). These algorithms are classified on the basis of multiple salient features measures that include distance measures, angle measures, correlation measures, encoding measures, feature-based matching measures, information measures. While (Shanmugam and Srinivasaperumal, 2014) do not recommend any particular spectral matching algorithm, they advise the use of a combination of two or more spectral matching techniques in conjunction with a well-built and specialized spectral library for better performance in target recognition. In this research only Spectral Angle Mapper (SAM) was employed. The choice of this algorithm was informed by its wide use in classifying hyperspectral imagery (Christovam et al., 2019).

Spectral Angle Mapper (SAM) algorithm matches different spectra by measuring differences in the angle between the unknown (image) spectra and reference spectra (Padma and Sanjeevi, 2014), such as other known spectra or spectra contained in a spectral library. It treats spectra as vectors in a space with dimensionality 'n' equal to the number of bands (Kruse et al., 1993, Jollineau and Howarth, 2008). The degree in the similarity of spectra between the reference spectrum 'r' and image spectrum 't' in an n-dimensional space is expressed in terms of the mean angle (α) between the two spectra for each band measured in radians (van der Meer, 2006, Kayet and Chakrabarty, 2016) (figure 3.10). Smaller angles indicate that the image and reference spectra are more closely matched (Eckert and Kneubühler, 2004).

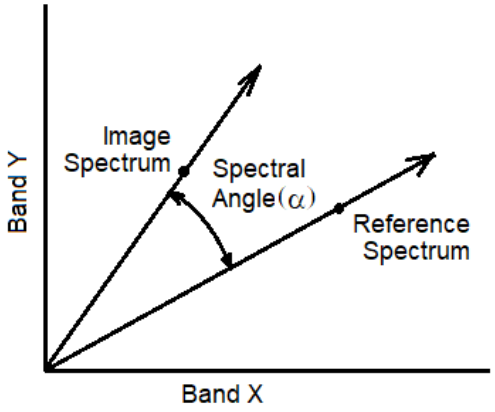

Figure 3.10: Spectral Angle (α) between image and reference spectra in Spectral Angle Mapper (SAM)

Mathematically, for n-dimensional space, the measured spectral angle is given as

$$\alpha = cos^{-1}\left(\frac{\vec{t}.\vec{r}}{\|\vec{t}\|.\|\vec{r}\|}\right) \ldots\ldots\ldots\ldots\ldots\ldots\ldots\ldots\ldots\ldots\ldots\ldots\ldots\ldots\ldots\ldots\ldots\ldots\ldots\ldots\ldots\ldots\ldots\ldots (3.5)$$

Which also can be written as

$$\alpha = cos^{-1}\left(\frac{\sum_{i=1}^{n} t_i r_i}{\left(\sum_{i=1}^{n} {t_i}^2\right)^{1/2}.\left(\sum_{i=1}^{n} {r_i}^2\right)^{1/2}}\right) \ldots\ldots\ldots\ldots\ldots\ldots\ldots\ldots\ldots\ldots\ldots\ldots\ldots\ldots\ldots\ldots\ldots\ldots\ldots\ldots\ldots\ldots\ldots\ldots (3.6)$$

Where α = spectral angle, t = image spectrum, r = reference spectrum and n = number of bands

When using SAM, not all endmembers need to be identified while only the spectra direction, and not their length, is used, making it insensitive to albedo and illumination effects (Eckert and Kneubühler, 2004, Jollineau and Howarth, 2008). Thus all possible illumination conditions are treated alike with pixels that are poorly illuminated falling near the origin while the vector length relates only to how well the pixel is illuminated (Darvishi Boloorani, 2008). SAM works on the assumption that data has been converted to apparent reflectance with dark current and path radiance removed (Darvishi Boloorani, 2008, Sahoo et al., 2013).

When using spectra in a spectral library, a spectral angle is computed for every image spectrum pixel in the hyperspectral image and each reference (library) spectrum selected (Sahoo et al., 2013). The computed angle, measured in radians, is allocated to the corresponding pixel in the output SAM image, yielding one output image for each reference spectrum. The resulting spectral angle images create a new data cube with the number of bands corresponding to the number of reference spectra used in the processing (Sahoo et al., 2013).

ENVI's version of the SAM algorithm (used in this research) takes a number of 'training classes' or reference spectra from ASCII files, spectral libraries, or ROIs as input. It then determines the angular separation between each image pixel spectrum and that of the reference spectra (endmembers) in n-dimensions. The output is a classification image depicting the best SAM match at each pixel and a 'rule' image for each endmember showing the actual angular separation in radians between reference spectrum and each spectrum in the image. Darker pixels in the rule images depict smaller angles between image and reference, indicating strong similarity. The resulting rule images can be used with different thresholds to decide which pixels are included in the subsequent SAM classifications (Sahoo et al., 2013).

An additional limitation for the use of SAM, besides being applied to data reduced to apparent reflectance with dark-current and path-radiance biases removed, the features within the same angle space are inseparable while pixels falling outside the threshold defined by the user are designated as unclassified (Jollineau and Howarth, 2008).

3.3.7 Post Classification Accuracy Assessment of Classified Imagery

The quality of maps created using remotely sensed data must be evaluated and expressed in a meaningful way. This is important not only for the purposes of serving as a guide to the quality of its fitness but also to understand errors and their probable implications, especially if propagated through analyses linking the map to other data sets (Foody, 2021).

When applied to mapping from remotely sensed data, the term' accuracy' expresses the degree of ‘correctness’ of a map or classification (Foody, 2021). An image derived from classification can thus be considered accurate if it depicts reality with no bias. Therefore, image classification accuracy is the degree to which the resultant classified image agrees with reality or conforms to the ‘truth' (Tiwari et al., 2021). Conversely, a classification error thus occurs when the situation depicted on the map differs from reality. The reality, usually referred to as ‘reference data’, with which classified data is compared (Malinowski et al., 2015b) may take different forms inclusive of existing maps, images, field-collected data such as the location of samples, spectra of features, etc.

Various methods of assessing accuracy have been presented in the remote sensing literature (Foody, 2021). Currently, the confusion or error matrix is at the heart of accuracy evaluation, though there is plenty of room to expand the analysis beyond its use (Foody, 2021). The use of a confusion matrix and the metrics derived from it, have therefore been used as means of accuracy assessment in this research.

A confusing matrix is a simple cross-tabulation of the mapped class mark against that observed for a sample of instances at specific locations in the ground or reference data. It provides a clear basis for classification accuracy assessment, allowing for the description of classification accuracy and characterization of errors to help refinement of classification or estimates derived from it. The confusion matrix may reveal confusion among classes which could be resolved with the addition of more discriminatory information.

A confusion matrix provides various measures of classification accuracy. The percentage of cases correctly assigned being the most popular, as it provides an easy-to-understand indication of the classification's overall accuracy. The percentage of cases correctly assigned for individual classes may be derived from the confusion matrix by comparing the number of correctly assigned cases

to the total number of cases of that class. The resultant percentage may be the user's or producer's accuracy, depending on whether the calculations are based upon the matrix's row or column marginal (Foody, 2021).

Despite being considered informative, measures obtainable from a confusion matrix such as the percentage of correctly classified cases have often been criticized. This is because it is argued that some cases may have been assigned to the correct class purely by chance (Foody, 2021). Cohen's kappa coefficient, therefore, has often been used to accommodate for the effects of chance agreement. In fact, some commentators contend that it should, in certain circumstances, be adopted as a standard measure for classification accuracy (Tiwari et al., 2021). The Cohen's kappa coefficient is considered to have multiple attractive features that merit it to serve as an index of classification accuracy, thus making some compensation for chance agreement. A variance term may also be calculated for it, allowing for the statistical testing of the significance of the difference between two coefficients (Foody, 2021). This is often considered essential for the comparison of classifications differences and hence, the matrices.

The use of the Cohen Kappa, however, has often been questioned by various researchers citing among other reasons the fact that it is not representative of the entire data set in a confusion matrix as it is calculated on the basis of its marginals and main diagonal, not from the whole matrix (Stehman and Wickham, 2020). Despite its limitations, the use of the kappa coefficient and associated approaches has encouraged a more rigorous and quantitative assessment of classification accuracy, which should be viewed as a useful, if slightly incorrect, step toward a more appropriate evaluation method (Foody, 2020). Accuracy assessment, as a topic, therefore, has matured to a level where there have been calls for standardization of both the evaluation method and reporting style, often with thresholds for target accuracy specified (Foody, 2021). The specified threshold is usually expressed as a minimum level of overall accuracy expressed numerically by some index, such as the percentage of cases correctly allocated and a desire for each class to be classified with comparable accuracy. An overall accuracy target of 85% with no class less than 70% accurate, for example, has been stated as acceptable (Foody, 2021). Additional features required meeting include the provision of more than one measure of classification accuracy with associated confidence limits in conjunction with a confusion matrix. Despite the lack of a standardized method, there is a reasonable level of agreement on the general format in which accuracy assessments and associated reporting should be conducted, with some of the techniques suggested becoming virtual standards that are widely used (Congalton and Green, 2019).

3.4 Chapter Summary

This chapter presented an overview of the various techniques employed for vegetation mapping, including ground, aerial, and space-based. It, however, focused on the use of space-based hyperspectral imagery. Examples of similar research were presented. Hyperion imagery processing was discussed in detail being the imagery used for this research. The steps involved in radiometric pre-processing were discussed, highlighting various approaches. The chapter, however, discussed in detail, the Hyperion pre-processing workflow proposed by (Aneece et al., 2019). In terms of this workflow, Hyperion imagery was subjected to a number of pre-processing steps that include; (1) VNIR and SWIR separation, (2) Converting Digital Numbers to radiance, (3) Removing problematic bands, (4) Smile correction separately on VNIR and SWIR, (5) Merging VNIR and SWIR, (6) De-striping, (7) Atmospheric correction and (8) Cloud removal and spectral polishing/smoothing. Each of these pre-processing steps was discussed in detail, highlighting the different approaches available where several exist. The chapter also mentioned the importance of sampling for ground-truthing data.

The essence of geometric correction was also discussed, providing details on when in the imagery processing chain, it is convenient to georeference an image to avoid the change of radiometric data unnecessarily.

The need to develop a spectral library and select wavebands most suitable for spectral matching were also discussed, indicating their relevance for processing hyperspectral imagery due to the many bands contained in the imagery, which in most cases are strongly correlated, creating unnecessary duplications. It is usually advisable that a spectral library be accessible to allow for the use of its constituent spectra by multiple users. Various techniques available for optimal waveband selection were highlighted, but the focus was placed on the Random Forest (RF) tree ensemble and variable elimination both interactively and automatically as step-wise backward variable elimination and AIC, respectively.

The chapter also discussed spectral matching techniques with a focus on Spectral Angle Mapper (SAM) algorithm. Post-classification accuracy assessment was also discussed, highlighting the measures available for its accomplishment.

The subsequent chapter presented an overview of the characteristics of the Mfabeni wetland, which was identified as a study area.

Chapter 4

Mfabeni Wetland

4.1 Introduction

The study area for this research is the Mfabeni wetland. Mfabeni wetland is a type of 'Fen' wetland. The choice of the Mfabeni wetland as a study area was facilitated by a research collaboration between the Isimangaliso World Heritage Wetland Park and one of the researcher's supervisors.

4.2 Location of the Mfabeni Wetland

Mfabeni wetland, also known as Mfabeni swamp, is situated on the eastern shores of St Lucia Lake, near Cape Vidal, in the Isimangaliso World Heritage Wetland Park located along the north-eastern coast of KwaZulu-Natal stretching from south of the St Lucia town, northwards to the Mozambique border. It is a peatland, situated between the lake and the tall, coastal dunes (Fig 4.1) in the Hlabisa district at 24°09'44"S, 32°31 '64"E and an average altitude of 20m.

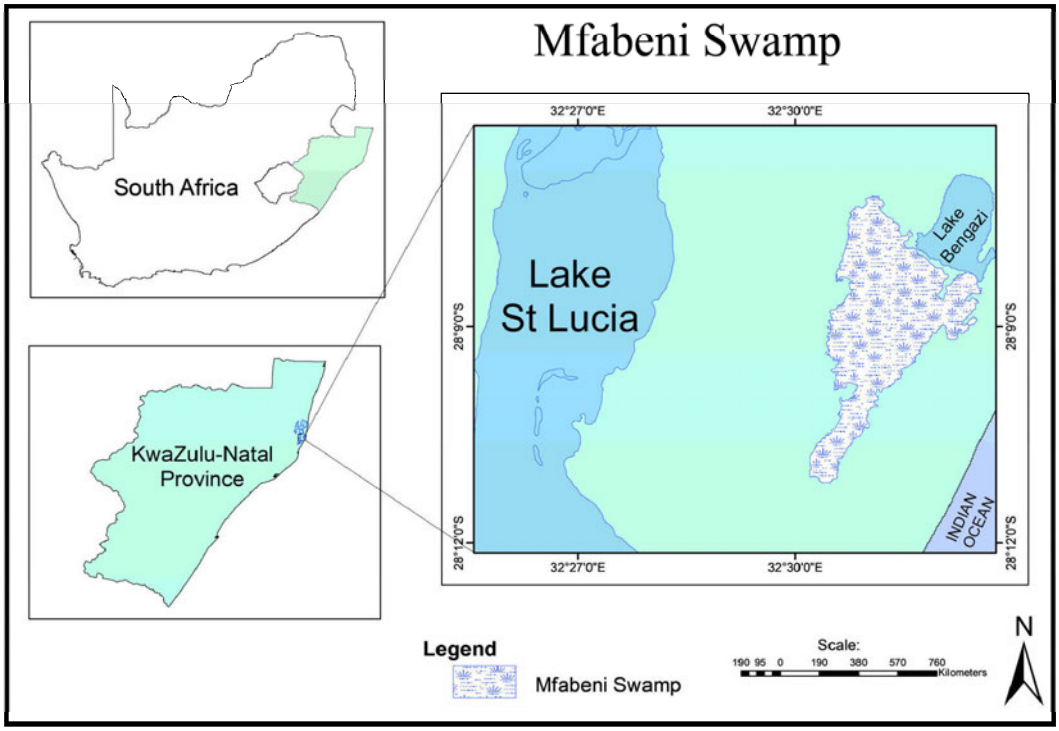

Figure 4.1: Location of Mfabeni Wetland

4.3 Climate

The account below on the climate of the Mfabeni wetland was modified from an article written by (Kelbe, N.D) for the Isimangaliso Wetland Park.

Located in the Isimangaliso Wetland Park, within Africa's subtropical climatic zone, Mfabeni wetland experiences weather systems from both tropical and temperate regions. The differences in temperature between summer and winter as well as between daily minimum and maximum are influenced by the Agulhas current's warming effect. Summers are hot while winters are mild, with occasional cold spells brought in by the Antarctic cold fronts. While there are days when it is extremely hot, temperatures are usually very mild. The mean temperature during summer is 26°C. The relative humidity is extremely high, exceeding 90% for much of the year. Summer's high humidity, lasting from January to March, can be highly uncomfortable. However, for much of the year, prevailing north-easterly winds blow parallel to the coast, peaking in August and troughing in May, reducing humidity.

During the winter months, between May and July, cold fronts sweep over the subcontinent, with a cool Southern Ocean air and widespread light rainfall which could last several days. This winter rainfall can contribute up to 20% of the region's annual rainfall. In spring very large thunderstorms, generally in the late afternoon, can arise from strong upper-level winds, heating of the surface, low-level inversions, and invading frontal systems. Although only a small percentage of these storms produce hail, they can cause river flooding. In the mid-to-late summer, these storms' intensity usually decreases, but in the late summer, subtropical winds continue to cause frequent smaller storms.

Although rainfall is highly variable, the spring and summer months, from September to March, account for roughly 60% of total rainfall. Most rains fall from January to March, with the least experienced from May to September. Cut-off lows frequently cause heavy rains. Rainfall declines steeply from the east (1200mm mean annual rainfall at Cape Vidal on the coast) to the west (650mm mean annual rainfall at uMkhuze in the far west) of the park while increasing to 800mm in the Lubombo Mountains.

Tropical cyclones (large storms) moving down the Mozambique Channel occasionally cause periodic floods in late summer. These tropical cyclones could dump over 700mm of rain in a few days, causing major flooding and widespread devastation. Throughout the year, thunderstorms form over the warm offshore ocean current and occasionally move inland, bringing additional rain to the coastal dunes. These convective storms are partly the reason there is a vast disparity in rainfall between the drier interior and the wet coast. While annual average rainfall is just over

1000mm, there have been instances when it has exceeded 3000mm and fallen below 500mm. Cyclones' induced floods and droughts play a significant role in the region's hydro-ecology. Evaporation is high, particularly in early spring and the drier winter periods. The annual average evaporation is around 1300 mm per year in the Lake St Lucia system. Due to this high evaporation rate, the region has an annual negative water balance, i.e., more water leaving the system than entering.

4.4 Geology and Soils (Geomorphology)

The Mfabeni wetland is the thickest peatland (ten meters) and also the oldest (45,000 years) in South Africa (Grundling et al., 2015). Like other peat wetlands in the iSimangaliso Wetland Park, the peat substrate is underlain by Aerion sand of the marine origin (Grundling et al., 1998). Mfabeni wetland lies within an interdunal that runs parallel to the Indian Ocean coastline and extending 10 × 3 km in size with peat thickness of up to 11 m (Baker et al., 2014). It is part of the greater Natal Mire Complex (NMC) (figure 4.2) that extends from southern Mozambique to the south of Richards Bay (Smuts, 1992). The NMC falls within the coastal Cenozoic deposits of the Maputaland group, constrained to the west by the Lebombo monocline and the uMkhuze and uPongola River valleys (Baker et al., 2014).

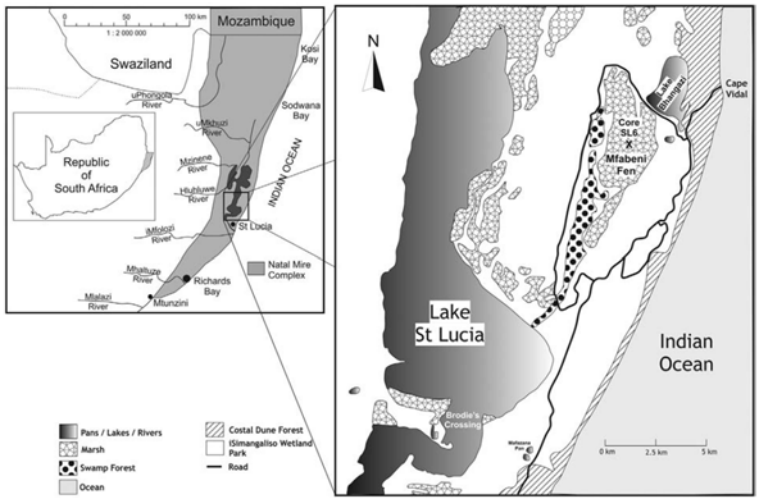

Figure 4.2: Location of Mfabeni Peatland within the Natal Mire Complex (Baker et al., 2014)

The Mfabeni peatland was formed by valley infilling on an intertidal and lacustrine non-permeable clay layer (Grundling et al., 2013) within the reworked late Pleistocene Kwa Mbonambi Formation coastal dune depression (Smuts, 1992). The infilling was a result of a blockage of the Kazama palaeo-channel and sustained groundwater input from the Maputaland aquifer (Grundling et al., 2013). However, the wetland lacks the KwaMbonambi Formation's underlying dune topography, which is common in Maputaland's underneath peatlands (Venter, 2003).

The peat is located in a valley-bottom setting, on clay material, flanked by an 80–100 m tall vegetated coastal dune cordon (known as the eastern dunes) to the east and the 15–70 m tall Embomveni sand dune ridge (known as the western dunes) to the west (Figure 4.3). It is separated from Lake Bangazi and Lake St. Lucia in the north and south, respectively, by beach ridges (Grundling et al., 2013). To the south and north, the peat deposit thins out, and reworked aeolian marine sands lie beneath it (Grundling et al., 2013). Research carried out by (Grundling et al., 2013) by coring in and next to the Mfabeni wetland (Figure 4.3) established the presence of grey clay material at present-day sea level and was not found to occur beyond the Mfabeni Mire valley-bottom width though it might extend along the peatland length.

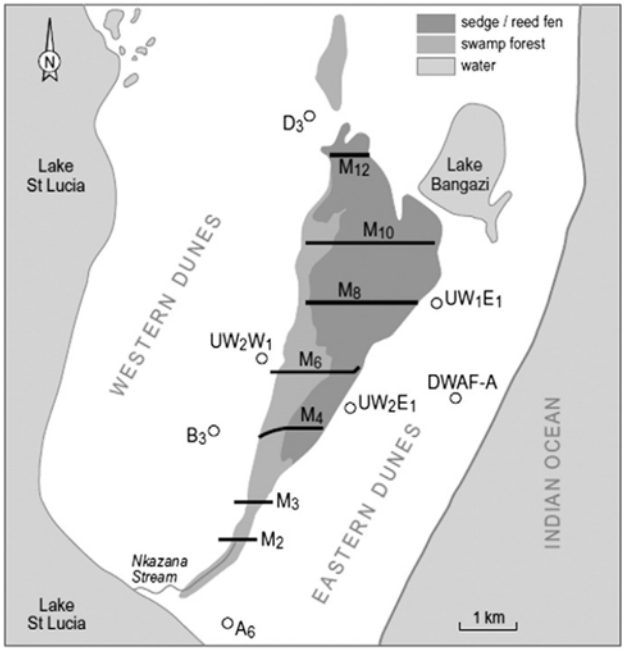

Figure 4.3: Coring sample sites in and adjacent to the Mfabeni mire. Lines M2 to M12 show transects 600 –1000 m apart across the mire where samples were taken at about 100 – 200 m spacing. Hollow circles represent samples taken outside, but adjacent to the Mfabeni mire (Grundling et al., 2013)

(Grundling et al. 2013) describe Mfabeni Mire morphology as complex, with a deep central depression oriented North-South, and a smaller depression oriented east-west of the main depression. The Mfabeni Mire morphology is complex, consisting of a deep depression in the centre oriented North-South, and a smaller depression oriented east-west of the main depression. The peat body may be up to 10.8 m thick in the main basin, with depths not exceeding 2.5m in the lateral basins. The peatland's surface slopes down in a southerly direction from the peatland's central region, with a very gentle slope from West to East. Towards the south, the peat surface steepens (between transects M3 and M2 in figure 4.3) with an incision of the present Nkazana stream channel into the peat surface as it drains towards Lake St. Lucia.

Sandy layers of about 0.2 m in thickness (not shown in figure 4.4) occasionally separate the peat layers, particularly in the eastern part of the peatland where the peat layer is decomposed. Thin ash layers, not shown in figure 4.4, are found in the western part of the mire, as well as in the northern peat deposits, which are more shallow (Grundling et al., 2013).

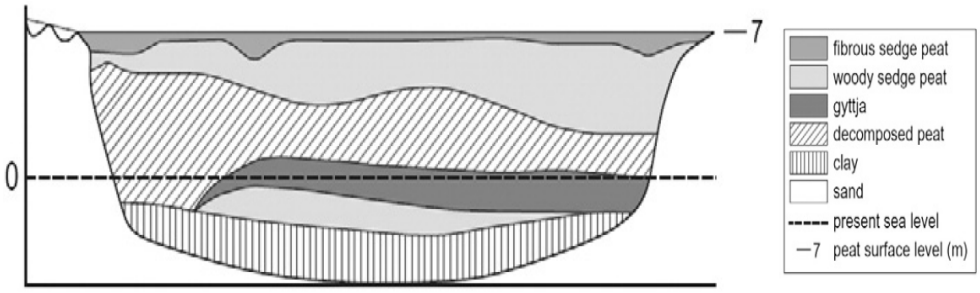

Figure 4. 4: Representative Stratigraphy of the Mfabeni Mire along M8 transect taken from west to east showing five distinct peat layers recognized by (Grundling et al., 2013)

4.5 Hydrology (Geo-hydrology)

The Mfabeni Mire water balance (Figure 4.5), like that of similar peatland, is determined by the various factors that include precipitation, groundwater seepage, surface drainage and evapotranspiration (Grundling et al., 2015).

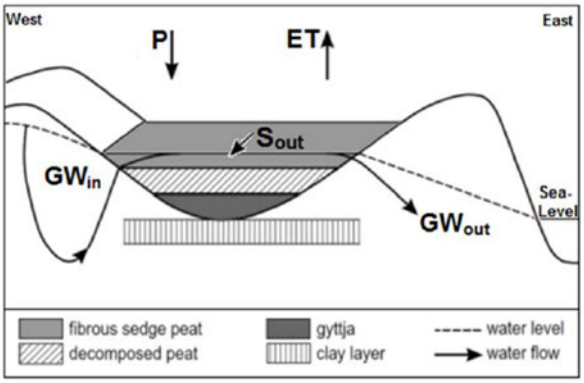

Figure 4.5: Schematic diagram of the water balance of the Mfabeni wetland (Grundling et al., 2015)

Precipitation, in the form of rainfall, is the major source of water in the Mfabeni wetland (Grundling et al., 2015). (Grundling et al., 2015) citing (Taylor et al., 2006) reported the existence of a strong rainfall gradient between the eastern coastal dunes and Lake St Lucia (figure 4.3).

A regional mound of groundwater (figure 4.5) beneath the western dune complex is the major recharge area that discharges groundwater within the seepage area defined by the swamp forest

into the peatland (Grundling et al., 2013). Groundwater finds its way into the fen portion of the wetland directly from the western dune mound and *via* the swamp forest (Rawlins and Kelbe, 1991). The groundwater drains towards the peatland's center, where it flows over the surface of the mire and through shallow subsurface layers along a gentle slope to the east (Grundling et al., 2015).. As groundwater drains down the eastern section of the peatland, it gets recharged before sloping steeply eastwards towards the coastal dune complex (Grundling et al., 2015). This conceptualized flow of water is illustrated in figure 4.5.

Surface drainage in Mfabeni wetland occurs southwards to Lake St. Lucia, largely by way of the Nkazana Stream within the swamp forest, with irregular water exchanges to or from Lake Bangazi which are dependent on lake levels (Grundling et al., 2015).

The regional water table, the level of which varies seasonally, slopes from the western dunes to the peatland and from the peatland to the Indian Ocean. (Rawlins and Kelbe, 1991) (figure 4.4). Within the sedge/reed fen section of the peatland, the water table drops gently to the east, then sharply between the eastern edge of the peatland and the coastal dune (Grundling et al., 2015).

(Grundling, 2014), focusing only on the area to the east of the western dunes from which the water table slopes towards the Indian Ocean (figure 4.4), provides an account of the Mfabeni wetland water table distribution based on the February 2009 (summer) water table data provided by the KwaZulu-Natal Wildlife Research Office of iSimangaliso Wetland Park.

The location of the Mfabeni wetland in the subtropics, a water-scarce region with persistent droughts, makes ET a frequent dominant in maintaining the water balance of the wetland. Total evaporation in the Mfabeni wetland plays a crucial role in its hydrology and has been shown to surpass rainfall amounts during droughts (Grundling et al., 2015).

4.6 Topography

Topography, geology, storage, and transmission properties of the geologic materials and soils of a catchment govern groundwater flow to peatlands (Grundling, 2014). Topography, therefore, can contribute to complex groundwater flow patterns into peatlands (Nijp et al., 2019) where prominent or high relief landscapes tend to develop local flow systems in comparison to flatter landscapes with relatively simpler regional flow systems (Grundling, 2014) citing (Winter, 1999). The extent of the swamp forest in the Mfabeni wetland, for example, is linked to areas with sloping topography and evident groundwater discharge (Grundling, 2014). A persistent and stable water supply, with no inundation (damming) on the surface, therefore are considered favorable

for colonization of swamp forests. These requirements are supported by (Grundling, 2014) who observed an extensive swamp forest dying-back resulting from a rise in water level of just 0.2 m when a low-level bridge north of the Mfabeni wetland in the Isimangaliso Wetland Park caused damming of a swamp forest.

Topographically, the Mfabeni wetland is located in a low-lying depression bordered by the eastern dunes and western dunes (figure 4.3). The elevation change over the wetland itself is generally low, ranging from about 6 – 14m above Mean Sea level as determined from the generated Digital Elevation Model (DEM).

A relationship between groundwater level and topography for Mfabeni wetland provided in figure 4.4 shows a positive correlation between them on the western dunes and over the peatland. They are negatively correlated on the eastern dune cordon towards the ocean, possibly due to the effect of the underlying geological strata and other minor aquitards affecting groundwater flow.

The gentle downwards sloping of the water table to the east within the sedge/reed fen section of the Mfabeni peatland (Grundling et al., 2015), the impermeability of the peatland and possible shallowness of the water table (Haitjema and Mitchell-Bruker, 2005), and its closeness to sea level low-lying altitude (flatness) in a topographical depression served as a justification for using elevation as a substitute for water level in this research.

4.7 Vegetation

The Mfabeni wetland is a sedge/reed fen and swamp forest peatland (appendix 4.1). According to (Venter, 2003), the swamp forest is dominated by *Syzygium cordatum* and *Stenochlaena tenuifolia* in the northern parts. In the central parts, the *Ficus trichopoda* and *Nephrolepis biserrata* are dominant while *Barringtonia racemosa* and *Bridelia micrantha* dominate the southern parts of the swamp forest where Nkazana streamflow occurs (Grundling et al., 2015). *Syzygium cordatum* trees can grow to 30m high while the *Stenochlaena tenuifolia* (Blechnaceae) fern can climb 10m up tree stems (Grundling et al., 2015). A stand of impenetrable *Nephrolepis biserrata*, a fern which can grow to a height of 2.5m, occupies the forest floor (Clulow et al., 2013).

(Venter, 2003), using aerial imagery and on-site ground sampling, described Mfabeni wetland major plant communities *" in terms of distribution, broad habitat, diagnostic species, species with significant indicator value and dominant species."* According to (Venter, 2003) plant community names were based on diagnostic and/or dominant species with the structural component of the

name based and adapted from (Edwards, 1983) classification. (Venter, 2003) did not attempt to formalize plant community names in terms of the International Code for Syntaxonomic Nomenclature due to limited knowledge on peatland vegetation on the community level in southern Africa.

According to (Venter, 2003) fourteen (14) communities were identified, with some classified further into sub-communities and sub-sub-communities. The spatial distribution of the identified 14 communities is as provided on a map of the Mfabeni wetland (figure 4.6). The numbers assigned to the communities are provided as a legend on the map (figure 4.6). Community names matched to the numbers provided on the map legend, including sub-classes and variants (where applicable) as assigned by (Venter, 2003) are provided in appendix 4.1.

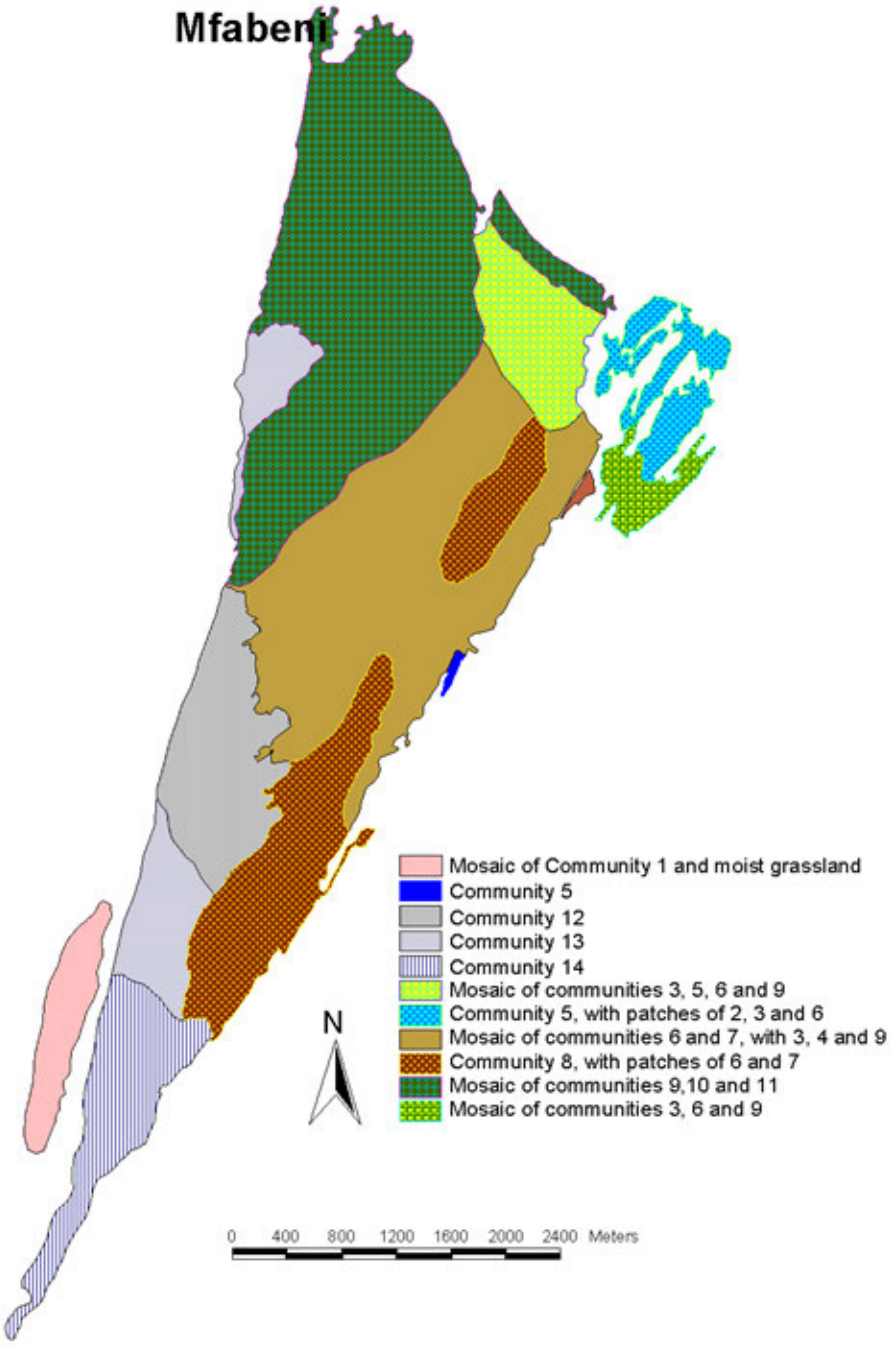

Figure 4.6: Spatial Distribution of Vegetation Communities of the Mfabeni Wetland (Venter, 2003)

A detailed description of each of the vegetation communities, their sub-communities and variants (where identified) as given on appendix 4.1 are provided by (Venter, 2003).

4.8 Chapter Summary

The chapter discussed the characteristics of the Mfabeni wetland in terms of its location, climate, geology and soils, hydrology, topography, and vegetation.

Mfabeni wetland's location in the subtropics and on the Eastern seaboard bordering the Indian Ocean renders it a climate characterized by weather systems from both tropical and temperate regions. Summers are hot while winters are mild, with occasional cold spells brought in by the Antarctic cold fronts. The relative humidity is extremely high for much of the year. Mfabeni wetland receives rainfall highly variable with the spring and summer months, accounting for roughly 60% of total rainfall. Cut-off lows frequently cause heavy rains, with tropical cyclones causing major flooding and widespread devastation. The cyclones' induced floods and droughts play a significant role in the region's hydro-ecology. Evaporation is high, particularly in early spring and the drier winter periods causing the region to have an annual negative water balance where more water leaves the wetland than entering.

Mfabeni wetland is the thickest peatland (ten meters) and also the oldest (45,000 years) in South Africa (Grundling et al., 2015), underlain by Aerion sand of the marine origin (Grundling et al., 1998).

The Mfabeni wetland hydrology is dominated by rainfall as the major source of water, while a regional mound of groundwater (figure 4.5) beneath the western dune complex serves as the major recharge area that discharges groundwater within the seepage area defined by the Mfabeni swamp forest into the peatland (Grundling et al., 2013). The surface and shallow subsurface water flow along the gradient keep the peatland wet and maintain its functions while draining southwards to Lake St. Lucia, largely by way of the Nkazana Stream located in the swamp forest.

The seasonally varying regional water table slopes from the western dunes to the peatland and from the peatland to the Indian Ocean (figure 4.4). Within the sedge/reed fen section of the peatland, the water table drops gently to the east, then sharply between the eastern edge of the peatland and the coastal dune (Grundling et al., 2015).

Topographically, the Mfabeni wetland is located in a low-lying depression bordered by the eastern dunes and western dunes (figure 4.3). The elevation change over the wetland itself is generally low, established to vary between about 6 – 14m above Mean Sea level based on the Digital Elevation Model (DEM) generated from a 5m interval contour map of the area.

The chapter established that a relationship between groundwater level and topography for Mfabeni wetland exists, as provided in figure 4.4. The gentle downwards sloping of the water table within the sedge/reed fen section of the Mfabeni peatland (Grundling et al., 2015), the impermeability of the peatland, and possible shallowness of the water table (Haitjema and Mitchell-Bruker, 2005), and its closeness to sea level low-lying altitude (flatness) in a topographical depression served as a justification for using elevation as a substitute for the water level in this research.

The vegetation of the Mfabeni wetland consists of sedge/reed fen and swamp forest peatland. A detailed composition of the Mfabeni wetland vegetation is given in appendix 4.1 with further details obtainable from (venter, 2003).

Chapter 5

Methods

5.1 Introduction

This section describes the methodology employed to collect data used in this research, how the data was processed, analyzed and the results obtained presented. Figure 5.1 shows a schematic representation of the process followed to get the anticipated results.

5.2 Data Collection

Data needed to undertake this research included; satellite imagery, ground truthing and Elevation of the study area. A field trip was undertaken to the Mfabeni Wetland of the Isimangaliso Wetland Park, where ground-truthing data was collected following the acquisition of Hyperion hyperspectral imagery sourced from the United States Geological Survey (USGS). A decision to use Hyperion Hyperspectral imagery was deliberately made to allow for the investigation of its applicability to this research.

The field data collected were considered insufficient to produce meaningful and reliable results. An existing vegetation map of the Mfabeni wetland described in chapter 4 was therefore used as a secondary source of ground truthing data. The Shuttle Radar Topography Mission (SRTM) Digital Elevation Model (DEM) acquired from (http://glcf.umiacs.umd.edu) was initially contemplated for use as a source of elevation data. Its low spatial resolution of 30m, however, made it unsuitable for reliable characterization of the wetland vegetation in terms of elevation change over a gently undulating wetland such as the Mfabeni wetland. A more detailed DEM generated from a 5m contour map of the Mfabeni was therefore used instead. Each of these data sets is described below.

5.2.1 Satellite imagery

Hyperion hyperspectral imagery of the Mfabeni Wetland (figure 5.2) was captured on 21 July 2012 following a Data Acquisition Request (DAR) submitted to the USGS. Hyperion imagery is 30m x 30m medium spatial resolution imagery captured by the Hyperion sensor onboard the Earth Observation (EO)-1 satellite launched as an experimental mission to study the use of hyperspectral space imagery. The mission, however, got extended due to popular demand. Once the mission ended, the sensors onboard the EO-1 satellite continued to capture imagery only on request using Data Acquisition Requests (DAR).

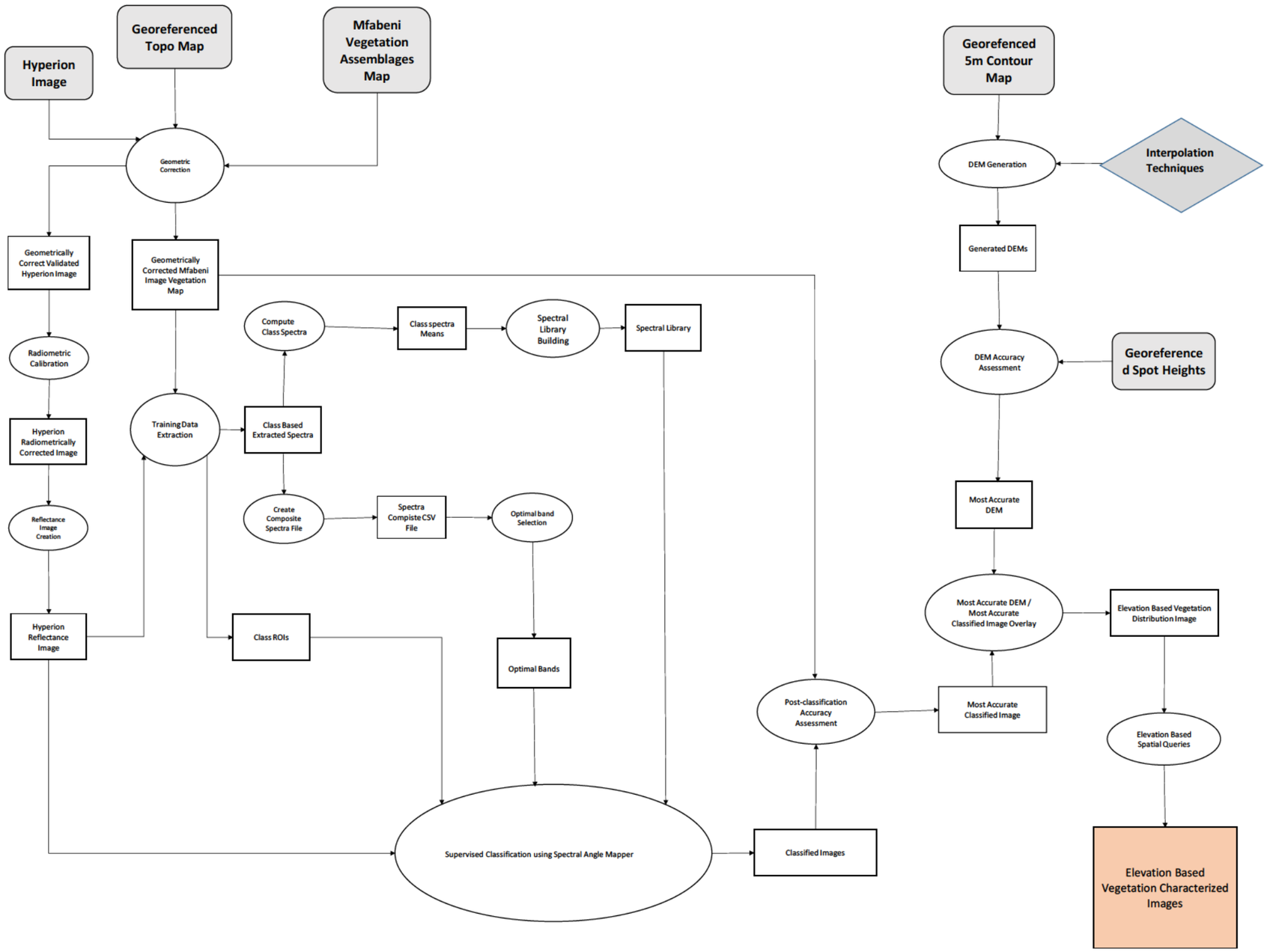

Figure 5. 1: Schematic representation of the research approach

The Hyperion image made available for download was pre-processed to level 1 radiance as L1R, L1Gst and L1T (Kumar and Yarrakula, 2017), and supplied in Hierarchical Data Format (HDF) and GeoTIFF formats along with the gain, offset, mean band centre and mean wavelength information.

The L1T format was used for the processing of Hyperion imagery for this research. While L1Gst could have been equally used, its geometric accuracy is sometimes considered questionable due to the fact that even though it was systematically geometrically corrected, no ground control points were used. L1T was geometrically corrected by use of ground control points.

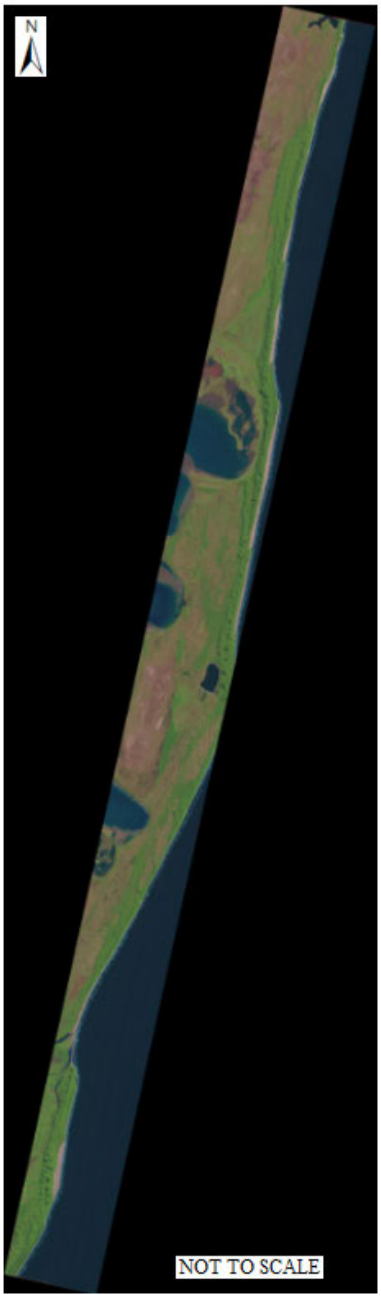

Figure 5.2: Hyperion Imagery captured over the Isimangaliso Wetland Park

5.2.2 Ground-Truthing Data

Ground truthing used in this research included primary data collected in the field and secondary data based on an existing vegetation map of the Mfabeni wetland.

5.2.2.1 Primary Sources of Ground Truthing Data

Primary sources included field spectral measurements taken with a spectralradiometer, Geographic locations and digital images of different vegetation assemblages observed by walking across the wetland. Spectral measurements of the Mfabeni wetland vegetation assemblages were taken on 2 August 2012, 12 days after satellite imagery of the study area had been captured. This was in agreement with the requirements for vegetation analysis using satellite imagery and corresponding field spectra which, according to (Govender M et al., 2008), must be captured within 15 days of satellite imagery acquisition so as to reflect the ground situation at the time of satellite imagery capture, provided no serious disturbance to the vegetation occurs over the concerned period. The Isimangaliso Wetland Park office confirmed the non-existence of any serious event having taken place between the dates of satellite imagery capture and field data collection.

Prior to 2 August 2012, spectral measurements had been taken over a preceding 2-day period at 2 other sites of the Isimangaliso Wetland Park (figure 5.3). The spectral measurements from these sites were used during model validation to select an optimal model using the Random Forest algorithm and the findings published in (Chilufya, et al, 2014). All three days were generally sunny, with measurements taken between 12:00 pm and 1:30 pm at site 1, 12:30 pm and 2:30 pm at site 2, and 11:30 am and 2:30 pm at site 3.

It was only possible to collect the field data over these three days when a security officer was made available to accompany the researcher to avoid the risk of possible attack by wild animals; hence limiting the amount of field data that could be collected for the research.

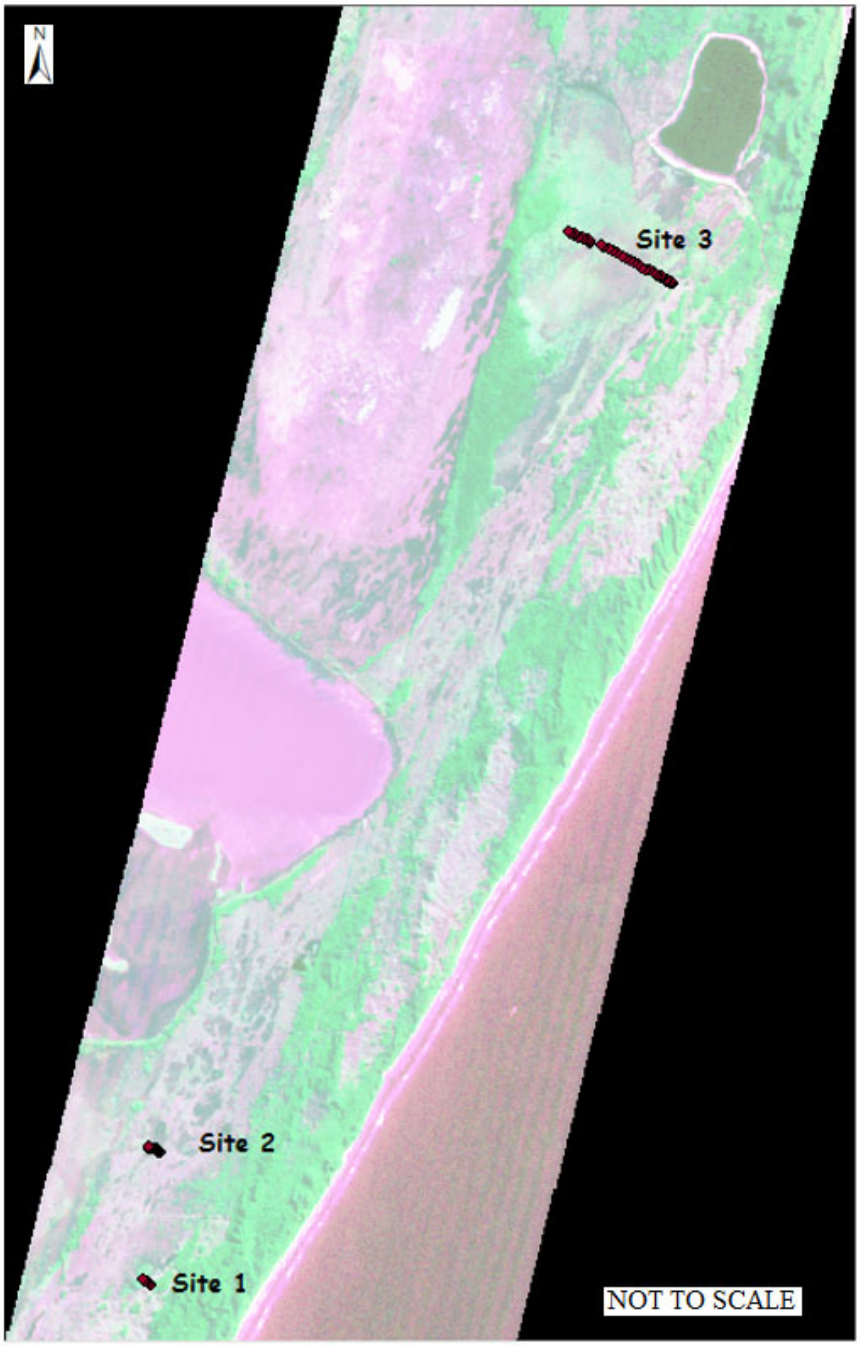

Figure 5.3: Location of the Study Area in the Isimangaliso Wetland Park showing data collection sites 1 to 3 (site 3 is the Mfabeni wetland)

Spectral reflectance measurement of vegetation assemblages was captured using an Analytical Spectral Devices (ASD) FieldSpec® 3 Spectralradiometer. The FieldSpec® 3 Spectralradiometer has a spectral range of 350–2500nm with a resolution of 1.4nm in the 350–1000nm range and 2.0nm for the spectral region 1000–2500nm (Analytical Spectral Devices (ASD), 2005). The measurements were taken at nadir using an 8° field of view lens attachment held at the height of about half a meter (figure 5.4).

Figure 5.4: Taking Field Spectral Measurements with an Analytical Spectral Devices (ASD) FieldSpec® 3 Spectralradiometer under the watch of a Game Ranger

The short height separation was due to the tall grass and the absence of a hoisting facility. The instrument was configured to make 20 repeated measurements, then record the average for each measurement of the reflectance spectra, which was then stored. Repeat measurements ranging from 2 to 4 were made for every identifiable vegetation assemblage and later averaged during processing and analysis.

For every vegetation assemblage field spectral measurement had been taken, a digital image (figure 5.5) of each sample measured was taken using a hand-held digital camera. The captured images were required for the identification of vegetation assemblages.

Figure 5.5: Sample digital image of Vegetation assemblage for which spectral measurements were taken.

Geographic locations (table 5.1) were also obtained for every site at which vegetation assemblage spectral measurements were taken using GNSS. At some sites, only one GNSS location was measured for a set of spectral measurements of the same vegetation assemblage located in the close vicinity. The geographic location of each sample measured was taken as Latitude and Longitude coordinates using Trimble GNSS R4 Receivers in differential mode with the reference station set up near the start of the transect using 'here' (autonomous) global coordinates with positional accuracy of approximately 5 metres. Each of the vegetation assemblages measured GNSS location, having been determined in differential mode, was therefore considered to have been established with a geometric accuracy of 5 metres.

The vegetation encountered showed no areas that could be described as being homogeneous patches of specific vegetation species. All were mixtures of various grass species interspaced with shrubs in certain areas (figure 5.5). However, certain grass species appeared dominant, though not in quantities to be described as covering the entire patch.

Both digital images and GNSS captured geographic locations were used during the interpretation, classification, and analysis of the Hyperion satellite imagery.

Table 5.1: GPS Coordinates of Spectral measurements Locations

4	S28.152993	E032.530212
5	S28.153040	E032.530257
6	S28.152988	E032.530136
7	S28.152841	E032.529960
8	S28.152632	E032.529668
9	S28.152587	E032.529352
10	S28.152477	E032.529170
11	S28.152481	E032.529178
12	S28.152347	E032.529243
13	S28.152347	E032.529243
14	S28.151989	E032.528573
15	S28.151929	E032.528342
16	S28.151816	E032.528213
17	S28.151641	E032.527721
18	S28.151505	E032.527536
19	S28.151249	E032.527022
20	S28.150875	E032.526654
21	S28.150763	E032.526092
22	S28.150518	E032.525462
23	S28.150029	E032.524799
24	S28.149964	E032.524668
25	S28.149716	E032.524313
26	S28.149647	E032.524072
27	S28.149270	E032.523708
28	S28.149114	E032.522934
29	S28.148816	E032.522468
30	S28.148297	E032.521598
31	S28.147978	E032.520852
32	S28.147644	E032.520199
33	S28.147303	E032.519466
34	S28.147029	E032.519128
35	S28.146542	E032.517457
36	S28.146542	E032.517459
37	S28.146357	E032.517287
38	S28.146208	E032.516892
39	S28.146015	E032.516403
40	S28.145889	E032.516165
41	S28.145730	E032.515627
42	S28.145478	E032.515019
43	S28.145209	E032.514822
44	S28.145147	E032.514367
45	S28.144992	E032.514143

5.2.2.2 Secondary Sources of Ground Truthing Data

Secondary data source was in form of a vegetation map of the Mfabeni wetland (figure 4.6) compiled by Venter (2003). This was the only vegetation map of the Mfabeni Wetland ever compiled to this detail level of vegetation assemblages at the time of conducting this research. Even at this level of detail, most of the mapped vegetation assemblages were combinations of multiple plant species as reflected on the map legend (figure 4.6).

The Mfabeni wetland vegetation was compiled in 2003 as part of a MSc research undertaken by Catharina Elizabethe Venter at the University of Pretoria, South Africa. The research was based on digital aerial photographs of the Mfabeni wetland and field measurements. A detailed

description of the methodology used in compiling this vegetation map is provided as part of the dissertation available via the University of Pretoria Library Services, Theses and Dissertations repository, accesssible (in July 2023) using the link
https://repository.up.ac.za/bitstream/handle/2263/24480/dissertation.pdf?sequence=1&isAllowed=y

Venter (2003) admits that during field sampling, heterogeneity of plant communities existed; hence sample plots were placed in areas where the vegetation was relatively homogeneous and where it differed visibly from the other adjacent areas. She further stated that differences in vegetation often occurred over a very small area and that this variation could not be observed on the aerial photographs used (venter 2003).

It can be argued, therefore that this vegetation map may not have been so accurate. However, despite these shortcomings, it was the only vegetation map of the Mfabeni wetland with the comprehensive detail of vegetation communities' distribution ever compiled at the time of conducting this research. It was for this reason that it was adopted as a secondary source of reference data for this research. It had been recently used as a reference for a study to compile a database of the South African national wetland vegetation (Sieben, et al, 2014).

5.2.3 Elevation Data

Height data was required for the characterization of grass assemblages in terms of Elevation used as an indirect means of establishing the wetland hydrological regime. A 30m-by-30m spatial resolution Shuttle Radar Topography Mission (SRTM) Digital Elevation Model (DEM) (figure 5.6) of the 27°S and 31°E degree square had been downloaded from (http://glcf.umiacs.umd.edu), but was not used for the final processing due to its low spatial resolution of 30m in relation to a gently undulating wetland used as the study area for this research.

Figure 5.6: Shuttle Radar Topographic Mission (SRTM) Digital Elevation Model (DEM) over the Study Area

A 5m contour map (figure 5.7) of the Mfabeni wetland and the surrounding, compiled by the South African Directorate of National Geospatial Information (NGI), was used to generate a DEM used for processing and analysis. A map of spot-heights (figure 5.7) covering the same area as the 5m contour map was used for accuracy assessment of the generated DEM prior to its use in the analysis.

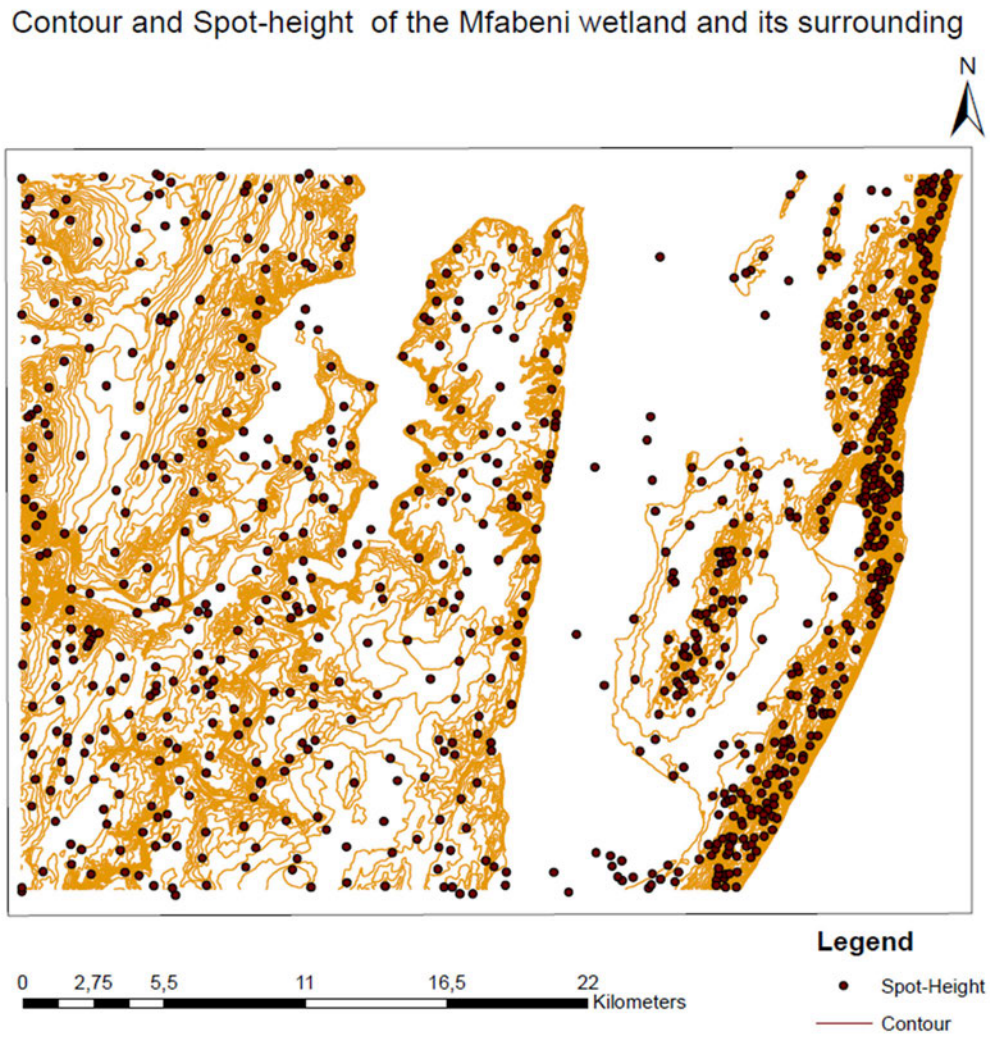

Figure 5.7: Contour and Spot-height of the Mfabeni wetland and its surrounding

5.3 Geometric correction and validation of the Mfabeni Wetland Hyperion Imagery

The L1T Hyperion image used for processing in this research had already been corrected for geometric errors with the help of control points picked from the area covered by the scene, prior to making it available for download (Kumar and Yarrakula, 2017). Its geometric accuracy was, however, validated using check points picked on a ring road that runs around the Mfabeni wetland (figure 5.8).

Figure 5.8: Hyperion image superimposed over the Topographic map of the Mfabeni wetland showing checkpoints used to validate the geometric accuracy of the L1T Hyperion image.

5.4 Formulation of Vegetation Assemblages Classes

The various vegetation communities reflected on the Mfabeni wetland vegetation map were identified as the classes representing different vegetation assemblages. Each of the mapped vegetation communities was allocated a class number, as depicted on figure 5.9 and tabulated on table 5.2. One vegetation community was not described on the vegetation map. It was therefore given class '0' and added to the legend.

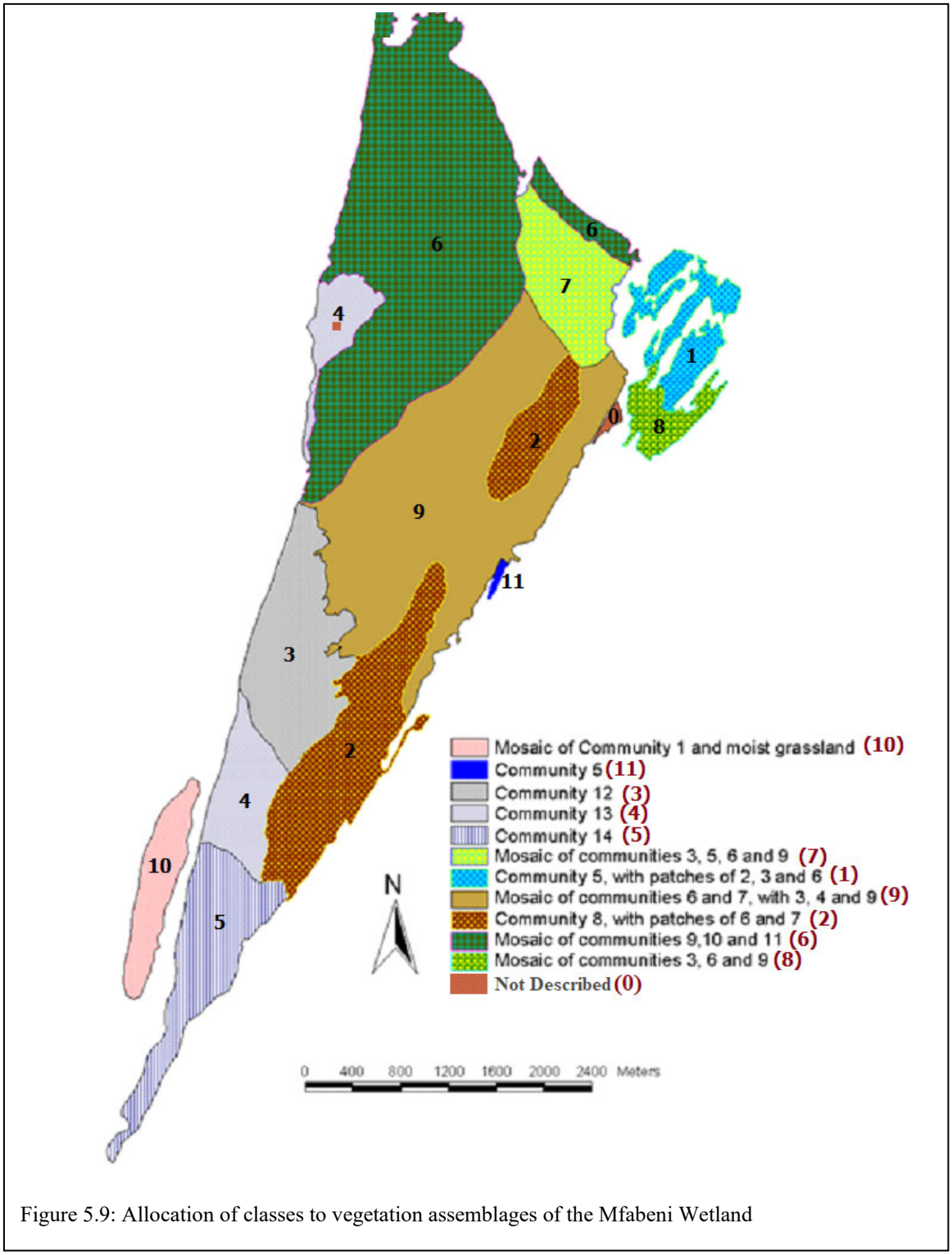

Figure 5.9: Allocation of classes to vegetation assemblages of the Mfabeni Wetland

Prior to the assignment of classes to vegetation assemblages, the vegetation map of Mfabeni wetland was registered to a digital copy of a topographic map of the study area obtained from the South African National Geospatial Information (NGI) and compiled in 2017 which served as a base map.

Table 5. 2: Classes Representing vegetation assemblages of the Mfabeni wetland

Class	Vegetation Assemblage
0	Not Described
1	Community 5, with patches of 2, 3 and 6
2	Community 8, with patches of 6 and 7
3	Community 12
4	Community 13
5	Community 14
6	Mosaic of communities 9, 10 and 11
7	Mosaic of communities 3, 5, 6 and 9
8	Mosaic of communities 3, 6 and 9
9	Mosaic of communities 6 and 7, with 3, 4 and 9
10	Mosaic of community 1 and moist grassland
11	Community 5
11	Community 5

5.5 Data Processing and Analysis

This section discusses how hyperspectral imagery, ground truthing and elevation data were processed and analyzed. The Spectral Angle Mapper (SAM) algorithm used for Hyperion image classification performs better when applied to image data for which atmospheric correction to extract apparent surface reflectance data has been performed (Gopinath et al., 2020). Radiometric calibration to obtain an apparent surface reflectance image was therefore performed on the image, despite the fact that no comparison with the field collected spectra was required as spectra was extracted directly from the image with field collected spectra having been established as insufficient to serve as a basis for reliable and conclusive results. The methodology presented here is, therefore, based on the use of secondary data were such was required.

5.5.1 Spatial Subsetting of the Hyperion Image

The Hyperion image far exceeded the study area spatial extent. It was, therefore spatially subset to the size of the study area to allow for speedy processing. Spectral subsetting was not done to allow for the removal of unwanted bands later. Figure 5.10 shows the resulting image covering the Mfabeni Wetland following spatial subsetting.

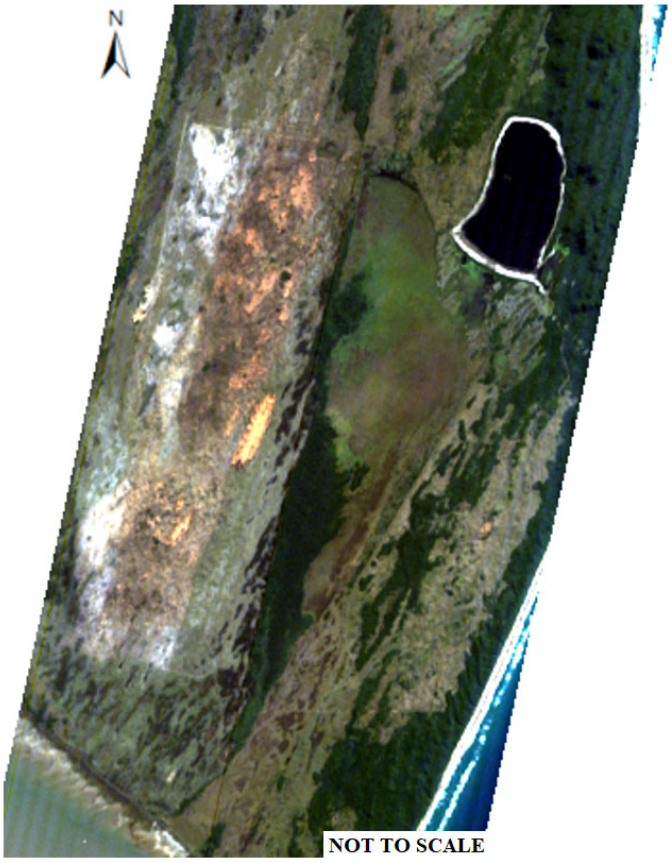

Figure 5.10: Spatial subset image of the study area

5.5.2 Hyperion Image Radiometric Calibration

Radiometric calibration was done to convert the raw image to spectral radiance, then converting the resultant image into a reflectance image that depicted the apparent surface reflectance.

5.3.2.1 Spectral Radiance Calibration

Hyperion image was radiometrically calibrated to obtain the actual radiance data in radiance units using a radiometric calibration procedure provided in ENVI Tutorial (L3Harris Geospatial, N.D). The procedure entailed multiplying bands 1-70 (visible/near-infrared (VNIR) bands) by a gain value of 0.025 to each pixel in this band range. This is similar to the conventional approach of

dividing each pixel in this band range by 40. Each pixel in the bands 71-242 (shortwave-infrared (SWIR) bands) was multiplied by a gain value of 0.0125, which is the same as dividing each pixel value by 80.

As the radiometrically calibrated image was required to be converted to an equivalent reflectance image using FLAASH, each pixel in both VNIR and SWIR was scaled so as to represent radiance units in $\mu W/(cm^2 * sr * nm)$. This was achieved automatically by applying a scale factor of 0.10 to each of the pixels. The output interleave was also changed from 'BSQ' to 'BIL' format used by the FLAASH algorithm.

The procedure is designed to exclude the zero bands; bands 1-7, 58-76 and 225-242, which result from either not being illuminated or corresponding to areas of low sensitivity of the spectrometer material leaving behind 198 of the total 242 bands. Strong water absorption bands (121-126, 167-180 and 222-224) were also subsequently removed leaving 175 of the total 242 bands (Zhang et al., 2021b).

De-striping of the Hyperion imagery was not undertaken as part of the radiometric calibration process because it produces an image with pixels that may have interpolated values. The research was based on working with pixels not altered in any way.

5.3.2.2 Surface Reflectance Calibration

The resultant spectral calibrated image was further calibrated to apparent surface reflectance to allow for data to be properly processed using SAM. Calibrating the image to apparent surface reflectance accounted for the removal of the atmospheric effect, inclusive of water vapour, oxygen, carbon dioxide, methane, ozone absorption, molecular and aerosol scattering, on spectra detected and recorded by the Hyperion sensor. FLAASH was considered the most ideal of the models available in ENVI for creating an apparent surface reflectance image out of a spectra-calibrated image created under 5.5.2.1 and therefore was used for this purpose. Figure 5.11 shows the parameters provided to FLAASH in order to derive an apparent surface reflectance image from the spectra calibrated image.

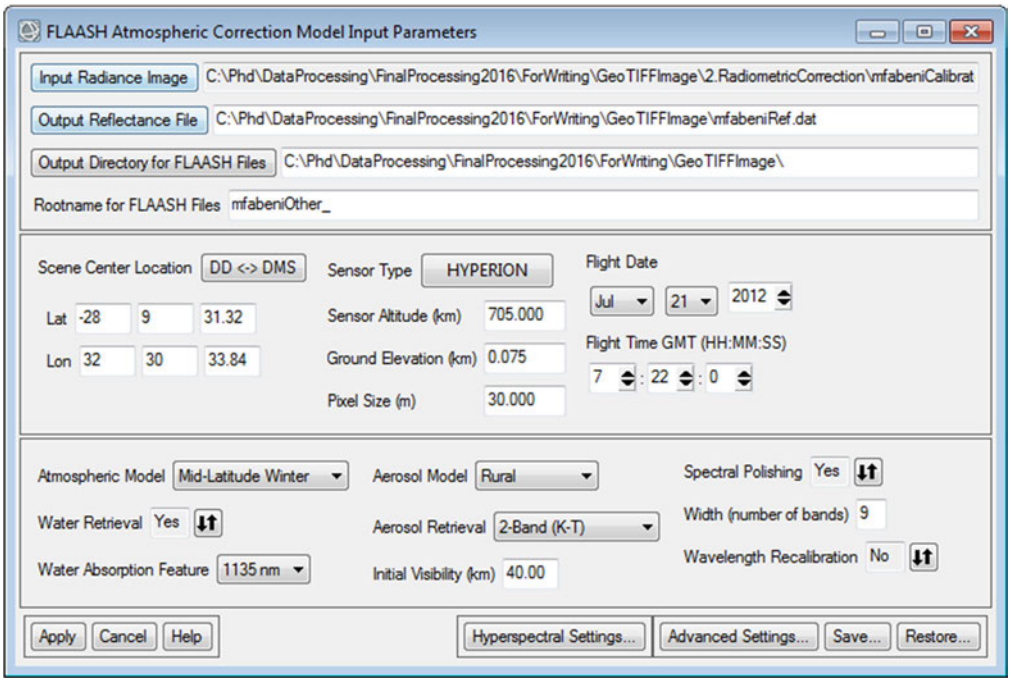

Figure 5.11: Parameters provided to FLAASH

Several of the parameters required by FLAASH were obtainable from the image and loaded automatically by the software. The sensor altitude was, however, entered interactively while other parameters were chosen from the drop-down selection lists provided by the software.

The image was captured on 21 July 2012 which is wintertime in South Africa. Hence 'Mid-Latitude Winter' was selected as an Atmospheric Model, the site being located around 28° 9'. 'Rural' was selected for Aerosol Model as the study area is located in the rural area of South Africa. Water Retrieval was required, and therefore it was indicated as 'Yes'. The rest of the parameters remained unchanged as 'Hyperion' is a known sensor, and consequently, they had been automatically populated in advance.

The ground elevation for the model was estimated as the mean of the Elevation of the image coverage obtained from the north-south and east-west elevation profiles drawn over the image after it had been overlain on Google Earth imagery (figure 5.12).

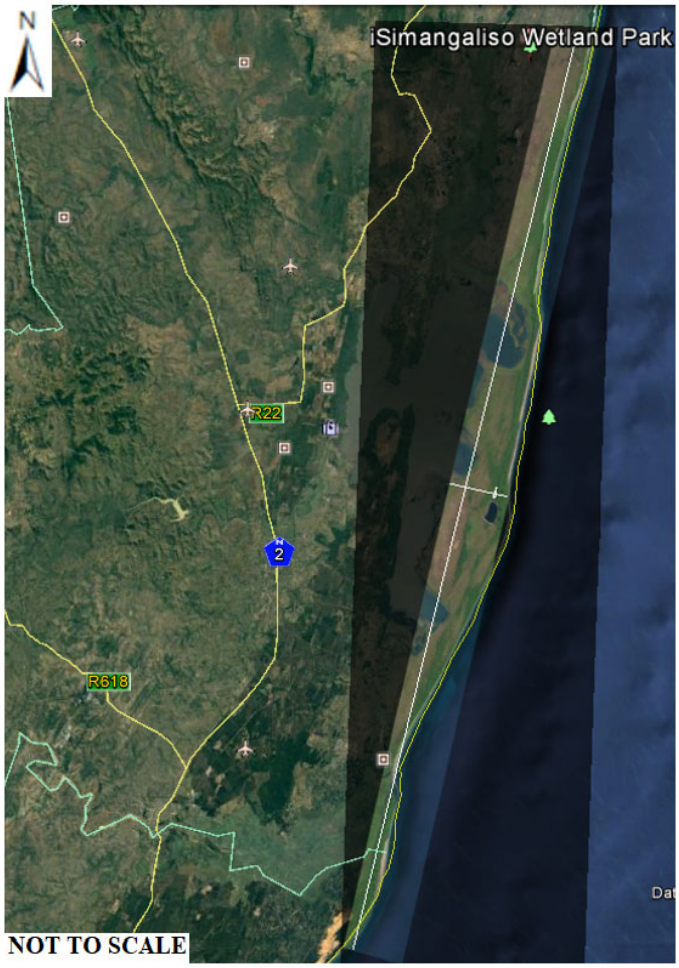

Figure 5.12: Hyperion Image overlain over Google Earth imagery for determination of image mean elevation.

The north-south elevation profile taken across the image length of 109km showed the lowest and highest elevation values of 0m and 150m, while that of east-west, across the image width of 6.88km, were 6m and 79m, respectively. Consequently, the ground elevation over the image was taken as 75m, the mean, and entered as 0.075km on the FLAASH parameter dialog box.

5.6 Extraction of Training Data

The vegetation map of the Mfabeni wetland (fig 4.6) was firstly registered to a topographic base map of the area compiled on a South African coordinate system. Following registration, it was then transformed to the coordinate system (WGS_1984_UTM_Zone_36S) of the Hyperion image and then superimposed over it.

The boundaries of the Mfabeni and vegetation assemblages were then digitized to create a shape file of the Vegetation assemblages' classes. The image region falling inside each of the digitized vegetation assemblage was then considered as belonging to the corresponding class.

Training data was then extracted using two approaches; (i) the conventional approach of digitizing areas of pure contiguous pixels representing each of the classes to create Regions of Interest (ROI) and (2) randomly extracting spectra of multiple individual pixels inside each of the classes and subsequently using the extracted spectra to compute class means for each of the vegetation assemblages. The spectra extracted in the latter cases were also used to identify the optimal bands for discriminating the vegetation assemblages through the data dimensionality reduction process using Random Forest and variable elimination. Appendix 5.1 shows a text file of 85 spectra of pixels extracted for class 1. Each column, with the exception of the first, represents spectrum of a single pixel across all remaining wavelengths contained in the Hyperion image. The first column represents the wavelengths contained in the image.

A minimum of 50 pixels was required for each class to ensure representativity (Beck, 2003). Table 5.3 show the number of spectra extracted for each of the classes. Classes 0 and 11 were not included. They could not meet the minimum required 50 pixels. The computed class means were used in conjunction with the identified optimal wavebands to classify the Hyperion image.

Table 5.3: Spectra Extracted for each Class Representing vegetation assemblages of the Mfabeni wetland

Class	Vegetation Assemblage	Number of spectra Extracted
0	Not Described	0
1	Community 5, with patches of 2, 3 and 6	85
2	Community 8, with patches of 6 and 7	114
3	Community 12	100
4	Community 13	78
5	Community 14	103
6	Mosaic of communities 9, 10 and 11	120
7	Mosaic of communities 3, 5, 6 and 9	107
8	Mosaic of communities 3, 6 and 9	89
9	Mosaic of communities 6 and 7, with 3, 4 and 9	125
10	Mosaic of community 1 and moist grassland	90
11	Community 5	0

Before the training data could be used for classification, spectral separability among the ROIs depicting the various classes was computed using two measures available in ENVI, namely, Jeffries-Matusita and Transformed Divergence separability.

The minimum and maximum values for each of these two measures are 0 and 2.0 and indicate how well the selected ROI pairs are statistically separate. Values greater than 1.9 indicate that the concerned ROI pairs have good separability. It is advisable that separability be improved for ROI pairs with lower separability values by editing the ROIs or selecting new ROIs. ROI pairs with separability values of less than 1 should be combined (Wicaksono, 2020).

The ROIs were then also visualized using the n-D Visualizer to give an idea about the purity of the pixels making ROIs.

The training data created from spectra of the randomly sampled image pixels, having not been defined as ROIs, could not be checked for spectral separability. Instead, they were used to create a spectral library.

5.7 Spectral Library Development

Image pixels spectra representing each of the classes of vegetation assemblages extracted as training data could be saved as a text file (appendix 5.1) or spectral library (figure 5.13). A spectral library of randomly extracted spectra of a single class as in figure 5.13 would be meaningless as it contains spectra of the same data. Hence extracted class spectra were saved as text files. The text files were required for further processing to determine class spectra means and to identify suitable bands for discriminating vegetation assemblages. The extracted spectra were therefore exported into MS-Excel where they were organized, transposed and the spectra mean for each class subsequently computed.

The computed spectra means were saved as a text file and then used to create a spectral library of the Mfabeni wetland vegetation assemblages.

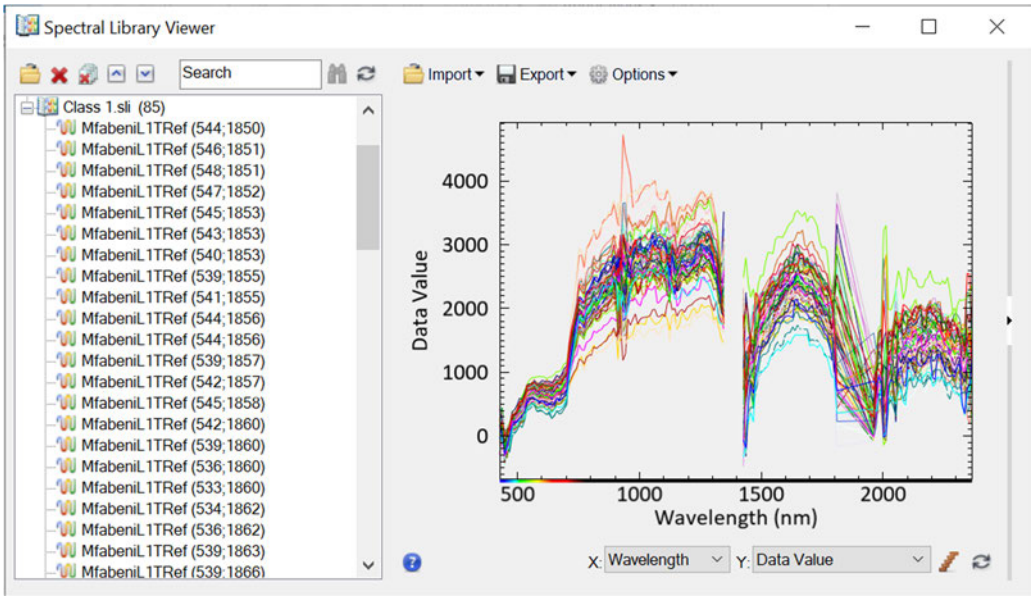

Figure 5.13: Spectral Library of Class 1 spectra displayed in the spectral library viewer

5.8 Identification of Optimal Wavebands

According to (Merentitis et al., 2014), a commensurate number of wavelengths for classification is required to avoid the 'curse of dimensionality. Too many wavebands for very few features (end members) would lead to poor classification. To avoid this problem, it is considered necessary to reduce the dimensionality of the data being processed. Various techniques, inclusive of principle component analysis, minimum noise fraction and machine learning, among others, may be used for this. The resultant data is considered the most suitable for deployment in image classification and hence can be viewed as optimal.

In this research, such data are the wavebands considered most suitable for discriminating vegetation assemblages. Some wavebands in the Hyperion image are highly correlated and hence, redundant. Random Forest and variable elimination were envisaged to remove such redundancy leaving behind only those wavebands considered optimal for subsequent image classification. Hence, they were used.

The process of identifying these wavebands involved several stages; preparing spectra for optimal waveband selection, identifying an optimal model for selecting optimal wavebands, and selection of optimal wavebands.

5.8.1 Preparing Hyperion Image Extracted Spectra for Optimal Waveband Selection

Once spectra for each class had been extracted and saved as a text file, it was exported into MS-Excel where it was combined with that of other classes to create a composite file. The resultant composite file was then transposed. In the transposed file, the first column represented the wavebands, while each of the remaining columns represented extracted vegetation assemblages' wavebands of extracted spectra. An extra column depicting 'class' was then added as the first column of the data file. The resultant file was subsequently saved as a Comma Separated Value (CSV) file.

5.8.2 Optimal Model determination using Random Forest

Identification of optimal wavebands most suitable for discriminating vegetation assemblages, using Random Forest, was performed on spectra extracted from the Hyperion image itself. RF was implemented using the 'R Analytical Tool To Learn Easily' (Rattle) package, a graphical data mining application written in R which serves as a pathway into R (figure 5.14). RF implemented on Rattle requires very few inputs. The user supplies the number of trees (nTree) to be created and the number of split variables to be permutated per node (mTry). If necessary, the user may have to indicate the number of samples. This was not required in this research as all the variables contained the same number of entries (Chilufya et al., 2014).

For a good model capable of providing the required optimal bands, five hundred (500) is recommended as a good number of trees (nTree) to be built and is provided as the default value in Rattle. Similarly, the square root ($p^{½}$) and one-third (p/3) of the total number of available variables (p) are recommended as the number of split variables to be permutated per node (mTry) for classification and regression, respectively (Liaw and Wiener, 2002). Rattle provides the square root as the default mTry value for classification, but does not display recommended default for regression. These recommended values do not always result in a good model for all data sets. (Liaw and Wiener, 2002) citing (Breiman, 2001) therefore, recommend the use of half and double the default mTry value in addition to the default. Both 'classification' and 'regression' may be used if required. Only 'classification' was used in this research.

In order to obtain the highest accuracy for classification, the RF model was optimized based on OOB estimate of error rate (Breiman, 2001) using various randomly selected nTree and mTry values, in addition to the recommended.

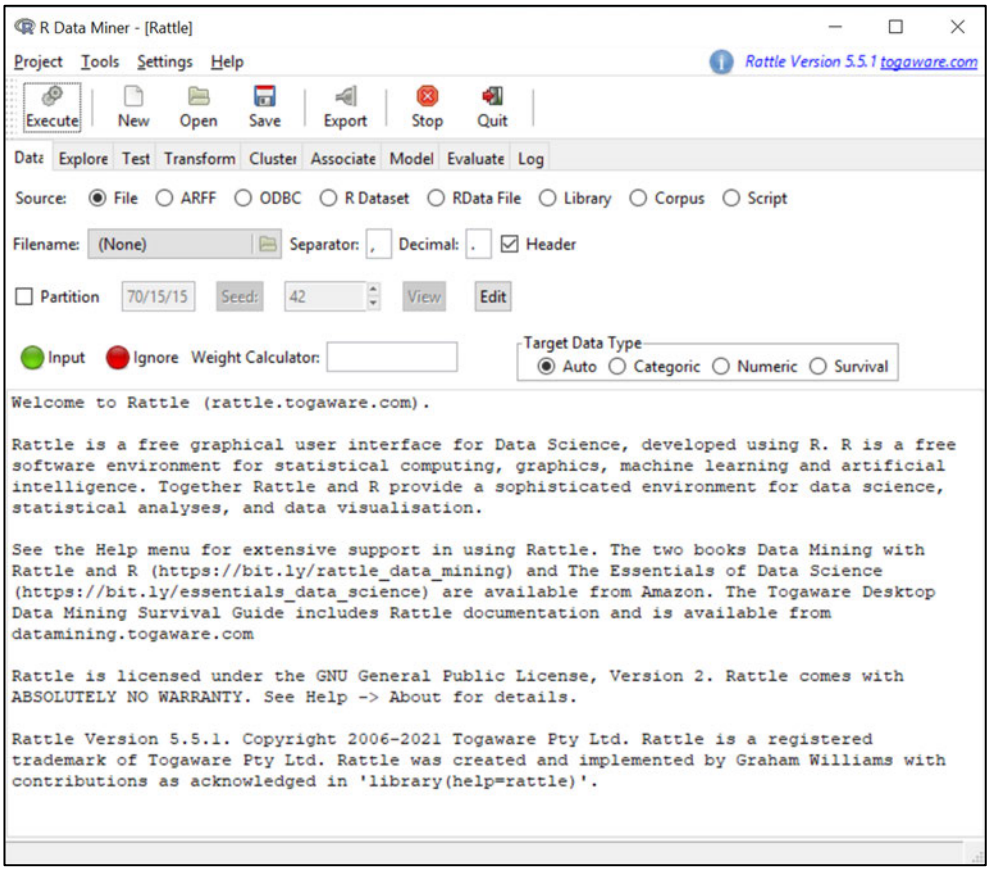

Figure 5. 14: R Analytical Tool To Learn Easily' (Rattle) package Graphical User Interface (GUI)

For every mTree, the algorithm was run repetitively with different randomly selected mTry values. The process was repeated for every mTry in turn.

During model optimization, the 'class' column was used as the 'dependant' variable, while all spectral bands for the extracted spectra served as independent variables. The data was partitioned into 70/15/15 for training/validation/testing, respectively, to allow for the validation and testing of the created model (figure 5.15).

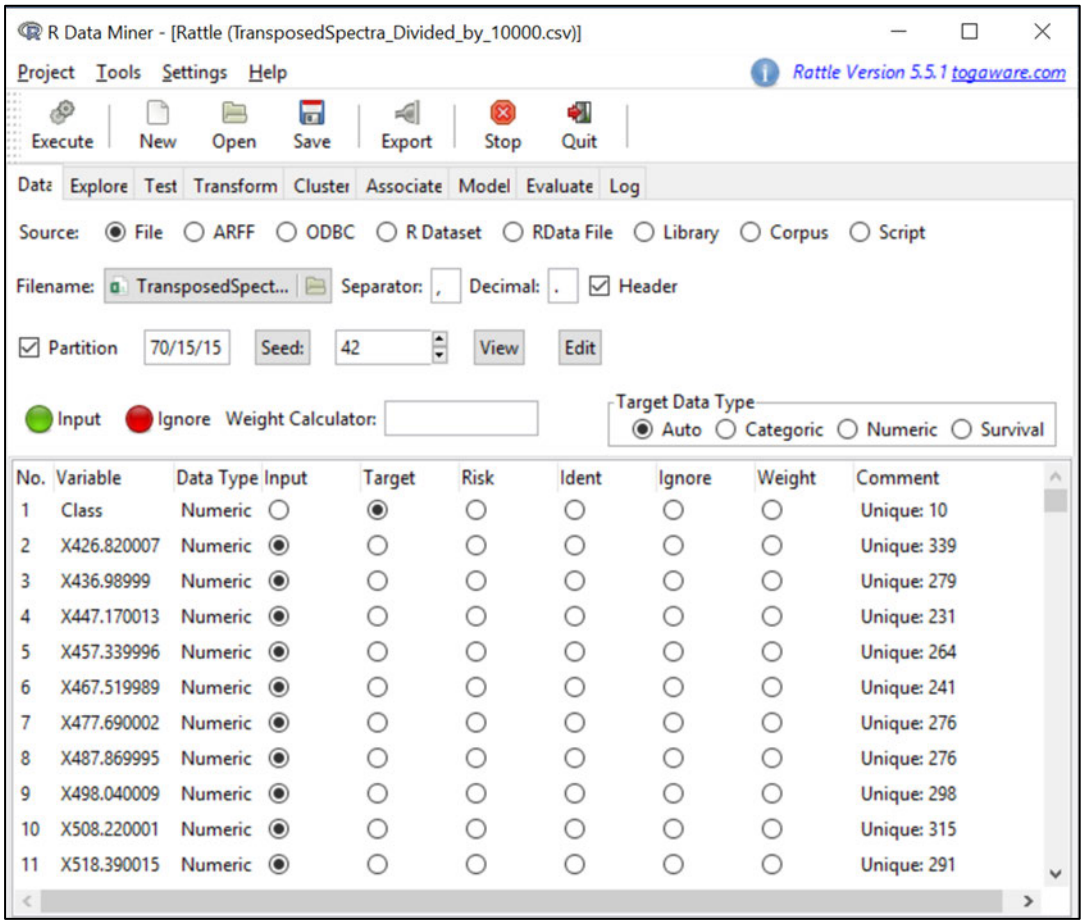

Figure 5.15: Specification of variable roles during RF Classification

The mean decrease accuracy (MDA) measured using the 'out-of-bag' (OOB) samples (figure 5.16) was used to identify the optimal model. The model with the lowest OOB error was adopted as optimal under the circumstances.

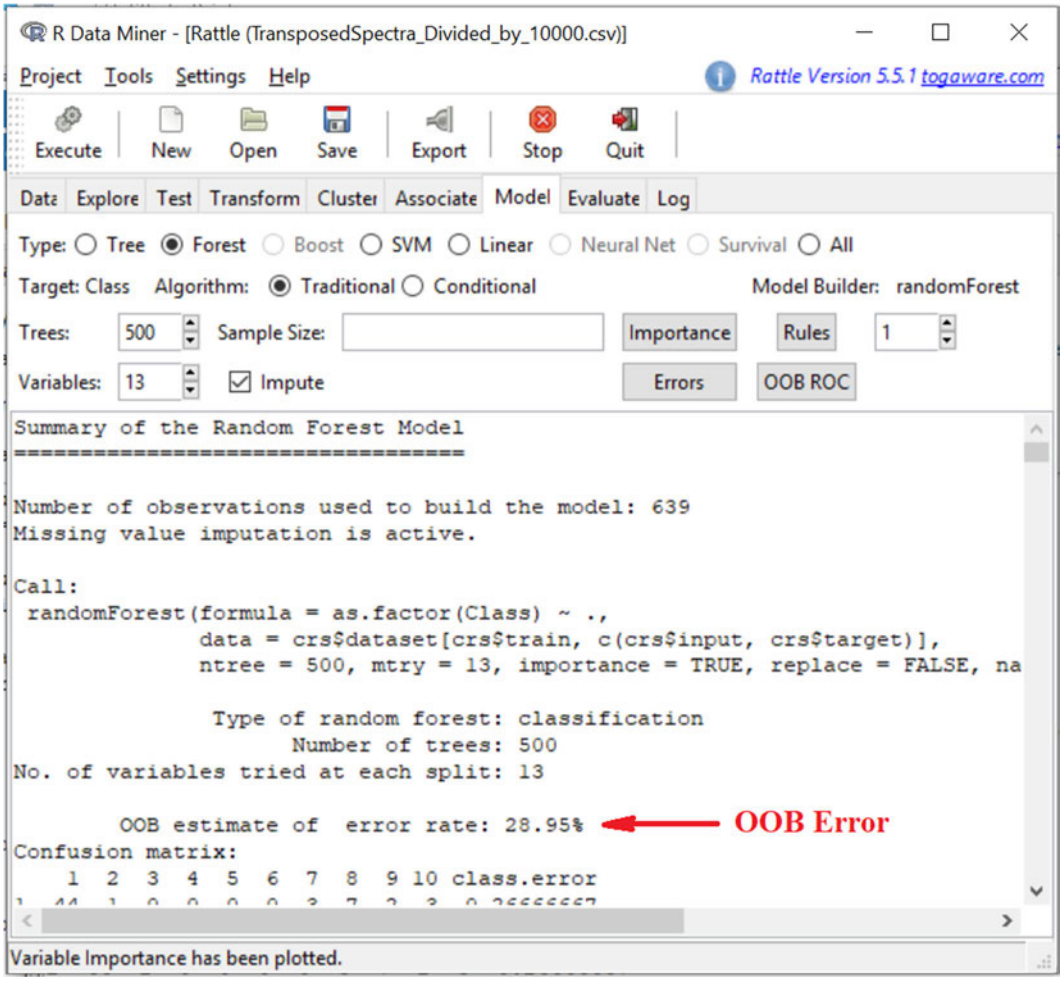

Figure 5.16: OOB Estimate of Error as a measure of RF Classification Accuracy

5.8.3 Performance Evaluation of RF Classification Models

In order to identify which of the optimal model is the most optimal, their performance was evaluated by comparing the overall accuracy values obtained from error matrices for the training, validation, testing, and full datasets involving 2/3 (70%), 1/6 (15%), 1/6 (15%) and 100% of the total data used to develop the model.

5.8.4 Selection of Optimal Wavebands of the Identified RF Optimal Model

Following identification of the most optimal RF classification model, it was subsequently used to identify optimal wavebands. Optimal wavebands were identified as the top waveband ranked according to variable importance determined in terms of MDA for the RF classification model. These were the wavebands considered most suitable for discriminating among the various vegetation assemblages (Chilufya et al., 2014).

A list of wavebands showing variable importance as listed under the mean decreasing accuracy (MDA) was copied as text from Rattle into MS Excel. The wavebands output generated by Rattle displayed with an 'X' prefix (figure 5.17) which had to be removed in order to obtain wavebands as numbers.

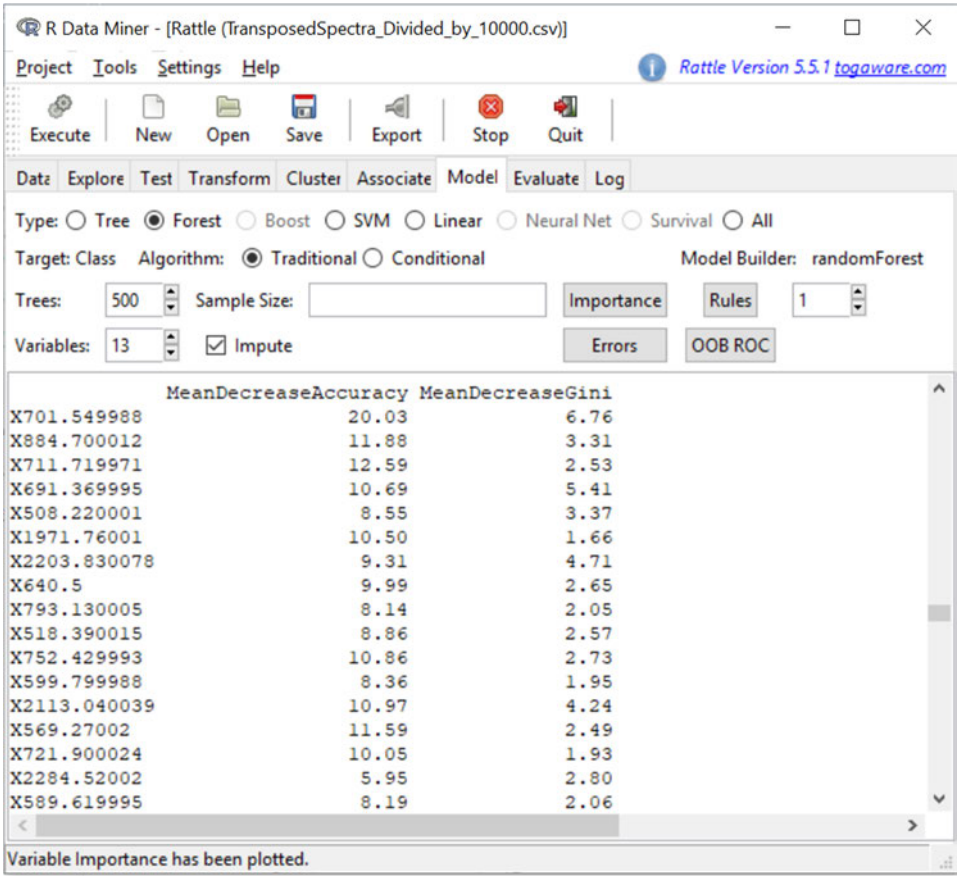

Figure 5.17: A listing of important wavebands with ‘X’ as a prefix

The resultant waveband numbers were then ranked in order of the descending MDA, with the largest MDA displayed at the top. The top 30 ranked wavebands of the identified optimal model were then extracted and subjected to variable elimination.

5.8.5 Optimal wavebands selection using Variable Elimination

The optimal wavebands identified using RF classification do not automatically select the optimal number of variables that produce the best accuracy when used for classification (Adam and Mutanga, 2009). There is, therefore, a need to subject these variables to 'variable elimination' to determine the most optimal of the wavebands obtained from RF classification model.

Backward variable elimination (stepwise based) and Akaike Information Criterion (AIC) (criterion based) were used to identify the most optimal of the 30 wavebands identified by RF classification. Optimal wavebands selection by 'backward variable elimination' was done interactively based on a 0.05 significance level as opposed to the criterion-based equivalent which required no user intervention. The AIC algorithm only stopped running once AIC value of all the remaining wavebands was less than a threshold value determined by the algorithm.

5.9 Image classification

Supervised Image classification was performed using the spectra means computed for each of the classes and used to create a spectral library as training data on the one hand and the wavebands identified as optimal for discriminating among different vegetation assemblages on the other. In an effort to obtain the best classified image, various optimal waveband numbers were explored including all the 175 wavebands making up the image.

Classification based on training data obtained using the conventional approach of extracting contiguous pixels of each vegetation assemblage class was also explored. Spectral Angle Mapper (SAM) was used as a classification algorithm.

5.10 Classification Accuracy Assessment

Each of the classified images was subjected to a post classification accuracy assessment to establish which one of them performed the best. The assessment was based on comparing the pixels correctly classified against the total number of pixels making up each of the vegetation assemblage classes. The classified image with the best classification accuracy was then adopted as representing the best distribution of vegetation assemblages of the Mfabeni wetland and subsequently used for the characterization of vegetation assemblages along an altitudinal gradient.

5.11 Digital Elevation Model (DEM) generation and Accuracy Assessment

Several DEMs were generated from the 5m contour map using various interpolation algorithms available in ArcGIS inclusive of Inverse Distance Weighted Average (IDW), Kriging, Natural neighbor, spline, Trend and Topo to Raster. The spatial resolution for all DEMs generated was 30m, deliberately chosen to match that of the Hyperion image.

Each generated DEM was then subjected to an accuracy assessment using spot-heights available in the study area. A total of 844 randomly spatially distributed spot-heights was used for accuracy

assessment. The accuracy measures used for assessment included; Mean Error, Root Mean Square Error (RMSE), Standard Deviation and Standard Error (Equations 5.1 – 5.4).

Mean Error

$$\hat{\mu} = \frac{1}{n}\sum_{i=1}^{n} \Delta h_i \ldots\ldots\ldots\ldots\ldots\ldots\ldots\ldots\ldots\ldots\ldots\ldots\ldots \text{(5.1)}$$

Root Mean Square Error

$$\widehat{RMSE} = \sqrt{\frac{1}{n}\sum_{i=1}^{n} \Delta h_i^2} \ldots\ldots\ldots\ldots\ldots\ldots\ldots\ldots\ldots \text{(5.2)}$$

Standard Deviation

$$\hat{\sigma} = \sqrt{\frac{1}{(n-1)}\sum_{i=1}^{n}(\Delta h_i - \hat{\mu})^2 5.3)} \ldots\ldots\ldots\ldots\ldots\ldots\ldots\ldots \text{(5.3)}$$

Standard Error

$$\hat{\sigma}_{\bar{x}} = \sqrt{\frac{1}{n(n-1)}\sum_{i=1}^{n}(\Delta h_i - \hat{\mu})^2 5.4)} \ldots\ldots\ldots\ldots\ldots\ldots\ldots\ldots \text{(5.4)}$$

Where 'i' is a point, n is the number of checkpoints and h is height difference

The DEM with the best result was considered the most accurate and hence was to be adopted for vegetation assemblages' characterization. In this research, however, the interpolation method that produced the best result faired badly when the interpolated DEM values at checkpoints inside and in the vicinity of the wetland were compared with the corresponding known ground values. The DEM that produced the best results based on the checkpoints inside and in the vicinity of the wetland was adopted for use instead.

5.12 Characterization of Vegetation Assemblages in terms of Elevation

Characterization of Mfabeni wetland vegetation was done in terms of variation in the spatial distribution of vegetation assemblages with respect to elevation on an altitudinal gradient. The best of the classified images identified under 5.10 was overlain with the DEM of the Mfabeni wetland adopted in 5.11. The resultant combined image was then used to display the spatial distribution of vegetation assemblages in terms of elevation across the wetland and along an altitudinal (elevation) gradient of selected transects.

5.12.1 Spatial distribution of vegetation assemblages at different elevations

The combined vegetation assemblages and DEM image was queried on each of the wetland elevations represented to produce spatial vegetation assemblage distribution maps.

5.12.2 Statistical distribution of vegetation assemblages at different elevations

Data from an accompanying attribute table of the combined vegetation assemblages and DEM image was used to quantify the distribution of vegetation assemblages at each Elevation in terms of the pixel count.

5.12.3 Spatial distribution of vegetation assemblages along Mfabeni wetland altitudinal (Elevation) gradient

The spatial distribution of vegetation assemblages along the altitudinal gradient of the Mfabeni wetland was determined by creating two separate layers of points depicting pixel centroids for all pixels making up, firstly, the vegetation assemblages and secondly, the adopted DEM of the Mfabeni wetland. This approach was able to use the extracted elevation point values that depicted the actual values (integers) as opposed to whole-number pixel values generated when the vegetation assemblages and DEM were combined prior to the extraction of points.

The elevation point layer was then used to convert the resultant 2D composite image into a 3D layer to allow for the creation of profiles across the wetland.

Once all image pixels had been converted to 3D points depicting their centroids, four (4) sets of transects with different orientations were then created. A point profile for each transect was subsequently created.

Transects were considered an ideal means of establishing a relationship between vegetation and elevations along an altitudinal gradient. Each transect was used to depict continuous variation in vegetation at every 30m (Hyperion image pixel spatial resolution) interval representing pixel centres along an elevation profile.

5.13 Validation of Change in Elevation and Vegetation assemblages against Vegetation Moisture Distribution in Mfabeni Wetland

Moisture distribution of the vegetation assemblages in the Mfabeni wetland was estimated from the Moisture Stress Index (MSI) computed as a ratio between reflectance in wavebands (ρ) 1599 and 819 using equation 5.5.

$$MSI = \frac{\rho_{1599}}{\rho_{819}} \quad (5.5)$$

MSI is a reflectance measurement sensitive to the increase in leaf water content. The strength of the absorption around 1599nm increases with an increase in vegetation water content, resulting in less reflectance. At 819nm, absorption remains nearly unaffected by changing water content.

Computation of the MSI was done repetitively, creating various classes in intervals of 0.1 over the 0 – 2. This was used to explore the threshold values for classifying moist conditions. Subsequently, the classes were then reclassified into three classes; 0 – 0.5, 0.51 – 1.0 and 1.01 – 2. MSI values beyond 2 were not computed and hence remained as blank areas on the MSI image. They were, however, included as part of the class with MSI above 1 in the reclassified image.

5.14 Presentation of Results

Results for this research were presented using a variety of formats dictated by the nature of the results. Graphics in the form of maps and graphs were used where considered most appropriate for conveying results better. Textual presentations, usually in the form of tables, were used where results merited this, especially for statistical analysis.

5.15 Chapter Summary

This chapter describes the data collected for the research, how it was pre-processed, processed, analysed, and results presented.

The field data originally collected for the research, inclusive of spectral measurements of wetland vegetation assemblages, GNSS locations of where spectral measurements were taken, and digital imagery showing the vegetation assemblages for which spectral measurement had been taken were not used for the final processing for this research due to its insufficiency to produce meaningful and reliable results. A vegetation image of the Mfabeni wetland compiled by (Venter, 2003) was used instead.

Processing of the data discussed included Hyperion imagery spatial subsetting to downsize it to the study area for processing efficiency, spectral radiance calibration and calibrating for apparent surface reflectance values. The process of formulating classes to represent vegetation assemblages was described and so was the process of extracting training data using two approaches. Process of creating a spectral library was then discussed. The chapter also presented how optimal wavebands were identified using Random Forest and variable elimination, and how they were used in the classification of the Hyperion image. The process of assessing the accuracy of classified images in order to come with the best was then presented. The most accurate classified image was then used in conjunction with a DEM to characterize the vegetation assemblages in terms of elevation. The DEM used had been identified as the best of the several generated from a 5m interval contour map using various interpolation techniques and assessed for accuracy using spot-height values of the area as checkpoints.

The resultant combined image of vegetation assemblages and elevations was then used to draw up profiles across the wetland to assess the distribution of vegetation along the elevation gradient. A MSI value map was finally used to validate the distribution of elevation and vegetation assemblages across the Mfabeni wetland.

The discussion of how the results of the research should be presented was also discussed. The next chapter presents the results obtained.

Chapter 6

Results

6.1 Introduction

This chapter presents the results obtained from the various aspects of processing undertaken for the research. The results presented include those obtained from the processing of the acquired Hyperion hyperspectral imagery, ground-truthing and elevation data. Where the original raw data produced results that needed further processing, the results arising from the follow up processing have also been presented leading to the final results expected from the research.

6.2 Geometrically Corrected and validated Mfabeni Wetland Hyperion Imagery

Table 6.1(a) shows coordinate values of checkpoints used to validate the geometric accuracy of the L1T Hyperion image of the Mfabeni wetland. A RMSE of 3,08248m was obtained based on the location of the selected points.

Table 6.1(a): Coordinates of checkpoints used to validate the geometric accuracy of the L1T Hyperion image of the Mfabeni wetland and RMSE Obtained.

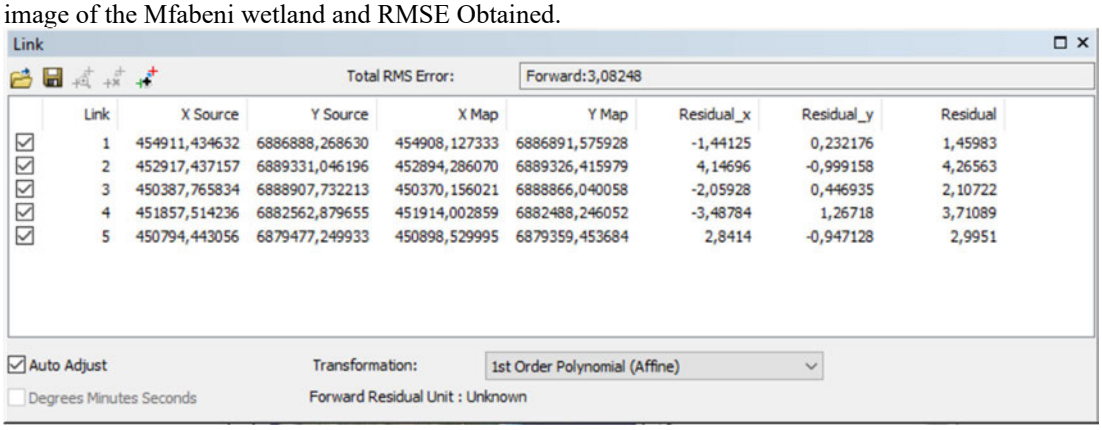

Link	X Source	Y Source	X Map	Y Map	Residual_x	Residual_y	Residual
1	454911,434632	6886888,268630	454908,127333	6886891,575928	-1,44125	0,232176	1,45983
2	452917,437157	6889331,046196	452894,286070	6889326,415979	4,14696	-0,999158	4,26563
3	450387,765834	6888907,732213	450370,156021	6888866,040058	-2,05928	0,446935	2,10722
4	451857,514236	6882562,879655	451914,002859	6882488,246052	-3,48784	1,26718	3,71089
5	450794,443056	6879477,249933	450898,529995	6879359,453684	2,8414	-0,947128	2,9951

6.3 Vegetation Assemblage Classes

The RMSE was used as an accuracy measure of registering a vegetation map to the Hyperion image. Table 6.1(b) shows a RMSE of 0.812802m obtained and the coordinate values of the points used for registration.

Table 6.1(b): Point Coordinates used register a Vegetation map of the Mfabeni wetland to the Spatial Reference System of the Hyperion image showing the RMSE

Link

Total RMS Error: Forward:0,812802

Link	X Source	Y Source	X Map	Y Map	Residual_x	Residual_y	Residual
1	1,609768	1,520954	450304,813431	6880205,446271	-0,902267	-1,86265e-09	0,902267
2	3,044707	8,305652	451667,875090	6887249,983404	0,0322336	9,31323e-10	0,0322336
3	2,801149	3,367364	451456,648973	6882158,066971	1,28619	-1,86265e-09	1,28619
4	5,403051	7,753072	453963,958543	6886785,949171	-0,416155	1,86265e-09	0,416155

Auto Adjust

Transformation: 1st Order Polynomial (Affine)

Degrees Minutes Seconds

Forward Residual Unit : Unknown

Figure 6.1 shows a map of vegetation assemblages with the allocated classes superimposed over the Hyperion image of the Mfabeni wetland.

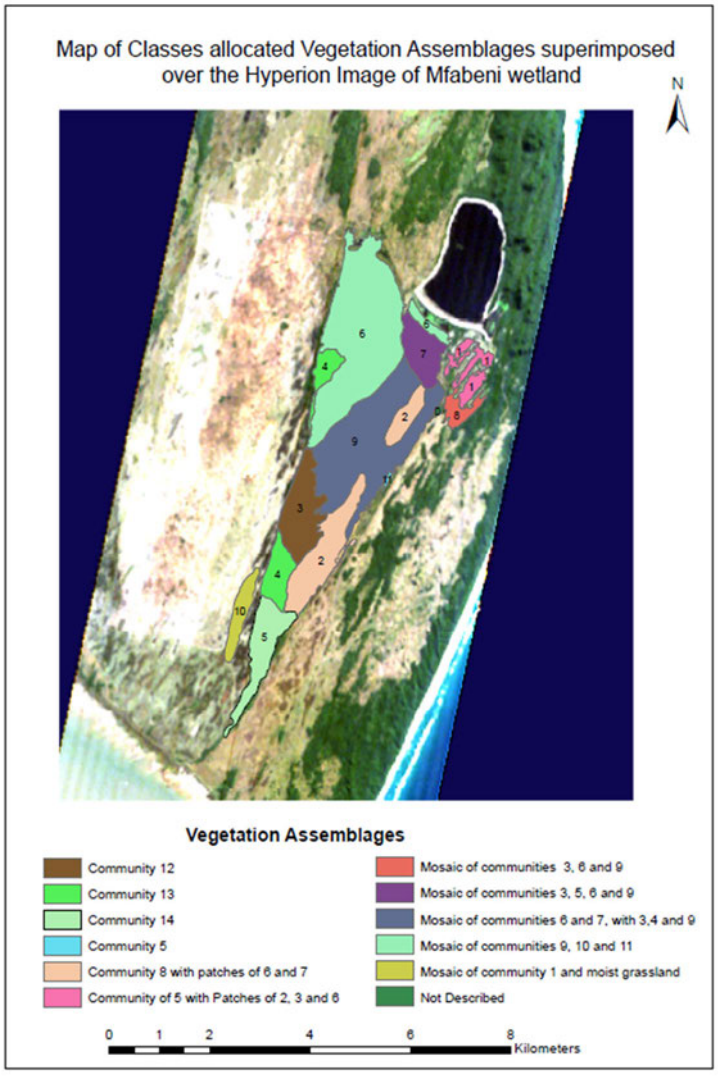

Figure 6.1: Classes allocated to Vegetation Assemblages superimposed over the Hyperion Image

6.4 Apparent Surface Reflectance Hyperion Image of the Mfabeni Wetland

Figure 6.2 shows an apparent surface reflectance spatially subset image of the Mfabeni wetland. The image consisted of 175 bands once the zero and strong water absorption bands had been removed (Zhang et al., 2021b). The figure shows the difference in values (enclosed in red) in three bands (29 for red, 20 for green 12 for blue) over the same crosshair location (193.4750, 195.6925) when the original image, radiometric calibrated, and reflectance images were subjected to a cursor inquiry. This was confirmation that the values do change once subjected to radiometric calibration. The resultant surface reflectance values were very small. They were therefore scaled by multiplying by 10000 for display purposes.

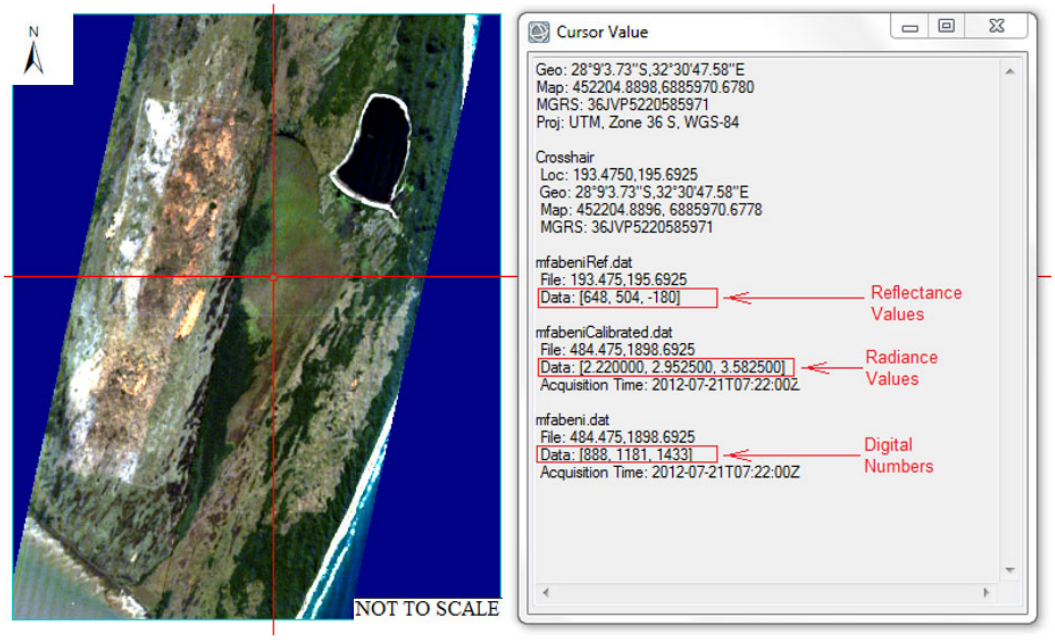

Figure 6.2: Apparent Surface Reflectance Image showing Reflectance Values, Digital Numbers (DN) and Radiance Values

Calibrating the Mfabeni wetland imagery to apparent surface reflectance was necessary for the effective deployment of the Spectral Angle Map algorithm. FLAASH created several output files, inclusive of a cloud mask image, a water vapor image, a journal file with processing results, a template file with the parameters defined, and the reflectance file. While all other resultant files supported the interpretation of the reflectance image, only the results of the reflectance file were used and hence presented here.

6.5 Training Data

Training data was extracted using the conventional approach of digitizing areas of pure contiguous pixels representing each class and by random sampling of pixels inside each

vegetation assemblage class. Spectra extracted using the latter approach were then subjected to data dimension reduction using a combination of Random Forest and variable elimination.

6.5.1 Training data based on the Conventional Approach

Figure 6.3 shows the Regions of Interest (ROI) digitized for each of the vegetation assemblage classes. Each color depicts one class of vegetation assemblage.

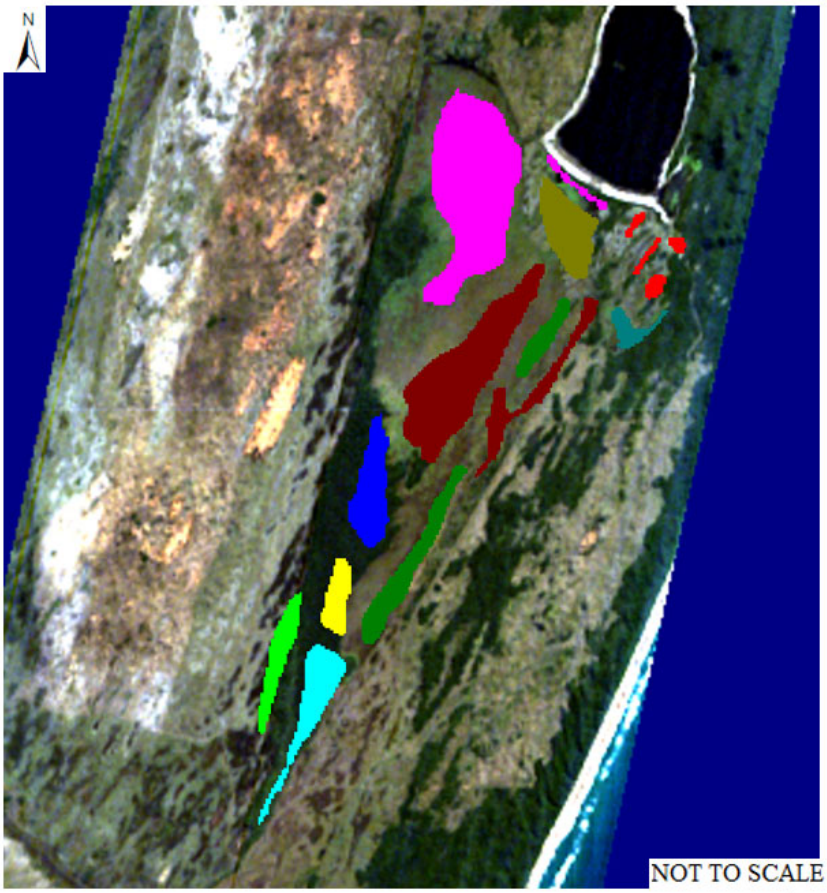

Figure 6.3: Digitized Regions of Interest (ROI) representing each of the vegetation Assemblage

Once the ROIs had been created, a spectra separability assessment was undertaken using the Jeffries-Matusita and Transformed Divergence value measures of separability. Table 6.2 shows a display of the end portion of a spectra separability report indicating the ROIs pair separability values listed from the least separable pair to the most separable. Appendix 6.1 shows a full ROI Separability Report.

Table 6. 2: Separability between pairs of Vegetation Assemblages classes of the Mfabeni Wetland

```
Pair Separation (least to most):

ROI #10 and ROI #8 - 0.00000000
ROI #3 and ROI #1 - 0.00000000
ROI #4 and ROI #1 - 0.00000000
ROI #2 and ROI #1 - 0.00000000
ROI #6 and ROI #1 - 0.00000000
ROI #8 and ROI #3 - 0.00000000
ROI #10 and ROI #1 - 0.00000000
ROI #9 and ROI #8 - 0.00000000
ROI #8 and ROI #5 - 0.00000000
ROI #9 and ROI #1 - 0.00000000
ROI #8 and ROI #7 - 0.00000000
ROI #8 and ROI #6 - 0.00000000
ROI #8 and ROI #4 - 0.00000000
ROI #8 and ROI #2 - 0.00000000
ROI #8 and ROI #1 - 0.00000000
ROI #5 and ROI #1 - 0.00000000
ROI #7 and ROI #1 - 0.00000000
ROI #10 and ROI #9 - 2.00000000
ROI #10 and ROI #7 - 2.00000000
ROI #10 and ROI #6 - 2.00000000
ROI #10 and ROI #5 - 2.00000000
ROI #10 and ROI #4 - 2.00000000
ROI #10 and ROI #3 - 2.00000000
ROI #10 and ROI #2 - 2.00000000
ROI #9 and ROI #7 - 2.00000000
ROI #9 and ROI #6 - 1.99999728
ROI #9 and ROI #5 - 2.00000000
ROI #9 and ROI #4 - 2.00000000
ROI #9 and ROI #3 - 2.00000000
ROI #9 and ROI #2 - 1.99999986
ROI #7 and ROI #6 - 2.00000000
ROI #7 and ROI #5 - 2.00000000
ROI #7 and ROI #4 - 2.00000000
ROI #7 and ROI #3 - 2.00000000
ROI #7 and ROI #2 - 2.00000000
ROI #6 and ROI #5 - 2.00000000
ROI #6 and ROI #4 - 2.00000000
ROI #6 and ROI #3 - 2.00000000
ROI #6 and ROI #2 - 2.00000000
ROI #5 and ROI #4 - 2.00000000
ROI #5 and ROI #3 - 2.00000000
ROI #5 and ROI #2 - 2.00000000
ROI #4 and ROI #3 - 2.00000000
ROI #4 and ROI #2 - 2.00000000
ROI #3 and ROI #2 - 2.00000000
```

Figure 6.4 shows n-D Visualizer captions of the same training data ROIs, depicting poor spectral separability among pixels representing vegetation assemblage classes.

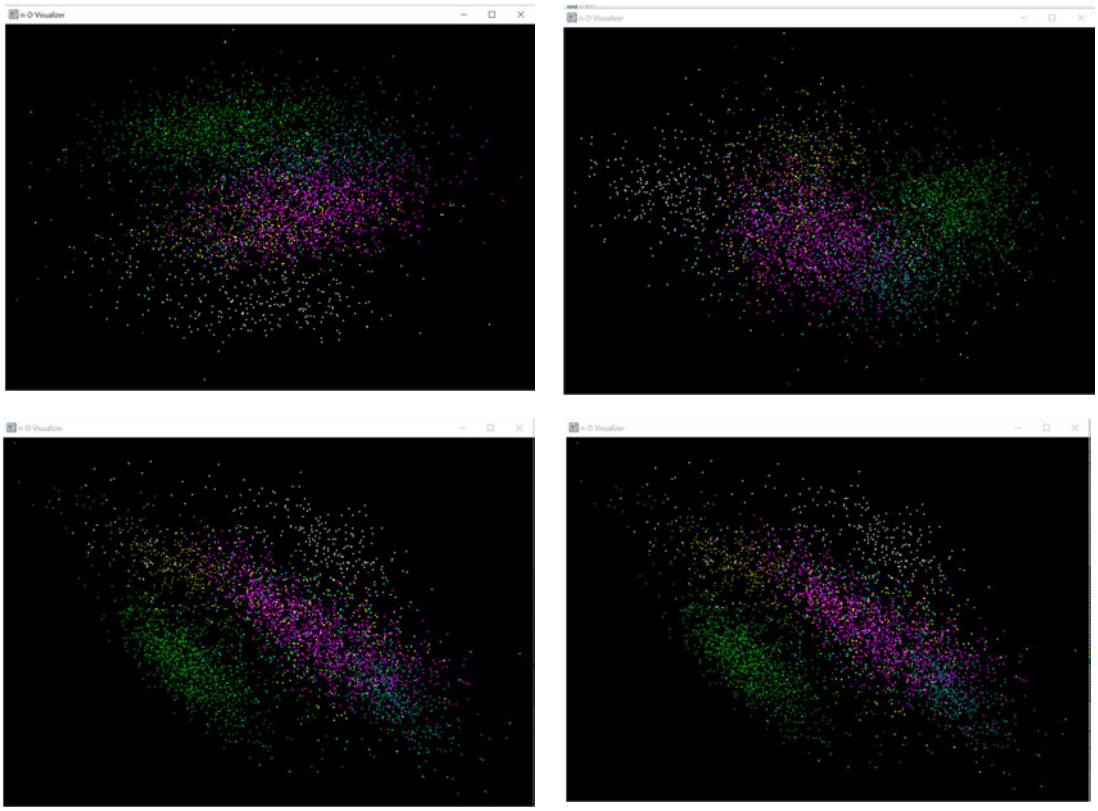

Figure 6.4: n-D Visualizer of the Regions of Interest (ROI) representing vegetation Assemblage classes.

6.5.2 Training data based on Randomly extracted Image Pixels spectra

Figure 6.5 shows an example of randomly selected pixel locations and spectral plots for class 7. A corresponding record of the extracted spectra similar to that of class 1 (appendix 5.1) was saved as a text file. This file combined with that for other classes, served as input data, for the creation of a spectral library and optimal wavebands identification using random forest and variable elimination.

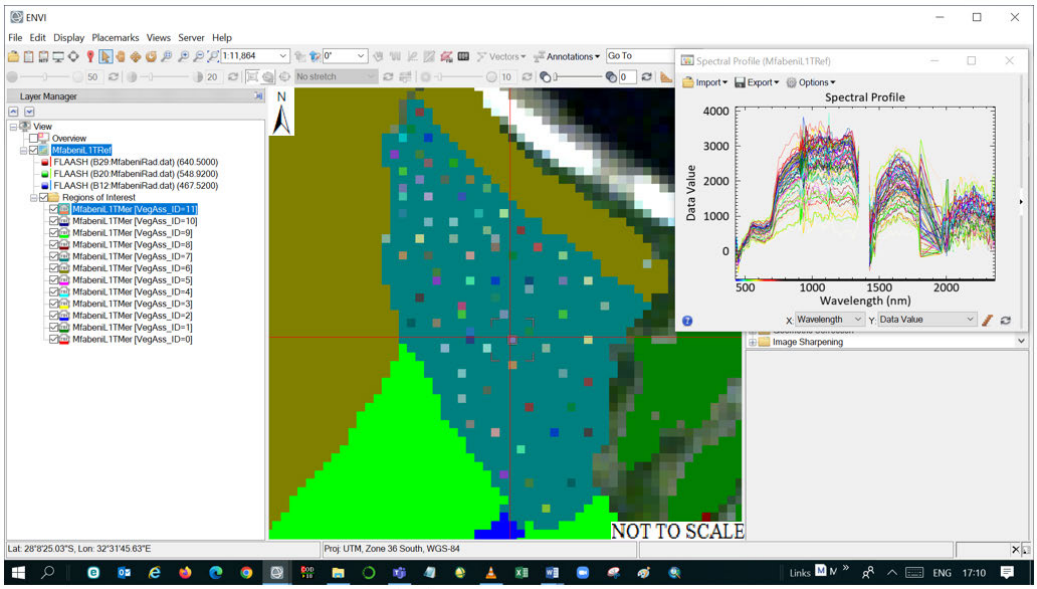

Figure 6.5: Randomly selected pixel locations and spectral plot for class 7

6.6 Spectral Library

Spectral library stores spectra of features usually referred to as endmembers, which serve as reference data for spectral matching. The data used for the spectral library creation may be based on field measurements or extracted from the image itself. In this research the latter was used.

The spectra extracted for each of the classes was used to compute the class means to serve as endmembers for vegetation assemblage classes. The class means were then consolidated into a single file. Table 6.3 shows a portion of the consolidated file of class spectra means, while (appendix 6.2) shows a complete file of spectra means for all vegetation assemblage classes.

Table 6.3: Portion of a file of class means serving as class endmembers

Class	426,82	436,99	447,17	457,34	467,52	477,69	487,87	498,04	508,22	518,39	528,57
Class 1 Mean	137,72	75,80	-192,55	-85,60	23,07	216,31	218,27	277,26	346,54	377,11	454,05
Class 2 Mean	-50,03	-88,11	-421,34	-275,69	-168,79	42,85	36,15	88,32	158,30	168,44	233,41
Class 3 Mean	-239,58	-231,39	-613,60	-454,45	-279,49	-119,25	-149,41	-105,26	-54,38	-50,73	24,70
Class 4 Mean	-230,46	-199,85	-610,35	-451,90	-272,40	-100,92	-140,97	-90,10	-34,36	-34,96	28,76
Class 5 Mean	-169,71	-175,75	-566,64	-404,79	-237,46	-74,19	-93,26	-53,48	13,99	21,05	93,26
Class 6 Mean	-43,16	-79,98	-434,97	-263,87	-130,92	40,92	25,38	90,31	157,88	191,06	276,49
Class 7 Mean	42,29	-15,70	-326,13	-153,04	-71,52	116,11	117,00	170,66	258,77	268,58	353,63
Class 8 Mean	71,09	-2,20	-320,22	-184,66	-96,10	112,15	105,37	150,07	210,48	245,45	331,04
Class 9 Mean	-3,96	-47,86	-383,67	-213,83	-120,74	83,80	89,19	139,04	209,37	232,35	306,00
Class 10 Mean	-35,98	-58,80	-445,47	-295,18	-150,82	47,04	16,13	79,70	135,71	142,88	195,64

Once combined, the file of class spectra means was then used to create a spectral library that served as reference for the classification of the Hyperion image of Mfabeni wetland (figure 6.6)

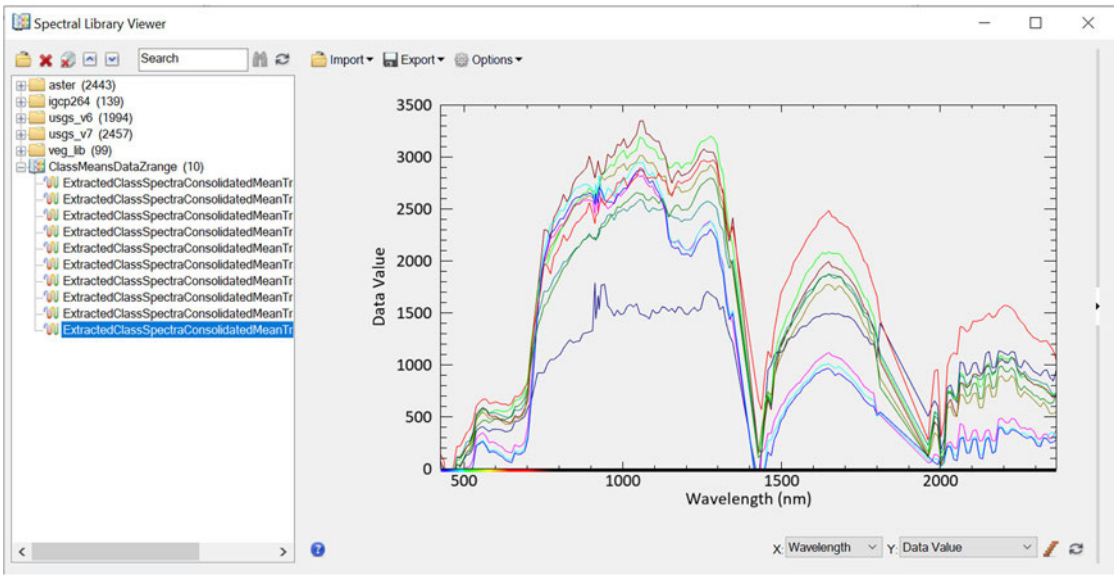

Figure 6.6: Display of a spectral Library Viewer of the Mfabeni Vegetation Assemblages' classes spectral means as endmembers

A look at figure 6.6 shows that the spectral curves depicting class spectra means exhibited shapes characteristic of vegetation. One curve depicting class 10, however, displayed lower in the 500 – 1500 nm region than all others.

6.7 Optimal Wavebands for Image Classification

Suitable wavebands were needed for spectral matching with reference spectra of vegetation assemblages' classes contained in the created spectral library. The results of the stages involved; preparing spectra for optimal waveband selection, identifying an optimal model for selecting optimal wavebands, and selection of optimal wavebands, are presented below.

6.7.1 Spectra for Optimal Waveband Selection

Table 6.4 shows a portion of a combined transposed pixel image extracted spectra used for optimal waveband selection. A full file of the consolidated spectra consists of 481 pages of an MS-Word document and hence could not be included as part of the appendices, but can be viewed as a softcopy document if required.

Table 6.4: Portion of the combined extracted pixels image spectra file showing the first few rows and columns of wavebands (column 1) and spectral measurements (columns 2, 3, 4,….)

Class	426,82	436,99	447,17	457,34	467,52	477,69	487,87	498,04	508,22	518,39	528,57	538,74	548,92	559,09
1	117	225	7	4	160	330	353	401	518	561	593	776	779	815
1	196	116	-223	59	178	315	347	407	488	584	676	774	820	822
1	165	18	-286	-148	-1	160	226	218	273	312	385	521	575	606
1	66	-79	-220	-218	-138	119	129	162	243	264	276	442	463	520
1	-20	-66	-316	-187	5	244	228	318	367	389	458	611	682	707
1	189	5	-208	-349	-44	112	110	164	224	221	312	479	497	513
1	-102	13	-232	-294	-197	62	55	91	171	134	238	426	461	506
1	276	75	-91	10	108	267	335	359	458	507	599	733	726	736
1	220	176	-169	88	25	251	258	314	405	389	472	626	641	679
2	85	80	-418	-133	-49	85	96	139	218	217	294	484	515	539
2	245	-229	-346	-232	-200	75	59	126	197	173	286	443	490	516
2	-3	-53	-418	-239	-127	100	127	120	239	200	276	445	515	537
2	-259	-208	-436	-299	-74	82	102	128	228	208	292	442	506	527
2	124	77	-382	-109	-104	128	82	185	199	217	335	496	543	583
2	-136	44	-313	-247	-92	130	127	147	229	244	280	456	499	541
2	-143	-172	-547	-185	-149	84	78	149	190	231	308	484	502	532
2	83	-64	-403	-177	-147	69	75	99	192	150	274	447	504	493
2	170	51	-307	-182	-118	57	119	120	224	183	258	435	429	490
2	-221	-134	-406	-234	-54	64	100	122	152	167	282	463	452	532
2	51	-131	-364	-120	-204	96	92	87	184	196	254	433	486	495
2	273	111	-331	-211	-51	141	94	130	256	233	232	449	449	523
2	-71	-66	-427	-258	-113	100	78	139	205	177	262	408	463	470
2	-30	-85	-415	-219	-156	82	112	110	224	184	213	383	481	483
2	85	124	-397	-117	-51	71	82	137	207	244	274	477	458	516
2	157	-263	-337	-260	-104	71	115	147	192	229	256	397	440	498
2	136	49	-346	-130	-72	117	123	157	201	202	276	477	493	498
2	-85	-38	-388	-333	-165	53	96	101	226	179	240	397	442	491
2	-6	-118	-352	-229	-234	60	73	93	245	210	294	438	468	546

6.7.2 Optimized RF Model for Optimal Wavebands Selection

Table 6.4 shows the OOB estimates of error results of the several RF classification models created in an attempt to obtain an optimized model. The number of trees (nTree) from 100 to 8,000 with variable intervals of 50, 100, and 500 were used, while the number of variables tried (mTry) at each split or node used ranged from 5 to 26 inclusive of 6, 13, and 26 which corresponded to the recommended mTry values of the square root, half and total number of variables (Brownlee, 2016).

A total number of 85 models consisting of seventeen (17) and five (5) randomly selected nTree and mTry, respectively, were created. Two (2) models with the lowest OOB estimate of error value of 27.86% at nTree by mTry of 500 by 6 and 6500 by 5 were identified as optimal (table 6.5). This implied that whenever each of these models was applied to a new set of observations, it would predict the accuracy with an error of 27.86%. The models' accuracy, therefore, was 72.14%.

Table 6.5: RF Models showing two (highlighted) models identified as optimal

RF Classification OOB					
	mTry				
nTree	5	6	10	13	26
100	28,95	28,95	30,36	30,05	29,89
500	29,73	27,86	29,26	29,58	28,64
1000	28,79	28,17	29,26	29,58	28,95
1500	28,17	28,95	28,95	29,58	28,64
2000	28,01	28,17	29,26	29,89	28,95
2500	28,33	28,48	29,11	29,58	28,95
3000	28,01	28,33	29,26	29,42	28,48
3500	28,64	28,17	29,11	29,58	28,64
4000	28,17	28,17	29,42	29,42	28,33
4500	28,79	28,33	29,11	29,58	28,79
5000	28,64	28,33	28,48	29,58	28,64
5500	28,48	28,33	28,64	29,58	28,48
6000	28,01	28,33	28,64	29,58	28,79
6500	27,86	28,33	28,79	29,42	28,64
7000	28,33	28,17	28,79	29,73	28,48
7500	28,33	28,48	28,79	29,73	28,79
8000	28,48	28,48	28,64	29,73	28,79

Figure 6.7 shows a graphical representation of the change in OOB for a given nTree with change in mTry, while figure 6.8 showing a similar representation for a given mTry with change in nTree.

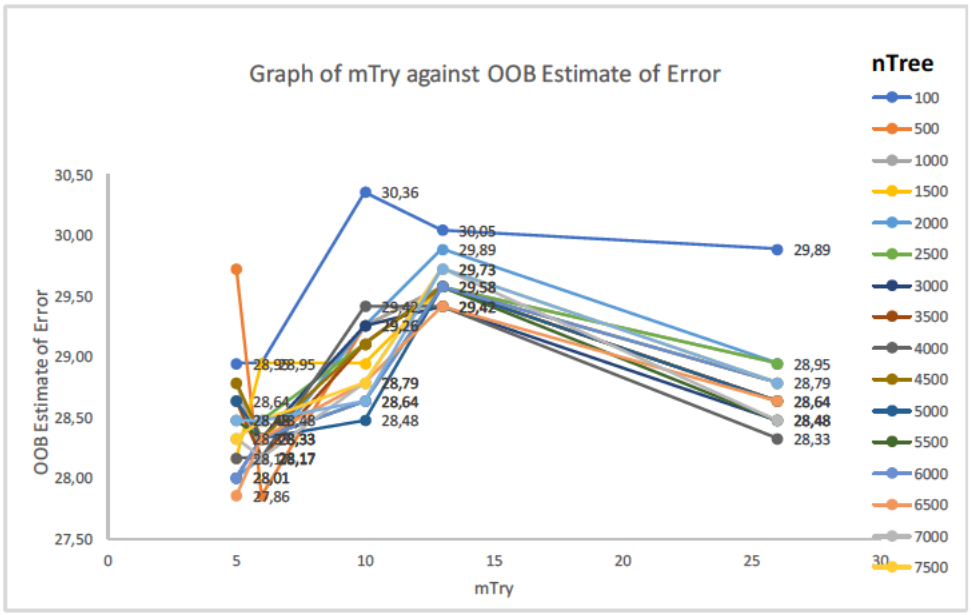

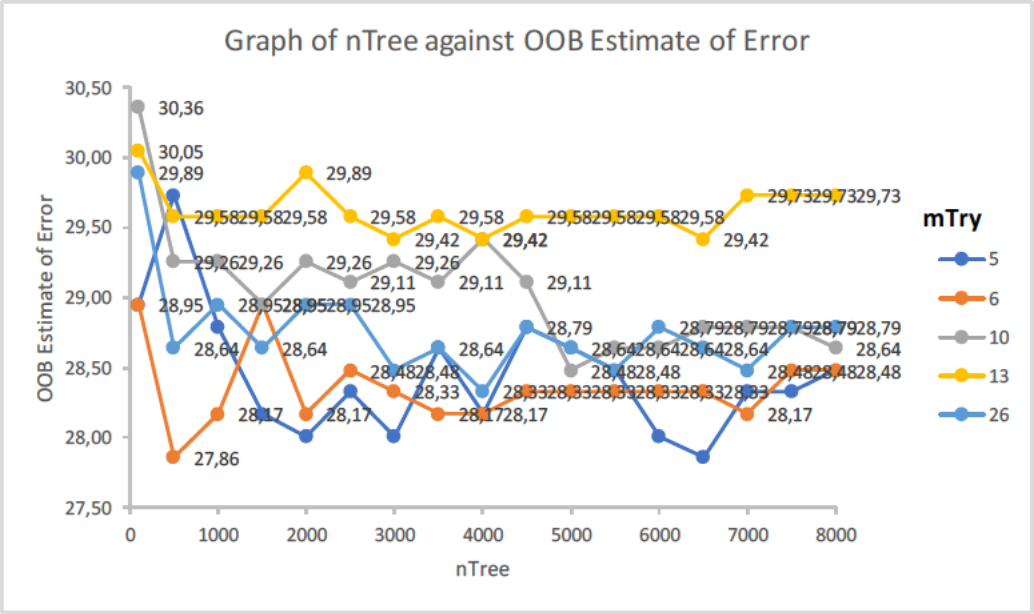

6.7.3 Performance of Evaluated Classification Models

Table 6.6 shows a summary of the results obtained once the two models identified by RF classification had been subjected to an evaluation to select one subsequently used to determine the optimal wavebands for grass assemblages' discrimination.

Table 6.6: Calculated Prediction Accuracy of the five optimal RF Classification Models

Dataset	Model	
	500 by 6	6500 by 5
Training	100.00	100.00
Validation	78,9	78.1
Testing	68.1	68
Full	92	91.9
Full	92	91.9

Calculated Prediction Accuracy was used as a basis for comparison of model performance. Both models produced the same value for the training datasets, but they had marginally different values for the validation, testing and full datasets. The differences are so small for the testing and full dataset that they can be considered to be the same. Despite the similarities, the '500 by 6' model having slightly better values, was adopted as the model for use in the identification of optimal wavebands necessary for spectral matching.

6.7.4 Selected Optimal Wavebands using Random Forest

The order of importance of variables given by the 'mean decrease accuracy' (MDA) for RF classification was used as a means of identifying the wavebands critical to the discrimination of pixels representing vegetation assemblages. Figure 6.9 shows waveband importance plotted across the spectral range covered by spectra for the '500 by 6' model identified as optimal while appendix 6. 3 is a summary of the '500 by 6' Random Forest Model identified as optimal.

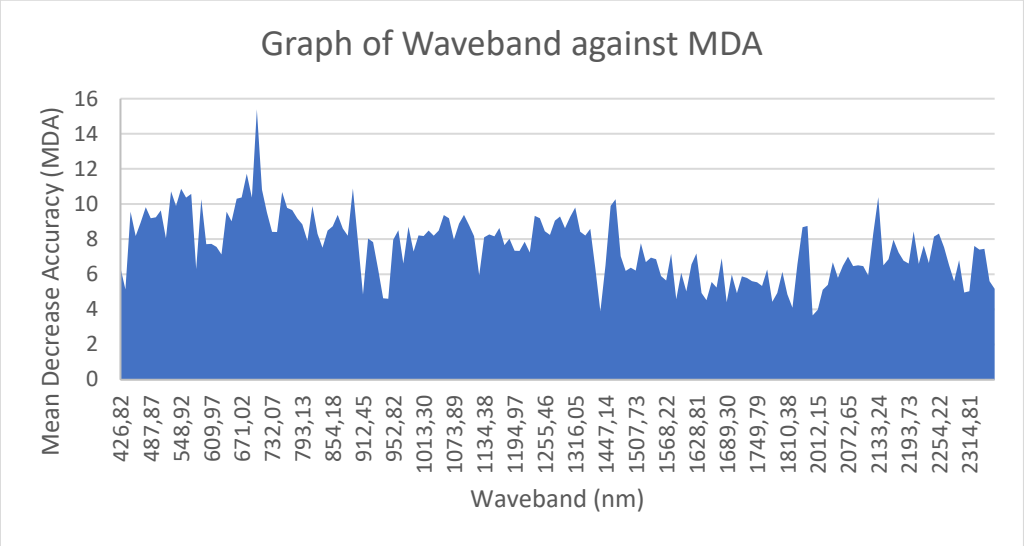

Figure 6.7: Waveband importance expressed in terms of Mean Decrease Accuracy for 500 by 6 RF classification model

Figure 6.10 shows a plot of the spectral location of the top 30 of these wavebands ranked according to variable importance in terms of the MDA when plotted over the 426.82 – 2375.3nm spectra range.

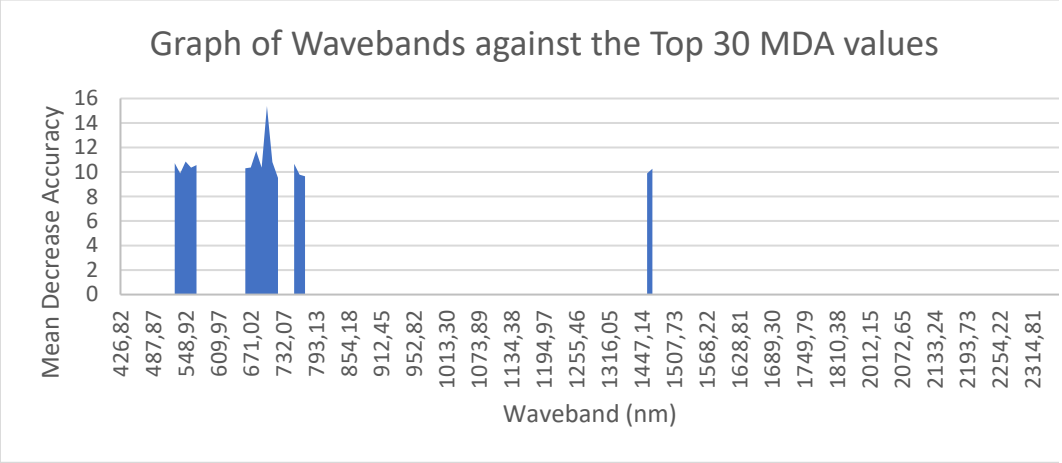

Figure 6.8: Location of the top 30 important wavebands over spectra range 426.82 – 2375.30nm

6.7.5 Most Optimal Wavebands Selected from RF Classification based Optimal Wavebands using Variable Elimination

Backward variable elimination identified 11 wavebands from the 30 optimal wavebands selected with RF classification (figure 6.11). All identified wavebands had a significant level of less than 0.05, indicated as Pr (>|t|) on figure 6.11.

```
> p=update(p,.~.-X548.919983)
> summary(p)

Call:
lm(formula = Class ~ X508.220001 + X528.570007 + X559.090027 +
    X691.369995 + X701.549988 + X711.719971 + X772.780029 + X1053.689941 +
    X1235.270020 + X2133.239990 + X721.900024, data = (g))

Residuals:
    Min      1Q  Median      3Q     Max
-5.8186 -1.6484 -0.1064  2.0306  6.8634

Coefficients:
              Estimate Std. Error t value Pr(>|t|)
(Intercept)   3.8742100  0.7324989   5.289 1.54e-07 ***
X508.220001  -0.0094921  0.0029597  -3.207 0.001388 **
X528.570007  -0.0104868  0.0030423  -3.447 0.000593 ***
X559.090027   0.0170303  0.0034671   4.912 1.07e-06 ***
X691.369995  -0.0113095  0.0026751  -4.228 2.60e-05 ***
X701.549988   0.0156131  0.0028172   5.542 3.92e-08 ***
X711.719971  -0.0083360  0.0038897  -2.143 0.032371 *
X772.780029  -0.0076196  0.0009634  -7.909 7.54e-15 ***
X1053.689941  0.0057087  0.0008333   6.851 1.36e-11 ***
X1235.270020 -0.0058382  0.0008129  -7.182 1.44e-12 ***
X2133.239990  0.0017815  0.0004896   3.638 0.000290 ***
X721.900024   0.0111387  0.0036472   3.054 0.002324 **
---
Signif. codes:  0 '***' 0.001 '**' 0.01 '*' 0.05 '.' 0.1 ' ' 1

Residual standard error: 2.52 on 902 degrees of freedom
Multiple R-squared:  0.2379,    Adjusted R-squared:  0.2287
F-statistic:  25.6 on 11 and 902 DF,  p-value: < 2.2e-16
```

Figure 6.9: Eleven (11) optimal wavebands selected by Backward variable elimination

The significant codes used by the algorithm are as given in table 6.7. On figure 6.11, only waveband 711.719971 is indicated to have been determined at a significance level of between 0.05 and 0.01. All other wavebands were selected with a significance level of better than 0.01. Appendix 6.4 shows the results of each of the iterations executed on the data to arrive at the results presented in figure 6.11.

Table 6.7: Interpretation of Significance Codes used by Backward Variable Elimination Algorithm.

Significance Code	Percentage Range
0 '***' 0.001	100 and 99.9%
0.001'**' 0.01	99.9 and 99%
0.01 '*' 0.05	99 and 95%
0.05 '.' 0.1	95 and 90%
0.1 ' ' 1	90 and 0%

Figure 6.12 shows the spectral location of these 11 wavebands plotted over the 426.82 – 2375.3nm spectra range.

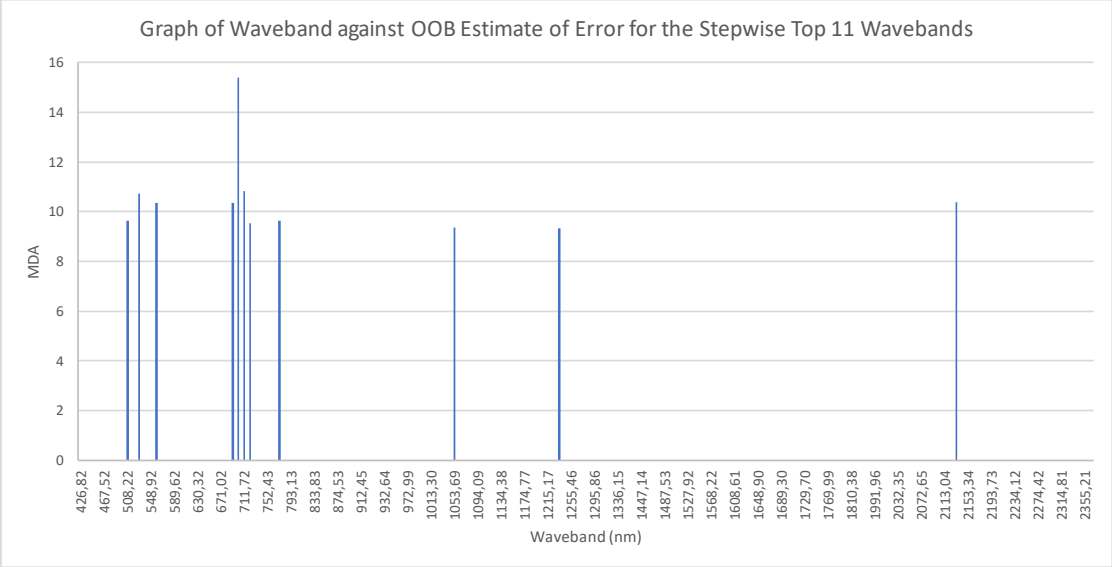

Figure 6.10: Location of 11 wavebands identified as optimal using stepwise backward variable elimination

Figure 6.13 shows AIC results with sixteen (16) wavebands selected as optimal, while figure 6.14 shows the spectral location of the identified 16 wavebands plotted over the 426.82 – 2375.3nm spectra range. Appendix 6.5 shows the iterations involved in obtaining the results given in figure 6.13.

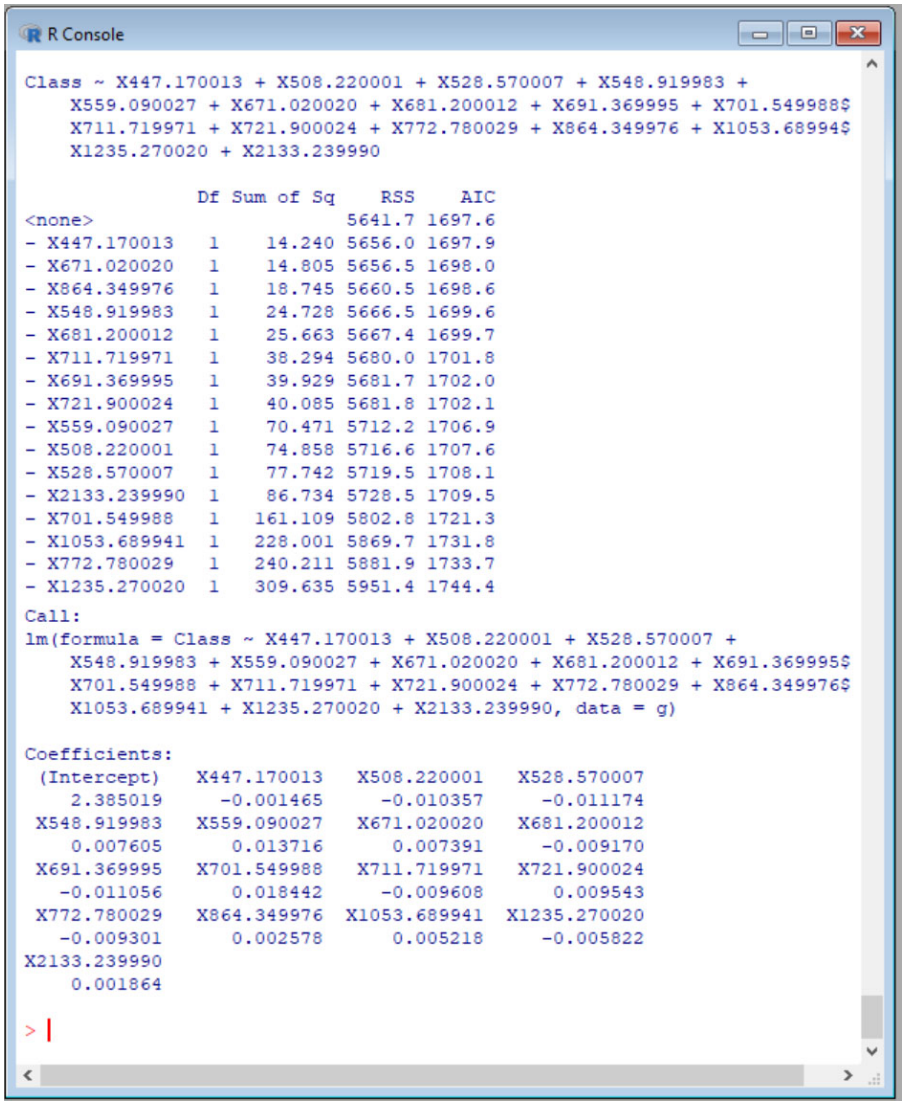

Figure 6.11: Sixteen (16) optimal wavebands selected by AIC with a backward direction

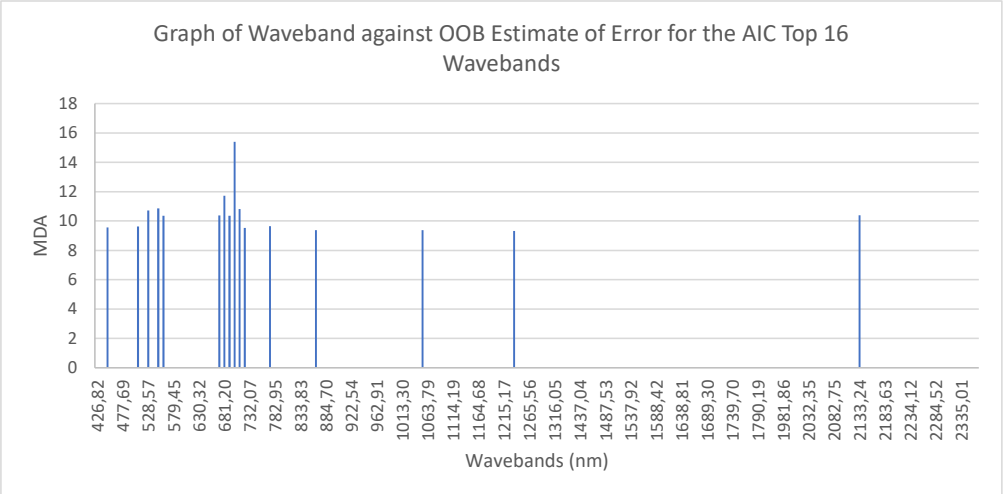

Figure 6.12: Location of 16 wavebands identified by AIC as optimal plotted over the 426.82 – 2375.30nm spectral range

Generally, AIC produces more reliable results as it incorporates variables on the borderline not clear as to whether they should be included when stepwise elimination is used. Hence (Faraway, 2002) used a criterion-based method. In this research, all the 11 optimal wavebands identified using the stepwise backward variable elimination method were also selected by the AIC.

Both the 11 and 16 wavebands were used in conjunction with the 10 class spectra means saved as endmembers in the spectral library to classify the Hyperion image of the Mfabeni wetland.

Variable elimination results confirmed the order of variable importance provided by RF as not necessarily corresponding to the statistical significance of each waveband in discriminating among different elements (Table 6.8). The order of variable importance provided in table 6.8 (a) does not correspond to that in (b) and (c). Waveband 894.88 and 569.27, for instance, do not appear as statistically significant on (b) and (c) despite having been ranked as variables of higher importance by RF classification.

Table 6.8: Comparison of Variable importance provided by RF and Statistical significance provided by the Variable Elimination methods

(a)

RF Top 30 Order of variable Importance

Waveband	MDA
701,549988	15,39
681,200012	11,72
894,880005	10,88
711,719971	10,82
569,27002	10,57
2133,23999	10,39
671,02002	10,37
691,369995	10,36
660,849976	10,3
589,619995	10,27
477,690002	9,82
772,780029	9,65
508,220001	9,63
640,5	9,56
721,900024	9,52
1094,089966	9,38
1063,790039	9,19
782,950012	9,18
650,669983	9,01
793,130005	8,84
1991,959961	8,75
884,700012	8,19
1033,48999	8,19
518,390015	8,05
1517,829956	7,77
609,969971	7,73
599,799988	7,71
620,150024	7,56
1769,98999	6,27
1487,530029	6,19

(b)

AIC 17 bands

Waveband	MDA
447,170013	9,82
671,02002	10,37
864,349976	9,38
548,919983	10,86
681,200012	11,72
711,719971	10,82
691,369995	10,36
721,900024	9,52
559,090027	10,36
508,220001	9,63
528,570007	10,72
2133,23999	10,39
701,549988	15,39
1053,689941	9,37
772,780029	9,65
1235,27002	9,32

(c)

Backward Stepwise 11

Waveband	MDA
508,220001	9,63
528,570007	10,72
559,090027	10,36
691,369995	10,36
701,549988	15,39
711,719971	10,82
772,780029	9,65
1053,68994	9,37
1235,27002	9,32
2133,23999	10,39
721,900024	9,52

6.8 Classified Images

Classification of images was done using the Spectral Angle Mapper (SAM) algorithm. Two different approaches of extracting training data, nine (9) different spectral angles of separation and three different sets of waveband numbers were used.

6.8.1 Classified Images Based on the Conventional Method of Extracting Training Data

Figures 6.15(a) and 6.15(b) show sample classified images created from conventionally digitized training data and training data based on class spectra means of pixel based extracted spectra saved in the spectral library respectively. In both cases optimal bands identified by RF and variable elimination were applied to all 175 wavebands using a spectral angle of separation of 0.6 radians. The process was then repeated for each of the nine (0.1 – 0.9 radian) spectral angle of separation for both conventionally extracted and class spectra means training data giving rise to 18 separate classified images.

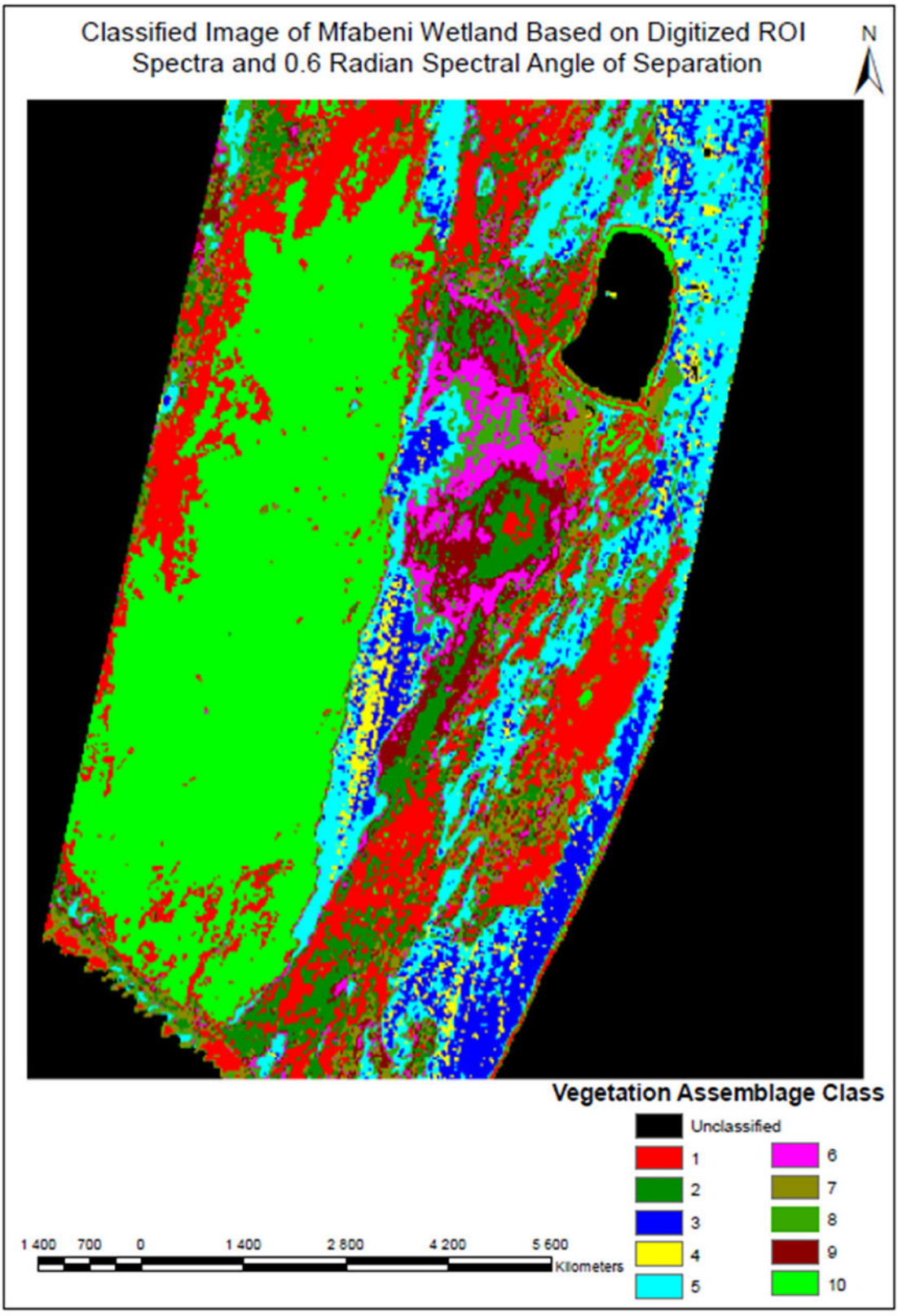

Figure 6.15(a): Classified image based on conventional extracted Training data

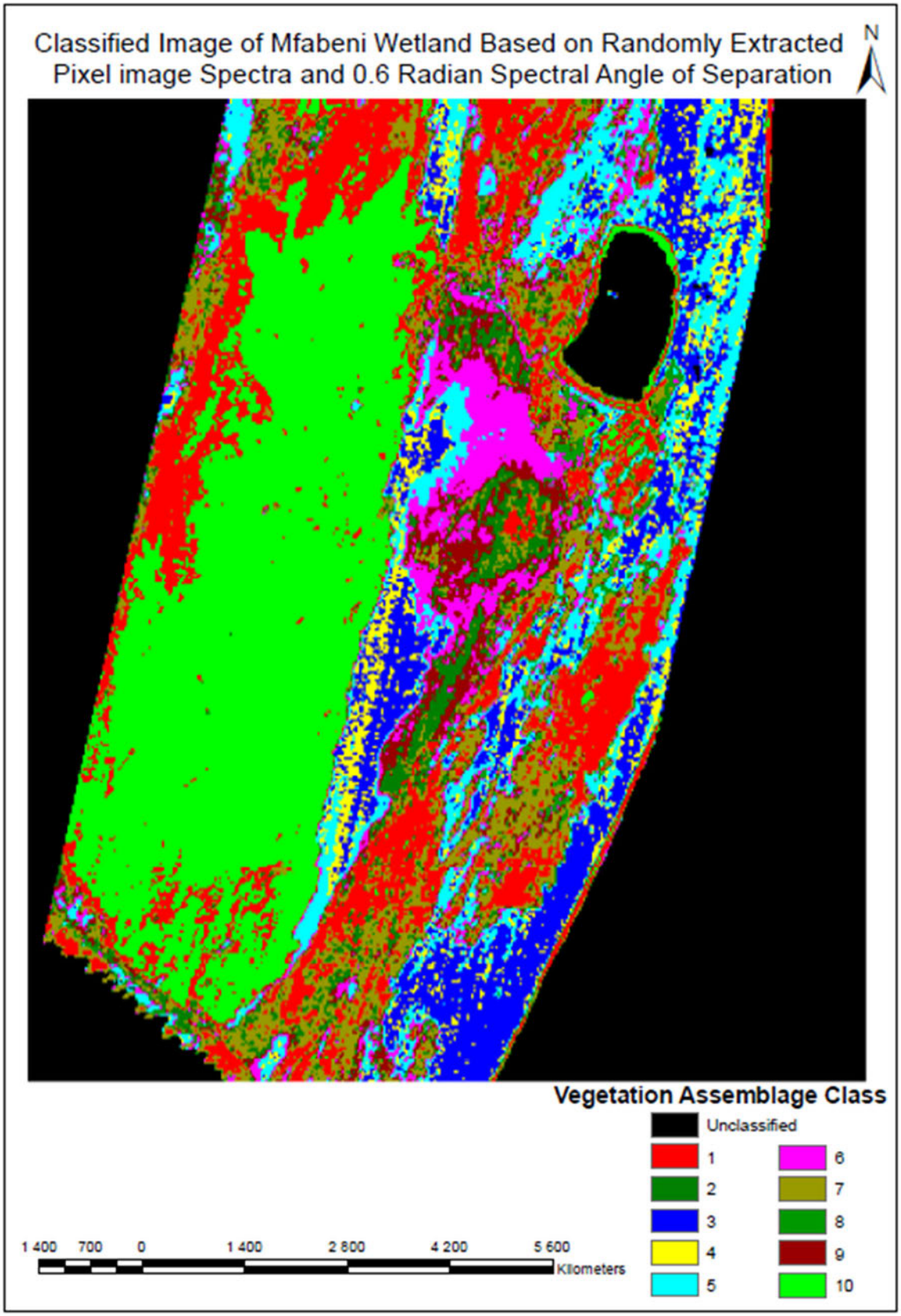

Figure 6.15(b): Classified image based on Randomly extracted pixels image based spectra Training data

Table 6.9 shows the pixel count and associated percentages allocated to each of the vegetation assemblage classes for each of the two methods of extracting training data.

Table 6.9: Pixel count and percentages allocated to each of the vegetation assemblage classes for each of the two methods of extracting training data

Class	Method of Extracting Training Data				Difference	
	Convention		Pixel spectra Based			
	Pixel Count	Percent	Pixel Count	Percent	Pixel Count	Percent
Unclaasified	64112	37,5	64110	37,5	2	0,0
1	17572	10,3	19244	11,3	-1672	-1,0
2	4589	2,7	8665	5,1	-4076	-2,4
3	10644	6,2	7151	4,2	3493	2,0
4	4797	2,8	2424	1,4	2373	1,4
5	10114	5,9	13987	8,2	-3873	-2,3
6	6587	3,9	4191	2,5	2396	1,4
7	11616	6,8	5771	3,4	5845	3,4
8	3177	1,9	6224	3,6	-3047	-1,8
9	4879	2,9	5201	3,0	-322	-0,2
10	32667	19,1	33786	19,8	-1119	-0,7
Total	170754	100,0	170754	100,0	0	0,0

6.8.2 Classified images based on the difference in spectral angle of separation

Figure 6.16(a) and (b) show differences in classified images due to change in the spectral angle of separation of an image using image pixels extracted training data and 16 optimal wavebands.

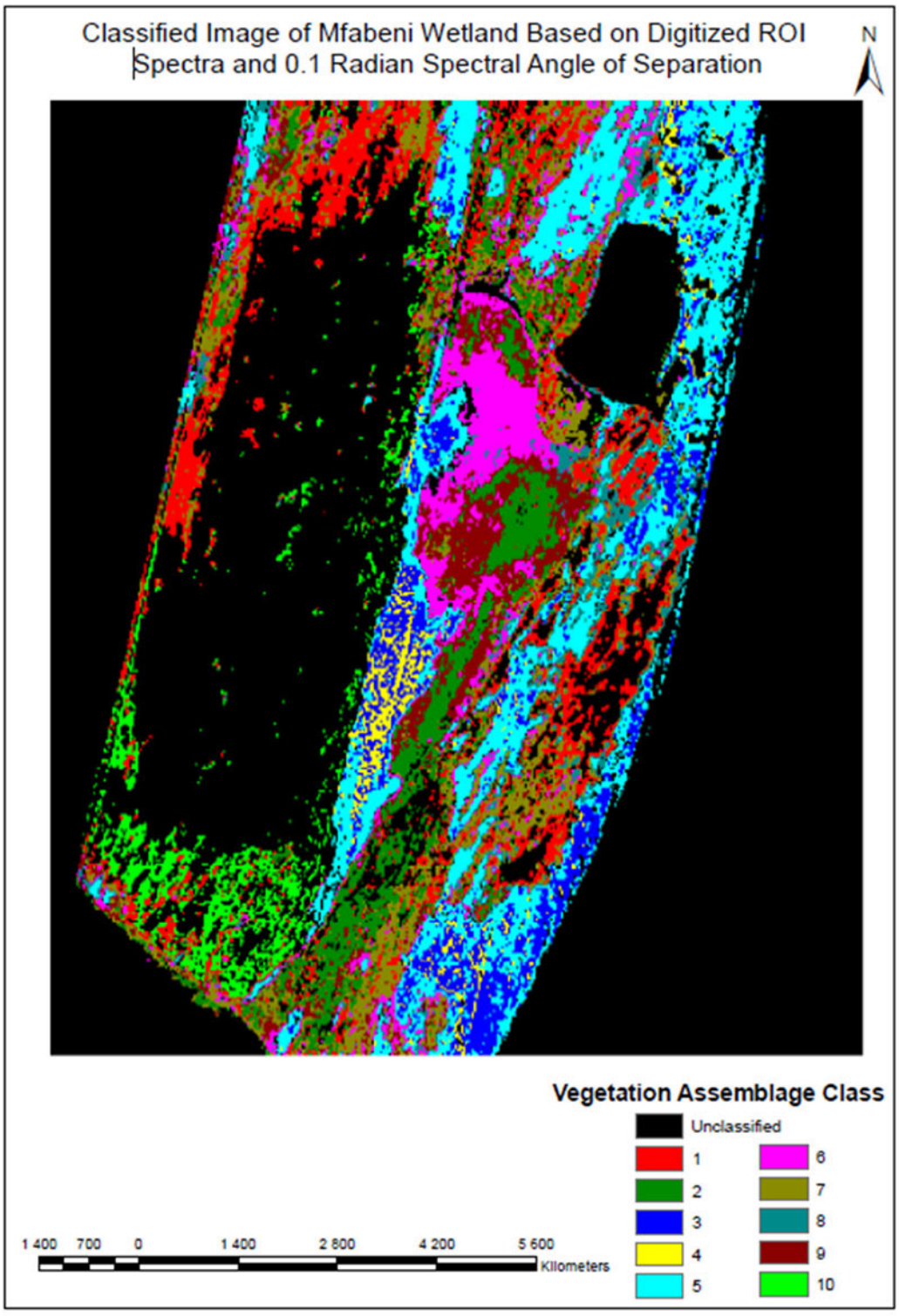

Figure 6.16(a): Classified image based on 0.1 Radian Spectral Angle of Separation

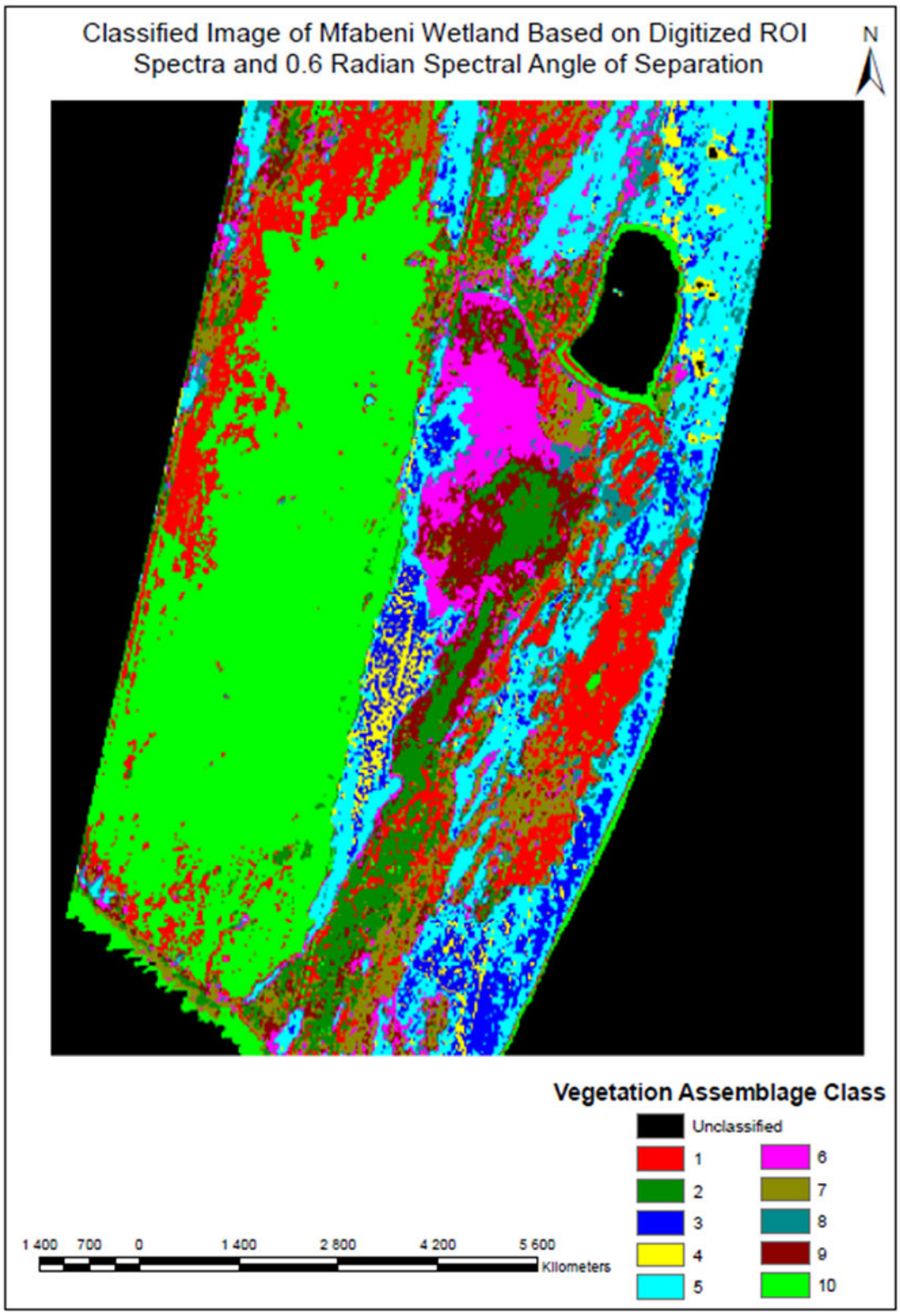

Figure 6.16(b): Classified image based on 0.6 Radian Spectral Angle of Separation

Table 6.10 shows the pixel count and associated percentages allocated to each of the vegetation assemblage classes for each of the spectral angles of separation for a conventionally trained data using all 175 image wavebands.

Table 6.10: Pixel count and corresponding percentage composition of each of the vegetation assemblages in the images classified according to the spectral angle of separation for classification with conventionally trained data all 175 image wavebands

Class	Spectral Angle Separation (Radians)																	
	0.1		0.2		0.3		0.4		0.5		0.6		0.7		0.8		0.9	
	Pixel Count	%	Pixel Count	%	Pixel Count	%	Pixel Count	%	Pixel Count	%	Pixel Count	%	Pixel Count	%	Pixel Count	%	Pixel Count	%
Unclassified	128798	75,4	81370	47,7	66203	38,8	64551	37,8	64300	37,7	64110	37,5	63942	37,4	63764	37,3	63527	37,2
1	7975	4,7	18453	10,8	19038	11,1	19198	11,2	19229	11,3	19244	11,3	19246	11,3	19248	11,3	19250	11,3
2	4621	2,7	8571	5,0	8648	5,1	8655	5,1	8663	5,1	8665	5,1	8671	5,1	8672	5,1	8672	5,1
3	5700	3,3	7087	4,2	7131	4,2	7147	4,2	7151	4,2	7151	4,2	7156	4,2	7159	4,2	7159	4,2
4	1419	0,8	2199	1,3	2289	1,3	2351	1,4	2394	1,4	2424	1,4	2453	1,4	2502	1,5	2551	1,5
5	8474	5,0	13761	8,1	13920	8,2	13952	8,2	13973	8,2	13987	8,2	14003	8,2	14020	8,2	14042	8,2
6	2984	1,7	4145	2,4	4178	2,4	4183	2,4	4187	2,5	4191	2,5	4192	2,5	4196	2,5	4196	2,5
7	3331	2,0	5149	3,0	5459	3,2	5620	3,3	5702	3,3	5771	3,4	5810	3,4	5836	3,4	5847	3,4
8	3052	1,8	5978	3,5	6090	3,6	6149	3,6	6189	3,6	6224	3,6	6271	3,7	6326	3,7	6457	3,8
9	3816	2,2	5181	3,0	5201	3,0	5201	3,0	5201	3,0	5201	3,0	5201	3,0	5201	3,0	5201	3,0
10	584	0,3	18860	11,0	32597	19,1	33747	19,8	33765	19,8	33786	19,8	33809	19,8	33830	19,8	33852	19,8

6.8.3 Classified images based on the difference in the number of spectral wavebands

Figure 6.17 shows the differences in images classified on the basis of (a) all 175 wavebands, (b) 11 and (c) 16 optimal wavebands obtained from the stepwise and AIC variable elimination method performed on the 30 wavebands selected by RF. Each of the classified images were created with 0.6 radian angle of separation.

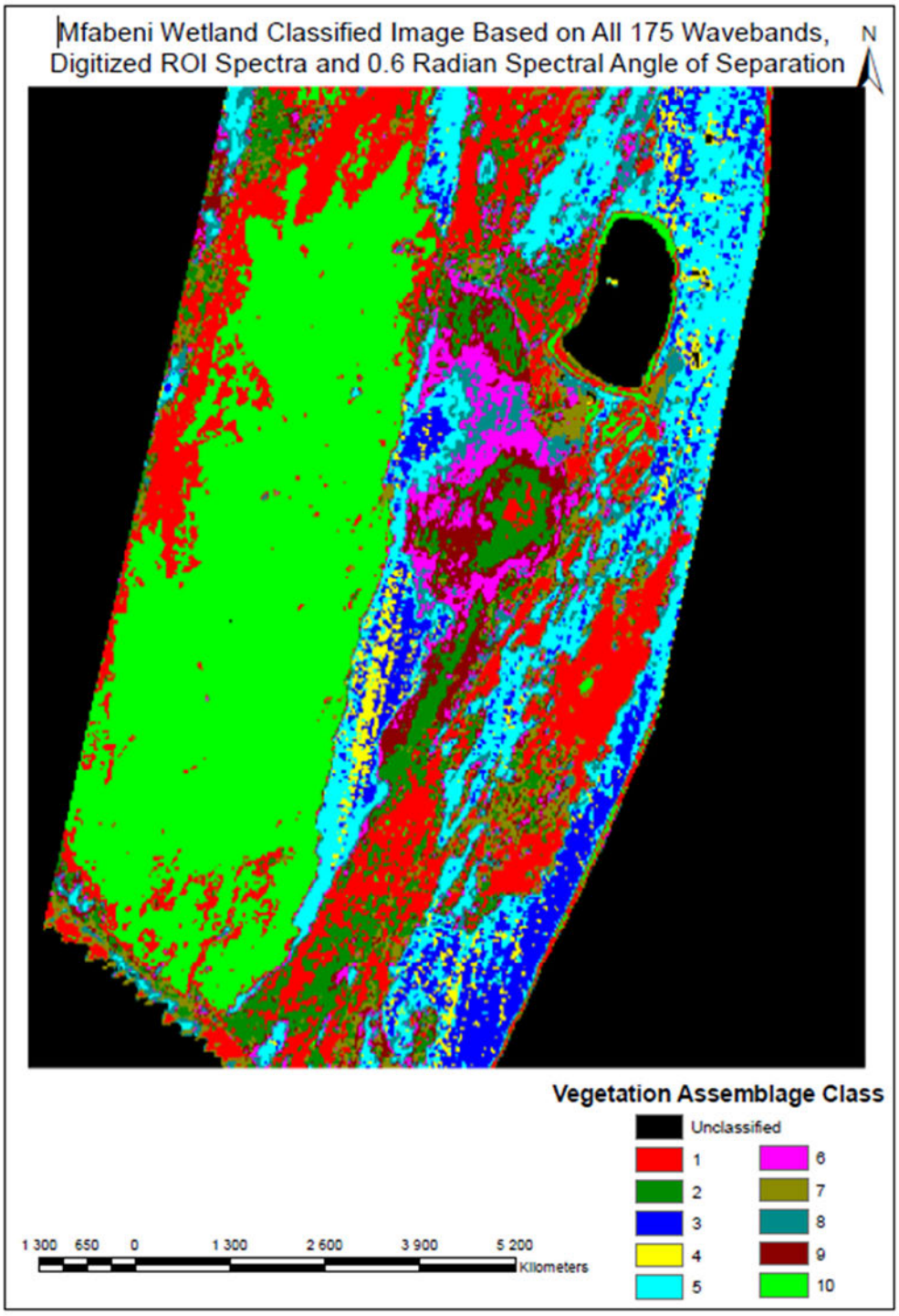

Figure 6.17(a): Classified image based on all 175 bands with 0.6 Radian spectral angle of separation

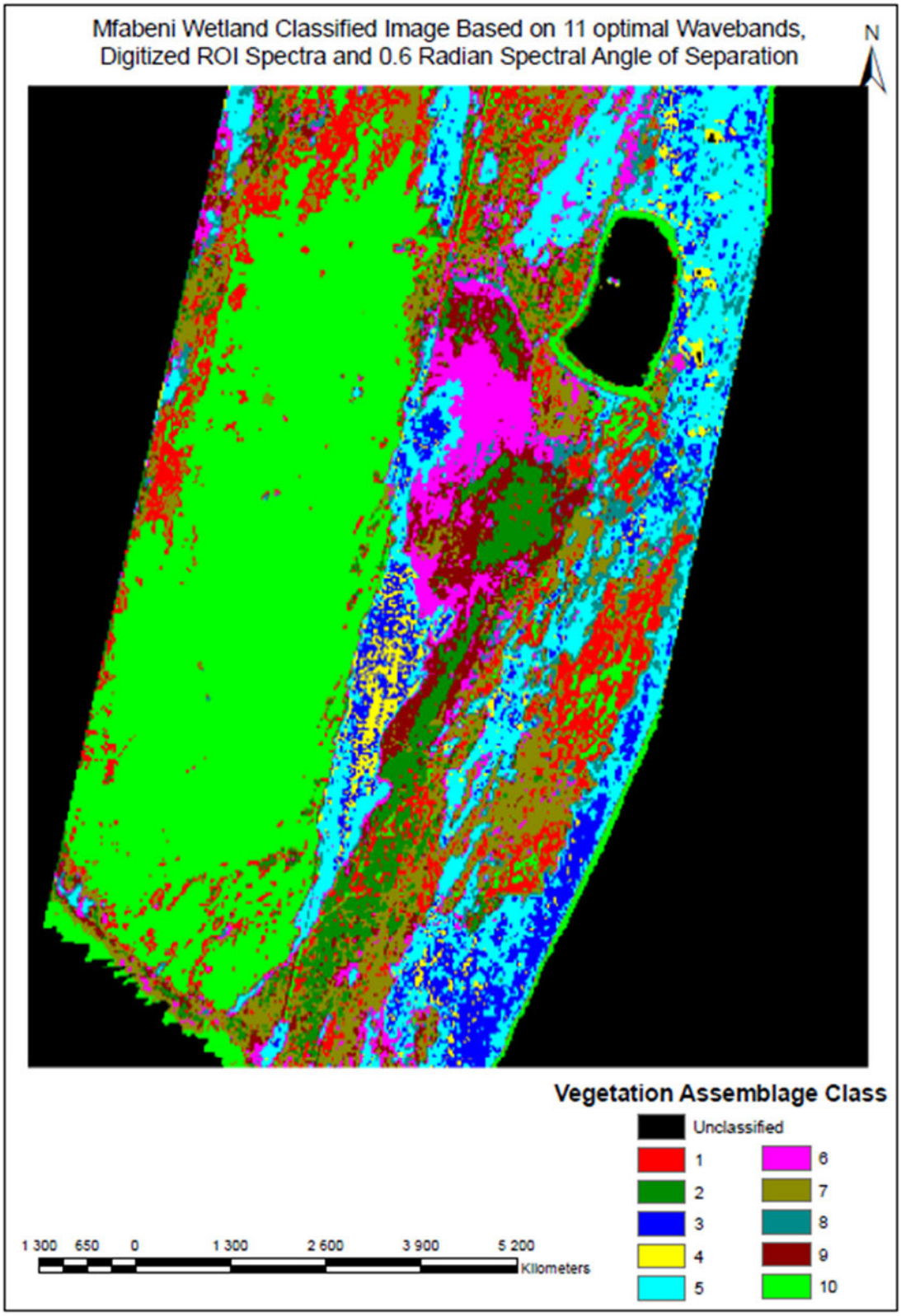

Figure 6.17(b): Classified image based 11 optimal bands with 0.6 Radian spectral angle of separation

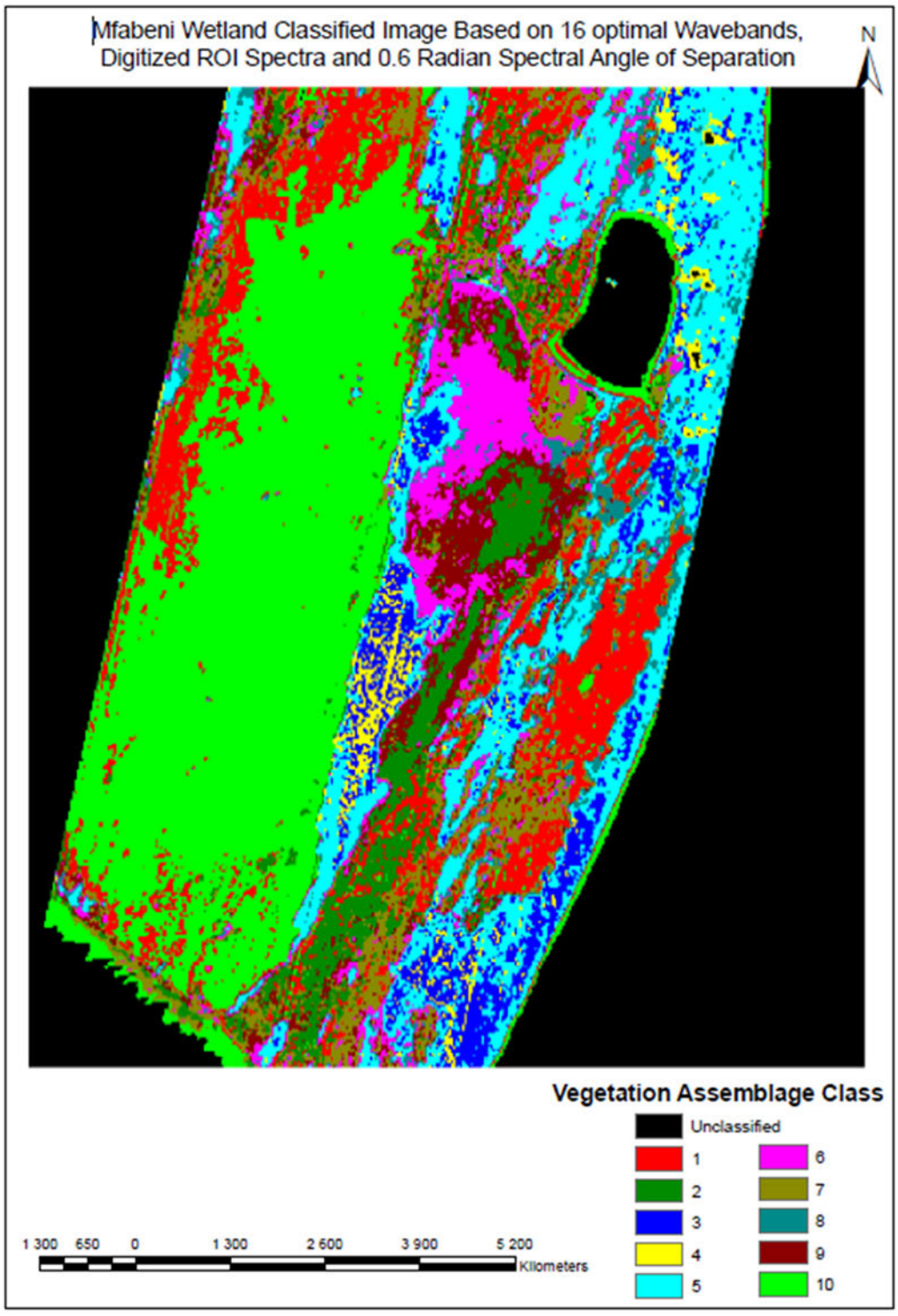

Figure 6.17(c): Classified image based 16 optimal bands with 0.6 Radian spectral angle of separation

Table 6.11 shows the pixel count and percentages for 0.6 radians angle of separation applied to each of the three images classified using all 175 bands, 11 bands and 16 bands. Each of these images was repeatedly classified for each of the spectral angle of separation 0.1 to 0.9 radians, generating a total of 27 images.

Table 6.11: Pixel count and corresponding percentage composition of each of the vegetation assemblages in the images classified with regard to the number of wavebands using 0.6 radians angle of separation.

Class	Number of Bands Used					
	All 175		11 Optimal		16 Optimal	
	Pixel Count	Percent	Pixel Count	Percent	Pixel Count	Percent
0	64110	37.545241	64177	37.584478	64308	37.661197
1	19244	11.270014	9706	5.684201	14156	8.290289
2	8665	5.074552	6357	3.722900	7805	4.570903
3	7151	4.187896	6231	3.649109	5627	3.295384
4	2424	1.419586	2127	1.245652	2264	1.325884
5	13987	8.191316	14930	8.743573	15652	9.166403
6	4191	2.454408	6280	3.677805	6202	3.632126
7	5771	3.379716	12888	7.547700	9332	5.465172
8	6224	3.645010	4940	2.893051	4667	2.733172
9	5201	3.045902	5379	3.150146	5577	3.266102
10	33786	19.786359	37739	22.101386	35164	20.593368

6.9 Post-Classification Accuracy Assessment

Each of the classified images was assessed for post-classification accuracy. The correctly classified pixels were compared against the total number of pixels making up a given vegetation assemblage. Table 6.12 shows percentage overall accuracy values obtained for each of the images classified for each of the two methods used, nine (0.1- 0.9) spectral angles of separation values and three different wavebands (all 175 bands, 11 optimal bands, and 16 optimal bands). Appendix 6.6 is a sample file of the results of an accuracy assessment for extracted spectra training data, 16 optimal wavebands, and 0.6 radians spectral angle of separation.

Table 6.12: Percentage (%) overall accuracy of each of the images classified using the different methods of extracting training data, spectral angles of separation and number of wavebands.

Spectra Angle	Conventional Extracted Training Data			Image Pixel Based Training Data		
	All 175 bands	11 Optimal	16 Optimal	All 175 bands	11 Optimal	16 Optimal
0,1	25,1589	43,1109	44,1985	25,679	42,4766	44,6608
0,2	37,6112	44,6839	48,567	38,5358	44,9902	48,359
0,3	38,5358	44,7995	48,9541	39,5008	45,1057	48,7808
0,4	38,6802	44,8168	48,9599	39,651	45,1231	48,7865
0,5	38,6976	44,8342	48,9657	39,6741	45,1404	48,7923
0,6	38,6976	44,8342	48,9657	39,6857	45,1404	48,7923
0,7	38,6976	44,8399	48,9657	39,6857	45,1462	48,7923
0,8	38,6976	44,8399	48,9657	39,6857	45,1462	48,7923
0,9	38,6976	44,8399	48,9657	39,6857	45,1462	48,7923

Based on the post-classification accuracy assessment results presented in table 6.12 the best overall accuracy was obtained for the image classified with conventionally extracted training data using 16 optimal bands and 0.5 – 0.9 spectral angle of separation. The purpose of repeating the classification using various parameters was to identify the image with the best classification accuracy. With five classified images identified as most accurate, any one of these could be used. The image with 0,5 radians spectral angle of separation was, however, adopted for subsequent analysis. Other images with similar accuracy were therefore considered redundant. The spectral angle of separation' like for other parameters, was adjusted in order to identify the classified image with the best accuracy. For the images with same accuracy, the one with the lowest spectral angle of separation was adopted. Figure 6.18, therefore, shows the classified image adopted for subsequent processing reduced to the spatial extent of the Mfabeni wetland. It was based on conventionally extracted training spectra, 16 optimal bands identified using RF and AIC and 0,5 radians angle of separation.

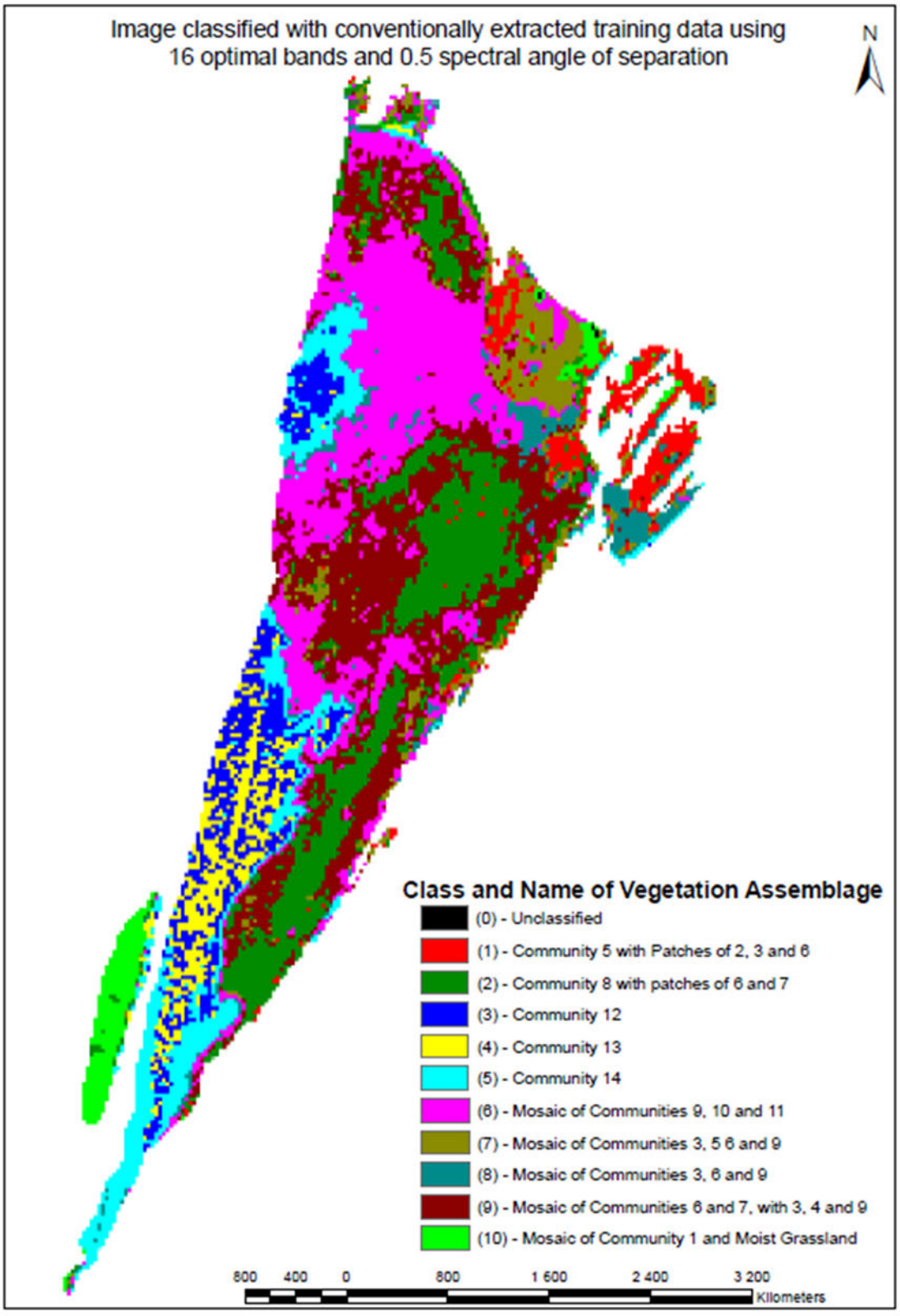

Figure 6.18: Classified image adopted for characterization of vegetation assemblages along an altitudinal

Table 6.13 shows the pixel count and percentage for each of the vegetation assemblage classes of the five classified images (table 6.12) of the Mfabeni wetland found to have had the best accuracy.

Table 6.13: Pixel count and corresponding percentage composition of each of the vegetation assemblages in the five images (table 6.12) with the best classification accuracy

Class	Spectral angle of separation (Radian)									
	0,50		0,6		0,7		0,8		0,9	
	Count	Percent	Count	Percent	Count	Percent	Count	Percent	Count	Percent
0	26	0,2	17	0,1	13	0,1	7	0,0	5	0,0
1	715	4,5	715	4,5	715	4,5	715	4,5	715	4,5
2	2678	17,0	2678	17,0	2678	17,0	2678	17,0	2678	17,0
3	1165	7,4	1165	7,4	1165	7,4	1165	7,4	1165	7,4
4	799	5,1	800	5,1	801	5,1	802	5,1	803	5,1
5	1430	9,1	1430	9,1	1430	9,1	1430	9,1	1430	9,1
6	3553	22,5	3553	22,5	3553	22,5	3553	22,5	3553	22,5
7	968	6,1	968	6,1	968	6,1	968	6,1	968	6,1
8	659	4,2	659	4,2	659	4,2	659	4,2	659	4,2
9	3291	20,9	3291	20,9	3291	20,9	3291	20,9	3291	20,9
10	499	3,2	507	3,2	510	3,2	515	3,3	516	3,3
Total	15783	100,0	15783	100,0	15783	100,0	15783	100,0	15783	100,0

Comparison of change in pixel count between consecutive spectral angles of separation for the five images displayed in table 6.13 showed marginal differences (Table 6.14).

Table 6.14: Differences in Pixels between consecutive Spectral angle of separation (Radian)

Class	0,6 - 0,5	0,7 - 0,6	0,8 - 0,7	0,9 - 0,8
	Pixel Count difference	Pixel Count difference	Pixel Count difference	Pixel Count difference
0	-9	-4	-6	-2
1	0	0	0	0
2	0	0	0	0
3	0	0	0	0
4	1	1	1	1
5	0	0	0	0
6	0	0	0	0
7	0	0	0	0
8	0	0	0	0
9	0	0	0	0
10	8	3	5	1

6.10 Digital Elevation Model and its Accuracy

Figure 6.19 shows a DEM adopted for subsequent characterization of the Mfabeni wetland in terms of elevation reduced to the spatial extent of the Mfabeni wetland boundary. It was based on a Topo-to-Raster interpolation which exhibited more reasonable results over a number of spot heights inside and in the vicinity of Mfabeni wetland used to validate the accuracy of the DEM accuracy (figure 6.20). Appendix 6.7 shows the DEMs generated using the various interpolation techniques.

Figure 6.19: DEM of Mfabeni wetland Generated Using Topo-to-Raster Interpolation Technique

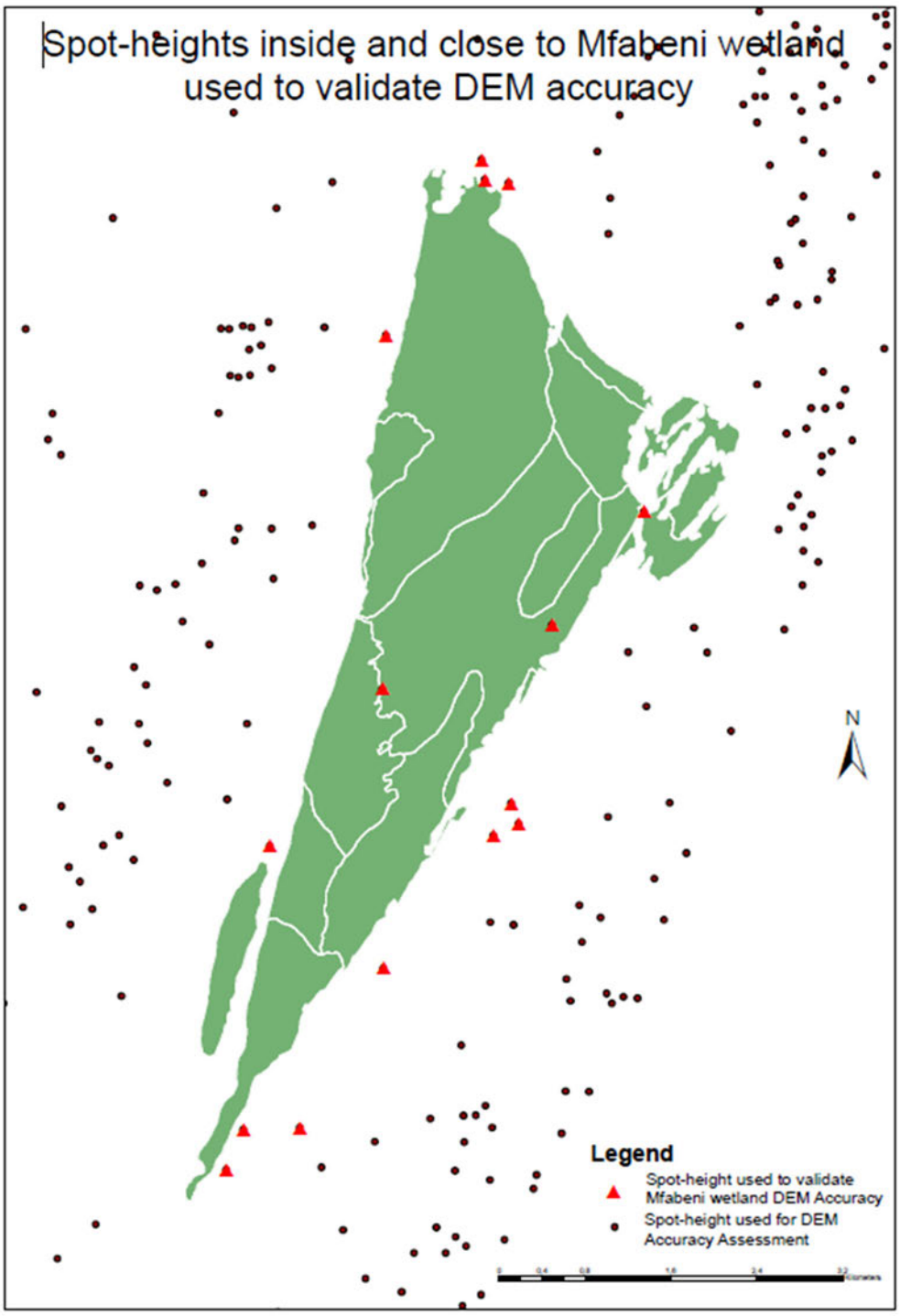

Figure 6.20: Location of spot-heights used as checkpoints to validate the accuracy of the DEM generated using various interpolation techniques.

Table 6.15 shows the DEM accuracy values obtained using the formulae given in equations 5.1-5.4 for each of the DEMs generated. The table shows natural neighbor with the best RMSE. However, Topo-to-Raster, despite its poor RMSE, featured the best when inspected for accuracy using the validation points (figure 6.20) and hence was used for subsequent processing and analysis.

Table 6.15: Accuracy of generated DEMs using spot-heights of in Mfabeni wetland and its surroundings

	Topo_To_Raster	IDW	Kriging_Ord-Spherical	Kriging_Ord-Exponential	Kriging_Ord-Linear	Natural Neighbour	Spline	Trend_Linear
Sum of Differences	-429,023	-252,04	-291,95875	-291,9767	-291,937327	-247,0455	-311,145284	-1409,85743
Sum of Differences squares	8603,73	6077,54	7325,26	7323,80	7326,80	5119,76	5195,75	229667,40
Sum of Residuals squares	7785,68	5795,21	6946,41	6944,91	6948,01	4848,51	4765,48	220833,18
Mean Error	-1,91	-1,12	-1,30	-1,30	-1,30	-1,10	-1,38	-6,27
RMSE	6,18	5,20	5,71	5,71	5,71	4,77	4,81	31,95
Standard Deviation	5,90	5,09	5,57	5,57	5,57	4,65	4,61	31,40
Standard Error	0,39	0,34	0,37	0,37	0,37	0,31	0,31	2,09

6.11 Distribution of Vegetation Assemblages of the Mfabeni Wetland in terms of Elevation

An overlay of the classified image of vegetation assemblages identified as suitable for characterization (figure 6.18) over the DEM of Mfabeni wetland (figure 6.19) considered ideal for vegetation characterization, produced an image with 77 different combinations, each one representing a unique combination of vegetation assemblage and elevation to the nearest 1m (figure 6.21).

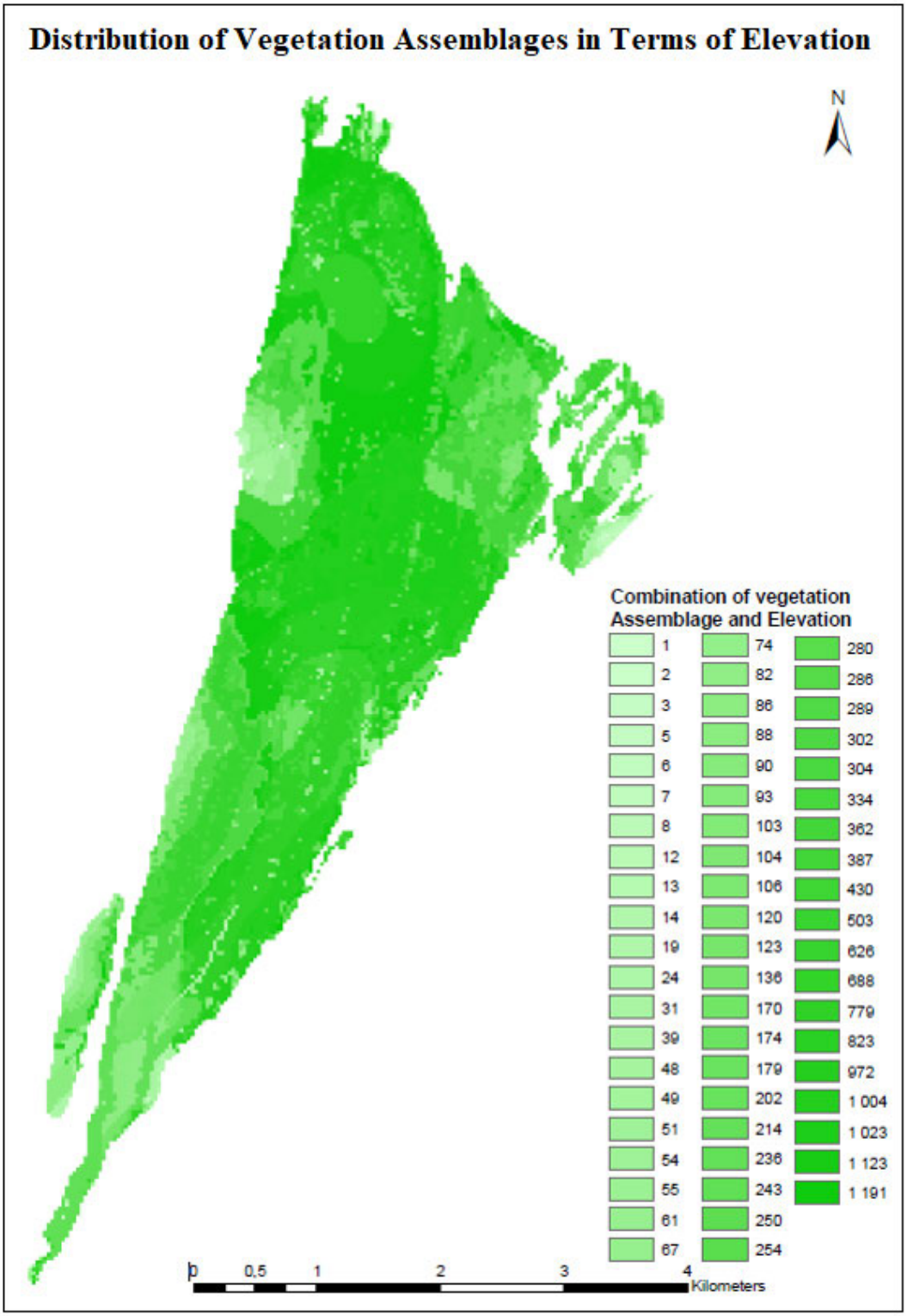

Figure 6.21: Combinations of different Vegetation Assemblages and elevation

Table 6.16 shows a portion of the table showing the pixel count for each of the vegetation assemblages thriving at each indicated elevations.

Table 6.16: Part of the combined Vegetation Assemblages/Elevation attribute table showing pixel count for each vegetation assemblage at a given elevation

Table

Extract_Com_T_to_R

Pixel Count	Elevation (m)	Class *	Vegetation Assemblage - Name
302	8	3	Community 12
55	12	3	Community 12
7	14	3	Community 12
51	11	5	Community 14
250	9	5	Community 14
90	8	8	Mosaic of communities 3, 6 and 9
48	7	8	Mosaic of communities 3, 6 and 9
236	6	5	Community 14
1	6	1	Community 5, with patces of 2, 3 and 6
24	6	10	Mosaic of community 1 and moist grassland
5	6	7	Mosaic of communities 3, 5, 6 and 9
86	6	4	Community 13
626	9	3	Community 12
14	13	3	Community 12
1	13	10	Mosaic of community 1 and moist grassland
74	8	10	Mosaic of community 1 and moist grassland
90	10	5	Community 14
688	7	6	Mosaic of communities 9, 10 and 11
39	6	2	Community 8, with patces of 6 and 7
31	6	6	Mosaic of communities 9, 10 and 11
289	10	3	Community 12
19	12	10	Mosaic of community 1 and moist grassland
88	7	10	Mosaic of community 1 and moist grassland
243	7	5	Community 14
2	6	8	Mosaic of communities 3, 6 and 9
123	7	4	Community 13
61	11	10	Mosaic of community 1 and moist grassland
254	8	5	Community 14
13	12	8	Mosaic of communities 3, 6 and 9
49	12	5	Community 14
49	7	1	Community 5, with patces of 2, 3 and 6
31	11	8	Mosaic of communities 3, 6 and 9
86	11	3	Community 12
82	6	3	Community 12
54	7	7	Mosaic of communities 3, 5, 6 and 9

71 (0 out of 77 Selected)

Extract_Com_T_to_R

Elevation values were converted to integer values automatically when merged with the selected classified vegetation assemblage image. Figure 6.22 shows the distribution of elevation to the nearest 1m across the Mfabeni wetland.

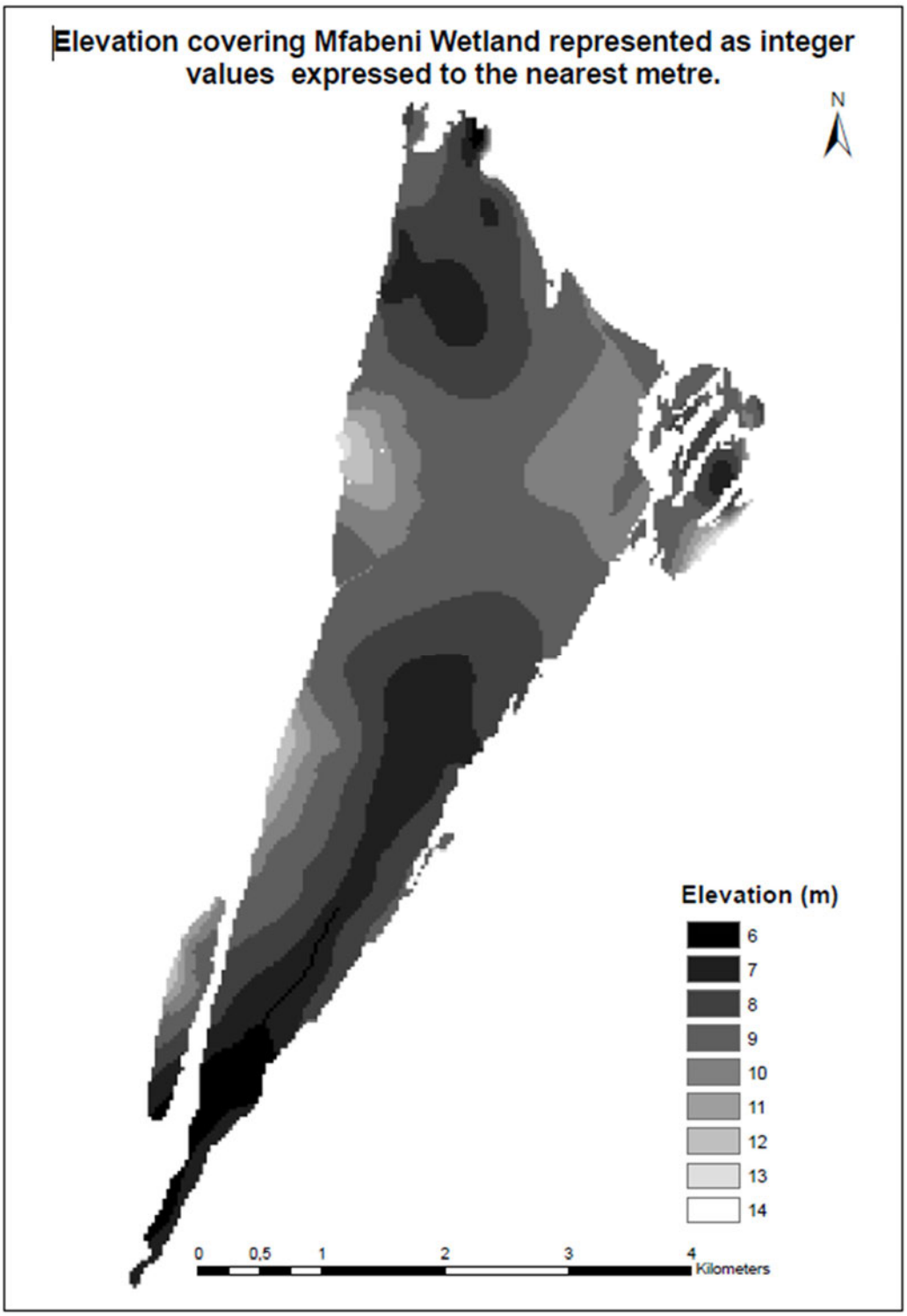

Figure 6.22: Representation of Elevation as integer values across Mfabeni wetland

Spatial queries subsequently performed on the combined image revealed variation in vegetation assemblage thriving at each of the different nine (6m – 14m) elevation levels covering the wetland. Figures 6.23 (a) – (i) show the spatial distribution of these vegetation assembles at each elevation.

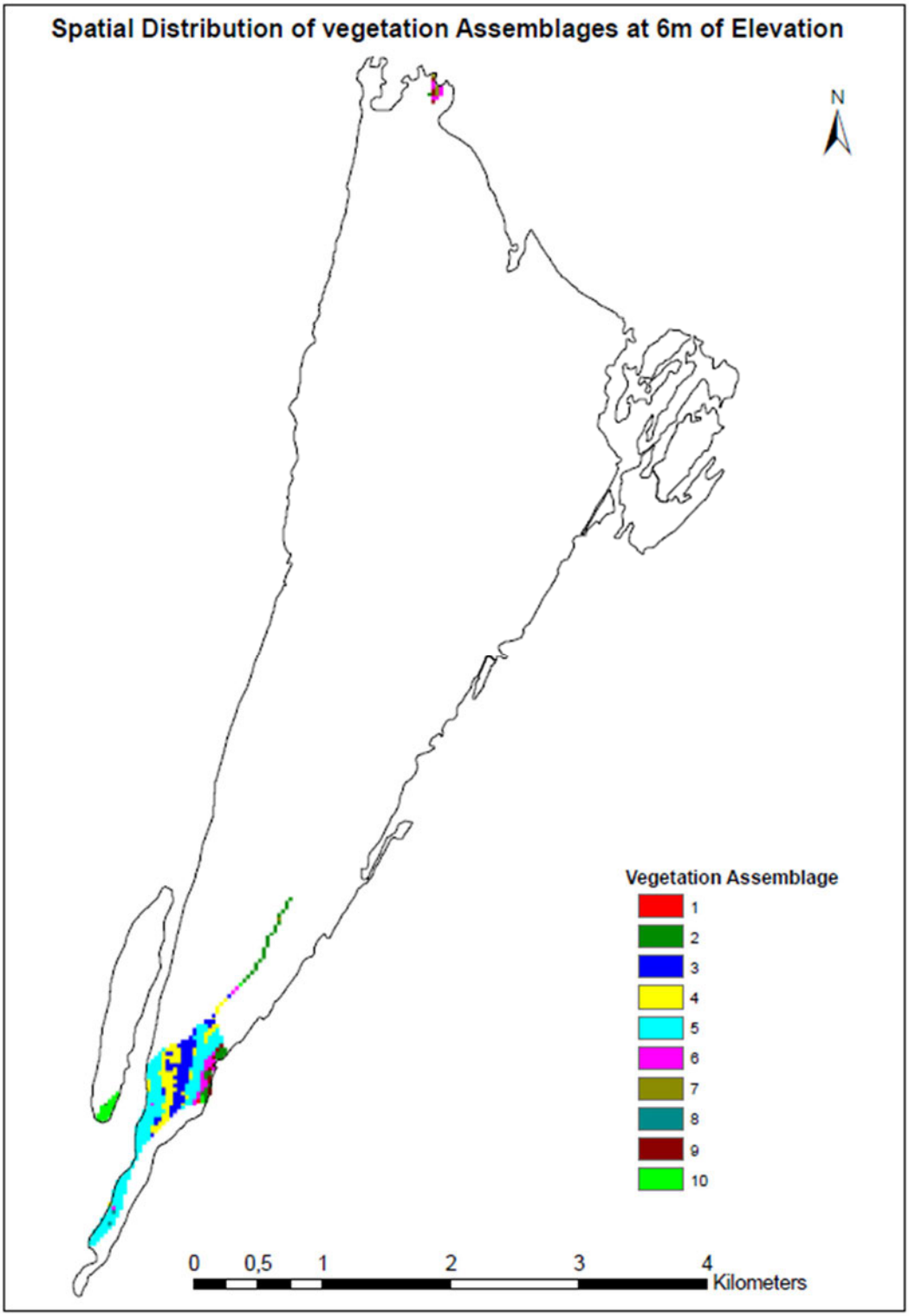

Figure 6.23(a): Spatial distribution of vegetation assemblages at 6m Elevation of Mfabeni Wetland

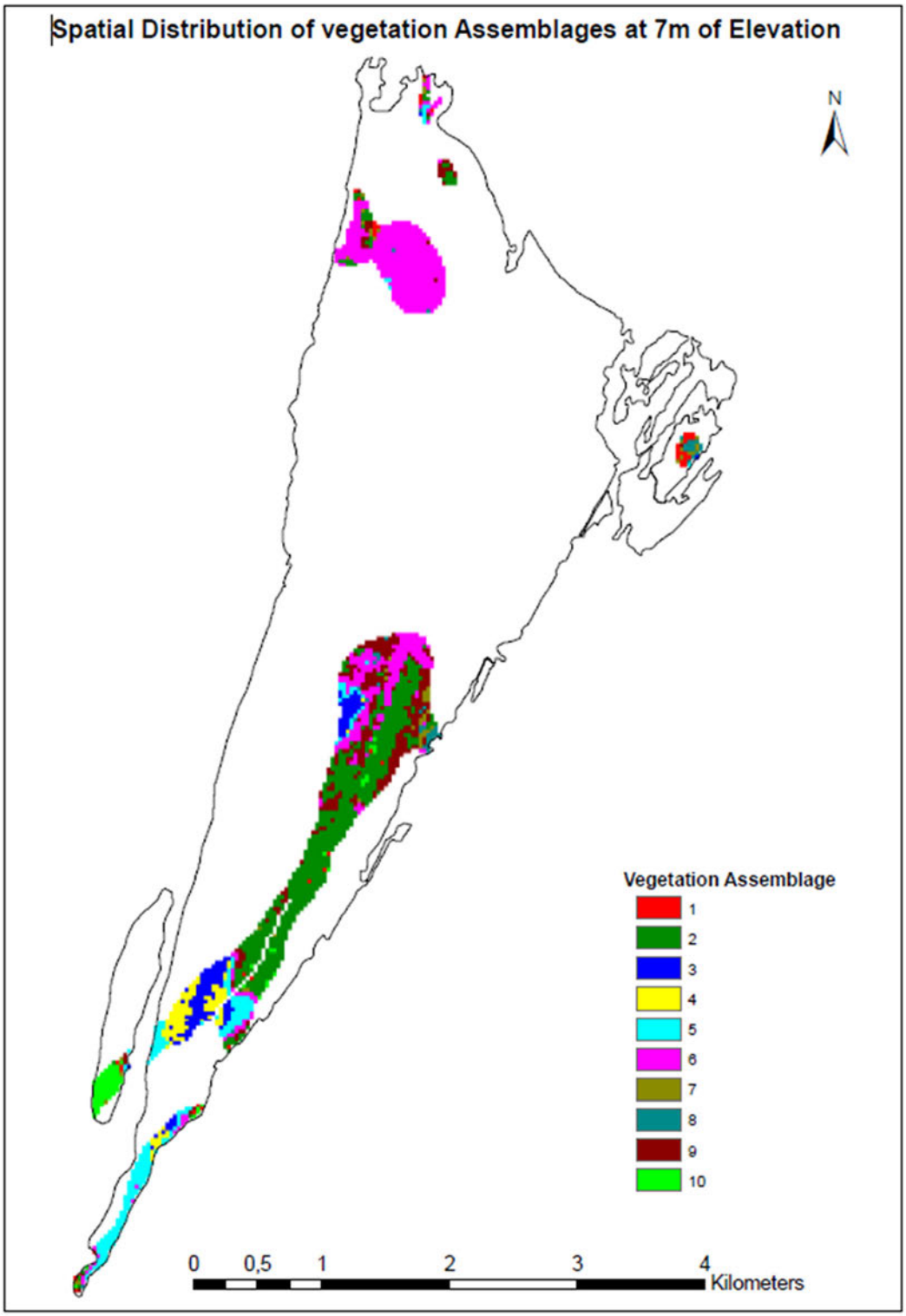

Figure 6.23(b): Spatial distribution of vegetation assemblages at 7m Elevation of Mfabeni Wetland

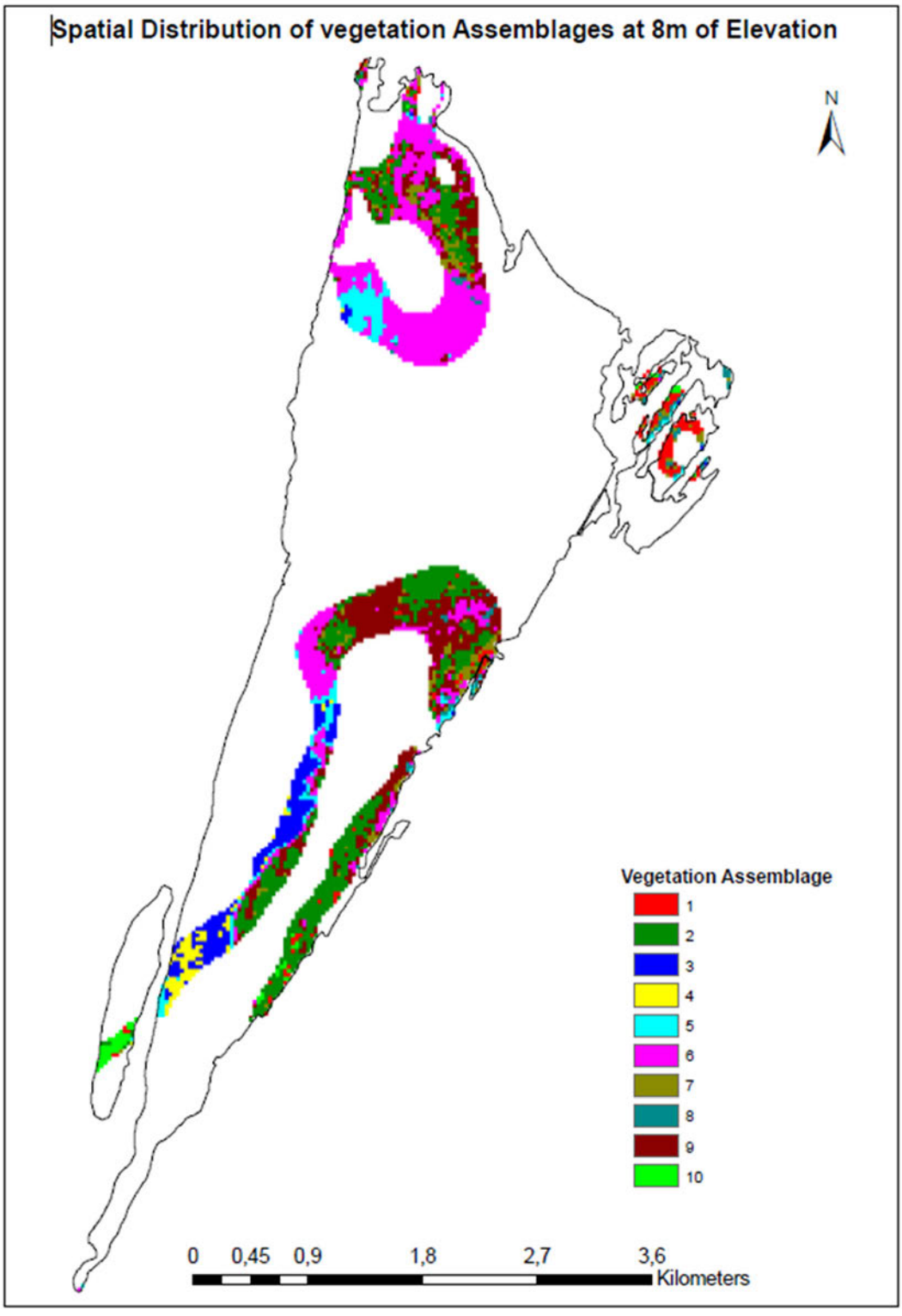

Figure 6.23(c): Spatial distribution of vegetation assemblages at 8m Elevation of Mfabeni Wetland

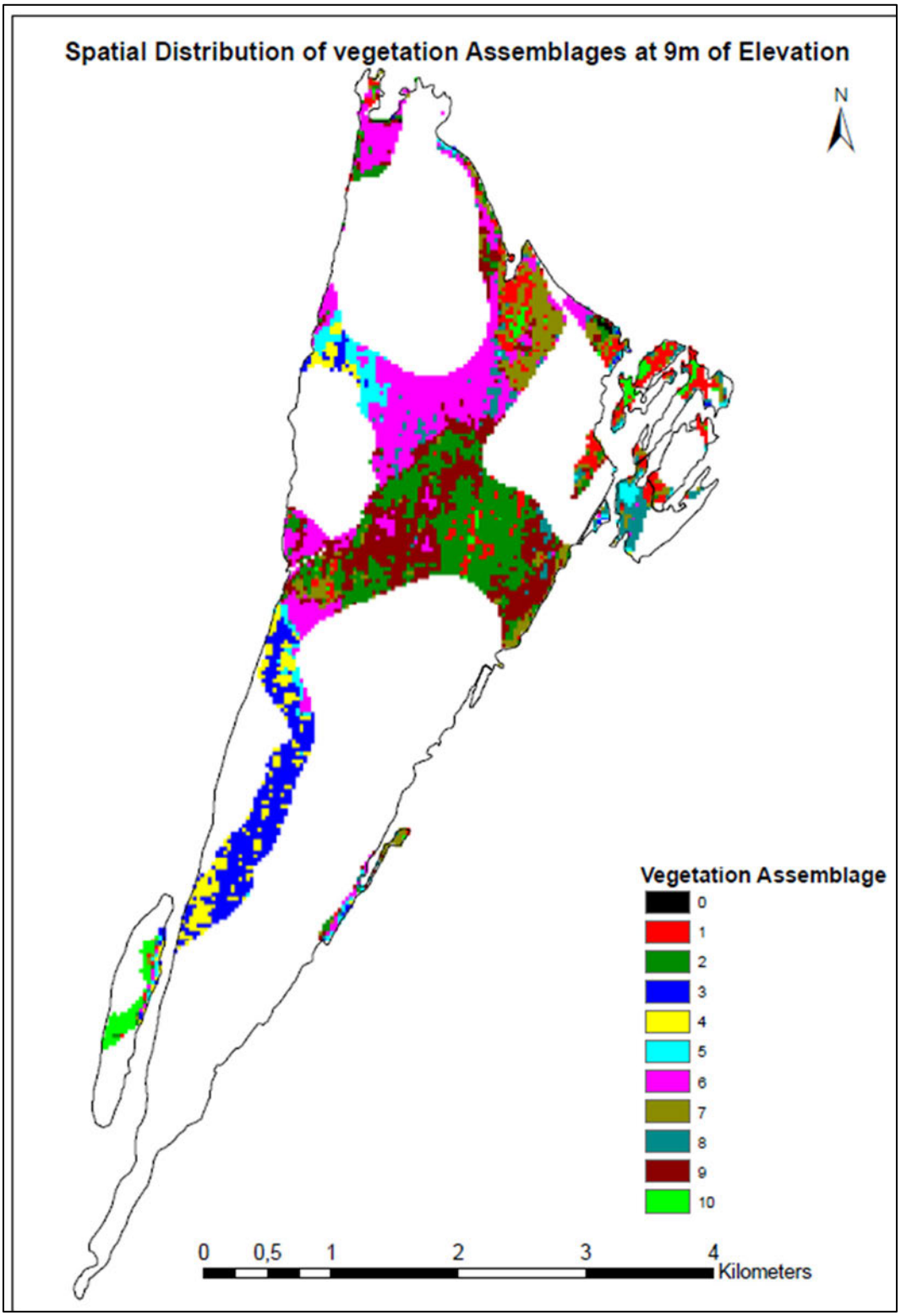

Figure 6.23(d): Spatial distribution of vegetation assemblages at 9m Elevation of Mfabeni Wetland

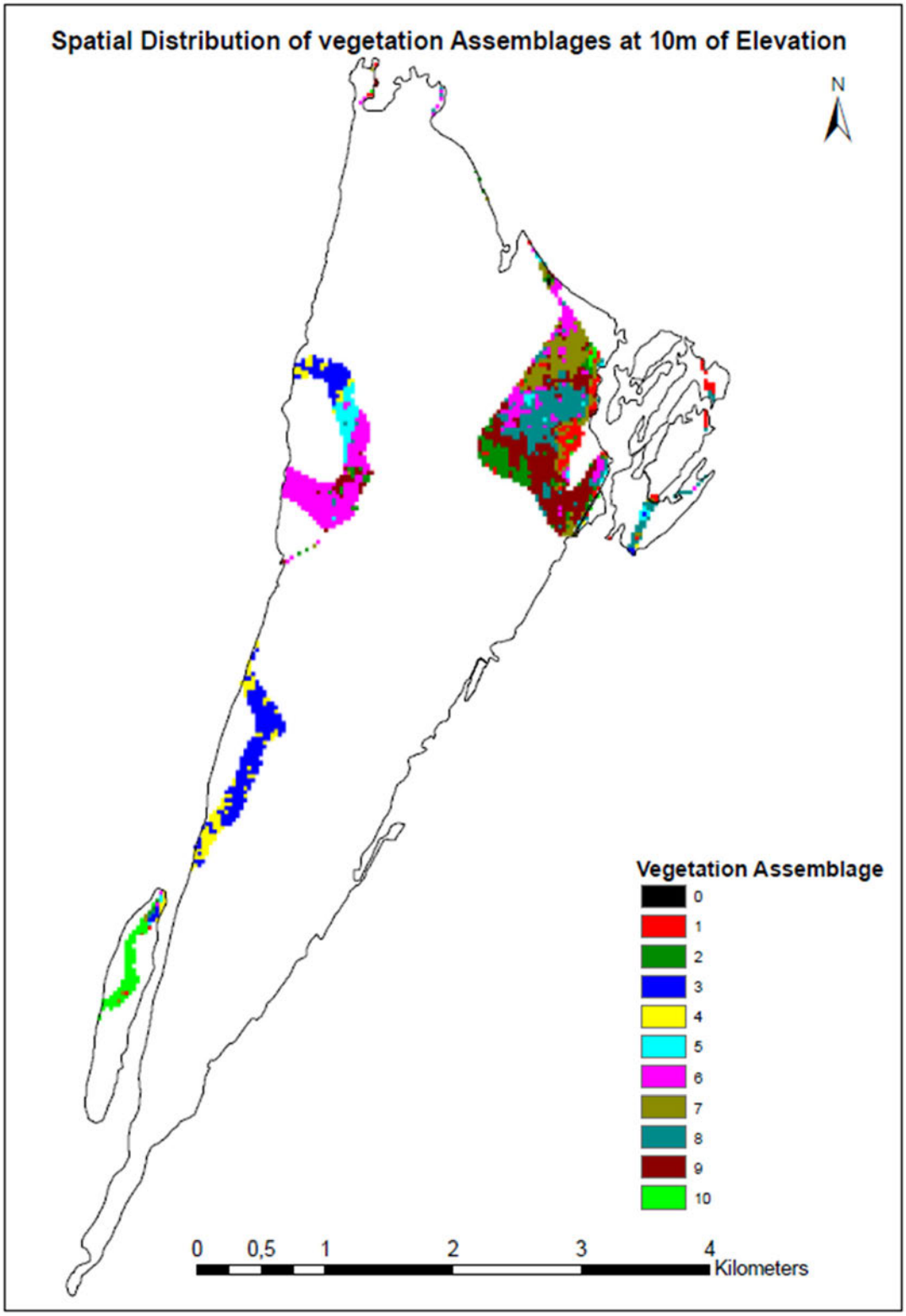

Figure 6.23(e): Spatial distribution of vegetation assemblages at 10m Elevation of Mfabeni Wetland

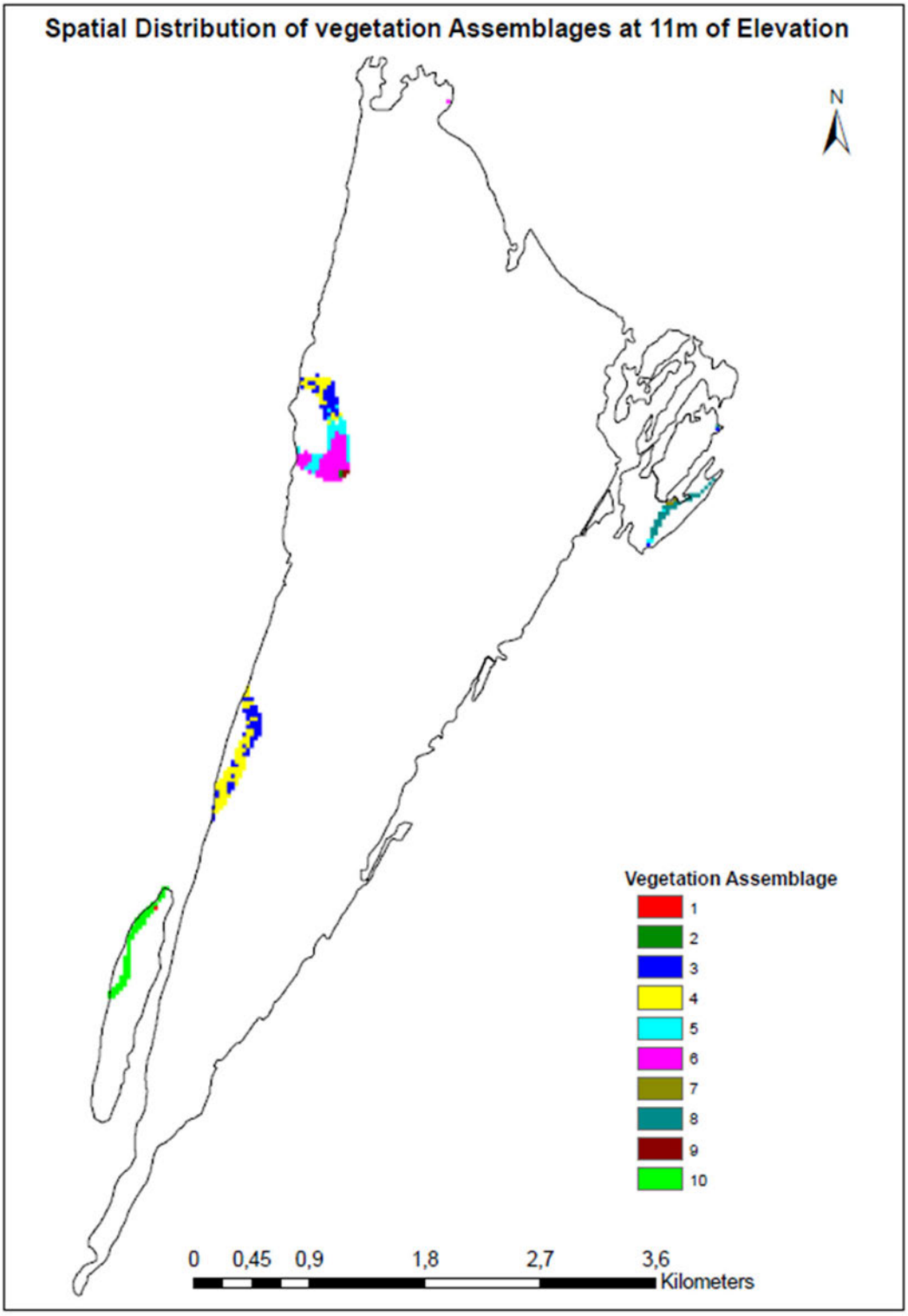

Figure 6.23(f): Spatial distribution of vegetation assemblages at 11m Elevation of Mfabeni Wetland

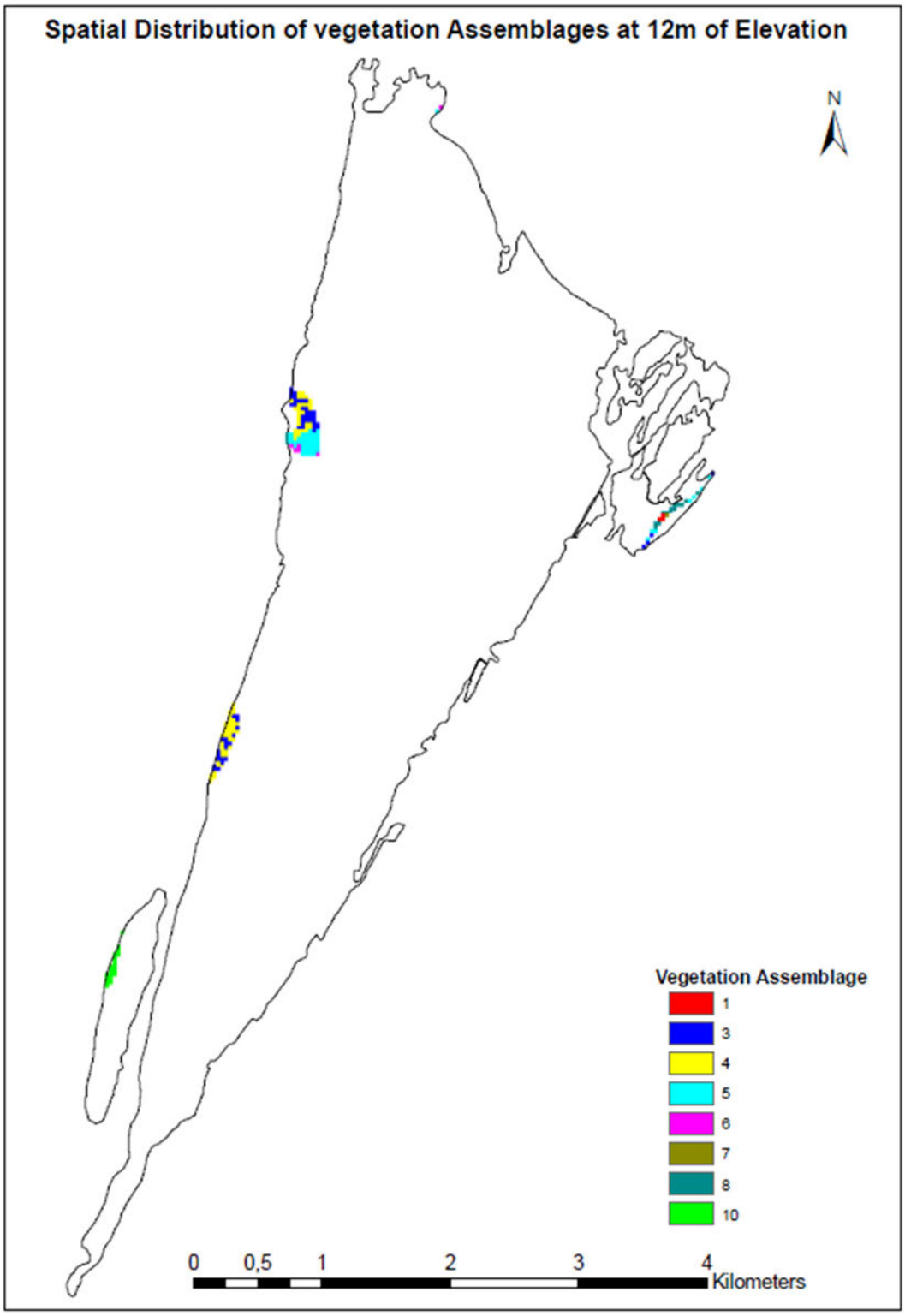

Figure 6.23(g): Spatial distribution of vegetation assemblages at 12m Elevation of Mfabeni Wetland

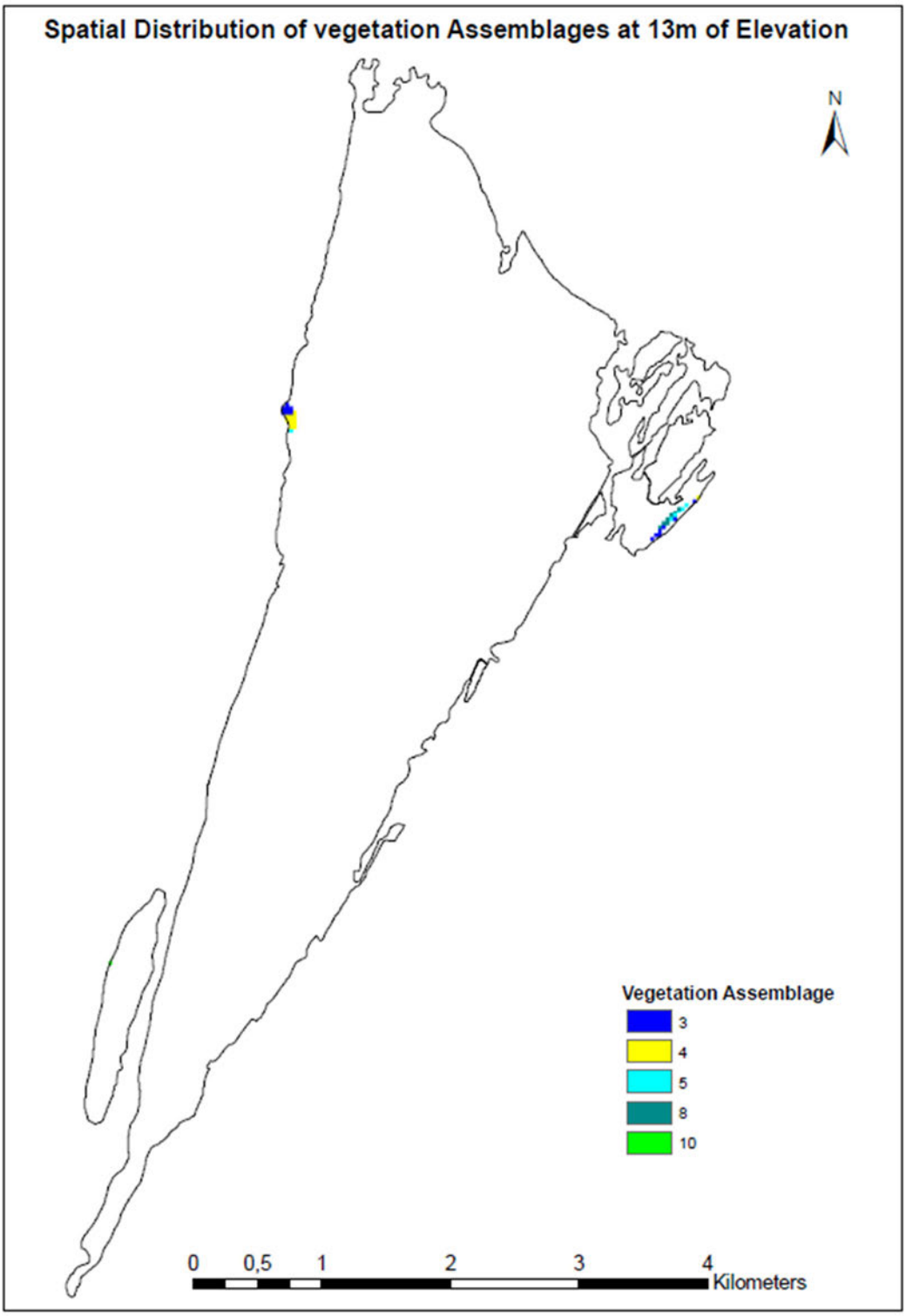

Figure 6.23(h): Spatial distribution of vegetation assemblages at 13m Elevation of Mfabeni Wetland

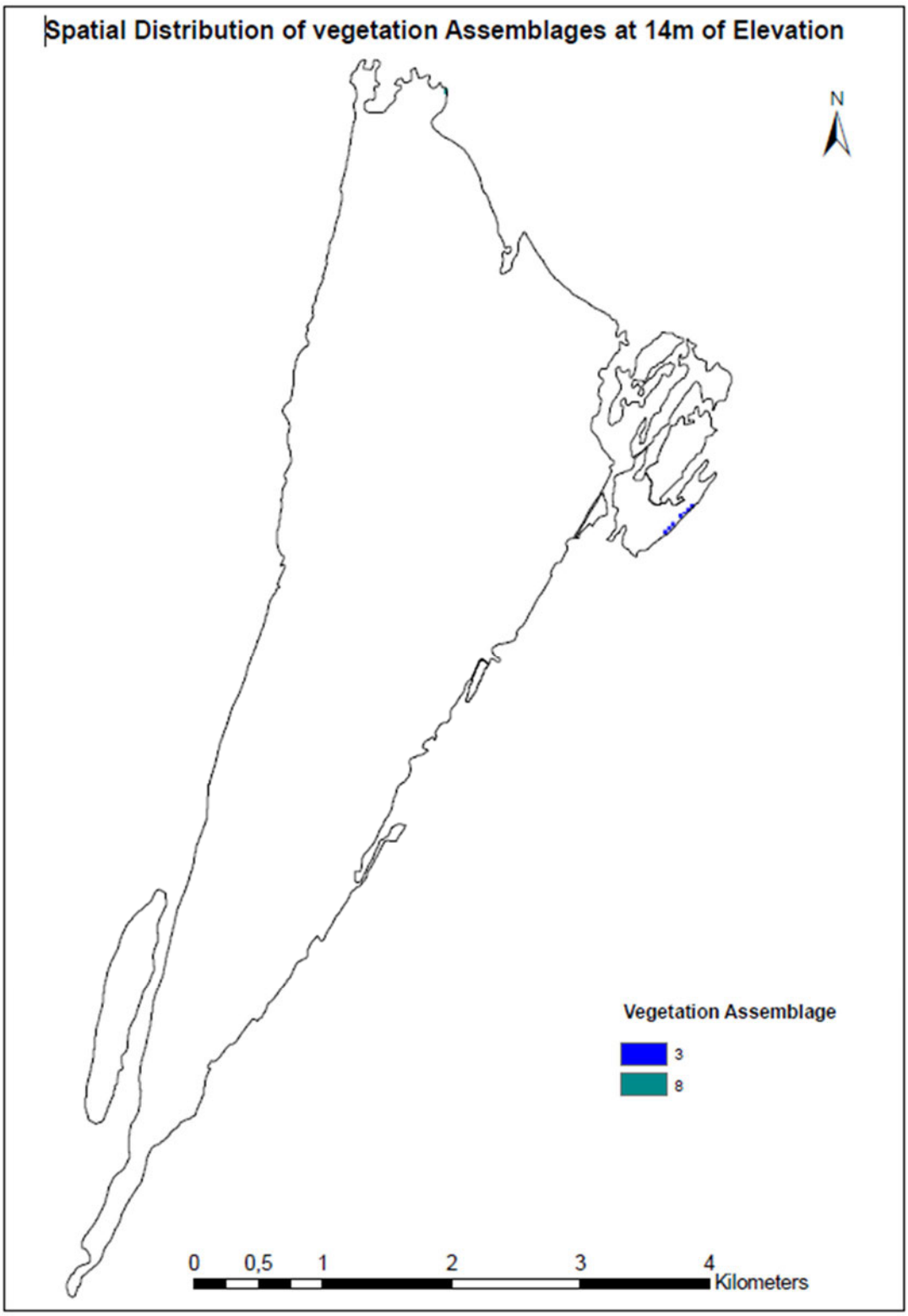

Figure 6.23(i): Spatial distribution of vegetation assemblages at 14m Elevation of Mfabeni Wetland

Table 6.17 provides a summary of each vegetation assemblage pixel count at each elevation covered by the Mfabeni wetland.

Table 6.17: Vegetation Assemblages Pixel Count at each Elevation of the Mfabeni Wetland

	Class	Elevation (m)									Sum	Max	Min
		6	7	8	9	10	11	12	13	14			
Vegetation Assemblage	0	0	0	0	8	2	0	0	0	0	10	8	0
	1	1	49	174	430	104	1	411	0	0	1170	430	0
	2	39	779	972	1023	136	2	0	0	0	2951	1023	0
	3	82	170	302	626	289	86	9	14	7	1585	626	7
	4	86	123	103	304	120	106	354	12	0	1208	354	0
	5	236	243	254	250	90	51	180	6	0	1310	254	0
	6	31	688	1123	1191	387	82	246	0	0	3748	1191	0
	7	5	54	214	503	202	3	378	0	0	1359	503	0
	8	2	48	90	286	280	31	165	7	2	911	286	2
	9	13	334	823	1004	362	3	0	0	0	2539	1004	0
	10	24	88	74	179	93	61	123	1	0	643	179	0
	Sum	519	2576	4129	5804	2065	426	1866	40	9	17434		
	Max	236	779	1123	1191	387	106	411	14	7			
	Min	0	0	0	8	2	0	0	0	0			

6.12 Spatial Distribution of Vegetation Assemblages along the Mfabeni wetland elevation gradient

Figure 6.24 shows part of a point layer created to allow for the creation of elevation gradient profiles. The figure show pixel centroids extracted from the vegetation assemblages and elevation images.

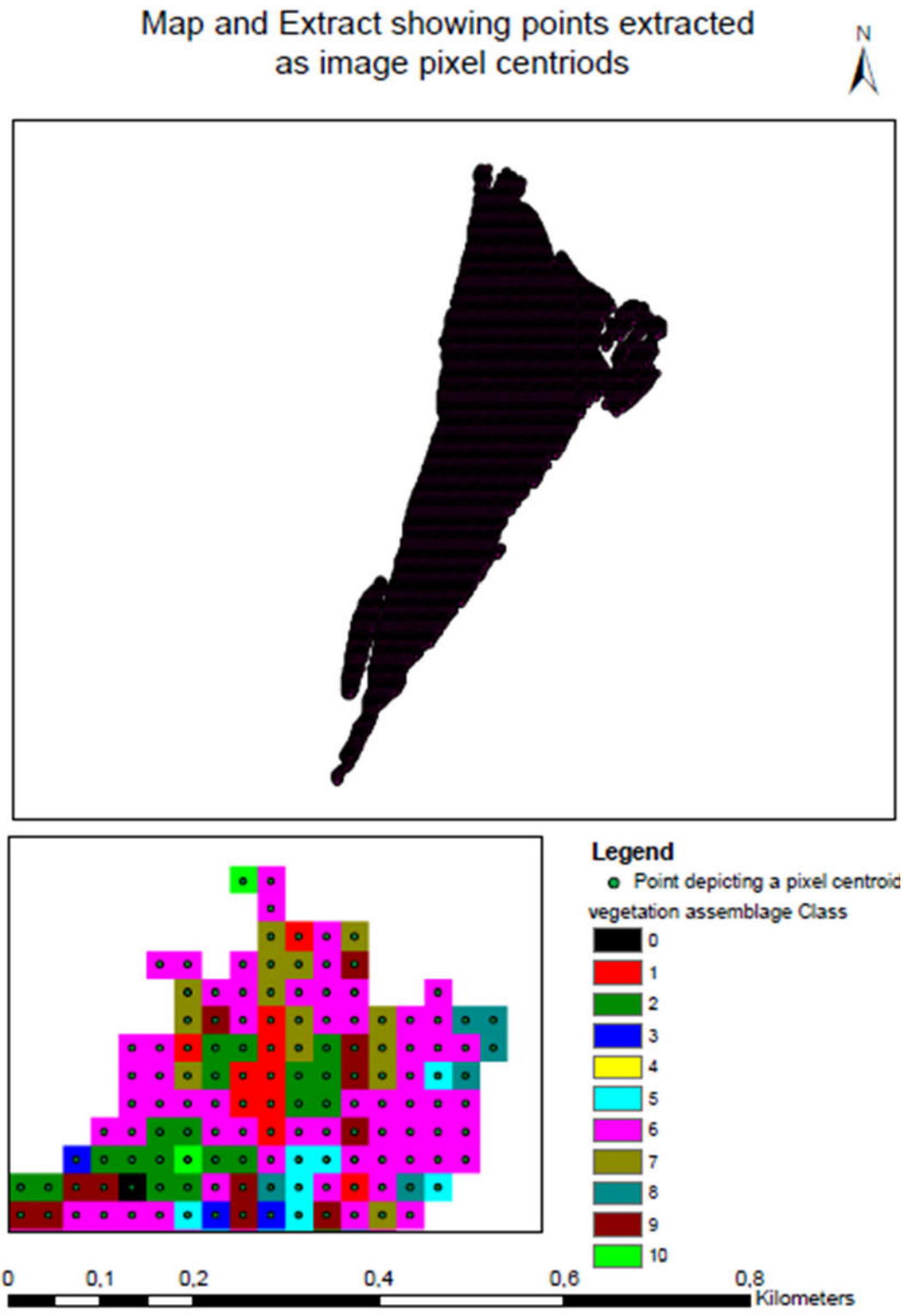

Figure 6.24: Points extracted as image pixel centroids

Table 6.18 shows a portion of an attribute table corresponding extracted centroids displaying the shape attributes with a 'Z' added to the shape column as confirmation that it was converted to 3D to allow for the creation of elevation profiles.

Table 6.18: Part of an attribute table showing elevation attributes converted for creation of profiles.

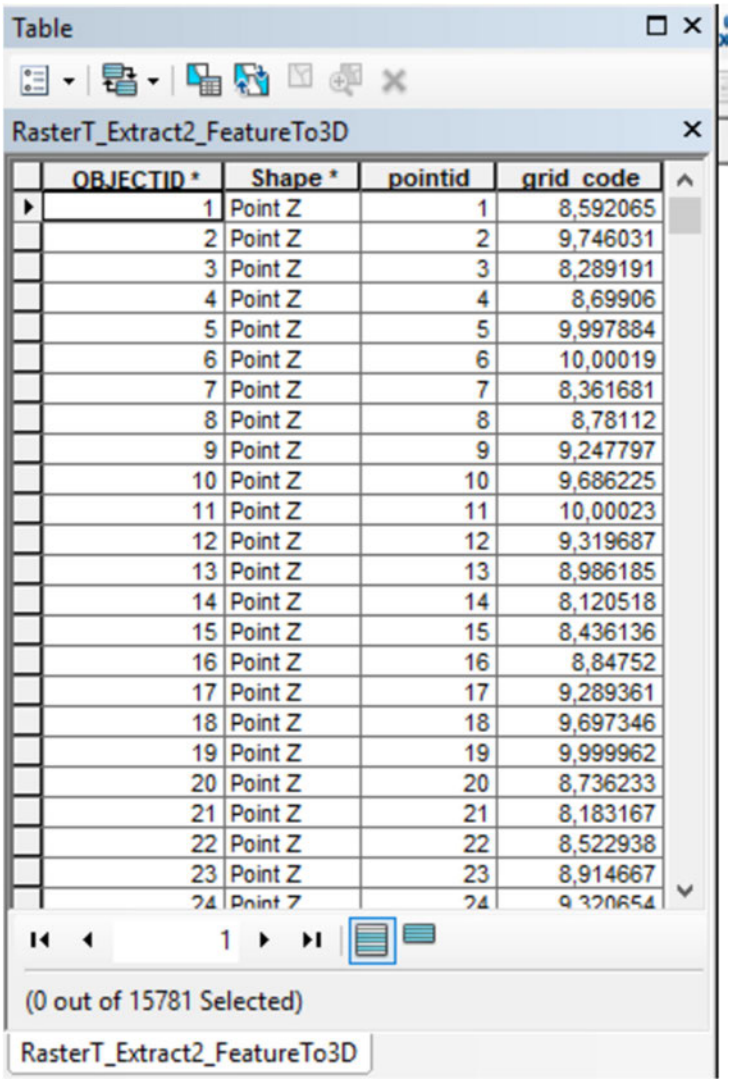

OBJECTID *	Shape *	pointid	grid_code
1	Point Z	1	8,592065
2	Point Z	2	9,746031
3	Point Z	3	8,289191
4	Point Z	4	8,69906
5	Point Z	5	9,997884
6	Point Z	6	10,00019
7	Point Z	7	8,361681
8	Point Z	8	8,78112
9	Point Z	9	9,247797
10	Point Z	10	9,686225
11	Point Z	11	10,00023
12	Point Z	12	9,319687
13	Point Z	13	8,986185
14	Point Z	14	8,120518
15	Point Z	15	8,436136
16	Point Z	16	8,84752
17	Point Z	17	9,289361
18	Point Z	18	9,697346
19	Point Z	19	9,999962
20	Point Z	20	8,736233
21	Point Z	21	8,183167
22	Point Z	22	8,522938
23	Point Z	23	8,914667
24	Point Z	24	9,320654

Once all image pixels had been converted to 3D points depicting their centroids, four (4) sets of transects with different orientations were created (figure 6.25). Figure 6.26(a) – (d) show separate sets (1- 4) of the transects created and the names assigned to each one of them. Each transect was created to cut across one line of points only. The use of transects oriented differently was considered essential to allow for the investigation of the elevation gradient that would satisfy the principle of zonation in terms of vegetation distribution along an altitudinal gradient.

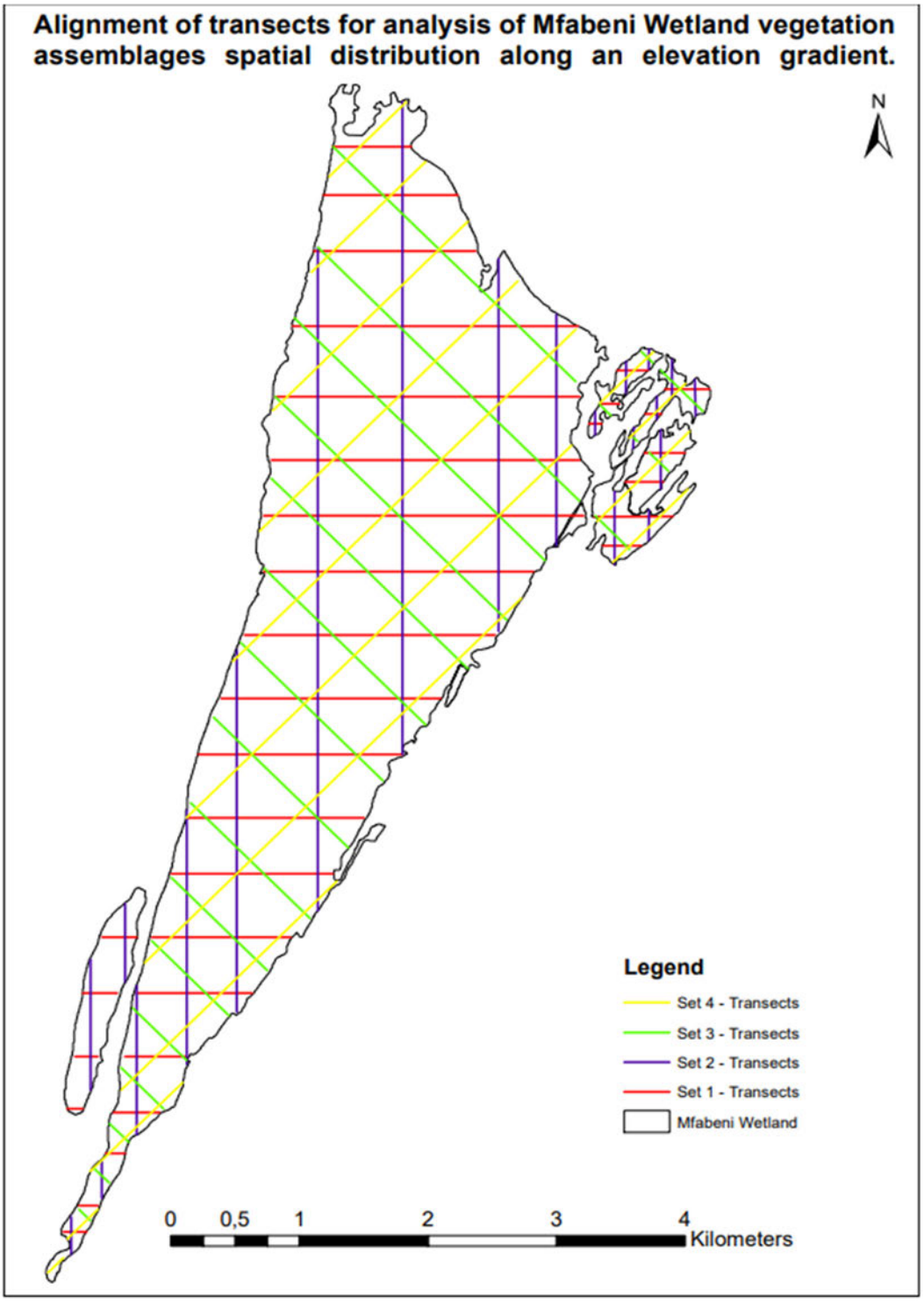

Figure 6.25: Alignment of transects used to analyze spatial distribution of vegetation assemblages on the Mfabeni Wetland elevation gradient.

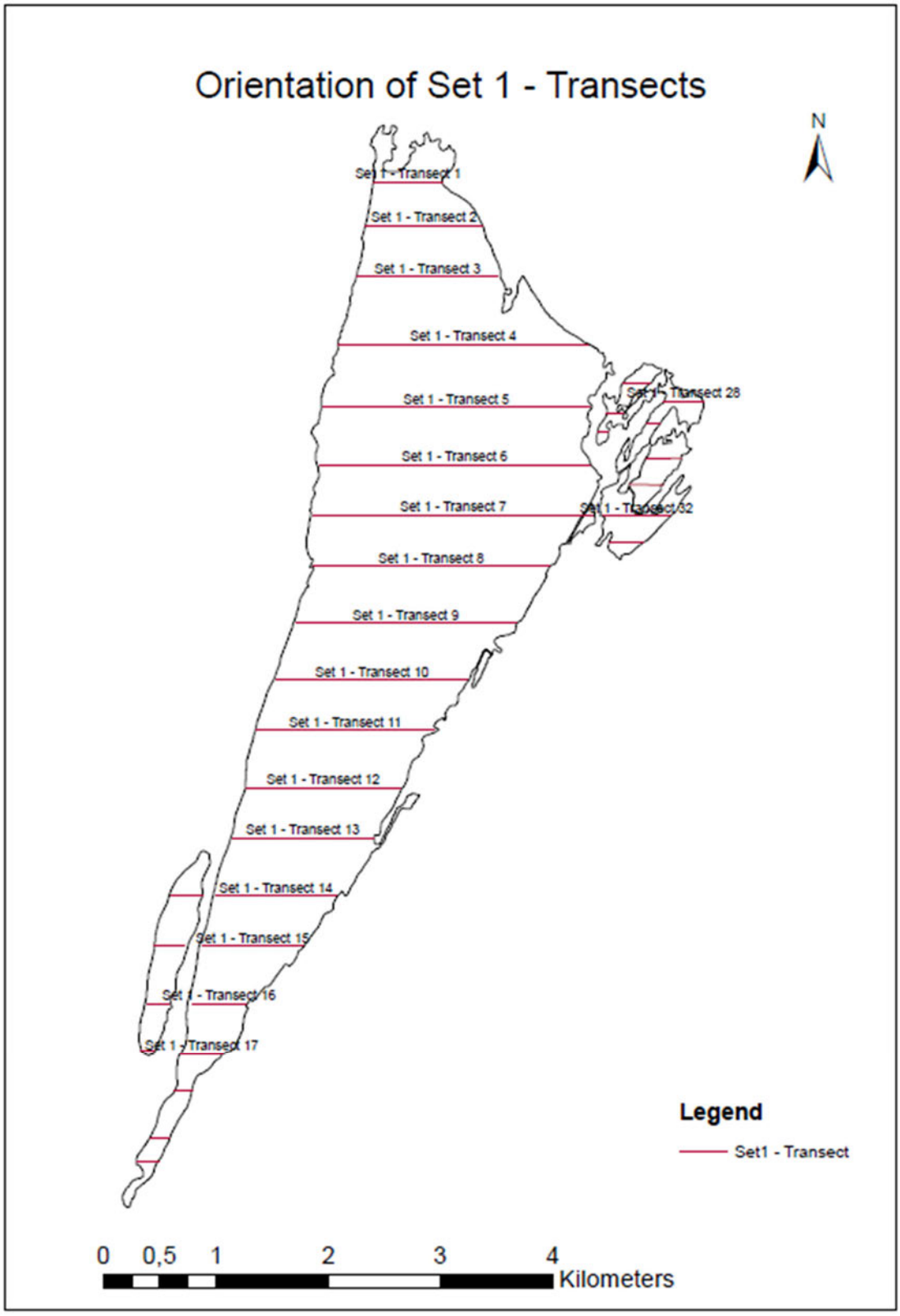

Figure 6.26(a): Alignment and names of set 1 transects used to analyze spatial distribution of vegetation assemblages on a Mfabeni Wetland elevation gradient.

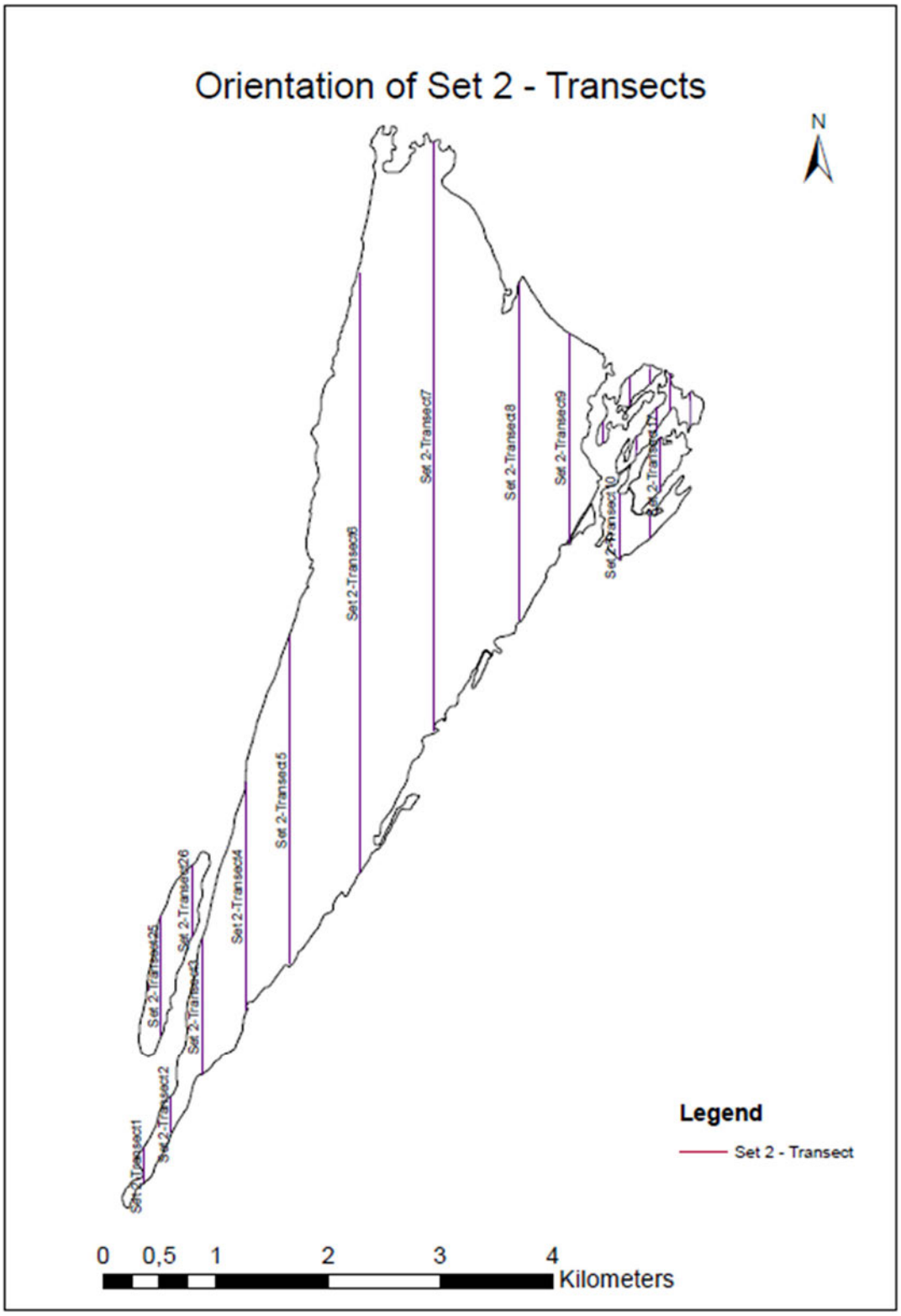

Figure 6.26(b): Alignment and names of set 2 transects used to analyze spatial distribution of vegetation assemblages on a Mfabeni Wetland elevation gradient.

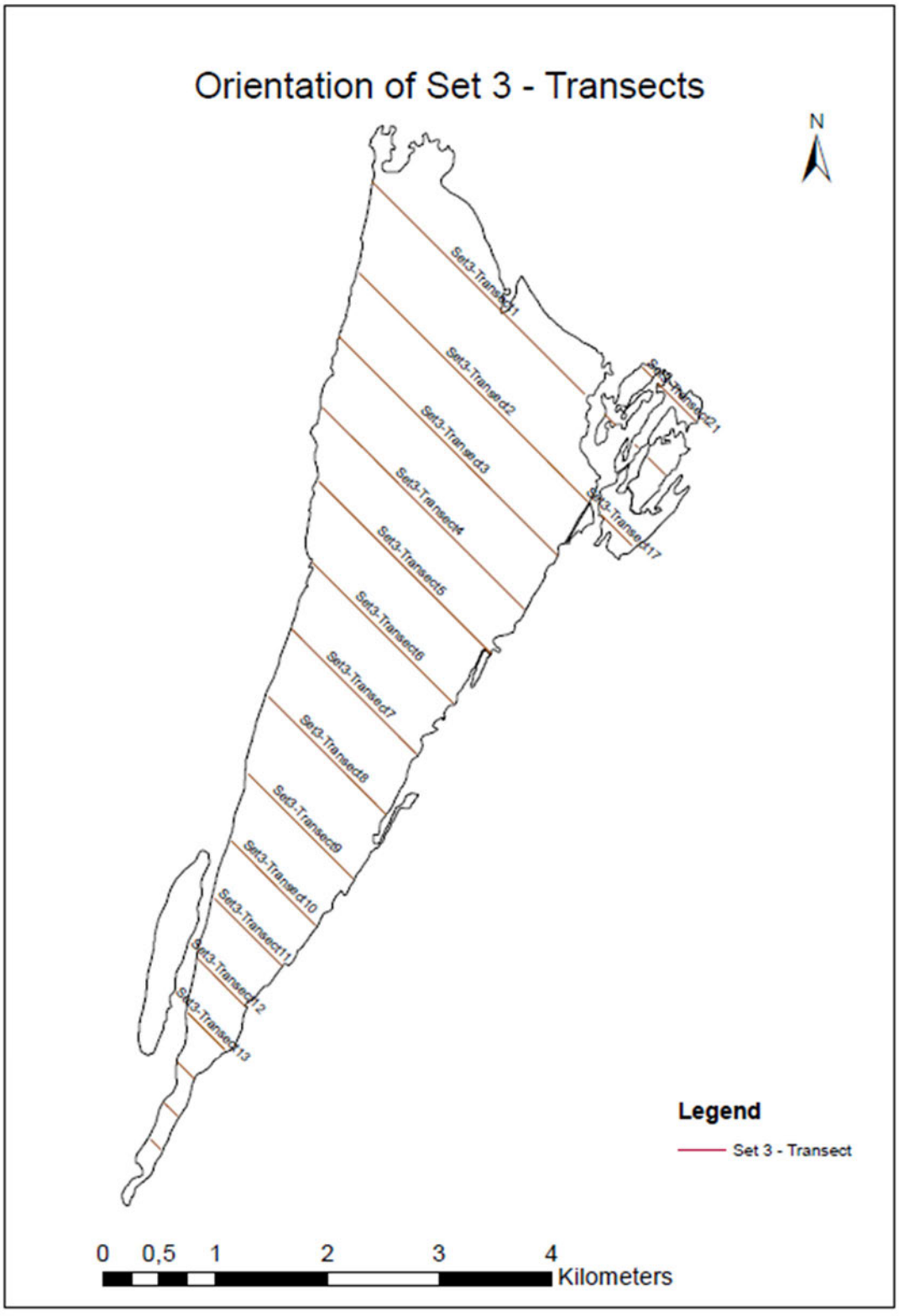

Figure 6.26(c): Alignment and names of set 3 transects used to analyze spatial distribution of vegetation assemblages on a Mfabeni Wetland elevation gradient.

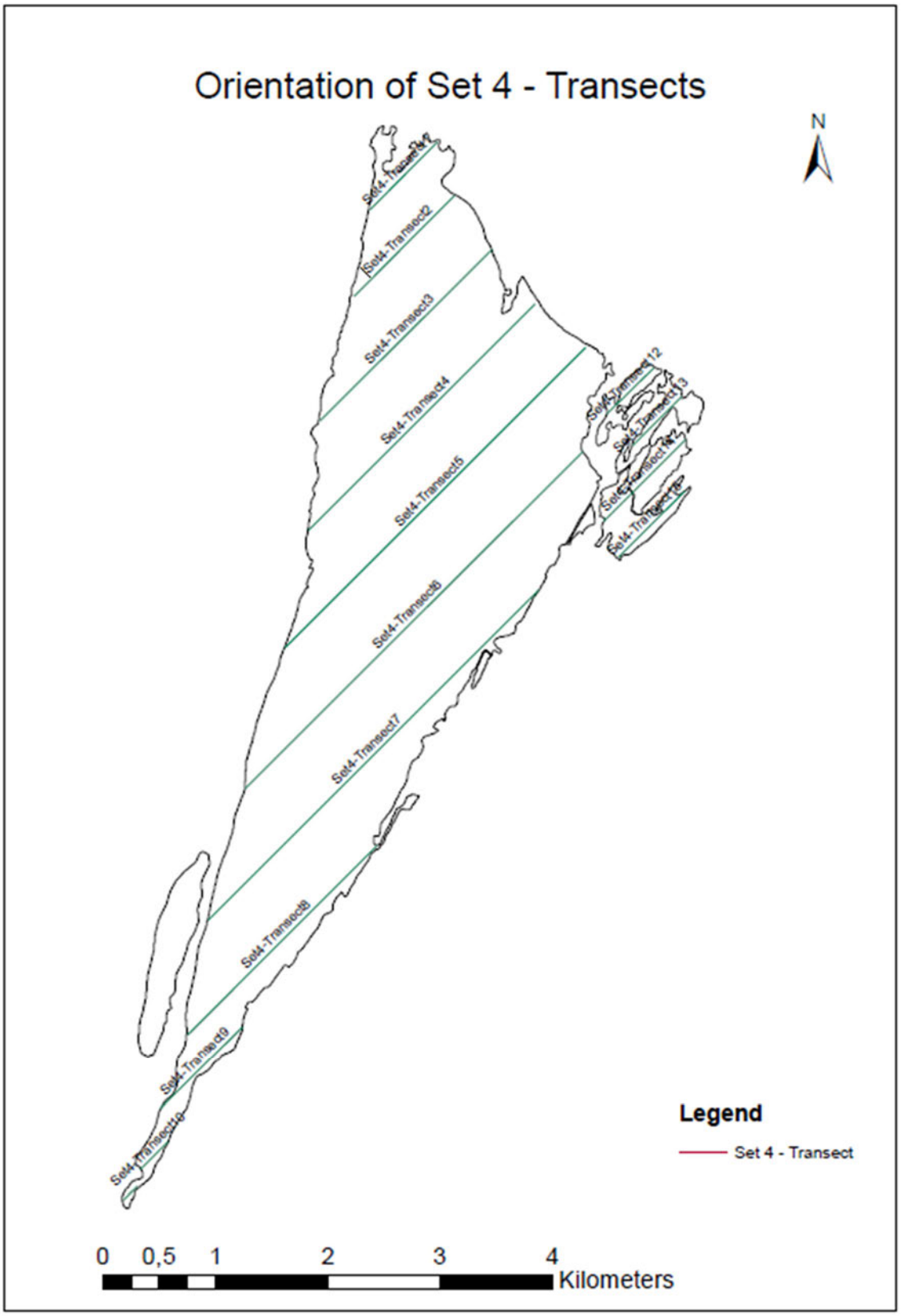

Figure 6.26(d): Alignment and names of set 4 transects used to analyze spatial distribution of vegetation assemblages on a Mfabeni Wetland elevation gradient.

A point profile for each transect was created by selecting the concerned transect line, then using the selected line to extract points on and alongside the line to a separate layer specifying a buffer distance of 15m to ensure that points alongside are not left out. Using ArcGIS' 3D Analyst's 'point profile tool', a line was then drawn over the concerned transect line to select all the points extracted earlier to the newly created layer. The accumulative distance from the beginning of the profile and the corresponding elevation data making up the profile (profile data) were then displayed in the form of a table, copied and exported to MS-Excel, where vegetation assemblages' data were added. An equivalent line profile through the selected points was then created.

Figure 6.27 shows how this was done using transect 5 of set 1 as an example along with a corresponding point profile and table of profile data. The beginning and end of the profile line are denoted by A and B, respectively, on figure 6.27.

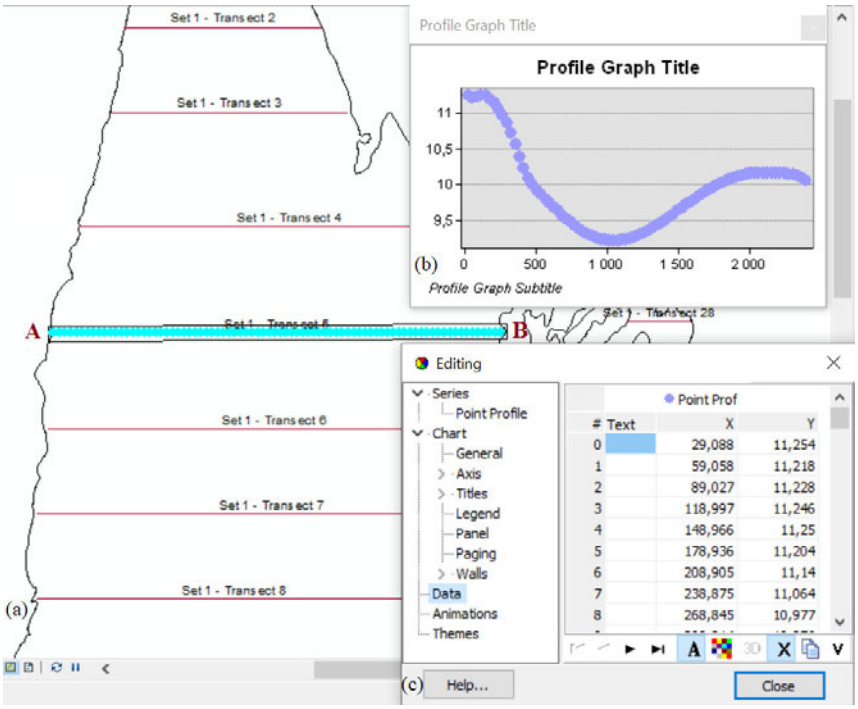

Figure 6. 27: Point profile along a transect across the wetland: (a) location of set1-transect 6; (b) plot of accumulative distance from the beginning of the transect against elevation for set1- transect 5 (c) profile data for set1-transect 6 with X and Y representing accumulative horizontal distance and elevation respectively

Figures 6.28(a) - (d) show sample line elevation profiles from each of the transect sets with vegetation assemblages indicating vegetation distribution on the elevation gradient labelled on them. Appendix 6.8 shows other transect profiles in each of the sets created across the Mfabeni wetland. The beginning and end of profiles were the opposite ends of the wetland boundary with the direction of the transect run corresponding to the direction of transect names alignment as labelled on figures 6.26(a) – 6.26(d).

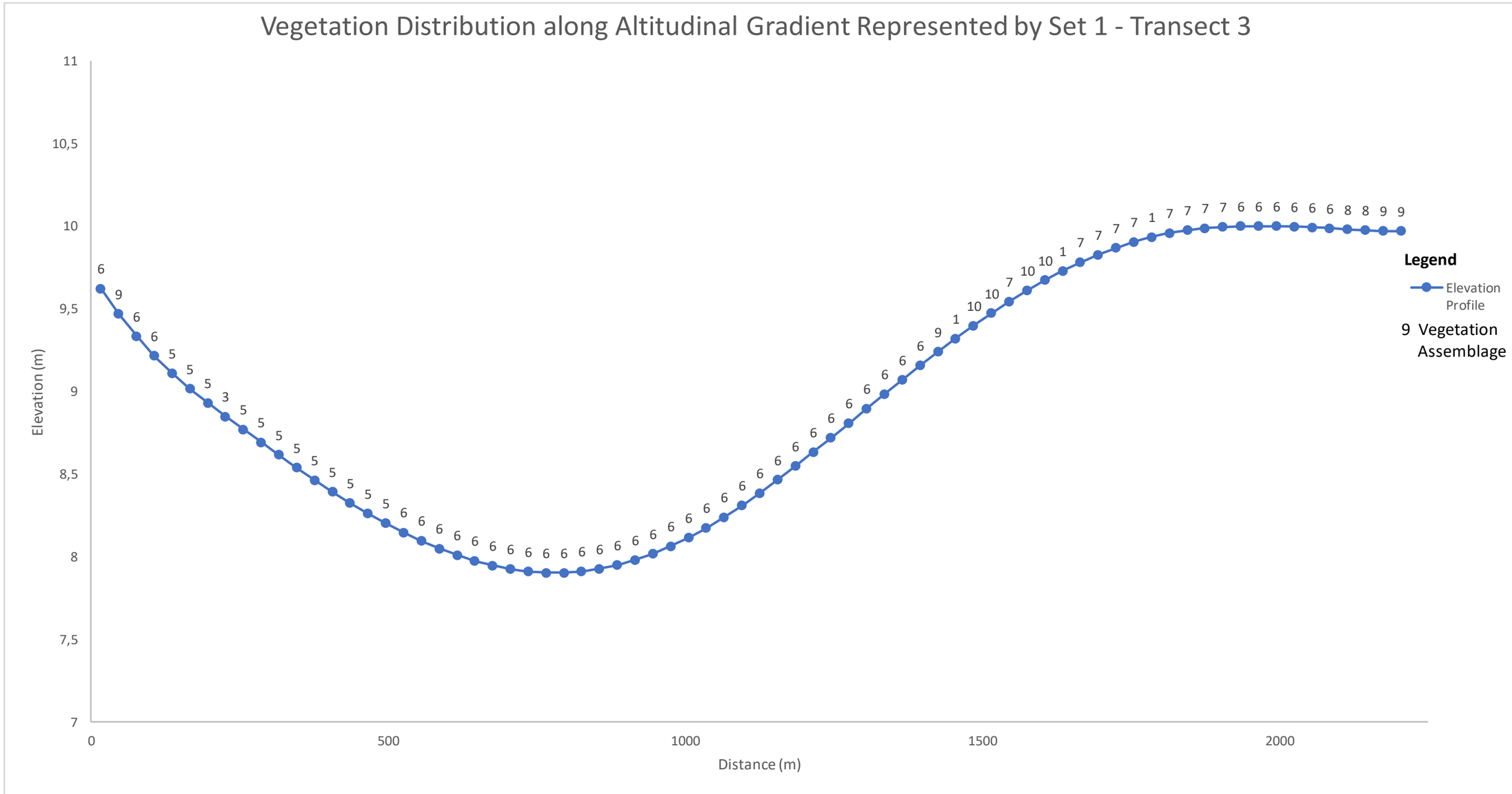

Figure 6.28(a): Line profile showing distribution of vegetation assemblages along Set 1-Transect 3 of the Mfabeni wetland

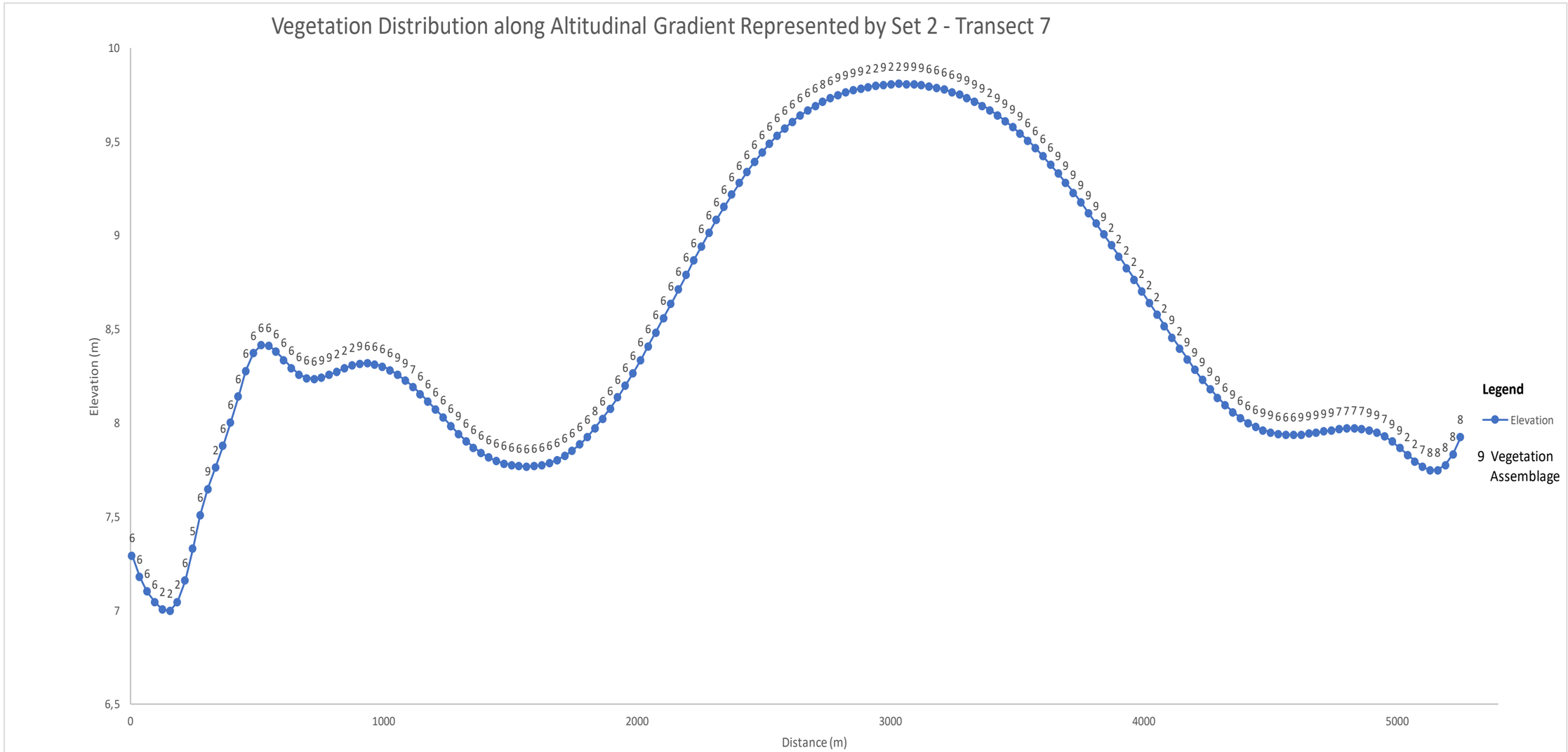

Figure 6.28(b): Line profile showing distribution of vegetation assemblages along Set 2-Transect 9 of the Mfabeni wetland

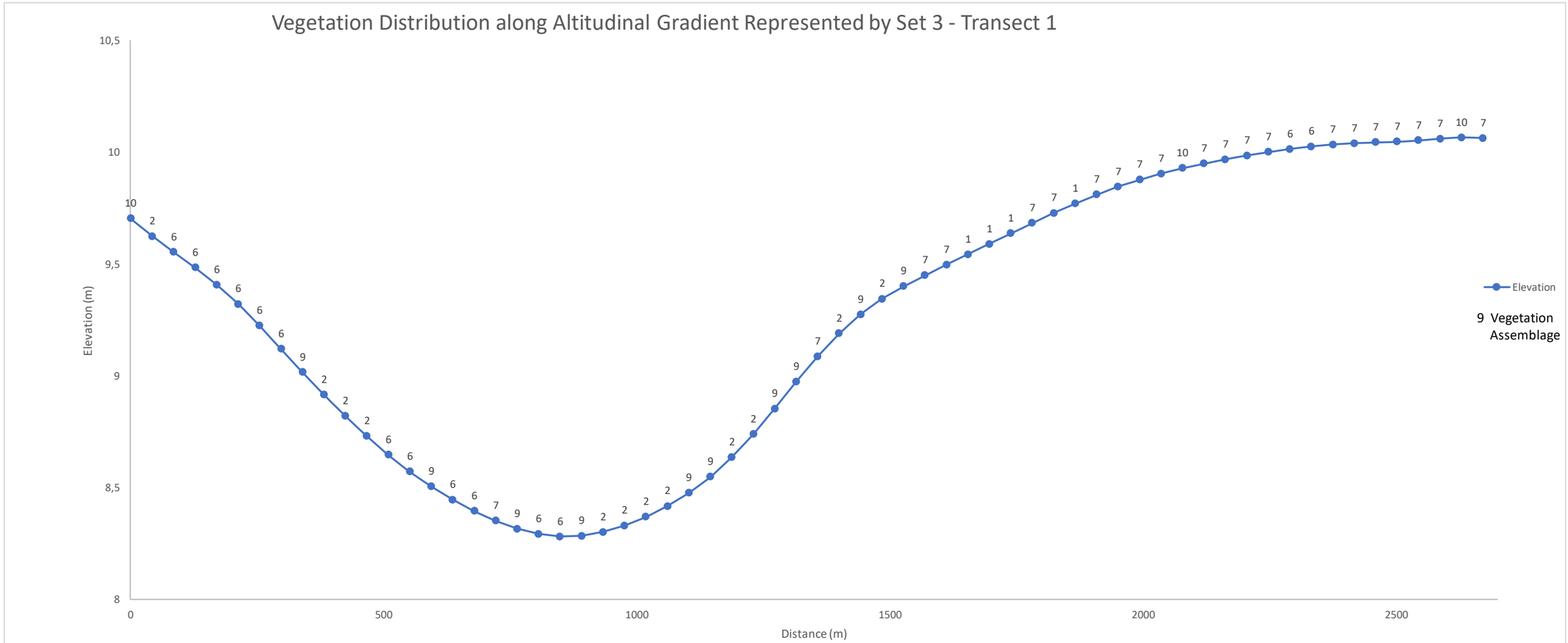

Figure 6.28(c): Line profile showing distribution of vegetation assemblages along Set 3-Transect 4 of the Mfabeni wetland

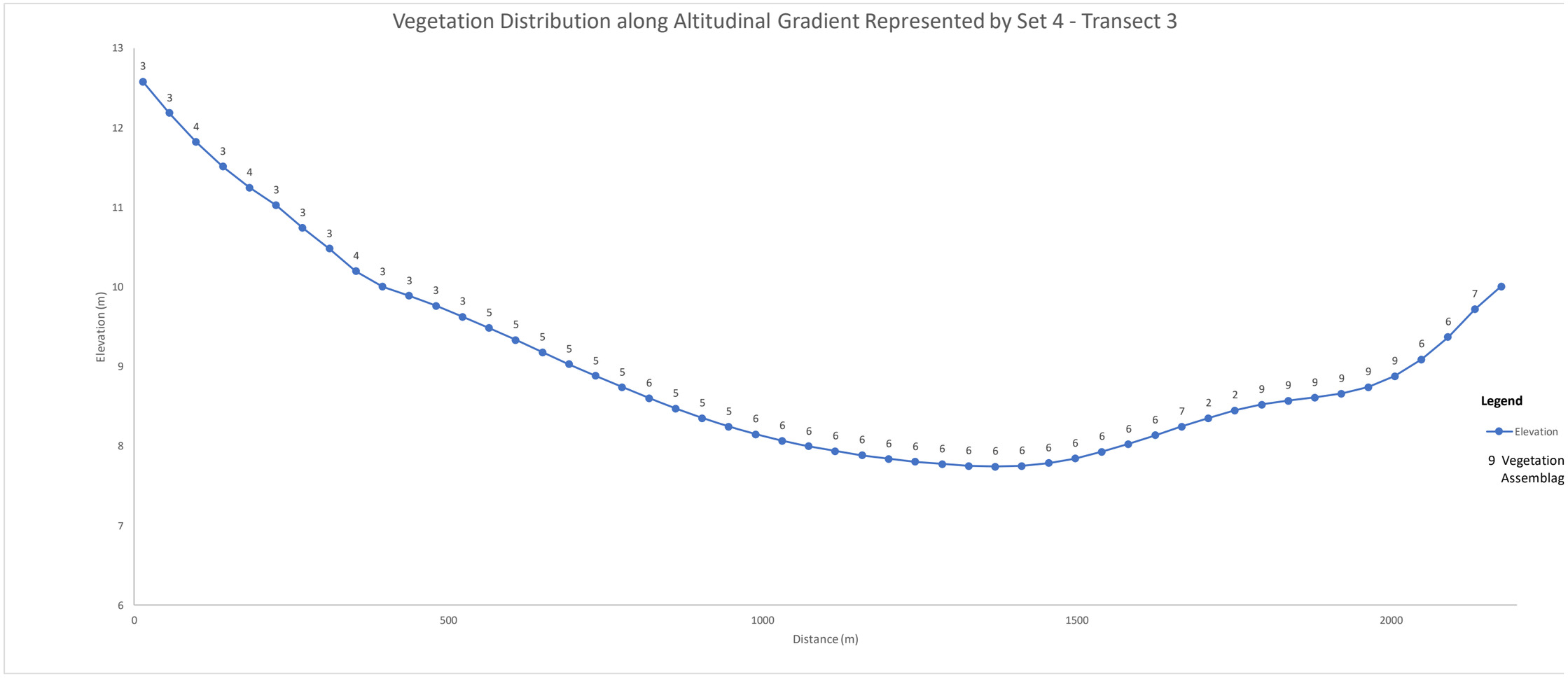

Figure 6.28(d): Line profile showing distribution of vegetation assemblages along Set 4-Transect 6 of the Mfabeni wetland

6.13 Relationship between Elevation change and Vegetation Moisture in Mfabeni Wetland

Figure 6.29 shows a Moisture Stress Index (MSI) image of the Mfabeni wetland generated using equation 5.2. The MSI was repetitively computed to create an image with different moisture classes. The blank areas (white) on the image represent MSI values of greater than 2.

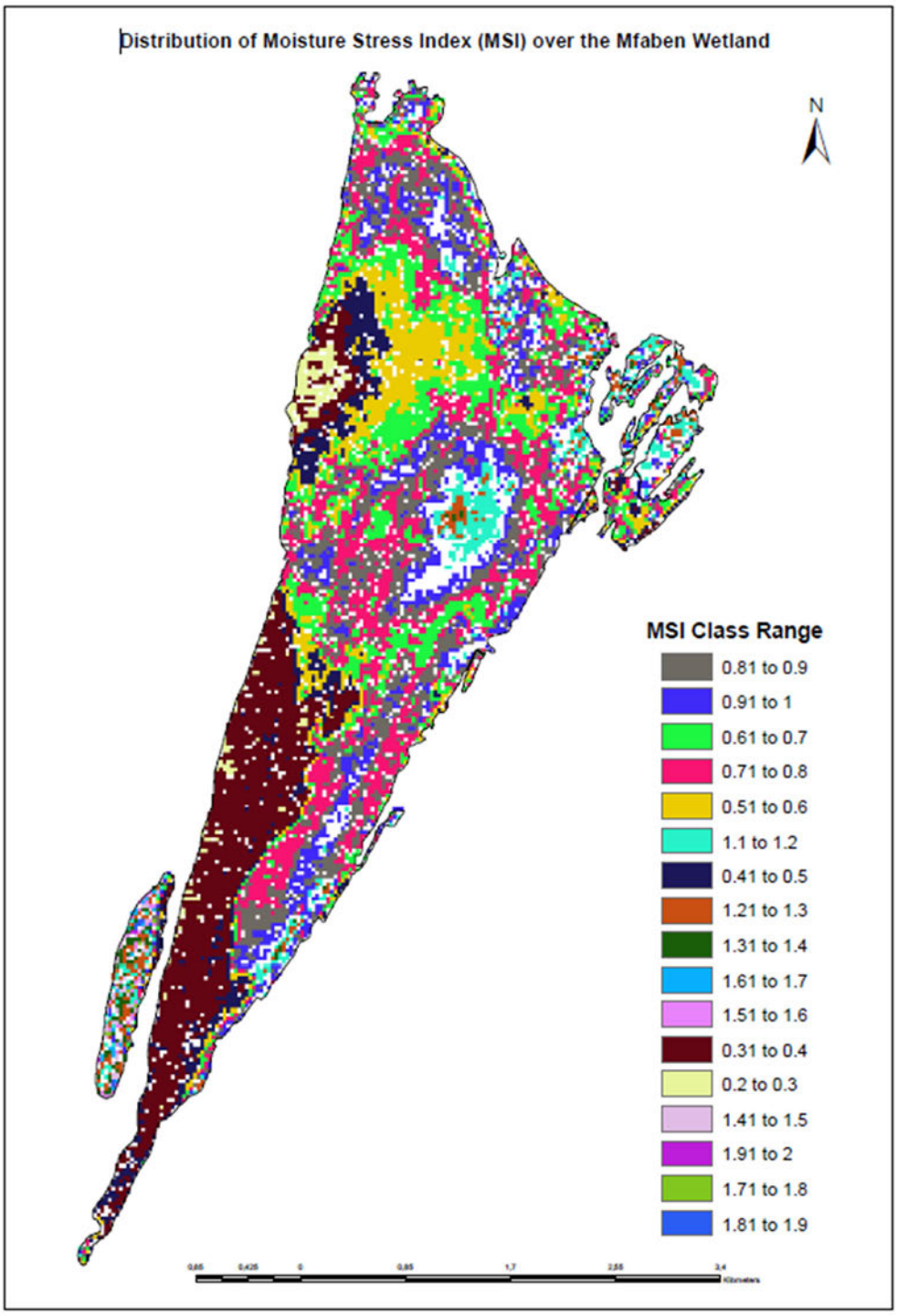

Figure 6.29: Vegetation Moisture Stress Index (MSI) Distribution over the Mfabeni wetland

For comparison with elevation change and vegetation assemblages' spatial distribution, the image was reclassified to create an image with three classes; namely highly moist (MSI, 0.1 – 0.5), moderately moist (MSI; 0.51 – 1.0) and less moist (MSI greater than 1.0) (figure 6.30).

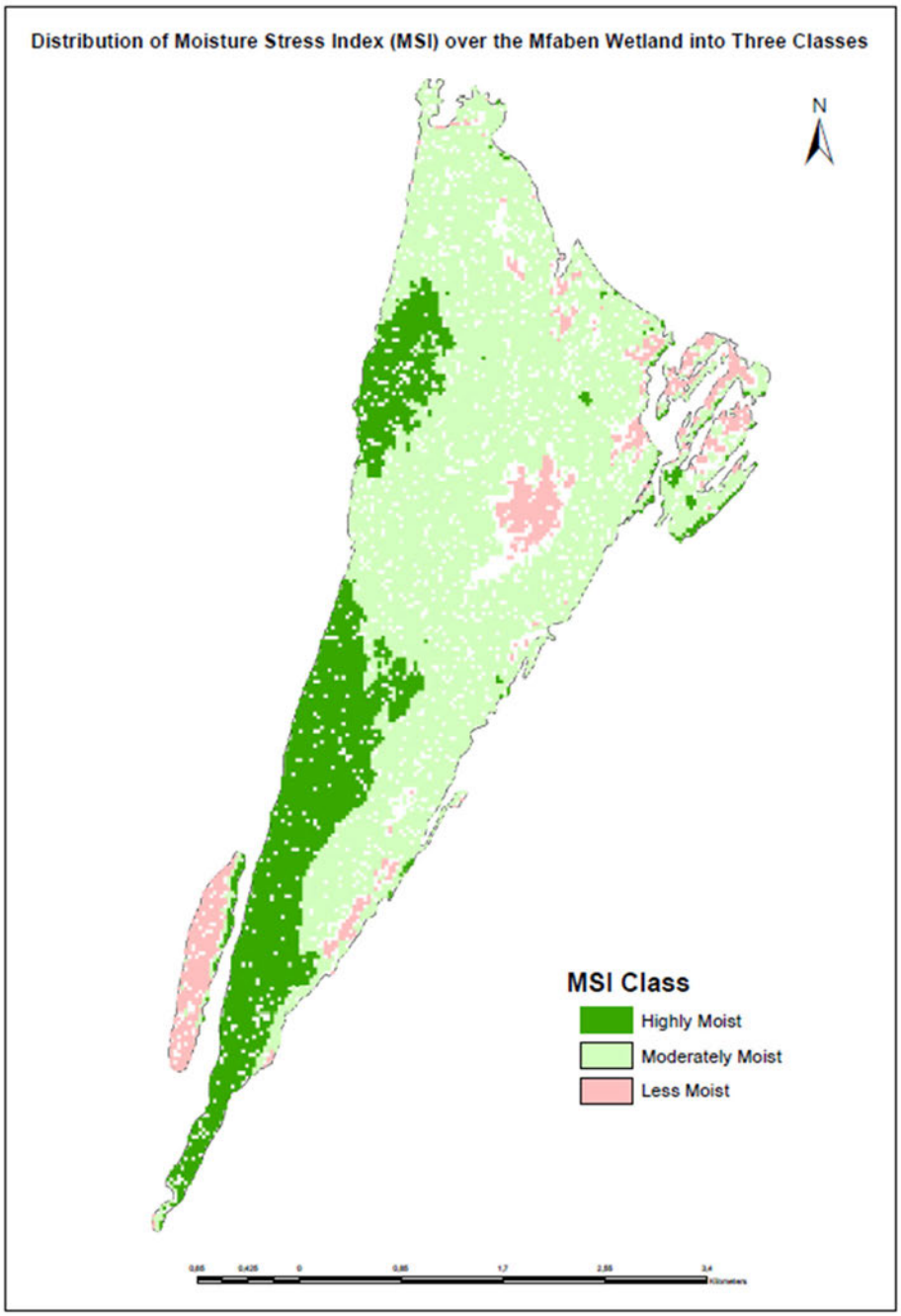

Figure 6.30: Distribution of Vegetation Assemblages in terms of Moisture Stress Index (MSI) Into three classes.

The results of an overlay of point files depicting centroids of the classified MSI with elevation undertaken to explore the relationship between MSI and elevation are presented in Table 6.19.

Table 6.19: Relationship between Elevation and MSI classes

Elevation	MSI			Grand Total
	Highly Moist	Moderately Moist	Less Moist	
6	350	85	24	459
7	483	1681	90	2254
8	632	2676	197	3505
9	1081	3286	547	4914
10	451	1201	130	1782
11	235	97	53	385
12	153	18	19	190
13	20	11	1	32
14	6	2		8
Grand Total	3411	9057	1061	13529

Table 6.19 shows that there was no positive correlation between moisture condition and elevation. High moisture areas did not appear to have been restricted to areas with lower elevation values. The majority in fact existed at medium elevation with the least at high elevations. As moisture was derived from the vegetation assemblages. It can be deduced that there is equally no positive correlation between vegetation assemblages' distribution and elevation.

Table 6.20 shows a similar table for the overlay of points depicting centroids for MSI and vegetation assemblages.

Table 6.20: Relationship between Vegetation Assemblages and MSI classes.

Vegetation Assemblage	MSI			
	Highly Moist	Moderately Moist	Less Moist	Grand Total
0		9		9
1		185	314	499
2	1	2015	281	2297
3	1505	5	1	1511
4	854			854
5	886	159		1045
6	156	3000		3156
7	1	711	38	750
8	7	683		690
9	1	2261	3	2265
10		29	424	453
Grand Total	3411	9057	1061	13529

Table 6.20 shows the different moist conditions the vegetation assemblages thrived in. Vegetation assemblages 3, 4 and 5 appeared to have predominantly thrived under highly moist conditions with 4 in fact not thriving under other moisture conditions. Vegetation assemblages 2, 6, 7, 8 and 9 appeared to predominantly thrive under moderately moist conditions. Only vegetation 1 and 10 could be said to be predominant under less moist conditions.

Figure 6.31(a) – (c) show results of the Mfabeni wetland vegetation assemblages spatially distributed in terms of the vegetation moisture stress index computed using equation 5.2 and reclassified to highly moist, moderately moist and less moist.

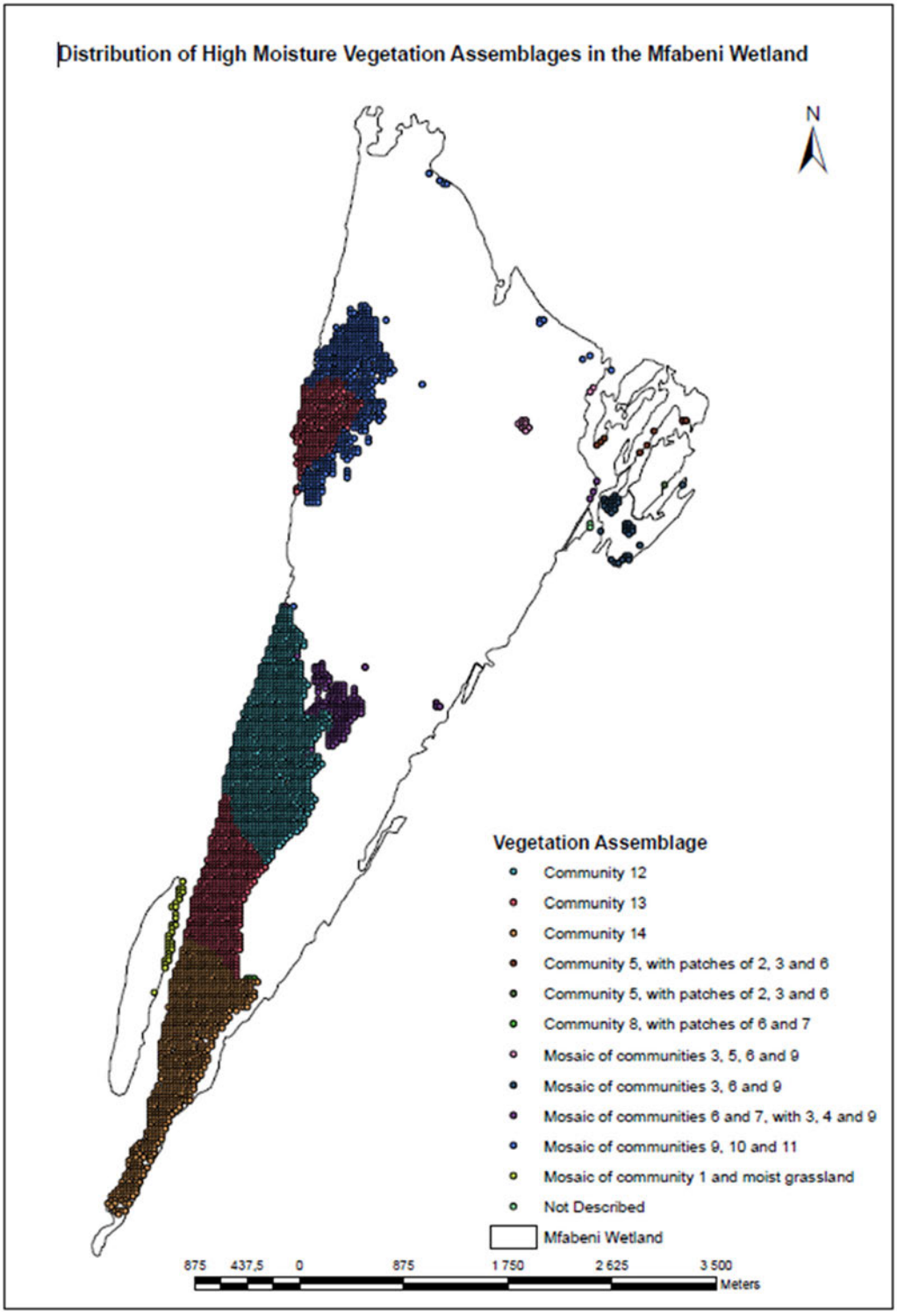

Figure 6.31(a): Distribution of Vegetation assemblages with high moisture content in the Mfabeni Wetland.

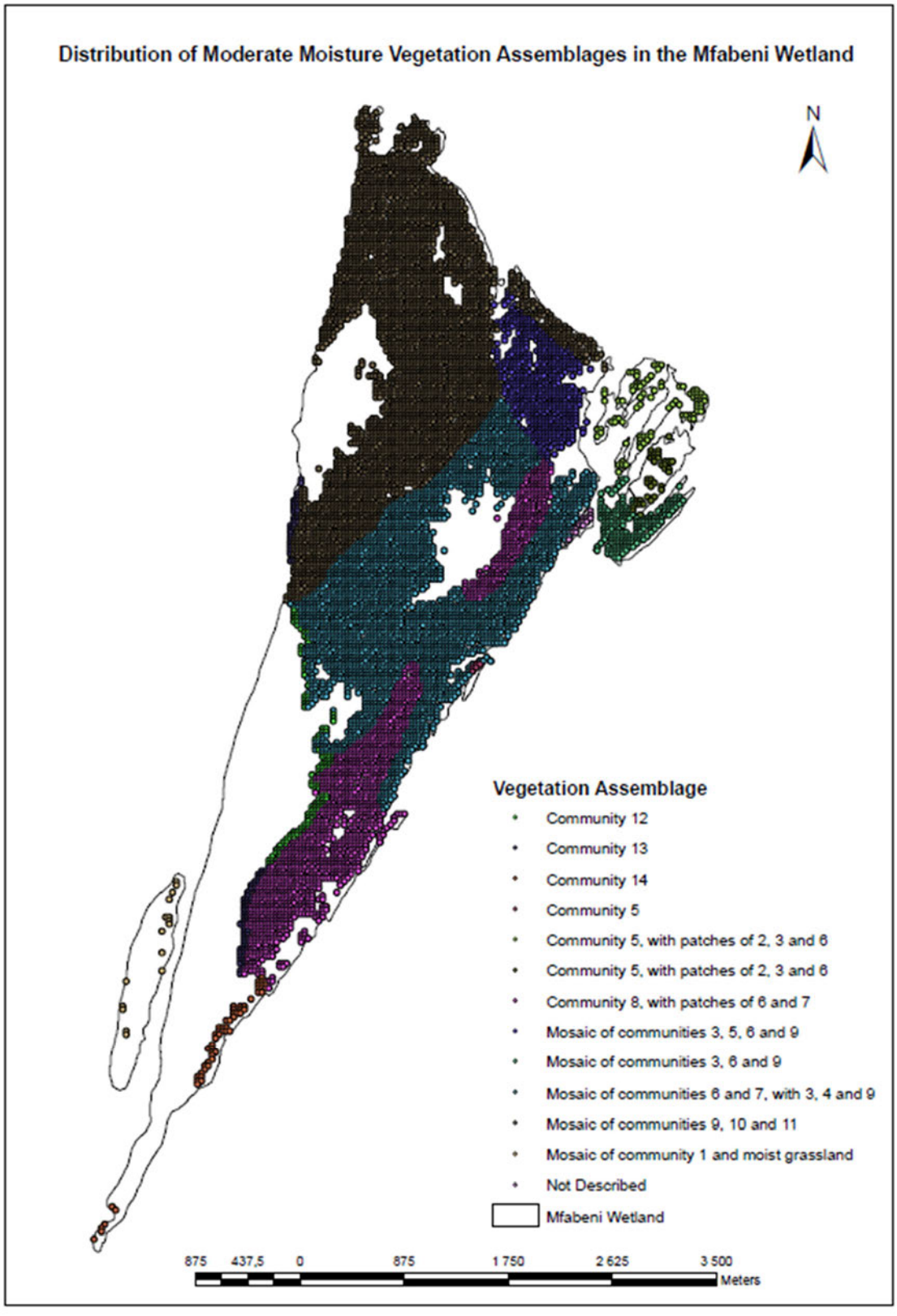

Figure 6.31(b): Distribution of Vegetation assemblages with moderate moisture content in the Mfabeni Wetland.

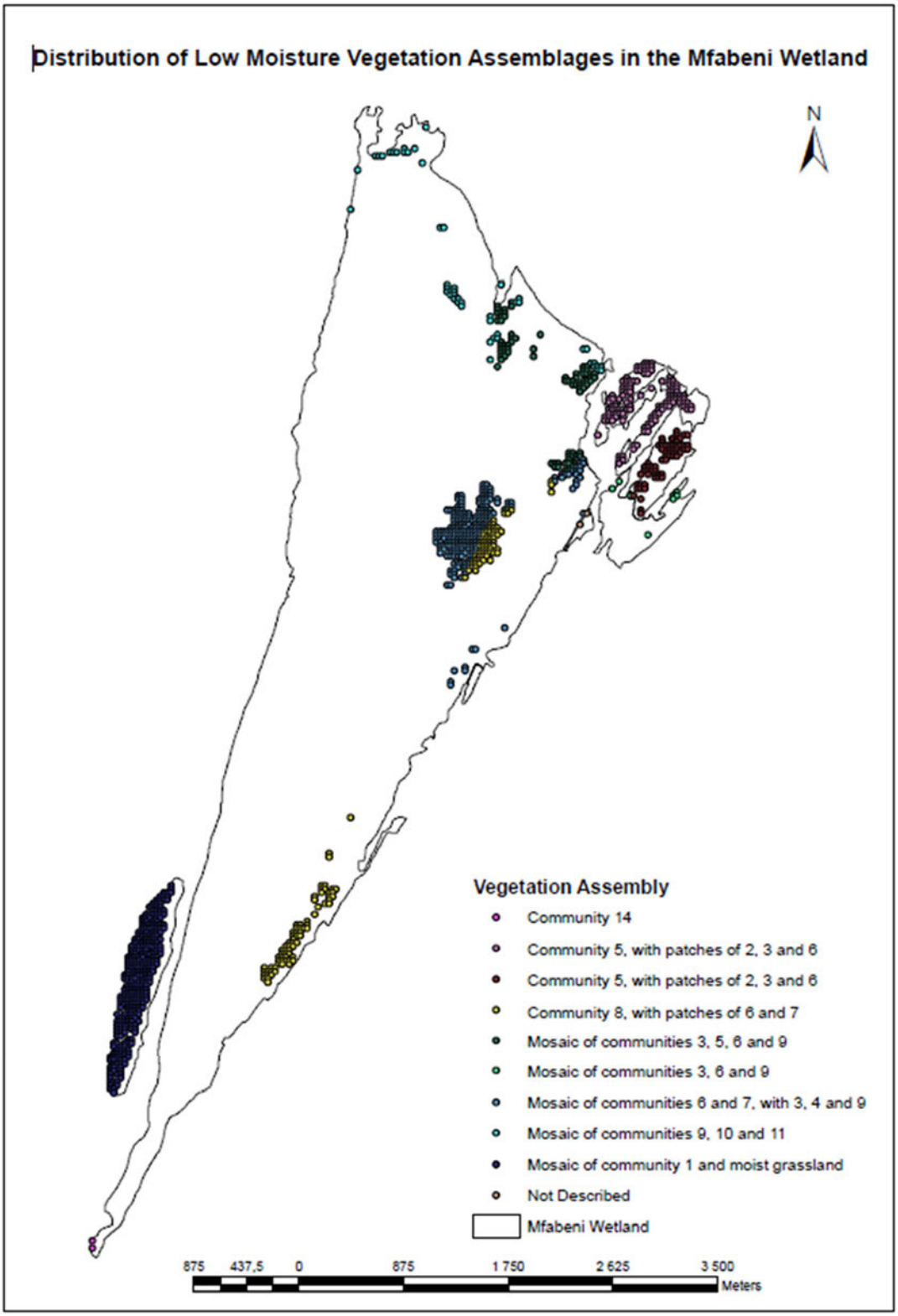

Figure 6.31(c): Distribution of Vegetation assemblages with less moisture content in the Mfabeni Wetland.

An overlay of MSI and vegetation assemblages was expected to have given a true picture of the distribution of vegetation assemblages in terms of the moisture content. A Visual inspection of the original image displayed in true color (figure 5.10) and the MSI image (figure 6.29) appear to show a correlation between areas with greener appearance and those depicted to have had high moisture on the MSI image and vice-versa.

6.14 Chapter Summary

This chapter presented the results obtained from the various stages of the research execution, inclusive of the Hyperion imagery geometric corrections, vegetation assemblages' classes, apparent surface reflectance Hyperion image of the Mfabeni wetland, training data, spectral library, optimal wavebands identified by means of Random Forest and variable elimination.

The presented results also include images classified using Spectral Angle Mapper and their related post-classification accuracy assessment, inclusive of the classified image identified for characterization of vegetation assemblages in terms of elevation. DEMs generated using various interpolation techniques were also presented along with results of their accuracy assessment and the subsequent validation to identify the most suitable used for the characterization of vegetation assemblages.

The combined image obtained from the overlay of the identified classified vegetation assemblages' image and the DEM identified as most suitable was also presented along with various maps showing the distribution of vegetation assemblages in terms of elevation. Using the resultant image from this combination and accompanying attribute data, various profiles aligned with randomly created transects of different orientations were created, showing the distribution of vegetation assemblages along the altitudinal gradient of the Mfabeni wetland.

Results of the relationship between the elevation, vegetation assemblages and the moisture distribution of the Mfabeni wetland determined as vegetation Moisture Stress Index (MSI) was established and presented as maps and tables.

With the results presented in this chapter, the subsequent chapter discussed their implication.

Chapter 7

Discussion

7.1 Introduction

This research was born out of the need to investigate the effectiveness of satellite hyperspectral sensing in discriminating among various wetland vegetation assemblages thriving along an altitudinal gradient. In an attempt to do so, the research question formulated as;

> *How can satellite hyperspectral imagery be used to characterize wetland vegetation in terms of the hydrological regime by indirectly relating spatial coverage of vegetation assemblages to change in Elevation?*

was answered by investigating three subservient questions, structured as;

1. *Can wetland vegetation assemblages of the Mfabeni wetland be distinguished on the basis of spectra extracted from the Hyperion image pixels?*
2. *Is there a relationship between the classification accuracy obtained using random forest and the post-classification accuracy of the classified Hyperion image of the Mfabeni wetland?*
3. *Can the distribution of wetland vegetation along an altitudinal gradient be explained in terms of its hydrological regime by indirectly relating it to change in elevation?*

The relevant data were collected and georeferenced where required. Classes representing vegetation assemblages were formulated, and the Hyperion image of the Mfabeni wetland radiometrically pre-processed to obtain an apparent surface reflectance image.

Training data for subsequent classification of the Hyperion image were created using two approaches; extracting spectra of contiguous image pixels inside each of the defined classes representing vegetation assemblages to create Regions of Interest (ROI) on one hand and extraction of spectra of randomly selected pixels inside each of the classes, on the other. The training data created using the former approach was subjected to a spectral separability assessment using two parameters built into ENVI, namely, Jeffries-Matusita and Transformed Divergence values. The training data obtained using the latter method was processed in two different ways; namely, obtaining class spectral means used to create a spectral library and to identify the most suitable (optimal) wavebands, using Random Forest and Variable Elimination, for subsequent classification of the Hyperion image.

Image classification of the Hyperion image was performed using the Spectral Angle Mapper (SAM) algorithm, allowing for the use of various spectral angles of separation (0.1 - 0.9 radians) in order to identify one capable of producing the best results. Identification of the most accurate classified image was achieved by means of post-classification accuracy assessment performed on each of the classified images using the percentage overall accuracy as a determinant.

A DEM of the Mfabeni wetland was generated from a 5m interval contour layer compiled by the NGI and subsequently assessed for accuracy and validated with the help of spot heights of the area, also compiled by the NGI.

The distribution of the vegetation assemblages in terms of elevation was then assessed using the classified image and DEM identified in the earlier steps. This was then followed by an assessment of the spatial distribution of vegetation along elevation profiles corresponding to a number of transects of different orientations created across the Mfabeni wetland.

As a means of validating the results obtained, an evaluation of a correlation between elevation and vegetation Moisture Stress Index (MSI) was undertaken on the one hand, and MSI and vegetation assemblages on the other. Vegetation assemblages were ultimately mapped in terms of three MSI classes, namely High Moist, Moderately Moist.

7.2 Datasets

Hyperion hyperspectral imagery was used as the satellite imagery for this research. The choice to use Hyperion imagery was deliberate so as to investigate the use of hyperspectral imagery collected from space for wetland vegetation mapping. Once the mission had been extended to provide hyperspectral data due to popular demand, imagery could only be obtained by means of Data Acquisition Requests (DAR). Three attempts were made available for each data request to capture the requested imagery, failure to which it would not be captured. The requester was only informed of the imagery availability once it had been captured. This posed a challenge for the collection of associated field data, especially for time-critical applications such as for this research.

Field spectral measurements of vegetation assemblages and other related data, therefore, were only collected close to two weeks following imagery capture due to time delay in receiving communication of its capture as well as field trip preparation logistical constraints. (Govender M et al., 2008), however, support a difference of up to 15 days between imagery capture and field campaign for vegetation ground-truthing data collection provided no severe disturbance to the

vegetation occurs between the dates of image capture and field data collection. Inquiries made to establish whether there had been any serious event such as heavy rains in the area over the concerned period revealed that there had been none. Hyperion imagery was therefore intended to be processed with the assumption that the time-lapse between the dates of imagery capture and ground-truthing field campaign did not negatively impact the quality of data and the results obtained. It was equally assumed that the Hyperion imagery being the only satellite-based hyperspectral imagery freely in circulation at the time of the research, the approach used in its processing its processing to obtain the envisaged results could be relevant to any other hyperspectral imagery, space or aerial based, subject to customization for imagery specific requirements.

The constraints associated with field data collection, particularly the fact that a security official to accompany the researcher was only made available for three days, implied that field data could only be collected for a maximum period of three days. With the first two days of field data collection having been spent at other sites (sites 1 and 2 on figure 5.3), the single day of data collection spent in the Mfabeni wetland was not enough to collect data capable of being used for meaningful and reliable results.

A vegetation map of the Mfabeni wetland compiled by (Venter, 2003), the only most detailed vegetation map of the area available at the time of conducting this research, was used as a secondary source of reference data.

The elevation data in the form of the Shuttle Radar Topography Mission (SRTM) Digital Elevation Model (DEM) though available was not used for the final processing due to its low spatial resolution of 30m when applied to a gently undulating wetland such as the study area for this research. The elevation data used was generated from a 5m interval contour layer and assessed for accuracy using spot heights of the same area.

7.3 Discussion of Results

The Hyperion imagery L1T format was used for processing in this research. While L1Gst could have been equally used, its geometric accuracy is sometimes considered questionable due to the fact that even though it was systematically geometrically corrected, no ground control points were used. L1T was geometrically corrected by use of ground control points.

The L1T format for the Hyperion image used for this research is supplied geometrically corrected using ground control points picked from the area covered by the scene (Kumar and Yarrakula, 2017). The L1T is arguably considered much more geometrically correct than the other Hyperion imagery formats. Despite this affirmation, L1T geometric accuracy was validated using clearly identified check points on a ring road (figure 5.8) located around the Mfabeni wetland obtaining a RMSE of 3.08248m. This result is far more accurate than the maximum 15m geometric accuracy expected of a 30m resolution image such the Hyperion judging from the fact that the maximum acceptable geometric accuracy of registering an image is half the spatial resolution. The results, could be this good because the area is relatively flat and that the control points originally used to register the L1T to the spatial reference system must have been accurately picked.

Existing literature supports the use of L1Gst as a reference for performing geometric correction of LIR (Adiri et al., 2020, Canbaz et al., 2021), however. This is confirmation that L1Gst is fairly geometrically accurate though systematically geometrically corrected based on locations derived from spacecraft ephemeris data with terrain correction based on a 90-meter Digital Elevation Model (DEM) for topographic accuracy (USGS-EROS, 2021), implying that its geometric accuracy should be acceptable, especially in the absence of the L1T format imagery.

No georeferenced digital map was readily available for use to define classes for the Mfabeni wetland vegetation assemblages. A digital image of the vegetation map had to be registered to the spatial reference system of the topographic base map and then spatially transformed to the spatial reference system of the Hyperion image. The RMSE of 0.812802m obtained in this image registration process was considered satisfactory as the maximum allowable for Hyperion imagery should be 15m. Accordingly, the RMSE for the accuracy of the classes digitized to represent vegetation assemblages was equally considered acceptable.

FLAASH used to correct the Hyperion image atmospheric effects was considered the most suitable of the various models available in ENVI software for creating an apparent surface reflectance image. Its choice was informed by a comparative study undertaken by (Rani et al., 2017, Somdatta and Chakrabarti, 2011). The study investigated the use of QUAC and FLAASH for atmospheric correction on hyperspectral imagery. FLAASH was found to be better, and thus, its use for atmospheric correction and correct interpretation and identification of composition of any object or minerals was recommended over QUAC. FLAASH is further considered suitable because it employs the full MODTRAN radiative-transfer code to model the scattering and transmission properties of the atmosphere at the time of image capture. It also fully accounts for adjacency effects (the scattering from adjacent pixels into the current pixel-sensor line of sight) associated with atmospheric scattering.

The two approaches used to obtain the training data for classification of the Hyperion image of the Mfabeni wetland, despite being different, use the mean of the collected spectra as representative (reference) spectra of the concerned class. The mean of the image pixels extracted spectra for each class was computed directly and stored as endmembers in the spectral library created in the first approach. The spectral extracted as a collection of one or multiple regions of interest (ROI) for each class were also used to obtain the mean of the class spectra in the other approach. The only difference is that, in the latter, the algorithm does so without the user's involvement. In both cases, the difference is only in terms of the actual values assigned to each waveband that make up the reference spectra. Consequently, the differences in classified images based on these mean spectra, all other things being equal, can only be attributed to the differences in the training data. An analysis of spectral separability performed on spectra created from the ROI of contiguous pixels using the Jeffries-Matusita and Transformed Divergence values showed very poor separability between various class pairs (table 6.2). A value of at least 1.9 was required for the classes to be considered spectrally separable, and those between 1 and 1.9 should have their ROIs either edited or dropped and new ones defined instead. ROIs with separability values of less than 1 should be combined into a single ROI (Wicaksono and Aryaguna, 2020). A look at table 6.2 shows that several class pairs would have been combined, pointing to the non-homogeneity of the vegetation assemblages. This was not done, however, to avoid reducing the number of vegetation assemblages to be mapped. Instead, they were allowed to be used as such in the classification of the Hyperion image of the Mfabeni wetland, though it was clear that some of the classes mapped separately should have been combined on the basis of the spectra similarity. This was not surprising as the vegetation communities on the map (figure 5.9) show the existence of certain sub-vegetation communities in multiple vegetation assemblages. The display of the n-D visualizer of the digitized ROI (figure 6.4) also showed that it was clearly not feasible to easily separate spectra of some of the vegetation assemblages.

The training data created from spectra of the randomly sampled image pixels, having not been defined as ROIs, could not be checked for spectral separability. Instead, they were used to create a spectral library. A spectral library created was based on class spectra means. When visualized using a spectral library viewer (figure 6.6), all curves exhibited very similar shapes characteristic of vegetation with the exception of that for class 10, which displayed lower in the 500 – 1500 nm region compared to all other bands. With these curves as endmembers depicting vegetation assemblages, it was obvious that mapping vegetation assemblages effectively would be challenging, requiring special techniques for separating spectra.

RF and variable elimination techniques were used as data dimension reduction techniques, and in so doing, identifying optimal wavebands for Hyperion image classification by eliminating redundant correlated wavebands and avoiding the 'curse of dimensionality' (Merentitis et al., 2014). The most optimal model for the subsequent selection of optimal bands was identified using RF classification. The choice of RF over other Tree ensembles being informed by its popularity in providing better predictive accuracy for both classification and regression (Ismail and Mutanga, 2009). The most optimal RF classification models with the lowest OOB estimate of error (Khan et al., 2021; Liu et al., 2021) were identified separately by means of optimization accomplished through an iterative process of nTree and mTry. Two (2) models, '500 by 6' and 6500 by 5' (table 6.5) with the lowest OOB estimate of error value of 27.86% (72.14% accuracy) were identified, from which the '500 by 6' was identified as the most optimal based on validation process based on the training, test, validation and full data sets.

The nTree and mTry combination that produces the best model has been established to vary. (Odebiri et al., 2020) recommend the use of 100 – 500 nTree and square root of the variables number for mTry except when data has noise, in which case the mTry could be increased. (Thabeng et al., 2019) used 500 to 10000 nTree in 500 intervals with mTry of 1 to 8. In this research, a different range was used for both nTree and mTry (table 6.5).

Change in OOB Estimate of Error with change in mTry for a given nTree and conversely change in OOB Estimate of Error with change in nTree for a given mTry were explored exhaustively to confirm that no OOB accuracy lower than that obtained for the used dataset existed. Graphs depicted in figures 6.7 and 6.8 were used to observe the change in the OOB estimate of error for a given nTree as mTry changed and conversely for a given mTry as nTree changed. Models that exhibited a downward or near downward trend for the used maximum nTree and mTry were meant to be extended further to check their performance beyond the maximum value used. This was considered necessary to ensure that none represented a model with OOB estimate of error less than the minimum obtained already (Chilufya et al., 2014).

Results obtained from RF classification satisfied the accuracy other researchers have obtained. (Fraser and Congalton, 2021) obtained an OOB error of 29.38%, giving an accuracy of 70.62% in Monitoring Fine-Scale Forest Health Using Unmanned Aerial Systems (UAS) Multispectral Models. (Worsham, 2020) obtained OOB error of 27.8% in An Examination of an Enhanced Remote Sensing Method for Agent Attribution of Forest Disturbance.

The ‘500 by 6’ model having produced marginally better results than the 6500 by 5 was adopted as the better of the two optimized models and hence was used to identify the wavebands most suitable for discriminating among the vegetation assemblages. Their performance being so close to each other, however, leaves the concern that both should have been investigated further. It is the wish of the researcher that in the circumstances where the results of the models' performance are close to each other, all the involved models be investigated to identify one that produces wavebands with the best image classification results.

The order of importance of variables given by the 'mean decrease accuracy' (MDA) for the optimal ‘500 by 6’ RF classification model was used as a means of identifying the wavebands critical to the discrimination of vegetation assemblages. The associated wavebands accordingly were identified as the most optimal in the order they were listed. The top 30 of these wavebands ranked according to variable importance for RF classification (MDA) were as provided in appendix 6.3 while figure 6.10 shows their spectral location when plotted over the spectral range 426.82 – 2375.3nm.

According to (Adam and Mutanga, 2009) the optimal wavebands identified using RF classification did not automatically select the optimal number of variables that produce the best accuracy when used for classification. The most optimal of the wavebands obtained from RF classification model, therefore, were determined using the variable elimination method. Backward variable elimination (stepwise based) and Akaike Information Criterion (AIC) (criterion-based) were used. The wavebands identified as common to both and that identified by the AIC were considered optimal and used in the subsequent spectral matching by supervised classification. All wavebands identified by the backward stepwise variable elimination method were identified by the AIC. Backward variable elimination selected 11 wavebands and AIC 16 wavebands from the 30 optimal wavebands selected with RF classification at a significant level of less than 0.05 (figure 6.11, figure 6.12; table 6.7 and appendix 6.4) and a cut-off of 1697.59 (figure 6.13, figure 6.14 and appendix 6.5) for backward variable elimination and AIC respectively. These bands were subsequently used separately for spectral matching.

Comparison of variable elimination and results from RF classification confirmed the order of variable importance provided by RF as not necessarily corresponding to the statistical significance of each waveband in discriminating among different elements (table 6.8) in agreement with (Adam and Mutanga, 2009).

The various classified images created using the Spectral Angle Mapper (SAM) algorithm were done in an effort to establish the approach, spectral angle of separation, and number of wavebands capable of producing a classified image with the best accuracy. In terms of the approach, classified images included that based on training data created using the conventional approach of digitizing areas of contiguous pixels as Regions of Interest (ROI) and that based on spectra randomly extracted from the images as pixel spectra. The spectral angle of separation between classes used ranged from 0.1 – 0.9 radians in steps of 0.1 radians. The bands employed included all 175 that remained once zero and strong water absorption bands had been removed as well as the optimal 11 and 16 wavebands obtained from the backward stepwise and AIC variable elimination methods performed on the 30 wavebands selected by RF classification. The classified images obtained were compared in terms of these parameters and, ultimately, one with the best classification accuracy adopted for subsequent characterization of the vegetation assemblages in terms of elevation.

Table 6.9 shows the difference in the pixel count and associated percentages allocated to each of the classes depicting vegetation assemblages when the two approaches were applied based on the same number of wavebands and the same spectral angle of separation. The differences were quite significant for classes 7, 2, 5, and 3 in that order. For the rest of the wavebands, the differences were quite low. It was also noticed that differences were both positive and negative, implying that one method allocated more pixels to a class in one instance and fewer in the other. Based on the same number of wavebands and spectral angle of separation, the difference can only be attributed to the difference in the mean spectra used as reference spectral for assigning pixels to each class.

The differences in the pixel count and associated percentages among the classified images obtained using different spectral angles of separation given in table 6.10 show that there is a threshold spectral angle of separation beyond which there is either no or insignificant difference in pixels assigned to the classes. Such a threshold value was found not to be the same for different image classification results based on different methods of classification and the number of wavebands used. One way of establishing such a threshold used in this research was to repetitively adjust the spectral angle of separation until there was no difference in the overall accuracy of the post-classification accuracy assessment results between two consecutive classified images. It was further noticed that even when the overall accuracy value remained the same, the re-assignment of pixels between different classes continued (tables 6.13 and 6.14), albeit small in number, hence affecting the producer's and user's accuracies. The spectral angle of separation value that first produced the best overall accuracy, therefore, was adopted as the threshold.

The pixel count and associated percentages in table 6.11 show that there were differences among the three classified images based on different numbers of wavebands. The differences are not easily discernible by simply looking at the images themselves, which otherwise visually looked very similar. The best of the three images was also only established by means of accuracy assessment.

The percentage overall accuracy values presented in table 6.12 show that there were multiple instances where the values remained the same. The exact spectral angle of separation at which the first best overall accuracy occurred for each listed number of bands and the approach used differed somehow. For the conventionally extracted training data, they occurred at 0.5 radians for all numbers of wavebands used. For the image pixels-based training data approach, they occurred at 0.6, 0.7, and 0,5 for all 175 bands, 11 optimal bands, and 16 optimal bands, respectively. This serves as confirmation that it is difficult to know in advance which spectral angle of separation would be most suitable for a given dataset.

Various DEM interpolation techniques were used in an effort to identify one that represented the topography of the Mfabeni wetland the best. A total of 844 checkpoints used was considered sufficiently large in agreement with (Höhle and Höhle, 2009). An inspection of the results of the accuracy assessment, however, demonstrated that the DEM with the best values for the accuracy measures faired poorly when assessed using checkpoints located inside and close to the wetland. These rather unusual results are supported by previous research, which indicates the accuracy of DEM to be affected by various factors, inclusive of terrain morphological characteristics such as slope (Liu et al., 2020). Furthermore, certain interpolation techniques are known to perform better under certain conditions than others. The poor accuracy assessment results can also be attributed to the fact that the checkpoints used are spot-heights which are salient points and hence prone to significant errors. According to (Höhle and Höhle, 2009), checkpoints located along break lines, at steep slopes, at the position of a sudden slope change, close to the building, etc., may lead to large errors.

An overlay of the adopted suitable classified image of vegetation assemblages (figure 6.18) over the Mfabeni wetland DEM (figure 6.19) generated an image with 77 different combinations between vegetation assemblages and elevation (figure 6.21).

Based on figure 6.21 and associated statistical data (table 6.16), the distribution of vegetation assemblages over each elevation value was displayed spatially in the form of maps (figures 6.23(a) – 6.23(i) and numerically quantified in terms of the pixel count (table 6.17), in relation to elevation.

Based on the results presented in figures 6.23(a) – 6.23(i) and table 6.17, the following were established about the distribution of Mfabeni wetland vegetation assemblages in relation to elevation;

i). The wetland analyzed consisted of a total of 17434 pixels equivalent to approximately 1569 Hectares (Ha) spatial coverage.
ii). no single vegetation assemblage existed exclusively at any given single elevation occupied by the wetland.
iii). Vegetation assemblage represented by class 6 was the most dominant in Mfabeni wetland, accounting for 3748 pixels (337 Ha)
iv). Vegetation assemblage 10 was the least dominant in Mfabeni wetland, accounting for 643 pixels (58 Ha).
v). The majority of vegetation assemblages, represented by a total pixel count of 5804 thrived at an elevation of 9m of the wetland followed by that at 8m with a pixel count of 4129.
vi). The least number of vegetation assemblages occurred at 14m with a total pixel count of 9 followed by 13m with a total pixel count of 40.

Transects of superimposed points of vegetation assemblages and elevation made out of pixel centroids and established at different orientations (figures 6.25 and 6.26 (a) – (d)) for extracting profiles (figure 6.28 (a) – (d)) and appendix 6.8 to investigate the principle of zonation exhibited characteristics of the idealized elevation gradient along certain transects. An analysis of the distribution of vegetation assemblages along an altitudinal gradient aligned with these transects revealed inconsistencies in the distribution of vegetation assemblages along the Mfabeni wetland elevation gradient.

The profile in figure 6.28(a) for example, showed vegetation assemblage 6 as dominant in the trough (lowest elevation), but appeared present on the incline towards the right side of the trough while to the left side of the trough there was vegetation assemblage 5 existing at the same elevation as vegetation assemblage 6 to the right. Figure 6.28(c) shows a mix of vegetation assemblages 6, 7 and 2 both in the trough and on the incline. An inspection of many other profiles showed the similar varying pattern.

Soil moisture measurements originally meant to be collected in the field as part of the ground truthing data were intended to be used to characterize wetland vegetation in terms of the hydrological regime. The soil moisture measurements should then have been compared with elevation to establish whether the envisaged relationship existed. In the absence of such soil

measurements, the vegetation moisture stress index (MSI) distribution was used to establish a relationship with elevation and then with the vegetation assemblages' distribution.

Based on the results in (table 6.19) it was deduced that there was no correlation between MSI and elevation. It had been anticipated that areas at lower elevations should have lower MSI values corresponding to areas with lower reflectance due to high moisture content as these are not only expected to hold moisture longer but that they should be closer to underground water sources; hence they, should remain moist most of the time. Similarly, areas on high ground (high elevation) should have higher MSI values indicative of lower moisture content.

A similar assessment between MSI and vegetation assemblages (table 6.20) showed that some of vegetation assemblages existed across two moist conditions with others across all three, differing only in quantity. Vegetation assemblages 6 and 10, for example, had dominance under moderately moist and less moist over highly moist and moderately moist conditions respectively, while assemblages 2, 3, 7 and 9 showed presence at all moist conditions. Vegetation assemblage 4, however, was only present under highly moist conditions.

(White, 2007) used MSI to establish a significant correlation between moisture in vegetation and levels of pine beetle damage. MSI and other remotely sensed-based moisture indices have been used in various studies (Kureel et al., 2022, Zhang and Zhou, 2019, Khellouk et al., 2020). In this research, it was envisaged that areas at lower elevations should have more water, and hence vegetation thriving at these elevations should exhibit more moisture with the consequence that reflectance would be low. Accordingly, the computed MSI values over these areas should be less in comparison to high-elevation areas with less water and hence high MSI values.

7.4 Limitations

The methodology employed in this research is capable of delivering reliable results. The reliability of the results obtained, however, are subject to various factors, predominantly, the questionable accuracy of the Mfabeni vegetation map used as a secondary source of reference data.

The vegetation map was compiled using unrectified aerial photographs and field data obtained using a sampling approach which the researcher admitted to have been challenging due to the mixed nature of vegetation communities which left no choice, but to place sample plots in areas where the vegetation was relatively homogeneous and where it differed visibly from the other adjacent areas (Venter, 2003). There was further stated that differences in vegetation often

occurred over a very small area and that this variation could not be observed on the aerial photographs used (Venter 2003).

These shortcomings inevitably resulted in a vegetation map that clearly showed overlaps in plant species found to be present across multiple mapped vegetation communities. While these overlaps were apparent, there were no attempts made to combine vegetation communities for the purpose of this research as this inevitably could have resulted in manipulation of the source reference data. The vegetation map was therefore used with the full knowledge of these shortcomings. The consequences of these shortcomings manifested in the resultant classified images which could not be reclassified to avoid tempering with the results. The obtained results may inevitably have been partly responsible for the classification accuracy obtained in this research being lower than is expected for vegetation mapping.

7.5 Chapter Summary

This chapter presented a discussion of the results of the research and their implications. An overview of the datasets used for the research was presented first, and then the results obtained were discussed.

The chapter highlighted the fact that the field data originally collected to serve as ground-truthing for Hyperion imagery processing had been found short of providing reliable results and that secondary reference data in the form of a vegetation map of the study area was used instead.

The geometric accuracy of the Hyperion image used for the study was checked and validated. Similarly, it was highlighted that while the use of secondary data implied that there was no need to use apparent surface reflectance values of the Hyperion image, as a comparison with field-measured spectra was not required, an image with apparent surface reflectance values was created because the Spectral Angle Mapper (SAM) algorithm used for classification performs optimally when used on reflectance data. FLAASH as the preferred model used for atmospheric correction to generate an apparent surface reflectance Hyperion image of the Mfabeni wetland required for vegetation characterization was also presented, but its accuracy was not evaluated.

Vegetation assemblage classes were formulated according to the conventional approach of assigning a number to each vegetation assemblage and the requirement that a minimum number of pixels be met to constitute a class was observed. Consequently, one vegetation assemblage did not meet a minimum of 50 pixels considered suitable for proper processing. The two approaches for extracting training data employed in this research were discussed and how the resultant data

was employed in the development of a spectral library and the identification of optimal bands relevant for image classification.

The resultant classified images were subjected to an accuracy assessment to identify the most accurate, which in turn was overlain with the most accurate DEM to obtain a combined image used for the characterization of vegetation assemblages in terms of elevation. The combined image created from this image and the corresponding DEM along with the accompanying statistical data were used to analyze the relationship between the Mfabeni wetland vegetation assemblages and their elevation.

The profiles made across the wetland exhibited similarity to the idealized altitudinal gradient at certain locations and orientations. Hence it was possible to investigate the principle of zonation on an altitudinal gradient.

The results discussed in this chapter demonstrated that the methodology employed in this research could be used to confirm the principle of zonation through the characterization of the wetland vegetation in terms of elevation along an altitudinal gradient.

The developed methodology showed that satellite Hyperion hyperspectral imagery could be used to characterize wetland vegetation in terms of the hydrological regime by indirectly relating spatial coverage of vegetation assemblages to change in elevation.

The research established that the topography of the Mfabeni was ideal for directly relating the water table to elevation and so suitable to use elevation as a substitute for the water table. However, validation using MSI demonstrated that elevation did not necessarily correlate with moisture distribution in the wetland, but that it was possible that some vegetation assemblages appeared to have been thriving only where certain moisture conditions prevailed as determined using the MSI.

Chapter 8

Conclusions and Recommendations

8.1 Introduction

Satellite imagery has been used to map different aspects of the earth surface with varying degrees of accuracy. This research investigated the use of satellite imagery, with a particular focus on Hyperion hyperspectral imagery in characterizing wetland vegetation along an altitudinal gradient in terms of the hydrological regime indirectly determined by means of change in elevation. The underlying premise was to use hyperspectral imagery in conjunction with field spectral measurements and hydrological regime determined indirectly by elevation to confirm the principle of shoreline zonation. According to the principle of shoreline zonation, vegetation on the shorelines is closely connected with water levels. In turn, the distribution of animals is related to the zonation of wetland plants. Zonation patterns, hence, summarize much of the spatial variation in wetlands and, therefore can be used as models in the study of wetlands (Schoolmaster Jr and Stagg, 2018).

The original intention was to measure soil moisture at every location or at some representative location in the vicinity of every site where vegetation assemblage spectra were measured. The device for measuring moisture malfunctioned during field data collection, and due to its age, it could not be repaired to be used again during the same field campaign. The study being time critical with field data being collected at the end of the field data collection window recommended (Govender M et al., 2008), it was not feasible to visit the site to collect moisture. Under the circumstances, elevation change was used as an indirect measure of soil moisture content linked to the level of the water table. According to (Haitjema and Mitchell-Bruker, 2005), water level (water table) and the topography are always related, as water table lows occur at surface waters, which in turn occur in topographically low areas. This is especially said to be true in areas with relatively low-permeable and/or anisotropic aquifers subjected to unusually high areal recharge rates and/or areas with shallow aquifers in flat or gently rolling terrain, making the Mfabeni wetland used for this research, an ideal study site.

Vegetation Moisture Stress Index (MSI) distribution for the Mfabeni wetland was also determined based on the same Hyperion image to serve as a proxy for the soil moisture that was never collected.

8.2 Conclusions

The aim of this research was set as; '…. to characterize wetland vegetation distribution along an altitudinal gradient in terms of the hydrological regime determined indirectly from elevation change using satellite hyperspectral imagery'. In order to achieve this aim, three objectives were pursued; (1) To establish whether vegetation assemblages in the Mfabeni wetland could be separated on the basis of the spectra extracted from the Hyperion image pixels, (2) To establish whether there was a relationship between the classification accuracy obtained using random forest and the post-classification accuracy obtained once the Hyperion image has been classified and (3) to investigate the existence of a positive correlation between the distribution of wetland vegetation along an altitudinal gradient and the hydrological regime determined indirectly by means of the change in elevation.

Objective 1: To establish whether vegetation assemblages in the Mfabeni wetland could be separated on the basis of the spectra extracted from the Hyperion image pixels.

This objective was achieved by the development of a Random Forest (RF) predictive model with acceptable accuracy for selecting optimal wavebands in conjunction with variable elimination methods for discriminating among various spectra representing vegetation assemblages. The RF model developed had a 27.86% OOB estimate of error, translating into an accuracy of 72.14% considered acceptable as it matched accuracies obtained for other studies (Fraser and Congalton, 2021, Worsham, 2020).

Objective 2: To establish whether there was a relationship between the classification accuracy obtained using random forest and the post-classification accuracy obtained once the Hyperion image has been classified.

This objective was achieved by comparing the accuracy of 72.14% obtained from the use of Random Forest on image pixels extracted spectra against 48.9657% overall accuracy for the best post-classification accuracy assessment. This significant drop in post-classification accuracy can be attributed to, among other reasons, the similarity in vegetation composition, making up the vegetation assemblages that gave rise to the image pixels spectra used in the classification process. Some of this vegetation existed among multiple vegetation assemblages, as could be seen from the names of the vegetation assemblages (table 5.2). These similarities among vegetation assemblages were supported by poor spectral separability between classes (table 6.2 and figure 6.4). These overlaps between multiple vegetation communities were a result of the difficulties in the sampling process undertaken in the field due to the mixed nature of the vegetation being mapped as acknowledged by (Venter, 2003). The post-classification accuracy assessment would

have been improved had the classes with similar spectra been merged. This was not done in order to allow for the classification without interfering with the vegetation assemblages represented on the Mfabeni wetland vegetation map (figure 4.6).

Objective 3: To investigate the existence of a positive correlation between the distribution of wetland vegetation along an altitudinal gradient and the hydrological regime determined indirectly by means of the change in elevation

This objective was achieved by creating altitudinal gradient profiles (figures 6.28(a) - 6.28(d) and appendix 6.8) along certain transects across the Mfabeni wetland. Some of the profiles conformed to the idealized appearance of an altitudinal (elevation) gradient (e.g. figures 6.28(a), 6.28(c) and 6.28(d)). When analysed for the distribution of vegetation assemblages in terms of elevation, however, an inconsistent pattern was observed.

Figure 6.28(a), for example, showed vegetation assemblage 6 as dominant in the trough (lowest elevation), but was seen to exist on the high elevation to the right side of the trough also, while to the left side of the trough vegetation assemblage 5 existed at the same elevation as vegetation assemblage 6 to the right. Figure 6.28(c) shows some vegetation assemblages co-existing at different elevations. In this case vegetation assemblages 6, 7 and 2 appeared to co-exist both in the trough at lower elevation and on the incline at higher elevation.

A further investigation undertaken to establish whether a relationship between elevation and the hydrological regime existed in the Mfabeni wetland using the vegetation moisture distribution computed as MSI values using the same Hyperion image, in place of field soil moisture measurements which were never collected, showed that no correlation existed (table 6.19).

A similar assessment between MSI values and vegetation assemblages (table 6.20) showed varying results. Some of the vegetation assemblages existed across two moist conditions while others exhibited presence across all three moist conditions, differing only in quantity with vegetation assemblage 4 being an exception thriving under highly moist conditions only.

In conclusion, all the three objectives being achieved, the research aim of characterizing wetland vegetation distribution along an altitudinal gradient in terms of the hydrological regime determined indirectly from elevation change using satellite hyperspectral imagery was therefore achieved.

The aim of the research, having been achieved, implied that the research question and its associated sub-questions were also achieved.

The set hypothesis, *'Wetland vegetation distribution along an altitudinal gradient can be characterized in terms of its hydrological regime by indirectly relating it to change in elevation using satellite hyperspectral imagery'*, can be said to have tested false.

The results of the profiles analysis along the transects across the wetland failed to establish a consistent pattern were moisture had a positive correlation with elevation. It had been envisaged that areas at lower elevation should have more moisture and vice versa. This research revealed an inconsistent pattern where different moisture conditions were found to be present at any elevation in total contrast with the idealized situation.

These results, however, may not be the norm under all conditions as the circumstances under which this research was conducted could be different for similar research that may be undertaken either on the same site or elsewhere. The poor results obtained for image classification, in particular can be attributed to among other things, the shortcomings in the vegetation map of the Mfabeni wetland used as a source of reference data.

8.3 Recommendations

The methodology used in this research has demonstrated that it is possible to characterize wetland vegetation in terms of elevation on an altitudinal gradient, despite the results obtained particularly the classified images and subsequently the analyses based on them being unreliable. However, in order to improve the results, the underlisted are recommended for further research;

- Use of field-measured spectra of vegetation assemblages for a comparable approach to compare the results
- Use of sub-pixel spectral matching analysis with vegetation assemblages' spectra measurements as end members. Treating individual or combinations of spectra measured in the field as corresponding to image spectra over a corresponding pixel may not yield good results. Relating spectral measures over specific portions of a pixel may provide better results.
- Exploring aggregating field spectra of specific vegetation assemblages using some statistical measure (median, mode, etc.) other than the mean and subsequently using these as spectral representations of respective vegetation assemblages for analysis.
- Exploring the difference in the results obtainable from all RF models found to be optimal by classifying images based on their optimal bands and comparing the results

- Investigating inconsistencies in the distribution of vegetation assemblages along different profiles on an altitudinal gradient.
- Assessing post classification accuracy using a sample of the total spectra extracted from randomly selected Hyperion pixels of each class as a test and compare the results with that obtained for this research.
- Merging vegetation classes of the Mfabeni wetland vegetation map compiled by Venter (2003) and used as a source of reference data with similar plant species and subjecting to processing and analyses used in this project.
- Investigating a relationship between the vegetation map compiled by (Venter 2003) and a Digital Elevation Model (DEM) of Mfabeni wetland.

References

ADAM, E. & MUTANGA, O. 2009. Spectral discrimination of papyrus vegetation (Cyperus papyrus L) in swamp wetlands using field spectrometry. *ISPRS Journal of Photogrammetry and remote Sensing,* 64.

ADAM, E., MUTANGA, O., RUGEGE, D. & ISMAIL, R. 2009. Field Spectrometry Of Papyrus Vegetation (Cyperus Papyrus L.) In Swamp Wetlands Of St Lucia, South Africa IGARSS, IEEE International,.

ADAME, M. F., ROBERTS, M. E., HAMILTON, D. P., NDEHEDEHE, C. E., REIS, V., LU, J., GRIFFITHS, M., CURWEN, G. & RONAN, M. 2019. Tropical coastal wetlands ameliorate nitrogen export during floods. *Frontiers in Marine Science,* 6**,** 671.

ADELABU, S., MUTANGA, O., ADAM, E. & SEBEGO, R. 2014. Spectral Discrimination of Insect Defoliation Levels in Mopane Woodland Using Hyperspectral Data. *IEEE Journal of Selected Topics in Applied Earth Observations and Remote Sensing* 7**,** 177-186.

ADIRI, Z., EL HARTI, A., JELLOULI, A., MAACHA, L., AZMI, M., ZOUHAIR, M. & BACHAOUI, E. M. 2020. Mapping copper mineralization using EO-1 Hyperion data fusion with Landsat 8 OLI and Sentinel-2A in Moroccan Anti-Atlas. *Geocarto international,* 35**,** 781-800.

AHANGARHA, M., SEYDI, S. T. & SHAHHOSEINI, R. 2019. Hyperspectral change detection in wetland and water-body areas based on machine learning. *The International Archives of Photogrammetry, Remote Sensing and Spatial Information Sciences,* 42**,** 19-24.

ANEECE, I., THENKABAIL, P., LYON, J., HUETE, A. & SLONECKER, T. 2019. Spaceborne Hyperspectral EO-1 Hyperion data Pre-processing, Methods, Approaches and Algorithms. *In:* THENKABAIL, P., LYON, J. & HUETE, A. (eds.) *Hyperspectral Remote Sensing of vegetation - Fundamentals, Sensor Systems, Spectral Libraries and Data Mining for Vegetation.* 2 ed. FL: Taylor & Francis.

ATZBERGER, C., DARVISHZADEH, R., IMMITZER, M., SCHLERF, M., SKIDMORE, A. & LE MAIRE, G. 2015. Comparative Analysis of Different Retrieval Methods for Mapping Grassland Leaf Area Index Uisng Airborne Imaging Spectroscopy. *International Journal of Applied Earth Observation and Geoinformation,* 43**,** 19-31.

AYYANDURAI, R. & VENKATESWARAN, S. 2021. Appraisal of groundwater potential zonation mapping in coastal track of Cuddalore district using geospatial techniques in Tamil Nadu India. *Indian Journal of Ecology,* 48**,** 1011-1018.

BAIAMONTE, G. 2021. Simplified Interception/Evaporation Model. *Hydrology,* 8**,** 99.

BAKER, A., ROUTH, J., BLAAUW, M. & ROYCHOUDHURY, A. 2014. Geochemical records of palaeoenvironmental controls on peat forming processes in the Mfabeni peatland, Kwazulu Natal, South Africa since the Late Pleistocene. *Palaeogeography, Palaeoclimatology, Palaeoecology,* 395**,** 95 - 106.

BALWAN, W. K. & KOUR, S. 2021. Wetland-An Ecological Boon for the Environment. *East African Scholars J. Agri. and Life Sci,* 4**,** 38-48.

BANNARI, A., STAENZ, K., CHAMPAGNE, C. & KHURSHID, K. 2015. Spatial Variability Mapping of Crop Residue Using Hyperion (EO-1) Hyperspectral Data *Remote Sensing,* 7**,** 8107 - 8127.

BAO, Y., LIU, T., DUAN, L., TONG, X., ZHANG, L., SINGH, V., LEI, H. & WANG, G. 2021. Comparison of an improved Penman-Monteith model and SWH model for estimating evapotranspiration in a meadow wetland in a semiarid region. *Science of the Total Environment,* 795**,** 148736.

BARRY, P. 2001. EO-1/Hyperion Science Data User's Guide Level 1_B Relando Beach, Califonia, USA: TRW Space, Defense & Information Systems.

BARTON, K. E., WESTERBAND, A., OSTERTAG, R., STACY, E., WINTER, K., DRAKE, D. R., FORTINI, L. B., LITTON, C. M., CORDELL, S. & KRUSHELNYCKY, P. 2021. Hawai 'i forest review: synthesizing the ecology, evolution, and conservation of a model system. *Perspectives in Plant Ecology, Evolution and Systematics,* 52**,** 125631.

BECK, R. 2003. EO-1 User Guide. Cincinnati, Ohio: University of Cincinnati.

BEGG, G. 1990. Policy Proposals for the Wetlands of Natal and KwaZulu. Pietermaritzburg: Natal Town and regional Planning Commission, Pietermaritzburg.

BELTRAN-ABUNZA. 2009. *Method Development to Process Hyper-Temporal Remote Sensing (RS) Images for Change Mapping.*

BISWAS, H., ZHANG, K., ROSS, M. S. & GANN, D. 2020. Delineation of tree patches in a mangrove-marsh transition zone by watershed segmentation of aerial photographs. *Remote Sensing,* 12**,** 2086.

BOTHMA, J. D. P. 1996. *Game Ranch Management,* Pretoria, J.L. van Schaik.

BRAND, R., DU PREEZ, P. & BROWN, L. 2013. High Altitude Montane Wetland Vegetation Classificatio of The Eastern Free State, South Africa. *South African Journal of Botany,* 88**,** 223-236.

BRASHER, M. G., GIOCOMO, J. J., AZURE, D. A., BARTUSZEVIGE, A. M., FLASPOHLER, M. E., HARRIGAL, D. E., OLSON, B. W., PITRE, J. M., RENNER, R. W. & STEPHENS, S. E. 2019. The history and importance of private lands for North American waterfowl conservation. *Wildlife Society Bulletin,* 43**,** 338-354.

BREIMAN, L. 2001. Random Forests. *Machine Learning* 4**,** 5-32.

BROGEA, N. & LEBLANCB, E. 2000. Comparing prediction power and stability of broadband and hyperspectralvegetation indices for estimation of green leaf area index and canopychlorophyll density. *Remote Sensing of Environme,* 76**,** 156 - 172.

BROWNLEE, J. 2016. Bagging and Random Forest Ensemble Algorithms for Machine Learning. *Machine Learning Mastery* [Online]. Available from: https://machinelearningmastery.com/bagging-and-random-forest-ensemble-algorithms-for-machine-learning/ 2019].

BUSTAMANTE, J., ARAGONE'S, D., AF'AN, I., LUQUE, C., VA'ZQUES, A., CASTELLANOS, E. & DI'AZ-DELGADO, R. 2016. Hyperspectral Sensors as a Management Tool to Prevent the Invasion of the Exotic Cordgrass Spartina densiflora in the Don'ana Wetlands. *Remote Sensing,* 8.

CANBAZ, O., GÜRSOY, Ö., KARAMAN, M., ÇALıŞKAN, A. B. & GÖKCE, A. 2021. Hydrothermal alteration mapping using EO-1 Hyperion hyperspectral data in Kösedağ, Central-Eastern Anatolia (Sivas-Turkey). *Arabian Journal of Geosciences,* 14**,** 1-23.

CARTER, C. & LIANG, S. 2019. Evaluation of ten machine learning methods for estimating terrestrial evapotranspiration from remote sensing. *International Journal of Applied Earth Observation and Geoinformation,* 78**,** 86-92.

CHANDRAN, G. & JOJY, C. 2015. A Survey of Cloud Detection Techniques For Satellite Images *International Research Journal of Engineering and Technology* 2.

CHARMAN, D. 2002. *Peatlands and Environmental Change,* Chichester, John Wiley & Sons.

CHAVEZ, J., P 1996. Image based Atmospheric Corrections-Revisited and Improved. *Photogrammetric Engineering & Remote Sensing,* 62**,** 1025-1036.

CHEN, L. N.D. Basic Ensemble Learning (Random Forest, AdaBoost, Gradient Boosting)- Step by Step Explained - A step by step explanation of top 3 tree-based ensemble learning algorithms. Available from: https://towardsdatascience.com/basic-ensemble-learning-random-forest-adaboost-gradient-boosting-step-by-step-explained-95d49d1e2725.

CHEN, S., FANG, L., LIU, Q., CHEN, L. & TONG, Q. The design and development of spectral library of featured crops of South China. Geoscience and Remote Sensing Symposium, 2005 Seoul, South Korea. IEEE.

CHILUFYA, M., AKOMBELWA, M. & STRETCH, D. Identification of Optimal Field Spectral Measurements Wavebands for Discriminating among Spatial Features in support of Mapping Using Hyper-spectral Imagery. *In:* WHITTAL, J. M., S, ed. AfricaGeo2014, 2014 Cape Town. CONSAS.

CHOMBA, I. C., BANDA, K. E., WINSEMIUS, H. C., CHOMBA, M. J., MATAA, M., NGWENYA, V., SICHINGABULA, H. M., NYAMBE, I. A. & ELLENDER, B. 2021. A review of coupled hydrologic-hydraulic models for floodplain assessments in Africa: Opportunities and challenges for floodplain wetland management. *Hydrology,* 8**,** 44.

CHOWDHURY, R., SUTRADHAR, T., BEGAM, M., MUKHERJEE, C., CHATTERJEE, K., BASAK, S. K. & RAY, K. 2019. Effects of nutrient limitation, salinity increase, and associated stressors on mangrove forest cover, structure, and zonation across Indian Sundarbans. *Hydrobiologia,* 842**,** 191-217.

CHRISTOVAM, L., PESSOA, G., SHIMABUKURO, M. & GALO, M. 2019. LAND USE AND LAND COVER CLASSIFICATION USING HYPERSPECTRAL IMAGERY: EVALUATING THE PERFORMANCE OF SPECTRAL ANGLE MAPPER, SUPPORT VECTOR MACHINE AND RANDOM FOREST. *International Archives of the Photogrammetry, Remote Sensing & Spatial Information Sciences*.

CIĘŻKOWSKI, W., BEREZOWSKI, T., KLENIEWSKA, M., SZPORAK-WASILEWSKA, S. & CHORMAŃSKI, J. 2018. Modelling wetland growing season rainfall interception losses based on maximum canopy storage measurements. *Water,* 10**,** 41.

CLULOW, A., EVERSON, C., PRICE, J., JEWITT, G. & SCOTT-SHAW, B. 2013. Water-use dynamics of a peat swamp forest and a dune forest in Maputaland,

. *South Africa. Hydrology and Earth System Sciences,* 17**,** 2053–2067.

COLLINS, N. 2005. Wetlands: The basics and some more. Free State, South Africa: Free State Department of Tourism, Environmental and Economic Affairs

CONGALTON, R. 1991. A review of assessing the accuracy of classifications of remotely sensed data. *Remote Sensing of Environment,* 37**,** 35– 46

CONGALTON, R. G. & GREEN, K. 2019. Assessing the accuracy of remotely sensed data: principles and practices, CRC press.

CONGALTON, R. Accuracy assessment of remotely sensed data: future needs and directions. Pecora 12 land information from space-based systems, 1994 Bethesda. ASPRS, 383 – 388.

COWARDIN, L., CARTER, V., GOLET, F. & LAROE, E. 1979. *Classification of Wetlands and Deepwater Habitats of the United States. ,* Washington, D.C., U. S. Department of the Interior, Fish and Wildlife Service, .

DARVISHI BOLOORANI, A. 2008. *Remotely Sensed Data Fusion as A Basis For Environmental Studies: Concepts, Techniques and Applications.* PhD, The Georg-August-Universität zu Göttingen.

DATT, B. & JUPP, D. 2004. Hyperion Data Processing Workshop: Hands-On Processing Instructions. Canberra: CSIRO Office of Space Science & Applications Earth Observation Centre.

DATT, B., MCVICAR, T., VAN NIEL, T., JUPP, D. & PEARLMAN, J. 2003. Preprocessing EO-1 Hyperion Hyperspectral Data toSupport the Application of Agricultural Indexes. *IEEE TRANSACTIONS ON GEOSCIENCE AND REMOTE SENSING,* 41.

DEPARTMENT OF ENVIRONMENT AND CONSERVATION 2012. *A guide to managing and restoring wetlands in Western Australia. ,* Perth, Western Australia, Department of Environment and Conservation, .

DINI, J. & COWAN, G. South African National Wetland Inventory. Proposed wetland classification system for South Africa. *In:* FINLAYSON, C., DAVIDSON, N. & STEVENSON, N., eds. 2nd International Conference on Wetlands and Development., 8 -14 November 1998 Dakar, Senegal.

DOBHAL, S. 2008. *Performance analysis of high-resolution and hyperspectral data fusion for classification and linear feature extraction* Master of Science in Geo-information Science, University of Twente.

DUNKERLEY, D. 2021. Light and low-intensity rainfalls: A review of their classification, occurrence, and importance in landsurface, ecological and environmental processes. *Earth-Science Reviews,* 214**,** 103529.

DURGAN, S. D., ZHANG, C., DUECASTER, A., FOURNEY, F. & SU, H. 2020. Unmanned aircraft system photogrammetry for mapping diverse vegetation species in a heterogeneous coastal wetland. *Wetlands,* 40**,** 2621-2633.

ECKERT, S. & KNEUBÜHLER, M. 2004. Application of HYPERION data to agricultural land classification and vegetation properties estimation in Switzerland. *XXth ISPRS Congress.* Istanbul, Turkey: ISPRS.

EDWARDS, D. 1983. A broad scale classification of vegetation for practical purposes. *Bothalia,* 14**,** 705 - 712.

EID, A. N. M., OLATUBARA, C., EWEMOJE, T., FAROUK, H. & EL-HENNAWY, M. T. 2020. Coastal wetland vegetation features and digital Change Detection Mapping based on remotely sensed imagery: El-Burullus Lake, Egypt. *International Soil and Water Conservation Research,* 8**,** 66-79.

EIGEMEIER, E., HEISKANEN, J., RAUTIAINEN, M., MÕTTUS, M., VESANTO, V., MAJASALMI, T. & STENBERG, P. 2012. Narrowband Vegetation Indices for Estimating Boreal Forest Leaf Area Index, Remote Sensing *In:* (ED.), D. B. E. (ed.) *Remote Sensing - Applications,.* InTech.

FARAWAY, J. 2002. Practical Regression and Anova using R.

FARIFTEH, J., NIEUWENHUIS, W. & GARCÍA-MELÉNDEZ, E. 2013. Mapping spatial variations of iron oxide by-product minerals from EO-1 Hyperion. *InternationalJournal of Remote Sensing,* 34**,** 682-699.

FAULKNER, S. P. & RICHARDSON, C. J. 2020. Physical and chemical characteristics of freshwater wetland soils. *Constructed wetlands for wastewater treatment***,** 41-72.

FOODY, G. M. 2020. Explaining the unsuitability of the kappa coefficient in the assessment and comparison of the accuracy of thematic maps obtained by image classification. Remote Sensing of Environment, 239, 111630.

FOODY, G. M. 2021. Impacts of ignorance on the accuracy of image classification and thematic mapping. Remote Sensing of Environment, 259, 112367.

FOODY, G. 2004. Thematic map comparison: evaluating the statistical significance of differences in classification accuracy. *Photogrammetric Engineering and Remote Sensing,* 70**,** 627–633.

FRASER, B. T. & CONGALTON, R. G. 2021. Monitoring Fine-Scale Forest Health Using Unmanned Aerial Systems (UAS) Multispectral Models. *Remote Sensing,* 13**,** 4873.

FREEZE, R. & CHERRY, J. 1979. *Groundwater,* Englewood Cliffs, NJ, Prentice-Hall.

FRIEDAL, M., BUSCEMA, M., VICENTE, L., LWASHITA, F. & KOGA-VICENTE, A. 2017. Mapping Fractional landscape Soild and Vegetation Components from Hyperion Satellite Imagery Using an Unsupervised Machine-learning Workflow *International Journal of Digital Earth* [Online].

FU, H., YUAN, G., JEPPESEN, E., GE, D., ZOU, D., LOU, Q., DAI, T., LI, W., ZHONG, J. & HUANG, Z. 2019. Multiple stabilizing pathways in wetland plant communities subjected to an elevation gradient. *Ecological Indicators,* 104**,** 704-710.

GAO, H., SABO, J. L., CHEN, X., LIU, Z., YANG, Z., REN, Z. & LIU, M. 2018. Landscape heterogeneity and hydrological processes: a review of landscape-based hydrological models. *Landscape ecology,* 33**,** 1461-1480.

GETIRANA, A., KUMAR, S. V., KONAPALA, G. & NDEHEDEHE, C. E. 2021. Impacts of fully coupling land surface and flood models on the simulation of large wetlands' water dynamics: The case of the Inner Niger Delta. *Journal of Advances in Modeling Earth Systems,* 13**,** e2021MS002463.

GIBSON, J., EBY, P., BIRKS, S., TWITCHELL, C., GRAY, C. & KARIYEVA, J. 2022. Isotope-based water balance assessment of open water wetlands across Alberta: Regional trends with emphasis on the oil sands region. *Journal of Hydrology: Regional Studies,* 40**,** 101036.

GINZARLY, M., HOUBART, C. & TELLER, J. 2019. The Historic Urban Landscape approach to urban management: a systematic review. *International Journal of Heritage Studies,* 25**,** 999-1019.

GOODENOUGH, D. G., DYK, A., NIEMANN, K. O., PEARLMAN, J. S., CHEN, H., HAN, T. & WEST, C. 2003. Processing Hyperion and ALI for forest classification. Geoscience and Remote Sensing. *IEEE Transactions,* 41**,** 1321-1331.

GOPINATH, G., SASIDHARAN, N. & SURENDRAN, U. 2020. Landuse classification of hyperspectral data by spectral angle mapper and support vector machine in humid tropical region of India. *Earth Science Informatics,* 13**,** 633-640.

GOVENDER M, CHETTY K, V, N. & BULCOCK, H. 2008. A Comparison of satellite hyperspectral and multispectral remote sensing imagery for improved classification and mapping of vegetation. *Water SA*

GRANGER, J. E., MAHDIANPARI, M., PUESTOW, T., WARREN, S., MOHAMMADIMANESH, F., SALEHI, B. & BRISCO, B. 2021. Object-based random forest wetland mapping in Conne River, Newfoundland, Canada. *Journal of Applied Remote Sensing,* 15**,** 038506.

GRASEL, D., GIEHL, E. L. H., WITTMANN, F. & JARENKOW, J. A. 2021. Patterns of plant diversity and composition in wetlands across a subtropical landscape: comparisons among ponds, streambanks and riverbanks. *Wetlands,* 41**,** 1-13.

GRENFELL, M. C., AALTO, R., GRENFELL, S. E. & ELLERY, W. N. 2019. Ecosystem engineering by hummock-building earthworms in seasonal wetlands of eastern South Africa: insights into the mechanics of biomorphodynamic feedbacks in wetland ecosystems. *Earth Surface Processes and Landforms,* 44**,** 354-366.

GRIFFIN, M. & BURKE, H. 2003. Compensation of Hyperspectral Data for Atmospheric Effects. *Lincoln Laboratory Journal,* 14.

GRUNDLING, P. 2014. *Genesis and Hydrological Function of an African Mire: Understanding the Role of Peatlands in Providing Ecosystem Services in Semi-arid Climate.* PhD University of Waterloo, Ontario, Canada.

GRUNDLING, P., CLULOW, A., PRICE, J. & EVERSON, C. 2015. Quantifying the water balance of Mfabeni Mire (iSimangaliso Wetland Park, South Africa) to understand its importance, functioning and vulnerability. *Mires and Peat,* 16**,** 1-18.

GRUNDLING, P., GROOTJANS, A., PRICE, J. & ELLERY, W. 2013. Development and persistence of an African mire: How the oldestSouth African fenhas survived in a marginal climate. *Catena,* 110**,** 176 - 183.

GRUNDLING, P., MAZUS, H. & BAARTMAN, L. 1998. Peat Resources in Northern KwaZulu-Natal Wetlands: Maputaland. Pretoria: Department of Environmental Affairs and Tourism.

GUZZI, D., LASTRI, C., NARDINO, V., PIPPI, I. & RAIMOND, V. 2019. Performance evaluation of destriping algorithms: a test procedure based on simulated images. *International Journal of Remote Sensing*.

HAITJEMA, H. & MITCHELL-BRUKER, S. 2005. Are Water Tables a Subdued Replica of the Topography? *Ground Water,* 43**,** 781-786.

HAMADACHE, Z. & SMARA, Y. 2014. Destriping methods for EO-1 Hyperion Hyperspectral Sensor. *Journées sur les signaux et systèmes,.* Guelma, Algerie.

HAPFELMEIER, A., HOTHORN, T., ULM, K. & STROBL, C. 2014. A new variable importance measure for random forests with missing data. *Statistics and Computing,* 24**,** 21 - 34.

HASANLOU, M. & SEYDI, S. T. 2021. Use of multispectral and hyperspectral satellite imagery for monitoring waterbodies and wetlands. *Southern Iraq's Marshes.* Springer.

HEMBA, S., ELEKWACHI, W., NWANKWOALA, H. O. & VICTORIA, E. 2020. Ecosystem destruction and disaster risk incubation-A case of wetland loss and flood disasters in Makurdi town of Nigeria. *Central Asian Journal of Environmental Science and Technology Innovation,* 1**,** 226-236.

HERLIHY, A. T., KENTULA, M. E., MAGEE, T. K., LOMNICKY, G. A., NAHLIK, A. M. & SERENBETZ, G. 2019. Striving for consistency in the National Wetland Condition Assessment: developing a reference condition approach for assessing wetlands at a continental scale. *Environmental Monitoring and Assessment,* 191**,** 1-20.

HÖHLE, J. & HÖHLE, M. 2009. Accuracy assessment of digital elevation models by means of robust statistical methods. *ISPRS Journal of Photogrammetry and Remote Sensing,* 64**,** 398-406.

HUSSAIN, M., KHAN, S., ABD_ALLAH, E., UL HAQ, Z., ALSHAHRANI, T., ALQARAWI, A., UR RAHMAN, I., IQBAL, M. & ABDULLAH–AHMAD, H. 2019. Assessment of Plant communities and identification of indicator species of an ecotonal forest zone at durand line, district Kurram, Pakistan. *Appl. Ecol. Environ. Res,* 17**,** 6375-6396.

ISMAIL, R. 2010. *Remote sensing of forest health: the detection and mapping of Pinus patula trees infested by Sirex noctilio.* PhD, University of KwaZulu-Natal.

ISMAIL, R. & MUTANGA, O. 2009. A Comparison of Regression Tree Ensembles: Predicating Sirex noctilio induced water stress in Pinus patual forests of KwaZulu-Natal, South Africa. *International Journal of Applied Earth Observation and Geoinformation,* 12S**,** S45-S51.

JEZIORSKA, J. 2019. UAS for wetland mapping and hydrological modeling. *Remote Sensing,* 11**,** 1997.

JIN, S., WANG, Q. & DARDANELLI, G. 2022. A Review on Multi-GNSS for Earth Observation and Emerging Applications. *Remote Sensing,* 14**,** 3930.

JOHNSON, J. A. 2018. Surface Water/Groundwater Interaction. *State of the Science and Practice***,** 72.

JOLLINEAU, M. & HOWARTH, P. 2008. Mapping an inland wetland complex using hyperspectral imagery. *International Journal of Remote Sensing,* 29**,** 3609 - 3631.

JUPP, D., DATT, B., LOVELL, J., S, C., KING, E., [A]STV, T. & OTHERS..... 2004. Discussions around Hyperion Data: Background Notes for the Hyperion Data Users Workshop. CSIRO Earth Observation Centre.

KADLEC, R. H. 2020. Hydrologic factors in wetland water treatment. *Constructed wetlands for wastewater treatment.* CRC Press.

KALACSKA, M., BOHLMAN, S., SANCHEZ-AZOFEIFA, G., CASTRO, K. & CAELLI, T. 2007. Hyperspectral discrimination of tropical dry forest lianas and trees: Comparative data reduction approaches at the leaf and canopy levels *Remote Sensensing of Environment,* 109**,** 407 - 415.

KAYET, N. & CHAKRABARTY, A. 2016. Hyper spectral Image processing for Forest types Mapping and forest health monitoring: A case study in the buffer zones of iron mining belts of Saranda forest, Jharkhand, India. *Journal of GeoPython,* 1.

KEDDY, P. 2010. *Wetland Ecology: Principles and Conservation,* Cambridge, Cambridge University Press.

KEDDY, P. & REZNICEK, A. 2018. Vegetation dynamics, buried seeds, and water level fluctuations on the shorelines of the Great Lakes. *Coastal wetlands.* CRC Press.

KELBE, B. N.D. *Climate - Isimangaliso Wetland Park* [Online]. Available: https://isimangaliso.com/useful-information/climate/ [Accessed 15 January 2021].

KHAN, Z., GUL, N., FAIZ, N., GUL, A., ADLER, W. & LAUSEN, B. 2021. Optimal trees selection for classification via out-of-bag assessment and sub-bagging. *IEEE Access,* 9**,** 28591-28607.

KHELLOUK, R., BARAKAT, A., BOUDHAR, A., HADRIA, R., LIONBOUI, H., EL JAZOULI, A., RAIS, J., EL BAGHDADI, M. & BENABDELOUAHAB, T. 2020. Spatiotemporal monitoring of surface soil moisture using optical remote sensing data: a case study in a semi-arid area. *Journal of Spatial Science,* 65**,** 481-499.

KHURSHID, S., STAENZ, K., SUN, L., NEVILLE, R., PETER WHITE, H., BANNARI, A., CHAMPAGNE, C. & HITCHCOCK, R. 2006. Preprocessing of EO-1 Hyperion Data. *Canadian Journal of Remote Sensing,* 32**,** 84-97.

KIM, J., RYU, Y., JIANG, C. & HWANG, Y. 2019. Continuous observation of vegetation canopy dynamics using an integrated low-cost, near-surface remote sensing system. *Agricultural and forest meteorology,* 264**,** 164-177.

KLEMAS, V. 2014. Remote Sensing of Riaperian and Wetland Buffers: An Overview. *Journal of Coastal Research,* 30**,** 869 - 880.

KOEHRSEN, W. 2017. Random Forest Simple Explanation. Available from: https://medium.com/@williamkoehrsen/random-forest-simple-explanation-377895a60d2d.

KOTZE, D., HUGHES, J., BREEN, C. & KLUG, J. 1994. The Development of a Wetland Soils Classification System for KwaZulu/Natal. *In:* COMMISSION, W. R. (ed.) *WRC Report No. 501/4/94.* Pretoria.

KRUSE, F., LEFKOFF, A., BOARDMAN, J., HEIDEEBRECHT, K., SHAPIRO, A., BARLOON, J. & GOETZ, A. 1993. The Spectral Image Processing system (SIPS) - Intercative Visualization and Analysis of Imaging Spectrometer. *Remote Sensensing of Environment,* 44**,** 145 - 163.

KUCERA, S. B. 2021. *Soil Moisture Dynamics, Runoff Generation, and Streamflow Response in a Prairie Hillslope See System, Texas.* Texas Christian University.

KUMAR, M. & YARRAKULA, K. 2017. Comparison of efficeint Techniques of Hyper-spectral Image Preprocessing for Mineralogy and Vegetation Studies. *Indian Journal of Geo Marine Sciences,* 46**,** 1008 - 1021.

KUREEL, N., SARUP, J., MATIN, S., GOSWAMI, S. & KUREEL, K. 2022. Modelling vegetation health and stress using hypersepctral remote sensing data. *Modeling Earth Systems and Environment,* 8**,** 733-748.

L3HARRIS GEOSPATIAL. N.D. *EO-1 Hyperion Vegetation Analysis Tutorial* [Online]. Available: https://www.l3harrisgeospatial.com/docs/hyperionvegetationanalysistutorial.html [Accessed 18 September 2018].

LALTAIKA, E. 2022. Indigenous peoples' participation and the management of wetlands in Africa: a review of the Ramsar Convention. *Fundamentals of Tropical Freshwater Wetlands***,** 711-726.

LAROCQUE, A., PHIRI, C., LEBLON, B., PIROTTI, F., CONNOR, K. & HANSON, A. 2020. Wetland Mapping with Landsat 8 OLI, Sentinel-1, ALOS-1 PALSAR, and LiDAR Data in Southern New Brunswick, Canada. *Remote Sensing,* 12**,** 2095.

LEWIS, K. 2018. *Wetland characteristics and wintering passerellidae occupancy on Agricultural Conservation Easement Program wetlands in West Virginia*, West Virginia University.

LI, N., WANG, R., ZHAO, H. & WEI, W. AN IMPROVED FEATURE EXTRACTION METHOD BASED ON CONTEXT FEATURES FOR MULTI-SPECTRAL REMOTE SENSING IMAGERY. 2019 IEEE International Conference on Signal, Information and Data Processing (ICSIDP), 2019. IEEE, 1-4.

LI, W., TAN, R., WANG, J. & YANG, Y. 2014. Plant diversity as a good indicator of vegetation stability in a typical plateau wetland. *Journal of Mountain Science,* 11.

LIAW, A. & WIENER, M. 2002. Classification and Regression by Random Forest. *R News,* 3**,** 18-22.

LILLESAND, T. M. & KIEFER, R. W. 2000. *Remote Sensing and Image Interpretation*, John Wiley & Sons, Inc.

LIU, Y., XU, P., CAO, C., SHAN, B., ZHU, K., MA, Q., ZHANG, Z. & YIN, H. 2021. A comparative evaluation of machine learning algorithms and an improved optimal model for landslide susceptibility: a case study. *Geomatics, Natural Hazards and Risk,* 12**,** 1973-2001.

LIU, Z., ZHU, J., FU, H., ZHOU, C. & ZUO, T. 2020. Evaluation of the vertical accuracy of open global dems over steep terrain regions using icesat data: A case study over hunan province, china. *Sensors,* 20**,** 4865.

LYONS, M. B., KEITH, D. A., PHINN, S. R., MASON, T. J. & ELITH, J. 2018. A comparison of resampling methods for remote sensing classification and accuracy assessment. Remote Sensing of Environment, 208, 145-153.

MACUS, W. 2001. Mapping of stream microhabitats with high spatial resolution hyperspectral imagery. *Journal of Geographic Systems.*

MAHDAVI, S., SALEHI, B., AMANI, M., GRANGER, J., BRISCO, B. & HUANG, W. 2019. A dynamic classification scheme for mapping spectrally similar classes: Application to wetland classification. *International Journal of Applied Earth Observation and Geoinformation,* 83**,** 101914.

MAHDAVI, S., SALEHI, B., GRANGER, J., AMANI, M., BRISCO, B. & HUANG, W. 2018. Remote sensing for wetland classification: A comprehensive review. *GIScience & Remote Sensing,* 55**,** 623-658.

MAHDIANPARI, M., BRISCO, B., GRANGER, J. E., MOHAMMADIMANESH, F., SALEHI, B., BANKS, S., HOMAYOUNI, S., BOURGEAU-CHAVEZ, L. & WENG, Q. 2020. The second generation Canadian wetland inventory map at 10 meters resolution using Google Earth Engine. *Canadian Journal of Remote Sensing,* 46**,** 360-375.

MALINOWSKI, R., GROOM, G., SCHWANGHART, W. & HECKRATH, G. 2015a. Detection and Delineation of Localized Flooding from WorldView-2 Mulitispectral Data. *Remote Sensing,* 7**,** 14853-14875.

MALINOWSKI, R., GROOM, G., SCHWANGHART, W. & HECKRATH, G. 2015b. Detection and Delineation of Localized Flooding from WorldView-2 Multispectral Data. *Remote Sensensing,* 7**,** 14853 - 14875.

MALTBY, E. & BARKER, T. 2009. *The wetland handbook*, John Wiley & Sons.

MANDLAZI, N. 2017. *HYDROLOGICAL CHARACTERISATION OF WETLANDS: UNDERSTANDING WETLANDS-CATCHMENT LINKAGES.* MSc, University of Western Cape.

MANJUNATH, K., KUMAR, A., MEENAKSHI, M., RENU, R., UNIYAL, S., SINGH, R., AHUJA, P., RAY, S. & PANIGRAHY, S. 2014. Developing Spectral Library of Major Plant Species of Western Himalayas Using Ground Observations. *Journal of the Indian Society of Remote Sensing,* 42**,** 201 - 216.

MANSOUR, K., MUTANGA, O., EVERSON, T. & ADAM, E. 2012. Discriminating indicator grass species for rangelend degradation assessment using hyperspectral data resampled to AISA resolution. *ISPRS Journal of Photogrammetry and Remote Sensing,* 70**,** 56-65.

MARCELLO, J., EUGENIO, F., PERDOMO, U. & MEDINA, A. 2016. Assessment of Atmospheric Algorithms to Retrieve Vegetation in Natural Protected Areas Using Multispectral High Resolution Imagery. *Sensors,* 16.

MASWANGANYE, S. E., DUBE, T., JOVANOVIC, N., KAPANGAZIWIRI, E. & MAZVIMAVI, D. 2022. Using the water balance approach to understand pool dynamics along non-perennial rivers in the semi-arid areas of South Africa. *Journal of Hydrology: Regional Studies,* 44**,** 101244.

MAUA, J. O., MBUVI, M. T. E., MATIKU, P., MUNGUTI, S., MATECHE, E. & OWILI, M. 2022. The difficult choice-to conserve the living filters or utilizing the full potential of wetlands: Insights from the Yala swamp, Kenya. *Environmental Challenges,* 6**,** 100427.

MERENTITIS, A., DEBES, C. & HEREMANS, R. 2014. Ensemble Learning in Hyperspectral Image Classification: Toward Selecting a Favorable Bias-Variance Tradeoff. *IEEE Journal of Selected Topics in Applied Earth Observations and Remote Sensing,* 7**,** 1089 - 1102.

MILEWSKI, R., CHABRILLAT, S. & BEHLING, R. 2017. Analyses of Recent Sediment Surface Dynamic of a Namibian Kalahari Salt Pan Based on Multitemporal Landsat and Hyperspectral Hyperion Data. *Remote Sensing,* 9.

MISHRA, N. B. 2020. Wetlands: remote sensing. *Wetlands and Habitats.* CRC Press.

MITSCH, W. & GOSSELINK, J. 2015. *Wetlands,* New Jersey, John Wiley & Sons, Inc.

MITTELBACH, G. G. & MCGILL, B. J. 2019. *Community ecology*, Oxford University Press.

MORA, P.-N. A. 2014. *HYPERSPECTRAL REMOTE SENSING FOR DETECTING VEGETATION AFFECTED BY HYDROCARBONS IN THE AMAZON FOREST.* PhD, University of Leicester.

MUSSA, K. R., MJEMAH, I. C. & MUZUKA, A. N. N. 2020. A review on the state of knowledge, conceptual and theoretical contentions of major theories and principles governing groundwater flow modeling. Applied Water Science, 10, 1-10.

MUTANGA, O. & SKIDMORE, A. 2004. Hyperspectral band depth analysis for a better estimation of grass biomass (Cenchrus ciliaris) measured under controlled laboratory conditions. . *International Journal of Applied Earth Observation and Geoinformation,* 5**,** 87-96.

NA, X., LI, X., LI, W. & WU, C. 2021. Wetland Mapping Using HJ-1A/B Hyperspectral Images and an Adaptive Sparse Constrained Least Squares Linear Spectral Mixture Model. *Remote Sensing,* 13**,** 751.

NASA-EARTHDATA-CMR-SEARCH. ND. *Earth Observing-1 Hyperion V1* [Online]. Available: https://cmr.earthdata.nasa.gov/search/concepts/C1379758136-USGS_EROS.html [Accessed 12 December 2020].

NASARUDIN, N. & SHAFRI, H. 2011. Development and Utilization of Urban Spectral Library for Remote Sensing of Urban Environment *Journal of Urban and Environmental Engineering,* 5**,** 44-56.

NEVILLE, R., SUN, L. & STAENZ, K. Detection of keystone in imaging spectrometer data. SPIE, 2004.

NIJP, J. J., METSELAAR, K., LIMPENS, J., BARTHOLOMEUS, H. M., NILSSON, M. B., BERENDSE, F. & VAN DER ZEE, S. E. 2019. High-resolution peat volume change in a northern peatland: Spatial variability, main drivers, and impact on ecohydrology. Ecohydrology, 12, e2114.

NISHII, R. & TANAKA, S. 1999. Accuracy and inaccuracy assessments in land-cover classification. *IEEE Transactions on Geoscience and Remote Sensing,* 37**,** 491–498.

NYARKO, B. K. 2020. Wetland river flow interaction in a sedimentary formation of the White Volta Basin of Ghana.

NYAROBI, H. 2022. *Morphological and physiological responses of the invasive plant gutenbergia cordifolia to varying biophysical conditions.* NM-AIST.

O'CONNOR, M. T., CARDENAS, M. B., NEILSON, B. T., NICHOLAIDES, K. D. & KLING, G. W. 2019. Active layer groundwater flow: The interrelated effects of stratigraphy, thaw, and topography. *Water Resources Research,* 55**,** 6555-6576.

ODEBIRI, O., MUTANGA, O., ODINDI, J., PEERBHAY, K. & DOVEY, S. 2020. Predicting soil organic carbon stocks under commercial forest plantations in KwaZulu-Natal province, South Africa using remotely sensed data. *GIScience & remote sensing,* 57**,** 450-463.

OWETHU PANTSHWA, A. & BUSCHKE, F. T. 2019. Ecosystem services and ecological degradation of communal wetlands in a South African biodiversity hotspot. *Royal Society open science,* 6**,** 181770.

PADMA, S. & SANJEEVI, S. 2014. Jefferies- matusista-Spectral Angle Mapper (JM-SAM) Spectral Matching For Species Level Mapping at Bhitarkanika, Muthupet ans Pichavaram Magroves. *The International Archives of the Photogrammetry, Remote Sensing and Spatial Information Sciences,* XL.

PAOLO, P. 2011. *EVALUATION OF A REMOTE SENSING BASED METHOD FOR THE ASSESSMENT OF AGRICULTURAL CROP RESIDUES ON THE SOIL SURFACE.* PhD, University of Milan.

PARK DAMS, J. V. R. 2019. Aquatic study, wetland delineation and dam assessment.

PARK, K., KI HONG, Y., HWAN KIM, G. & LEE, J. 2018. Classification of apple leaf conditions in hyper-spectral images for diagnosis of Marssonina blotch using mRMR and deep neural network. *Computers and Electronics in Agriculture,* 148**,** 179-187.

PEARLMAN, J. S., BARRY, P., SEGAL, C. C., SHEPANSKI, J., BEISO, D. & CARMAN, S. L. 2003. Hyperion, a space-based imaging spectrometer. *IEEE Transactions on Geoscience and Remote Sensing,* 41**,** 1160-1173.

PEDDINTI, V., MANDLA, V., MESAPAM, S. & KANCHERLA, S. 2021. Simulation of hyperspectral image with existing Sentinel and AVIRIS data using distance functions. Arab J Geosci, 14.

PERVEZ, W., KHAN, S. & VALIUDDIN 2015. Hyperspectral Hyperion Imagery Analysis and its Application Using Spectral Analysis. *The International Archives of the Photogrammetry, Remote Sensing and Spatial Information Sciences,* XL-3/W2.

PIMPLE, U., LEADPRATHOM, K., SIMONETTI, D., SITTHI, A., PETERS, R., PUNGKUL, S., PRAVINVONGVUTHI, T., DESSARD, H., BERGER, U. & SIRI-ON, K. 2022. Assessing mangrove species diversity, zonation and functional indicators in response to natural, regenerated, and rehabilitated succession. *Journal of Environmental Management,* 318**,** 115507.

PONTIUS, R. G. 2000. Quantification error versus location error in comparison of categorical maps. *Photogrammetric Engineering and Remote Sensing,* 66**,** 1011–1016.

POONA, K. & ISMAIL, R. 2013. Reducing Hyperspectral Data Diminesionality Uisng Random Forest Based Wrappers. . *IGARSS 2013.* IEEE International.

POULIOT, D., LATIFOVIC, R., PASHER, J. & DUFFE, J. 2019. Assessment of convolution neural networks for wetland mapping with landsat in the central Canadian boreal forest region. *Remote Sensing,* 11**,** 772.

PREETHA, P. P., JOSEPH, N. & NARASIMHAN, B. 2021. Quantifying Surface Water and Ground Water Interactions using a Coupled SWAT_FEM Model: Implications of Management Practices on Hydrological Processes in Irrigated River Basins. *Water Resources Management,* 35**,** 2781-2797.

PRETORIOUS, M. 2016. *SELECTED SOIL PROPERTIES AND VEGETATION COMPOSITION OF FIVE WETLAND SYSTEMS ON THE MAPUTALAND COASTAL PLAIN, KWAZULU-NATAL.* PhD, University of South Africa.

PRISLEY, S. P., TURNER, J. A., BROWN, M. J., SCHILLING, E. & LAMBERT, S. G. 2020. Uncertainty of Forested Wetland Maps Derived from Aerial Photography. *Photogrammetric Engineering & Remote Sensing,* 86**,** 609-617.

PROSPERE, K., MCLAREN, K. & WILSON, B. 2014. Plant Species Discrimination in a Tropical Wetland Using In-Situ Hyperspectral Data. *Remote Sensing,* 6**,** 8494-8523.

RAMA RAO, N. 2008. Development of a crop-specific spectral library and discrimination of various agricultural crop varieties using hyperspectral imagery. *International Journal of Remote Sensing,* 29**,** 131-144.

RAMA RAO, N. & BERND, Z. 2011. Use of field reflectance data for crop mapping using airborne hyperspectral image. *ISPRS Journal of Photogrammetry and Remote Sensing,* 66**,** 683 - 691.

RAMATSABANA, P., TANNER, J., MANTEL, S., PALMER, A. & EZENNE, G. 2019. Evaluation of remote-sensing based estimates of actual evapotranspiration over (diverse shape and sized) Palmiet wetlands. *Geosciences,* 9**,** 491.

RANI, N., MANDLA, V. & SINGH, T. 2017. Evaluation of atmospheric corrections on hyperspectral data with

special reference to mineral mapping. *Geoscience Frontiers,* 8**,** 797 - 808.

RASAIAH, B., JONES, S., BELLMAN, C. & MALTHUS, T. 2014. Critical metadata for spectroscopy field campaign. *Remote Sensing,* 6**,** 3662 – 3680.

RASAIAH, B., JONES, S., BELLMAN, C., MALTHUS, T. & HUENI, A. 2015. Assessing Field Spectroscopy Metadata Quality *Remote Sensing,* 7**,** 4499 - 4526.

RASMY, M., SAYAMA, T. & KOIKE, T. 2019. Development of water and energy Budget-based Rainfall-Runoff-Inundation model (WEB-RRI) and its verification in the Kalu and Mundeni River Basins, Sri Lanka. *Journal of Hydrology,* 579**,** 124163.

RAWLINS, B. & KELBE, B. 1991. *Case study on the hydrological response of a shallow coastal aquifer to afforestation.,* Wallingford, UK, International Association of Hydrological Sciences (IAHS) Publication 202, IAHS Press,.

REYNOLDS, E. M., COWAN JR, J. H., LEWIS, K. A. & SIMONSEN, K. A. 2018. Method for estimating relative abundance and species composition around oil and gas platforms in the northern Gulf of Mexico, USA. *Fisheries Research,* 201**,** 44-55.

ROGASS, C., GUANTER, L., MIELKE, C., SCHEFFLER, D., BOESCHE, N., LUBITZ, C., BRELL, M., SPENGLER, D. & SEGL, K. An automated processing chain for the retrieval of georeferenced reflectance data from hyperspectral EO-1 HYPERION acquisitions *In:* ZAGAJEWSKI, B., KYCKO, M. & REUTER, R., eds. EARSeL 34th Symposium 16-20 June 2014 2014 Warsaw, Poland.

ROLLS, R. J., HEINO, J., RYDER, D. S., CHESSMAN, B. C., GROWNS, I. O., THOMPSON, R. M. & GIDO, K. B. 2018. Scaling biodiversity responses to hydrological regimes. *Biological Reviews,* 93**,** 971-995.

ROSENFIELD, G. & FITZPATRICK-LINS, K. 1986. A coefficient of agreement as a measure of thematic classification accuracy. *Photogrammetric Engineering and Remote Sensing,* 52**,** 223–227.

RUPASINGHE, P. A. & CHOW-FRASER, P. 2019. Identification of most spectrally distinguishable phenological stage of invasive Phragmites australis in Lake Erie wetlands (Canada) for accurate mapping using multispectral satellite imagery. *Wetlands Ecology and Management,* 27**,** 513-538.

SAC 2007. A report on use of hyperspectral remote sensing in agricultural applications: Ground based studies. Ahmedabad: Space Applications Centre.

SAHOO, R., PARGAL, S., PRADHAN, S., KRISHNA, G. & GUPTA, V. 2013. *Processing of Hyperspectral Remote Sensing Data,* New Delhi-110 012, Division of Agricultural Physics, Indian Agricultural Research Institute,.

SAN, B. & SUZEN, M. 2010. Evaluation of Different Atmospheric Correction Algorithms for EO-1 Hyperion Imagery. *International Archives of the Photogrammetry, Remote Sensing and Spatial Information Science.* Kyoto Japan.

SCHMIDT, S. A. & AHN, C. 2019. A comparative review of methods of using soil colors and their patterns for wetland ecology and management. *Communications in Soil Science and Plant Analysis,* 50**,** 1293-1309.

SCHOOLMASTER JR, D. R. & STAGG, C. L. 2018. Resource competition model predicts zonation and increasing nutrient use efficiency along a wetland salinity gradient. *Ecology,* 99**,** 670-680.

SEIDEL, F., KOKHANOVSKY, A. & SCHAEPMAN, M. 2010. Fast and simple model for atmospheric radiative transfer. *Atmospheric Measurements Techniques,* 3**,** 1129 - 11411.

SEMENIUK, C. A. & SEMENIUK, V. 2018. Wetland Classification: Geomorphic-Hydrologic System. *In:* FINLAYSON, C. M., EVERARD, M., IRVINE, K., MCINNES, R. J., MIDDLETON, B. A., VAN DAM, A. A. & DAVIDSON, N. C. (eds.) *The Wetland Book: I: Structure and Function, Management, and Methods.* Dordrecht: Springer Netherlands.

SHAFI, U., MUMTAZ, R., GARCÍA-NIETO, J., HASSAN, S. A., ZAIDI, S. A. R. & IQBAL, N. 2019. Precision agriculture techniques and practices: From considerations to applications. *Sensors,* 19**,** 3796.

SHANMUGAM, S. & SRINIVASAPERUMAL, P. 2014. Spectral matching approaches in hyperspectral image processing. *International Journal of Remote Sensing,* 35**,** 8217-8251,.

SHANO, L., RAGHUVANSHI, T. K. & METEN, M. 2020. Landslide susceptibility evaluation and hazard zonation techniques–a review. *Geoenvironmental Disasters,* 7**,** 1-19.

SHEN, G., YANG, X., JIN, Y., XU, B. & ZHOU, Q. 2019. Remote sensing and evaluation of the wetland ecological degradation process of the Zoige Plateau Wetland in China. *Ecological Indicators,* 104**,** 48-58.

SHEN, X., LIU, Y., ZHANG, J., WANG, Y., MA, R., LIU, B., LU, X. & JIANG, M. 2022. Asymmetric impacts of diurnal warming on vegetation carbon sequestration of marshes in the Qinghai Tibet Plateau. *Global Biogeochemical Cycles,* 36**,** e2022GB007396.

SHEPARD, J. P., BRADY, S. J., COST, N. D. & STORRS, C. G. 2019. Classification and inventory. *Southern Forested Wetlands.* Routledge.

SHIPPERT, P. 2004. Why Use Hyperspectral Imagery? *Photogrammetric Engineering and Remote Sensing***,** 377-380.

SIEBEN, E., GLEN, R., VAN DEVENTER, H. & DAYARAM, A. 2021. The contribution of wetland flora to regional floristic diversity across a wide range of climatic conditions in southern Africa. *Biodiversity and Conservation,* 30**,** 575-596.

SIEBEN, E. J. J., MTSHALI, H. & JANKS, M. 2014. National wetland vegetation database: classification and analysis of wetland vegetation types for conservation planning and monitoring. *WRC Report K5/1980.* Water Research Commission.

SILVA MOTA, G., LUZ, G., NAYARA, M., COUTINHO, E., VELOSO, M. & FERNANDES, G. 2017. Changes in Species Composistion, Vegetation Structure, and Life forms along an Altitudinal gardient of Rupestrian Grassland in South Eastern Brazil. *Flora*.

SINGH, M., SARKAR, B., BOLAN, N. S., OK, Y. S. & CHURCHMAN, G. J. 2019. Decomposition of soil organic matter as affected by clay types, pedogenic oxides and plant residue addition rates. *Journal of hazardous materials,* 374**,** 11-19.

SINGH, M. & SINHA, R. 2021. Hydrogeomorphic indicators of wetland health inferred from multi-temporal remote sensing data for a new Ramsar site (Kaabar Tal), India. *Ecological Indicators,* 127**,** 107739.

SMITH, K. E., TERRANO, J. F., PITCHFORD, J. L. & ARCHER, M. J. 2021. Coastal wetland shoreline change monitoring: A comparison of shorelines from high-resolution WorldView Satellite imagery, aerial Imagery, and field surveys. *Remote Sensing,* 13**,** 3030.

SMITH, R. 2006. *Introduction To Hyperspectral Imaging with TNTmips*, MicroImages, Inc.

SMITS, P., DELLEPIANE, S. & SCHOWENGERDT, R. 1999. Quality assessment of image classification algorithms for land-cover mapping: a review and proposal for a cost-based approach. *International Journal of Remote Sensing,* 20**,** 1461–1486.

SMUTS, W. 1992. Peatlands of the Natal Mire Complex: geomorphology and characterization. *South African Journal of Science,* 88**,** 9 - 10.

SOMDATTA, C. & CHAKRABARTI, S. 2011. Preprocessing of Hyperspectral Data: A case study of Henry and Lothian Islands in Sunderban Region, West Bengal, India. *INTERNATIONAL JOURNAL OF GEOMATICS AND GEOSCIENCES* 2.

SOPHOCLEOUS, M. 2002. Interactions between groundwater and surface water: the state of the science. *Hydrogeology Journal,* 10**,** 52–67.

STANTURF, J. A. & SCHOENHOLTZ, S. H. 2019. Soils and landforms. *Southern Forested Wetlands.* Routledge.

STEHMAN, S. & WICKHAM, J. 2020. A guide for evaluating and reporting map data quality: Affirming Shao et al."Overselling overall map accuracy misinforms about research reliability". Landscape ecology, 35, 1263-1267.

STEWART, A., RIOUX, D., BOYER, F., GIELLY, L., POMPANON, F., SAILLARD, A., THUILLER, W., VALAY, J.-G., MARECHAL, E. & COISSAC, E. 2021. Altitudinal zonation of green algae biodiversity in the French Alps. *Frontiers in plant science,* 12**,** 679428.

TAYLOR, R., KELBE, B., HALDORSEN, S., BOTHA, G., WEJDEN, B., VAERET, L. & SIMONSEN, M. 2006. Groundwater-dependent ecology of the shoreline of the subtropical Lake St Lucia estuary. *Environmental Geology,* 49**,** 586–600.

THABENG, O. L., MERLO, S. & ADAM, E. 2019. High-resolution remote sensing and advanced classification techniques for the prospection of archaeological sites' markers: The case of dung deposits in the Shashi-Limpopo Confluence area (southern Africa). *Journal of Archaeological Science,* 102**,** 48-60.

THENKABAIL, P., SMITH, R. & DE PAUW, E. 2002. Evaluation of Narrowband and Broadband Vegetation Indices for Determining Optimal Hyperspectral Wavebands for Agricultural Crop Characterization *Photogrammetric Engineering & Remote Sensing,* 68**,** 607 - 621.

THULIN, S. 2008. *Hypesctral Remote Sensing of Temperate Pasture Quality.* PhD, RMIT University of Melbourne.

THULIN, S., HILL, M., HELD, A., JONES, S. & WOODGATE, P. 2014. Digestibility, Lignin and Cellulose in Temperate Pastures Using Hyperspectral Image Data *American Journal of Plant Sciences,,* 5**,** 997 - 1019.

TIAN, S., ZHANG, X., TIAN, J. & SUN, Q. 2016. Random Forest Classification of Wetland Landcovers from Multi-Sensor Data in the Arid Region of Xinjiang, China. *Remote Sensing,* 8.

TINER, R. W. 1991. The concept of a hydrophyte for wetland identification-individual plants adapt to wet environment. . *BioSciencesBioSciences,* 41**,** 236-247.

TIWARI, J., SHARMA, S. & PATIL, R. 2021. Accuracy assessment of land use land cover mapping of a watershed of Narmada basin using Remote sensing and Geographical Information System. JNKVV, 42

TOLLETTE, D. G., MORTAZAVI, B., TATARIW, C., FLOURNOY, N. & SOBECKY, P. A. 2022. Water Accommodated Fraction of Macondo Oil Has Limited Effects on Nitrate Reduction in Northern Gulf of Mexico Salt Marsh Sediments Regardless of Prior Oiling History. *Water, Air, & Soil Pollution,* 233**,** 1-16.

TURK, G. 2002. Map Evaluation and Chance Correction. *Photogrammetric Engineering and Remote Sensing,* 68**,** 123–133.

USGS-EROS. ND. *USGS EROS Archive - Earth Observing One (EO-1)* [Online]. Available: https://www.usgs.gov/centers/eros/science/usgs-eros-archive-earth-observing-one-eo-1?qt-science_center_objects=0#qt-science_center_objects [Accessed 4 March 2019].

USGS-EROS. 2021. *USGS EROS Archive - Earth Observing One (EO-1)* [Online]. Available: https://www.usgs.gov/centers/eros/science/usgs-eros-archive-earth-observing-one-eo-1?qt-science_center_objects=0#qt-science_center_objects [Accessed 12 November 2022].

USGS. 2017. *Earth Observing 1 (EO-1)* [Online]. [Accessed 14 September 2017].

VAN DER MEER, F. 2006. The effectiveness of spectral similarity measures for the analysis of hyperspectral imagery. *International journal of applied earth observation and geoinformation,* 8**,** 3 - 17.

VAN DER VALK, A. G. 2020. Wetlands: Classification. Wetlands and Habitats. CRC Press.

VANNESTE, T., GOVAERT, S., DE KESEL, W., VAN DEN BERGE, S., VANGANSBEKE, P., MEEUSSEN, C., BRUNET, J., COUSINS, S. A., DECOCQ, G. & DIEKMANN, M. 2020. Plant diversity in hedgerows and road verges across Europe. *Journal of Applied Ecology,* 57**,** 1244-1257.

VARGA, K., SZABO', S., SZABO', G., DE'VAI, G. & TO'THME'RE'SZ, B. 2015. Improve land Cover Mapping Using Aerial Photograps and satellite Images. *De Gruyter*.

VENTER, C. 2003. *The Vegetation Ecology of Mfabeni Peat Swamp, St Lucia, KwaZulu-Natal.* MSc, University of Pretoria.

VERRY, E. 2018. Hydrological processes of natural, northern forested wetlands. *Northern forested wetlands.* Routledge.

VESELKA IV, W., KORDEK, W. S. & ANDERSON, J. T. 2021. Using multiple taxa and wetland classification schemes for enhanced detection of biological response signatures to human impairment. *Ecological Indicators,* 133**,** 108391.

WESTERFELT, P. & FRIBERG, G. 2022. Digital mapping of retention zones around wetlands.

WETLAND HYDROLOGY. ND. Available: https://www.hilarispublisher.com/scholarly/wetland-hydrology-journals-articles-ppts-list-2337.html [Accessed 30 December 2020 2020].

WHITE, H., KHURSHID, K., HITCHCOCK, R., NEVILLE, R., SUN, L., CHAMPAGNE, C. & STAENZ, K. From at-sensor observations to at-surface reflectance-calibration steps for earth observations hyperspectral sensors. . IEEE International Geoscience and Remote Sensing Symposium, 2004 Anchorage, Alaska. Piscataway, N.J: IEEE, 3241-3244.

WHITESIDE, T. & BARTOLO, R. 2015. Mapping Aquatic Vegetationnin a Tropical Wetland Using High Spatial Resolution Multispectral Satellite Imagery. *Remote Sensing,* 7**,** 11664-11694.

WICAKSONO, P. & ARYAGUNA, P. A. 2020. Analyses of inter-class spectral separability and classification accuracy of benthic habitat mapping using multispectral image. *Remote Sensing Applications: Society and Environment,* 19**,** 100335.

WILLIAMS, G. 2011. *Data Mining with Rattle and R - The Art of Excavating data for Knowledge Discovery,* New York, Springer.

WINTER, T. 1999. Relation of streams, lakes and wetlands to groundwater flow system. *Hydrogeology Journal,* 7**,** 28-45.

WORSHAM, H. M. 2020. An Examination of an Enhanced Remote Sensing Method for Agent Attribution of Forest Disturbance. *bioRxiv*.

XIN, P., WILSON, A., SHEN, C., GE, Z., MOFFETT, K. B., SANTOS, I. R., CHEN, X., XU, X., YAU, Y. Y. & MOORE, W. 2022. Surface water and groundwater interactions in salt marshes and their impact on plant ecology and coastal biogeochemistry. *Reviews of Geophysics,* 60**,** e2021RG000740.

XU, T., WENG, B., YAN, D., WANG, K., LI, X., BI, W., LI, M., CHENG, X. & LIU, Y. 2019. Wetlands of international importance: Status, threats, and future protection. *International Journal of Environmental Research and Public Health,* 16**,** 1818.

YANG, W., YOU, Q., FANG, N., XU, L., ZHOU, Y., WU, N., NI, C., LIU, Y., LIU, G. & YANG, T. 2018. Assessment of wetland health status of Poyang Lake using vegetation-based indices of biotic integrity. *Ecological Indicators,* 90**,** 79-89.

YANG, X., YU, Y. & FAN, W. 2015. Chlorophyll content retrieval from hyperspectral remote sensing imagery. *Environmental Monitoring and Assessment,* 187.

YASEEF, N., YAKIR, D., ROTENBERG, E., SCHILLER, G. & COHEN, S. 2009. Ecohydrology of a semi-arid forest: partitioning among water balance components and its implications for predicted precipitation changes. *Ecohydrology*.

YE, X.-C., MENG, Y.-K., XU, L.-G. & XU, C.-Y. 2019. Net primary productivity dynamics and associated hydrological driving factors in the floodplain wetland of China's largest freshwater lake. *Science of the Total Environment,* 659**,** 302-313.

YEO, I.-Y., LEE, S., LANG, M. W., YETEMEN, O., MCCARTY, G. W., SADEGHI, A. M. & EVENSON, G. 2019. Mapping landscape-level hydrological connectivity of headwater wetlands to downstream waters: A catchment modeling approach-Part 2. *Science of the Total Environment,* 653**,** 1557-1570.

ZHANG, F. & ZHOU, G. 2019. Estimation of vegetation water content using hyperspectral vegetation indices: A comparison of crop water indicators in response to water stress treatments for summer maize. *BMC ecology,* 19**,** 1-12.

ZHANG, G., BAI, J., TEBBE, C. C., ZHAO, Q., JIA, J., WANG, W., WANG, X. & YU, L. 2021a. Salinity controls soil microbial community structure and function in coastal estuarine wetlands. *Environmental microbiology,* 23**,** 1020-1037.

ZHANG, Y., LI, W., SUN, G. & KING, J. S. 2019. Coastal wetland resilience to climate variability: A hydrologic perspective. *Journal of Hydrology,* 568**,** 275-284.

ZHANG, Y., WANG, A., YUAN, F., GUAN, D. & WU, J. 2021b. The application of EO-1 Hyperion hyperspectral data to estimate the GPP of temperate forest in Changbai Mountain, Northeast China. *Environmental Earth Sciences,* 80**,** 1-11.

ZHANG, Z., BORTOLOTTI, L. E., LI, Z., ARMSTRONG, L. M., BELL, T. W. & LI, Y. 2021c. Heterogeneous changes to wetlands in the Canadian prairies under future climate. *Water Resources Research,* 57**,** e2020WR028727.

ZHAO, S., ZHUANG, L., WANG, C., LI, Y., WANG, S. & ZHU, G. 2018. High-throughput analysis of anammox bacteria in wetland and dryland soils along the altitudinal gradient in Qinghai–Tibet Plateau. *Microbiologyopen,* 7**,** e00556.

ZOMER, R., TRABUCCO, A. & USTIN, S. 2009. Building Spectral Libraries for Wetland Land Cover Classification and Hyperspectral Remote Sensing. *Journal of Envornmental Management,* 90**,** 2170 - 2177.

Appendices

Appendix 4.1: Vegetation of the Mfabeni wetland

Spatial Distribution of vegetation communities in the Mfabeni Wetland

"Sedge/reed fen vegetation communities (0.3–1.5 m tall) cover the northern and eastern parts of the wetland and include the sedges; Cladium mariscus, Fimbristylis bivalvis, Rhynchospora holo-schoenoides and Phragmites australis with the grasses; Panicum glandulopaniculatum and Ischaemum fasciculatum" (Grundling et al., 2015). The western and southern parts of the wetland are covered by swamp forest with an intermediate canopy 6–15 meters above ground level.

Vegetation Community Names

Community names matched to the numbers provided on the map legend, including sub-classes and variants (where applicable) as assigned by (Venter, 2003) are as provided below:

1. *Restio zuluensis – Andropogon appendiculatus closed low sedge and grass peatland*
2. *Scleria poiformis closed tall sedge peatland*
    - 2.1. *Scleria poiformis typical sub-community*
    - 2.2. *Scleria poiformis – Dactylotenium species sub-community*
    - 2.3. *Scleria poiformis – Leersia hexandra sub-community*
3. *Rhynchospora holoschoenoides open to closed short sedge peatland*
    - 3.1. *Rhynchospora holoschoenoides – Panicum brevifolium sub-community*
    - 3.2. *Rhynchospora holoschoenoides – Pycreus nitidus sub-community*
4. *Typha capensis – Ludwigia octovalvis closed high peatland*
5. *Eleocharis dulcis closed tall sedge peatland*
    - 5.1. *Nymphaea nouchali – Utricularia species sub-community*
    - 5.2. *Eleocharis dulcis – Schoenoplectus brachyceras sub-community*
6. *Rhynchospora corymbosa closed low sedge peatland*
7. *Fimbristylis bivalvis open to closed short sedge peatland*
    - 7.1. *Fimbristylis bivalvis – Schoenoplectus brachyceras sub-community*
    - 7.2. *Fimbristylis bivalvis – typical sub-community*
8. *Sphagnum truncatum – Xyris natalensis closed short moss peatland*
    - 8.1. *Sphagnum truncatum – Xyris natalensis sub-community*
        - 8.1.1. *Andropogon huillensis variant*
        - 8.1.2. *Fimbristylis bivalvis variant*
        - 8.1.3. *Xyris natalensis variant*
        - 8.1.4. *Eulophia angolensis variant*
    - 8.2. *Sphagnum truncatum – Laurembergia repens sub-community*
9. *Cladium mariscus closed high sedge peatland*
    - 9.1. *Cladium mariscus – Cynodon dactylon sub-community*

Appendix 5.1: Spectra for 85 pixels randomly sampled from Class 1

ENVI ASCII Plot File [Sat Aug 13 16:51:20 2022]

Column 1: Wavelength

Column 2: MfabeniL1TRef (544,1850)~~2##255,0,0

Column 3: MfabeniL1TRef (546,1851)~~22##0,128,0

Column 4: MfabeniL1TRef (548,1851)~~4##0,0,255

Column 5: MfabeniL1TRef (547,1852)~~6##0,255,255

Column 6: MfabeniL1TRef (545,1853)~~7##255,0,255

Column 7: MfabeniL1TRef (543,1853)~~28##128,128,0

Column 8: MfabeniL1TRef (540,1853)~~31##0,128,128

Column 9: MfabeniL1TRef (539,1855)~~19##128,0,0

Column 10: MfabeniL1TRef (541,1855)~~3##0,255,0

Column 11: MfabeniL1TRef (544,1856)~~25##0,0,128

Column 12: MfabeniL1TRef (544,1856)~~11##255,127,80

Column 13: MfabeniL1TRef (539,1857)~~15##127,255,0

Column 14: MfabeniL1TRef (542,1857)~~13##238,130,238

Column 15: MfabeniL1TRef (545,1858)~~18##220,20,60

Column 16: MfabeniL1TRef (542,1860)~~9##46,139,87

Column 17: MfabeniL1TRef (539,1860)~~25##25,25,112

Column 18: MfabeniL1TRef (536,1860)~~41##255,165,0

Column 19: MfabeniL1TRef (533,1860)~~12##127,255,212

Column 20: MfabeniL1TRef (534,1862)~~13##218,112,214

Column 21: MfabeniL1TRef (536,1862)~~16##216,191,216

Column 22: MfabeniL1TRef (539,1863)~~16##221,160,221

Column 23: MfabeniL1TRef (539,1866)~~40##75,0,130

Column 24: MfabeniL1TRef (536,1865)~~39##65,105,225

Column 25: MfabeniL1TRef (534,1865)~~31##70,130,180

Column 26: MfabeniL1TRef (533,1868)~~48##230,230,250

Column 27: MfabeniL1TRef (533,1870)~~1##240,255,255

Column 28: MfabeniL1TRef (533,1870)~~30##64,224,208

Column 29: MfabeniL1TRef (531,1871)~~1##240,255,240

Column 30: MfabeniL1TRef (551,1856)~~9##34,139,34

Column 31: MfabeniL1TRef (553,1856)~~15##124,252,0

Column 32: MfabeniL1TRef (555,1857)~~1##255,255,240

Column 33: MfabeniL1TRef (556,1858)~~48##240,230,140

Column 34: MfabeniL1TRef (558,1859)~~48##245,222,179

Column 35: MfabeniL1TRef (558,1859)~~5##255,215,0

Column 36: MfabeniL1TRef (554,1860)~~1##255,248,220

Column 37: MfabeniL1TRef (551,1860)~~48##255,228,181

Column 38: MfabeniL1TRef (552,1858)~~48##255,218,185

Column 39: MfabeniL1TRef (556,1862)~~46##210,105,30

Column 40: MfabeniL1TRef (556,1862)~~14##160,82,45

Column 41: MfabeniL1TRef (559,1862)~~48##255,228,225

Column 42: MfabeniL1TRef (561,1860)~~11##250,128,114

Column 43: MfabeniL1TRef (559,1865)~~11##255,99,71

Column 44: MfabeniL1TRef (555,1864)~~16##255,192,203

Column 45: MfabeniL1TRef (551,1862)~~14##165,42,42

Column 46: MfabeniL1TRef (548,1863)~~14##178,34,34

Column 47: MfabeniL1TRef (549,1865)~~49##192,192,192

Column 48: MfabeniL1TRef (547,1865)~~2##255,0,0

Column 49: MfabeniL1TRef (547,1867)~~22##0,128,0

Column 50: MfabeniL1TRef (545,1869)~~4##0,0,255

Column 51: MfabeniL1TRef (545,1871)~~5##255,255,0

Column 52: MfabeniL1TRef (545,1871)~~6##0,255,255

Column 53: MfabeniL1TRef (542,1870)~~7##255,0,255

Column 54: MfabeniL1TRef (543,1872)~~28##128,128,0

Column 55: MfabeniL1TRef (542,1875)~~31##0,128,128

Column 56: MfabeniL1TRef (541,1873)~~19##128,0,0

Column 57: MfabeniL1TRef (539,1874)~~3##0,255,0

Column 58: MfabeniL1TRef (540,1876)~~25##0,0,128

Column 59: MfabeniL1TRef (539,1877)~~11##255,127,80

Column 60: MfabeniL1TRef (537,1878)~~15##127,255,0

Column 61: MfabeniL1TRef (542,1884)~~13##238,130,238

Column 62: MfabeniL1TRef (542,1884)~~18##220,20,60

Column 63: MfabeniL1TRef (542,1887)~~9##46,139,87

Column 64: MfabeniL1TRef (543,1891)~~25##25,25,112

Column 65: MfabeniL1TRef (545,1888)~~41##255,165,0

Column 66: MfabeniL1TRef (545,1885)~~12##127,255,212

Column 67: MfabeniL1TRef (545,1885)~~13##218,112,214

Column 68: MfabeniL1TRef (544,1881)~~16##216,191,216

Column 69: MfabeniL1TRef (547,1882)~~16##221,160,221

Column 70: MfabeniL1TRef (548,1886)~~40##75,0,130

Column 71: MfabeniL1TRef (550,1881)~~39##65,105,225

Column 72: MfabeniL1TRef (547,1879)~~31##70,130,180

Column 73: MfabeniL1TRef (547,1875)~~48##230,230,250

Column 74: MfabeniL1TRef (549,1877)~~1##240,255,255

Column 75: MfabeniL1TRef (553,1878)~~30##64,224,208

Column 76: MfabeniL1TRef (554,1875)~~1##240,255,240

Column 77: MfabeniL1TRef (550,1875)~~9##34,139,34

Column 78: MfabeniL1TRef (549,1871)~~15##124,252,0

Column 79: MfabeniL1TRef (549,1871)~~1##255,255,240

Column 80: MfabeniL1TRef (552,1871)~~48##240,230,140

Column 81: MfabeniL1TRef (552,1871)~~48##245,222,179

Column 82: MfabeniL1TRef (555,1872)~~5##255,215,0

Column 83: MfabeniL1TRef (555,1872)~~1##255,248,220

Column 84: MfabeniL1TRef (556,1875)~~48##255,228,181

Column 85: MfabeniL1TRef (555,1870)~~48##255,218,185

Column 86: MfabeniL1TRef (546,1867)~~46##210,105,30

426.820007 117.000000 196.000000 165.000000 66.000000 -20.000000 189.000000 -102.000000
276.000000 220.000000 -51.000000 -51.000000 47.000000 76.000000 39.000000 -44.000000
419.000000 250.000000 568.000000 83.000000 136.000000 382.000000 201.000000 -22.000000
257.000000 13.000000 -238.000000 -238.000000 191.000000 245.000000 27.000000 211.000000
201.000000 313.000000 313.000000 184.000000 -30.000000 300.000000 472.000000 472.000000
281.000000 30.000000 81.000000 332.000000 59.000000 163.000000 32.000000 233.000000
349.000000 78.000000 269.000000 269.000000 -300.000000 112.000000 37.000000 -259.000000 -
71.000000 291.000000 -109.000000 117.000000 438.000000 438.000000 182.000000 141.000000
112.000000 -13.000000 -13.000000 233.000000 -25.000000 95.000000 153.000000 -73.000000
199.000000 6.000000 339.000000 131.000000 66.000000 44.000000 44.000000 168.000000
168.000000 230.000000 230.000000 -66.000000 245.000000 407.000000

436.989990 225.000000 116.000000 18.000000 -79.000000 -66.000000 5.000000 13.000000
75.000000 176.000000 28.000000 28.000000 214.000000 10.000000 111.000000 212.000000
222.000000 21.000000 88.000000 235.000000 52.000000 325.000000 235.000000 196.000000
44.000000 -61.000000 -136.000000 -136.000000 13.000000 225.000000 80.000000 -22.000000
181.000000 271.000000 271.000000 101.000000 -105.000000 21.000000 305.000000 305.000000
284.000000 -213.000000 101.000000 199.000000 -48.000000 217.000000 238.000000 132.000000
444.000000 137.000000 147.000000 147.000000 41.000000 -51.000000 -89.000000 -43.000000
28.000000 -97.000000 163.000000 212.000000 168.000000 168.000000 -89.000000 158.000000 -
48.000000 -69.000000 -69.000000 230.000000 -169.000000 13.000000 -120.000000 -48.000000
57.000000 -12.000000 220.000000 116.000000 -20.000000 -151.000000 -151.000000 -27.000000 -
27.000000 21.000000 21.000000 52.000000 308.000000 145.000000

447.170013 7.000000 -223.000000 -286.000000 -220.000000 -316.000000 -208.000000 -232.000000 -
91.000000 -169.000000 -274.000000 -274.000000 -229.000000 -256.000000 -10.000000 85.000000
25.000000 -160.000000 40.000000 -187.000000 10.000000 -34.000000 -130.000000 -205.000000 -
214.000000 -349.000000 -355.000000 -355.000000 -271.000000 -58.000000 -91.000000 -184.000000 -
1.000000 -187.000000 -187.000000 -211.000000 -202.000000 -193.000000 55.000000 55.000000 -
46.000000 -304.000000 -130.000000 -73.000000 -274.000000 -184.000000 -34.000000 -82.000000 -
43.000000 -145.000000 -67.000000 -67.000000 -235.000000 -319.000000 -382.000000 -421.000000 -
139.000000 -304.000000 -217.000000 -115.000000 -100.000000 -100.000000 -325.000000 -265.000000 -
274.000000 -442.000000 -442.000000 -139.000000 -400.000000 -343.000000 -331.000000 -175.000000 -
214.000000 -220.000000 -196.000000 -268.000000 -292.000000 -232.000000 -232.000000 -325.000000 -
325.000000 -334.000000 -334.000000 -235.000000 -88.000000 -70.000000

457.339996 4.000000 59.000000 -148.000000 -218.000000 -187.000000 -349.000000 -294.000000
10.000000 88.000000 -182.000000 -182.000000 30.000000 -161.000000 114.000000 106.000000 -
26.000000 -31.000000 56.000000 -31.000000 -23.000000 124.000000 83.000000 -47.000000 -
96.000000 -166.000000 -380.000000 -380.000000 -114.000000 -10.000000 143.000000 -86.000000
75.000000 59.000000 59.000000 18.000000 -231.000000 -7.000000 12.000000 12.000000
15.000000 -234.000000 -112.000000 44.000000 -57.000000 4.000000 -60.000000 18.000000
33.000000 -62.000000 -34.000000 -34.000000 -286.000000 -198.000000 -237.000000 -185.000000 -
106.000000 -96.000000 -192.000000 0.000000 -44.000000 -44.000000 -23.000000 -31.000000 -
166.000000 -250.000000 -250.000000 -57.000000 -229.000000 -182.000000 -148.000000 -190.000000 -
255.000000 -93.000000 -106.000000 -33.000000 -213.000000 -54.000000 -54.000000 -88.000000 -
88.000000 -192.000000 -192.000000 -244.000000 -2.000000 28.000000

467.519989 160.000000 178.000000 -1.000000 -138.000000 5.000000 -44.000000 -197.000000
108.000000 25.000000 -42.000000 -42.000000 101.000000 21.000000 142.000000 144.000000
149.000000 67.000000 128.000000 105.000000 133.000000 204.000000 140.000000 44.000000
44.000000 -133.000000 -163.000000 -163.000000 5.000000 160.000000 222.000000 74.000000
156.000000 78.000000 78.000000 140.000000 -49.000000 94.000000 156.000000 156.000000
62.000000 -108.000000 39.000000 74.000000 10.000000 37.000000 -8.000000 110.000000
110.000000 99.000000 62.000000 62.000000 -44.000000 -94.000000 -254.000000 -101.000000 -
44.000000 35.000000 -72.000000 42.000000 60.000000 60.000000 -35.000000 19.000000 -
26.000000 -149.000000 -149.000000 19.000000 -74.000000 -65.000000 -67.000000 -90.000000 -
106.000000 -3.000000 58.000000 65.000000 10.000000 92.000000 92.000000 44.000000
44.000000 -56.000000 -56.000000 -67.000000 44.000000 35.000000

477.690002 330.000000 315.000000 160.000000 119.000000 244.000000 112.000000 62.000000
267.000000 251.000000 168.000000 168.000000 301.000000 185.000000 339.000000 317.000000
380.000000 349.000000 324.000000 287.000000 339.000000 326.000000 255.000000 226.000000
289.000000 141.000000 77.000000 77.000000 192.000000 292.000000 351.000000 266.000000
310.000000 285.000000 285.000000 296.000000 203.000000 298.000000 330.000000 330.000000
307.000000 105.000000 278.000000 276.000000 223.000000 216.000000 193.000000 260.000000

258.000000 210.000000 230.000000 230.000000 135.000000 105.000000 -6.000000 109.000000
119.000000 214.000000 135.000000 267.000000 232.000000 232.000000 209.000000 184.000000
177.000000 123.000000 123.000000 153.000000 128.000000 125.000000 169.000000 77.000000
123.000000 209.000000 173.000000 234.000000 189.000000 214.000000 214.000000 184.000000
184.000000 189.000000 189.000000 132.000000 276.000000 234.000000

487.869995 353.000000 347.000000 226.000000 129.000000 228.000000 110.000000 55.000000
335.000000 258.000000 180.000000 180.000000 302.000000 203.000000 316.000000 302.000000
411.000000 322.000000 335.000000 304.000000 372.000000 374.000000 320.000000 256.000000
291.000000 215.000000 1.000000 1.000000 199.000000 258.000000 421.000000 221.000000
283.000000 281.000000 281.000000 293.000000 121.000000 310.000000 289.000000 289.000000
246.000000 124.000000 258.000000 256.000000 234.000000 205.000000 209.000000 258.000000
273.000000 227.000000 170.000000 170.000000 90.000000 92.000000 40.000000 166.000000
118.000000 203.000000 178.000000 267.000000 248.000000 248.000000 170.000000 184.000000
186.000000 127.000000 127.000000 182.000000 112.000000 118.000000 125.000000 145.000000
125.000000 234.000000 160.000000 252.000000 147.000000 277.000000 277.000000 229.000000
229.000000 168.000000 168.000000 83.000000 267.000000 209.000000

498.040009 401.000000 407.000000 218.000000 162.000000 318.000000 164.000000 91.000000
359.000000 314.000000 237.000000 237.000000 284.000000 261.000000 422.000000 411.000000
489.000000 363.000000 370.000000 328.000000 426.000000 426.000000 349.000000 303.000000
362.000000 189.000000 53.000000 53.000000 251.000000 376.000000 461.000000 297.000000
357.000000 322.000000 322.000000 361.000000 197.000000 314.000000 414.000000 414.000000
386.000000 178.000000 336.000000 301.000000 282.000000 235.000000 268.000000 353.000000
332.000000 316.000000 299.000000 299.000000 262.000000 134.000000 82.000000 189.000000
228.000000 278.000000 232.000000 318.000000 297.000000 297.000000 239.000000 282.000000
184.000000 216.000000 216.000000 247.000000 155.000000 234.000000 187.000000 172.000000
203.000000 289.000000 251.000000 280.000000 232.000000 314.000000 314.000000 234.000000
234.000000 176.000000 176.000000 159.000000 299.000000 289.000000

508.220001 518.000000 488.000000 273.000000 243.000000 367.000000 224.000000 171.000000
458.000000 405.000000 277.000000 277.000000 379.000000 313.000000 545.000000 507.000000
594.000000 458.000000 501.000000 430.000000 503.000000 511.000000 435.000000 381.000000
407.000000 288.000000 171.000000 171.000000 320.000000 418.000000 529.000000 401.000000
443.000000 433.000000 433.000000 399.000000 267.000000 458.000000 428.000000 428.000000
414.000000 277.000000 390.000000 373.000000 331.000000 316.000000 339.000000 433.000000
316.000000 337.000000 331.000000 331.000000 262.000000 184.000000 166.000000 211.000000
292.000000 326.000000 264.000000 375.000000 362.000000 362.000000 294.000000 314.000000
324.000000 254.000000 254.000000 303.000000 143.000000 244.000000 197.000000 250.000000
248.000000 318.000000 297.000000 390.000000 245.000000 420.000000 420.000000 363.000000
363.000000 296.000000 296.000000 241.000000 384.000000 354.000000

518.390015 561.000000 584.000000 312.000000 264.000000 389.000000 221.000000 134.000000
507.000000 389.000000 327.000000 327.000000 345.000000 322.000000 530.000000 557.000000
575.000000 488.000000 519.000000 441.000000 555.000000 488.000000 501.000000 465.000000
470.000000 304.000000 161.000000 161.000000 360.000000 465.000000 617.000000 422.000000
474.000000 472.000000 472.000000 459.000000 256.000000 505.000000 501.000000 501.000000
486.000000 316.000000 451.000000 399.000000 370.000000 343.000000 356.000000 439.000000
410.000000 368.000000 354.000000 354.000000 327.000000 206.000000 142.000000 300.000000
291.000000 385.000000 322.000000 395.000000 397.000000 397.000000 302.000000 339.000000
329.000000 298.000000 298.000000 339.000000 233.000000 298.000000 252.000000 291.000000
279.000000 356.000000 302.000000 383.000000 316.000000 439.000000 439.000000 356.000000
356.000000 314.000000 314.000000 209.000000 420.000000 383.000000

528.570007 593.000000 676.000000 385.000000 276.000000 458.000000 312.000000 238.000000
599.000000 472.000000 367.000000 367.000000 482.000000 383.000000 682.000000 597.000000
623.000000 516.000000 615.000000 506.000000 607.000000 629.000000 496.000000 536.000000
547.000000 361.000000 234.000000 234.000000 421.000000 522.000000 706.000000 526.000000
538.000000 621.000000 621.000000 585.000000 318.000000 530.000000 619.000000 619.000000
627.000000 387.000000 540.000000 522.000000 433.000000 359.000000 437.000000 524.000000
524.000000 450.000000 421.000000 421.000000 377.000000 252.000000 248.000000 361.000000
395.000000 472.000000 389.000000 490.000000 492.000000 492.000000 413.000000 383.000000
363.000000 330.000000 330.000000 411.000000 338.000000 349.000000 363.000000 334.000000
344.000000 443.000000 363.000000 453.000000 429.000000 528.000000 528.000000 456.000000
456.000000 304.000000 304.000000 336.000000 534.000000 472.000000

538.739990 776.000000 774.000000 521.000000 442.000000 611.000000 479.000000 426.000000
733.000000 626.000000 569.000000 569.000000 604.000000 592.000000 807.000000 763.000000
804.000000 671.000000 747.000000 634.000000 747.000000 719.000000 682.000000 643.000000
677.000000 482.000000 413.000000 413.000000 541.000000 678.000000 811.000000 618.000000
707.000000 806.000000 806.000000 735.000000 496.000000 730.000000 740.000000 740.000000
784.000000 574.000000 749.000000 678.000000 606.000000 530.000000 585.000000 645.000000
634.000000 597.000000 562.000000 562.000000 511.000000 444.000000 405.000000 497.000000
592.000000 580.000000 542.000000 629.000000 608.000000 608.000000 571.000000 574.000000
542.000000 498.000000 498.000000 548.000000 449.000000 496.000000 495.000000 507.000000
496.000000 548.000000 546.000000 675.000000 514.000000 636.000000 636.000000 592.000000
592.000000 474.000000 474.000000 484.000000 638.000000 576.000000

548.919983 779.000000 820.000000 575.000000 463.000000 682.000000 497.000000 461.000000
726.000000 641.000000 598.000000 598.000000 637.000000 609.000000 801.000000 769.000000
820.000000 715.000000 785.000000 671.000000 815.000000 811.000000 735.000000 660.000000
714.000000 509.000000 456.000000 456.000000 577.000000 730.000000 880.000000 721.000000
744.000000 777.000000 777.000000 753.000000 491.000000 781.000000 806.000000 806.000000
815.000000 621.000000 776.000000 710.000000 628.000000 562.000000 619.000000 632.000000
678.000000 600.000000 577.000000 577.000000 536.000000 461.000000 417.000000 509.000000
598.000000 676.000000 598.000000 650.000000 643.000000 643.000000 571.000000 614.000000
570.000000 543.000000 543.000000 616.000000 483.000000 548.000000 561.000000 559.000000
541.000000 618.000000 596.000000 666.000000 584.000000 726.000000 726.000000 626.000000
626.000000 509.000000 509.000000 506.000000 696.000000 623.000000

559.090027 815.000000 822.000000 606.000000 520.000000 707.000000 513.000000 506.000000
736.000000 679.000000 592.000000 592.000000 688.000000 647.000000 833.000000 769.000000
792.000000 760.000000 822.000000 698.000000 813.000000 801.000000 759.000000 741.000000
775.000000 567.000000 479.000000 479.000000 606.000000 755.000000 914.000000 771.000000
757.000000 872.000000 872.000000 752.000000 486.000000 759.000000 845.000000 845.000000
859.000000 658.000000 838.000000 748.000000 640.000000 583.000000 626.000000 734.000000
686.000000 670.000000 640.000000 640.000000 539.000000 488.000000 463.000000 530.000000
617.000000 652.000000 610.000000 686.000000 686.000000 686.000000 642.000000 633.000000
612.000000 578.000000 578.000000 606.000000 504.000000 583.000000 562.000000 592.000000
591.000000 658.000000 628.000000 699.000000 621.000000 700.000000 700.000000 651.000000
651.000000 529.000000 529.000000 571.000000 698.000000 665.000000

569.270020 835.000000 826.000000 591.000000 509.000000 702.000000 514.000000 481.000000
751.000000 698.000000 578.000000 578.000000 676.000000 606.000000 833.000000 799.000000
875.000000 760.000000 816.000000 713.000000 839.000000 833.000000 775.000000 732.000000
760.000000 556.000000 464.000000 464.000000 610.000000 769.000000 919.000000 773.000000
790.000000 863.000000 863.000000 769.000000 505.000000 814.000000 859.000000 859.000000
867.000000 698.000000 887.000000 726.000000 670.000000 563.000000 643.000000 717.000000

689.000000 664.000000 623.000000 623.000000 552.000000 496.000000 468.000000 550.000000
635.000000 687.000000 614.000000 698.000000 670.000000 670.000000 612.000000 612.000000
610.000000 593.000000 593.000000 638.000000 516.000000 559.000000 574.000000 572.000000
593.000000 643.000000 636.000000 720.000000 565.000000 709.000000 709.000000 647.000000
647.000000 529.000000 529.000000 555.000000 705.000000 651.000000

579.450012 785.000000 805.000000 559.000000 463.000000 638.000000 443.000000 388.000000
691.000000 608.000000 565.000000 565.000000 618.000000 571.000000 805.000000 740.000000
805.000000 738.000000 760.000000 695.000000 811.000000 786.000000 699.000000 693.000000
699.000000 510.000000 392.000000 392.000000 597.000000 734.000000 928.000000 681.000000
748.000000 854.000000 854.000000 716.000000 500.000000 797.000000 834.000000 834.000000
852.000000 608.000000 785.000000 712.000000 635.000000 510.000000 590.000000 632.000000
665.000000 630.000000 596.000000 596.000000 514.000000 439.000000 384.000000 502.000000
585.000000 652.000000 573.000000 652.000000 648.000000 648.000000 577.000000 585.000000
575.000000 527.000000 527.000000 608.000000 504.000000 510.000000 508.000000 579.000000
512.000000 608.000000 571.000000 683.000000 547.000000 712.000000 712.000000 606.000000
606.000000 478.000000 478.000000 498.000000 657.000000 636.000000

589.619995 757.000000 781.000000 527.000000 437.000000 662.000000 464.000000 405.000000
724.000000 636.000000 547.000000 547.000000 651.000000 582.000000 811.000000 766.000000
829.000000 725.000000 777.000000 745.000000 815.000000 828.000000 684.000000 697.000000
749.000000 553.000000 422.000000 422.000000 556.000000 732.000000 934.000000 691.000000
788.000000 822.000000 822.000000 739.000000 477.000000 776.000000 815.000000 815.000000
870.000000 591.000000 800.000000 703.000000 622.000000 541.000000 594.000000 646.000000
618.000000 630.000000 585.000000 585.000000 536.000000 441.000000 390.000000 531.000000
586.000000 671.000000 577.000000 672.000000 623.000000 623.000000 589.000000 613.000000
568.000000 557.000000 557.000000 577.000000 486.000000 508.000000 510.000000 549.000000
497.000000 620.000000 584.000000 665.000000 536.000000 697.000000 697.000000 619.000000
619.000000 493.000000 493.000000 493.000000 658.000000 622.000000

599.799988 791.000000 835.000000 548.000000 485.000000 678.000000 469.000000 403.000000
777.000000 682.000000 549.000000 549.000000 640.000000 567.000000 808.000000 808.000000
872.000000 752.000000 789.000000 730.000000 839.000000 848.000000 720.000000 720.000000
736.000000 530.000000 408.000000 408.000000 582.000000 738.000000 931.000000 721.000000
730.000000 799.000000 799.000000 795.000000 496.000000 792.000000 846.000000 846.000000
863.000000 594.000000 809.000000 722.000000 594.000000 532.000000 577.000000 656.000000
638.000000 661.000000 598.000000 598.000000 577.000000 448.000000 394.000000 517.000000
583.000000 624.000000 611.000000 698.000000 687.000000 687.000000 599.000000 636.000000
590.000000 560.000000 560.000000 600.000000 486.000000 525.000000 539.000000 550.000000
565.000000 577.000000 594.000000 678.000000 538.000000 728.000000 728.000000 637.000000
637.000000 475.000000 475.000000 488.000000 687.000000 628.000000

609.969971 787.000000 785.000000 528.000000 430.000000 633.000000 464.000000 364.000000
720.000000 655.000000 544.000000 544.000000 620.000000 564.000000 829.000000 796.000000
860.000000 765.000000 762.000000 731.000000 831.000000 818.000000 693.000000 700.000000
769.000000 515.000000 393.000000 393.000000 575.000000 769.000000 927.000000 711.000000
782.000000 791.000000 791.000000 756.000000 480.000000 822.000000 831.000000 831.000000
827.000000 569.000000 778.000000 734.000000 596.000000 560.000000 616.000000 644.000000
606.000000 620.000000 584.000000 584.000000 508.000000 457.000000 364.000000 506.000000
578.000000 655.000000 564.000000 693.000000 691.000000 691.000000 626.000000 613.000000
577.000000 548.000000 548.000000 602.000000 475.000000 497.000000 522.000000 569.000000
558.000000 615.000000 580.000000 678.000000 553.000000 716.000000 716.000000 615.000000
615.000000 477.000000 477.000000 477.000000 642.000000 586.000000

620.150024 758.000000 792.000000 475.000000 424.000000 636.000000 482.000000 334.000000
711.000000 614.000000 533.000000 533.000000 595.000000 574.000000 803.000000 798.000000
845.000000 749.000000 771.000000 704.000000 837.000000 790.000000 674.000000 709.000000
792.000000 525.000000 362.000000 362.000000 563.000000 713.000000 897.000000 681.000000
741.000000 796.000000 796.000000 777.000000 471.000000 766.000000 884.000000 884.000000
895.000000 567.000000 781.000000 745.000000 593.000000 538.000000 557.000000 655.000000
610.000000 589.000000 540.000000 540.000000 495.000000 409.000000 338.000000 477.000000
555.000000 621.000000 597.000000 631.000000 655.000000 655.000000 608.000000 593.000000
576.000000 495.000000 495.000000 593.000000 478.000000 520.000000 507.000000 510.000000
512.000000 591.000000 569.000000 676.000000 559.000000 683.000000 683.000000 589.000000
589.000000 492.000000 492.000000 479.000000 627.000000 608.000000

630.320007 780.000000 786.000000 499.000000 421.000000 621.000000 427.000000 387.000000
726.000000 625.000000 501.000000 501.000000 651.000000 523.000000 826.000000 781.000000
859.000000 790.000000 776.000000 720.000000 812.000000 834.000000 688.000000 702.000000
796.000000 537.000000 365.000000 365.000000 537.000000 749.000000 924.000000 674.000000
753.000000 790.000000 790.000000 739.000000 466.000000 770.000000 831.000000 831.000000
851.000000 576.000000 806.000000 741.000000 635.000000 521.000000 560.000000 653.000000
645.000000 635.000000 584.000000 584.000000 501.000000 423.000000 348.000000 501.000000
592.000000 615.000000 592.000000 702.000000 664.000000 664.000000 570.000000 607.000000
572.000000 534.000000 534.000000 568.000000 458.000000 452.000000 503.000000 525.000000
483.000000 605.000000 580.000000 676.000000 552.000000 678.000000 678.000000 621.000000
621.000000 509.000000 509.000000 397.000000 645.000000 645.000000

640.500000 785.000000 739.000000 482.000000 361.000000 605.000000 400.000000 272.000000
714.000000 655.000000 537.000000 537.000000 624.000000 540.000000 782.000000 758.000000
834.000000 745.000000 781.000000 702.000000 809.000000 819.000000 688.000000 657.000000
805.000000 525.000000 342.000000 342.000000 546.000000 723.000000 929.000000 680.000000
744.000000 803.000000 803.000000 736.000000 464.000000 775.000000 840.000000 840.000000
861.000000 556.000000 774.000000 703.000000 620.000000 542.000000 542.000000 645.000000
636.000000 573.000000 519.000000 519.000000 544.000000 387.000000 272.000000 486.000000
537.000000 626.000000 589.000000 700.000000 642.000000 642.000000 589.000000 564.000000
559.000000 528.000000 528.000000 597.000000 466.000000 446.000000 491.000000 497.000000
456.000000 585.000000 569.000000 676.000000 491.000000 676.000000 676.000000 598.000000
598.000000 474.000000 474.000000 454.000000 616.000000 618.000000

650.669983 792.000000 801.000000 473.000000 414.000000 619.000000 426.000000 323.000000
786.000000 621.000000 503.000000 503.000000 644.000000 546.000000 870.000000 793.000000
883.000000 787.000000 807.000000 732.000000 842.000000 832.000000 705.000000 720.000000
820.000000 508.000000 364.000000 364.000000 569.000000 734.000000 967.000000 666.000000
756.000000 771.000000 771.000000 785.000000 492.000000 805.000000 846.000000 846.000000
855.000000 575.000000 800.000000 738.000000 607.000000 552.000000 550.000000 647.000000
647.000000 619.000000 560.000000 560.000000 519.000000 414.000000 312.000000 505.000000
551.000000 692.000000 608.000000 715.000000 667.000000 667.000000 616.000000 633.000000
586.000000 531.000000 531.000000 623.000000 469.000000 484.000000 517.000000 524.000000
514.000000 601.000000 545.000000 703.000000 520.000000 725.000000 725.000000 604.000000
604.000000 510.000000 510.000000 447.000000 632.000000 639.000000

660.849976 827.000000 853.000000 598.000000 465.000000 679.000000 533.000000 390.000000
839.000000 709.000000 598.000000 598.000000 739.000000 630.000000 881.000000 859.000000
953.000000 840.000000 870.000000 807.000000 921.000000 920.000000 788.000000 782.000000
835.000000 608.000000 384.000000 384.000000 621.000000 802.000000 1012.000000 723.000000
845.000000 826.000000 826.000000 845.000000 577.000000 860.000000 935.000000 935.000000
922.000000 643.000000 842.000000 813.000000 703.000000 643.000000 616.000000 780.000000

696.000000 674.000000 629.000000 629.000000 613.000000 504.000000 398.000000 593.000000
604.000000 726.000000 653.000000 790.000000 741.000000 741.000000 681.000000 696.000000
644.000000 594.000000 594.000000 679.000000 558.000000 558.000000 577.000000 602.000000
579.000000 699.000000 652.000000 780.000000 615.000000 723.000000 723.000000 701.000000
701.000000 568.000000 568.000000 496.000000 684.000000 705.000000

671.020020 824.000000 813.000000 555.000000 447.000000 674.000000 503.000000 386.000000
809.000000 705.000000 568.000000 568.000000 721.000000 633.000000 889.000000 889.000000
919.000000 844.000000 899.000000 842.000000 912.000000 921.000000 741.000000 797.000000
869.000000 570.000000 431.000000 431.000000 622.000000 816.000000 1008.000000 741.000000
804.000000 788.000000 788.000000 824.000000 580.000000 872.000000 908.000000 908.000000
883.000000 622.000000 858.000000 779.000000 687.000000 656.000000 597.000000 712.000000
665.000000 705.000000 624.000000 624.000000 611.000000 496.000000 344.000000 573.000000
606.000000 703.000000 645.000000 811.000000 759.000000 759.000000 707.000000 688.000000
665.000000 593.000000 593.000000 660.000000 568.000000 548.000000 573.000000 620.000000
532.000000 705.000000 638.000000 775.000000 609.000000 768.000000 768.000000 687.000000
687.000000 562.000000 562.000000 485.000000 707.000000 696.000000

681.200012 861.000000 876.000000 583.000000 456.000000 705.000000 514.000000 418.000000
821.000000 741.000000 654.000000 654.000000 790.000000 636.000000 938.000000 894.000000
967.000000 878.000000 870.000000 869.000000 910.000000 958.000000 729.000000 801.000000
914.000000 616.000000 432.000000 432.000000 638.000000 865.000000 1047.000000 756.000000
863.000000 830.000000 830.000000 870.000000 601.000000 905.000000 958.000000 958.000000
939.000000 645.000000 894.000000 807.000000 692.000000 678.000000 634.000000 765.000000
721.000000 707.000000 643.000000 643.000000 647.000000 543.000000 361.000000 623.000000
629.000000 738.000000 696.000000 847.000000 798.000000 798.000000 749.000000 725.000000
690.000000 605.000000 605.000000 683.000000 587.000000 572.000000 599.000000 625.000000
610.000000 690.000000 678.000000 790.000000 683.000000 779.000000 779.000000 703.000000
703.000000 585.000000 585.000000 545.000000 718.000000 729.000000

691.369995 940.000000 926.000000 624.000000 505.000000 773.000000 611.000000 462.000000
922.000000 823.000000 662.000000 662.000000 856.000000 686.000000 1001.000000 954.000000
1061.000000 942.000000 972.000000 936.000000 1014.000000 992.000000 801.000000 859.000000
924.000000 631.000000 459.000000 459.000000 673.000000 932.000000 1137.000000 846.000000
948.000000 898.000000 898.000000 936.000000 690.000000 944.000000 1065.000000 1065.000000
1029.000000 748.000000 973.000000 897.000000 769.000000 694.000000 673.000000 833.000000
749.000000 805.000000 679.000000 679.000000 720.000000 556.000000 427.000000 674.000000
678.000000 811.000000 720.000000 890.000000 837.000000 837.000000 773.000000 773.000000
767.000000 690.000000 690.000000 752.000000 643.000000 621.000000 654.000000 676.000000
649.000000 785.000000 741.000000 862.000000 727.000000 879.000000 879.000000 774.000000
774.000000 641.000000 641.000000 600.000000 814.000000 787.000000

701.549988 993.000000 987.000000 691.000000 588.000000 839.000000 665.000000 542.000000
940.000000 861.000000 733.000000 733.000000 876.000000 729.000000 1045.000000 1011.000000
1096.000000 1008.000000 1049.000000 976.000000 1056.000000 1066.000000 893.000000 948.000000
974.000000 729.000000 557.000000 557.000000 787.000000 972.000000 1142.000000 849.000000
942.000000 981.000000 981.000000 960.000000 656.000000 999.000000 1036.000000 1036.000000
1093.000000 748.000000 1016.000000 921.000000 807.000000 710.000000 712.000000 848.000000
783.000000 785.000000 720.000000 720.000000 756.000000 599.000000 489.000000 694.000000
763.000000 855.000000 802.000000 962.000000 895.000000 895.000000 811.000000 822.000000
801.000000 712.000000 712.000000 802.000000 679.000000 635.000000 707.000000 718.000000
708.000000 803.000000 765.000000 875.000000 719.000000 887.000000 887.000000 828.000000
828.000000 643.000000 643.000000 602.000000 807.000000 807.000000

711.719971 1363.000000 1314.000000 1067.000000 888.000000 1161.000000 939.000000 901.000000
1272.000000 1168.000000 1054.000000 1054.000000 1051.000000 1084.000000 1462.000000
1266.000000 1379.000000 1298.000000 1394.000000 1157.000000 1376.000000 1358.000000
1313.000000 1309.000000 1297.000000 991.000000 986.000000 986.000000 1091.000000 1228.000000
1472.000000 1225.000000 1261.000000 1533.000000 1533.000000 1340.000000 747.000000
1258.000000 1444.000000 1444.000000 1560.000000 1180.000000 1523.000000 1290.000000
1096.000000 826.000000 1076.000000 1085.000000 1083.000000 1108.000000 1100.000000
1100.000000 903.000000 924.000000 951.000000 983.000000 1156.000000 1257.000000 1190.000000
1218.000000 1215.000000 1215.000000 1147.000000 1085.000000 1141.000000 1075.000000
1075.000000 1098.000000 899.000000 1042.000000 1038.000000 1028.000000 1056.000000
1121.000000 1081.000000 1179.000000 1008.000000 1230.000000 1230.000000 1129.000000
1129.000000 760.000000 760.000000 974.000000 1059.000000 1029.000000

721.900024 1615.000000 1531.000000 1340.000000 1162.000000 1400.000000 1163.000000
1224.000000 1502.000000 1375.000000 1309.000000 1309.000000 1217.000000 1296.000000
1695.000000 1454.000000 1589.000000 1473.000000 1671.000000 1310.000000 1590.000000
1592.000000 1560.000000 1498.000000 1495.000000 1197.000000 1278.000000 1278.000000
1354.000000 1460.000000 1673.000000 1479.000000 1446.000000 1909.000000 1909.000000
1556.000000 853.000000 1403.000000 1670.000000 1670.000000 1835.000000 1521.000000
1835.000000 1556.000000 1295.000000 919.000000 1333.000000 1271.000000 1328.000000
1296.000000 1315.000000 1315.000000 1082.000000 1126.000000 1349.000000 1164.000000
1393.000000 1536.000000 1434.000000 1414.000000 1394.000000 1394.000000 1329.000000
1300.000000 1325.000000 1280.000000 1280.000000 1306.000000 1113.000000 1307.000000
1253.000000 1193.000000 1323.000000 1288.000000 1304.000000 1367.000000 1180.000000
1429.000000 1429.000000 1318.000000 1318.000000 897.000000 897.000000 1199.000000
1243.000000 1207.000000

732.070007 1780.000000 1711.000000 1590.000000 1394.000000 1574.000000 1348.000000
1457.000000 1653.000000 1542.000000 1481.000000 1481.000000 1378.000000 1500.000000
1874.000000 1570.000000 1750.000000 1625.000000 1898.000000 1453.000000 1715.000000
1740.000000 1757.000000 1705.000000 1640.000000 1384.000000 1609.000000 1609.000000
1535.000000 1648.000000 1848.000000 1669.000000 1641.000000 2157.000000 2157.000000
1735.000000 929.000000 1542.000000 1874.000000 1874.000000 2044.000000 1782.000000
2110.000000 1791.000000 1465.000000 1004.000000 1535.000000 1385.000000 1528.000000
1440.000000 1552.000000 1552.000000 1229.000000 1320.000000 1676.000000 1327.000000
1588.000000 1697.000000 1627.000000 1512.000000 1595.000000 1595.000000 1499.000000
1424.000000 1487.000000 1493.000000 1493.000000 1439.000000 1270.000000 1540.000000
1398.000000 1353.000000 1528.000000 1475.000000 1480.000000 1533.000000 1315.000000
1525.000000 1525.000000 1491.000000 1491.000000 976.000000 976.000000 1463.000000
1412.000000 1338.000000

742.250000 1944.000000 1893.000000 1842.000000 1612.000000 1729.000000 1496.000000
1688.000000 1762.000000 1688.000000 1650.000000 1650.000000 1450.000000 1727.000000
2070.000000 1692.000000 1947.000000 1779.000000 2102.000000 1538.000000 1863.000000
1905.000000 1965.000000 1875.000000 1794.000000 1482.000000 1875.000000 1875.000000
1701.000000 1844.000000 2030.000000 1906.000000 1833.000000 2532.000000 2532.000000
1963.000000 980.000000 1696.000000 2098.000000 2098.000000 2371.000000 2114.000000
2462.000000 2081.000000 1628.000000 1060.000000 1732.000000 1546.000000 1690.000000
1623.000000 1760.000000 1760.000000 1270.000000 1441.000000 2058.000000 1421.000000
1754.000000 1902.000000 1810.000000 1644.000000 1711.000000 1711.000000 1658.000000
1608.000000 1653.000000 1682.000000 1682.000000 1572.000000 1393.000000 1793.000000
1558.000000 1501.000000 1763.000000 1622.000000 1673.000000 1693.000000 1474.000000
1703.000000 1703.000000 1700.000000 1700.000000 1043.000000 1043.000000 1723.000000
1537.000000 1454.000000

752.429993 2150.000000 2073.000000 2148.000000 1889.000000 1916.000000 1658.000000
1857.000000 1996.000000 1855.000000 1882.000000 1882.000000 1604.000000 1964.000000
2368.000000 1872.000000 2125.000000 1939.000000 2349.000000 1686.000000 2042.000000
2096.000000 2184.000000 2081.000000 2012.000000 1644.000000 2127.000000 2127.000000
1876.000000 2121.000000 2305.000000 2171.000000 2077.000000 2942.000000 2942.000000
2230.000000 1106.000000 1928.000000 2387.000000 2387.000000 2699.000000 2443.000000
2829.000000 2395.000000 1857.000000 1208.000000 2014.000000 1721.000000 1918.000000
1799.000000 2025.000000 2025.000000 1432.000000 1686.000000 2387.000000 1625.000000
1981.000000 2115.000000 2044.000000 1853.000000 1964.000000 1964.000000 1866.000000
1824.000000 1943.000000 1918.000000 1918.000000 1811.000000 1579.000000 2119.000000
1838.000000 1704.000000 2006.000000 1851.000000 1933.000000 1926.000000 1673.000000
1905.000000 1905.000000 1943.000000 1943.000000 1187.000000 1187.000000 1991.000000
1761.000000 1631.000000

762.599976 2099.000000 2039.000000 2153.000000 1833.000000 1941.000000 1633.000000
1858.000000 1912.000000 1795.000000 1963.000000 1963.000000 1563.000000 1919.000000
2267.000000 1830.000000 2102.000000 1944.000000 2283.000000 1614.000000 2010.000000
2055.000000 2163.000000 2083.000000 1934.000000 1684.000000 2068.000000 2068.000000
1846.000000 2090.000000 2286.000000 2185.000000 2099.000000 2885.000000 2885.000000
2229.000000 1139.000000 1953.000000 2359.000000 2359.000000 2670.000000 2470.000000
2835.000000 2388.000000 1865.000000 1186.000000 1976.000000 1687.000000 1915.000000
1760.000000 2007.000000 2007.000000 1354.000000 1700.000000 2435.000000 1563.000000
1934.000000 2042.000000 1995.000000 1795.000000 1941.000000 1941.000000 1846.000000
1808.000000 1944.000000 1925.000000 1925.000000 1773.000000 1605.000000 2061.000000
1817.000000 1659.000000 2020.000000 1852.000000 1938.000000 1947.000000 1649.000000
1877.000000 1877.000000 1906.000000 1906.000000 1253.000000 1253.000000 2017.000000
1785.000000 1598.000000

772.780029 2077.000000 1988.000000 2079.000000 1806.000000 1879.000000 1602.000000
1852.000000 1874.000000 1810.000000 1823.000000 1823.000000 1528.000000 1903.000000
2227.000000 1808.000000 2079.000000 1903.000000 2279.000000 1637.000000 1947.000000
2054.000000 2087.000000 2000.000000 1982.000000 1606.000000 2112.000000 2112.000000
1845.000000 1998.000000 2169.000000 2002.000000 1949.000000 2724.000000 2724.000000
2101.000000 1022.000000 1808.000000 2229.000000 2229.000000 2539.000000 2281.000000
2644.000000 2285.000000 1726.000000 1128.000000 1907.000000 1623.000000 1831.000000
1693.000000 1916.000000 1916.000000 1344.000000 1633.000000 2349.000000 1522.000000
1953.000000 2050.000000 1996.000000 1759.000000 1850.000000 1850.000000 1798.000000
1742.000000 1815.000000 1841.000000 1841.000000 1687.000000 1515.000000 1971.000000
1734.000000 1594.000000 1876.000000 1713.000000 1829.000000 1839.000000 1561.000000
1773.000000 1773.000000 1817.000000 1817.000000 1101.000000 1101.000000 1879.000000
1645.000000 1563.000000

782.950012 2205.000000 2137.000000 2247.000000 1964.000000 2045.000000 1747.000000
1985.000000 2051.000000 1929.000000 2013.000000 2013.000000 1649.000000 2045.000000
2381.000000 1923.000000 2248.000000 2067.000000 2383.000000 1791.000000 2082.000000
2174.000000 2265.000000 2153.000000 2087.000000 1749.000000 2275.000000 2275.000000
1979.000000 2180.000000 2358.000000 2218.000000 2156.000000 2960.000000 2960.000000
2320.000000 1173.000000 1940.000000 2438.000000 2438.000000 2790.000000 2566.000000
2937.000000 2489.000000 1901.000000 1229.000000 2043.000000 1772.000000 2008.000000
1843.000000 2040.000000 2040.000000 1468.000000 1769.000000 2554.000000 1659.000000
2140.000000 2194.000000 2127.000000 1955.000000 2035.000000 2035.000000 1942.000000
1874.000000 1993.000000 2019.000000 2019.000000 1866.000000 1690.000000 2141.000000
1909.000000 1734.000000 2098.000000 1901.000000 2032.000000 2008.000000 1732.000000

1963.000000 1963.000000 2002.000000 2002.000000 1261.000000 1261.000000 2098.000000
1792.000000 1660.000000

793.130005 2279.000000 2160.000000 2303.000000 1991.000000 2041.000000 1807.000000
2056.000000 2063.000000 1929.000000 2066.000000 2066.000000 1707.000000 2079.000000
2422.000000 1929.000000 2236.000000 2082.000000 2544.000000 1808.000000 2155.000000
2233.000000 2301.000000 2218.000000 2085.000000 1776.000000 2276.000000 2276.000000
2033.000000 2260.000000 2408.000000 2266.000000 2190.000000 3033.000000 3033.000000
2342.000000 1196.000000 2021.000000 2488.000000 2488.000000 2825.000000 2626.000000
2999.000000 2563.000000 1911.000000 1266.000000 2118.000000 1805.000000 2063.000000
1861.000000 2084.000000 2084.000000 1492.000000 1830.000000 2642.000000 1722.000000
2149.000000 2272.000000 2202.000000 1976.000000 2057.000000 2057.000000 2019.000000
1930.000000 2073.000000 2066.000000 2066.000000 1922.000000 1743.000000 2212.000000
1962.000000 1823.000000 2133.000000 1912.000000 2038.000000 2047.000000 1725.000000
2005.000000 2005.000000 2060.000000 2060.000000 1303.000000 1303.000000 2165.000000
1802.000000 1725.000000

803.299988 2293.000000 2172.000000 2392.000000 2089.000000 2075.000000 1855.000000
2083.000000 2129.000000 2041.000000 2110.000000 2110.000000 1712.000000 2198.000000
2488.000000 1968.000000 2317.000000 2151.000000 2522.000000 1858.000000 2236.000000
2282.000000 2320.000000 2237.000000 2224.000000 1839.000000 2428.000000 2428.000000
2120.000000 2265.000000 2479.000000 2349.000000 2243.000000 3121.000000 3121.000000
2423.000000 1219.000000 2047.000000 2557.000000 2557.000000 2952.000000 2671.000000
3085.000000 2599.000000 1976.000000 1271.000000 2171.000000 1848.000000 2119.000000
1920.000000 2176.000000 2176.000000 1533.000000 1877.000000 2650.000000 1780.000000
2181.000000 2310.000000 2236.000000 2028.000000 2169.000000 2169.000000 2087.000000
1977.000000 2124.000000 2144.000000 2144.000000 1987.000000 1777.000000 2262.000000
2024.000000 1859.000000 2214.000000 1973.000000 2122.000000 2126.000000 1860.000000
2026.000000 2026.000000 2083.000000 2083.000000 1351.000000 1351.000000 2201.000000
1882.000000 1776.000000

813.479980 2346.000000 2274.000000 2500.000000 2172.000000 2187.000000 1981.000000
2227.000000 2231.000000 2097.000000 2227.000000 2227.000000 1846.000000 2259.000000
2617.000000 2131.000000 2456.000000 2172.000000 2652.000000 1971.000000 2308.000000
2386.000000 2452.000000 2374.000000 2331.000000 1906.000000 2479.000000 2479.000000
2186.000000 2421.000000 2518.000000 2440.000000 2354.000000 3216.000000 3216.000000
2503.000000 1364.000000 2176.000000 2732.000000 2732.000000 3069.000000 2833.000000
3235.000000 2731.000000 2072.000000 1398.000000 2260.000000 1935.000000 2196.000000
2003.000000 2229.000000 2229.000000 1649.000000 1989.000000 2795.000000 1918.000000
2347.000000 2457.000000 2366.000000 2136.000000 2219.000000 2219.000000 2197.000000
2072.000000 2203.000000 2233.000000 2233.000000 2086.000000 1915.000000 2353.000000
2109.000000 1954.000000 2273.000000 2114.000000 2285.000000 2238.000000 1966.000000
2087.000000 2087.000000 2194.000000 2194.000000 1425.000000 1425.000000 2332.000000
1998.000000 1856.000000

823.650024 2314.000000 2226.000000 2416.000000 2166.000000 2172.000000 1958.000000
2152.000000 2157.000000 2034.000000 2107.000000 2107.000000 1790.000000 2203.000000
2569.000000 2073.000000 2419.000000 2220.000000 2561.000000 1922.000000 2250.000000
2308.000000 2499.000000 2331.000000 2285.000000 1931.000000 2376.000000 2376.000000
2160.000000 2329.000000 2516.000000 2344.000000 2251.000000 3145.000000 3145.000000
2443.000000 1292.000000 2099.000000 2635.000000 2635.000000 2970.000000 2693.000000
3085.000000 2621.000000 2013.000000 1370.000000 2178.000000 1909.000000 2124.000000
1938.000000 2163.000000 2163.000000 1617.000000 2003.000000 2746.000000 1826.000000
2293.000000 2364.000000 2332.000000 2061.000000 2203.000000 2203.000000 2153.000000

2092.000000 2179.000000 2176.000000 2176.000000 2044.000000 1825.000000 2312.000000
2066.000000 1922.000000 2246.000000 2045.000000 2161.000000 2138.000000 1878.000000
2044.000000 2044.000000 2149.000000 2149.000000 1370.000000 1370.000000 2233.000000
1924.000000 1817.000000

833.830017 2359.000000 2281.000000 2461.000000 2125.000000 2148.000000 1985.000000
2194.000000 2184.000000 2106.000000 2190.000000 2190.000000 1811.000000 2242.000000
2594.000000 2078.000000 2432.000000 2263.000000 2616.000000 1992.000000 2293.000000
2405.000000 2434.000000 2346.000000 2326.000000 1967.000000 2533.000000 2533.000000
2260.000000 2417.000000 2526.000000 2380.000000 2342.000000 3183.000000 3183.000000
2477.000000 1322.000000 2190.000000 2623.000000 2623.000000 3038.000000 2780.000000
3138.000000 2649.000000 2079.000000 1408.000000 2226.000000 1936.000000 2183.000000
2034.000000 2199.000000 2199.000000 1658.000000 1978.000000 2740.000000 1856.000000
2277.000000 2435.000000 2384.000000 2139.000000 2288.000000 2288.000000 2232.000000
2105.000000 2212.000000 2252.000000 2252.000000 2066.000000 1886.000000 2367.000000
2090.000000 2013.000000 2314.000000 2086.000000 2191.000000 2165.000000 1933.000000
2120.000000 2120.000000 2187.000000 2187.000000 1411.000000 1411.000000 2337.000000
1972.000000 1802.000000

844.000000 2413.000000 2390.000000 2589.000000 2221.000000 2253.000000 1978.000000
2244.000000 2249.000000 2145.000000 2296.000000 2296.000000 1861.000000 2321.000000
2697.000000 2204.000000 2549.000000 2297.000000 2742.000000 2067.000000 2369.000000
2440.000000 2548.000000 2479.000000 2399.000000 2046.000000 2584.000000 2584.000000
2238.000000 2529.000000 2640.000000 2472.000000 2437.000000 3297.000000 3297.000000
2614.000000 1322.000000 2241.000000 2822.000000 2822.000000 3188.000000 2898.000000
3288.000000 2799.000000 2171.000000 1435.000000 2325.000000 2005.000000 2227.000000
2062.000000 2259.000000 2259.000000 1670.000000 2050.000000 2842.000000 1961.000000
2411.000000 2521.000000 2393.000000 2230.000000 2334.000000 2334.000000 2310.000000
2179.000000 2283.000000 2338.000000 2338.000000 2162.000000 1942.000000 2490.000000
2184.000000 2068.000000 2336.000000 2203.000000 2300.000000 2252.000000 1971.000000
2208.000000 2208.000000 2250.000000 2250.000000 1420.000000 1420.000000 2385.000000
2003.000000 1925.000000

854.179993 2392.000000 2408.000000 2633.000000 2344.000000 2279.000000 2033.000000
2336.000000 2238.000000 2171.000000 2379.000000 2379.000000 1942.000000 2359.000000
2704.000000 2148.000000 2565.000000 2375.000000 2750.000000 2077.000000 2453.000000
2559.000000 2625.000000 2528.000000 2434.000000 2077.000000 2665.000000 2665.000000
2338.000000 2550.000000 2712.000000 2533.000000 2524.000000 3351.000000 3351.000000
2657.000000 1370.000000 2293.000000 2834.000000 2834.000000 3271.000000 2969.000000
3393.000000 2849.000000 2185.000000 1473.000000 2419.000000 2021.000000 2257.000000
2126.000000 2384.000000 2384.000000 1733.000000 2097.000000 2886.000000 1974.000000
2393.000000 2533.000000 2480.000000 2208.000000 2400.000000 2400.000000 2335.000000
2246.000000 2396.000000 2380.000000 2380.000000 2151.000000 1975.000000 2542.000000
2272.000000 2138.000000 2410.000000 2212.000000 2314.000000 2355.000000 2053.000000
2194.000000 2194.000000 2316.000000 2316.000000 1473.000000 1473.000000 2453.000000
2057.000000 1925.000000

864.349976 2488.000000 2411.000000 2710.000000 2328.000000 2351.000000 2087.000000
2349.000000 2326.000000 2200.000000 2242.000000 2242.000000 1911.000000 2381.000000
2717.000000 2233.000000 2664.000000 2379.000000 2736.000000 2064.000000 2456.000000
2507.000000 2599.000000 2537.000000 2460.000000 2059.000000 2671.000000 2671.000000
2309.000000 2560.000000 2694.000000 2569.000000 2481.000000 3401.000000 3401.000000
2687.000000 1380.000000 2300.000000 2845.000000 2845.000000 3276.000000 3021.000000
3401.000000 2847.000000 2154.000000 1495.000000 2374.000000 2040.000000 2279.000000

2189.000000 2358.000000 2358.000000 1746.000000 2145.000000 2928.000000 1955.000000
2518.000000 2599.000000 2481.000000 2261.000000 2423.000000 2423.000000 2351.000000
2295.000000 2409.000000 2418.000000 2418.000000 2189.000000 2050.000000 2555.000000
2376.000000 2140.000000 2427.000000 2263.000000 2402.000000 2360.000000 2033.000000
2237.000000 2237.000000 2346.000000 2346.000000 1514.000000 1514.000000 2462.000000
2052.000000 1957.000000

874.530029 2482.000000 2516.000000 2739.000000 2356.000000 2372.000000 2071.000000
2452.000000 2413.000000 2225.000000 2354.000000 2354.000000 1950.000000 2443.000000
2822.000000 2262.000000 2705.000000 2381.000000 2803.000000 2159.000000 2475.000000
2560.000000 2551.000000 2558.000000 2505.000000 2133.000000 2668.000000 2668.000000
2409.000000 2567.000000 2771.000000 2629.000000 2523.000000 3508.000000 3508.000000
2693.000000 1443.000000 2317.000000 2872.000000 2872.000000 3253.000000 3049.000000
3469.000000 2934.000000 2282.000000 1573.000000 2418.000000 2103.000000 2333.000000
2214.000000 2402.000000 2402.000000 1785.000000 2179.000000 2959.000000 2081.000000
2491.000000 2581.000000 2579.000000 2301.000000 2418.000000 2418.000000 2388.000000
2317.000000 2452.000000 2441.000000 2441.000000 2250.000000 2083.000000 2615.000000
2397.000000 2136.000000 2457.000000 2344.000000 2466.000000 2438.000000 2142.000000
2278.000000 2278.000000 2395.000000 2395.000000 1592.000000 1592.000000 2491.000000
2113.000000 1996.000000

884.700012 2522.000000 2532.000000 2714.000000 2328.000000 2391.000000 2103.000000
2488.000000 2356.000000 2302.000000 2406.000000 2406.000000 1987.000000 2442.000000
2806.000000 2244.000000 2622.000000 2406.000000 2907.000000 2179.000000 2507.000000
2604.000000 2668.000000 2591.000000 2524.000000 2177.000000 2640.000000 2640.000000
2369.000000 2632.000000 2739.000000 2675.000000 2523.000000 3540.000000 3540.000000
2771.000000 1462.000000 2324.000000 2968.000000 2968.000000 3348.000000 3093.000000
3471.000000 2976.000000 2285.000000 1581.000000 2425.000000 2176.000000 2294.000000
2237.000000 2451.000000 2451.000000 1857.000000 2222.000000 2990.000000 2165.000000
2495.000000 2613.000000 2567.000000 2355.000000 2444.000000 2444.000000 2501.000000
2414.000000 2446.000000 2513.000000 2513.000000 2315.000000 2161.000000 2657.000000
2417.000000 2161.000000 2524.000000 2285.000000 2526.000000 2451.000000 2190.000000
2278.000000 2278.000000 2427.000000 2427.000000 1634.000000 1634.000000 2502.000000
2079.000000 2022.000000

894.880005 2672.000000 2464.000000 2837.000000 2484.000000 2553.000000 2269.000000
2608.000000 2412.000000 2356.000000 2468.000000 2468.000000 1954.000000 2583.000000
3003.000000 2410.000000 2807.000000 2498.000000 2930.000000 2243.000000 2503.000000
2708.000000 2769.000000 2678.000000 2578.000000 2128.000000 2794.000000 2794.000000
2454.000000 2740.000000 2938.000000 2776.000000 2646.000000 3690.000000 3690.000000
2832.000000 1589.000000 2415.000000 3157.000000 3157.000000 3491.000000 3137.000000
3641.000000 3082.000000 2378.000000 1698.000000 2489.000000 2240.000000 2465.000000
2244.000000 2504.000000 2504.000000 1841.000000 2313.000000 3065.000000 2179.000000
2696.000000 2737.000000 2721.000000 2514.000000 2532.000000 2532.000000 2581.000000
2423.000000 2516.000000 2580.000000 2580.000000 2432.000000 2281.000000 2739.000000
2474.000000 2324.000000 2614.000000 2423.000000 2629.000000 2464.000000 2362.000000
2435.000000 2435.000000 2611.000000 2611.000000 1638.000000 1638.000000 2540.000000
2215.000000 2104.000000

905.049988 2496.000000 2446.000000 2758.000000 2387.000000 2510.000000 2150.000000
2480.000000 2274.000000 2320.000000 2266.000000 2266.000000 2050.000000 2534.000000
2777.000000 2241.000000 2604.000000 2444.000000 2858.000000 2271.000000 2470.000000
2634.000000 2686.000000 2659.000000 2639.000000 2130.000000 2693.000000 2693.000000
2459.000000 2683.000000 2736.000000 2710.000000 2421.000000 3520.000000 3520.000000

2658.000000 1547.000000 2308.000000 2960.000000 2960.000000 3349.000000 3109.000000
3472.000000 2848.000000 2130.000000 1544.000000 2475.000000 2116.000000 2403.000000
2250.000000 2442.000000 2442.000000 1800.000000 2221.000000 2970.000000 2047.000000
2607.000000 2561.000000 2622.000000 2312.000000 2460.000000 2460.000000 2494.000000
2328.000000 2389.000000 2425.000000 2425.000000 2381.000000 2102.000000 2602.000000
2473.000000 2159.000000 2508.000000 2340.000000 2465.000000 2455.000000 2322.000000
2215.000000 2215.000000 2480.000000 2480.000000 1613.000000 1613.000000 2531.000000
2094.000000 1971.000000

912.450012 2646.000000 2360.000000 2550.000000 1960.000000 2581.000000 1666.000000
2632.000000 2016.000000 2071.000000 2809.000000 2809.000000 2218.000000 2428.000000
2944.000000 1974.000000 2720.000000 2121.000000 2678.000000 1917.000000 2429.000000
2566.000000 2374.000000 2681.000000 2724.000000 1988.000000 2361.000000 2361.000000
2014.000000 2792.000000 2679.000000 2277.000000 2495.000000 3655.000000 3655.000000
3196.000000 1433.000000 2536.000000 2914.000000 2914.000000 2978.000000 3131.000000
3320.000000 3159.000000 1445.000000 1731.000000 2513.000000 1914.000000 1960.000000
2287.000000 1688.000000 1688.000000 1942.000000 2239.000000 2764.000000 1958.000000
2400.000000 2606.000000 2256.000000 1873.000000 2516.000000 2516.000000 2734.000000
2193.000000 2368.000000 2395.000000 2395.000000 2816.000000 1881.000000 2664.000000
2206.000000 1771.000000 2374.000000 1933.000000 2222.000000 2562.000000 2167.000000
2453.000000 2453.000000 2136.000000 2136.000000 1205.000000 1205.000000 2722.000000
1686.000000 1747.000000

915.229980 2516.000000 2416.000000 2780.000000 2292.000000 2360.000000 2165.000000
2490.000000 2200.000000 2409.000000 2374.000000 2374.000000 2046.000000 2528.000000
2718.000000 2239.000000 2542.000000 2542.000000 2526.000000 2469.000000 2568.000000
2572.000000 2603.000000 2802.000000 2537.000000 2234.000000 2737.000000 2737.000000
2435.000000 2646.000000 2864.000000 2545.000000 2536.000000 3322.000000 3322.000000
2583.000000 1589.000000 2147.000000 2793.000000 2793.000000 3151.000000 2979.000000
3301.000000 2996.000000 2161.000000 1536.000000 2422.000000 2001.000000 2291.000000
2079.000000 2484.000000 2484.000000 1762.000000 2342.000000 2884.000000 1994.000000
2490.000000 2706.000000 2589.000000 2219.000000 2537.000000 2537.000000 2391.000000
2316.000000 2295.000000 2492.000000 2492.000000 2302.000000 1952.000000 2490.000000
2291.000000 2186.000000 2520.000000 2138.000000 2487.000000 2365.000000 2321.000000
2300.000000 2300.000000 2575.000000 2575.000000 1513.000000 1513.000000 2549.000000
2114.000000 2108.000000

922.539978 2770.000000 2268.000000 2703.000000 2252.000000 2533.000000 1891.000000
2750.000000 2294.000000 2173.000000 2803.000000 2803.000000 2291.000000 2473.000000
3160.000000 2178.000000 3076.000000 2284.000000 2759.000000 2008.000000 2591.000000
2553.000000 2456.000000 2727.000000 2463.000000 2230.000000 2583.000000 2583.000000
2072.000000 3112.000000 2834.000000 2287.000000 2653.000000 3790.000000 3790.000000
3253.000000 1578.000000 2679.000000 2979.000000 2979.000000 3367.000000 3148.000000
3663.000000 3124.000000 1686.000000 1932.000000 2741.000000 1968.000000 2196.000000
2336.000000 1700.000000 1700.000000 2155.000000 2197.000000 2872.000000 2128.000000
2511.000000 2627.000000 2480.000000 2038.000000 2329.000000 2329.000000 2764.000000
2298.000000 2530.000000 2634.000000 2634.000000 2940.000000 1993.000000 2615.000000
2346.000000 1863.000000 2469.000000 2019.000000 2429.000000 2606.000000 1811.000000
2602.000000 2602.000000 1964.000000 1964.000000 1492.000000 1492.000000 2710.000000
1638.000000 1748.000000

925.409973 2580.000000 2537.000000 2639.000000 2026.000000 2273.000000 2237.000000
2456.000000 2432.000000 2172.000000 2648.000000 2648.000000 1971.000000 2663.000000
2715.000000 2514.000000 2723.000000 2624.000000 2605.000000 2249.000000 2634.000000

2451.000000 2756.000000 2607.000000 2914.000000 2269.000000 2795.000000 2795.000000
2391.000000 2689.000000 2646.000000 2718.000000 2690.000000 3374.000000 3374.000000
2540.000000 1537.000000 2377.000000 2962.000000 2962.000000 3407.000000 3075.000000
3511.000000 2737.000000 2578.000000 1566.000000 2234.000000 2363.000000 2463.000000
2228.000000 2576.000000 2576.000000 2088.000000 2193.000000 3243.000000 2179.000000
2912.000000 2555.000000 2586.000000 2294.000000 2512.000000 2512.000000 2695.000000
2317.000000 2322.000000 2530.000000 2530.000000 2474.000000 2077.000000 2653.000000
2770.000000 2317.000000 2737.000000 2253.000000 2537.000000 2786.000000 2218.000000
2090.000000 2090.000000 2713.000000 2713.000000 1799.000000 1799.000000 2786.000000
2525.000000 2100.000000

932.640015 3165.000000 2344.000000 2730.000000 2237.000000 2874.000000 2158.000000
2749.000000 3148.000000 2830.000000 3162.000000 3162.000000 2866.000000 2779.000000
2635.000000 2722.000000 2282.000000 2371.000000 3328.000000 2587.000000 2927.000000
2942.000000 2337.000000 2498.000000 3652.000000 2324.000000 3205.000000 3205.000000
2551.000000 2174.000000 3069.000000 2558.000000 2827.000000 3288.000000 3288.000000
2534.000000 1562.000000 2451.000000 3136.000000 3136.000000 4198.000000 3650.000000
4724.000000 2562.000000 2635.000000 1188.000000 1553.000000 3185.000000 2127.000000
1803.000000 2518.000000 2518.000000 2017.000000 1623.000000 2210.000000 2031.000000
3126.000000 2126.000000 2705.000000 3079.000000 2513.000000 2513.000000 2315.000000
2308.000000 2757.000000 2559.000000 2559.000000 2106.000000 2490.000000 1962.000000
1969.000000 1951.000000 2122.000000 2632.000000 2583.000000 3135.000000 2264.000000
2287.000000 2287.000000 2839.000000 2839.000000 2378.000000 2378.000000 3095.000000
1716.000000 1566.000000

942.729980 3072.000000 2384.000000 2612.000000 1886.000000 2679.000000 2080.000000
2647.000000 2887.000000 2502.000000 2951.000000 2951.000000 2897.000000 2854.000000
2853.000000 2674.000000 1994.000000 2571.000000 3085.000000 2607.000000 2882.000000
2608.000000 2207.000000 2200.000000 3656.000000 2221.000000 3164.000000 3164.000000
2570.000000 2335.000000 2716.000000 2491.000000 2722.000000 3316.000000 3316.000000
2463.000000 1440.000000 2184.000000 3097.000000 3097.000000 4001.000000 3339.000000
4428.000000 2570.000000 2224.000000 1285.000000 1616.000000 3072.000000 2139.000000
1847.000000 2275.000000 2275.000000 1882.000000 1763.000000 2404.000000 2516.000000
2988.000000 2280.000000 2689.000000 2962.000000 2280.000000 2280.000000 2519.000000
2468.000000 2715.000000 2392.000000 2392.000000 2064.000000 2488.000000 1932.000000
2161.000000 2236.000000 2071.000000 2564.000000 2514.000000 3003.000000 2275.000000
2346.000000 2346.000000 2765.000000 2765.000000 2007.000000 2007.000000 2854.000000
1949.000000 1578.000000

952.820007 2901.000000 2780.000000 2494.000000 1953.000000 2807.000000 2317.000000
2831.000000 2820.000000 2347.000000 2638.000000 2638.000000 2392.000000 3048.000000
2742.000000 2625.000000 2655.000000 2374.000000 2809.000000 2490.000000 2765.000000
2490.000000 2663.000000 2624.000000 2730.000000 2257.000000 2947.000000 2947.000000
2424.000000 2839.000000 3166.000000 2493.000000 2709.000000 3802.000000 3802.000000
3006.000000 1544.000000 2348.000000 3429.000000 3429.000000 3207.000000 3474.000000
4250.000000 2445.000000 2308.000000 1835.000000 2376.000000 2645.000000 2536.000000
2128.000000 2175.000000 2175.000000 1990.000000 2234.000000 3168.000000 2031.000000
2525.000000 2947.000000 3105.000000 2503.000000 3152.000000 3152.000000 2906.000000
2553.000000 2438.000000 2411.000000 2411.000000 2366.000000 2602.000000 2533.000000
2396.000000 2111.000000 2366.000000 2259.000000 2421.000000 2137.000000 2170.000000
2434.000000 2434.000000 2107.000000 2107.000000 1516.000000 1516.000000 2677.000000
2283.000000 2193.000000

962.909973 2834.000000 2843.000000 2545.000000 2231.000000 2689.000000 2380.000000
2825.000000 2604.000000 2252.000000 2459.000000 2459.000000 2384.000000 2716.000000
2895.000000 2545.000000 2984.000000 2458.000000 2896.000000 2505.000000 2793.000000
2631.000000 2730.000000 2636.000000 2708.000000 2375.000000 2898.000000 2898.000000
2560.000000 2805.000000 3213.000000 2590.000000 2705.000000 3762.000000 3762.000000
3113.000000 1633.000000 2568.000000 3349.000000 3349.000000 3373.000000 3391.000000
4070.000000 2740.000000 2416.000000 1736.000000 2411.000000 2414.000000 2384.000000
2313.000000 2232.000000 2232.000000 2133.000000 2295.000000 3202.000000 2214.000000
2678.000000 2895.000000 2921.000000 2519.000000 3161.000000 3161.000000 2924.000000
2483.000000 2581.000000 2414.000000 2414.000000 2405.000000 2495.000000 2636.000000
2555.000000 2284.000000 2373.000000 2336.000000 2457.000000 2436.000000 2319.000000
2602.000000 2602.000000 2291.000000 2291.000000 1568.000000 1568.000000 2737.000000
2206.000000 2192.000000

972.989990 2966.000000 2785.000000 2828.000000 2418.000000 2497.000000 2438.000000
2860.000000 2459.000000 2546.000000 2594.000000 2594.000000 2457.000000 2808.000000
2924.000000 2516.000000 2875.000000 2698.000000 2961.000000 2556.000000 2827.000000
2922.000000 2775.000000 2813.000000 2789.000000 2376.000000 2651.000000 2651.000000
2543.000000 2939.000000 3071.000000 2807.000000 2730.000000 3815.000000 3815.000000
3094.000000 1516.000000 2561.000000 3290.000000 3290.000000 3483.000000 3225.000000
3583.000000 3244.000000 2507.000000 1831.000000 2376.000000 2435.000000 2433.000000
2401.000000 2248.000000 2248.000000 2117.000000 2385.000000 2814.000000 2356.000000
2702.000000 2871.000000 2957.000000 2679.000000 2839.000000 2839.000000 3013.000000
2756.000000 2675.000000 2676.000000 2676.000000 2672.000000 2252.000000 2810.000000
2709.000000 2437.000000 2670.000000 2447.000000 2733.000000 2712.000000 2371.000000
2187.000000 2187.000000 2626.000000 2626.000000 1592.000000 1592.000000 2737.000000
2363.000000 2129.000000

983.080017 3086.000000 2898.000000 2952.000000 2439.000000 2553.000000 2497.000000
2976.000000 2400.000000 2550.000000 2734.000000 2734.000000 2486.000000 2843.000000
3034.000000 2666.000000 2942.000000 2759.000000 3030.000000 2635.000000 2847.000000
2899.000000 2873.000000 2884.000000 2865.000000 2499.000000 2709.000000 2709.000000
2614.000000 3023.000000 3277.000000 2894.000000 2787.000000 3863.000000 3863.000000
3148.000000 1573.000000 2691.000000 3347.000000 3347.000000 3738.000000 3248.000000
3672.000000 3308.000000 2620.000000 1917.000000 2484.000000 2488.000000 2570.000000
2502.000000 2409.000000 2409.000000 2166.000000 2451.000000 2875.000000 2410.000000
2805.000000 2854.000000 3075.000000 2795.000000 2884.000000 2884.000000 3073.000000
2844.000000 2824.000000 2841.000000 2841.000000 2795.000000 2348.000000 2961.000000
2878.000000 2558.000000 2809.000000 2600.000000 2852.000000 2800.000000 2560.000000
2203.000000 2203.000000 2752.000000 2752.000000 1762.000000 1762.000000 2828.000000
2436.000000 2228.000000

993.169983 2794.000000 2866.000000 2928.000000 2575.000000 2584.000000 2476.000000
2888.000000 2224.000000 2560.000000 2683.000000 2683.000000 2342.000000 2765.000000
3094.000000 2612.000000 2854.000000 2757.000000 3092.000000 2587.000000 2768.000000
2849.000000 2828.000000 2844.000000 2988.000000 2438.000000 2915.000000 2915.000000
2595.000000 2985.000000 3228.000000 2911.000000 2901.000000 3781.000000 3781.000000
3190.000000 1674.000000 2870.000000 3255.000000 3255.000000 3577.000000 3281.000000
3685.000000 3337.000000 2523.000000 1757.000000 2676.000000 2252.000000 2518.000000
2611.000000 2347.000000 2347.000000 2077.000000 2460.000000 3072.000000 2449.000000
2673.000000 3097.000000 2844.000000 2618.000000 2949.000000 2949.000000 2856.000000
2808.000000 2975.000000 2929.000000 2929.000000 2694.000000 2497.000000 2869.000000
2884.000000 2651.000000 2904.000000 2663.000000 2784.000000 2809.000000 2603.000000

2608.000000 2608.000000 2771.000000 2771.000000 1751.000000 1751.000000 2765.000000
2480.000000 2254.000000

1003.299988 2849.000000 2861.000000 2916.000000 2540.000000 2583.000000 2477.000000
2977.000000 2303.000000 2553.000000 2746.000000 2746.000000 2385.000000 2877.000000
3078.000000 2626.000000 3033.000000 2752.000000 3198.000000 2572.000000 2902.000000
2935.000000 2870.000000 2855.000000 3042.000000 2454.000000 2927.000000 2927.000000
2670.000000 2959.000000 3234.000000 2952.000000 2916.000000 3946.000000 3946.000000
3239.000000 1646.000000 2849.000000 3319.000000 3319.000000 3579.000000 3391.000000
3793.000000 3398.000000 2602.000000 1832.000000 2699.000000 2378.000000 2632.000000
2695.000000 2514.000000 2514.000000 2041.000000 2503.000000 3132.000000 2453.000000
2784.000000 3111.000000 2911.000000 2695.000000 3067.000000 3067.000000 2887.000000
2848.000000 2931.000000 2979.000000 2979.000000 2736.000000 2572.000000 2954.000000
2950.000000 2644.000000 2902.000000 2726.000000 2915.000000 2969.000000 2631.000000
2556.000000 2556.000000 2812.000000 2812.000000 1762.000000 1762.000000 2804.000000
2532.000000 2409.000000

1013.299988 2838.000000 2854.000000 2950.000000 2474.000000 2550.000000 2579.000000
2888.000000 2515.000000 2468.000000 2602.000000 2602.000000 2332.000000 2742.000000
3096.000000 2558.000000 2954.000000 2615.000000 3132.000000 2547.000000 2664.000000
2750.000000 2817.000000 2906.000000 2716.000000 2410.000000 2852.000000 2852.000000
2597.000000 2771.000000 3058.000000 2892.000000 2862.000000 3829.000000 3829.000000
3077.000000 1569.000000 2704.000000 3376.000000 3376.000000 3631.000000 3305.000000
3853.000000 3286.000000 2549.000000 1859.000000 2453.000000 2512.000000 2484.000000
2645.000000 2562.000000 2562.000000 2171.000000 2546.000000 3062.000000 2471.000000
2770.000000 2783.000000 2831.000000 2518.000000 2846.000000 2846.000000 2876.000000
2518.000000 2770.000000 2750.000000 2750.000000 2650.000000 2391.000000 2802.000000
2854.000000 2475.000000 2577.000000 2672.000000 2918.000000 2778.000000 2511.000000
2447.000000 2447.000000 2742.000000 2742.000000 1760.000000 1760.000000 2745.000000
2521.000000 2204.000000

1023.400024 2814.000000 2944.000000 2962.000000 2544.000000 2595.000000 2570.000000
2917.000000 2489.000000 2511.000000 2653.000000 2653.000000 2353.000000 2715.000000
3161.000000 2504.000000 2941.000000 2678.000000 3065.000000 2521.000000 2761.000000
2811.000000 2818.000000 2940.000000 2749.000000 2433.000000 2817.000000 2817.000000
2585.000000 2872.000000 3070.000000 2917.000000 2849.000000 3878.000000 3878.000000
3095.000000 1548.000000 2750.000000 3281.000000 3281.000000 3684.000000 3373.000000
3919.000000 3304.000000 2676.000000 1863.000000 2495.000000 2487.000000 2493.000000
2639.000000 2530.000000 2530.000000 2205.000000 2545.000000 3115.000000 2486.000000
2702.000000 2899.000000 2784.000000 2550.000000 2828.000000 2828.000000 2891.000000
2487.000000 2815.000000 2798.000000 2798.000000 2638.000000 2456.000000 2836.000000
2922.000000 2573.000000 2597.000000 2726.000000 2905.000000 2769.000000 2547.000000
2481.000000 2481.000000 2781.000000 2781.000000 1744.000000 1744.000000 2865.000000
2486.000000 2240.000000

1033.489990 2737.000000 2795.000000 2919.000000 2609.000000 2508.000000 2493.000000
2936.000000 2663.000000 2472.000000 2715.000000 2715.000000 2411.000000 2811.000000
3081.000000 2467.000000 3008.000000 2692.000000 2938.000000 2620.000000 2776.000000
2813.000000 2923.000000 2929.000000 2843.000000 2507.000000 2941.000000 2941.000000
2553.000000 3020.000000 3255.000000 2840.000000 2830.000000 3883.000000 3883.000000
3031.000000 1622.000000 2830.000000 3355.000000 3355.000000 3671.000000 3465.000000
3937.000000 3342.000000 2569.000000 1868.000000 2752.000000 2326.000000 2722.000000
2639.000000 2480.000000 2480.000000 2317.000000 2687.000000 3193.000000 2588.000000
2600.000000 3019.000000 2860.000000 2559.000000 2866.000000 2866.000000 2736.000000

2884.000000 2853.000000 2925.000000 2925.000000 2716.000000 2467.000000 2806.000000
2911.000000 2656.000000 2837.000000 2760.000000 2870.000000 2817.000000 2595.000000
2572.000000 2572.000000 2679.000000 2679.000000 1881.000000 1881.000000 2840.000000
2615.000000 2464.000000

1043.589966 2768.000000 2773.000000 2986.000000 2614.000000 2523.000000 2607.000000
2968.000000 2626.000000 2412.000000 2763.000000 2763.000000 2426.000000 2804.000000
3086.000000 2539.000000 2985.000000 2659.000000 2977.000000 2612.000000 2749.000000
2829.000000 2854.000000 2927.000000 2847.000000 2481.000000 3005.000000 3005.000000
2623.000000 3053.000000 3197.000000 2932.000000 2833.000000 3895.000000 3895.000000
3130.000000 1687.000000 2857.000000 3418.000000 3418.000000 3729.000000 3442.000000
3924.000000 3339.000000 2532.000000 1887.000000 2744.000000 2380.000000 2816.000000
2721.000000 2486.000000 2486.000000 2302.000000 2715.000000 3240.000000 2576.000000
2738.000000 3064.000000 2924.000000 2596.000000 3013.000000 3013.000000 2773.000000
2882.000000 2857.000000 2882.000000 2882.000000 2698.000000 2454.000000 2847.000000
2978.000000 2720.000000 2840.000000 2744.000000 2880.000000 2819.000000 2609.000000
2595.000000 2595.000000 2769.000000 2769.000000 1870.000000 1870.000000 2847.000000
2604.000000 2598.000000

1053.689941 2999.000000 2855.000000 3153.000000 2594.000000 2661.000000 2570.000000
3145.000000 2575.000000 2519.000000 2732.000000 2732.000000 2460.000000 2912.000000
3186.000000 2622.000000 3022.000000 2916.000000 3309.000000 2606.000000 3042.000000
3006.000000 2984.000000 3048.000000 3006.000000 2616.000000 3093.000000 3093.000000
2725.000000 3109.000000 3412.000000 3073.000000 3014.000000 4008.000000 4008.000000
3255.000000 1666.000000 2909.000000 3529.000000 3529.000000 3831.000000 3470.000000
3957.000000 3596.000000 2594.000000 1979.000000 2670.000000 2547.000000 2724.000000
2683.000000 2711.000000 2711.000000 2296.000000 2612.000000 3252.000000 2486.000000
2983.000000 2978.000000 3019.000000 2732.000000 3052.000000 3052.000000 3083.000000
2716.000000 2939.000000 2986.000000 2986.000000 2868.000000 2784.000000 2983.000000
3145.000000 2670.000000 2958.000000 2847.000000 3004.000000 3075.000000 2807.000000
2581.000000 2581.000000 2829.000000 2829.000000 1815.000000 1815.000000 2898.000000
2609.000000 2466.000000

1063.790039 2914.000000 2851.000000 2991.000000 2557.000000 2669.000000 2460.000000
3223.000000 2527.000000 2646.000000 2764.000000 2764.000000 2441.000000 2816.000000
3169.000000 2571.000000 3080.000000 2931.000000 3285.000000 2654.000000 3007.000000
3120.000000 2985.000000 2985.000000 3061.000000 2666.000000 3086.000000 3086.000000
2689.000000 3135.000000 3505.000000 3025.000000 3047.000000 3956.000000 3956.000000
3187.000000 1687.000000 2925.000000 3510.000000 3510.000000 3804.000000 3518.000000
4008.000000 3614.000000 2582.000000 1989.000000 2726.000000 2512.000000 2728.000000
2672.000000 2707.000000 2707.000000 2358.000000 2580.000000 3257.000000 2532.000000
2885.000000 3059.000000 2926.000000 2684.000000 3027.000000 3027.000000 3134.000000
2730.000000 2942.000000 2942.000000 2942.000000 2836.000000 2811.000000 2989.000000
3136.000000 2566.000000 2910.000000 2863.000000 2985.000000 3020.000000 2733.000000
2535.000000 2535.000000 2827.000000 2827.000000 1753.000000 1753.000000 2907.000000
2606.000000 2446.000000

1073.890015 2952.000000 2868.000000 3101.000000 2507.000000 2633.000000 2451.000000
3062.000000 2584.000000 2582.000000 2773.000000 2773.000000 2338.000000 2830.000000
3139.000000 2719.000000 2933.000000 2736.000000 3093.000000 2533.000000 2841.000000
2909.000000 2891.000000 2917.000000 2911.000000 2555.000000 3036.000000 3036.000000
2584.000000 3034.000000 3302.000000 2833.000000 2930.000000 3821.000000 3821.000000
2943.000000 1613.000000 2879.000000 3198.000000 3198.000000 3701.000000 3425.000000
3759.000000 3259.000000 2706.000000 1875.000000 2657.000000 2307.000000 2694.000000

2652.000000 2553.000000 2553.000000 2083.000000 2551.000000 3133.000000 2477.000000
2848.000000 3000.000000 2956.000000 2643.000000 2939.000000 2939.000000 2903.000000
2715.000000 2971.000000 2913.000000 2913.000000 2698.000000 2774.000000 2788.000000
2910.000000 2736.000000 2763.000000 2815.000000 2965.000000 2876.000000 2625.000000
2548.000000 2548.000000 2800.000000 2800.000000 1771.000000 1771.000000 2785.000000
2553.000000 2384.000000

1083.989990 2923.000000 2831.000000 3123.000000 2562.000000 2556.000000 2429.000000
2994.000000 2519.000000 2559.000000 2714.000000 2714.000000 2280.000000 2819.000000
3162.000000 2731.000000 3062.000000 2715.000000 3141.000000 2537.000000 2829.000000
2928.000000 2866.000000 2933.000000 2855.000000 2582.000000 2993.000000 2993.000000
2654.000000 3077.000000 3224.000000 2870.000000 2821.000000 3779.000000 3779.000000
3009.000000 1608.000000 2784.000000 3228.000000 3228.000000 3818.000000 3292.000000
3713.000000 3245.000000 2639.000000 1876.000000 2655.000000 2367.000000 2705.000000
2652.000000 2567.000000 2567.000000 2108.000000 2614.000000 3175.000000 2456.000000
2807.000000 2925.000000 2905.000000 2676.000000 3000.000000 3000.000000 3003.000000
2753.000000 2954.000000 2968.000000 2968.000000 2710.000000 2668.000000 2791.000000
2959.000000 2721.000000 2796.000000 2793.000000 2908.000000 2861.000000 2687.000000
2439.000000 2439.000000 2870.000000 2870.000000 1788.000000 1788.000000 2839.000000
2526.000000 2506.000000

1094.089966 2739.000000 2651.000000 3118.000000 2560.000000 2556.000000 2365.000000
3015.000000 2569.000000 2728.000000 2646.000000 2646.000000 2372.000000 2758.000000
3040.000000 2513.000000 3037.000000 2906.000000 3205.000000 2609.000000 2797.000000
2917.000000 3029.000000 2993.000000 2941.000000 2637.000000 2945.000000 2945.000000
2691.000000 3040.000000 3143.000000 2932.000000 2905.000000 3811.000000 3811.000000
3090.000000 1731.000000 2751.000000 3328.000000 3328.000000 3695.000000 3380.000000
3703.000000 3354.000000 2555.000000 1912.000000 2751.000000 2563.000000 2743.000000
2633.000000 2478.000000 2478.000000 2179.000000 2642.000000 3157.000000 2496.000000
2941.000000 2899.000000 2832.000000 2694.000000 2877.000000 2877.000000 3001.000000
2873.000000 2820.000000 2957.000000 2957.000000 2715.000000 2640.000000 2806.000000
2944.000000 2616.000000 2829.000000 2685.000000 2926.000000 2952.000000 2766.000000
2503.000000 2503.000000 2799.000000 2799.000000 1879.000000 1879.000000 2901.000000
2558.000000 2501.000000

1104.189941 2711.000000 2580.000000 3048.000000 2539.000000 2489.000000 2514.000000
2963.000000 2567.000000 2730.000000 2575.000000 2575.000000 2284.000000 2813.000000
2969.000000 2484.000000 3028.000000 2886.000000 3253.000000 2605.000000 2813.000000
2934.000000 2988.000000 3042.000000 2816.000000 2621.000000 2891.000000 2891.000000
2731.000000 3074.000000 3118.000000 2858.000000 2833.000000 3790.000000 3790.000000
2965.000000 1718.000000 2736.000000 3362.000000 3362.000000 3709.000000 3324.000000
3715.000000 3324.000000 2507.000000 1868.000000 2818.000000 2665.000000 2718.000000
2591.000000 2513.000000 2513.000000 2196.000000 2620.000000 3156.000000 2492.000000
2981.000000 2899.000000 2821.000000 2849.000000 2866.000000 2866.000000 2950.000000
2946.000000 2752.000000 2956.000000 2956.000000 2634.000000 2630.000000 2748.000000
2880.000000 2528.000000 2879.000000 2706.000000 2941.000000 2874.000000 2731.000000
2494.000000 2494.000000 2789.000000 2789.000000 1925.000000 1925.000000 2847.000000
2532.000000 2438.000000

1114.189941 2862.000000 2749.000000 2754.000000 2660.000000 2433.000000 2587.000000
2881.000000 2567.000000 2365.000000 2543.000000 2543.000000 2317.000000 2778.000000
3123.000000 2562.000000 2919.000000 2722.000000 3068.000000 2563.000000 2802.000000
2627.000000 2617.000000 2947.000000 2913.000000 2898.000000 3218.000000 3218.000000
2689.000000 2997.000000 3263.000000 3405.000000 2892.000000 3881.000000 3881.000000

3121.000000 1784.000000 2838.000000 3556.000000 3556.000000 3657.000000 3399.000000
3851.000000 3451.000000 2554.000000 2077.000000 2596.000000 2710.000000 2832.000000
2733.000000 2870.000000 2870.000000 2240.000000 2768.000000 3386.000000 2209.000000
2615.000000 2901.000000 2944.000000 2612.000000 3209.000000 3209.000000 3155.000000
2779.000000 2936.000000 2964.000000 2964.000000 2804.000000 2609.000000 3027.000000
3114.000000 2741.000000 2795.000000 2843.000000 2892.000000 2897.000000 2752.000000
2542.000000 2542.000000 2998.000000 2998.000000 1842.000000 1842.000000 2847.000000
2411.000000 2607.000000

1124.280029 2715.000000 2970.000000 2509.000000 2435.000000 2262.000000 2528.000000
3035.000000 2683.000000 2091.000000 2808.000000 2808.000000 2301.000000 2682.000000
3083.000000 2501.000000 2826.000000 2808.000000 2851.000000 2521.000000 2829.000000
2436.000000 2306.000000 2573.000000 2790.000000 2946.000000 3047.000000 3047.000000
2626.000000 3058.000000 3012.000000 3351.000000 2814.000000 3759.000000 3759.000000
3174.000000 1486.000000 2873.000000 3687.000000 3687.000000 3313.000000 3249.000000
3765.000000 3489.000000 2401.000000 2172.000000 2461.000000 2747.000000 2862.000000
2742.000000 2796.000000 2796.000000 2318.000000 2632.000000 3230.000000 2172.000000
2544.000000 2961.000000 3119.000000 2327.000000 3408.000000 3408.000000 3167.000000
2639.000000 2982.000000 2854.000000 2854.000000 2776.000000 2390.000000 3053.000000
2975.000000 2814.000000 2804.000000 2764.000000 2805.000000 2838.000000 2534.000000
2295.000000 2295.000000 2855.000000 2855.000000 1656.000000 1656.000000 2552.000000
2302.000000 2584.000000

1134.380005 3017.000000 2949.000000 2827.000000 2309.000000 2615.000000 2464.000000
2777.000000 2482.000000 2517.000000 2826.000000 2826.000000 2347.000000 2751.000000
3128.000000 2879.000000 2954.000000 2818.000000 3144.000000 2613.000000 2824.000000
3052.000000 2891.000000 2926.000000 2943.000000 2475.000000 2608.000000 2608.000000
2607.000000 2873.000000 3064.000000 2825.000000 2746.000000 3461.000000 3461.000000
3102.000000 1868.000000 2884.000000 3308.000000 3308.000000 3458.000000 3338.000000
3456.000000 3157.000000 2510.000000 1979.000000 2696.000000 2425.000000 2554.000000
2431.000000 2548.000000 2548.000000 2376.000000 2249.000000 2825.000000 2655.000000
2923.000000 2860.000000 2944.000000 2768.000000 3226.000000 3226.000000 2972.000000
2743.000000 2856.000000 2971.000000 2971.000000 2690.000000 2497.000000 2663.000000
2799.000000 2594.000000 2582.000000 2689.000000 2791.000000 2953.000000 2856.000000
2549.000000 2549.000000 2923.000000 2923.000000 1883.000000 1883.000000 2762.000000
2661.000000 2403.000000

1144.479980 2903.000000 2936.000000 2632.000000 2151.000000 2641.000000 2426.000000
2716.000000 2412.000000 2448.000000 2534.000000 2534.000000 2426.000000 2649.000000
3163.000000 2688.000000 2836.000000 2728.000000 3105.000000 2589.000000 2652.000000
2953.000000 2673.000000 2707.000000 2856.000000 2375.000000 2464.000000 2464.000000
2609.000000 2679.000000 3071.000000 2731.000000 2624.000000 3391.000000 3391.000000
3074.000000 1803.000000 2799.000000 3357.000000 3357.000000 3341.000000 3210.000000
3298.000000 2996.000000 2473.000000 2004.000000 2592.000000 2320.000000 2510.000000
2227.000000 2367.000000 2367.000000 2385.000000 2218.000000 2504.000000 2498.000000
2715.000000 2787.000000 2771.000000 2839.000000 3089.000000 3089.000000 2787.000000
2704.000000 2742.000000 2829.000000 2829.000000 2668.000000 2411.000000 2550.000000
2633.000000 2502.000000 2468.000000 2676.000000 2749.000000 2917.000000 2762.000000
2523.000000 2523.000000 2892.000000 2892.000000 1914.000000 1914.000000 2589.000000
2631.000000 2304.000000

1154.579956 2781.000000 2513.000000 2594.000000 2141.000000 2512.000000 2395.000000
2785.000000 2419.000000 2602.000000 2267.000000 2267.000000 2549.000000 2510.000000
2856.000000 2574.000000 2871.000000 2724.000000 2983.000000 2614.000000 2791.000000

2827.000000 2717.000000 2710.000000 2858.000000 2430.000000 2459.000000 2459.000000
2499.000000 2938.000000 3113.000000 2803.000000 2716.000000 3315.000000 3315.000000
2972.000000 1709.000000 2726.000000 3162.000000 3162.000000 3196.000000 2978.000000
3477.000000 2949.000000 2463.000000 1878.000000 2386.000000 2492.000000 2433.000000
2406.000000 2355.000000 2355.000000 2033.000000 2368.000000 2672.000000 2272.000000
2648.000000 2786.000000 2619.000000 2655.000000 2962.000000 2962.000000 2906.000000
2710.000000 2708.000000 2562.000000 2562.000000 2607.000000 2552.000000 2680.000000
2787.000000 2483.000000 2516.000000 2638.000000 2633.000000 2701.000000 2658.000000
2366.000000 2366.000000 2807.000000 2807.000000 1677.000000 1677.000000 2462.000000
2428.000000 2291.000000

1164.680054 2869.000000 2662.000000 2679.000000 2175.000000 2553.000000 2415.000000
2802.000000 2520.000000 2563.000000 2394.000000 2394.000000 2529.000000 2516.000000
2980.000000 2648.000000 2979.000000 2730.000000 3005.000000 2717.000000 2762.000000
2914.000000 2773.000000 2821.000000 3005.000000 2600.000000 2514.000000 2514.000000
2598.000000 2987.000000 3258.000000 2968.000000 2877.000000 3480.000000 3480.000000
3125.000000 1715.000000 2824.000000 3385.000000 3385.000000 3372.000000 3066.000000
3601.000000 3147.000000 2661.000000 1958.000000 2476.000000 2552.000000 2518.000000
2586.000000 2493.000000 2493.000000 2088.000000 2438.000000 2670.000000 2300.000000
2674.000000 2787.000000 2675.000000 2731.000000 3038.000000 3038.000000 2976.000000
2770.000000 2845.000000 2706.000000 2706.000000 2664.000000 2557.000000 2746.000000
2953.000000 2600.000000 2607.000000 2736.000000 2724.000000 2792.000000 2750.000000
2474.000000 2474.000000 2856.000000 2856.000000 1757.000000 1757.000000 2531.000000
2509.000000 2458.000000

1174.770020 2941.000000 2846.000000 2750.000000 2330.000000 2633.000000 2541.000000
2774.000000 2689.000000 2588.000000 2587.000000 2587.000000 2521.000000 2649.000000
3139.000000 2815.000000 2990.000000 2894.000000 3062.000000 2664.000000 2837.000000
2992.000000 2815.000000 3003.000000 2928.000000 2440.000000 2536.000000 2536.000000
2610.000000 2971.000000 3327.000000 2894.000000 3001.000000 3623.000000 3623.000000
3275.000000 1724.000000 2875.000000 3471.000000 3471.000000 3512.000000 3151.000000
3538.000000 3314.000000 2679.000000 1986.000000 2583.000000 2490.000000 2611.000000
2566.000000 2433.000000 2433.000000 2306.000000 2479.000000 2649.000000 2450.000000
2676.000000 2911.000000 2959.000000 2878.000000 3044.000000 3044.000000 2811.000000
2734.000000 2878.000000 2743.000000 2743.000000 2750.000000 2478.000000 2650.000000
3001.000000 2648.000000 2620.000000 2764.000000 2875.000000 2931.000000 2799.000000
2530.000000 2530.000000 2867.000000 2867.000000 1949.000000 1949.000000 2610.000000
2691.000000 2480.000000

1184.869995 2978.000000 2819.000000 2685.000000 2245.000000 2607.000000 2506.000000
2764.000000 2655.000000 2530.000000 2517.000000 2517.000000 2525.000000 2596.000000
3121.000000 2833.000000 2992.000000 2909.000000 3088.000000 2630.000000 2853.000000
2950.000000 2748.000000 2990.000000 2913.000000 2520.000000 2515.000000 2515.000000
2565.000000 3045.000000 3342.000000 2871.000000 2900.000000 3496.000000 3496.000000
3236.000000 1704.000000 2923.000000 3343.000000 3343.000000 3429.000000 3055.000000
3530.000000 3191.000000 2674.000000 1940.000000 2615.000000 2459.000000 2548.000000
2510.000000 2403.000000 2403.000000 2299.000000 2447.000000 2593.000000 2443.000000
2661.000000 2809.000000 2930.000000 2854.000000 3025.000000 3025.000000 2811.000000
2739.000000 2871.000000 2783.000000 2783.000000 2700.000000 2508.000000 2574.000000
2899.000000 2664.000000 2633.000000 2758.000000 2859.000000 2917.000000 2865.000000
2555.000000 2555.000000 2782.000000 2782.000000 1871.000000 1871.000000 2525.000000
2641.000000 2442.000000

1194.969971 2918.000000 2982.000000 2645.000000 2205.000000 2664.000000 2376.000000
2737.000000 2565.000000 2530.000000 2485.000000 2485.000000 2408.000000 2534.000000
3190.000000 2849.000000 2909.000000 2834.000000 3044.000000 2817.000000 2882.000000
2927.000000 2732.000000 2844.000000 2961.000000 2530.000000 2586.000000 2586.000000
2590.000000 2989.000000 3454.000000 2993.000000 2988.000000 3560.000000 3560.000000
3243.000000 1747.000000 2968.000000 3517.000000 3517.000000 3495.000000 3117.000000
3631.000000 3349.000000 2740.000000 2017.000000 2529.000000 2551.000000 2601.000000
2575.000000 2465.000000 2465.000000 2189.000000 2444.000000 2556.000000 2513.000000
2602.000000 2944.000000 2883.000000 2773.000000 3052.000000 3052.000000 2961.000000
2747.000000 2877.000000 2808.000000 2808.000000 2782.000000 2610.000000 2732.000000
2984.000000 2617.000000 2598.000000 2837.000000 2867.000000 2946.000000 2821.000000
2596.000000 2596.000000 2854.000000 2854.000000 1816.000000 1816.000000 2545.000000
2566.000000 2492.000000

1205.069946 2950.000000 3024.000000 2685.000000 2211.000000 2687.000000 2427.000000
2769.000000 2544.000000 2564.000000 2537.000000 2537.000000 2472.000000 2608.000000
3221.000000 2887.000000 2941.000000 2804.000000 3121.000000 2803.000000 2885.000000
2955.000000 2712.000000 2887.000000 2963.000000 2522.000000 2563.000000 2563.000000
2551.000000 2995.000000 3384.000000 2880.000000 2936.000000 3628.000000 3628.000000
3193.000000 1719.000000 2930.000000 3475.000000 3475.000000 3549.000000 3138.000000
3604.000000 3312.000000 2729.000000 2047.000000 2538.000000 2508.000000 2558.000000
2609.000000 2451.000000 2451.000000 2263.000000 2482.000000 2577.000000 2552.000000
2606.000000 2982.000000 2883.000000 2820.000000 3116.000000 3116.000000 2882.000000
2836.000000 2842.000000 2824.000000 2824.000000 2754.000000 2585.000000 2729.000000
2931.000000 2591.000000 2651.000000 2843.000000 2880.000000 2964.000000 2838.000000
2515.000000 2515.000000 2814.000000 2814.000000 1869.000000 1869.000000 2643.000000
2632.000000 2506.000000

1215.170044 2914.000000 3034.000000 2673.000000 2295.000000 2683.000000 2492.000000
2792.000000 2613.000000 2570.000000 2614.000000 2614.000000 2490.000000 2608.000000
3242.000000 2759.000000 3023.000000 2806.000000 3103.000000 2734.000000 2795.000000
2980.000000 2725.000000 2983.000000 2994.000000 2534.000000 2611.000000 2611.000000
2659.000000 3022.000000 3449.000000 2924.000000 2875.000000 3587.000000 3587.000000
3219.000000 1847.000000 2910.000000 3382.000000 3382.000000 3471.000000 3096.000000
3516.000000 3246.000000 2751.000000 2057.000000 2652.000000 2624.000000 2636.000000
2585.000000 2424.000000 2424.000000 2285.000000 2534.000000 2768.000000 2582.000000
2661.000000 2951.000000 2853.000000 2837.000000 2986.000000 2986.000000 2942.000000
2798.000000 2937.000000 2878.000000 2878.000000 2800.000000 2664.000000 2780.000000
2993.000000 2699.000000 2738.000000 2961.000000 2841.000000 3014.000000 2882.000000
2618.000000 2618.000000 2894.000000 2894.000000 1967.000000 1967.000000 2648.000000
2708.000000 2558.000000

1225.170044 2908.000000 3006.000000 2767.000000 2302.000000 2679.000000 2475.000000
2822.000000 2627.000000 2613.000000 2599.000000 2599.000000 2549.000000 2598.000000
3257.000000 2694.000000 3027.000000 2829.000000 3118.000000 2754.000000 2803.000000
3050.000000 2763.000000 2996.000000 2946.000000 2536.000000 2592.000000 2592.000000
2692.000000 3085.000000 3534.000000 3020.000000 2940.000000 3723.000000 3723.000000
3248.000000 1925.000000 3027.000000 3409.000000 3409.000000 3517.000000 3224.000000
3617.000000 3283.000000 2843.000000 2109.000000 2714.000000 2648.000000 2712.000000
2725.000000 2533.000000 2533.000000 2343.000000 2570.000000 2781.000000 2612.000000
2606.000000 2982.000000 2853.000000 2844.000000 3088.000000 3088.000000 3031.000000
2888.000000 3028.000000 2975.000000 2975.000000 2832.000000 2763.000000 2809.000000
3081.000000 2847.000000 2794.000000 2948.000000 2859.000000 3007.000000 2873.000000

2763.000000 2763.000000 2944.000000 2944.000000 2009.000000 2009.000000 2684.000000
2735.000000 2663.000000

1235.270020 2966.000000 2959.000000 2957.000000 2375.000000 2698.000000 2431.000000
2856.000000 2694.000000 2645.000000 2570.000000 2570.000000 2604.000000 2633.000000
3278.000000 2788.000000 3000.000000 3006.000000 3188.000000 2837.000000 2937.000000
3054.000000 2880.000000 3120.000000 3022.000000 2604.000000 2580.000000 2580.000000
2756.000000 3118.000000 3569.000000 3022.000000 3208.000000 3758.000000 3758.000000
3321.000000 1847.000000 3018.000000 3629.000000 3629.000000 3626.000000 3310.000000
3701.000000 3577.000000 2851.000000 2133.000000 2710.000000 2663.000000 2676.000000
2829.000000 2585.000000 2585.000000 2284.000000 2657.000000 2795.000000 2503.000000
2692.000000 2999.000000 2973.000000 2865.000000 3210.000000 3210.000000 3052.000000
2921.000000 3042.000000 2995.000000 2995.000000 2882.000000 2801.000000 2817.000000
3155.000000 2837.000000 2790.000000 2983.000000 3067.000000 3119.000000 2888.000000
2732.000000 2732.000000 2919.000000 2919.000000 1923.000000 1923.000000 2724.000000
2706.000000 2620.000000

1245.359985 3003.000000 3097.000000 3024.000000 2482.000000 2822.000000 2534.000000
2921.000000 2706.000000 2659.000000 2699.000000 2699.000000 2659.000000 2685.000000
3349.000000 2798.000000 3159.000000 3079.000000 3194.000000 2881.000000 2968.000000
3152.000000 2838.000000 3156.000000 3133.000000 2723.000000 2706.000000 2706.000000
2810.000000 3215.000000 3646.000000 3099.000000 3226.000000 3829.000000 3829.000000
3380.000000 1891.000000 3111.000000 3693.000000 3693.000000 3723.000000 3297.000000
3775.000000 3615.000000 2885.000000 2155.000000 2810.000000 2706.000000 2718.000000
2883.000000 2614.000000 2614.000000 2301.000000 2704.000000 2836.000000 2619.000000
2714.000000 3121.000000 3088.000000 2897.000000 3243.000000 3243.000000 3097.000000
3019.000000 3125.000000 3076.000000 3076.000000 2968.000000 2883.000000 2885.000000
3193.000000 2902.000000 2890.000000 3087.000000 3123.000000 3203.000000 2991.000000
2769.000000 2769.000000 2986.000000 2986.000000 1966.000000 1966.000000 2786.000000
2779.000000 2633.000000

1255.459961 3075.000000 3143.000000 2994.000000 2494.000000 2840.000000 2604.000000
3021.000000 2822.000000 2809.000000 2633.000000 2633.000000 2688.000000 2775.000000
3313.000000 2934.000000 3212.000000 3146.000000 3169.000000 2916.000000 3005.000000
3219.000000 3010.000000 3086.000000 3227.000000 2717.000000 2712.000000 2712.000000
2662.000000 3188.000000 3622.000000 3075.000000 3240.000000 3865.000000 3865.000000
3350.000000 1890.000000 3049.000000 3701.000000 3701.000000 3669.000000 3408.000000
3837.000000 3572.000000 2793.000000 2165.000000 2743.000000 2706.000000 2801.000000
2834.000000 2594.000000 2594.000000 2474.000000 2795.000000 2926.000000 2610.000000
2877.000000 3170.000000 3023.000000 3081.000000 3204.000000 3204.000000 3217.000000
2918.000000 3018.000000 2999.000000 2999.000000 2903.000000 2751.000000 2936.000000
3261.000000 2842.000000 2863.000000 3075.000000 3148.000000 3190.000000 3067.000000
2777.000000 2777.000000 2984.000000 2984.000000 2068.000000 2068.000000 2743.000000
2816.000000 2730.000000

1265.560059 3048.000000 3179.000000 2932.000000 2448.000000 2939.000000 2567.000000
2981.000000 2847.000000 2808.000000 2698.000000 2698.000000 2701.000000 2710.000000
3328.000000 2905.000000 3149.000000 3088.000000 3246.000000 2978.000000 3021.000000
3161.000000 2987.000000 3173.000000 3307.000000 2853.000000 2716.000000 2716.000000
2737.000000 3166.000000 3559.000000 3096.000000 3221.000000 3644.000000 3644.000000
3401.000000 1952.000000 3044.000000 3623.000000 3623.000000 3583.000000 3392.000000
3806.000000 3565.000000 2798.000000 2159.000000 2716.000000 2570.000000 2734.000000
2825.000000 2591.000000 2591.000000 2497.000000 2719.000000 2826.000000 2640.000000
2832.000000 3194.000000 3048.000000 3106.000000 3152.000000 3152.000000 3157.000000

2908.000000 2999.000000 2971.000000 2971.000000 2850.000000 2765.000000 2947.000000
3239.000000 2807.000000 2874.000000 3026.000000 3118.000000 3093.000000 3023.000000
2706.000000 2706.000000 3041.000000 3041.000000 2010.000000 2010.000000 2746.000000
2761.000000 2682.000000

1275.660034 3159.000000 3027.000000 2974.000000 2433.000000 2797.000000 2579.000000
2902.000000 2768.000000 2742.000000 2726.000000 2726.000000 2642.000000 2805.000000
3322.000000 2954.000000 3194.000000 3155.000000 3277.000000 2976.000000 3024.000000
3113.000000 2978.000000 3186.000000 3286.000000 2807.000000 2856.000000 2856.000000
2867.000000 3137.000000 3577.000000 3034.000000 3094.000000 3788.000000 3788.000000
3433.000000 1899.000000 2979.000000 3641.000000 3641.000000 3730.000000 3326.000000
3704.000000 3477.000000 2813.000000 2143.000000 2684.000000 2683.000000 2683.000000
2900.000000 2650.000000 2650.000000 2407.000000 2683.000000 2839.000000 2652.000000
2839.000000 3049.000000 3084.000000 3065.000000 3204.000000 3204.000000 3135.000000
2914.000000 3025.000000 3012.000000 3012.000000 2935.000000 2830.000000 2904.000000
3204.000000 2811.000000 2769.000000 3067.000000 3089.000000 3129.000000 3039.000000
2689.000000 2689.000000 2995.000000 2995.000000 2033.000000 2033.000000 2855.000000
2779.000000 2649.000000

1285.760010 3159.000000 3090.000000 2905.000000 2366.000000 2829.000000 2526.000000
2924.000000 2761.000000 2751.000000 2783.000000 2783.000000 2662.000000 2782.000000
3332.000000 2994.000000 3116.000000 3183.000000 3221.000000 2891.000000 3041.000000
3108.000000 2957.000000 3211.000000 3192.000000 2728.000000 2794.000000 2794.000000
2813.000000 3232.000000 3709.000000 3079.000000 3123.000000 3746.000000 3746.000000
3421.000000 1867.000000 3018.000000 3754.000000 3754.000000 3764.000000 3398.000000
3751.000000 3550.000000 2874.000000 2207.000000 2793.000000 2713.000000 2762.000000
2833.000000 2604.000000 2604.000000 2444.000000 2624.000000 2773.000000 2662.000000
2850.000000 3116.000000 3059.000000 3022.000000 3221.000000 3221.000000 3152.000000
3024.000000 3075.000000 3085.000000 3085.000000 3017.000000 2884.000000 2902.000000
3242.000000 2867.000000 2850.000000 3117.000000 3124.000000 3176.000000 3058.000000
2714.000000 2714.000000 3035.000000 3035.000000 2043.000000 2043.000000 2863.000000
2777.000000 2659.000000

1295.859985 3007.000000 3119.000000 2873.000000 2274.000000 2817.000000 2427.000000
2913.000000 2696.000000 2621.000000 2683.000000 2683.000000 2648.000000 2677.000000
3227.000000 2897.000000 3081.000000 2970.000000 3295.000000 2929.000000 2987.000000
3106.000000 2826.000000 3112.000000 3137.000000 2706.000000 2652.000000 2652.000000
2729.000000 3144.000000 3521.000000 2995.000000 3096.000000 3840.000000 3840.000000
3328.000000 1869.000000 3065.000000 3739.000000 3739.000000 3711.000000 3308.000000
3802.000000 3519.000000 2792.000000 2060.000000 2717.000000 2663.000000 2608.000000
2758.000000 2570.000000 2570.000000 2431.000000 2559.000000 2707.000000 2683.000000
2734.000000 3134.000000 3067.000000 3001.000000 3244.000000 3244.000000 3094.000000
2945.000000 3066.000000 3056.000000 3056.000000 2918.000000 2840.000000 2893.000000
3145.000000 2901.000000 2803.000000 2951.000000 3108.000000 3181.000000 3008.000000
2780.000000 2780.000000 3004.000000 3004.000000 2001.000000 2001.000000 2767.000000
2767.000000 2571.000000

1305.959961 2879.000000 2950.000000 2707.000000 2141.000000 2618.000000 2303.000000
2704.000000 2569.000000 2492.000000 2492.000000 2492.000000 2541.000000 2502.000000
3105.000000 2831.000000 2964.000000 2807.000000 3093.000000 2808.000000 2855.000000
2906.000000 2678.000000 2907.000000 2972.000000 2529.000000 2454.000000 2454.000000
2591.000000 2906.000000 3355.000000 2836.000000 2919.000000 3395.000000 3395.000000
3143.000000 1757.000000 2884.000000 3443.000000 3443.000000 3516.000000 3071.000000
3565.000000 3253.000000 2606.000000 1965.000000 2509.000000 2482.000000 2439.000000

2622.000000 2385.000000 2385.000000 2286.000000 2415.000000 2541.000000 2504.000000
2629.000000 2970.000000 2888.000000 2874.000000 3075.000000 3075.000000 2907.000000
2732.000000 2797.000000 2732.000000 2732.000000 2731.000000 2663.000000 2679.000000
2960.000000 2692.000000 2577.000000 2816.000000 2858.000000 2827.000000 2802.000000
2562.000000 2562.000000 2859.000000 2859.000000 1824.000000 1824.000000 2599.000000
2555.000000 2383.000000

1316.050049 2744.000000 2888.000000 2595.000000 2106.000000 2645.000000 2319.000000
2570.000000 2546.000000 2492.000000 2420.000000 2420.000000 2489.000000 2501.000000
3078.000000 2747.000000 2867.000000 2820.000000 2911.000000 2779.000000 2706.000000
2970.000000 2641.000000 2869.000000 2914.000000 2512.000000 2289.000000 2289.000000
2497.000000 2874.000000 3343.000000 2756.000000 2793.000000 3271.000000 3271.000000
3030.000000 1824.000000 2711.000000 3305.000000 3305.000000 3211.000000 2969.000000
3375.000000 3132.000000 2550.000000 2121.000000 2415.000000 2589.000000 2483.000000
2591.000000 2362.000000 2362.000000 2329.000000 2388.000000 2492.000000 2535.000000
2631.000000 2872.000000 2818.000000 2803.000000 2926.000000 2926.000000 2890.000000
2734.000000 2691.000000 2721.000000 2721.000000 2698.000000 2518.000000 2493.000000
2893.000000 2585.000000 2507.000000 2774.000000 2733.000000 2775.000000 2690.000000
2469.000000 2469.000000 2792.000000 2792.000000 1872.000000 1872.000000 2435.000000
2521.000000 2446.000000

1326.050049 2421.000000 2685.000000 2278.000000 1794.000000 2383.000000 2079.000000
2293.000000 2270.000000 2212.000000 2209.000000 2209.000000 2301.000000 2224.000000
2821.000000 2515.000000 2611.000000 2578.000000 2599.000000 2512.000000 2486.000000
2743.000000 2425.000000 2612.000000 2655.000000 2305.000000 2003.000000 2003.000000
2232.000000 2582.000000 2976.000000 2355.000000 2476.000000 2893.000000 2893.000000
2625.000000 1641.000000 2384.000000 3042.000000 3042.000000 2882.000000 2591.000000
3032.000000 2803.000000 2246.000000 1893.000000 2183.000000 2355.000000 2222.000000
2263.000000 2093.000000 2093.000000 2227.000000 2161.000000 2211.000000 2310.000000
2345.000000 2672.000000 2509.000000 2542.000000 2683.000000 2683.000000 2617.000000
2426.000000 2309.000000 2344.000000 2344.000000 2455.000000 2190.000000 2189.000000
2494.000000 2293.000000 2251.000000 2423.000000 2424.000000 2507.000000 2414.000000
2185.000000 2185.000000 2442.000000 2442.000000 1706.000000 1706.000000 2137.000000
2243.000000 2251.000000

1336.150024 2248.000000 2243.000000 2158.000000 1751.000000 2247.000000 2046.000000
2056.000000 2076.000000 2091.000000 1943.000000 1943.000000 2017.000000 2051.000000
2437.000000 2305.000000 2401.000000 2234.000000 2449.000000 2434.000000 2411.000000
2416.000000 2151.000000 2454.000000 2517.000000 2179.000000 1920.000000 1920.000000
2206.000000 2283.000000 2542.000000 2334.000000 2434.000000 2558.000000 2558.000000
2564.000000 1651.000000 2255.000000 2577.000000 2577.000000 2721.000000 2399.000000
2569.000000 2430.000000 2216.000000 1777.000000 2076.000000 2128.000000 2242.000000
2228.000000 1882.000000 1882.000000 1859.000000 2155.000000 2166.000000 2191.000000
2075.000000 2653.000000 2593.000000 2485.000000 2508.000000 2508.000000 2445.000000
2402.000000 2191.000000 2155.000000 2155.000000 2224.000000 2205.000000 2137.000000
2440.000000 2184.000000 1989.000000 2339.000000 2231.000000 2259.000000 2469.000000
2145.000000 2145.000000 2332.000000 2332.000000 1517.000000 1517.000000 2005.000000
1999.000000 2289.000000

1346.250000 1760.000000 2331.000000 2335.000000 1779.000000 2594.000000 2188.000000
1975.000000 1874.000000 2285.000000 1863.000000 1863.000000 1782.000000 2028.000000
2408.000000 2066.000000 2460.000000 1840.000000 2828.000000 2738.000000 2371.000000
2371.000000 1947.000000 2425.000000 2344.000000 2171.000000 1767.000000 1767.000000
2241.000000 2177.000000 2014.000000 2750.000000 2704.000000 2341.000000 2341.000000

```
2802.000000  2060.000000  2124.000000  2178.000000  2178.000000  3053.000000  2936.000000
2117.000000  1939.000000  2700.000000  1927.000000  2282.000000  2166.000000  2769.000000
2576.000000  1742.000000  1742.000000  1679.000000  2642.000000  2425.000000  2541.000000
1878.000000  3522.000000  3108.000000  2702.000000  2580.000000  2580.000000  2784.000000
3086.000000  2251.000000  2489.000000  2489.000000  2184.000000  2687.000000  2521.000000
3259.000000  2530.000000  2122.000000  2484.000000  2171.000000  2504.000000  3016.000000
2463.000000  2463.000000  2932.000000  2932.000000  1460.000000  1460.000000  2068.000000
1618.000000  2677.000000

  1416.939941    0.000000    0.000000    0.000000    0.000000    0.000000    0.000000    0.000000
0.000000    0.000000    0.000000    0.000000    0.000000    0.000000    0.000000    0.000000    0.000000
0.000000    0.000000    0.000000    0.000000    0.000000    0.000000    0.000000    0.000000    0.000000
0.000000    0.000000    0.000000    0.000000    0.000000    0.000000    0.000000    0.000000    0.000000
0.000000    0.000000    0.000000    0.000000    0.000000    0.000000    0.000000    0.000000    0.000000
0.000000    0.000000    0.000000    0.000000    0.000000    0.000000    0.000000    0.000000    0.000000
0.000000    0.000000    0.000000    0.000000    0.000000    0.000000    0.000000    0.000000    0.000000
0.000000    0.000000    0.000000    0.000000    0.000000    0.000000    0.000000    0.000000    0.000000
0.000000    0.000000    0.000000    0.000000    0.000000    0.000000    0.000000    0.000000    0.000000
0.000000    0.000000    0.000000    0.000000    0.000000    0.000000

  1426.939941  1897.000000  1786.000000   -52.000000  -328.000000  -100.000000  1061.000000   -38.000000
1698.000000    83.000000   200.000000   200.000000  1550.000000  -220.000000   843.000000  1573.000000
1061.000000   -38.000000   719.000000   -40.000000   219.000000  -478.000000  -458.000000  1448.000000
501.000000   983.000000  -161.000000  -161.000000  -393.000000   859.000000  2486.000000   489.000000
1229.000000   -61.000000   -61.000000  2488.000000  -161.000000  1288.000000  1157.000000  1157.000000
194.000000  1793.000000  -160.000000  1212.000000   574.000000   427.000000   382.000000   771.000000
771.000000   739.000000   639.000000   639.000000   598.000000  1240.000000   564.000000  2316.000000
877.000000   -99.000000   750.000000   629.000000  1488.000000  1488.000000   847.000000   664.000000
273.000000  1046.000000  1046.000000   904.000000  -267.000000    72.000000   259.000000   893.000000
1003.000000   464.000000   848.000000    92.000000   351.000000   664.000000   664.000000  1158.000000
1158.000000   955.000000   955.000000    -8.000000   296.000000   332.000000

  1437.040039   595.000000   858.000000  -192.000000  -106.000000   558.000000  -152.000000  1337.000000
2088.000000   953.000000   511.000000   511.000000  1915.000000  -151.000000  1212.000000   506.000000
2251.000000   905.000000  -280.000000   695.000000  1142.000000  2188.000000  1255.000000  1489.000000
1032.000000   226.000000  -150.000000  -150.000000   169.000000   613.000000  2797.000000   287.000000
716.000000   598.000000   598.000000   721.000000   -22.000000   642.000000  1454.000000  1454.000000
853.000000   745.000000  1244.000000   378.000000   472.000000   627.000000  -107.000000  1234.000000
152.000000    89.000000   682.000000   682.000000   675.000000   170.000000    -9.000000   -57.000000
183.000000    85.000000   182.000000  1281.000000   822.000000   822.000000   379.000000  -323.000000
617.000000  -146.000000  -146.000000   481.000000   -23.000000   -34.000000   223.000000    17.000000
310.000000   538.000000   649.000000   451.000000   135.000000   390.000000   390.000000   453.000000
453.000000  -107.000000  -107.000000   411.000000   814.000000   282.000000

  1447.140015  1055.000000  1218.000000   502.000000   243.000000  1052.000000   501.000000
1046.000000  1884.000000  1201.000000   860.000000   860.000000  1649.000000   491.000000  1402.000000
1046.000000  1824.000000  1279.000000  1063.000000  1123.000000  1439.000000  1919.000000
1329.000000  1557.000000  1321.000000   591.000000   348.000000   348.000000   573.000000  1060.000000
2384.000000   765.000000   810.000000   810.000000   810.000000  1080.000000   792.000000   997.000000
1496.000000  1496.000000   942.000000   818.000000  1132.000000   904.000000   947.000000   898.000000
346.000000  1364.000000   614.000000   848.000000   665.000000   665.000000   968.000000   612.000000
342.000000   573.000000   967.000000   901.000000   866.000000  1176.000000  1203.000000  1203.000000
771.000000   402.000000   935.000000   274.000000   274.000000   668.000000   581.000000   327.000000
```

375.000000 541.000000 578.000000 965.000000 971.000000 705.000000 781.000000 729.000000
729.000000 775.000000 775.000000 171.000000 171.000000 521.000000 1211.000000 846.000000

1457.229980 1584.000000 1511.000000 817.000000 368.000000 1167.000000 878.000000 702.000000
1298.000000 989.000000 959.000000 959.000000 1531.000000 1085.000000 1471.000000 1587.000000
1409.000000 1597.000000 1813.000000 1742.000000 1654.000000 1191.000000 1181.000000
1388.000000 1825.000000 1068.000000 740.000000 740.000000 1293.000000 1398.000000
2174.000000 1004.000000 902.000000 1049.000000 1049.000000 1458.000000 962.000000
1409.000000 1501.000000 1501.000000 1242.000000 751.000000 1027.000000 1240.000000
1168.000000 1168.000000 1105.000000 1477.000000 843.000000 1034.000000 698.000000 698.000000
1253.000000 671.000000 455.000000 938.000000 679.000000 1444.000000 985.000000 1272.000000
1379.000000 1379.000000 1149.000000 1178.000000 945.000000 896.000000 896.000000 1309.000000
757.000000 924.000000 897.000000 955.000000 754.000000 1290.000000 713.000000 1130.000000
1339.000000 1132.000000 1132.000000 1322.000000 1322.000000 795.000000 795.000000 634.000000
1213.000000 978.000000

1467.329956 1790.000000 1494.000000 666.000000 218.000000 1138.000000 803.000000 535.000000
1318.000000 897.000000 1075.000000 1075.000000 1448.000000 993.000000 1363.000000
1365.000000 1180.000000 1511.000000 2071.000000 1925.000000 1643.000000 1016.000000
1145.000000 1455.000000 1948.000000 1091.000000 702.000000 702.000000 1371.000000
1445.000000 2306.000000 852.000000 861.000000 944.000000 944.000000 1254.000000 803.000000
1420.000000 1434.000000 1434.000000 1322.000000 699.000000 1072.000000 1048.000000
1018.000000 1168.000000 1065.000000 1333.000000 774.000000 796.000000 643.000000 643.000000
1206.000000 549.000000 438.000000 984.000000 457.000000 1359.000000 862.000000 1113.000000
1106.000000 1106.000000 1114.000000 1233.000000 682.000000 777.000000 777.000000 1336.000000
615.000000 797.000000 798.000000 811.000000 727.000000 1249.000000 438.000000 983.000000
1288.000000 1038.000000 1038.000000 1267.000000 1267.000000 889.000000 889.000000 495.000000
1029.000000 760.000000

1477.430054 2249.000000 1402.000000 949.000000 859.000000 1383.000000 1284.000000
865.000000 1672.000000 1736.000000 1273.000000 1273.000000 1692.000000 1268.000000
1677.000000 1965.000000 1946.000000 1593.000000 1829.000000 1824.000000 1818.000000
2223.000000 1646.000000 1548.000000 1634.000000 989.000000 666.000000 666.000000 1108.000000
1805.000000 2042.000000 1357.000000 1479.000000 969.000000 969.000000 1633.000000 889.000000
1633.000000 2014.000000 2014.000000 1269.000000 880.000000 1196.000000 1343.000000
1097.000000 1302.000000 1103.000000 1598.000000 1287.000000 1337.000000 953.000000
953.000000 1336.000000 970.000000 695.000000 1221.000000 1614.000000 1429.000000 1313.000000
1983.000000 1570.000000 1570.000000 1566.000000 1321.000000 885.000000 818.000000 818.000000
1275.000000 724.000000 1103.000000 1085.000000 903.000000 722.000000 1288.000000 1335.000000
1454.000000 1196.000000 1275.000000 1275.000000 1488.000000 1488.000000 1042.000000
1042.000000 880.000000 1399.000000 1360.000000

1487.530029 2177.000000 1741.000000 1174.000000 996.000000 1551.000000 1309.000000
1004.000000 1727.000000 1781.000000 1413.000000 1413.000000 1906.000000 1388.000000
1911.000000 2097.000000 2037.000000 1746.000000 1921.000000 1947.000000 1909.000000
2232.000000 1648.000000 1703.000000 1765.000000 1247.000000 778.000000 778.000000
1340.000000 1912.000000 2378.000000 1502.000000 1782.000000 1292.000000 1292.000000
1897.000000 1127.000000 1838.000000 2153.000000 2153.000000 1549.000000 1132.000000
1509.000000 1619.000000 1433.000000 1472.000000 1296.000000 1692.000000 1425.000000
1580.000000 1179.000000 1179.000000 1499.000000 1185.000000 848.000000 1332.000000
1621.000000 1601.000000 1438.000000 2006.000000 1682.000000 1682.000000 1591.000000
1514.000000 1190.000000 1043.000000 1043.000000 1437.000000 915.000000 1275.000000
1270.000000 1162.000000 965.000000 1539.000000 1390.000000 1605.000000 1450.000000

1460.000000 1460.000000 1660.000000 1660.000000 1055.000000 1055.000000 1047.000000
1543.000000 1592.000000

1497.630005 1837.000000 1988.000000 1379.000000 990.000000 1753.000000 1365.000000
1227.000000 1939.000000 1595.000000 1386.000000 1386.000000 1992.000000 1351.000000
2158.000000 2089.000000 2159.000000 2102.000000 2017.000000 2204.000000 2076.000000
2110.000000 1669.000000 1855.000000 2240.000000 1572.000000 1110.000000 1110.000000
1624.000000 1948.000000 2516.000000 1790.000000 1825.000000 1672.000000 1672.000000
2132.000000 1441.000000 2058.000000 2184.000000 2184.000000 1804.000000 1390.000000
1853.000000 1855.000000 1797.000000 1733.000000 1412.000000 2011.000000 1687.000000
1771.000000 1471.000000 1471.000000 1748.000000 1307.000000 1014.000000 1602.000000
1375.000000 1664.000000 1541.000000 1837.000000 1941.000000 1941.000000 1618.000000
1665.000000 1466.000000 1342.000000 1342.000000 1618.000000 1384.000000 1306.000000
1462.000000 1484.000000 1327.000000 1924.000000 1487.000000 1710.000000 1700.000000
1725.000000 1725.000000 1855.000000 1855.000000 1341.000000 1341.000000 1284.000000
1772.000000 1739.000000

1507.729980 1907.000000 2042.000000 1397.000000 1019.000000 1783.000000 1430.000000
1281.000000 2040.000000 1702.000000 1506.000000 1506.000000 2074.000000 1410.000000
2252.000000 2136.000000 2219.000000 2165.000000 2077.000000 2218.000000 2135.000000
2156.000000 1752.000000 1941.000000 2269.000000 1556.000000 1141.000000 1141.000000
1665.000000 2056.000000 2514.000000 1819.000000 1959.000000 1749.000000 1749.000000
2179.000000 1468.000000 2094.000000 2296.000000 2296.000000 1878.000000 1434.000000
1943.000000 2014.000000 1875.000000 1774.000000 1505.000000 2072.000000 1754.000000
1794.000000 1531.000000 1531.000000 1871.000000 1358.000000 1016.000000 1647.000000
1467.000000 1758.000000 1590.000000 1920.000000 2116.000000 2116.000000 1671.000000
1681.000000 1558.000000 1465.000000 1465.000000 1716.000000 1390.000000 1504.000000
1528.000000 1547.000000 1369.000000 1985.000000 1525.000000 1780.000000 1799.000000
1769.000000 1769.000000 1842.000000 1842.000000 1400.000000 1400.000000 1367.000000
1850.000000 1888.000000

1517.829956 2181.000000 2215.000000 1431.000000 1066.000000 1899.000000 1438.000000
1284.000000 2130.000000 1812.000000 1453.000000 1453.000000 2267.000000 1525.000000
2250.000000 2272.000000 2194.000000 2279.000000 2137.000000 2284.000000 2187.000000
2149.000000 1806.000000 2110.000000 2215.000000 1557.000000 1084.000000 1084.000000
1741.000000 2080.000000 2730.000000 1823.000000 2024.000000 1815.000000 1815.000000
2326.000000 1621.000000 2196.000000 2366.000000 2366.000000 1894.000000 1510.000000
1877.000000 1991.000000 1988.000000 1851.000000 1670.000000 2041.000000 1754.000000
1800.000000 1511.000000 1511.000000 1765.000000 1419.000000 1072.000000 1615.000000
1446.000000 1811.000000 1765.000000 1981.000000 2054.000000 2054.000000 1687.000000
1861.000000 1656.000000 1557.000000 1557.000000 1834.000000 1544.000000 1542.000000
1554.000000 1642.000000 1486.000000 2084.000000 1676.000000 2000.000000 1853.000000
1877.000000 1877.000000 1879.000000 1879.000000 1452.000000 1452.000000 1413.000000
1955.000000 1880.000000

1527.920044 2257.000000 2286.000000 1501.000000 1107.000000 1961.000000 1481.000000
1321.000000 2152.000000 1867.000000 1462.000000 1462.000000 2330.000000 1549.000000
2308.000000 2310.000000 2202.000000 2271.000000 2206.000000 2379.000000 2219.000000
2241.000000 1877.000000 2080.000000 2296.000000 1626.000000 1132.000000 1132.000000
1795.000000 2117.000000 2882.000000 1910.000000 2163.000000 1946.000000 1946.000000
2391.000000 1671.000000 2286.000000 2443.000000 2443.000000 1961.000000 1564.000000
1901.000000 2102.000000 2046.000000 1934.000000 1689.000000 2053.000000 1806.000000
1852.000000 1526.000000 1526.000000 1810.000000 1490.000000 1142.000000 1652.000000
1510.000000 1863.000000 1790.000000 2045.000000 2134.000000 2134.000000 1829.000000

1919.000000 1698.000000 1633.000000 1633.000000 1914.000000 1696.000000 1584.000000
1649.000000 1725.000000 1551.000000 2161.000000 1704.000000 2092.000000 1897.000000
1937.000000 1937.000000 1954.000000 1954.000000 1495.000000 1495.000000 1447.000000
2092.000000 1962.000000

1537.920044 2365.000000 2156.000000 1603.000000 1245.000000 2091.000000 1740.000000
1456.000000 2216.000000 2034.000000 1619.000000 1619.000000 2318.000000 1704.000000
2464.000000 2392.000000 2265.000000 2325.000000 2251.000000 2321.000000 2241.000000
2397.000000 1966.000000 2289.000000 2435.000000 1771.000000 1298.000000 1298.000000
1824.000000 2272.000000 2874.000000 2093.000000 2245.000000 2068.000000 2068.000000
2394.000000 1623.000000 2227.000000 2497.000000 2497.000000 2168.000000 1637.000000
2037.000000 2343.000000 2018.000000 1951.000000 1778.000000 2191.000000 1900.000000
2015.000000 1746.000000 1746.000000 1944.000000 1544.000000 1246.000000 1754.000000
1701.000000 1992.000000 1896.000000 2229.000000 2388.000000 2388.000000 1961.000000
1993.000000 1781.000000 1763.000000 1763.000000 1995.000000 1744.000000 1660.000000
1776.000000 1836.000000 1630.000000 2265.000000 1838.000000 2121.000000 2076.000000
2000.000000 2000.000000 2122.000000 2122.000000 1612.000000 1612.000000 1513.000000
2157.000000 2088.000000

1548.020020 2441.000000 2234.000000 1652.000000 1267.000000 2200.000000 1790.000000
1499.000000 2296.000000 2043.000000 1654.000000 1654.000000 2422.000000 1703.000000
2550.000000 2425.000000 2358.000000 2383.000000 2259.000000 2351.000000 2282.000000
2517.000000 2053.000000 2341.000000 2502.000000 1790.000000 1348.000000 1348.000000
1916.000000 2416.000000 2859.000000 2170.000000 2268.000000 2110.000000 2110.000000
2436.000000 1652.000000 2289.000000 2531.000000 2531.000000 2194.000000 1732.000000
2086.000000 2379.000000 2008.000000 2012.000000 1858.000000 2238.000000 1950.000000
2072.000000 1816.000000 1816.000000 2056.000000 1604.000000 1296.000000 1801.000000
1741.000000 2039.000000 1920.000000 2257.000000 2379.000000 2379.000000 2031.000000
2073.000000 1847.000000 1861.000000 1861.000000 2037.000000 1792.000000 1654.000000
1861.000000 1838.000000 1726.000000 2222.000000 1900.000000 2156.000000 2107.000000
2026.000000 2026.000000 2163.000000 2163.000000 1617.000000 1617.000000 1546.000000
2250.000000 2104.000000

1558.119995 2278.000000 2371.000000 1746.000000 1331.000000 2290.000000 1739.000000
1600.000000 2304.000000 2133.000000 1796.000000 1796.000000 2383.000000 1839.000000
2525.000000 2419.000000 2329.000000 2408.000000 2482.000000 2444.000000 2319.000000
2526.000000 2200.000000 2275.000000 2390.000000 1839.000000 1259.000000 1259.000000
1936.000000 2296.000000 3082.000000 2135.000000 2474.000000 2095.000000 2095.000000
2610.000000 1703.000000 2456.000000 2682.000000 2682.000000 2163.000000 1835.000000
2264.000000 2484.000000 2302.000000 1956.000000 1877.000000 2318.000000 2053.000000
2135.000000 1763.000000 1763.000000 2093.000000 1685.000000 1421.000000 1982.000000
1771.000000 2054.000000 1911.000000 2243.000000 2368.000000 2368.000000 1925.000000
2021.000000 1913.000000 1816.000000 1816.000000 1953.000000 1888.000000 1848.000000
2020.000000 1996.000000 1810.000000 2374.000000 1967.000000 2246.000000 2224.000000
2170.000000 2170.000000 2221.000000 2221.000000 1545.000000 1545.000000 1577.000000
2256.000000 2193.000000

1568.219971 2361.000000 2397.000000 1792.000000 1364.000000 2305.000000 1849.000000
1627.000000 2358.000000 2140.000000 1829.000000 1829.000000 2386.000000 1974.000000
2603.000000 2458.000000 2398.000000 2471.000000 2494.000000 2442.000000 2419.000000
2544.000000 2228.000000 2277.000000 2475.000000 1849.000000 1364.000000 1364.000000
1946.000000 2357.000000 3130.000000 2219.000000 2493.000000 2118.000000 2118.000000
2679.000000 1788.000000 2465.000000 2784.000000 2784.000000 2372.000000 1909.000000
2401.000000 2468.000000 2344.000000 2041.000000 1904.000000 2349.000000 2070.000000

2231.000000 1807.000000 1807.000000 2152.000000 1809.000000 1478.000000 1990.000000
1829.000000 2015.000000 1978.000000 2337.000000 2378.000000 2378.000000 2010.000000
2099.000000 1981.000000 1872.000000 1872.000000 1997.000000 1921.000000 1924.000000
2081.000000 2098.000000 1872.000000 2412.000000 2062.000000 2340.000000 2368.000000
2142.000000 2142.000000 2271.000000 2271.000000 1618.000000 1618.000000 1699.000000
2328.000000 2199.000000

1578.319946 2567.000000 2439.000000 1761.000000 1336.000000 2270.000000 1886.000000
1746.000000 2307.000000 2233.000000 1861.000000 1861.000000 2431.000000 1853.000000
2711.000000 2530.000000 2514.000000 2493.000000 2447.000000 2522.000000 2477.000000
2609.000000 2105.000000 2390.000000 2592.000000 1989.000000 1563.000000 1563.000000
1964.000000 2451.000000 3123.000000 2273.000000 2454.000000 2355.000000 2355.000000
2748.000000 1778.000000 2582.000000 2826.000000 2826.000000 2504.000000 1910.000000
2418.000000 2553.000000 2368.000000 2083.000000 2004.000000 2422.000000 2178.000000
2281.000000 1889.000000 1889.000000 2154.000000 1774.000000 1403.000000 2002.000000
1795.000000 2200.000000 2101.000000 2427.000000 2493.000000 2493.000000 2216.000000
2059.000000 2116.000000 1872.000000 1872.000000 2162.000000 1881.000000 1992.000000
2029.000000 2199.000000 1968.000000 2438.000000 2145.000000 2364.000000 2219.000000
2285.000000 2285.000000 2405.000000 2405.000000 1757.000000 1757.000000 1819.000000
2397.000000 2352.000000

1588.420044 2596.000000 2493.000000 1819.000000 1382.000000 2285.000000 1895.000000
1828.000000 2427.000000 2246.000000 1883.000000 1883.000000 2459.000000 1867.000000
2682.000000 2573.000000 2573.000000 2534.000000 2517.000000 2573.000000 2530.000000
2640.000000 2187.000000 2458.000000 2628.000000 2041.000000 1567.000000 1567.000000
2084.000000 2544.000000 3115.000000 2323.000000 2540.000000 2449.000000 2449.000000
2800.000000 1875.000000 2595.000000 2918.000000 2918.000000 2516.000000 2008.000000
2414.000000 2701.000000 2299.000000 2142.000000 2102.000000 2493.000000 2225.000000
2359.000000 1917.000000 1917.000000 2194.000000 1812.000000 1434.000000 2037.000000
1793.000000 2281.000000 2151.000000 2486.000000 2565.000000 2565.000000 2285.000000
2158.000000 2146.000000 1984.000000 1984.000000 2213.000000 1886.000000 1992.000000
2098.000000 2166.000000 2012.000000 2437.000000 2221.000000 2465.000000 2241.000000
2311.000000 2311.000000 2449.000000 2449.000000 1784.000000 1784.000000 1803.000000
2453.000000 2359.000000

1598.510010 2632.000000 2746.000000 1870.000000 1423.000000 2485.000000 2001.000000
1786.000000 2490.000000 2321.000000 1950.000000 1950.000000 2477.000000 1895.000000
2754.000000 2628.000000 2570.000000 2603.000000 2623.000000 2515.000000 2523.000000
2734.000000 2283.000000 2569.000000 2658.000000 1992.000000 1499.000000 1499.000000
2051.000000 2640.000000 3195.000000 2341.000000 2564.000000 2467.000000 2467.000000
2736.000000 1844.000000 2619.000000 2922.000000 2922.000000 2509.000000 2012.000000
2442.000000 2631.000000 2450.000000 2235.000000 2147.000000 2577.000000 2295.000000
2379.000000 1983.000000 1983.000000 2228.000000 1933.000000 1588.000000 2034.000000
2068.000000 2300.000000 2152.000000 2523.000000 2548.000000 2548.000000 2367.000000
2350.000000 2147.000000 2189.000000 2189.000000 2211.000000 2042.000000 2075.000000
2184.000000 2177.000000 2029.000000 2496.000000 2223.000000 2471.000000 2345.000000
2294.000000 2294.000000 2387.000000 2387.000000 1802.000000 1802.000000 1831.000000
2480.000000 2430.000000

1608.609985 2673.000000 2775.000000 1885.000000 1496.000000 2534.000000 2000.000000
1767.000000 2513.000000 2297.000000 1953.000000 1953.000000 2504.000000 1932.000000
2800.000000 2665.000000 2534.000000 2572.000000 2610.000000 2623.000000 2487.000000
2716.000000 2275.000000 2580.000000 2644.000000 2059.000000 1593.000000 1593.000000
2144.000000 2694.000000 3282.000000 2406.000000 2541.000000 2503.000000 2503.000000

2808.000000 1885.000000 2579.000000 3020.000000 3020.000000 2575.000000 2050.000000
2525.000000 2630.000000 2444.000000 2308.000000 2177.000000 2605.000000 2305.000000
2406.000000 2084.000000 2084.000000 2301.000000 1936.000000 1619.000000 2080.000000
2093.000000 2377.000000 2216.000000 2568.000000 2618.000000 2618.000000 2440.000000
2334.000000 2122.000000 2177.000000 2177.000000 2296.000000 2101.000000 2190.000000
2257.000000 2173.000000 2067.000000 2520.000000 2224.000000 2499.000000 2385.000000
2228.000000 2228.000000 2410.000000 2410.000000 1809.000000 1809.000000 1902.000000
2503.000000 2436.000000

1618.709961 2668.000000 2620.000000 1882.000000 1441.000000 2364.000000 2035.000000
1802.000000 2569.000000 2300.000000 2083.000000 2083.000000 2597.000000 2031.000000
2845.000000 2821.000000 2661.000000 2677.000000 2680.000000 2709.000000 2613.000000
2757.000000 2384.000000 2617.000000 2733.000000 2083.000000 1602.000000 1602.000000
2316.000000 2757.000000 3342.000000 2399.000000 2676.000000 2732.000000 2732.000000
2865.000000 1983.000000 2760.000000 3053.000000 3053.000000 2660.000000 2103.000000
2684.000000 2812.000000 2524.000000 2223.000000 2259.000000 2640.000000 2396.000000
2383.000000 2123.000000 2123.000000 2219.000000 1927.000000 1622.000000 2063.000000
2115.000000 2348.000000 2344.000000 2581.000000 2713.000000 2713.000000 2344.000000
2416.000000 2279.000000 2243.000000 2243.000000 2424.000000 2167.000000 2143.000000
2255.000000 2359.000000 2087.000000 2620.000000 2275.000000 2564.000000 2524.000000
2427.000000 2427.000000 2688.000000 2688.000000 1854.000000 1854.000000 1982.000000
2600.000000 2572.000000

1628.810059 2704.000000 2732.000000 1857.000000 1532.000000 2488.000000 2046.000000
1805.000000 2560.000000 2339.000000 2138.000000 2138.000000 2620.000000 2058.000000
3022.000000 2781.000000 2701.000000 2684.000000 2656.000000 2680.000000 2616.000000
2857.000000 2387.000000 2620.000000 2688.000000 2106.000000 1576.000000 1576.000000
2311.000000 2696.000000 3374.000000 2439.000000 2712.000000 2704.000000 2704.000000
2921.000000 1985.000000 2836.000000 3037.000000 3037.000000 2716.000000 2130.000000
2680.000000 2808.000000 2575.000000 2282.000000 2246.000000 2676.000000 2499.000000
2379.000000 2082.000000 2082.000000 2315.000000 1990.000000 1713.000000 2178.000000
2142.000000 2415.000000 2419.000000 2632.000000 2777.000000 2777.000000 2391.000000
2403.000000 2395.000000 2246.000000 2246.000000 2463.000000 2230.000000 2118.000000
2298.000000 2415.000000 2082.000000 2599.000000 2286.000000 2576.000000 2568.000000
2479.000000 2479.000000 2720.000000 2720.000000 1877.000000 1877.000000 1977.000000
2563.000000 2668.000000

1638.810059 2658.000000 2931.000000 2146.000000 1587.000000 2531.000000 2048.000000
1937.000000 2706.000000 2403.000000 2057.000000 2057.000000 2680.000000 2095.000000
2949.000000 2911.000000 2859.000000 2684.000000 2679.000000 2740.000000 2672.000000
2894.000000 2279.000000 2667.000000 2829.000000 2176.000000 1638.000000 1638.000000
2155.000000 2568.000000 3498.000000 2611.000000 2815.000000 2640.000000 2640.000000
2909.000000 1941.000000 2854.000000 3089.000000 3089.000000 2692.000000 2261.000000
2739.000000 2905.000000 2555.000000 2243.000000 2158.000000 2671.000000 2436.000000
2500.000000 2154.000000 2154.000000 2343.000000 1975.000000 1651.000000 2155.000000
2087.000000 2565.000000 2351.000000 2783.000000 2842.000000 2842.000000 2475.000000
2381.000000 2350.000000 2162.000000 2162.000000 2491.000000 2261.000000 2209.000000
2435.000000 2286.000000 2030.000000 2768.000000 2312.000000 2564.000000 2653.000000
2427.000000 2427.000000 2730.000000 2730.000000 1932.000000 1932.000000 1979.000000
2564.000000 2679.000000

1648.900024 2668.000000 2994.000000 2119.000000 1587.000000 2544.000000 2077.000000
1948.000000 2690.000000 2514.000000 2034.000000 2034.000000 2716.000000 2098.000000
3011.000000 2887.000000 2892.000000 2712.000000 2779.000000 2806.000000 2772.000000

3017.000000 2343.000000 2750.000000 2875.000000 2193.000000 1681.000000 1681.000000
2222.000000 2612.000000 3541.000000 2577.000000 2774.000000 2675.000000 2675.000000
2864.000000 1917.000000 2885.000000 3198.000000 3198.000000 2761.000000 2285.000000
2783.000000 2914.000000 2572.000000 2246.000000 2156.000000 2732.000000 2552.000000
2611.000000 2174.000000 2174.000000 2377.000000 2055.000000 1738.000000 2163.000000
2000.000000 2591.000000 2377.000000 2763.000000 2956.000000 2956.000000 2543.000000
2436.000000 2409.000000 2173.000000 2173.000000 2560.000000 2256.000000 2122.000000
2383.000000 2354.000000 2058.000000 2773.000000 2427.000000 2650.000000 2611.000000
2435.000000 2435.000000 2667.000000 2667.000000 2019.000000 2019.000000 2041.000000
2654.000000 2779.000000

1659.000000 2842.000000 2880.000000 2002.000000 1578.000000 2526.000000 1973.000000
1853.000000 2552.000000 2397.000000 2084.000000 2084.000000 2582.000000 1964.000000
2987.000000 2860.000000 2779.000000 2800.000000 2662.000000 2791.000000 2724.000000
2844.000000 2337.000000 2710.000000 2736.000000 2110.000000 1723.000000 1723.000000
2152.000000 2794.000000 3486.000000 2459.000000 2656.000000 2669.000000 2669.000000
2870.000000 1959.000000 2879.000000 3179.000000 3179.000000 2656.000000 2241.000000
2661.000000 2788.000000 2553.000000 2202.000000 2189.000000 2649.000000 2366.000000
2455.000000 2134.000000 2134.000000 2281.000000 1964.000000 1681.000000 2166.000000
1994.000000 2509.000000 2256.000000 2680.000000 2881.000000 2881.000000 2413.000000
2387.000000 2330.000000 2227.000000 2227.000000 2468.000000 2156.000000 2188.000000
2270.000000 2293.000000 2057.000000 2720.000000 2296.000000 2515.000000 2596.000000
2407.000000 2407.000000 2570.000000 2570.000000 1834.000000 1834.000000 1979.000000
2451.000000 2494.000000

1669.099976 2854.000000 2841.000000 2002.000000 1588.000000 2492.000000 1938.000000
1868.000000 2593.000000 2370.000000 2043.000000 2043.000000 2602.000000 1955.000000
2937.000000 2868.000000 2798.000000 2728.000000 2775.000000 2781.000000 2703.000000
2834.000000 2340.000000 2680.000000 2702.000000 2126.000000 1667.000000 1667.000000
2221.000000 2731.000000 3445.000000 2429.000000 2665.000000 2643.000000 2643.000000
2843.000000 2024.000000 2905.000000 3232.000000 3232.000000 2691.000000 2163.000000
2656.000000 2847.000000 2577.000000 2198.000000 2189.000000 2670.000000 2304.000000
2486.000000 2080.000000 2080.000000 2252.000000 1977.000000 1680.000000 2104.000000
2008.000000 2444.000000 2322.000000 2628.000000 2889.000000 2889.000000 2396.000000
2382.000000 2355.000000 2211.000000 2211.000000 2460.000000 2146.000000 2140.000000
2276.000000 2299.000000 2063.000000 2669.000000 2307.000000 2525.000000 2538.000000
2411.000000 2411.000000 2547.000000 2547.000000 1823.000000 1823.000000 1997.000000
2473.000000 2491.000000

1679.199951 2720.000000 2716.000000 1954.000000 1575.000000 2401.000000 1964.000000
1835.000000 2544.000000 2289.000000 2017.000000 2017.000000 2633.000000 2039.000000
2917.000000 2753.000000 2673.000000 2557.000000 2707.000000 2695.000000 2647.000000
2749.000000 2271.000000 2570.000000 2753.000000 2142.000000 1713.000000 1713.000000
2159.000000 2658.000000 3511.000000 2371.000000 2585.000000 2527.000000 2527.000000
2835.000000 1962.000000 2732.000000 2991.000000 2991.000000 2599.000000 2171.000000
2577.000000 2727.000000 2563.000000 2220.000000 2091.000000 2578.000000 2297.000000
2385.000000 2091.000000 2091.000000 2195.000000 1986.000000 1674.000000 2120.000000
2044.000000 2383.000000 2307.000000 2601.000000 2788.000000 2788.000000 2248.000000
2408.000000 2362.000000 2144.000000 2144.000000 2386.000000 2154.000000 2135.000000
2188.000000 2274.000000 2109.000000 2709.000000 2265.000000 2519.000000 2528.000000
2474.000000 2474.000000 2577.000000 2577.000000 1824.000000 1824.000000 1895.000000
2394.000000 2462.000000

1689.300049 2749.000000 2785.000000 1912.000000 1594.000000 2396.000000 1946.000000
1810.000000 2524.000000 2360.000000 1946.000000 1946.000000 2651.000000 2018.000000
2949.000000 2805.000000 2729.000000 2574.000000 2685.000000 2692.000000 2611.000000
2775.000000 2264.000000 2537.000000 2724.000000 2123.000000 1721.000000 1721.000000
2168.000000 2661.000000 3358.000000 2373.000000 2659.000000 2505.000000 2505.000000
2818.000000 1930.000000 2628.000000 2964.000000 2964.000000 2655.000000 2165.000000
2597.000000 2762.000000 2505.000000 2241.000000 2105.000000 2621.000000 2362.000000
2369.000000 2047.000000 2047.000000 2213.000000 1909.000000 1673.000000 2132.000000
2092.000000 2328.000000 2333.000000 2542.000000 2764.000000 2764.000000 2235.000000
2380.000000 2268.000000 2105.000000 2105.000000 2429.000000 2043.000000 2100.000000
2190.000000 2207.000000 2034.000000 2649.000000 2215.000000 2492.000000 2492.000000
2350.000000 2350.000000 2578.000000 2578.000000 1815.000000 1815.000000 1938.000000
2401.000000 2512.000000

1699.400024 2683.000000 2636.000000 1840.000000 1414.000000 2358.000000 1946.000000
1862.000000 2626.000000 2344.000000 2011.000000 2011.000000 2649.000000 1969.000000
2814.000000 2695.000000 2663.000000 2677.000000 2631.000000 2648.000000 2557.000000
2777.000000 2245.000000 2723.000000 2695.000000 2124.000000 1583.000000 1583.000000
2216.000000 2644.000000 3444.000000 2412.000000 2669.000000 2501.000000 2501.000000
2880.000000 1942.000000 2726.000000 3035.000000 3035.000000 2516.000000 2086.000000
2559.000000 2808.000000 2505.000000 2122.000000 2034.000000 2551.000000 2205.000000
2347.000000 2062.000000 2062.000000 2202.000000 1860.000000 1491.000000 2049.000000
1965.000000 2428.000000 2208.000000 2494.000000 2694.000000 2694.000000 2224.000000
2322.000000 2290.000000 2084.000000 2084.000000 2321.000000 2181.000000 2036.000000
2247.000000 2213.000000 2003.000000 2603.000000 2212.000000 2474.000000 2395.000000
2435.000000 2435.000000 2483.000000 2483.000000 1782.000000 1782.000000 1875.000000
2427.000000 2369.000000

1709.500000 2665.000000 2660.000000 1789.000000 1434.000000 2392.000000 1959.000000
1832.000000 2550.000000 2330.000000 2051.000000 2051.000000 2574.000000 1949.000000
2860.000000 2626.000000 2627.000000 2647.000000 2572.000000 2636.000000 2517.000000
2717.000000 2241.000000 2699.000000 2690.000000 2041.000000 1546.000000 1546.000000
2162.000000 2556.000000 3439.000000 2334.000000 2639.000000 2465.000000 2465.000000
2844.000000 1982.000000 2722.000000 3053.000000 3053.000000 2500.000000 2078.000000
2550.000000 2777.000000 2469.000000 2148.000000 2032.000000 2630.000000 2241.000000
2329.000000 2062.000000 2062.000000 2254.000000 1845.000000 1515.000000 2066.000000
1925.000000 2441.000000 2208.000000 2515.000000 2683.000000 2683.000000 2238.000000
2300.000000 2313.000000 2041.000000 2041.000000 2293.000000 2152.000000 2010.000000
2165.000000 2210.000000 1963.000000 2594.000000 2232.000000 2485.000000 2418.000000
2453.000000 2453.000000 2427.000000 2427.000000 1767.000000 1767.000000 1893.000000
2451.000000 2392.000000

1719.599976 2628.000000 2587.000000 1816.000000 1423.000000 2295.000000 1916.000000
1792.000000 2452.000000 2271.000000 1889.000000 1889.000000 2476.000000 1899.000000
2792.000000 2716.000000 2631.000000 2564.000000 2514.000000 2573.000000 2526.000000
2732.000000 2140.000000 2577.000000 2619.000000 2049.000000 1509.000000 1509.000000
2051.000000 2538.000000 3384.000000 2323.000000 2501.000000 2399.000000 2399.000000
2742.000000 1902.000000 2573.000000 2927.000000 2927.000000 2426.000000 2084.000000
2469.000000 2599.000000 2439.000000 2147.000000 2015.000000 2478.000000 2170.000000
2297.000000 1965.000000 1965.000000 2149.000000 1882.000000 1493.000000 1992.000000
1967.000000 2229.000000 2116.000000 2425.000000 2597.000000 2597.000000 2244.000000
2125.000000 2177.000000 1968.000000 1968.000000 2332.000000 2010.000000 2021.000000
2231.000000 2199.000000 1963.000000 2595.000000 2119.000000 2375.000000 2350.000000

2356.000000 2356.000000 2395.000000 2395.000000 1812.000000 1812.000000 1812.000000
2447.000000 2335.000000

1729.699951 2526.000000 2509.000000 1786.000000 1384.000000 2253.000000 1876.000000
1703.000000 2407.000000 2168.000000 1870.000000 1870.000000 2406.000000 1847.000000
2666.000000 2641.000000 2492.000000 2476.000000 2454.000000 2523.000000 2491.000000
2631.000000 1993.000000 2522.000000 2540.000000 1994.000000 1421.000000 1421.000000
2012.000000 2468.000000 3294.000000 2252.000000 2439.000000 2417.000000 2417.000000
2643.000000 1876.000000 2557.000000 2892.000000 2892.000000 2436.000000 1981.000000
2416.000000 2557.000000 2421.000000 2105.000000 2004.000000 2433.000000 2164.000000
2214.000000 1978.000000 1978.000000 2072.000000 1905.000000 1502.000000 1935.000000
1892.000000 2173.000000 2135.000000 2351.000000 2580.000000 2580.000000 2149.000000
2094.000000 2115.000000 1943.000000 1943.000000 2247.000000 1898.000000 1988.000000
2149.000000 2106.000000 1913.000000 2564.000000 2140.000000 2387.000000 2297.000000
2249.000000 2249.000000 2345.000000 2345.000000 1840.000000 1840.000000 1797.000000
2414.000000 2309.000000

1739.699951 2470.000000 2564.000000 1758.000000 1434.000000 2326.000000 1765.000000
1676.000000 2374.000000 2183.000000 1880.000000 1880.000000 2484.000000 1818.000000
2676.000000 2525.000000 2495.000000 2506.000000 2341.000000 2575.000000 2433.000000
2578.000000 2102.000000 2397.000000 2493.000000 1919.000000 1488.000000 1488.000000
2015.000000 2488.000000 3052.000000 2164.000000 2383.000000 2339.000000 2339.000000
2632.000000 1740.000000 2461.000000 2783.000000 2783.000000 2292.000000 1875.000000
2301.000000 2469.000000 2260.000000 2001.000000 1920.000000 2441.000000 2086.000000
2191.000000 1932.000000 1932.000000 2099.000000 1788.000000 1463.000000 1959.000000
1798.000000 2220.000000 2020.000000 2305.000000 2489.000000 2489.000000 2078.000000
2136.000000 2060.000000 1862.000000 1862.000000 2155.000000 1895.000000 1962.000000
1968.000000 2010.000000 1883.000000 2395.000000 2038.000000 2253.000000 2321.000000
2193.000000 2193.000000 2375.000000 2375.000000 1691.000000 1691.000000 1757.000000
2204.000000 2219.000000

1749.790039 2358.000000 2485.000000 1709.000000 1392.000000 2198.000000 1695.000000
1606.000000 2280.000000 2106.000000 1804.000000 1804.000000 2411.000000 1820.000000
2580.000000 2452.000000 2484.000000 2367.000000 2401.000000 2497.000000 2272.000000
2517.000000 2014.000000 2263.000000 2337.000000 1860.000000 1374.000000 1374.000000
1999.000000 2342.000000 2948.000000 2069.000000 2254.000000 2303.000000 2303.000000
2551.000000 1686.000000 2365.000000 2735.000000 2735.000000 2186.000000 1797.000000
2227.000000 2378.000000 2181.000000 1951.000000 1804.000000 2285.000000 1998.000000
2096.000000 1844.000000 1844.000000 2016.000000 1690.000000 1388.000000 1915.000000
1789.000000 2088.000000 1927.000000 2272.000000 2411.000000 2411.000000 1973.000000
2037.000000 1954.000000 1817.000000 1817.000000 2044.000000 1856.000000 1856.000000
1884.000000 1921.000000 1756.000000 2326.000000 1993.000000 2262.000000 2193.000000
2097.000000 2097.000000 2247.000000 2247.000000 1681.000000 1681.000000 1653.000000
2247.000000 2147.000000

1759.890015 2285.000000 2449.000000 1601.000000 1258.000000 2082.000000 1682.000000
1528.000000 2193.000000 1972.000000 1710.000000 1710.000000 2203.000000 1656.000000
2579.000000 2382.000000 2356.000000 2344.000000 2341.000000 2329.000000 2268.000000
2380.000000 1885.000000 2210.000000 2377.000000 1810.000000 1310.000000 1310.000000
1852.000000 2185.000000 2970.000000 2073.000000 2258.000000 2072.000000 2072.000000
2445.000000 1657.000000 2346.000000 2600.000000 2600.000000 2111.000000 1792.000000
2167.000000 2301.000000 2075.000000 1883.000000 1676.000000 2282.000000 1948.000000
2044.000000 1747.000000 1747.000000 1976.000000 1605.000000 1291.000000 1870.000000
1658.000000 1994.000000 1900.000000 2148.000000 2296.000000 2296.000000 1922.000000

1855.000000 1893.000000 1649.000000 1649.000000 2014.000000 1791.000000 1696.000000
1795.000000 1901.000000 1650.000000 2310.000000 1842.000000 2121.000000 2065.000000
2033.000000 2033.000000 2192.000000 2192.000000 1575.000000 1575.000000 1574.000000
2175.000000 2077.000000

1769.989990 2360.000000 2339.000000 1568.000000 1253.000000 2041.000000 1664.000000
1531.000000 2211.000000 2003.000000 1647.000000 1647.000000 2228.000000 1596.000000
2542.000000 2405.000000 2292.000000 2278.000000 2314.000000 2286.000000 2296.000000
2402.000000 1919.000000 2165.000000 2407.000000 1760.000000 1321.000000 1321.000000
1877.000000 2203.000000 2894.000000 2031.000000 2139.000000 2036.000000 2036.000000
2381.000000 1578.000000 2305.000000 2516.000000 2516.000000 2131.000000 1763.000000
2145.000000 2240.000000 2066.000000 1868.000000 1726.000000 2258.000000 1862.000000
2003.000000 1736.000000 1736.000000 1920.000000 1591.000000 1233.000000 1775.000000
1657.000000 1930.000000 1867.000000 2121.000000 2308.000000 2308.000000 1902.000000
1870.000000 1837.000000 1618.000000 1618.000000 1951.000000 1737.000000 1637.000000
1733.000000 1845.000000 1639.000000 2272.000000 1786.000000 2034.000000 2031.000000
2050.000000 2050.000000 2063.000000 2063.000000 1478.000000 1478.000000 1491.000000
2083.000000 2008.000000

1780.089966 2246.000000 2211.000000 1452.000000 1093.000000 2101.000000 1501.000000
1403.000000 1917.000000 1813.000000 1594.000000 1594.000000 2233.000000 1520.000000
2326.000000 2302.000000 2197.000000 2179.000000 2066.000000 2231.000000 2269.000000
2269.000000 1794.000000 1954.000000 2243.000000 1736.000000 1160.000000 1160.000000
1678.000000 2099.000000 2489.000000 1946.000000 2070.000000 1806.000000 1806.000000
2296.000000 1542.000000 1954.000000 2303.000000 2303.000000 1944.000000 1641.000000
1902.000000 2081.000000 1954.000000 1775.000000 1600.000000 2204.000000 1847.000000
1826.000000 1588.000000 1588.000000 1900.000000 1556.000000 1248.000000 1729.000000
1697.000000 1871.000000 1731.000000 2016.000000 2232.000000 2232.000000 1848.000000
1840.000000 1634.000000 1592.000000 1592.000000 1835.000000 1550.000000 1528.000000
1638.000000 1658.000000 1547.000000 1996.000000 1694.000000 1899.000000 1905.000000
1814.000000 1814.000000 2013.000000 2013.000000 1508.000000 1508.000000 1429.000000
1987.000000 2039.000000

1790.189941 2076.000000 2101.000000 1230.000000 928.000000 2032.000000 1565.000000
1256.000000 1663.000000 1913.000000 1596.000000 1596.000000 2068.000000 1515.000000
2203.000000 2282.000000 2093.000000 2171.000000 1894.000000 2284.000000 2197.000000
2106.000000 1705.000000 1909.000000 2173.000000 1724.000000 1036.000000 1036.000000
1653.000000 1990.000000 2299.000000 1870.000000 2069.000000 1673.000000 1673.000000
2267.000000 1530.000000 1797.000000 2194.000000 2194.000000 1758.000000 1511.000000
1735.000000 1952.000000 1880.000000 1593.000000 1514.000000 2016.000000 1793.000000
1737.000000 1460.000000 1460.000000 1845.000000 1426.000000 1187.000000 1713.000000
1758.000000 1765.000000 1575.000000 1819.000000 2143.000000 2143.000000 1869.000000
1758.000000 1502.000000 1561.000000 1561.000000 1836.000000 1480.000000 1471.000000
1531.000000 1634.000000 1415.000000 1880.000000 1526.000000 1731.000000 1764.000000
1659.000000 1659.000000 1964.000000 1964.000000 1359.000000 1359.000000 1261.000000
1783.000000 1905.000000

1800.290039 1690.000000 2153.000000 1094.000000 909.000000 1565.000000 1640.000000
1548.000000 2180.000000 2161.000000 1230.000000 1230.000000 2499.000000 1346.000000
2244.000000 1920.000000 2376.000000 1548.000000 1937.000000 2558.000000 2586.000000
2492.000000 1705.000000 1675.000000 1899.000000 1109.000000 960.000000 960.000000
1858.000000 2135.000000 2311.000000 1960.000000 1655.000000 1763.000000 1763.000000
1879.000000 1477.000000 2177.000000 1923.000000 1923.000000 1896.000000 1471.000000
2062.000000 1421.000000 1453.000000 1747.000000 1757.000000 1933.000000 1360.000000

1526.000000 1391.000000 1391.000000 1594.000000 1027.000000 1416.000000 1903.000000
1333.000000 1720.000000 1726.000000 1848.000000 2142.000000 2142.000000 1407.000000
1995.000000 1704.000000 1598.000000 1598.000000 1278.000000 1560.000000 913.000000
1226.000000 1718.000000 627.000000 1833.000000 1290.000000 1236.000000 1384.000000
1550.000000 1550.000000 1979.000000 1979.000000 1487.000000 1487.000000 882.000000
1487.000000 1245.000000

1810.380005 882.000000 2080.000000 709.000000 357.000000 725.000000 1573.000000 1072.000000
2533.000000 2408.000000 725.000000 725.000000 2993.000000 556.000000 2388.000000 1044.000000
3327.000000 822.000000 2644.000000 3653.000000 3823.000000 3125.000000 1445.000000
229.000000 1135.000000 397.000000 204.000000 204.000000 1878.000000 2858.000000 1851.000000
1960.000000 1224.000000 1683.000000 1683.000000 1894.000000 1194.000000 3149.000000
1591.000000 1591.000000 1322.000000 868.000000 2190.000000 535.000000 430.000000 1398.000000
2194.000000 2045.000000 645.000000 837.000000 903.000000 903.000000 1648.000000 539.000000
1470.000000 2046.000000 1071.000000 1552.000000 1645.000000 1893.000000 1826.000000
1826.000000 663.000000 1833.000000 1500.000000 1817.000000 1817.000000 764.000000
1618.000000 645.000000 769.000000 1317.000000 -159.000000 1557.000000 714.000000 113.000000
1134.000000 1063.000000 1063.000000 1727.000000 1727.000000 1794.000000 1794.000000
381.000000 786.000000 1014.000000

1961.660034 297.000000 487.000000 859.000000 424.000000 -18.000000 310.000000 -18.000000
113.000000 -18.000000 -18.000000 -18.000000 968.000000 -18.000000 869.000000 372.000000
508.000000 1100.000000 485.000000 1026.000000 1316.000000 1316.000000 -18.000000 241.000000
1617.000000 177.000000 -19.000000 -19.000000 -18.000000 230.000000 401.000000 -19.000000 -
80.000000 -19.000000 -19.000000 -19.000000 -81.000000 101.000000 713.000000 713.000000
224.000000 -19.000000 -19.000000 336.000000 1365.000000 461.000000 40.000000 736.000000 -
82.000000 587.000000 40.000000 40.000000 -83.000000 304.000000 440.000000 -18.000000 -
18.000000 177.000000 -18.000000 178.000000 305.000000 305.000000 -19.000000 -19.000000
399.000000 -20.000000 -20.000000 -19.000000 -19.000000 1100.000000 -20.000000 -19.000000 -
81.000000 517.000000 -19.000000 102.000000 286.000000 159.000000 159.000000 -80.000000 -
80.000000 41.000000 41.000000 407.000000 1019.000000 232.000000

1971.760010 998.000000 962.000000 782.000000 381.000000 262.000000 425.000000 173.000000
751.000000 785.000000 352.000000 352.000000 1126.000000 513.000000 1174.000000 1032.000000
1162.000000 1019.000000 925.000000 1247.000000 1171.000000 1334.000000 620.000000 888.000000
1356.000000 675.000000 169.000000 169.000000 243.000000 798.000000 1331.000000 165.000000
612.000000 251.000000 251.000000 475.000000 342.000000 1009.000000 1047.000000 1047.000000
632.000000 305.000000 497.000000 810.000000 1262.000000 799.000000 405.000000 1082.000000
450.000000 734.000000 424.000000 424.000000 492.000000 599.000000 406.000000 388.000000
317.000000 532.000000 478.000000 838.000000 743.000000 743.000000 434.000000 380.000000
660.000000 130.000000 130.000000 342.000000 499.000000 773.000000 145.000000 411.000000
167.000000 949.000000 545.000000 701.000000 755.000000 694.000000 694.000000 460.000000
460.000000 408.000000 408.000000 563.000000 1065.000000 608.000000

1981.859985 1060.000000 1146.000000 926.000000 587.000000 945.000000 608.000000 576.000000
1618.000000 838.000000 672.000000 672.000000 1515.000000 824.000000 1415.000000 1292.000000
1330.000000 1428.000000 1283.000000 1434.000000 1360.000000 1261.000000 965.000000
1345.000000 1501.000000 945.000000 629.000000 629.000000 863.000000 1224.000000 1697.000000
1008.000000 870.000000 627.000000 627.000000 1145.000000 956.000000 1292.000000 1137.000000
1137.000000 683.000000 388.000000 622.000000 831.000000 1046.000000 1004.000000 764.000000
1207.000000 1046.000000 1039.000000 702.000000 702.000000 863.000000 787.000000 683.000000
912.000000 860.000000 793.000000 761.000000 1033.000000 1038.000000 1038.000000 728.000000
1025.000000 792.000000 708.000000 708.000000 795.000000 667.000000 568.000000 703.000000

826.000000 709.000000 1158.000000 629.000000 830.000000 959.000000 1065.000000 1065.000000 1138.000000 1138.000000 672.000000 672.000000 461.000000 905.000000 1121.000000

1991.959961 949.000000 1139.000000 858.000000 744.000000 931.000000 577.000000 577.000000 1678.000000 829.000000 635.000000 635.000000 1600.000000 752.000000 1462.000000 1344.000000 1215.000000 1452.000000 1298.000000 1492.000000 1519.000000 1221.000000 915.000000 1447.000000 1656.000000 1049.000000 611.000000 611.000000 955.000000 1235.000000 1737.000000 1151.000000 775.000000 631.000000 631.000000 1107.000000 1147.000000 1324.000000 1110.000000 1110.000000 619.000000 417.000000 418.000000 727.000000 975.000000 1061.000000 746.000000 1283.000000 1035.000000 1006.000000 805.000000 805.000000 779.000000 808.000000 783.000000 961.000000 858.000000 887.000000 680.000000 1021.000000 1164.000000 1164.000000 701.000000 1064.000000 786.000000 772.000000 772.000000 667.000000 637.000000 540.000000 725.000000 956.000000 782.000000 1216.000000 459.000000 705.000000 822.000000 1160.000000 1160.000000 1182.000000 1182.000000 662.000000 662.000000 329.000000 792.000000 1108.000000

2002.060059 2129.000000 611.000000 -21.000000 -21.000000 -20.000000 -20.000000 -20.000000 -20.000000 1003.000000 1129.000000 1129.000000 -148.000000 106.000000 738.000000 106.000000 1514.000000 2538.000000 -21.000000 489.000000 1393.000000 2549.000000 361.000000 106.000000 2789.000000 234.000000 231.000000 231.000000 -20.000000 -147.000000 3218.000000 -146.000000 227.000000 -21.000000 -21.000000 352.000000 -147.000000 103.000000 353.000000 353.000000 -21.000000 -21.000000 -21.000000 101.000000 351.000000 -146.000000 477.000000 -147.000000 -21.000000 -21.000000 -21.000000 -21.000000 -20.000000 -20.000000 -20.000000 -20.000000 -20.000000 -20.000000 -20.000000 -20.000000 -20.000000 -20.000000 -21.000000 -21.000000 351.000000 475.000000 475.000000 -147.000000 859.000000 101.000000 -22.000000 104.000000 -21.000000 -22.000000 -21.000000 -21.000000 103.000000 226.000000 226.000000 103.000000 103.000000 -21.000000 -21.000000 -21.000000 -21.000000 -21.000000

2012.150024 1630.000000 777.000000 9.000000 95.000000 10.000000 -75.000000 10.000000 -75.000000 1556.000000 1039.000000 1039.000000 -75.000000 95.000000 351.000000 1125.000000 1642.000000 2844.000000 9.000000 696.000000 1043.000000 2421.000000 1039.000000 181.000000 1983.000000 353.000000 947.000000 947.000000 10.000000 -75.000000 3303.000000 -74.000000 770.000000 9.000000 9.000000 601.000000 179.000000 1109.000000 602.000000 602.000000 94.000000 9.000000 9.000000 430.000000 854.000000 600.000000 601.000000 -75.000000 180.000000 9.000000 9.000000 9.000000 10.000000 10.000000 10.000000 10.000000 96.000000 96.000000 10.000000 267.000000 10.000000 10.000000 9.000000 350.000000 853.000000 346.000000 346.000000 -75.000000 1199.000000 93.000000 9.000000 264.000000 9.000000 262.000000 9.000000 9.000000 348.000000 853.000000 853.000000 433.000000 433.000000 9.000000 9.000000 9.000000 179.000000 265.000000

2022.250000 1121.000000 1457.000000 768.000000 578.000000 1239.000000 1031.000000 485.000000 1644.000000 646.000000 1127.000000 1127.000000 1674.000000 998.000000 1569.000000 1512.000000 1273.000000 1385.000000 1200.000000 1271.000000 1275.000000 1034.000000 693.000000 1255.000000 1432.000000 806.000000 434.000000 434.000000 644.000000 1246.000000 1985.000000 844.000000 986.000000 732.000000 732.000000 1241.000000 704.000000 1273.000000 1051.000000 1051.000000 1051.000000 671.000000 1180.000000 1047.000000 906.000000 1049.000000 685.000000 1471.000000 897.000000 955.000000 1003.000000 1003.000000 1205.000000 500.000000 452.000000 918.000000 1031.000000 1272.000000 951.000000 1176.000000 1286.000000 1286.000000 818.000000 881.000000 763.000000 620.000000 620.000000 975.000000 688.000000 840.000000 777.000000 672.000000 719.000000 937.000000 733.000000 1019.000000 972.000000 842.000000 842.000000 1036.000000 1036.000000 734.000000 734.000000 876.000000 1067.000000 992.000000

2032.349976 1375.000000 1509.000000 883.000000 624.000000 1234.000000 974.000000 569.000000 1564.000000 897.000000 1119.000000 1119.000000 1650.000000 1128.000000 1673.000000 1572.000000 1370.000000 1438.000000 1451.000000 1408.000000 1392.000000 1189.000000

935.000000 1292.000000 1399.000000 984.000000 557.000000 557.000000 876.000000 1277.000000
1980.000000 976.000000 1148.000000 765.000000 765.000000 1340.000000 940.000000 1455.000000
1226.000000 1226.000000 1149.000000 709.000000 1198.000000 1222.000000 1119.000000
1186.000000 842.000000 1518.000000 1018.000000 1120.000000 1014.000000 1014.000000
1223.000000 664.000000 540.000000 1042.000000 1061.000000 1235.000000 1022.000000
1293.000000 1330.000000 1330.000000 904.000000 913.000000 965.000000 678.000000 678.000000
1065.000000 671.000000 849.000000 830.000000 815.000000 748.000000 1089.000000 938.000000
1082.000000 1140.000000 1070.000000 1070.000000 1216.000000 1216.000000 881.000000
881.000000 804.000000 1216.000000 999.000000

2042.449951 1725.000000 1118.000000 844.000000 547.000000 1074.000000 704.000000 453.000000
1552.000000 1516.000000 787.000000 787.000000 1659.000000 1014.000000 1464.000000
1741.000000 1647.000000 1277.000000 1796.000000 1634.000000 1302.000000 1804.000000
1085.000000 1228.000000 1396.000000 799.000000 357.000000 357.000000 1263.000000 1355.000000
2098.000000 1115.000000 1233.000000 901.000000 901.000000 1684.000000 1129.000000
1553.000000 1483.000000 1483.000000 1008.000000 724.000000 962.000000 1243.000000
1339.000000 1173.000000 1162.000000 1415.000000 1070.000000 1186.000000 877.000000
877.000000 1025.000000 775.000000 632.000000 644.000000 943.000000 752.000000 835.000000
1265.000000 1192.000000 1192.000000 1071.000000 1011.000000 1102.000000 805.000000
805.000000 962.000000 701.000000 1053.000000 804.000000 1128.000000 796.000000 1315.000000
949.000000 1068.000000 1234.000000 1351.000000 1351.000000 1329.000000 1329.000000 783.000000
783.000000 534.000000 1293.000000 1201.000000

2052.449951 1957.000000 783.000000 848.000000 501.000000 829.000000 480.000000 306.000000
1810.000000 1853.000000 349.000000 349.000000 1875.000000 916.000000 1283.000000 1961.000000
1526.000000 1352.000000 2326.000000 1809.000000 1244.000000 2117.000000 1068.000000
1329.000000 1351.000000 698.000000 392.000000 392.000000 1459.000000 1434.000000 2320.000000
1215.000000 1150.000000 998.000000 998.000000 2039.000000 1087.000000 1627.000000
1584.000000 1584.000000 1042.000000 695.000000 847.000000 1083.000000 1366.000000
1106.000000 1193.000000 1457.000000 935.000000 1237.000000 759.000000 759.000000 871.000000
523.000000 327.000000 284.000000 981.000000 218.000000 720.000000 1439.000000 1242.000000
1242.000000 1001.000000 957.000000 1170.000000 867.000000 867.000000 869.000000 696.000000
1083.000000 801.000000 1108.000000 739.000000 1344.000000 977.000000 912.000000 1237.000000
1279.000000 1279.000000 1215.000000 1215.000000 738.000000 738.000000 326.000000 1324.000000
1218.000000

2062.550049 1751.000000 1658.000000 1025.000000 672.000000 1252.000000 880.000000
842.000000 1701.000000 1309.000000 1271.000000 1271.000000 1943.000000 1345.000000
1658.000000 1923.000000 1663.000000 1813.000000 1862.000000 1718.000000 1890.000000
1553.000000 1382.000000 1718.000000 1718.000000 1327.000000 1192.000000 1192.000000
1418.000000 1711.000000 2595.000000 1133.000000 1336.000000 1262.000000 1262.000000
1559.000000 1284.000000 1652.000000 1856.000000 1856.000000 1337.000000 948.000000
1301.000000 1131.000000 1410.000000 1447.000000 1503.000000 1917.000000 1378.000000
1300.000000 1263.000000 1263.000000 1213.000000 580.000000 823.000000 973.000000 1253.000000
1215.000000 1215.000000 1402.000000 1680.000000 1680.000000 1323.000000 1378.000000
1335.000000 1057.000000 1057.000000 1302.000000 1154.000000 890.000000 1001.000000
1413.000000 819.000000 1594.000000 1003.000000 1263.000000 1356.000000 1465.000000
1465.000000 1541.000000 1541.000000 1226.000000 1226.000000 707.000000 1208.000000
1397.000000

2072.649902 1805.000000 1628.000000 1084.000000 731.000000 1305.000000 923.000000
787.000000 1755.000000 1346.000000 1141.000000 1141.000000 1796.000000 1263.000000
1723.000000 1917.000000 1755.000000 1823.000000 1764.000000 1822.000000 1784.000000
1647.000000 1372.000000 1672.000000 1809.000000 1291.000000 1030.000000 1030.000000

1453.000000 1667.000000 2463.000000 1149.000000 1366.000000 1176.000000 1176.000000
1448.000000 1409.000000 1746.000000 1774.000000 1774.000000 1258.000000 824.000000
1286.000000 1229.000000 1487.000000 1542.000000 1393.000000 1804.000000 1424.000000
1407.000000 1271.000000 1271.000000 1276.000000 568.000000 732.000000 1032.000000
1196.000000 1223.000000 1087.000000 1387.000000 1780.000000 1780.000000 1275.000000
1383.000000 1229.000000 959.000000 959.000000 1355.000000 1083.000000 1012.000000 985.000000
1409.000000 920.000000 1527.000000 1000.000000 1258.000000 1353.000000 1406.000000
1406.000000 1421.000000 1421.000000 1231.000000 1231.000000 824.000000 1394.000000
1478.000000

2082.750000 2061.000000 1841.000000 811.000000 534.000000 1415.000000 1033.000000
546.000000 1578.000000 1416.000000 1265.000000 1265.000000 1798.000000 1241.000000
1992.000000 1890.000000 1856.000000 1543.000000 1783.000000 1786.000000 1602.000000
1649.000000 1125.000000 1415.000000 1647.000000 1044.000000 487.000000 487.000000 986.000000
1516.000000 2149.000000 1179.000000 1433.000000 1179.000000 1179.000000 1664.000000
1100.000000 1757.000000 1873.000000 1873.000000 1272.000000 960.000000 1261.000000
1432.000000 1583.000000 1421.000000 1029.000000 1760.000000 1366.000000 1249.000000
1202.000000 1202.000000 1345.000000 812.000000 581.000000 1172.000000 1126.000000
1195.000000 1056.000000 1311.000000 1461.000000 1461.000000 1216.000000 1366.000000
1005.000000 890.000000 890.000000 1227.000000 961.000000 1212.000000 993.000000 1123.000000
880.000000 1571.000000 1214.000000 1387.000000 1214.000000 1409.000000 1409.000000
1688.000000 1688.000000 1203.000000 1203.000000 902.000000 1595.000000 1459.000000

2092.840088 2041.000000 1955.000000 773.000000 483.000000 1485.000000 1130.000000
570.000000 1636.000000 1421.000000 1162.000000 1162.000000 1722.000000 1355.000000
1912.000000 1969.000000 1733.000000 1636.000000 1729.000000 1775.000000 1583.000000
1616.000000 1194.000000 1355.000000 1700.000000 1097.000000 450.000000 450.000000 924.000000
1588.000000 2292.000000 1136.000000 1436.000000 1189.000000 1189.000000 1672.000000
1116.000000 1757.000000 1951.000000 1951.000000 1329.000000 1040.000000 1308.000000
1520.000000 1521.000000 1457.000000 1167.000000 1739.000000 1353.000000 1232.000000
1232.000000 1232.000000 1430.000000 871.000000 678.000000 1227.000000 1184.000000
1248.000000 1076.000000 1345.000000 1516.000000 1516.000000 1246.000000 1353.000000
1135.000000 899.000000 899.000000 1234.000000 987.000000 1155.000000 1016.000000 1126.000000
869.000000 1542.000000 1200.000000 1479.000000 1383.000000 1488.000000 1488.000000
1640.000000 1640.000000 1265.000000 1265.000000 1029.000000 1640.000000 1525.000000

2102.939941 1987.000000 1875.000000 1232.000000 1039.000000 1541.000000 1154.000000
857.000000 1829.000000 1409.000000 1123.000000 1123.000000 1920.000000 1388.000000
1804.000000 1950.000000 1685.000000 1542.000000 1935.000000 1654.000000 1533.000000
1819.000000 1337.000000 1684.000000 1684.000000 1174.000000 590.000000 590.000000
1152.000000 1781.000000 2641.000000 1514.000000 1412.000000 1249.000000 1249.000000
1687.000000 1374.000000 1850.000000 1769.000000 1769.000000 1230.000000 904.000000
1332.000000 1481.000000 1859.000000 1564.000000 1391.000000 1772.000000 1629.000000
1534.000000 1270.000000 1270.000000 1489.000000 1234.000000 857.000000 1051.000000
1348.000000 1307.000000 1225.000000 1480.000000 1581.000000 1581.000000 1233.000000
1324.000000 1279.000000 954.000000 954.000000 1445.000000 997.000000 1065.000000 1115.000000
1282.000000 1027.000000 1695.000000 1097.000000 1453.000000 1403.000000 1594.000000
1594.000000 1535.000000 1535.000000 1199.000000 1199.000000 1046.000000 1667.000000
1833.000000

2113.040039 1969.000000 1868.000000 1170.000000 1020.000000 1497.000000 1143.000000
920.000000 1822.000000 1376.000000 1224.000000 1224.000000 1963.000000 1315.000000
1808.000000 1942.000000 1781.000000 1558.000000 2040.000000 1608.000000 1590.000000
1813.000000 1335.000000 1638.000000 1608.000000 1133.000000 625.000000 625.000000

1061.000000 1837.000000 2589.000000 1481.000000 1471.000000 1239.000000 1239.000000
1733.000000 1422.000000 1925.000000 1734.000000 1734.000000 1219.000000 907.000000
1371.000000 1540.000000 1843.000000 1571.000000 1329.000000 1686.000000 1595.000000
1370.000000 1259.000000 1259.000000 1415.000000 1263.000000 880.000000 1072.000000
1346.000000 1406.000000 1173.000000 1538.000000 1527.000000 1527.000000 1161.000000
1312.000000 1238.000000 946.000000 946.000000 1463.000000 998.000000 1106.000000 1056.000000
1251.000000 1029.000000 1631.000000 1118.000000 1481.000000 1371.000000 1732.000000
1732.000000 1492.000000 1492.000000 1179.000000 1179.000000 1028.000000 1713.000000
1817.000000

2123.139893 1777.000000 1838.000000 1238.000000 863.000000 1618.000000 1109.000000
763.000000 1914.000000 1435.000000 1038.000000 1038.000000 2056.000000 1170.000000
1980.000000 1913.000000 1730.000000 1751.000000 1716.000000 1770.000000 1762.000000
1956.000000 1180.000000 1790.000000 1821.000000 977.000000 619.000000 619.000000 1078.000000
1847.000000 2470.000000 1388.000000 1539.000000 1256.000000 1256.000000 1904.000000
1339.000000 2036.000000 1702.000000 1702.000000 1297.000000 953.000000 1156.000000
1365.000000 1519.000000 1640.000000 1296.000000 1949.000000 1573.000000 1570.000000
1307.000000 1307.000000 1444.000000 1271.000000 885.000000 1150.000000 1028.000000
1221.000000 1181.000000 1476.000000 1709.000000 1709.000000 1137.000000 1340.000000
1113.000000 1002.000000 1002.000000 1380.000000 1227.000000 1335.000000 1041.000000
1166.000000 1207.000000 1720.000000 1175.000000 1388.000000 1571.000000 1609.000000
1609.000000 1794.000000 1794.000000 1287.000000 1287.000000 861.000000 1571.000000
1736.000000

2133.239990 1823.000000 1823.000000 1245.000000 906.000000 1665.000000 1017.000000
778.000000 2034.000000 1565.000000 977.000000 977.000000 2144.000000 1176.000000 2022.000000
1874.000000 1755.000000 1665.000000 1743.000000 1804.000000 1706.000000 2035.000000
1186.000000 1744.000000 1814.000000 1017.000000 737.000000 737.000000 1066.000000
1763.000000 2478.000000 1403.000000 1522.000000 1194.000000 1194.000000 1901.000000
1294.000000 2110.000000 1811.000000 1811.000000 1284.000000 975.000000 1214.000000
1432.000000 1612.000000 1652.000000 1313.000000 1962.000000 1564.000000 1582.000000
1274.000000 1274.000000 1315.000000 1216.000000 967.000000 1097.000000 987.000000
1186.000000 1236.000000 1406.000000 1595.000000 1595.000000 1215.000000 1374.000000
1174.000000 1005.000000 1005.000000 1374.000000 1245.000000 1362.000000 1153.000000
1234.000000 1284.000000 1731.000000 1184.000000 1453.000000 1563.000000 1592.000000
1592.000000 1801.000000 1801.000000 1194.000000 1194.000000 876.000000 1662.000000
1703.000000

2143.340088 1930.000000 1950.000000 1133.000000 867.000000 1538.000000 1321.000000
897.000000 2001.000000 1695.000000 1341.000000 1341.000000 2011.000000 1291.000000
2049.000000 1932.000000 1833.000000 1952.000000 1733.000000 1764.000000 1765.000000
1863.000000 1380.000000 1715.000000 1932.000000 1311.000000 818.000000 818.000000
1183.000000 1743.000000 2342.000000 1338.000000 1624.000000 1240.000000 1240.000000
1653.000000 1329.000000 1889.000000 2008.000000 2008.000000 1427.000000 1093.000000
1477.000000 1554.000000 1594.000000 1683.000000 1240.000000 1743.000000 1546.000000
1486.000000 1260.000000 1260.000000 1547.000000 976.000000 887.000000 1193.000000
1252.000000 1449.000000 1242.000000 1548.000000 1754.000000 1754.000000 1231.000000
1280.000000 1210.000000 1014.000000 1014.000000 1497.000000 1132.000000 1141.000000
1092.000000 1221.000000 1113.000000 1741.000000 1201.000000 1565.000000 1339.000000
1594.000000 1594.000000 1624.000000 1624.000000 1289.000000 1289.000000 1093.000000
1644.000000 1645.000000

2153.340088 2040.000000 2060.000000 1088.000000 838.000000 1563.000000 1396.000000
987.000000 2057.000000 1616.000000 1311.000000 1311.000000 2014.000000 1364.000000

2019.000000 1971.000000 1899.000000 2035.000000 1830.000000 1772.000000 1743.000000
1827.000000 1405.000000 1740.000000 1908.000000 1207.000000 869.000000 869.000000
1310.000000 1766.000000 2334.000000 1325.000000 1616.000000 1210.000000 1210.000000
1617.000000 1338.000000 1887.000000 2065.000000 2065.000000 1461.000000 1107.000000
1493.000000 1572.000000 1512.000000 1709.000000 1314.000000 1819.000000 1611.000000
1575.000000 1273.000000 1273.000000 1603.000000 1028.000000 872.000000 1228.000000
1354.000000 1521.000000 1239.000000 1678.000000 1813.000000 1813.000000 1246.000000
1350.000000 1230.000000 1064.000000 1064.000000 1463.000000 1171.000000 1166.000000
1135.000000 1233.000000 1192.000000 1708.000000 1273.000000 1596.000000 1357.000000
1615.000000 1615.000000 1659.000000 1659.000000 1326.000000 1326.000000 1190.000000
1597.000000 1757.000000

2163.429932 1967.000000 1631.000000 1119.000000 911.000000 1320.000000 1297.000000
808.000000 1752.000000 1646.000000 1145.000000 1145.000000 1763.000000 1308.000000
1828.000000 1867.000000 1868.000000 1751.000000 1886.000000 1855.000000 1683.000000
2009.000000 1413.000000 1622.000000 1797.000000 1227.000000 759.000000 759.000000
1365.000000 1676.000000 2331.000000 1476.000000 1603.000000 1255.000000 1255.000000
1858.000000 1339.000000 1950.000000 2032.000000 2032.000000 1349.000000 1071.000000
1419.000000 1762.000000 1648.000000 1440.000000 1220.000000 1758.000000 1526.000000
1591.000000 1163.000000 1163.000000 1237.000000 1144.000000 761.000000 1122.000000
1297.000000 1308.000000 1076.000000 1565.000000 1691.000000 1691.000000 1271.000000
1235.000000 1358.000000 930.000000 930.000000 1374.000000 1188.000000 1299.000000
1299.000000 1280.000000 1165.000000 1844.000000 1383.000000 1406.000000 1674.000000
1636.000000 1636.000000 1766.000000 1766.000000 1233.000000 1233.000000 1036.000000
1673.000000 1676.000000

2173.530029 1965.000000 1656.000000 1128.000000 968.000000 1384.000000 1292.000000
856.000000 1684.000000 1649.000000 1154.000000 1154.000000 1810.000000 1234.000000
1862.000000 1855.000000 1798.000000 1833.000000 1885.000000 1947.000000 1673.000000
1961.000000 1441.000000 1602.000000 1855.000000 1315.000000 681.000000 681.000000
1405.000000 1666.000000 2450.000000 1514.000000 1662.000000 1342.000000 1342.000000
1948.000000 1356.000000 1834.000000 1972.000000 1972.000000 1366.000000 1126.000000
1435.000000 1786.000000 1742.000000 1445.000000 1193.000000 1793.000000 1472.000000
1491.000000 1160.000000 1160.000000 1279.000000 1199.000000 809.000000 1177.000000
1384.000000 1350.000000 1166.000000 1545.000000 1613.000000 1613.000000 1243.000000
1197.000000 1307.000000 930.000000 930.000000 1345.000000 1288.000000 1374.000000
1260.000000 1322.000000 1150.000000 1878.000000 1469.000000 1526.000000 1629.000000
1638.000000 1638.000000 1835.000000 1835.000000 1252.000000 1252.000000 1011.000000
1823.000000 1632.000000

2183.629883 1969.000000 1869.000000 1243.000000 998.000000 1606.000000 1215.000000
957.000000 1966.000000 1562.000000 1225.000000 1225.000000 1987.000000 1270.000000
2025.000000 2064.000000 1931.000000 1786.000000 1890.000000 1964.000000 1889.000000
1911.000000 1493.000000 1672.000000 1986.000000 1270.000000 797.000000 797.000000
1347.000000 1721.000000 2482.000000 1695.000000 1661.000000 1394.000000 1394.000000
1728.000000 1454.000000 1962.000000 2063.000000 2063.000000 1496.000000 1140.000000
1463.000000 1769.000000 1616.000000 1793.000000 1116.000000 1957.000000 1522.000000
1584.000000 1295.000000 1295.000000 1414.000000 1213.000000 901.000000 1360.000000
1293.000000 1438.000000 1181.000000 1573.000000 1727.000000 1727.000000 1367.000000
1277.000000 1271.000000 1082.000000 1082.000000 1632.000000 1242.000000 1236.000000
1158.000000 1331.000000 1119.000000 1859.000000 1462.000000 1584.000000 1552.000000
1637.000000 1637.000000 1762.000000 1762.000000 1329.000000 1329.000000 1162.000000
1662.000000 1734.000000

2193.729980 1988.000000 1823.000000 1236.000000 991.000000 1605.000000 1230.000000
900.000000 2042.000000 1677.000000 1358.000000 1358.000000 1994.000000 1194.000000
2011.000000 2063.000000 1947.000000 1747.000000 1916.000000 1957.000000 1855.000000
2008.000000 1534.000000 1687.000000 1782.000000 1182.000000 827.000000 827.000000
1263.000000 1845.000000 2598.000000 1723.000000 1688.000000 1408.000000 1408.000000
1758.000000 1423.000000 1945.000000 2133.000000 2133.000000 1502.000000 1176.000000
1468.000000 1720.000000 1757.000000 1827.000000 1221.000000 2092.000000 1588.000000
1665.000000 1326.000000 1326.000000 1451.000000 1251.000000 900.000000 1276.000000
1359.000000 1464.000000 1241.000000 1617.000000 1898.000000 1898.000000 1402.000000
1378.000000 1336.000000 1056.000000 1056.000000 1587.000000 1282.000000 1218.000000
1183.000000 1340.000000 1153.000000 1919.000000 1537.000000 1607.000000 1643.000000
1710.000000 1710.000000 1701.000000 1701.000000 1409.000000 1409.000000 1268.000000
1654.000000 1776.000000

2203.830078 1926.000000 1790.000000 911.000000 776.000000 1496.000000 1422.000000
1001.000000 1907.000000 1794.000000 1174.000000 1174.000000 2067.000000 1434.000000
2000.000000 2041.000000 1894.000000 1782.000000 2024.000000 2017.000000 1784.000000
2156.000000 1583.000000 1781.000000 1905.000000 1273.000000 911.000000 911.000000
1668.000000 1825.000000 2449.000000 1636.000000 1648.000000 1611.000000 1611.000000
1994.000000 1528.000000 1945.000000 1970.000000 1970.000000 1588.000000 1181.000000
1490.000000 1646.000000 1709.000000 1783.000000 1476.000000 2049.000000 1690.000000
1587.000000 1439.000000 1439.000000 1334.000000 950.000000 827.000000 1286.000000
1398.000000 1310.000000 1348.000000 1745.000000 1718.000000 1718.000000 1580.000000
1542.000000 1364.000000 1253.000000 1253.000000 1565.000000 1269.000000 1424.000000
1350.000000 1342.000000 1318.000000 1918.000000 1415.000000 1649.000000 1687.000000
1561.000000 1561.000000 1785.000000 1785.000000 1452.000000 1452.000000 1069.000000
1834.000000 1789.000000

2213.929932 1857.000000 1695.000000 886.000000 817.000000 1536.000000 1408.000000
1049.000000 1953.000000 1791.000000 1200.000000 1200.000000 2057.000000 1408.000000
1950.000000 2091.000000 1895.000000 1825.000000 1938.000000 1964.000000 1722.000000
2163.000000 1593.000000 1836.000000 1999.000000 1362.000000 932.000000 932.000000
1581.000000 1764.000000 2396.000000 1588.000000 1750.000000 1611.000000 1611.000000
1900.000000 1475.000000 1912.000000 1912.000000 1912.000000 1508.000000 1173.000000
1509.000000 1668.000000 1680.000000 1784.000000 1450.000000 1984.000000 1695.000000
1542.000000 1473.000000 1473.000000 1361.000000 1026.000000 864.000000 1316.000000
1339.000000 1339.000000 1327.000000 1733.000000 1720.000000 1720.000000 1545.000000
1545.000000 1391.000000 1207.000000 1207.000000 1613.000000 1301.000000 1425.000000
1345.000000 1336.000000 1313.000000 1807.000000 1312.000000 1646.000000 1682.000000
1553.000000 1553.000000 1785.000000 1785.000000 1346.000000 1346.000000 1081.000000
1866.000000 1764.000000

2224.030029 1758.000000 1874.000000 1291.000000 929.000000 1642.000000 1222.000000
1035.000000 1958.000000 1514.000000 1362.000000 1362.000000 1911.000000 1490.000000
1991.000000 2027.000000 1794.000000 1771.000000 1921.000000 1841.000000 1736.000000
1865.000000 1420.000000 1794.000000 2074.000000 1350.000000 929.000000 929.000000
1385.000000 1745.000000 2408.000000 1523.000000 1558.000000 1406.000000 1406.000000
1744.000000 1547.000000 1966.000000 2106.000000 2106.000000 1442.000000 1197.000000
1418.000000 1778.000000 1837.000000 1674.000000 1499.000000 1862.000000 1582.000000
1651.000000 1465.000000 1465.000000 1478.000000 1187.000000 907.000000 1455.000000
1374.000000 1584.000000 1304.000000 1561.000000 1689.000000 1689.000000 1326.000000
1466.000000 1371.000000 1150.000000 1150.000000 1477.000000 1291.000000 1289.000000
1347.000000 1372.000000 1174.000000 1802.000000 1255.000000 1663.000000 1581.000000

1674.000000 1674.000000 1745.000000 1745.000000 1197.000000 1197.000000 1197.000000
1814.000000 1746.000000

2234.120117 1689.000000 1898.000000 1272.000000 905.000000 1641.000000 1199.000000
1040.000000 1911.000000 1518.000000 1322.000000 1322.000000 1862.000000 1481.000000
1996.000000 1947.000000 1800.000000 1751.000000 1751.000000 1776.000000 1752.000000
1837.000000 1420.000000 1702.000000 2033.000000 1310.000000 856.000000 856.000000
1359.000000 1726.000000 2375.000000 1505.000000 1480.000000 1260.000000 1260.000000
1750.000000 1493.000000 1909.000000 2105.000000 2105.000000 1517.000000 1186.000000
1407.000000 1725.000000 1762.000000 1664.000000 1505.000000 1751.000000 1554.000000
1640.000000 1444.000000 1444.000000 1371.000000 1187.000000 844.000000 1432.000000
1371.000000 1543.000000 1285.000000 1592.000000 1690.000000 1690.000000 1297.000000
1444.000000 1284.000000 1161.000000 1161.000000 1432.000000 1235.000000 1161.000000
1394.000000 1383.000000 1162.000000 1848.000000 1223.000000 1615.000000 1505.000000
1664.000000 1664.000000 1689.000000 1689.000000 1174.000000 1174.000000 1174.000000
1775.000000 1714.000000

2244.219971 1587.000000 1774.000000 1133.000000 906.000000 1521.000000 1321.000000
907.000000 1668.000000 1534.000000 1174.000000 1174.000000 1721.000000 1280.000000
1867.000000 1841.000000 1641.000000 1467.000000 1814.000000 1855.000000 1548.000000
1935.000000 1334.000000 1494.000000 1815.000000 1080.000000 813.000000 813.000000
1387.000000 1814.000000 2440.000000 1626.000000 1546.000000 1586.000000 1586.000000
1920.000000 1467.000000 1773.000000 1653.000000 1653.000000 1426.000000 973.000000
1386.000000 1479.000000 1786.000000 1600.000000 1520.000000 1600.000000 1467.000000
1520.000000 1266.000000 1266.000000 1467.000000 1227.000000 1013.000000 1320.000000
1280.000000 1334.000000 1214.000000 1481.000000 1547.000000 1547.000000 1293.000000
1240.000000 1279.000000 1026.000000 1026.000000 1333.000000 1240.000000 1146.000000
1186.000000 1400.000000 1293.000000 1733.000000 1226.000000 1493.000000 1560.000000
1573.000000 1573.000000 1840.000000 1840.000000 1360.000000 1360.000000 1053.000000
1680.000000 1667.000000

2254.219971 1485.000000 1800.000000 1043.000000 828.000000 1443.000000 1243.000000
786.000000 1657.000000 1500.000000 1014.000000 1014.000000 1614.000000 1171.000000
1757.000000 1786.000000 1643.000000 1372.000000 1914.000000 1872.000000 1529.000000
1872.000000 1329.000000 1414.000000 1757.000000 1014.000000 771.000000 771.000000
1386.000000 1771.000000 2385.000000 1542.000000 1499.000000 1571.000000 1571.000000
1971.000000 1471.000000 1828.000000 1528.000000 1528.000000 1371.000000 928.000000
1342.000000 1442.000000 1756.000000 1542.000000 1499.000000 1585.000000 1457.000000
1414.000000 1299.000000 1299.000000 1471.000000 1114.000000 900.000000 1286.000000
1229.000000 1200.000000 1229.000000 1343.000000 1514.000000 1514.000000 1228.000000
1271.000000 1285.000000 1028.000000 1028.000000 1314.000000 1257.000000 1185.000000
1171.000000 1385.000000 1271.000000 1699.000000 1214.000000 1428.000000 1499.000000
1585.000000 1585.000000 1828.000000 1828.000000 1385.000000 1385.000000 1014.000000
1599.000000 1600.000000

2264.320068 1685.000000 1670.000000 963.000000 793.000000 1402.000000 1162.000000
836.000000 1813.000000 1459.000000 1218.000000 1218.000000 1883.000000 1317.000000
1883.000000 1685.000000 1813.000000 1615.000000 1897.000000 1728.000000 1686.000000
1813.000000 1331.000000 1529.000000 1728.000000 1148.000000 666.000000 666.000000
1261.000000 1543.000000 2489.000000 1260.000000 1472.000000 1203.000000 1203.000000
1656.000000 1416.000000 1825.000000 1769.000000 1769.000000 1274.000000 892.000000
1288.000000 1542.000000 1585.000000 1585.000000 1330.000000 1741.000000 1345.000000
1387.000000 1090.000000 1090.000000 1388.000000 935.000000 652.000000 1162.000000
1232.000000 1232.000000 1133.000000 1501.000000 1572.000000 1572.000000 1260.000000

1402.000000 1245.000000 1062.000000 1062.000000 1288.000000 1161.000000 1104.000000
1076.000000 1317.000000 1104.000000 1839.000000 1147.000000 1444.000000 1415.000000
1613.000000 1613.000000 1571.000000 1571.000000 1133.000000 1133.000000 935.000000
1726.000000 1458.000000

2274.419922 1561.000000 1659.000000 929.000000 831.000000 1294.000000 1168.000000
845.000000 1688.000000 1365.000000 1154.000000 1154.000000 1870.000000 1322.000000
1757.000000 1687.000000 1786.000000 1491.000000 1785.000000 1617.000000 1674.000000
1730.000000 1266.000000 1533.000000 1631.000000 1168.000000 760.000000 760.000000
1266.000000 1504.000000 2276.000000 1209.000000 1364.000000 1195.000000 1195.000000
1560.000000 1420.000000 1743.000000 1729.000000 1729.000000 1209.000000 844.000000
1209.000000 1462.000000 1490.000000 1602.000000 1293.000000 1659.000000 1294.000000
1350.000000 1139.000000 1139.000000 1336.000000 943.000000 578.000000 999.000000 1182.000000
1056.000000 1042.000000 1421.000000 1463.000000 1463.000000 1224.000000 1308.000000
1111.000000 985.000000 985.000000 1238.000000 1097.000000 1097.000000 998.000000 1223.000000
1027.000000 1700.000000 1097.000000 1251.000000 1336.000000 1504.000000 1504.000000
1588.000000 1588.000000 1013.000000 1013.000000 985.000000 1602.000000 1462.000000

2284.520020 1723.000000 1536.000000 957.000000 738.000000 1364.000000 879.000000 895.000000
1834.000000 1349.000000 1004.000000 1004.000000 1943.000000 1067.000000 1661.000000
1818.000000 1740.000000 1442.000000 1676.000000 1567.000000 1724.000000 1646.000000
1176.000000 1583.000000 1614.000000 1145.000000 707.000000 707.000000 1270.000000
1629.000000 1988.000000 1160.000000 1535.000000 1144.000000 1144.000000 1738.000000
1301.000000 1832.000000 1488.000000 1488.000000 1097.000000 816.000000 1051.000000
1456.000000 1457.000000 1316.000000 1238.000000 1676.000000 1395.000000 1410.000000
1035.000000 1035.000000 1208.000000 926.000000 770.000000 1145.000000 1004.000000
1114.000000 911.000000 1176.000000 1411.000000 1411.000000 973.000000 1332.000000
1003.000000 1050.000000 1050.000000 1144.000000 1035.000000 1159.000000 956.000000
1191.000000 1098.000000 1613.000000 1160.000000 1410.000000 1207.000000 1597.000000
1597.000000 1457.000000 1457.000000 1269.000000 1269.000000 832.000000 1582.000000
1348.000000

2294.610107 1781.000000 1451.000000 928.000000 667.000000 1382.000000 860.000000 825.000000
1766.000000 1278.000000 999.000000 999.000000 2010.000000 894.000000 1660.000000 1922.000000
1731.000000 1296.000000 1642.000000 1574.000000 1575.000000 1488.000000 1103.000000
1452.000000 1644.000000 1034.000000 754.000000 754.000000 1190.000000 1607.000000
1761.000000 1188.000000 1483.000000 1049.000000 1049.000000 1675.000000 1328.000000
1796.000000 1484.000000 1484.000000 1049.000000 771.000000 980.000000 1482.000000
1361.000000 1379.000000 1188.000000 1555.000000 1381.000000 1327.000000 962.000000
962.000000 1155.000000 859.000000 773.000000 1243.000000 930.000000 982.000000 860.000000
1156.000000 1347.000000 1347.000000 859.000000 1346.000000 996.000000 996.000000 996.000000
1067.000000 1032.000000 1083.000000 944.000000 1224.000000 1119.000000 1552.000000
1084.000000 1310.000000 1188.000000 1622.000000 1622.000000 1553.000000 1553.000000
1293.000000 1293.000000 840.000000 1553.000000 1398.000000

2304.709961 1608.000000 1608.000000 1099.000000 668.000000 1363.000000 977.000000
730.000000 1641.000000 1317.000000 1100.000000 1100.000000 1764.000000 1131.000000
1716.000000 1902.000000 1687.000000 1594.000000 1731.000000 1656.000000 1687.000000
1471.000000 1239.000000 1532.000000 1532.000000 1147.000000 699.000000 699.000000
1008.000000 1469.000000 2053.000000 1283.000000 1314.000000 914.000000 914.000000
1591.000000 1130.000000 1591.000000 1499.000000 1499.000000 1099.000000 930.000000
1268.000000 1206.000000 1576.000000 1422.000000 1022.000000 1762.000000 1053.000000
1283.000000 1145.000000 1145.000000 1316.000000 1023.000000 669.000000 962.000000 977.000000
1100.000000 1039.000000 1224.000000 1285.000000 1285.000000 946.000000 1084.000000

1021.000000 806.000000 806.000000 1284.000000 930.000000 960.000000 990.000000 1115.000000
853.000000 1560.000000 1068.000000 1361.000000 1345.000000 1268.000000 1268.000000
1669.000000 1669.000000 1053.000000 1053.000000 929.000000 1438.000000 1207.000000

2314.810059 1569.000000 1551.000000 1129.000000 656.000000 1360.000000 1044.000000
780.000000 1519.000000 1342.000000 1202.000000 1202.000000 1694.000000 1096.000000
1639.000000 1834.000000 1536.000000 1624.000000 1621.000000 1658.000000 1660.000000
1361.000000 1201.000000 1588.000000 1588.000000 1219.000000 656.000000 656.000000 902.000000
1515.000000 2144.000000 1076.000000 1321.000000 813.000000 813.000000 1654.000000
1077.000000 1601.000000 1461.000000 1461.000000 1023.000000 1058.000000 1146.000000
1145.000000 1531.000000 1443.000000 1040.000000 1779.000000 884.000000 1146.000000
1163.000000 1163.000000 1166.000000 867.000000 622.000000 991.000000 1061.000000 1149.000000
1061.000000 1167.000000 1148.000000 1148.000000 796.000000 1147.000000 1005.000000
865.000000 865.000000 1217.000000 954.000000 987.000000 952.000000 1024.000000 796.000000
1600.000000 1076.000000 1304.000000 1269.000000 1268.000000 1268.000000 1602.000000
1602.000000 1093.000000 1093.000000 883.000000 1461.000000 972.000000

2324.909912 1553.000000 1585.000000 506.000000 474.000000 1089.000000 992.000000 669.000000
1235.000000 1558.000000 927.000000 927.000000 1622.000000 1072.000000 1553.000000
1573.000000 1558.000000 1751.000000 1472.000000 1347.000000 1479.000000 1576.000000
1379.000000 1347.000000 1573.000000 960.000000 764.000000 764.000000 1217.000000 1471.000000
2124.000000 1227.000000 1435.000000 1162.000000 1162.000000 1580.000000 1117.000000
1660.000000 1629.000000 1629.000000 1083.000000 746.000000 1148.000000 1289.000000
1306.000000 1418.000000 1018.000000 1665.000000 1343.000000 1307.000000 1034.000000
1034.000000 1281.000000 813.000000 766.000000 1315.000000 1218.000000 1137.000000 928.000000
1380.000000 1362.000000 1362.000000 1006.000000 989.000000 841.000000 809.000000 809.000000
1261.000000 972.000000 1224.000000 904.000000 1245.000000 940.000000 1626.000000 906.000000
1243.000000 1324.000000 1546.000000 1546.000000 1645.000000 1645.000000 874.000000
874.000000 810.000000 1356.000000 1488.000000

2335.010010 1297.000000 1422.000000 348.000000 330.000000 977.000000 905.000000 690.000000
1211.000000 1569.000000 851.000000 851.000000 1695.000000 833.000000 1440.000000 1461.000000
1605.000000 1731.000000 1690.000000 1371.000000 1481.000000 1445.000000 1550.000000
1317.000000 1551.000000 1138.000000 831.000000 831.000000 1263.000000 1510.000000
2148.000000 1364.000000 1328.000000 1167.000000 1167.000000 1507.000000 1134.000000
1632.000000 1597.000000 1597.000000 1025.000000 704.000000 1151.000000 1415.000000
1417.000000 1399.000000 1007.000000 1690.000000 1493.000000 1364.000000 971.000000
971.000000 1334.000000 833.000000 923.000000 1264.000000 1264.000000 1300.000000 654.000000
1372.000000 1388.000000 1388.000000 1082.000000 992.000000 739.000000 881.000000 881.000000
1116.000000 1027.000000 1165.000000 1041.000000 1402.000000 937.000000 1701.000000
775.000000 1204.000000 1276.000000 1612.000000 1612.000000 1775.000000 1775.000000 847.000000
847.000000 811.000000 1275.000000 1707.000000

2345.110107 1490.000000 1294.000000 751.000000 600.000000 1235.000000 1301.000000
625.000000 1913.000000 1105.000000 1082.000000 1082.000000 1672.000000 1321.000000
1664.000000 2258.000000 1497.000000 1694.000000 1597.000000 1648.000000 1216.000000
1981.000000 1147.000000 1561.000000 1322.000000 1278.000000 773.000000 773.000000
1298.000000 1379.000000 2170.000000 1093.000000 1136.000000 1028.000000 1028.000000
1395.000000 1356.000000 1503.000000 1569.000000 1569.000000 1115.000000 316.000000
511.000000 1369.000000 1178.000000 1587.000000 1071.000000 2551.000000 730.000000 1201.000000
834.000000 834.000000 1472.000000 667.000000 363.000000 973.000000 1192.000000 973.000000
908.000000 1039.000000 1190.000000 1190.000000 817.000000 1359.000000 725.000000 897.000000
897.000000 858.000000 967.000000 1218.000000 895.000000 815.000000 685.000000 1306.000000

1201.000000 1482.000000 1051.000000 1306.000000 1306.000000 1094.000000 1094.000000
856.000000 856.000000 1137.000000 1504.000000 860.000000

2355.209961 1627.000000 1209.000000 809.000000 731.000000 1235.000000 1176.000000
655.000000 1778.000000 935.000000 1135.000000 1135.000000 1356.000000 1174.000000 1687.000000
2235.000000 1396.000000 1496.000000 1705.000000 1414.000000 1178.000000 1901.000000
1034.000000 1574.000000 1355.000000 1155.000000 929.000000 929.000000 1392.000000
1266.000000 2227.000000 1082.000000 1082.000000 904.000000 904.000000 1379.000000
1305.000000 1518.000000 1559.000000 1559.000000 1063.000000 192.000000 489.000000
1374.000000 1179.000000 1496.000000 1042.000000 2541.000000 790.000000 1161.000000
845.000000 845.000000 1292.000000 633.000000 454.000000 815.000000 1336.000000 835.000000
1015.000000 995.000000 1093.000000 1093.000000 831.000000 1487.000000 882.000000 645.000000
645.000000 868.000000 967.000000 1136.000000 920.000000 510.000000 510.000000 1237.000000
1083.000000 1538.000000 866.000000 961.000000 961.000000 1024.000000 1024.000000 786.000000
786.000000 984.000000 1618.000000 770.000000

2365.199951 1112.000000 1302.000000 1279.000000 943.000000 1139.000000 588.000000
885.000000 2035.000000 737.000000 970.000000 970.000000 1736.000000 736.000000 1408.000000
1478.000000 1544.000000 1417.000000 1618.000000 1139.000000 1804.000000 1079.000000
1032.000000 1627.000000 1182.000000 736.000000 436.000000 436.000000 734.000000 983.000000
2380.000000 936.000000 1083.000000 685.000000 685.000000 1209.000000 1214.000000 1377.000000
853.000000 853.000000 916.000000 644.000000 1212.000000 1434.000000 1165.000000 851.000000
412.000000 1364.000000 1301.000000 1314.000000 957.000000 957.000000 395.000000 1179.000000
800.000000 1012.000000 184.000000 779.000000 609.000000 673.000000 947.000000 947.000000
1176.000000 542.000000 683.000000 390.000000 390.000000 1214.000000 1151.000000 786.000000
1099.000000 1087.000000 414.000000 1436.000000 979.000000 1273.000000 1400.000000
1018.000000 1018.000000 1126.000000 1126.000000 1420.000000 1420.000000 748.000000
1105.000000 1533.000000

Appendix 6.1: Spectra Separability Report for Vegetation Assemblage Classes Regions of Interest (ROIs)

Input File: MfabeniL1T.dat

ROI Name: (Jeffries-Matusita, Transformed Divergence)

ROI #10:

ROI #9: (NaN 2.00000000)

ROI #8: (0.00000000 0.00000000)

ROI #7: (NaN 2.00000000)

ROI #6: (NaN 2.00000000)

ROI #5: (NaN 2.00000000)

ROI #4: (NaN 2.00000000)

ROI #3: (NaN 2.00000000)

ROI #2: (NaN 2.00000000)

ROI #1: (0.00000000 0.00000000)

ROI #9:

ROI #10: (NaN 2.00000000)

ROI #8: (0.00000000 0.00000000)

ROI #7: (NaN 2.00000000)

ROI #6: (NaN 1.99999728)

ROI #5: (NaN 2.00000000)

ROI #4: (NaN 2.00000000)

ROI #3: (NaN 2.00000000)

ROI #2: (NaN 1.99999986)

ROI #1: (0.00000000 0.00000000)

ROI #8:

ROI #10: (0.00000000 0.00000000)

ROI #9: (0.00000000 0.00000000)

ROI #7: (0.00000000 0.00000000)

ROI #6: (0.00000000 0.00000000)

ROI #5: (0.00000000 0.00000000)

ROI #4: (0.00000000 0.00000000)

ROI #3: (0.00000000 0.00000000)

ROI #2: (0.00000000 0.00000000)

ROI #1: (0.00000000 0.00000000)

ROI #7:

ROI #10: (NaN 2.00000000)

ROI #9: (NaN 2.00000000)

ROI #8: (0.00000000 0.00000000)

ROI #6: (NaN 2.00000000)

ROI #5: (NaN 2.00000000)

ROI #4: (NaN 2.00000000)

ROI #3: (NaN 2.00000000)

ROI #2: (NaN 2.00000000)

ROI #1: (0.00000000 0.00000000)

ROI #6:

ROI #10: (NaN 2.00000000)

ROI #9: (NaN 1.99999728)

ROI #8: (0.00000000 0.00000000)

ROI #7: (NaN 2.00000000)

ROI #5: (NaN 2.00000000)

ROI #4: (NaN 2.00000000)

ROI #3: (NaN 2.00000000)

ROI #2: (NaN 2.00000000)

ROI #1: (0.00000000 0.00000000)

ROI #5:

ROI #10: (NaN 2.00000000)

ROI #9: (NaN 2.00000000)

ROI #8: (0.00000000 0.00000000)

ROI #7: (NaN 2.00000000)

ROI #6: (NaN 2.00000000)

ROI #4: (NaN 2.00000000)

ROI #3: (NaN 2.00000000)

ROI #2: (NaN 2.00000000)

ROI #1: (0.00000000 0.00000000)

ROI #4:

ROI #10: (NaN 2.00000000)

ROI #9: (NaN 2.00000000)

ROI #8: (0.00000000 0.00000000)

ROI #7: (NaN 2.00000000)

ROI #6: (NaN 2.00000000)

ROI #5: (NaN 2.00000000)

ROI #3: (NaN 2.00000000)

ROI #2: (NaN 2.00000000)

ROI #1: (0.00000000 0.00000000)

ROI #3:

ROI #10: (NaN 2.00000000)

ROI #9: (NaN 2.00000000)

ROI #8: (0.00000000 0.00000000)

ROI #7: (NaN 2.00000000)

ROI #6: (NaN 2.00000000)

ROI #5: (NaN 2.00000000)

ROI #4: (NaN 2.00000000)

ROI #2: (NaN 2.00000000)

ROI #1: (0.00000000 0.00000000)

ROI #2:

ROI #10: (NaN 2.00000000)

ROI #9: (NaN 1.99999986)

ROI #8: (0.00000000 0.00000000)

ROI #7: (NaN 2.00000000)

ROI #6: (NaN 2.00000000)

ROI #5: (NaN 2.00000000)

ROI #4: (NaN 2.00000000)

ROI #3: (NaN 2.00000000)

ROI #1: (0.00000000 0.00000000)

ROI #1:

ROI #10: (0.00000000 0.00000000)

ROI #9: (0.00000000 0.00000000)

ROI #8: (0.00000000 0.00000000)

ROI #7: (0.00000000 0.00000000)

ROI #6: (0.00000000 0.00000000)

ROI #5: (0.00000000 0.00000000)

ROI #4: (0.00000000 0.00000000)

ROI #3: (0.00000000 0.00000000)

ROI #2: (0.00000000 0.00000000)

Pair Separation (least to most);

ROI #10 and ROI #8 - 0.00000000

ROI #3 and ROI #1 - 0.00000000

ROI #4 and ROI #1 - 0.00000000

ROI #2 and ROI #1 - 0.00000000

ROI #6 and ROI #1 - 0.00000000

ROI #8 and ROI #3 - 0.00000000

ROI #10 and ROI #1 - 0.00000000

ROI #9 and ROI #8 - 0.00000000

ROI #8 and ROI #5 - 0.00000000

ROI #9 and ROI #1 - 0.00000000

ROI #8 and ROI #7 - 0.00000000

ROI #8 and ROI #6 - 0.00000000

ROI #8 and ROI #4 - 0.00000000

ROI #8 and ROI #2 - 0.00000000

ROI #8 and ROI #1 - 0.00000000

ROI #5 and ROI #1 - 0.00000000

ROI #7 and ROI #1 - 0.00000000

ROI #10 and ROI #9 - 2.00000000

ROI #10 and ROI #7 - 2.00000000

ROI #10 and ROI #6 - 2.00000000

ROI #10 and ROI #5 - 2.00000000

ROI #10 and ROI #4 - 2.00000000

ROI #10 and ROI #3 - 2.00000000

ROI #10 and ROI #2 - 2.00000000

ROI #9 and ROI #7 - 2.00000000

ROI #9 and ROI #6 - 1.99999728

ROI #9 and ROI #5 - 2.00000000

ROI #9 and ROI #4 - 2.00000000

ROI #9 and ROI #3 - 2.00000000

ROI #9 and ROI #2 - 1.99999986

ROI #7 and ROI #6 - 2.00000000

ROI #7 and ROI #5 - 2.00000000

ROI #7 and ROI #4 - 2.00000000

ROI #7 and ROI #3 - 2.00000000

ROI #7 and ROI #2 - 2.00000000

ROI #6 and ROI #5 - 2.00000000

ROI #6 and ROI #4 - 2.00000000

ROI #6 and ROI #3 - 2.00000000

ROI #6 and ROI #2 - 2.00000000

ROI #5 and ROI #4 - 2.00000000

ROI #5 and ROI #3 - 2.00000000

ROI #5 and ROI #2 - 2.00000000

ROI #4 and ROI #3 - 2.00000000

ROI #4 and ROI #2 - 2.00000000

ROI #3 and ROI #2 - 2.00000000

Appendix 6.2: Consolidated File of Vegetation Assemblages Class Means

Class	426,82	436,99	447,17	457,34	467,52	477,69	487,87	498,04	508,22	518,39	528,57
	538,74	548,92	559,09	569,27	579,45	589,62	599,80	609,97	620,15	630,32	640,50
	650,67	660,85	671,02	681,20	691,37	701,55	711,72	721,90	732,07	742,25	752,43
	762,60	772,78	782,95	793,13	803,30	813,48	823,65	833,83	844,00	854,18	864,35
	874,53	884,70	894,88	905,05	912,45	915,23	922,54	925,41	932,64	942,73	952,82
	962,91	972,99	983,08	993,17	1003,30	1013,30	1023,40	1033,49	1043,59	1053,69	1063,79
	1073,89	1083,99	1094,09	1104,19	1114,19	1124,28	1134,38	1144,48	1154,58	1164,68	1174,77
	1184,87	1194,97	1205,07	1215,17	1225,17	1235,27	1245,36	1255,46	1265,56	1275,66	1285,76
	1295,86	1305,96	1316,05	1326,05	1336,15	1346,25	1416,94	1426,94	1437,04	1447,14	1457,23
	1467,33	1477,43	1487,53	1497,63	1507,73	1517,83	1527,92	1537,92	1548,02	1558,12	1568,22
	1578,32	1588,42	1598,51	1608,61	1618,71	1628,81	1638,81	1648,90	1659,00	1669,10	1679,20
	1689,30	1699,40	1709,50	1719,60	1729,70	1739,70	1749,79	1759,89	1769,99	1780,09	1790,19
	1800,29	1810,38	1961,66	1971,76	1981,86	1991,96	2002,06	2012,15	2022,25	2032,35	2042,45
	2052,45	2062,55	2072,65	2082,75	2092,84	2102,94	2113,04	2123,14	2133,24	2143,34	2153,34
	2163,43	2173,53	2183,63	2193,73	2203,83	2213,93	2224,03	2234,12	2244,22	2254,22	2264,32
	2274,42	2284,52	2294,61	2304,71	2314,81	2324,91	2335,01	2345,11	2355,21	2365,20	
Class 1 Mean		137,72	75,80	-192,55	-85,60	23,07	216,31	218,27	277,26	346,54	377,11
	454,05	603,68	639,20	668,29	671,58	629,56	632,38	644,28	633,72	620,21	624,33
	610,16	631,05	699,14	693,34	723,56	785,40	826,55	1151,48	1372,88	1554,18	1736,31
	1968,75	1950,56	1874,08	2041,85	2086,46	2146,05	2250,12	2191,81	2238,08	2318,58	2367,76
	2386,74	2433,06	2462,33	2561,26	2458,09	2358,26	2433,89	2459,42	2522,49	2605,81	2536,01
	2585,68	2619,32	2662,07	2752,94	2753,51	2804,68	2722,45	2741,60	2781,96	2806,76	2892,96
	2883,19	2798,75	2797,39	2805,25	2791,78	2843,45	2775,15	2769,32	2677,13	2618,44	2709,19
	2771,08	2741,36	2764,99	2772,68	2796,91	2843,35	2887,54	2952,62	2968,60	2951,07	2955,33
	2970,95	2922,85	2734,20	2671,51	2392,27	2229,25	2333,25	0,00	667,36	569,24	897,11
	1133,12	1066,98	1336,49	1504,06	1687,08	1754,98	1814,61	1876,42	1983,54	2032,48	2082,94
	2137,91	2201,48	2248,76	2294,25	2326,28	2394,55	2422,49	2450,13	2484,00	2424,28	2416,98
	2373,68	2359,85	2334,95	2322,51	2262,92	2213,67	2161,33	2082,75	1996,78	1962,66	1845,87
	1750,31	1662,47	1430,25	277,08	636,65	943,89	952,38	308,39	458,74	989,94	1087,09
	1116,64	1099,82	1369,48	1359,07	1317,18	1341,40	1421,40	1419,38	1427,25	1435,59	1469,76
	1498,14	1454,13	1468,87	1525,55	1554,38	1573,14	1563,64	1546,95	1515,29	1454,20	1414,78
	1384,47	1326,87	1294,86	1260,41	1248,67	1221,45	1230,05	1231,08	1186,52	1138,08	1046,42
Class 2 Mean		-50,03	-88,11	-421,34	-275,69	-168,79	42,85	36,15	88,32	158,30	168,44
	233,41	405,22	433,70	465,68	466,54	441,98	465,15	480,13	482,50	479,01	474,93
	489,50	515,43	597,99	603,41	631,09	682,53	785,82	1009,04	1199,66	1370,71	1458,12
	1569,91	1598,29	1681,63	1746,58	1800,07	1865,40	1931,35	1961,59	2021,66	2074,91	2117,97
	2142,91	2196,66	2211,07	2246,22	2216,44	2207,61	2207,01	2228,09	2314,04	2322,01	2331,82
	2371,98	2434,73	2445,49	2520,06	2513,95	2552,44	2570,02	2603,41	2631,54	2657,60	2644,09
	2640,55	2588,04	2581,12	2617,03	2590,84	2550,70	2601,53	2529,94	2420,15	2478,74	2529,15
	2537,13	2488,58	2492,82	2493,66	2530,45	2597,43	2667,61	2724,50	2750,02	2777,73	2795,76
	2786,83	2712,29	2546,41	2492,28	2205,85	2013,60	1972,88	0,00	106,29	145,26	505,43
	704,09	616,39	975,48	1097,02	1173,52	1235,26	1324,91	1365,81	1428,70	1477,99	1532,47
	1584,22	1645,34	1673,96	1706,54	1768,57	1812,53	1847,59	1848,12	1876,46	1844,08	1832,36
	1856,56	1838,56	1772,71	1739,09	1704,86	1665,81	1604,10	1545,39	1469,83	1449,09	1312,41
	1293,06	1054,85	785,94	109,80	301,04	509,88	477,62	52,96	118,53	728,38	730,71
	667,34	670,36	833,34	799,47	696,44	714,98	819,93	824,67	671,41	682,57	895,20
	922,19	769,33	791,04	975,19	989,79	937,20	933,12	974,12	936,68	803,83	754,41
	797,54	761,88	744,23	705,49	702,10	666,67	675,44	646,50	627,73	638,14	715,48

Class 3 Mean	-239,58	-231,39	-613,60	-454,45	-279,49	-119,25	-149,41	-105,26	-54,38	-50,73	
	24,70	222,54	241,98	263,70	218,39	157,76	167,29	159,76	134,37	119,71	85,85
	70,10	60,44	155,67	137,18	147,16	170,92	294,20	649,86	1052,93	1493,05	1809,53
	2022,16	2131,67	2269,72	2290,54	2343,03	2404,27	2406,22	2468,67	2526,12	2584,66	2608,85
	2613,77	2631,90	2632,25	2654,49	2637,21	2540,85	2646,13	2552,24	2711,78	2671,34	2583,83
	2566,94	2567,63	2550,13	2626,78	2655,42	2698,24	2697,72	2767,64	2815,10	2860,52	2872,27
	2867,18	2803,64	2747,95	2770,35	2699,35	2649,83	2569,49	2498,59	2227,39	2137,35	2120,46
	2128,36	2064,36	2063,45	2067,87	2040,12	2097,72	2171,63	2219,48	2249,18	2252,88	2304,70
	2264,02	2199,45	1987,35	1881,54	1597,46	1433,73	1497,49	0,00	-310,73	-143,62	-18,39
	162,38	125,82	285,86	351,49	461,61	503,18	581,25	623,64	662,45	707,99	731,69
	785,23	814,89	838,95	879,10	915,34	926,61	948,31	958,85	968,11	938,11	897,54
	919,33	901,27	876,54	851,32	831,75	793,33	757,31	715,73	665,58	634,67	608,96
	603,45	516,08	549,24	123,22	87,83	61,83	40,97	114,24	115,12	219,98	207,66
	92,18	78,24	291,20	300,07	151,73	154,43	284,01	286,86	107,82	96,73	280,82
	298,69	150,70	164,95	394,02	393,77	337,09	335,33	377,88	370,39	353,43	329,92
	306,98	295,21	309,65	280,66	222,96	213,75	299,86	289,51	250,73	257,92	276,90
Class 4 Mean	-230,46	-199,85	-610,35	-451,90	-272,40	-100,92	-140,97	-90,10	-34,36	-34,96	
	28,76	230,92	254,10	276,18	234,09	174,87	179,22	179,72	158,36	143,35	106,06
	91,21	83,36	178,15	157,72	163,05	195,12	327,27	709,92	1123,12	1568,40	1887,87
	2092,21	2212,77	2353,53	2366,72	2420,74	2485,03	2483,28	2546,69	2606,17	2669,60	2703,00
	2706,40	2731,42	2737,86	2722,06	2689,03	2576,78	2741,68	2611,74	2823,71	2695,55	2602,94
	2701,55	2676,01	2617,08	2697,88	2737,10	2787,31	2792,83	2858,79	2908,85	2938,47	2942,64
	2945,35	2864,31	2817,32	2852,49	2784,56	2701,27	2627,92	2539,22	2264,60	2181,85	2169,46
	2207,24	2150,42	2109,95	2105,14	2097,79	2151,79	2250,82	2301,10	2333,22	2344,47	2382,94
	2348,56	2263,05	2055,53	1934,99	1646,85	1466,72	1523,99	0,00	-274,40	-119,47	33,46
	272,73	274,81	362,32	415,29	498,94	539,53	619,15	671,22	694,08	742,96	770,56
	820,17	841,19	864,26	910,42	953,50	977,50	999,35	1001,26	1012,71	988,26	966,09
	984,36	964,72	931,55	904,00	874,08	842,68	800,26	754,38	717,18	692,14	671,54
	666,92	500,99	536,10	90,33	69,76	100,28	90,36	22,56	46,38	215,59	225,67
	137,03	123,85	295,47	309,14	171,87	178,73	299,76	308,33	133,62	137,88	300,04
	311,71	164,08	180,71	414,77	405,31	357,67	357,31	391,24	386,17	349,59	337,60
	345,04	318,67	315,00	297,58	255,10	237,36	293,63	291,55	342,35	353,22	274,82
Class 5 Mean	-169,71	-175,75	-566,64	-404,79	-237,46	-74,19	-93,26	-53,48	13,99	21,05	
	93,26	293,62	326,00	349,72	312,55	251,51	259,80	249,05	224,88	212,85	172,03
	162,65	152,92	235,20	213,38	221,75	259,77	418,77	826,81	1205,74	1592,86	1841,79
	1996,98	2103,46	2219,56	2233,22	2288,03	2343,29	2349,55	2406,74	2465,48	2521,94	2550,41
	2543,58	2581,47	2582,25	2584,66	2576,36	2446,16	2617,31	2466,71	2674,01	2572,36	2548,71
	2501,00	2524,35	2562,88	2649,03	2620,65	2658,41	2692,09	2740,18	2808,29	2838,55	2809,84
	2820,04	2752,44	2714,62	2716,86	2640,40	2612,99	2565,75	2455,64	2211,83	2175,49	2183,78
	2190,07	2139,54	2109,14	2101,66	2124,42	2170,59	2250,01	2299,55	2342,83	2363,83	2384,63
	2344,47	2269,12	2065,56	1963,07	1681,11	1474,57	1409,66	0,00	-268,01	156,46	199,24
	341,58	340,45	470,71	529,45	602,68	638,08	702,21	748,63	777,52	815,65	832,09
	882,79	915,19	952,89	996,54	1031,36	1054,72	1078,47	1100,81	1119,09	1088,64	1078,87
	1067,63	1054,44	1022,63	991,91	956,37	917,31	892,56	840,28	793,35	771,33	740,55
	730,28	547,69	518,45	58,98	65,05	141,34	132,41	71,91	88,07	244,73	260,18
	204,24	195,80	435,78	419,58	271,72	273,27	368,82	375,59	266,34	273,85	367,26
	376,69	268,76	270,96	479,37	486,20	449,12	442,36	484,25	478,79	428,27	389,64
	396,17	380,38	387,97	361,18	293,43	283,74	330,76	336,43	284,19	317,40	373,11
Class 6 Mean	-43,16	-79,98	-434,97	-263,87	-130,92	40,92	25,38	90,31	157,88	191,06	
	276,49	470,38	513,78	547,91	522,17	479,71	486,62	483,19	474,49	454,55	430,41
	427,40	436,27	498,73	484,25	494,00	551,39	745,01	1149,24	1460,11	1723,29	1875,53

1987,69	2041,15	2142,26	2178,81	2238,67	2298,24	2333,00	2386,25	2451,27	2507,91	2541,83	
2558,44	2600,23	2602,71	2630,86	2604,57	2641,99	2613,66	2678,54	2688,89	2811,45	2777,20	
2804,32	2817,51	2824,68	2892,22	2903,32	2938,05	2870,77	2920,88	2933,52	2952,86	3015,44	
3008,89	2955,24	2937,89	2945,92	2896,57	2818,41	2809,12	2815,30	2638,96	2643,92	2698,10	
2715,67	2658,99	2667,60	2672,15	2692,28	2734,09	2800,51	2851,16	2865,04	2869,46	2924,09	
2893,87	2827,46	2633,29	2551,30	2249,91	2012,26	1906,51	0,00	144,16	380,10	559,89	
741,45	708,45	883,49	996,88	1075,25	1141,47	1214,04	1258,80	1324,52	1382,90	1424,74	
1477,84	1542,31	1595,04	1633,63	1682,83	1695,51	1724,24	1767,04	1774,74	1757,76	1717,08	
1760,29	1746,87	1697,67	1666,08	1617,38	1570,29	1514,43	1449,10	1374,40	1337,04	1245,14	
1221,26	1037,72	876,52	114,23	209,83	349,34	316,74	80,96	115,83	588,11	602,08	
511,69	504,18	719,13	706,35	627,57	640,71	724,82	729,63	586,97	589,37	781,49	
813,86	688,31	698,08	880,56	894,78	843,42	848,00	898,80	867,15	730,08	689,74	
745,63	719,81	692,88	662,86	630,45	596,22	641,39	598,87	532,88	530,13	549,35	
Class 7 Mean	42,29	-15,70	-326,13	-153,04	-71,52	116,11	117,00	170,66	258,77	268,58	
353,63	528,90	562,03	590,90	574,54	534,01	537,87	537,67	524,52	511,86	500,99	
492,99	501,49	570,19	560,24	575,08	629,31	752,84	1058,53	1281,58	1465,23	1571,37	
1711,59	1704,88	1753,20	1833,14	1873,07	1919,82	1990,29	1995,65	2045,20	2089,22	2125,36	
2143,05	2199,80	2216,14	2263,78	2216,08	2228,91	2194,96	2264,01	2246,63	2352,29	2370,79	
2440,29	2450,05	2390,92	2467,63	2476,14	2501,32	2476,47	2516,45	2528,87	2558,49	2589,81	
2576,82	2498,30	2469,27	2511,46	2497,97	2486,84	2498,93	2527,42	2439,31	2430,87	2411,99	
2408,99	2375,59	2398,34	2393,52	2399,62	2439,58	2486,78	2529,70	2553,99	2573,09	2562,40	
2538,12	2504,92	2343,58	2293,22	2043,42	1927,43	2011,91	0,00	181,48	186,91	502,42	
699,21	595,64	986,54	1123,78	1216,79	1279,57	1357,13	1393,15	1468,97	1522,87	1558,08	
1612,75	1689,76	1713,99	1727,84	1775,53	1824,13	1848,01	1854,35	1869,41	1865,60	1861,11	
1842,67	1839,26	1787,60	1769,51	1744,68	1694,80	1642,09	1570,45	1504,46	1490,98	1426,52	
1364,05	1255,09	1109,26	224,95	372,91	544,57	511,48	146,99	211,10	729,96	742,99	
694,67	688,41	899,25	882,87	804,60	838,49	889,45	880,90	857,00	871,38	973,79	
992,02	912,41	933,51	1055,01	1066,03	1018,32	1018,20	1073,25	1057,13	935,85	893,90	
938,59	893,88	864,21	855,78	849,64	835,42	819,25	816,53	759,49	704,07	723,46	
Class 8 Mean	71,09	-2,20	-320,22	-184,66	-96,10	112,15	105,37	150,07	210,48	245,45	
331,04	505,29	548,18	582,26	570,64	514,38	504,58	505,66	485,15	465,74	459,62	
443,27	451,40	511,20	498,58	515,18	579,33	659,21	1110,12	1431,47	1712,11	1990,53	
2300,27	2293,16	2213,17	2414,17	2470,51	2537,54	2640,52	2569,53	2621,26	2742,21	2799,83	
2826,46	2860,87	2893,08	3008,97	2890,89	2795,25	2837,08	2963,47	2904,99	2826,98	2857,24	
3026,78	2991,35	3021,37	3119,88	3109,35	3176,81	3084,54	3115,00	3172,31	3214,56	3343,97	
3347,71	3221,87	3213,49	3174,49	3150,52	3149,34	3050,74	3002,02	2842,20	2746,88	2825,74	
2869,54	2816,19	2830,56	2843,82	2874,49	2923,20	2967,46	3039,25	3075,91	3048,64	3047,49	
3042,40	2963,35	2750,67	2644,16	2329,43	2187,82	2416,49	0,00	183,08	151,46	461,83	
668,35	566,91	881,52	1035,24	1187,51	1258,31	1308,21	1373,57	1489,73	1545,55	1601,29	
1665,53	1719,93	1768,02	1808,72	1853,52	1907,85	1941,60	1969,81	1993,25	1939,79	1938,43	
1920,66	1911,84	1871,12	1846,39	1804,73	1762,21	1704,09	1631,04	1550,44	1514,17	1417,45	
1341,25	1256,58	1032,09	126,22	293,10	451,65	409,34	27,79	71,98	613,30	670,18	
571,00	501,48	829,00	822,27	779,53	808,39	906,99	911,45	888,25	917,65	988,11	
995,89	915,19	940,55	1029,47	1050,29	1032,97	1022,02	1073,84	1039,21	953,67	919,25	
908,79	859,83	837,90	810,46	808,55	790,21	782,09	761,27	718,92	683,07	699,29	
Class 9 Mean	-3,96	-47,86	-383,67	-213,83	-120,74	83,80	89,19	139,04	209,37	232,35	
306,00	487,94	527,86	562,67	565,99	532,58	552,60	564,38	561,88	552,28	553,08	
564,77	588,55	662,47	663,20	684,92	744,99	877,77	1205,33	1456,32	1673,49	1810,81	
1965,48	1975,17	2072,86	2151,64	2216,02	2287,16	2350,27	2378,63	2447,32	2530,09	2563,03	
2593,69	2646,19	2652,31	2701,35	2658,34	2673,74	2637,69	2691,49	2671,18	2820,49	2847,57	
2887,35	2926,05	2911,83	2998,09	3034,47	3064,55	2982,89	3026,77	3046,03	3067,04	3189,17	

3175,89	3112,79	3089,25	3083,92	3059,17	2983,26	2972,57	2989,64	2889,51	2902,04	2941,02
2942,24	2886,81	2929,72	2942,04	2934,14	2989,85	3081,25	3143,80	3154,01	3168,44	3200,00
3180,53	3123,97	2925,63	2836,92	2507,47	2281,00	2156,75	0,00	151,86	279,01	628,72
748,65	647,80	1067,08	1214,37	1311,02	1380,18	1476,40	1524,64	1594,07	1653,00	1742,13
1814,44	1884,00	1919,14	1952,65	2010,36	2042,00	2078,20	2065,68	2084,93	2071,64	2070,45
2071,33	2047,56	1985,91	1954,98	1916,51	1863,07	1797,98	1725,27	1654,37	1628,18	1531,42
1467,45	1288,55	1073,32	162,95	323,99	553,24	535,61	86,38	160,92	737,71	757,99
699,63	652,77	923,40	902,22	785,57	815,29	910,23	909,06	784,25	803,32	995,45
1018,64	894,89	927,62	1074,39	1090,29	1058,71	1052,78	1078,35	1049,65	929,20	872,69
893,71	854,51	841,28	812,29	806,12	813,22	776,77	734,86	725,03	719,60	727,87
Class 10 Mean	-35,98	-58,80	-445,47	-295,18	-150,82	47,04	16,13	79,70	135,71	142,88
195,64	365,93	392,36	408,22	382,03	359,30	380,08	381,49	379,08	374,67	356,88
361,14	376,13	458,63	459,01	478,97	505,50	588,08	653,92	789,02	925,59	921,81
926,10	1008,19	1052,59	1051,79	1078,34	1102,84	1160,32	1203,91	1242,16	1212,83	1225,70
1229,71	1300,59	1307,82	1317,00	1327,66	1789,90	1441,84	1667,47	1532,40	1766,60	1773,91
1566,30	1531,32	1469,14	1526,58	1483,22	1494,46	1559,37	1581,87	1556,47	1588,33	1491,14
1482,19	1467,76	1442,34	1531,50	1495,90	1504,10	1559,61	1549,17	1515,63	1543,78	1501,39
1560,31	1544,57	1495,39	1483,22	1524,86	1552,91	1518,34	1535,63	1659,87	1708,43	1681,67
1655,11	1636,50	1530,40	1562,09	1397,11	1284,42	1215,88	0,00	-144,06	198,43	555,83
950,03	1000,13	1096,86	1127,86	1119,51	1150,51	1238,83	1263,38	1266,41	1300,73	1354,18
1372,33	1373,08	1407,31	1442,02	1462,33	1463,61	1484,52	1492,26	1487,27	1494,74	1488,49
1492,42	1477,09	1464,81	1465,74	1449,16	1424,03	1376,10	1328,91	1272,78	1261,03	1198,81
1201,48	1066,50	1403,23	504,40	593,34	657,00	603,42	185,39	283,79	784,27	808,34
710,11	636,78	1029,87	1014,58	898,42	923,27	1014,30	1022,37	920,01	917,28	1107,31
1129,79	972,03	976,71	1134,20	1127,11	1107,71	1093,88	1129,44	1120,38	993,86	971,86
1045,91	1014,43	972,76	935,38	919,83	895,32	943,82	953,12	879,32	844,43	948,37

Appendix 6.3: Summary of '500 by 6' Random Forest Model Identified as most optimal showing bands according to their Importance (Variable Importance)

Summary of the Random Forest Model

==========

Number of observations used to build the model: 639

Call:

randomForest(formula = as.factor(Class) ~ .,

data = crs$dataset[crs$train, c(crs$input, crs$target)],

ntree = 500, mtry = 6, importance = TRUE, replace = FALSE, na.action = na.omit)

Type of random forest: classification

Number of trees: 500

No. of variables tried at each split: 6

OOB estimate of error rate: 27.86%

Confusion matrix:

	1	2	3	4	5	6	7	8	9	10	class.error
1	45	1	0	0	0	0	2	7	2	3	0.25000000
2	0	70	0	0	0	0	0	1	12	1	0.16666667
3	0	1	59	8	8	0	0	2	0	0	0.24358974
4	0	2	17	26	4	1	0	2	1	0	0.50943396
5	0	0	9	2	41	0	2	1	0	0	0.25454545
6	0	8	0	0	0	38	4	1	6	1	0.34482759
7	11	3	0	0	0	1	37	4	4	2	0.40322581
8	9	1	0	0	1	1	1	48	2	0	0.23809524
9	2	13	0	0	0	8	1	0	39	0	0.38095238
10	1	0	2	1	0	0	1	0	0	58	0.07936508

Variable Importance

==========

	1	2	3	4	5	6	7	8	9	10
X701.549988	2.59	7.41	8.69	4.51	-1.86	10.37	7.94	9.62	8.59	2.51
X2133.239990	6.72	6.98	7.15	4.30	-1.67	5.66	3.76	7.30	3.88	6.33
X711.719971	2.93	3.72	7.09	2.44	-0.11	6.30	4.12	3.79	1.59	3.20
X894.880005	3.67	5.36	6.83	5.15	5.64	4.06	4.36	6.77	2.30	5.10
X640.500000	3.65	7.68	6.79	3.77	-1.17	5.21	4.95	5.14	5.27	2.98
X1991.959961	2.94	2.89	6.67	-4.43	2.32	1.49	2.87	3.54	3.37	2.60
X691.369995	5.38	10.10	6.63	4.87	2.20	5.41	5.68	6.83	7.62	4.36
X508.220001	6.28	7.13	6.61	3.80	-2.31	4.45	7.44	5.34	3.62	4.83
X1063.790039	4.95	4.49	6.00	2.32	3.82	4.64	4.00	5.56	4.12	6.26
X1769.989990	1.41	4.88	5.96	1.85	2.18	2.49	4.12	3.84	2.69	3.64
X772.780029	1.32	4.47	5.78	4.18	3.97	5.89	3.87	3.92	-1.04	3.27
X650.669983	3.75	7.68	5.71	5.30	-0.46	4.73	4.69	7.40	7.65	2.59
X518.390015	5.82	6.88	5.69	3.31	-2.68	4.38	5.37	5.03	1.44	3.79
X620.150024	3.79	5.41	5.67	3.43	-0.20	1.99	5.16	5.30	3.21	3.09
X609.969971	4.33	4.54	5.57	4.16	-0.23	4.33	4.23	5.40	4.16	3.41
X1487.530029	0.78	5.65	5.38	0.82	-0.81	4.04	2.93	3.22	3.01	4.83
X782.950012	4.96	4.47	5.34	3.54	2.93	3.64	2.78	4.67	4.14	5.00
X721.900024	1.98	3.53	5.31	3.95	0.55	6.51	5.61	4.52	3.06	3.07
X671.020020	5.68	9.87	5.28	3.84	2.18	4.46	5.84	6.45	7.74	4.03
X884.700012	3.80	4.56	5.25	4.14	3.80	4.31	5.54	5.08	1.52	4.69
X589.619995	3.92	4.67	5.08	4.28	-2.49	4.79	4.83	2.38	1.61	2.14
X477.690002	8.55	6.73	5.06	3.27	4.13	4.80	4.10	7.68	2.23	4.97
X1094.089966	4.68	2.81	4.99	2.64	5.83	4.01	3.89	3.96	2.34	5.05
X793.130005	2.78	5.40	4.96	3.98	4.35	2.39	4.24	4.94	0.32	4.91
X599.799988	4.18	3.75	4.95	4.15	-0.77	5.14	5.69	4.29	3.67	4.87
X660.849976	5.26	9.91	4.95	3.62	2.62	6.69	6.53	6.55	8.29	3.85
X569.270020	5.36	4.64	4.94	4.60	-0.94	2.97	4.57	3.95	3.84	4.40
X1517.829956	4.40	7.83	4.86	3.86	-2.03	5.27	4.78	4.93	5.28	4.30
X681.200012	4.65	10.44	4.85	5.13	2.34	5.18	4.87	7.88	7.65	4.03
X1033.489990	3.18	4.77	4.85	0.57	3.08	3.30	3.52	5.23	3.56	4.32
X1981.859985	4.44	2.84	4.85	-1.54	1.92	1.99	0.27	2.44	3.01	3.79

X1497.630005 4.75 6.57 4.84 4.46 0.29 4.84 3.74 5.53 3.17 4.37

X1043.589966 2.23 4.41 4.83 2.84 2.05 1.72 2.64 5.52 2.03 5.32

X752.429993 4.77 6.59 4.82 4.59 3.87 2.60 3.74 7.27 2.88 5.87

X833.830017 2.93 4.37 4.75 2.08 3.20 4.20 2.53 3.36 1.39 3.19

X922.539978 1.64 3.94 4.73 1.10 1.58 4.38 3.14 5.12 -1.06 1.69

X915.229980 1.34 5.14 4.71 3.48 3.95 3.07 4.45 3.49 1.97 3.62

X1467.329956 4.20 3.70 4.67 -0.55 -1.20 4.85 4.19 3.16 0.95 4.68

X803.299988 2.07 3.83 4.65 3.60 3.35 2.56 4.14 4.54 2.10 3.62

X1537.920044 3.35 4.74 4.65 2.55 1.73 3.00 4.51 4.86 3.81 1.19

X630.320007 3.72 6.03 4.63 2.91 0.43 2.38 3.72 5.72 6.15 3.76

X962.909973 2.19 4.93 4.58 1.32 2.22 3.42 2.78 3.49 3.72 3.45

X742.250000 2.23 5.14 4.55 3.82 2.87 4.90 3.32 4.00 -0.14 3.90

X1548.020020 2.71 4.21 4.55 0.55 0.59 3.72 2.71 2.50 3.15 2.43

X823.650024 3.43 4.49 4.54 4.21 4.17 1.47 4.55 4.40 1.98 4.29

X1507.729980 4.39 5.14 4.47 3.49 -0.96 4.39 2.83 4.03 4.36 3.83

X813.479980 2.63 5.52 4.46 3.58 5.29 3.69 4.11 6.79 2.35 5.43

X2234.120117 5.79 5.37 4.39 3.58 2.20 4.00 4.99 5.36 4.34 4.36

X1568.219971 3.63 3.79 4.36 3.11 2.56 2.31 2.03 3.48 3.48 3.07

X2224.030029 6.40 6.32 4.36 5.71 0.98 4.72 4.58 4.86 5.24 4.84

X487.869995 6.70 6.81 4.32 4.60 0.09 4.84 3.52 6.62 3.74 4.74

X864.349976 2.46 5.35 4.32 1.77 5.72 2.34 4.09 5.90 1.97 5.20

X1628.810059 3.46 4.59 4.29 0.99 1.57 2.61 3.19 2.66 3.97 2.75

X548.919983 4.31 7.44 4.28 5.09 -2.56 4.11 6.62 4.34 3.07 4.29

X952.820007 3.20 5.01 4.22 1.37 0.84 3.50 2.65 4.77 2.99 1.98

X732.070007 2.54 3.52 4.21 3.53 4.62 6.04 5.15 2.97 1.70 3.51

X2062.550049 4.41 1.42 4.20 -0.06 -1.27 3.84 -0.02 2.72 2.29 4.48

X1729.699951 3.03 4.76 4.17 1.77 2.17 3.42 1.20 5.56 4.57 3.28

X1104.189941 3.03 4.27 4.16 2.74 5.72 3.27 4.20 4.79 2.28 5.60

X1477.430054 0.70 2.91 4.14 -1.53 -1.41 3.07 3.52 3.01 2.59 3.83

X762.599976 1.74 6.93 4.12 5.11 5.08 5.74 5.30 6.16 1.40 4.03

X2153.340088 6.03 5.23 4.05 2.91 4.28 4.31 4.10 5.02 3.30 5.58

X844.000000 2.28 4.98 4.01 4.59 2.94 3.31 4.34 5.22 0.02 3.98

X498.040009 8.37 6.34 3.97 4.02 1.57 3.38 4.81 3.93 4.38 5.31

X1527.920044 4.44 5.13 3.97 3.10 0.40 3.68 4.89 4.32 4.37 5.00

X2193.729980 5.79 6.28 3.94 2.68 2.07 4.36 2.91 4.41 3.92 4.75

X1023.400024 2.60 4.14 3.87 2.87 5.23 3.73 4.92 3.30 3.55 4.85

X1285.760010 2.65 5.45 3.84 1.30 1.55 5.63 4.17 4.97 5.38 4.48

X2143.340088 5.09 5.77 3.84 0.21 1.15 3.44 3.00 5.06 2.31 5.03

X2304.709961 4.04 2.63 3.82 2.11 1.73 2.63 2.40 4.14 3.88 3.78

X1295.859985 2.46 4.03 3.78 1.98 1.81 3.21 2.26 3.70 6.06 4.32

X1558.119995 2.86 3.86 3.75 3.12 2.60 3.37 1.96 2.79 3.76 3.22

X1618.709961 2.65 4.04 3.72 2.21 1.81 4.16 3.59 4.70 5.48 3.20

X2042.449951 3.98 3.08 3.69 0.25 -0.64 4.47 2.18 4.55 1.25 3.34

X854.179993 3.92 4.43 3.68 4.21 4.56 3.06 3.32 4.24 2.50 5.51

X1790.189941 0.87 3.91 3.66 -0.86 1.61 4.81 2.76 4.03 1.85 2.45

X1305.959961 4.09 5.33 3.65 0.89 2.04 6.05 3.57 5.97 6.32 4.32

X579.450012 3.70 4.03 3.63 4.45 -1.68 3.51 5.35 2.17 0.26 3.38

X1053.689941 4.75 5.47 3.59 3.55 4.22 3.89 4.47 5.74 4.29 5.71

X559.090027 4.53 6.87 3.57 3.94 -2.63 4.61 6.27 3.38 0.80 4.03

X1457.229980 5.10 3.93 3.57 -1.78 2.12 5.41 1.32 3.59 2.49 4.30

X2082.750000 4.23 3.01 3.39 2.04 0.48 4.28 3.22 2.45 0.60 4.38

X1749.790039 4.15 5.29 3.32 3.57 3.52 3.36 1.63 4.51 3.77 3.33

X1759.890015 2.46 3.77 3.27 1.79 1.55 4.50 3.24 4.27 3.73 1.88

X2264.320068 6.17 6.15 3.27 3.80 2.62 3.06 3.28 7.00 2.10 6.14

X1709.500000 2.97 4.19 3.19 0.90 2.84 3.57 1.48 3.61 3.23 2.68

X1336.150024 3.39 5.61 3.16 1.81 1.35 1.04 2.08 5.00 4.17 5.21

X2123.139893 6.83 6.23 3.16 3.07 0.75 4.56 3.48 7.98 2.02 4.19

X538.739990 4.29 6.10 3.15 1.53 0.81 3.87 7.42 4.19 3.74 4.99

X1780.089966 0.91 2.88 3.15 0.81 -0.72 3.40 2.99 3.45 2.77 2.88

X1679.199951 1.97 4.55 3.10 3.95 0.98 0.25 2.74 4.07 4.25 1.70

X1003.299988 3.81 4.07 3.09 3.12 5.27 3.09 4.68 3.75 2.16 5.13

X925.409973 2.42 3.71 3.08 3.84 1.12 3.90 2.61 3.19 -1.10 3.57

X426.820007 3.22 5.81 3.06 1.09 -1.33 2.16 1.69 0.18 0.62 1.39

X1245.359985 3.81 5.31 3.05 1.37 3.69 3.76 3.96 3.86 5.52 5.44

X983.080017 3.17 4.43 2.99 3.21 4.35 4.63 4.19 6.08 2.12 3.26

X436.989990 2.73 2.79 2.83 -0.41 -0.44 2.24 1.40 1.40 2.35 1.36

X2052.449951 2.33 3.55 2.83 0.00 -0.73 1.65 2.12 3.74 -0.25 -0.71

X2314.810059 2.05 -0.04 2.82 0.87 1.79 1.46 3.33 4.09 2.17 2.55

X2284.520020 3.06 2.18 2.80 1.13 1.73 3.88 1.95 3.83 -0.01 4.05

X2183.629883 3.68 4.78 2.79 3.32 1.84 4.36 3.91 4.53 3.95 6.32

X1719.599976 1.82 4.32 2.78 2.28 3.80 2.94 3.63 4.44 5.15 3.24

X1659.000000 3.29 4.48 2.74 3.13 2.55 2.17 1.82 4.93 4.47 2.52

X2355.209961 0.69 0.26 2.74 -0.77 2.39 0.99 3.08 1.85 1.31 3.94

X1638.810059 3.28 3.24 2.73 3.07 3.44 1.98 3.07 4.02 3.76 2.55

X912.450012 0.50 2.56 2.72 2.60 2.27 2.63 1.56 2.38 1.16 -1.87

X1255.459961 3.42 5.86 2.69 3.12 3.82 3.36 4.48 4.00 4.54 4.63

X2274.419922 4.53 4.62 2.62 2.91 1.28 1.88 3.54 5.39 2.34 6.07

X2072.649902 4.13 4.73 2.61 1.89 0.00 3.38 2.11 3.06 0.14 3.90

X2092.840088 4.55 2.33 2.58 0.97 1.69 3.93 1.53 1.61 3.16 4.47

X1164.680054 2.95 4.46 2.57 3.14 2.94 6.26 2.32 3.00 4.60 4.08

X972.989990 1.82 3.77 2.56 0.84 1.88 3.09 3.24 4.93 0.20 2.88

X2345.110107 4.71 1.50 2.52 -2.22 2.75 3.04 2.23 2.83 2.83 3.33

X1235.270020 3.26 4.99 2.51 1.98 4.03 4.73 3.92 5.34 4.86 5.02

X1013.299988 2.56 4.17 2.46 2.04 5.09 4.01 3.15 3.59 2.40 4.98

X1669.099976 3.01 4.92 2.42 0.58 3.20 2.33 1.76 4.35 4.50 2.50

X2163.429932 6.20 5.18 2.31 0.86 2.16 3.73 3.30 4.34 3.47 5.42

X2365.199951 1.10 3.27 2.29 0.16 -0.51 1.52 1.96 2.46 0.03 3.51

X874.530029 4.30 5.04 2.23 3.54 4.64 2.37 3.04 4.73 3.12 5.58

X905.049988 2.79 3.57 2.23 3.49 3.79 2.51 3.78 4.40 2.23 4.46

X1265.560059 2.58 3.78 2.23 3.01 1.92 1.39 4.92 3.35 4.10 3.55

X1215.170044 3.24 5.57 2.21 3.06 1.57 4.00 4.17 5.11 5.03 4.51

X1739.699951 3.80 4.57 2.16 1.94 2.28 1.30 1.49 4.46 3.59 3.10

X1124.280029 0.52 2.83 2.13 0.99 3.60 2.27 2.29 1.77 3.35 2.88

X1225.170044 2.97 3.52 2.12 2.33 3.60 3.11 4.24 4.45 3.69 4.09

X1426.939941 3.96 3.03 2.12 0.63 1.26 0.64 1.14 4.46 -0.49 2.12

X1588.420044 3.83 3.35 2.09 2.74 2.95 2.51 0.61 4.31 3.79 2.32

X1699.400024 2.89 4.68 2.07 0.92 2.57 2.67 2.63 4.31 3.62 3.01

X1578.319946 3.13 4.23 2.06 2.00 3.27 2.68 3.77 3.70 4.27 1.64

X2102.939941 5.41 3.29 1.90 3.14 3.22 3.69 2.51 4.27 4.86 5.51

X2203.830078 5.85 5.44 1.89 2.56 -0.90 3.74 1.77 2.60 2.91 6.15

X1184.869995 3.17 3.49 1.88 0.09 3.71 5.43 3.03 4.97 3.64 4.18

X1608.609985 3.05 5.25 1.82 2.93 2.96 4.84 2.31 4.02 3.42 2.51

X1083.989990 4.93 5.19 1.80 3.00 5.46 3.85 4.94 5.23 4.69 5.54

X1689.300049 2.11 5.04 1.77 -0.01 2.84 3.55 0.75 3.50 3.97 1.61

X1154.579956 2.15 4.97 1.75 0.66 2.23 2.77 5.31 2.86 5.95 3.58

X457.339996 5.18 4.36 1.67 2.50 1.01 2.58 5.29 4.57 0.81 4.12

X1275.660034 3.05 6.28 1.67 1.94 3.53 6.07 4.08 4.63 5.42 4.62

X1326.050049 4.45 6.53 1.63 1.24 3.36 4.80 4.79 4.67 4.92 4.27

X2032.349976 3.22 3.32 1.61 0.22 3.45 2.81 3.44 2.60 1.22 3.06

X528.570007 5.26 7.38 1.59 5.17 0.49 3.91 6.09 4.17 2.37 4.60

X467.519989 6.27 4.49 1.53 1.12 -1.86 5.20 4.47 4.36 1.88 2.67

X993.169983 2.58 3.57 1.50 3.83 4.57 2.72 4.50 4.20 1.78 3.70

X1598.510010 3.17 4.72 1.48 3.17 2.04 2.84 1.71 3.67 2.91 1.78

X2012.150024 2.03 0.34 1.47 1.68 0.54 0.79 2.12 2.54 -0.35 1.40

X1174.770020 2.79 4.29 1.46 1.19 3.99 3.99 4.96 4.97 3.56 4.07

X1114.189941 3.20 5.34 1.44 0.48 4.32 2.86 3.43 5.86 2.78 4.19

X1073.890015 4.58 4.25 1.34 2.14 4.98 2.99 3.99 3.70 4.37 4.63

X1447.140015 2.27 1.85 1.33 1.96 -0.69 2.84 3.55 3.90 3.33 2.08

X1316.050049 3.81 6.92 1.30 1.79 3.58 5.77 3.48 5.82 5.96 4.64

X2113.040039 4.55 3.77 1.30 1.46 3.09 3.32 1.55 3.60 2.85 4.68

X1205.069946 1.91 3.12 1.22 1.65 2.85 4.58 3.82 4.20 4.27 3.81

X2294.610107 3.59 3.58 1.20 0.72 1.96 3.59 3.37 0.73 1.30 5.00

X1346.250000 3.46 3.61 1.18 -1.40 0.78 -0.12 0.73 7.48 -0.33 4.38

X2173.530029 6.02 6.10 1.17 1.00 1.70 3.91 4.11 3.43 3.02 5.20

X2213.929932 5.76 4.97 1.10 2.64 -0.06 4.11 1.88 2.44 3.45 5.29

X942.729980 1.22 2.70 1.02 0.92 1.15 3.74 0.26 1.35 0.71 -1.16

X1648.900024 1.78 5.27 0.93 3.71 1.05 2.59 0.22 3.27 3.64 1.77

X1144.479980 2.17 3.24 0.66 1.33 3.03 4.38 3.59 5.04 5.35 4.44

X1810.380005 2.62 2.00 0.62 -0.49 1.76 1.90 2.14 3.07 0.51 0.84

X1961.660034 0.95 1.86 0.59 1.32 1.32 2.12 1.65 1.07 0.45 2.66

X932.640015 1.19 4.82 0.53 0.12 -0.40 1.45 1.92 1.83 -1.34 1.05

X1800.290039 1.78 1.74 0.47 1.08 4.49 2.66 2.70 1.90 0.80 1.14

X2254.219971	6.33	5.63	0.45	3.02	3.17	4.22	-0.49	5.13	2.68	5.11
X2022.250000	3.47	4.17	0.25	1.41	2.27	2.06	0.81	2.87	-0.02	2.75
X1194.969971	2.16	3.97	0.23	2.15	2.19	4.18	2.71	4.34	4.20	4.05
X447.170013	6.35	5.23	0.11	0.81	2.88	2.49	3.01	5.35	2.22	3.35
X1437.040039	-0.13	0.42	-0.06	2.15	0.94	0.60	3.80	3.27	0.07	1.37
X1134.380005	3.39	5.47	-0.55	-0.45	4.20	4.17	1.63	5.10	2.89	5.66
X2002.060059	1.50	2.05	-0.56	-1.42	1.05	1.02	3.21	2.46	-0.23	1.63
X2335.010010	2.90	3.74	-1.05	0.76	4.16	2.52	2.03	1.23	1.35	3.20
X1971.760010	3.75	3.18	-1.10	0.93	2.65	0.88	-0.45	3.24	-0.71	3.77
X2244.219971	5.78	6.61	-2.26	1.78	2.83	4.40	1.24	6.16	0.22	4.42
X2324.909912	4.03	5.33	-2.89	1.99	4.15	2.98	1.54	2.58	0.47	4.61

	MeanDecreaseAccuracy	MeanDecreaseGini
X701.549988	15.39	5.10
X2133.239990	10.39	3.81
X711.719971	10.82	2.49
X894.880005	10.88	3.07
X640.500000	9.56	2.81
X1991.959961	8.75	1.49
X691.369995	10.36	4.33
X508.220001	9.63	3.18
X1063.790039	9.19	2.73
X1769.989990	6.27	1.85
X772.780029	9.65	2.21
X650.669983	9.01	3.43
X518.390015	8.05	2.72
X620.150024	7.56	2.28
X609.969971	7.73	2.21
X1487.530029	6.19	1.91
X782.950012	9.18	2.29
X721.900024	9.52	2.37
X671.020020	10.37	3.86
X884.700012	8.19	2.42
X589.619995	10.27	2.00

X477.690002	9.82	3.92
X1094.089966	9.38	2.40
X793.130005	8.84	2.37
X599.799988	7.71	1.99
X660.849976	10.30	4.02
X569.270020	10.57	2.43
X1517.829956	7.77	2.80
X681.200012	11.72	4.08
X1033.489990	8.19	2.02
X1981.859985	8.68	1.51
X1497.630005	6.37	2.79
X1043.589966	8.49	2.13
X752.429993	10.68	3.09
X833.830017	7.51	2.08
X922.539978	7.83	1.64
X915.229980	8.03	1.95
X1467.329956	10.27	2.30
X803.299988	7.90	2.03
X1537.920044	6.95	1.91
X630.320007	7.13	2.44
X962.909973	8.50	1.86
X742.250000	8.40	2.13
X1548.020020	6.85	1.48
X823.650024	8.30	2.18
X1507.729980	6.21	2.15
X813.479980	9.88	2.63
X2234.120117	6.64	2.58
X1568.219971	5.64	1.68
X2224.030029	7.63	2.94
X487.869995	9.19	3.33
X864.349976	9.38	2.49
X1628.810059	7.18	1.58
X548.919983	10.86	2.54

X952.820007	7.97	1.72
X732.070007	8.41	2.16
X2062.550049	6.48	1.56
X1729.699951	5.79	1.83
X1104.189941	8.79	2.44
X1477.430054	7.03	1.58
X762.599976	9.78	2.70
X2153.340088	6.85	2.85
X844.000000	8.49	2.19
X498.040009	9.24	2.93
X1527.920044	6.69	2.08
X2193.729980	6.61	2.70
X1023.400024	8.49	2.12
X1285.760010	9.29	2.38
X2143.340088	6.51	2.26
X2304.709961	4.96	1.98
X1295.859985	8.62	2.08
X1558.119995	5.90	1.59
X1618.709961	6.55	1.78
X2042.449951	6.68	1.47
X854.179993	8.73	2.37
X1790.189941	4.93	1.39
X1305.959961	9.26	2.38
X579.450012	6.29	1.81
X1053.689941	9.37	2.93
X559.090027	10.36	2.32
X1457.229980	9.89	2.00
X2082.750000	6.46	1.58
X1749.790039	5.54	1.79
X1759.890015	5.33	1.55
X2264.320068	7.54	3.10
X1709.500000	4.92	1.74
X1336.150024	8.20	1.82

X2123.139893	8.34	2.68
X538.739990	9.89	2.38
X1780.089966	4.43	1.32
X1679.199951	6.91	1.77
X1003.299988	8.21	2.37
X925.409973	6.26	1.61
X426.820007	6.36	1.44
X1245.359985	9.19	2.32
X983.080017	8.70	2.11
X436.989990	5.13	1.16
X2052.449951	5.80	1.25
X2314.810059	5.03	1.48
X2284.520020	5.60	1.67
X2183.629883	6.77	2.37
X1719.599976	5.88	1.83
X1659.000000	5.56	1.62
X2355.209961	5.61	1.19
X1638.810059	4.93	1.42
X912.450012	4.84	1.36
X1255.459961	8.45	2.26
X2274.419922	6.53	2.28
X2072.649902	7.00	1.56
X2092.840088	6.51	1.70
X1164.680054	8.63	2.08
X972.989990	6.61	1.70
X2345.110107	7.45	1.45
X1235.270020	9.32	2.24
X1013.299988	8.18	2.07
X1669.099976	5.24	1.46
X2163.429932	7.97	2.36
X2365.199951	5.17	1.16
X874.530029	8.60	2.51
X905.049988	7.93	2.10

X1265.560059	8.24	1.70
X1215.170044	7.85	2.20
X1739.699951	5.61	1.64
X1124.280029	5.93	1.34
X1225.170044	7.24	1.87
X1426.939941	6.30	1.39
X1588.420044	4.58	1.55
X1699.400024	5.98	1.36
X1578.319946	7.16	1.54
X2102.939941	6.46	2.08
X2203.830078	8.44	1.98
X1184.869995	8.02	1.89
X1608.609985	5.02	1.68
X1083.989990	8.88	3.02
X1689.300049	4.40	1.46
X1154.579956	8.16	2.01
X457.339996	8.18	2.00
X1275.660034	9.05	2.39
X1326.050049	8.42	2.44
X2032.349976	5.40	1.32
X528.570007	10.72	2.64
X467.519989	8.94	2.21
X993.169983	7.29	1.84
X1598.510010	6.08	1.53
X2012.150024	3.97	0.67
X1174.770020	7.66	1.82
X1114.189941	8.17	2.07
X1073.890015	7.97	2.44
X1447.140015	6.51	1.52
X1316.050049	9.80	2.40
X2113.040039	5.93	1.94
X1205.069946	7.33	2.00
X2294.610107	6.80	1.56

X1346.250000	8.59	1.62
X2173.530029	7.24	2.12
X2213.929932	6.59	2.16
X942.729980	4.60	1.16
X1648.900024	4.52	1.37
X1144.479980	8.27	2.11
X1810.380005	4.86	1.21
X1961.660034	4.09	0.79
X932.640015	4.63	1.22
X1800.290039	6.13	1.31
X2254.219971	8.31	2.21
X2022.250000	5.11	1.28
X1194.969971	7.34	1.92
X447.170013	9.56	1.92
X1437.040039	3.88	1.49
X1134.380005	8.10	2.59
X2002.060059	3.66	0.53
X2335.010010	7.40	1.55
X1971.760010	6.57	1.13
X2244.219971	8.14	2.22
X2324.909912	7.61	1.54

Time taken: 4.58 secs

Rattle timestamp: 2022-10-23 18:15:36 Chilufyam

==========

Appendix 6.4: Backward Stepwise Variable Elimination Iterations

```
R version 4.1.3 (2022-03-10) -- "One Push-Up"
Copyright (C) 2022 The R Foundation for Statistical Computing
Platform: x86_64-w64-mingw32/x64 (64-bit)

R is free software and comes with ABSOLUTELY NO WARRANTY.
You are welcome to redistribute it under certain conditions.
Type 'license()' or 'licence()' for distribution details.

  Natural language support but running in an English locale

R is a collaborative project with many contributors.
Type 'contributors()' for more information and
'citation()' on how to cite R or R packages in publications.

Type 'demo()' for some demos, 'help()' for on-line help, or
'help.start()' for an HTML browser interface to help.
Type 'q()' to quit R.

[Previously saved workspace restored]

> library (rattle)
Loading required package: tibble
Loading required package: bitops
Rattle: A free graphical interface for data science with R.
Version 5.5.1 Copyright (c) 2006-2021 Togaware Pty Ltd.
Type 'rattle()' to shake, rattle, and roll your data.
> rattle()

> g=read.csv(file.choose(),header=T)
> summary(g)
    Class       X447.170013     X477.690002      X508.220001
```

Min. : 1.000 Min. :-967.0 Min. :-233.00 Min. :-179.0

1st Qu.: 3.000 1st Qu.:-564.2 1st Qu.: -72.00 1st Qu.: -1.0

Median : 6.000 Median :-436.0 Median : 41.00 Median : 154.0

Mean : 5.503 Mean :-432.9 Mean : 35.33 Mean : 139.2

3rd Qu.: 8.000 3rd Qu.:-325.0 3rd Qu.: 112.00 3rd Qu.: 231.0

Max. :10.000 Max. : 85.0 Max. : 435.00 Max. : 624.0

X528.570007 X538.739990 X548.919983 X559.090027

Min. :-127.0 Min. : 78.0 Min. : 88.0 Min. :100.0

1st Qu.: 64.0 1st Qu.:256.0 1st Qu.:280.0 1st Qu.:293.0

Median : 242.0 Median :426.0 Median :459.0 Median :491.0

Mean : 228.7 Mean :410.6 Mean :443.1 Mean :470.8

3rd Qu.: 346.5 3rd Qu.:525.0 3rd Qu.:568.0 3rd Qu.:605.8

Max. : 743.0 Max. :846.0 Max. :916.0 Max. :943.0

X569.270020 X589.619995 X640.500000 X660.849976

Min. : 74.0 Min. : 39.0 Min. :-66.0 Min. : 60.0

1st Qu.:261.0 1st Qu.:219.0 1st Qu.:152.0 1st Qu.: 228.0

Median :475.0 Median :453.5 Median :416.0 Median : 496.5

Mean :451.2 Mean :416.3 Mean :371.6 Mean : 457.1

3rd Qu.:595.0 3rd Qu.:557.8 3rd Qu.:542.8 3rd Qu.: 632.0

Max. :923.0 Max. :934.0 Max. :929.0 Max. :1015.0

X671.020020 X681.200012 X691.369995 X701.549988

Min. : 23.0 Min. : 49.0 Min. : 54.0 Min. : 148.0

1st Qu.: 214.5 1st Qu.: 212.5 1st Qu.: 250.2 1st Qu.: 366.2

Median : 483.0 Median : 496.0 Median : 550.0 Median : 661.5

Mean : 447.6 Mean : 464.1 Mean : 511.0 Mean : 628.9

3rd Qu.: 633.0 3rd Qu.: 659.8 3rd Qu.: 718.0 3rd Qu.: 828.0

Max. :1008.0 Max. :1047.0 Max. :1137.0 Max. :1204.0

X711.719971 X721.900024 X752.429993 X762.599976 X772.780029

Min. : 61 Min. : 92 Min. : 61 Min. : 99 Min. : 92

1st Qu.: 677 1st Qu.:1011 1st Qu.:1644 1st Qu.:1658 1st Qu.:1698

Median :1015 Median :1267 Median :1913 Median :1963 Median :2037

Mean : 953 Mean :1237 Mean :1851 Mean :1899 Mean :1962

3rd Qu.:1173 3rd Qu.:1449 3rd Qu.:2155 3rd Qu.:2203 3rd Qu.:2287

```
 Max.   :1685   Max.   :2106   Max.   :3729   Max.   :3599   Max.   :3554
  X813.479980    X864.349976    X894.880005    X1053.689941   X1094.089966
 Min.   : 269   Min.   : 200   Min.   : 196   Min.   : 177   Min.   : 194
 1st Qu.:1976   1st Qu.:2142   1st Qu.:2226   1st Qu.:2530   1st Qu.:2470
 Median :2265   Median :2448   Median :2545   Median :2847   Median :2774
 Mean   :2187   Mean   :2373   Mean   :2467   Mean   :2779   Mean   :2701
 3rd Qu.:2508   3rd Qu.:2734   3rd Qu.:2829   3rd Qu.:3175   3rd Qu.:3089
 Max.   :4056   Max.   :4319   Max.   :4464   Max.   :4611   Max.   :4416
  X1235.270020   X1316.050049   X1457.229980    X1467.329956
 Min.   :  -4   Min.   : 222   Min.   :-142.0   Min.   :-188.0
 1st Qu.:2094   1st Qu.:1850   1st Qu.: 318.0   1st Qu.: 255.2
 Median :2580   Median :2319   Median : 624.0   Median : 548.5
 Mean   :2509   Mean   :2285   Mean   : 638.9   Mean   : 590.3
 3rd Qu.:3020   3rd Qu.:2764   3rd Qu.: 878.0   3rd Qu.: 837.5
 Max.   :3758   Max.   :3375   Max.   :2174.0   Max.   :2319.0
  X2133.239990
 Min.   : -29.0
 1st Qu.: 251.2
 Median : 658.0
 Mean   : 667.4
 3rd Qu.: 907.0
 Max.   :2478.0
> p=lm(Class~.,data=(g))
> summary(p)


Call:
lm(formula = Class ~ ., data = (g))

Residuals:
    Min      1Q  Median      3Q     Max
-6.1600 -1.6653 -0.0632  1.9376  7.0527
```

Coefficients:

	Estimate	Std. Error	t value	Pr(>|t|)	
(Intercept)	2.9965321	1.3119089	2.284	0.022602	*
X447.170013	-0.0015457	0.0010040	-1.540	0.124017	
X477.690002	0.0027758	0.0028565	0.972	0.331435	
X508.220001	-0.0106970	0.0031833	-3.360	0.000812	***
X528.570007	-0.0115772	0.0034215	-3.384	0.000747	***
X538.739990	-0.0019734	0.0040139	-0.492	0.623085	
X548.919983	0.0068487	0.0042420	1.614	0.106777	
X559.090027	0.0126349	0.0045841	2.756	0.005967	**
X569.270020	0.0019324	0.0047485	0.407	0.684153	
X589.619995	0.0033652	0.0049641	0.678	0.498010	
X640.500000	0.0045136	0.0042945	1.051	0.293539	
X660.849976	0.0042085	0.0047315	0.889	0.373996	
X671.020020	0.0053540	0.0050116	1.068	0.285665	
X681.200012	-0.0119508	0.0048523	-2.463	0.013970	*
X691.369995	-0.0123627	0.0046443	-2.662	0.007911	**
X701.549988	0.0132643	0.0046076	2.879	0.004089	**
X711.719971	-0.0091907	0.0040196	-2.286	0.022462	*
X721.900024	0.0104228	0.0038969	2.675	0.007619	**
X752.429993	-0.0034746	0.0033273	-1.044	0.296643	
X762.599976	-0.0014299	0.0026129	-0.547	0.584355	
X772.780029	-0.0066212	0.0019921	-3.324	0.000925	***
X813.479980	-0.0007823	0.0028032	-0.279	0.780244	
X864.349976	0.0031237	0.0021494	1.453	0.146500	
X894.880005	0.0015370	0.0014840	1.036	0.300592	
X1053.689941	0.0052063	0.0009809	5.307	0.000000141	***
X1094.089966	0.0001150	0.0010580	0.109	0.913433	
X1235.270020	-0.0065959	0.0013048	-5.055	0.000000523	***
X1316.050049	0.0008727	0.0012463	0.700	0.483969	
X1457.229980	-0.0002710	0.0011776	-0.230	0.818052	
X1467.329956	-0.0001314	0.0008583	-0.153	0.878345	
X2133.239990	0.0022347	0.0005821	3.839	0.000132	***

```
---Signif. codes:  0 ‘***’ 0.001 ‘**’ 0.01 ‘*’ 0.05 ‘.’ 0.1 ‘ ’ 1

Residual standard error: 2.515 on 883 degrees of freedom
Multiple R-squared:  0.2572,    Adjusted R-squared:  0.232
F-statistic: 10.19 on 30 and 883 DF,  p-value: < 2.2e-16

> p=update(g,.~.- X1094.089966)
Error in update.default(g, . ~ . - X1094.089966) :
  need an object with call component
> p=update(p,.~.-X1094.089966)
> summary(p)

Call:
lm(formula = Class ~ X447.170013 + X477.690002 + X508.220001 +
    X528.570007 + X538.739990 + X548.919983 + X559.090027 + X569.270020 +
    X589.619995 + X640.500000 + X660.849976 + X671.020020 + X681.200012 +
    X691.369995 + X701.549988 + X711.719971 + X721.900024 + X752.429993 +
    X762.599976 + X772.780029 + X813.479980 + X864.349976 + X894.880005 +
    X1053.689941 + X1235.270020 + X1316.050049 + X1457.229980 +
    X1467.329956 + X2133.239990, data = (g))

Residuals:
    Min      1Q  Median      3Q     Max
-6.1653 -1.6548 -0.0613  1.9359  7.0435

Coefficients:
             Estimate Std. Error t value      Pr(>|t|)
(Intercept)   3.0149984  1.3001442   2.319      0.020624 *
X447.170013  -0.0015408  0.0010024  -1.537      0.124618
X477.690002   0.0027813  0.0028545   0.974      0.330146
X508.220001  -0.0106825  0.0031787  -3.361      0.000811 ***
X528.570007  -0.0116037  0.0034109  -3.402      0.000699 ***
X538.739990  -0.0019856  0.0040101  -0.495      0.620616
```

```
X548.919983   0.0068425  0.0042393   1.614     0.106868
X559.090027   0.0126173  0.0045786   2.756     0.005978 **
X569.270020   0.0019313  0.0047459   0.407     0.684148
X589.619995   0.0033972  0.0049526   0.686     0.492927
X640.500000   0.0045193  0.0042918   1.053     0.292628
X660.849976   0.0041786  0.0047209   0.885     0.376328
X671.020020   0.0053518  0.0050087   1.068     0.285587
X681.200012  -0.0119338  0.0048470  -2.462     0.014003 *
X691.369995  -0.0123943  0.0046325  -2.675     0.007600 **
X701.549988   0.0132658  0.0046050   2.881     0.004063 **
X711.719971  -0.0092107  0.0040131  -2.295     0.021958 *
X721.900024   0.0104455  0.0038891   2.686     0.007370 **
X752.429993  -0.0034801  0.0033250  -1.047     0.295560
X762.599976  -0.0014412  0.0026094  -0.552     0.580883
X772.780029  -0.0066041  0.0019847  -3.327     0.000913 ***
X813.479980  -0.0007730  0.0028003  -0.276     0.782580
X864.349976   0.0031264  0.0021481   1.455     0.145896
X894.880005   0.0015494  0.0014788   1.048     0.295022
X1053.689941  0.0052507  0.0008913   5.891 0.00000000544 ***
X1235.270020 -0.0065566  0.0012531  -5.232 0.00000020898 ***
X1316.050049  0.0008867  0.0012390   0.716     0.474375
X1457.229980 -0.0002781  0.0011751  -0.237     0.812967
X1467.329956 -0.0001276  0.0008571  -0.149     0.881668
X2133.239990  0.0022362  0.0005816   3.845     0.000129 ***
---
Signif. codes:  0 ‘***’ 0.001 ‘**’ 0.01 ‘*’ 0.05 ‘.’ 0.1 ‘ ’ 1

Residual standard error: 2.513 on 884 degrees of freedom
Multiple R-squared:  0.2572,    Adjusted R-squared:  0.2329
F-statistic: 10.56 on 29 and 884 DF,  p-value: < 2.2e-16

> p=update(p,.~.-X1467.329956)
> summary(p)
```

```
Call:
lm(formula = Class ~ X447.170013 + X477.690002 + X508.220001 +
    X528.570007 + X538.739990 + X548.919983 + X559.090027 + X569.270020 +
    X589.619995 + X640.500000 + X660.849976 + X671.020020 + X681.200012 +
    X691.369995 + X701.549988 + X711.719971 + X721.900024 + X752.429993 +
    X762.599976 + X772.780029 + X813.479980 + X864.349976 + X894.880005 +
    X1053.689941 + X1235.270020 + X1316.050049 + X1457.229980 +
    X2133.239990, data = (g))

Residuals:
    Min      1Q  Median      3Q     Max
-6.1706 -1.6584 -0.0665  1.9316  7.0314

Coefficients:
             Estimate Std. Error t value      Pr(>|t|)
(Intercept)   3.0080861  1.2985971   2.316     0.020763 *
X447.170013  -0.0015448  0.0010015  -1.543     0.123299
X477.690002   0.0027616  0.0028498   0.969     0.332790
X508.220001  -0.0106416  0.0031651  -3.362     0.000806 ***
X528.570007  -0.0115833  0.0034063  -3.401     0.000702 ***
X538.739990  -0.0019950  0.0040074  -0.498     0.618726
X548.919983   0.0068172  0.0042335   1.610     0.107691
X559.090027   0.0126658  0.0045645   2.775     0.005640 **
X569.270020   0.0019419  0.0047427   0.409     0.682305
X589.619995   0.0033789  0.0049483   0.683     0.494890
X640.500000   0.0044575  0.0042694   1.044     0.296735
X660.849976   0.0041963  0.0047168   0.890     0.373897
X671.020020   0.0053896  0.0049995   1.078     0.281315
X681.200012  -0.0119608  0.0048410  -2.471     0.013670 *
X691.369995  -0.0123600  0.0046242  -2.673     0.007659 **
X701.549988   0.0132577  0.0046022   2.881     0.004063 **
X711.719971  -0.0091973  0.0040099  -2.294     0.022044 *
X721.900024   0.0104297  0.0038855   2.684     0.007405 **
```

```
X752.429993  -0.0034894  0.0033226  -1.050      0.293909
X762.599976  -0.0014361  0.0026078  -0.551      0.581967
X772.780029  -0.0066120  0.0019829  -3.334      0.000890 ***
X813.479980  -0.0007676  0.0027985  -0.274      0.783930
X864.349976   0.0031283  0.0021468   1.457      0.145430
X894.880005   0.0015455  0.0014777   1.046      0.295901
X1053.689941  0.0052545  0.0008904   5.901 0.00000000514 ***
X1235.270020 -0.0065496  0.0012515  -5.233 0.00000020786 ***
X1316.050049  0.0008899  0.0012381   0.719      0.472492
X1457.229980 -0.0004408  0.0004318  -1.021      0.307512
X2133.239990  0.0022447  0.0005785   3.880      0.000112 ***
---
Signif. codes:  0 '***' 0.001 '**' 0.01 '*' 0.05 '.' 0.1 ' ' 1

Residual standard error: 2.512 on 885 degrees of freedom
Multiple R-squared:  0.2572,    Adjusted R-squared:  0.2337
F-statistic: 10.94 on 28 and 885 DF,  p-value: < 2.2e-16

> p=update(p,.~.-X813.479980)
> summary(p)

Call:
lm(formula = Class ~ X447.170013 + X477.690002 + X508.220001 +
    X528.570007 + X538.739990 + X548.919983 + X559.090027 + X569.270020 +
    X589.619995 + X640.500000 + X660.849976 + X671.020020 + X681.200012 +
    X691.369995 + X701.549988 + X711.719971 + X721.900024 + X752.429993 +
    X762.599976 + X772.780029 + X864.349976 + X894.880005 + X1053.689941 +
    X1235.270020 + X1316.050049 + X1457.229980 + X2133.239990,
    data = (g))

Residuals:
   Min     1Q Median     3Q    Max
-6.147 -1.651 -0.076  1.960  6.997
```

Coefficients:

	Estimate	Std. Error	t value	Pr(>|t|)	
(Intercept)	2.9232435	1.2605605	2.319	0.020622	*
X447.170013	-0.0015660	0.0009980	-1.569	0.116977	
X477.690002	0.0027740	0.0028480	0.974	0.330317	
X508.220001	-0.0106267	0.0031630	-3.360	0.000813	***
X528.570007	-0.0115560	0.0034030	-3.396	0.000715	***
X538.739990	-0.0019308	0.0039984	-0.483	0.629300	
X548.919983	0.0068605	0.0042284	1.622	0.105054	
X559.090027	0.0126876	0.0045615	2.781	0.005526	**
X569.270020	0.0019227	0.0047397	0.406	0.685096	
X589.619995	0.0033889	0.0049456	0.685	0.493377	
X640.500000	0.0044470	0.0042670	1.042	0.297609	
X660.849976	0.0041732	0.0047136	0.885	0.376201	
X671.020020	0.0054796	0.0049862	1.099	0.272086	
X681.200012	-0.0119624	0.0048384	-2.472	0.013609	*
X691.369995	-0.0124792	0.0046014	-2.712	0.006816	**
X701.549988	0.0132410	0.0045993	2.879	0.004087	**
X711.719971	-0.0091917	0.0040077	-2.293	0.022054	*
X721.900024	0.0104522	0.0038826	2.692	0.007235	**
X752.429993	-0.0038855	0.0029909	-1.299	0.194251	
X762.599976	-0.0015480	0.0025743	-0.601	0.547774	
X772.780029	-0.0066340	0.0019803	-3.350	0.000842	***
X864.349976	0.0029750	0.0020717	1.436	0.151359	
X894.880005	0.0014487	0.0014342	1.010	0.312716	
X1053.689941	0.0052263	0.0008840	5.912	0.00000000481	***
X1235.270020	-0.0065067	0.0012410	-5.243	0.00000019766	***
X1316.050049	0.0008483	0.0012282	0.691	0.489911	
X1457.229980	-0.0004344	0.0004309	-1.008	0.313664	
X2133.239990	0.0022492	0.0005779	3.892	0.000107	***

Signif. codes: 0 ‘***’ 0.001 ‘**’ 0.01 ‘*’ 0.05 ‘.’ 0.1 ‘ ’ 1

```
Residual standard error: 2.51 on 886 degrees of freedom
Multiple R-squared:  0.2571,    Adjusted R-squared:  0.2345
F-statistic: 11.36 on 27 and 886 DF,  p-value: < 2.2e-16

> p=update(p,.~.-X569.270020)
> summary(p)

Call:
lm(formula = Class ~ X447.170013 + X477.690002 + X508.220001 +
    X528.570007 + X538.739990 + X548.919983 + X559.090027 + X589.619995 +
    X640.500000 + X660.849976 + X671.020020 + X681.200012 + X691.369995 +
    X701.549988 + X711.719971 + X721.900024 + X752.429993 + X762.599976 +
    X772.780029 + X864.349976 + X894.880005 + X1053.689941 +
    X1235.270020 + X1316.050049 + X1457.229980 + X2133.239990,
    data = (g))

Residuals:
    Min      1Q  Median      3Q     Max
-6.1581 -1.6376 -0.0806  1.9713  6.9683

Coefficients:
             Estimate Std. Error t value     Pr(>|t|)
(Intercept)   2.9664117  1.2554690   2.363     0.018353 *
X447.170013  -0.0015438  0.0009960  -1.550     0.121506
X477.690002   0.0028908  0.0028320   1.021     0.307651
X508.220001  -0.0106302  0.0031615  -3.362     0.000806 ***
X528.570007  -0.0114755  0.0033956  -3.379     0.000758 ***
X538.739990  -0.0015964  0.0039107  -0.408     0.683218
X548.919983   0.0071808  0.0041520   1.729     0.084072 .
X559.090027   0.0131065  0.0044409   2.951     0.003248 **
X589.619995   0.0037824  0.0048472   0.780     0.435414
X640.500000   0.0046134  0.0042452   1.087     0.277448
X660.849976   0.0043562  0.0046897   0.929     0.353207
```

```
X671.020020   0.0054678  0.0049837   1.097     0.272884
X681.200012  -0.0120351  0.0048328  -2.490     0.012946 *
X691.369995  -0.0125728  0.0045934  -2.737     0.006322 **
X701.549988   0.0132208  0.0045969   2.876     0.004124 **
X711.719971  -0.0090766  0.0039958  -2.272     0.023353 *
X721.900024   0.0104892  0.0038797   2.704     0.006991 **
X752.429993  -0.0037451  0.0029694  -1.261     0.207558
X762.599976  -0.0015167  0.0025719  -0.590     0.555525
X772.780029  -0.0067857  0.0019437  -3.491     0.000505 ***
X864.349976   0.0029966  0.0020701   1.448     0.148083
X894.880005   0.0014284  0.0014326   0.997     0.319017
X1053.689941  0.0051940  0.0008800   5.902 0.0000000051 ***
X1235.270020 -0.0064900  0.0012398  -5.235 0.0000002062 ***
X1316.050049  0.0008523  0.0012276   0.694     0.487686
X1457.229980 -0.0004529  0.0004283  -1.058     0.290566
X2133.239990  0.0022462  0.0005776   3.889     0.000108 ***
---
Signif. codes:  0 '***' 0.001 '**' 0.01 '*' 0.05 '.' 0.1 ' ' 1

Residual standard error: 2.509 on 887 degrees of freedom
Multiple R-squared:  0.257,     Adjusted R-squared:  0.2352
F-statistic:  11.8 on 26 and 887 DF,  p-value: < 2.2e-16

> p=update(p,.~.-X538.739990)
> summary(p)

Call:
lm(formula = Class ~ X447.170013 + X477.690002 + X508.220001 +
    X528.570007 + X548.919983 + X559.090027 + X589.619995 + X640.500000 +
    X660.849976 + X671.020020 + X681.200012 + X691.369995 + X701.549988 +
    X711.719971 + X721.900024 + X752.429993 + X762.599976 + X772.780029 +
    X864.349976 + X894.880005 + X1053.689941 + X1235.270020 +
    X1316.050049 + X1457.229980 + X2133.239990, data = (g))
```

Residuals:

Min	1Q	Median	3Q	Max
-6.1642	-1.6772	-0.0837	1.9704	6.9281

Coefficients:

	Estimate	Std. Error	t value	Pr(>|t|)	
(Intercept)	2.7766663	1.1657039	2.382	0.017430	*
X447.170013	-0.0015717	0.0009932	-1.582	0.113911	
X477.690002	0.0027542	0.0028109	0.980	0.327430	
X508.220001	-0.0107607	0.0031438	-3.423	0.000648	***
X528.570007	-0.0117530	0.0033253	-3.534	0.000430	***
X548.919983	0.0068290	0.0040597	1.682	0.092891	.
X559.090027	0.0127551	0.0043547	2.929	0.003487	**
X589.619995	0.0035900	0.0048220	0.744	0.456773	
X640.500000	0.0043959	0.0042096	1.044	0.296657	
X660.849976	0.0043267	0.0046870	0.923	0.356185	
X671.020020	0.0055371	0.0049785	1.112	0.266348	
X681.200012	-0.0118851	0.0048166	-2.468	0.013792	*
X691.369995	-0.0126039	0.0045906	-2.746	0.006162	**
X701.549988	0.0132960	0.0045911	2.896	0.003871	**
X711.719971	-0.0091540	0.0039894	-2.295	0.021991	*
X721.900024	0.0104810	0.0038778	2.703	0.007007	**
X752.429993	-0.0037965	0.0029654	-1.280	0.200789	
X762.599976	-0.0014545	0.0025662	-0.567	0.570996	
X772.780029	-0.0068208	0.0019409	-3.514	0.000463	***
X864.349976	0.0029964	0.0020691	1.448	0.147920	
X894.880005	0.0014589	0.0014300	1.020	0.307895	
X1053.689941	0.0051796	0.0008789	5.894	0.00000000536	***
X1235.270020	-0.0065080	0.0012384	-5.255	0.00000018532	***
X1316.050049	0.0009042	0.0012204	0.741	0.458958	
X1457.229980	-0.0004530	0.0004281	-1.058	0.290201	
X2133.239990	0.0022365	0.0005769	3.877	0.000114	***

```
Signif. codes:  0 ‘***’ 0.001 ‘**’ 0.01 ‘*’ 0.05 ‘.’ 0.1 ‘ ’ 1

Residual standard error: 2.508 on 888 degrees of freedom
Multiple R-squared:  0.2569,    Adjusted R-squared:  0.2359
F-statistic: 12.28 on 25 and 888 DF,  p-value: < 2.2e-16

> p=update(p,.~.-X762.599976)
> summary(p)

Call:
lm(formula = Class ~ X447.170013 + X477.690002 + X508.220001 +
    X528.570007 + X548.919983 + X559.090027 + X589.619995 + X640.500000 +
    X660.849976 + X671.020020 + X681.200012 + X691.369995 + X701.549988 +
    X711.719971 + X721.900024 + X752.429993 + X772.780029 + X864.349976 +
    X894.880005 + X1053.689941 + X1235.270020 + X1316.050049 +
    X1457.229980 + X2133.239990, data = (g))

Residuals:
    Min      1Q  Median      3Q     Max
-6.1339 -1.6660 -0.0976  1.9501  6.9263

Coefficients:
             Estimate Std. Error t value      Pr(>|t|)
(Intercept)   2.6997494  1.1573359   2.333     0.019885 *
X447.170013  -0.0015383  0.0009911  -1.552     0.120988
X477.690002   0.0026794  0.0028067   0.955     0.340029
X508.220001  -0.0106488  0.0031364  -3.395     0.000716 ***
X528.570007  -0.0116151  0.0033152  -3.504     0.000482 ***
X548.919983   0.0067659  0.0040566   1.668     0.095694 .
X559.090027   0.0126611  0.0043498   2.911     0.003696 **
X589.619995   0.0034633  0.0048150   0.719     0.472165
X640.500000   0.0042266  0.0041974   1.007     0.314230
X660.849976   0.0044151  0.0046826   0.943     0.345994
```

```
X671.020020   0.0057725  0.0049593   1.164      0.244746
X681.200012  -0.0119184  0.0048144  -2.476      0.013487 *
X691.369995  -0.0128032  0.0045754  -2.798      0.005249 **
X701.549988   0.0135171  0.0045727   2.956      0.003199 **
X711.719971  -0.0090409  0.0039829  -2.270      0.023451 *
X721.900024   0.0104216  0.0038749   2.690      0.007290 **
X752.429993  -0.0046698  0.0025327  -1.844      0.065546 .
X772.780029  -0.0072958  0.0017501  -4.169 0.00003360736 ***
X864.349976   0.0029432  0.0020662   1.424      0.154664
X894.880005   0.0014172  0.0014275   0.993      0.321100
X1053.689941  0.0051946  0.0008781   5.916 0.00000000471 ***
X1235.270020 -0.0065666  0.0012336  -5.323 0.00000012922 ***
X1316.050049  0.0009883  0.0012109   0.816      0.414630
X1457.229980 -0.0004921  0.0004223  -1.165      0.244283
X2133.239990  0.0022167  0.0005756   3.851      0.000126 ***
---
Signif. codes:  0 '***' 0.001 '**' 0.01 '*' 0.05 '.' 0.1 ' ' 1

Residual standard error: 2.507 on 889 degrees of freedom
Multiple R-squared:  0.2566,    Adjusted R-squared:  0.2365
F-statistic: 12.79 on 24 and 889 DF,  p-value: < 2.2e-16

> p=update(p,.~.-X589.619995)
> summary(p)

Call:
lm(formula = Class ~ X447.170013 + X477.690002 + X508.220001 +
    X528.570007 + X548.919983 + X559.090027 + X640.500000 + X660.849976 +
    X671.020020 + X681.200012 + X691.369995 + X701.549988 + X711.719971 +
    X721.900024 + X752.429993 + X772.780029 + X864.349976 + X894.880005 +
    X1053.689941 + X1235.270020 + X1316.050049 + X1457.229980 +
    X2133.239990, data = (g))
```

Residuals:

Min	1Q	Median	3Q	Max
-6.1607	-1.6944	-0.0659	1.9394	6.7865

Coefficients:

	Estimate	Std. Error	t value	Pr(>|t|)	
(Intercept)	2.7026100	1.1570152	2.336	0.019720	*
X447.170013	-0.0015457	0.0009908	-1.560	0.119088	
X477.690002	0.0028506	0.0027958	1.020	0.308205	
X508.220001	-0.0106426	0.0031355	-3.394	0.000719	***
X528.570007	-0.0111108	0.0032393	-3.430	0.000631	***
X548.919983	0.0075027	0.0039241	1.912	0.056203	.
X559.090027	0.0133172	0.0042520	3.132	0.001793	**
X640.500000	0.0047041	0.0041435	1.135	0.256558	
X660.849976	0.0045738	0.0046761	0.978	0.328277	
X671.020020	0.0060733	0.0049403	1.229	0.219269	
X681.200012	-0.0118613	0.0048124	-2.465	0.013899	*
X691.369995	-0.0127633	0.0045738	-2.791	0.005375	**
X701.549988	0.0136071	0.0045698	2.978	0.002983	**
X711.719971	-0.0087231	0.0039573	-2.204	0.027757	*
X721.900024	0.0104645	0.0038734	2.702	0.007032	**
X752.429993	-0.0047136	0.0025313	-1.862	0.062911	.
X772.780029	-0.0073540	0.0017477	-4.208	0.00002840069	***
X864.349976	0.0029573	0.0020655	1.432	0.152558	
X894.880005	0.0014474	0.0014265	1.015	0.310544	
X1053.689941	0.0052116	0.0008776	5.939	0.00000000412	***
X1235.270020	-0.0066418	0.0012288	-5.405	0.00000008331	***
X1316.050049	0.0010123	0.0012101	0.837	0.403078	
X1457.229980	-0.0004715	0.0004213	-1.119	0.263284	
X2133.239990	0.0022089	0.0005753	3.839	0.000132	***

Signif. codes: 0 ‘***’ 0.001 ‘**’ 0.01 ‘*’ 0.05 ‘.’ 0.1 ‘ ’ 1

```
Residual standard error: 2.506 on 890 degrees of freedom
Multiple R-squared:  0.2562,    Adjusted R-squared:  0.2369
F-statistic: 13.33 on 23 and 890 DF,  p-value: < 2.2e-16

> p=update(p,.~.-X1316.050049)
> summary(p)

Call:
lm(formula = Class ~ X447.170013 + X477.690002 + X508.220001 +
    X528.570007 + X548.919983 + X559.090027 + X640.500000 + X660.849976 +
    X671.020020 + X681.200012 + X691.369995 + X701.549988 + X711.719971 +
    X721.900024 + X752.429993 + X772.780029 + X864.349976 + X894.880005 +
    X1053.689941 + X1235.270020 + X1457.229980 + X2133.239990,
    data = (g))

Residuals:
    Min      1Q  Median      3Q     Max
-6.1109 -1.6712 -0.0712  1.9696  6.8280

Coefficients:
             Estimate Std. Error t value Pr(>|t|)
(Intercept)   2.7971005  1.1512943   2.430 0.015315 *
X447.170013  -0.0016263  0.0009859  -1.650 0.099384 .
X477.690002   0.0027125  0.0027905   0.972 0.331289
X508.220001  -0.0105580  0.0031334  -3.370 0.000785 ***
X528.570007  -0.0111581  0.0032383  -3.446 0.000596 ***
X548.919983   0.0074326  0.0039225   1.895 0.058435 .
X559.090027   0.0131205  0.0042447   3.091 0.002057 **
X640.500000   0.0044337  0.0041302   1.073 0.283344
X660.849976   0.0045587  0.0046753   0.975 0.329794
X671.020020   0.0062246  0.0049361   1.261 0.207624
X681.200012  -0.0117984  0.0048110  -2.452 0.014383 *
X691.369995  -0.0125459  0.0045657  -2.748 0.006119 **
```

```
X701.549988   0.0138503  0.0045597   3.038 0.002455 **
X711.719971  -0.0089367  0.0039483  -2.263 0.023850 *
X721.900024   0.0108659  0.0038429   2.827 0.004797 **
X752.429993  -0.0047660  0.0025301  -1.884 0.059925 .
X772.780029  -0.0075975  0.0017230  -4.409 1.16e-05 ***
X864.349976   0.0029272  0.0020648   1.418 0.156646
X894.880005   0.0016066  0.0014136   1.137 0.256036
X1053.689941  0.0052369  0.0008769   5.972 3.38e-09 ***
X1235.270020 -0.0058891  0.0008369  -7.037 3.92e-12 ***
X1457.229980 -0.0004024  0.0004130  -0.974 0.330138
X2133.239990  0.0022314  0.0005746   3.883 0.000111 ***
---
Signif. codes:  0 '***' 0.001 '**' 0.01 '*' 0.05 '.' 0.1 ' ' 1

Residual standard error: 2.506 on 891 degrees of freedom
Multiple R-squared:  0.2556,    Adjusted R-squared:  0.2372
F-statistic:  13.9 on 22 and 891 DF,  p-value: < 2.2e-16

> p=update(p,.~.-X477.690002)
> summary(p)

Call:
lm(formula = Class ~ X447.170013 + X508.220001 + X528.570007 +
    X548.919983 + X559.090027 + X640.500000 + X660.849976 + X671.020020 +
    X681.200012 + X691.369995 + X701.549988 + X711.719971 + X721.900024 +
    X752.429993 + X772.780029 + X864.349976 + X894.880005 + X1053.689941 +
    X1235.270020 + X1457.229980 + X2133.239990, data = (g))

Residuals:
    Min      1Q  Median      3Q     Max
-6.0525 -1.7182 -0.0792  1.9857  6.8519

Coefficients:
```

```
            Estimate Std. Error t value Pr(>|t|)
(Intercept)   2.5049028  1.1113247   2.254 0.024439 *
X447.170013  -0.0015015  0.0009775  -1.536 0.124873
X508.220001  -0.0097915  0.0030324  -3.229 0.001288 **
X528.570007  -0.0110498  0.0032362  -3.414 0.000668 ***
X548.919983   0.0078746  0.0038960   2.021 0.043556 *
X559.090027   0.0135306  0.0042236   3.204 0.001405 **
X640.500000   0.0041464  0.0041195   1.007 0.314425
X660.849976   0.0048788  0.0046635   1.046 0.295771
X671.020020   0.0059731  0.0049292   1.212 0.225914
X681.200012  -0.0116410  0.0048081  -2.421 0.015672 *
X691.369995  -0.0118387  0.0045072  -2.627 0.008771 **
X701.549988   0.0134943  0.0045449   2.969 0.003066 **
X711.719971  -0.0092768  0.0039327  -2.359 0.018544 *
X721.900024   0.0109478  0.0038419   2.850 0.004479 **
X752.429993  -0.0045455  0.0025198  -1.804 0.071581 .
X772.780029  -0.0077121  0.0017189  -4.487 8.18e-06 ***
X864.349976   0.0028918  0.0020645   1.401 0.161635
X894.880005   0.0015613  0.0014127   1.105 0.269384
X1053.689941  0.0052733  0.0008761   6.019 2.56e-09 ***
X1235.270020 -0.0059346  0.0008356  -7.103 2.50e-12 ***
X1457.229980 -0.0003736  0.0004119  -0.907 0.364627
X2133.239990  0.0022518  0.0005742   3.922 9.47e-05 ***
---
Signif. codes:  0 ‘***’ 0.001 ‘**’ 0.01 ‘*’ 0.05 ‘.’ 0.1 ‘ ’ 1

Residual standard error: 2.506 on 892 degrees of freedom
Multiple R-squared:  0.2548,    Adjusted R-squared:  0.2372
F-statistic: 14.52 on 21 and 892 DF,  p-value: < 2.2e-16

>
> p=update(p,.~.-X1457.229980)
> summary(p)
```

```
Call:
lm(formula = Class ~ X447.170013 + X508.220001 + X528.570007 +
    X548.919983 + X559.090027 + X640.500000 + X660.849976 + X671.020020 +
    X681.200012 + X691.369995 + X701.549988 + X711.719971 + X721.900024 +
    X752.429993 + X772.780029 + X864.349976 + X894.880005 + X1053.689941 +
    X1235.270020 + X2133.239990, data = (g))

Residuals:
    Min      1Q  Median      3Q     Max
-6.0268 -1.6621 -0.0637  1.9798  6.8363

Coefficients:
             Estimate Std. Error t value Pr(>|t|)
(Intercept)   2.5267511  1.1109533   2.274 0.023178 *
X447.170013  -0.0014789  0.0009771  -1.514 0.130467
X508.220001  -0.0096972  0.0030303  -3.200 0.001423 **
X528.570007  -0.0110897  0.0032356  -3.427 0.000637 ***
X548.919983   0.0076334  0.0038865   1.964 0.049830 *
X559.090027   0.0136804  0.0042199   3.242 0.001232 **
X640.500000   0.0039927  0.0041156   0.970 0.332229
X660.849976   0.0046509  0.0046563   0.999 0.318138
X671.020020   0.0061279  0.0049257   1.244 0.213803
X681.200012  -0.0115220  0.0048059  -2.397 0.016713 *
X691.369995  -0.0117494  0.0045056  -2.608 0.009267 **
X701.549988   0.0132958  0.0045391   2.929 0.003485 **
X711.719971  -0.0090341  0.0039232  -2.303 0.021522 *
X721.900024   0.0107653  0.0038363   2.806 0.005122 **
X752.429993  -0.0042947  0.0025043  -1.715 0.086710 .
X772.780029  -0.0079463  0.0016992  -4.676 3.37e-06 ***
X864.349976   0.0029004  0.0020642   1.405 0.160348
X894.880005   0.0016447  0.0014096   1.167 0.243617
X1053.689941  0.0052472  0.0008755   5.993 2.98e-09 ***
```

```
X1235.270020 -0.0059750  0.0008343  -7.162 1.67e-12 ***
X2133.239990  0.0020043  0.0005052   3.968 7.84e-05 ***
---
Signif. codes:  0 '***' 0.001 '**' 0.01 '*' 0.05 '.' 0.1 ' ' 1

Residual standard error: 2.506 on 893 degrees of freedom
Multiple R-squared:  0.2541,    Adjusted R-squared:  0.2374
F-statistic: 15.21 on 20 and 893 DF,  p-value: < 2.2e-16

> p=update(p,.~.-X640.500000)
> summary(p)

Call:
lm(formula = Class ~ X447.170013 + X508.220001 + X528.570007 +
    X548.919983 + X559.090027 + X660.849976 + X671.020020 + X681.200012 +
    X691.369995 + X701.549988 + X711.719971 + X721.900024 + X752.429993 +
    X772.780029 + X864.349976 + X894.880005 + X1053.689941 +
    X1235.270020 + X2133.239990, data = (g))

Residuals:
    Min      1Q  Median      3Q     Max
-6.0252 -1.7065 -0.0426  2.0188  6.7819

Coefficients:
             Estimate Std. Error t value Pr(>|t|)
(Intercept)   2.0729779  1.0076601   2.057 0.039955 *
X447.170013  -0.0014054  0.0009741  -1.443 0.149434
X508.220001  -0.0097674  0.0030294  -3.224 0.001309 **
X528.570007  -0.0111923  0.0032338  -3.461 0.000564 ***
X548.919983   0.0081425  0.0038508   2.115 0.034747 *
X559.090027   0.0143583  0.0041615   3.450 0.000586 ***
X660.849976   0.0055307  0.0045670   1.211 0.226205
X671.020020   0.0064462  0.0049146   1.312 0.189982
```

```
X681.200012  -0.0108206  0.0047510  -2.278 0.022990 *
X691.369995  -0.0113762  0.0044890  -2.534 0.011440 *
X701.549988   0.0141307  0.0044567   3.171 0.001573 **
X711.719971  -0.0088191  0.0039168  -2.252 0.024589 *
X721.900024   0.0104818  0.0038250   2.740 0.006260 **
X752.429993  -0.0041504  0.0024998  -1.660 0.097211 .
X772.780029  -0.0079559  0.0016992  -4.682 3.28e-06 ***
X864.349976   0.0028208  0.0020625   1.368 0.171765
X894.880005   0.0016633  0.0014094   1.180 0.238279
X1053.689941  0.0052450  0.0008755   5.991 3.02e-09 ***
X1235.270020 -0.0060039  0.0008337  -7.201 1.27e-12 ***
X2133.239990  0.0019914  0.0005050   3.944 8.66e-05 ***
---
Signif. codes:  0 '***' 0.001 '**' 0.01 '*' 0.05 '.' 0.1 ' ' 1

Residual standard error: 2.506 on 894 degrees of freedom
Multiple R-squared:  0.2533,    Adjusted R-squared:  0.2374
F-statistic: 15.96 on 19 and 894 DF,  p-value: < 2.2e-16

> p=update(p,.~.-X894.880005)
> summary(p)

Call:
lm(formula = Class ~ X447.170013 + X508.220001 + X528.570007 +
    X548.919983 + X559.090027 + X660.849976 + X671.020020 + X681.200012 +
    X691.369995 + X701.549988 + X711.719971 + X721.900024 + X752.429993 +
    X772.780029 + X864.349976 + X1053.689941 + X1235.270020 +
    X2133.239990, data = (g))

Residuals:
    Min      1Q  Median      3Q     Max
-5.9657 -1.6531 -0.0563  1.9943  6.8855
```

```
Coefficients:
             Estimate Std. Error t value Pr(>|t|)
(Intercept)   2.3102095  0.9876204   2.339 0.019546 *
X447.170013  -0.0014029  0.0009743  -1.440 0.150247
X508.220001  -0.0100425  0.0030211  -3.324 0.000923 ***
X528.570007  -0.0111234  0.0032340  -3.440 0.000610 ***
X548.919983   0.0079295  0.0038474   2.061 0.039590 *
X559.090027   0.0142245  0.0041609   3.419 0.000658 ***
X660.849976   0.0056108  0.0045675   1.228 0.219607
X671.020020   0.0063735  0.0049153   1.297 0.195082
X681.200012  -0.0103303  0.0047339  -2.182 0.029353 *
X691.369995  -0.0115637  0.0044872  -2.577 0.010124 *
X701.549988   0.0141652  0.0044576   3.178 0.001535 **
X711.719971  -0.0089499  0.0039161  -2.285 0.022521 *
X721.900024   0.0106165  0.0038241   2.776 0.005615 **
X752.429993  -0.0030442  0.0023179  -1.313 0.189415
X772.780029  -0.0085398  0.0016259  -5.252 1.88e-07 ***
X864.349976   0.0038835  0.0018560   2.092 0.036678 *
X1053.689941  0.0053634  0.0008699   6.165 1.06e-09 ***
X1235.270020 -0.0059564  0.0008329  -7.151 1.79e-12 ***
X2133.239990  0.0019547  0.0005041   3.877 0.000113 ***
---
Signif. codes:  0 ‘***’ 0.001 ‘**’ 0.01 ‘*’ 0.05 ‘.’ 0.1 ‘ ’ 1

Residual standard error: 2.506 on 895 degrees of freedom
Multiple R-squared:  0.2522,    Adjusted R-squared:  0.2371
F-statistic: 16.76 on 18 and 895 DF,  p-value: < 2.2e-16

> p=update(p,.~.-X660.849976)
> summary(p)

Call:
lm(formula = Class ~ X447.170013 + X508.220001 + X528.570007 +
```

```
    X548.919983 + X559.090027 + X671.020020 + X681.200012 + X691.369995 +
    X701.549988 + X711.719971 + X721.900024 + X752.429993 + X772.780029 +
    X864.349976 + X1053.689941 + X1235.270020 + X2133.239990,
    data = (g))

Residuals:
   Min     1Q Median     3Q    Max
-5.930 -1.685 -0.041  1.940  6.892

Coefficients:
             Estimate Std. Error t value Pr(>|t|)
(Intercept)   2.3316334  0.9877468   2.361 0.018461 *
X447.170013  -0.0013937  0.0009745  -1.430 0.153031
X508.220001  -0.0099086  0.0030200  -3.281 0.001074 **
X528.570007  -0.0105984  0.0032065  -3.305 0.000987 ***
X548.919983   0.0080365  0.0038475   2.089 0.037011 *
X559.090027   0.0146063  0.0041505   3.519 0.000455 ***
X671.020020   0.0075816  0.0048173   1.574 0.115880
X681.200012  -0.0087207  0.0045502  -1.917 0.055612 .
X691.369995  -0.0105090  0.0044056  -2.385 0.017267 *
X701.549988   0.0152292  0.0043738   3.482 0.000522 ***
X711.719971  -0.0090310  0.0039166  -2.306 0.021349 *
X721.900024   0.0101673  0.0038077   2.670 0.007717 **
X752.429993  -0.0030756  0.0023184  -1.327 0.184985
X772.780029  -0.0084842  0.0016257  -5.219 2.24e-07 ***
X864.349976   0.0040334  0.0018525   2.177 0.029719 *
X1053.689941  0.0053083  0.0008690   6.109 1.50e-09 ***
X1235.270020 -0.0059186  0.0008326  -7.108 2.40e-12 ***
X2133.239990  0.0019105  0.0005030   3.798 0.000155 ***
---
Signif. codes:  0 ‘***’ 0.001 ‘**’ 0.01 ‘*’ 0.05 ‘.’ 0.1 ‘ ’ 1

Residual standard error: 2.507 on 896 degrees of freedom
```

```
Multiple R-squared:  0.2509,    Adjusted R-squared:  0.2367
F-statistic: 17.65 on 17 and 896 DF,  p-value: < 2.2e-16

> p=update(p,.~.-X721.900024)
> summary(p)

Call:
lm(formula = Class ~ X447.170013 + X508.220001 + X528.570007 +
    X548.919983 + X559.090027 + X671.020020 + X681.200012 + X691.369995 +
    X701.549988 + X711.719971 + X752.429993 + X772.780029 + X864.349976 +
    X1053.689941 + X1235.270020 + X2133.239990, data = (g))

Residuals:
    Min      1Q  Median      3Q     Max
-6.0706 -1.6978 -0.0836  2.0667  6.7476

Coefficients:
             Estimate Std. Error t value Pr(>|t|)
(Intercept)   2.4129497  0.9906450   2.436 0.015055 *
X447.170013  -0.0014275  0.0009778  -1.460 0.144659
X508.220001  -0.0101798  0.0030285  -3.361 0.000809 ***
X528.570007  -0.0107226  0.0032171  -3.333 0.000894 ***
X548.919983   0.0090489  0.0038418   2.355 0.018719 *
X559.090027   0.0153630  0.0041549   3.698 0.000231 ***
X671.020020   0.0057190  0.0047828   1.196 0.232110
X681.200012  -0.0102897  0.0045275  -2.273 0.023280 *
X691.369995  -0.0106855  0.0044201  -2.417 0.015827 *
X701.549988   0.0177594  0.0042845   4.145 3.72e-05 ***
X711.719971  -0.0010813  0.0025536  -0.423 0.672064
X752.429993  -0.0023103  0.0023085  -1.001 0.317198
X772.780029  -0.0070487  0.0015395  -4.579 5.34e-06 ***
X864.349976   0.0040865  0.0018587   2.199 0.028162 *
X1053.689941  0.0052375  0.0008716   6.009 2.71e-09 ***
```

```
X1235.270020 -0.0058860  0.0008354  -7.046 3.67e-12 ***
X2133.239990  0.0018907  0.0005046   3.747 0.000191 ***
---
Signif. codes:  0 '***' 0.001 '**' 0.01 '*' 0.05 '.' 0.1 ' ' 1

Residual standard error: 2.515 on 897 degrees of freedom
Multiple R-squared:  0.2449,    Adjusted R-squared:  0.2315
F-statistic: 18.19 on 16 and 897 DF,  p-value: < 2.2e-16

> p=update(p,.~.+X721.900024)
> summary(p)

Call:
lm(formula = Class ~ X447.170013 + X508.220001 + X528.570007 +
    X548.919983 + X559.090027 + X671.020020 + X681.200012 + X691.369995 +
    X701.549988 + X711.719971 + X752.429993 + X772.780029 + X864.349976 +
    X1053.689941 + X1235.270020 + X2133.239990 + X721.900024,
    data = (g))

Residuals:
   Min     1Q Median     3Q    Max
-5.930 -1.685 -0.041  1.940  6.892

Coefficients:
             Estimate Std. Error t value Pr(>|t|)
(Intercept)   2.3316334  0.9877468   2.361 0.018461 *
X447.170013  -0.0013937  0.0009745  -1.430 0.153031
X508.220001  -0.0099086  0.0030200  -3.281 0.001074 **
X528.570007  -0.0105984  0.0032065  -3.305 0.000987 ***
X548.919983   0.0080365  0.0038475   2.089 0.037011 *
X559.090027   0.0146063  0.0041505   3.519 0.000455 ***
X671.020020   0.0075816  0.0048173   1.574 0.115880
X681.200012  -0.0087207  0.0045502  -1.917 0.055612 .
```

```
X691.369995  -0.0105090  0.0044056  -2.385 0.017267 *
X701.549988   0.0152292  0.0043738   3.482 0.000522 ***
X711.719971  -0.0090310  0.0039166  -2.306 0.021349 *
X752.429993  -0.0030756  0.0023184  -1.327 0.184985
X772.780029  -0.0084842  0.0016257  -5.219 2.24e-07 ***
X864.349976   0.0040334  0.0018525   2.177 0.029719 *
X1053.689941  0.0053083  0.0008690   6.109 1.50e-09 ***
X1235.270020 -0.0059186  0.0008326  -7.108 2.40e-12 ***
X2133.239990  0.0019105  0.0005030   3.798 0.000155 ***
X721.900024   0.0101673  0.0038077   2.670 0.007717 **
---
Signif. codes:  0 '***' 0.001 '**' 0.01 '*' 0.05 '.' 0.1 ' ' 1

Residual standard error: 2.507 on 896 degrees of freedom
Multiple R-squared:  0.2509,    Adjusted R-squared:  0.2367
F-statistic: 17.65 on 17 and 896 DF,  p-value: < 2.2e-16

> p=update(p,.~.-X752.429993)
> summary(p)

Call:
lm(formula = Class ~ X447.170013 + X508.220001 + X528.570007 +
    X548.919983 + X559.090027 + X671.020020 + X681.200012 + X691.369995 +
    X701.549988 + X711.719971 + X772.780029 + X864.349976 + X1053.689941 +
    X1235.270020 + X2133.239990 + X721.900024, data = (g))

Residuals:
    Min      1Q  Median      3Q     Max
-5.8752 -1.6635 -0.0719  1.9723  6.9432

Coefficients:
             Estimate Std. Error t value Pr(>|t|)
(Intercept)   2.3850187  0.9873446   2.416 0.015909 *
```

```
X447.170013  -0.0014648  0.0009735  -1.505 0.132763
X508.220001  -0.0103574  0.0030022  -3.450 0.000587 ***
X528.570007  -0.0111742  0.0031783  -3.516 0.000460 ***
X548.919983   0.0076048  0.0038353   1.983 0.047692 *
X559.090027   0.0137157  0.0040975   3.347 0.000850 ***
X671.020020   0.0073907  0.0048172   1.534 0.125325
X681.200012  -0.0091697  0.0045395  -2.020 0.043683 *
X691.369995  -0.0110563  0.0043881  -2.520 0.011921 *
X701.549988   0.0184418  0.0036438   5.061 5.06e-07 ***
X711.719971  -0.0096084  0.0038940  -2.467 0.013792 *
X772.780029  -0.0093015  0.0015051  -6.180 9.72e-10 ***
X864.349976   0.0025776  0.0014931   1.726 0.084624 .
X1053.689941  0.0052184  0.0008667   6.021 2.53e-09 ***
X1235.270020 -0.0058220  0.0008298  -7.016 4.49e-12 ***
X2133.239990  0.0018641  0.0005020   3.714 0.000217 ***
X721.900024   0.0095429  0.0037801   2.525 0.011756 *
---
Signif. codes:  0 '***' 0.001 '**' 0.01 '*' 0.05 '.' 0.1 ' ' 1

Residual standard error: 2.508 on 897 degrees of freedom
Multiple R-squared:  0.2494,    Adjusted R-squared:  0.236
F-statistic: 18.63 on 16 and 897 DF,  p-value: < 2.2e-16

> p=update(p,.~.-X447.170013)
> summary(p)

Call:
lm(formula = Class ~ X508.220001 + X528.570007 + X548.919983 +
    X559.090027 + X671.020020 + X681.200012 + X691.369995 + X701.549988 +
    X711.719971 + X772.780029 + X864.349976 + X1053.689941 +
    X1235.270020 + X2133.239990 + X721.900024, data = (g))
```

```
Residuals:
    Min      1Q  Median      3Q     Max
-5.9489 -1.6687 -0.0991  1.9512  6.8270

Coefficients:
             Estimate Std. Error t value Pr(>|t|)
(Intercept)   3.3004101  0.7781940   4.241 2.45e-05 ***
X508.220001  -0.0108390  0.0029872  -3.628 0.000301 ***
X528.570007  -0.0116537  0.0031645  -3.683 0.000245 ***
X548.919983   0.0073448  0.0038341   1.916 0.055727 .
X559.090027   0.0131405  0.0040825   3.219 0.001334 **
X671.020020   0.0073453  0.0048205   1.524 0.127917
X681.200012  -0.0092529  0.0045424  -2.037 0.041941 *
X691.369995  -0.0114585  0.0043830  -2.614 0.009091 **
X701.549988   0.0189408  0.0036312   5.216 2.27e-07 ***
X711.719971  -0.0092446  0.0038892  -2.377 0.017664 *
X772.780029  -0.0093658  0.0015055  -6.221 7.57e-10 ***
X864.349976   0.0026024  0.0014940   1.742 0.081872 .
X1053.689941  0.0052592  0.0008669   6.067 1.92e-09 ***
X1235.270020 -0.0059134  0.0008281  -7.141 1.92e-12 ***
X2133.239990  0.0019012  0.0005017   3.789 0.000161 ***
X721.900024   0.0095785  0.0037827   2.532 0.011504 *
---
Signif. codes:  0 ‘***’ 0.001 ‘**’ 0.01 ‘*’ 0.05 ‘.’ 0.1 ‘ ’ 1

Residual standard error: 2.51 on 898 degrees of freedom
Multiple R-squared:  0.2475,    Adjusted R-squared:  0.235
F-statistic: 19.69 on 15 and 898 DF,  p-value: < 2.2e-16

> p=update(p,.~.-X671.020020)
> summary(p)
```

```
Call:
lm(formula = Class ~ X508.220001 + X528.570007 + X548.919983 +
    X559.090027 + X681.200012 + X691.369995 + X701.549988 + X711.719971 +
    X772.780029 + X864.349976 + X1053.689941 + X1235.270020 +
    X2133.239990 + X721.900024, data = (g))

Residuals:
    Min      1Q  Median      3Q     Max
-5.8279 -1.6674 -0.1436  1.9978  6.9281

Coefficients:
             Estimate Std. Error t value Pr(>|t|)
(Intercept)   3.2174322  0.7768569   4.142 3.77e-05 ***
X508.220001  -0.0107043  0.0029881  -3.582 0.000359 ***
X528.570007  -0.0116551  0.0031669  -3.680 0.000247 ***
X548.919983   0.0076787  0.0038307   2.005 0.045313 *
X559.090027   0.0131362  0.0040855   3.215 0.001350 **
X681.200012  -0.0061575  0.0040658  -1.514 0.130261
X691.369995  -0.0090412  0.0040888  -2.211 0.027273 *
X701.549988   0.0204192  0.0035018   5.831 7.67e-09 ***
X711.719971  -0.0089407  0.0038870  -2.300 0.021667 *
X772.780029  -0.0093780  0.0015066  -6.224 7.40e-10 ***
X864.349976   0.0028246  0.0014880   1.898 0.057982 .
X1053.689941  0.0052642  0.0008675   6.068 1.91e-09 ***
X1235.270020 -0.0059988  0.0008268  -7.255 8.67e-13 ***
X2133.239990  0.0019419  0.0005014   3.873 0.000115 ***
X721.900024   0.0087582  0.0037469   2.337 0.019634 *
---
Signif. codes:  0 ‘***’ 0.001 ‘**’ 0.01 ‘*’ 0.05 ‘.’ 0.1 ‘ ’ 1

Residual standard error: 2.512 on 899 degrees of freedom
Multiple R-squared:  0.2456,    Adjusted R-squared:  0.2338
F-statistic:  20.9 on 14 and 899 DF,  p-value: < 2.2e-16
```

```
> p=update(p,.~.-X681.200012)
> summary(p)

Call:
lm(formula = Class ~ X508.220001 + X528.570007 + X548.919983 +
    X559.090027 + X691.369995 + X701.549988 + X711.719971 + X772.780029 +
    X864.349976 + X1053.689941 + X1235.270020 + X2133.239990 +
    X721.900024, data = (g))

Residuals:
    Min      1Q  Median      3Q     Max
-5.9570 -1.6368 -0.1085  1.9796  6.8532

Coefficients:
             Estimate Std. Error t value Pr(>|t|)
(Intercept)   3.2628238  0.7768362   4.200 2.93e-05 ***
X508.220001  -0.0105699  0.0029889  -3.536 0.000426 ***
X528.570007  -0.0121954  0.0031490  -3.873 0.000115 ***
X548.919983   0.0077550  0.0038331   2.023 0.043351 *
X559.090027   0.0129624  0.0040868   3.172 0.001567 **
X691.369995  -0.0132908  0.0029762  -4.466 8.99e-06 ***
X701.549988   0.0183700  0.0032321   5.684 1.78e-08 ***
X711.719971  -0.0089147  0.0038897  -2.292 0.022145 *
X772.780029  -0.0094699  0.0015065  -6.286 5.07e-10 ***
X864.349976   0.0025549  0.0014783   1.728 0.084299 .
X1053.689941  0.0052949  0.0008679   6.101 1.57e-09 ***
X1235.270020 -0.0059965  0.0008274  -7.247 9.16e-13 ***
X2133.239990  0.0018631  0.0004990   3.733 0.000201 ***
X721.900024   0.0099435  0.0036669   2.712 0.006821 **
---
Signif. codes:  0 ‘***’ 0.001 ‘**’ 0.01 ‘*’ 0.05 ‘.’ 0.1 ‘ ’ 1

Residual standard error: 2.513 on 900 degrees of freedom
```

```
Multiple R-squared:  0.2437,    Adjusted R-squared:  0.2327
F-statistic:  22.3 on 13 and 900 DF,  p-value: < 2.2e-16


> p=update(p,.~.-X864.349976)
> summary(p)


Call:
lm(formula = Class ~ X508.220001 + X528.570007 + X548.919983 +
   X559.090027 + X691.369995 + X701.549988 + X711.719971 + X772.780029 +
   X1053.689941 + X1235.270020 + X2133.239990 + X721.900024,
   data = (g))


Residuals:
   Min     1Q  Median     3Q    Max
-5.9020 -1.6580 -0.1535  2.0211  6.6700


Coefficients:
             Estimate Std. Error t value Pr(>|t|)
(Intercept)   3.3746999  0.7749871   4.355 1.49e-05 ***
X508.220001  -0.0103831  0.0029903  -3.472 0.000541 ***
X528.570007  -0.0121276  0.0031522  -3.847 0.000128 ***
X548.919983   0.0074706  0.0038338   1.949 0.051649 .
X559.090027   0.0127855  0.0040901   3.126 0.001829 **
X691.369995  -0.0110255  0.0026749  -4.122 4.11e-05 ***
X701.549988   0.0156092  0.0028128   5.549 3.77e-08 ***
X711.719971  -0.0084318  0.0038840  -2.171 0.030197 *
X772.780029  -0.0074690  0.0009650  -7.740 2.66e-14 ***
X1053.689941  0.0057269  0.0008321   6.883 1.10e-11 ***
X1235.270020 -0.0057280  0.0008136  -7.040 3.81e-12 ***
X2133.239990  0.0017006  0.0004906   3.466 0.000553 ***
X721.900024   0.0103847  0.0036620   2.836 0.004674 **
---
Signif. codes:  0 ‘***’ 0.001 ‘**’ 0.01 ‘*’ 0.05 ‘.’ 0.1 ‘ ’ 1
```

```
Residual standard error: 2.516 on 901 degrees of freedom
Multiple R-squared:  0.2411,    Adjusted R-squared:  0.231
F-statistic: 23.86 on 12 and 901 DF,  p-value: < 2.2e-16

> p=update(p,.~.-X548.919983)
> summary(p)

Call:
lm(formula = Class ~ X508.220001 + X528.570007 + X559.090027 +
    X691.369995 + X701.549988 + X711.719971 + X772.780029 + X1053.689941 +
    X1235.270020 + X2133.239990 + X721.900024, data = (g))

Residuals:
    Min      1Q  Median      3Q     Max
-5.8186 -1.6484 -0.1064  2.0306  6.8634

Coefficients:
             Estimate Std. Error t value Pr(>|t|)
(Intercept)   3.8742100  0.7324989   5.289 1.54e-07 ***
X508.220001  -0.0094921  0.0029597  -3.207 0.001388 **
X528.570007  -0.0104868  0.0030423  -3.447 0.000593 ***
X559.090027   0.0170303  0.0034671   4.912 1.07e-06 ***
X691.369995  -0.0113095  0.0026751  -4.228 2.60e-05 ***
X701.549988   0.0156131  0.0028172   5.542 3.92e-08 ***
X711.719971  -0.0083360  0.0038897  -2.143 0.032371 *
X772.780029  -0.0076196  0.0009634  -7.909 7.54e-15 ***
X1053.689941  0.0057087  0.0008333   6.851 1.36e-11 ***
X1235.270020 -0.0058382  0.0008129  -7.182 1.44e-12 ***
X2133.239990  0.0017815  0.0004896   3.638 0.000290 ***
X721.900024   0.0111387  0.0036472   3.054 0.002324 **
---
Signif. codes:  0 ‘***’ 0.001 ‘**’ 0.01 ‘*’ 0.05 ‘.’ 0.1 ‘ ’ 1
```

```
Residual standard error: 2.52 on 902 degrees of freedom
Multiple R-squared:  0.2379,    Adjusted R-squared:  0.2287
F-statistic:  25.6 on 11 and 902 DF,  p-value: < 2.2e-16

> p=update(p,.~.-X711.719971)
> summary(p)

Call:
lm(formula = Class ~ X508.220001 + X528.570007 + X559.090027 +
    X691.369995 + X701.549988 + X772.780029 + X1053.689941 +
    X1235.270020 + X2133.239990 + X721.900024, data = (g))

Residuals:
    Min      1Q  Median      3Q     Max
-5.8918 -1.6051 -0.0938  2.0667  6.5852

Coefficients:
             Estimate Std. Error t value Pr(>|t|)
(Intercept)   4.3996329  0.6916235   6.361 3.17e-10 ***
X508.220001  -0.0091249  0.0029606  -3.082 0.002118 **
X528.570007  -0.0108336  0.0030441  -3.559 0.000392 ***
X559.090027   0.0160571  0.0034441   4.662 3.60e-06 ***
X691.369995  -0.0118461  0.0026686  -4.439 1.02e-05 ***
X701.549988   0.0137272  0.0026815   5.119 3.75e-07 ***
X772.780029  -0.0066461  0.0008512  -7.808 1.61e-14 ***
X1053.689941  0.0057055  0.0008349   6.833 1.52e-11 ***
X1235.270020 -0.0060668  0.0008075  -7.513 1.39e-13 ***
X2133.239990  0.0019337  0.0004854   3.984 7.34e-05 ***
X721.900024   0.0047121  0.0020800   2.265 0.023726 *
---
Signif. codes:  0 ‘***’ 0.001 ‘**’ 0.01 ‘*’ 0.05 ‘.’ 0.1 ‘ ’ 1
```

Residual standard error: 2.525 on 903 degrees of freedom

Multiple R-squared: 0.2341, Adjusted R-squared: 0.2256

F-statistic: 27.6 on 10 and 903 DF, p-value: < 2.2e-16

>

Appendix 6.5: AIC Variable Elimination Iterations

```
R version 4.1.3 (2022-03-10) -- "One Push-Up"
Copyright (C) 2022 The R Foundation for Statistical Computing
Platform: x86_64-w64-mingw32/x64 (64-bit)

R is free software and comes with ABSOLUTELY NO WARRANTY.
You are welcome to redistribute it under certain conditions.
Type 'license()' or 'licence()' for distribution details.

  Natural language support but running in an English locale

R is a collaborative project with many contributors.
Type 'contributors()' for more information and
'citation()' on how to cite R or R packages in publications.

Type 'demo()' for some demos, 'help()' for on-line help, or
'help.start()' for an HTML browser interface to help.
Type 'q()' to quit R.

[Previously saved workspace restored]

> library (rattle)
Loading required package: tibble
Loading required package: bitops
Rattle: A free graphical interface for data science with R.
Version 5.5.1 Copyright (c) 2006-2021 Togaware Pty Ltd.
Type 'rattle()' to shake, rattle, and roll your data.
> rattle()

> g=read.csv(file.choose(),header=T)
> summary(g)
    Class        X447.170013     X477.690002      X508.220001
```

Min. : 1.000 Min. :-967.0 Min. :-233.00 Min. :-179.0

1st Qu.: 3.000 1st Qu.:-564.2 1st Qu.: -72.00 1st Qu.: -1.0

Median : 6.000 Median :-436.0 Median : 41.00 Median : 154.0

Mean : 5.503 Mean :-432.9 Mean : 35.33 Mean : 139.2

3rd Qu.: 8.000 3rd Qu.:-325.0 3rd Qu.: 112.00 3rd Qu.: 231.0

Max. :10.000 Max. : 85.0 Max. : 435.00 Max. : 624.0

X528.570007 X538.739990 X548.919983 X559.090027

Min. :-127.0 Min. : 78.0 Min. : 88.0 Min. :100.0

1st Qu.: 64.0 1st Qu.:256.0 1st Qu.:280.0 1st Qu.:293.0

Median : 242.0 Median :426.0 Median :459.0 Median :491.0

Mean : 228.7 Mean :410.6 Mean :443.1 Mean :470.8

3rd Qu.: 346.5 3rd Qu.:525.0 3rd Qu.:568.0 3rd Qu.:605.8

Max. : 743.0 Max. :846.0 Max. :916.0 Max. :943.0

X569.270020 X589.619995 X640.500000 X660.849976

Min. : 74.0 Min. : 39.0 Min. :-66.0 Min. : 60.0

1st Qu.:261.0 1st Qu.:219.0 1st Qu.:152.0 1st Qu.: 228.0

Median :475.0 Median :453.5 Median :416.0 Median : 496.5

Mean :451.2 Mean :416.3 Mean :371.6 Mean : 457.1

3rd Qu.:595.0 3rd Qu.:557.8 3rd Qu.:542.8 3rd Qu.: 632.0

Max. :923.0 Max. :934.0 Max. :929.0 Max. :1015.0

X671.020020 X681.200012 X691.369995 X701.549988

Min. : 23.0 Min. : 49.0 Min. : 54.0 Min. : 148.0

1st Qu.: 214.5 1st Qu.: 212.5 1st Qu.: 250.2 1st Qu.: 366.2

Median : 483.0 Median : 496.0 Median : 550.0 Median : 661.5

Mean : 447.6 Mean : 464.1 Mean : 511.0 Mean : 628.9

3rd Qu.: 633.0 3rd Qu.: 659.8 3rd Qu.: 718.0 3rd Qu.: 828.0

Max. :1008.0 Max. :1047.0 Max. :1137.0 Max. :1204.0

X711.719971 X721.900024 X752.429993 X762.599976 X772.780029

Min. : 61 Min. : 92 Min. : 61 Min. : 99 Min. : 92

1st Qu.: 677 1st Qu.:1011 1st Qu.:1644 1st Qu.:1658 1st Qu.:1698

Median :1015 Median :1267 Median :1913 Median :1963 Median :2037

Mean : 953 Mean :1237 Mean :1851 Mean :1899 Mean :1962

3rd Qu.:1173 3rd Qu.:1449 3rd Qu.:2155 3rd Qu.:2203 3rd Qu.:2287

```
 Max.   :1685   Max.   :2106   Max.   :3729   Max.   :3599   Max.   :3554
  X813.479980    X864.349976    X894.880005    X1053.689941   X1094.089966
 Min.   : 269   Min.   : 200   Min.   : 196   Min.   : 177   Min.   : 194
 1st Qu.:1976   1st Qu.:2142   1st Qu.:2226   1st Qu.:2530   1st Qu.:2470
 Median :2265   Median :2448   Median :2545   Median :2847   Median :2774
 Mean   :2187   Mean   :2373   Mean   :2467   Mean   :2779   Mean   :2701
 3rd Qu.:2508   3rd Qu.:2734   3rd Qu.:2829   3rd Qu.:3175   3rd Qu.:3089
 Max.   :4056   Max.   :4319   Max.   :4464   Max.   :4611   Max.   :4416
  X1235.270020   X1316.050049   X1457.229980    X1467.329956
 Min.   :  -4   Min.   : 222   Min.   :-142.0   Min.   :-188.0
 1st Qu.:2094   1st Qu.:1850   1st Qu.: 318.0   1st Qu.: 255.2
 Median :2580   Median :2319   Median : 624.0   Median : 548.5
 Mean   :2509   Mean   :2285   Mean   : 638.9   Mean   : 590.3
 3rd Qu.:3020   3rd Qu.:2764   3rd Qu.: 878.0   3rd Qu.: 837.5
 Max.   :3758   Max.   :3375   Max.   :2174.0   Max.   :2319.0
  X2133.239990
 Min.   : -29.0
 1st Qu.: 251.2
 Median : 658.0
 Mean   : 667.4
 3rd Qu.: 907.0
 Max.   :2478.0
> p=lm(Class~.,data=(g))
> summary(p)


Call:
lm(formula = Class ~ ., data = (g))

Residuals:
    Min      1Q  Median      3Q     Max
-6.1600 -1.6653 -0.0632  1.9376  7.0527
```

Coefficients:

	Estimate	Std. Error	t value	Pr(>|t|)	
(Intercept)	2.9965321	1.3119089	2.284	0.022602	*
X447.170013	-0.0015457	0.0010040	-1.540	0.124017	
X477.690002	0.0027758	0.0028565	0.972	0.331435	
X508.220001	-0.0106970	0.0031833	-3.360	0.000812	***
X528.570007	-0.0115772	0.0034215	-3.384	0.000747	***
X538.739990	-0.0019734	0.0040139	-0.492	0.623085	
X548.919983	0.0068487	0.0042420	1.614	0.106777	
X559.090027	0.0126349	0.0045841	2.756	0.005967	**
X569.270020	0.0019324	0.0047485	0.407	0.684153	
X589.619995	0.0033652	0.0049641	0.678	0.498010	
X640.500000	0.0045136	0.0042945	1.051	0.293539	
X660.849976	0.0042085	0.0047315	0.889	0.373996	
X671.020020	0.0053540	0.0050116	1.068	0.285665	
X681.200012	-0.0119508	0.0048523	-2.463	0.013970	*
X691.369995	-0.0123627	0.0046443	-2.662	0.007911	**
X701.549988	0.0132643	0.0046076	2.879	0.004089	**
X711.719971	-0.0091907	0.0040196	-2.286	0.022462	*
X721.900024	0.0104228	0.0038969	2.675	0.007619	**
X752.429993	-0.0034746	0.0033273	-1.044	0.296643	
X762.599976	-0.0014299	0.0026129	-0.547	0.584355	
X772.780029	-0.0066212	0.0019921	-3.324	0.000925	***
X813.479980	-0.0007823	0.0028032	-0.279	0.780244	
X864.349976	0.0031237	0.0021494	1.453	0.146500	
X894.880005	0.0015370	0.0014840	1.036	0.300592	
X1053.689941	0.0052063	0.0009809	5.307	0.000000141	***
X1094.089966	0.0001150	0.0010580	0.109	0.913433	
X1235.270020	-0.0065959	0.0013048	-5.055	0.000000523	***
X1316.050049	0.0008727	0.0012463	0.700	0.483969	
X1457.229980	-0.0002710	0.0011776	-0.230	0.818052	
X1467.329956	-0.0001314	0.0008583	-0.153	0.878345	
X2133.239990	0.0022347	0.0005821	3.839	0.000132	***

```
---
Signif. codes:  0 ‘***’ 0.001 ‘**’ 0.01 ‘*’ 0.05 ‘.’ 0.1 ‘ ’ 1

Residual standard error: 2.515 on 883 degrees of freedom
Multiple R-squared:  0.2572,    Adjusted R-squared:  0.232
F-statistic: 10.19 on 30 and 883 DF,  p-value: < 2.2e-16

> p=update(g,.~.- X1094.089966)
Error in update.default(g, . ~ . - X1094.089966) :
  need an object with call component
> p=update(p,.~.-X1094.089966)
> summary(p)

Call:
lm(formula = Class ~ X447.170013 + X477.690002 + X508.220001 +
    X528.570007 + X538.739990 + X548.919983 + X559.090027 + X569.270020 +
    X589.619995 + X640.500000 + X660.849976 + X671.020020 + X681.200012 +
    X691.369995 + X701.549988 + X711.719971 + X721.900024 + X752.429993 +
    X762.599976 + X772.780029 + X813.479980 + X864.349976 + X894.880005 +
    X1053.689941 + X1235.270020 + X1316.050049 + X1457.229980 +
    X1467.329956 + X2133.239990, data = (g))

Residuals:
    Min      1Q  Median      3Q     Max
-6.1653 -1.6548 -0.0613  1.9359  7.0435

Coefficients:
             Estimate Std. Error t value      Pr(>|t|)
(Intercept)   3.0149984  1.3001442   2.319      0.020624 *
X447.170013  -0.0015408  0.0010024  -1.537      0.124618
X477.690002   0.0027813  0.0028545   0.974      0.330146
X508.220001  -0.0106825  0.0031787  -3.361      0.000811 ***
X528.570007  -0.0116037  0.0034109  -3.402      0.000699 ***
```

```
X538.739990  -0.0019856  0.0040101  -0.495     0.620616
X548.919983   0.0068425  0.0042393   1.614     0.106868
X559.090027   0.0126173  0.0045786   2.756     0.005978 **
X569.270020   0.0019313  0.0047459   0.407     0.684148
X589.619995   0.0033972  0.0049526   0.686     0.492927
X640.500000   0.0045193  0.0042918   1.053     0.292628
X660.849976   0.0041786  0.0047209   0.885     0.376328
X671.020020   0.0053518  0.0050087   1.068     0.285587
X681.200012  -0.0119338  0.0048470  -2.462     0.014003 *
X691.369995  -0.0123943  0.0046325  -2.675     0.007600 **
X701.549988   0.0132658  0.0046050   2.881     0.004063 **
X711.719971  -0.0092107  0.0040131  -2.295     0.021958 *
X721.900024   0.0104455  0.0038891   2.686     0.007370 **
X752.429993  -0.0034801  0.0033250  -1.047     0.295560
X762.599976  -0.0014412  0.0026094  -0.552     0.580883
X772.780029  -0.0066041  0.0019847  -3.327     0.000913 ***
X813.479980  -0.0007730  0.0028003  -0.276     0.782580
X864.349976   0.0031264  0.0021481   1.455     0.145896
X894.880005   0.0015494  0.0014788   1.048     0.295022
X1053.689941  0.0052507  0.0008913   5.891 0.00000000544 ***
X1235.270020 -0.0065566  0.0012531  -5.232 0.00000020898 ***
X1316.050049  0.0008867  0.0012390   0.716     0.474375
X1457.229980 -0.0002781  0.0011751  -0.237     0.812967
X1467.329956 -0.0001276  0.0008571  -0.149     0.881668
X2133.239990  0.0022362  0.0005816   3.845     0.000129 ***
---
Signif. codes:  0 ‘***’ 0.001 ‘**’ 0.01 ‘*’ 0.05 ‘.’ 0.1 ‘ ’ 1

Residual standard error: 2.513 on 884 degrees of freedom
Multiple R-squared:  0.2572,    Adjusted R-squared:  0.2329
F-statistic: 10.56 on 29 and 884 DF,  p-value: < 2.2e-16

> p=update(p,.~.-X1467.329956)
```

```
> summary(p)

Call:
lm(formula = Class ~ X447.170013 + X477.690002 + X508.220001 +
    X528.570007 + X538.739990 + X548.919983 + X559.090027 + X569.270020 +
    X589.619995 + X640.500000 + X660.849976 + X671.020020 + X681.200012 +
    X691.369995 + X701.549988 + X711.719971 + X721.900024 + X752.429993 +
    X762.599976 + X772.780029 + X813.479980 + X864.349976 + X894.880005 +
    X1053.689941 + X1235.270020 + X1316.050049 + X1457.229980 +
    X2133.239990, data = (g))

Residuals:
    Min      1Q  Median      3Q     Max
-6.1706 -1.6584 -0.0665  1.9316  7.0314

Coefficients:
             Estimate Std. Error t value      Pr(>|t|)
(Intercept)  3.0080861  1.2985971   2.316     0.020763 *
X447.170013 -0.0015448  0.0010015  -1.543     0.123299
X477.690002  0.0027616  0.0028498   0.969     0.332790
X508.220001 -0.0106416  0.0031651  -3.362     0.000806 ***
X528.570007 -0.0115833  0.0034063  -3.401     0.000702 ***
X538.739990 -0.0019950  0.0040074  -0.498     0.618726
X548.919983  0.0068172  0.0042335   1.610     0.107691
X559.090027  0.0126658  0.0045645   2.775     0.005640 **
X569.270020  0.0019419  0.0047427   0.409     0.682305
X589.619995  0.0033789  0.0049483   0.683     0.494890
X640.500000  0.0044575  0.0042694   1.044     0.296735
X660.849976  0.0041963  0.0047168   0.890     0.373897
X671.020020  0.0053896  0.0049995   1.078     0.281315
X681.200012 -0.0119608  0.0048410  -2.471     0.013670 *
X691.369995 -0.0123600  0.0046242  -2.673     0.007659 **
X701.549988  0.0132577  0.0046022   2.881     0.004063 **
```

```
X711.719971  -0.0091973  0.0040099  -2.294      0.022044 *
X721.900024   0.0104297  0.0038855   2.684      0.007405 **
X752.429993  -0.0034894  0.0033226  -1.050      0.293909
X762.599976  -0.0014361  0.0026078  -0.551      0.581967
X772.780029  -0.0066120  0.0019829  -3.334      0.000890 ***
X813.479980  -0.0007676  0.0027985  -0.274      0.783930
X864.349976   0.0031283  0.0021468   1.457      0.145430
X894.880005   0.0015455  0.0014777   1.046      0.295901
X1053.689941  0.0052545  0.0008904   5.901 0.00000000514 ***
X1235.270020 -0.0065496  0.0012515  -5.233 0.00000020786 ***
X1316.050049  0.0008899  0.0012381   0.719      0.472492
X1457.229980 -0.0004408  0.0004318  -1.021      0.307512
X2133.239990  0.0022447  0.0005785   3.880      0.000112 ***
---
Signif. codes:  0 '***' 0.001 '**' 0.01 '*' 0.05 '.' 0.1 ' ' 1

Residual standard error: 2.512 on 885 degrees of freedom
Multiple R-squared:  0.2572,    Adjusted R-squared:  0.2337
F-statistic: 10.94 on 28 and 885 DF,  p-value: < 2.2e-16

> p=update(p,.~.-X813.479980)
> summary(p)

Call:
lm(formula = Class ~ X447.170013 + X477.690002 + X508.220001 +
    X528.570007 + X538.739990 + X548.919983 + X559.090027 + X569.270020 +
    X589.619995 + X640.500000 + X660.849976 + X671.020020 + X681.200012 +
    X691.369995 + X701.549988 + X711.719971 + X721.900024 + X752.429993 +
    X762.599976 + X772.780029 + X864.349976 + X894.880005 + X1053.689941 +
    X1235.270020 + X1316.050049 + X1457.229980 + X2133.239990,
    data = (g))

Residuals:
```

```
   Min     1Q Median     3Q    Max
-6.147 -1.651 -0.076  1.960  6.997


Coefficients:
             Estimate Std. Error t value      Pr(>|t|)
(Intercept)   2.9232435  1.2605605   2.319     0.020622 *
X447.170013  -0.0015660  0.0009980  -1.569     0.116977
X477.690002   0.0027740  0.0028480   0.974     0.330317
X508.220001  -0.0106267  0.0031630  -3.360     0.000813 ***
X528.570007  -0.0115560  0.0034030  -3.396     0.000715 ***
X538.739990  -0.0019308  0.0039984  -0.483     0.629300
X548.919983   0.0068605  0.0042284   1.622     0.105054
X559.090027   0.0126876  0.0045615   2.781     0.005526 **
X569.270020   0.0019227  0.0047397   0.406     0.685096
X589.619995   0.0033889  0.0049456   0.685     0.493377
X640.500000   0.0044470  0.0042670   1.042     0.297609
X660.849976   0.0041732  0.0047136   0.885     0.376201
X671.020020   0.0054796  0.0049862   1.099     0.272086
X681.200012  -0.0119624  0.0048384  -2.472     0.013609 *
X691.369995  -0.0124792  0.0046014  -2.712     0.006816 **
X701.549988   0.0132410  0.0045993   2.879     0.004087 **
X711.719971  -0.0091917  0.0040077  -2.293     0.022054 *
X721.900024   0.0104522  0.0038826   2.692     0.007235 **
X752.429993  -0.0038855  0.0029909  -1.299     0.194251
X762.599976  -0.0015480  0.0025743  -0.601     0.547774
X772.780029  -0.0066340  0.0019803  -3.350     0.000842 ***
X864.349976   0.0029750  0.0020717   1.436     0.151359
X894.880005   0.0014487  0.0014342   1.010     0.312716
X1053.689941  0.0052263  0.0008840   5.912 0.00000000481 ***
X1235.270020 -0.0065067  0.0012410  -5.243 0.00000019766 ***
X1316.050049  0.0008483  0.0012282   0.691     0.489911
X1457.229980 -0.0004344  0.0004309  -1.008     0.313664
X2133.239990  0.0022492  0.0005779   3.892     0.000107 ***
```

```
---
Signif. codes:  0 ‘***’ 0.001 ‘**’ 0.01 ‘*’ 0.05 ‘.’ 0.1 ‘ ’ 1

Residual standard error: 2.51 on 886 degrees of freedom
Multiple R-squared:  0.2571,    Adjusted R-squared:  0.2345
F-statistic: 11.36 on 27 and 886 DF,  p-value: < 2.2e-16

> p=update(p,.~.-X569.270020)
> summary(p)

Call:
lm(formula = Class ~ X447.170013 + X477.690002 + X508.220001 +
    X528.570007 + X538.739990 + X548.919983 + X559.090027 + X589.619995 +
    X640.500000 + X660.849976 + X671.020020 + X681.200012 + X691.369995 +
    X701.549988 + X711.719971 + X721.900024 + X752.429993 + X762.599976 +
    X772.780029 + X864.349976 + X894.880005 + X1053.689941 +
    X1235.270020 + X1316.050049 + X1457.229980 + X2133.239990,
    data = (g))

Residuals:
    Min      1Q  Median      3Q     Max
-6.1581 -1.6376 -0.0806  1.9713  6.9683

Coefficients:
             Estimate Std. Error t value     Pr(>|t|)
(Intercept)   2.9664117  1.2554690   2.363     0.018353 *
X447.170013  -0.0015438  0.0009960  -1.550     0.121506
X477.690002   0.0028908  0.0028320   1.021     0.307651
X508.220001  -0.0106302  0.0031615  -3.362     0.000806 ***
X528.570007  -0.0114755  0.0033956  -3.379     0.000758 ***
X538.739990  -0.0015964  0.0039107  -0.408     0.683218
X548.919983   0.0071808  0.0041520   1.729     0.084072 .
X559.090027   0.0131065  0.0044409   2.951     0.003248 **
```

```
X589.619995   0.0037824  0.0048472   0.780     0.435414
X640.500000   0.0046134  0.0042452   1.087     0.277448
X660.849976   0.0043562  0.0046897   0.929     0.353207
X671.020020   0.0054678  0.0049837   1.097     0.272884
X681.200012  -0.0120351  0.0048328  -2.490     0.012946 *
X691.369995  -0.0125728  0.0045934  -2.737     0.006322 **
X701.549988   0.0132208  0.0045969   2.876     0.004124 **
X711.719971  -0.0090766  0.0039958  -2.272     0.023353 *
X721.900024   0.0104892  0.0038797   2.704     0.006991 **
X752.429993  -0.0037451  0.0029694  -1.261     0.207558
X762.599976  -0.0015167  0.0025719  -0.590     0.555525
X772.780029  -0.0067857  0.0019437  -3.491     0.000505 ***
X864.349976   0.0029966  0.0020701   1.448     0.148083
X894.880005   0.0014284  0.0014326   0.997     0.319017
X1053.689941  0.0051940  0.0008800   5.902 0.0000000051 ***
X1235.270020 -0.0064900  0.0012398  -5.235 0.0000002062 ***
X1316.050049  0.0008523  0.0012276   0.694     0.487686
X1457.229980 -0.0004529  0.0004283  -1.058     0.290566
X2133.239990  0.0022462  0.0005776   3.889     0.000108 ***
---
Signif. codes:  0 ‘***’ 0.001 ‘**’ 0.01 ‘*’ 0.05 ‘.’ 0.1 ‘ ’ 1

Residual standard error: 2.509 on 887 degrees of freedom
Multiple R-squared:  0.257,     Adjusted R-squared:  0.2352
F-statistic:  11.8 on 26 and 887 DF,  p-value: < 2.2e-16

> p=update(p,.~.-X538.739990)
> summary(p)

Call:
lm(formula = Class ~ X447.170013 + X477.690002 + X508.220001 +
    X528.570007 + X548.919983 + X559.090027 + X589.619995 + X640.500000 +
    X660.849976 + X671.020020 + X681.200012 + X691.369995 + X701.549988 +
```

```
    X711.719971 + X721.900024 + X752.429993 + X762.599976 + X772.780029 +
    X864.349976 + X894.880005 + X1053.689941 + X1235.270020 +
    X1316.050049 + X1457.229980 + X2133.239990, data = (g))

Residuals:
    Min      1Q  Median      3Q     Max
-6.1642 -1.6772 -0.0837  1.9704  6.9281

Coefficients:
                Estimate Std. Error t value      Pr(>|t|)
(Intercept)    2.7766663  1.1657039   2.382      0.017430 *
X447.170013   -0.0015717  0.0009932  -1.582      0.113911
X477.690002    0.0027542  0.0028109   0.980      0.327430
X508.220001   -0.0107607  0.0031438  -3.423      0.000648 ***
X528.570007   -0.0117530  0.0033253  -3.534      0.000430 ***
X548.919983    0.0068290  0.0040597   1.682      0.092891 .
X559.090027    0.0127551  0.0043547   2.929      0.003487 **
X589.619995    0.0035900  0.0048220   0.744      0.456773
X640.500000    0.0043959  0.0042096   1.044      0.296657
X660.849976    0.0043267  0.0046870   0.923      0.356185
X671.020020    0.0055371  0.0049785   1.112      0.266348
X681.200012   -0.0118851  0.0048166  -2.468      0.013792 *
X691.369995   -0.0126039  0.0045906  -2.746      0.006162 **
X701.549988    0.0132960  0.0045911   2.896      0.003871 **
X711.719971   -0.0091540  0.0039894  -2.295      0.021991 *
X721.900024    0.0104810  0.0038778   2.703      0.007007 **
X752.429993   -0.0037965  0.0029654  -1.280      0.200789
X762.599976   -0.0014545  0.0025662  -0.567      0.570996
X772.780029   -0.0068208  0.0019409  -3.514      0.000463 ***
X864.349976    0.0029964  0.0020691   1.448      0.147920
X894.880005    0.0014589  0.0014300   1.020      0.307895
X1053.689941   0.0051796  0.0008789   5.894 0.00000000536 ***
X1235.270020  -0.0065080  0.0012384  -5.255 0.00000018532 ***
```

```
X1316.050049  0.0009042  0.0012204   0.741     0.458958
X1457.229980 -0.0004530  0.0004281  -1.058     0.290201
X2133.239990  0.0022365  0.0005769   3.877     0.000114 ***
---
Signif. codes:  0 '***' 0.001 '**' 0.01 '*' 0.05 '.' 0.1 ' ' 1

Residual standard error: 2.508 on 888 degrees of freedom
Multiple R-squared:  0.2569,    Adjusted R-squared:  0.2359
F-statistic: 12.28 on 25 and 888 DF,  p-value: < 2.2e-16

> p=update(p,.~.-X762.599976)
> summary(p)

Call:
lm(formula = Class ~ X447.170013 + X477.690002 + X508.220001 +
   X528.570007 + X548.919983 + X559.090027 + X589.619995 + X640.500000 +
   X660.849976 + X671.020020 + X681.200012 + X691.369995 + X701.549988 +
   X711.719971 + X721.900024 + X752.429993 + X772.780029 + X864.349976 +
   X894.880005 + X1053.689941 + X1235.270020 + X1316.050049 +
   X1457.229980 + X2133.239990, data = (g))

Residuals:
   Min     1Q  Median     3Q     Max
-6.1339 -1.6660 -0.0976  1.9501  6.9263

Coefficients:
             Estimate Std. Error t value      Pr(>|t|)
(Intercept)   2.6997494  1.1573359   2.333     0.019885 *
X447.170013  -0.0015383  0.0009911  -1.552     0.120988
X477.690002   0.0026794  0.0028067   0.955     0.340029
X508.220001  -0.0106488  0.0031364  -3.395     0.000716 ***
X528.570007  -0.0116151  0.0033152  -3.504     0.000482 ***
X548.919983   0.0067659  0.0040566   1.668     0.095694 .
```

```
X559.090027   0.0126611  0.0043498   2.911     0.003696 **
X589.619995   0.0034633  0.0048150   0.719     0.472165
X640.500000   0.0042266  0.0041974   1.007     0.314230
X660.849976   0.0044151  0.0046826   0.943     0.345994
X671.020020   0.0057725  0.0049593   1.164     0.244746
X681.200012  -0.0119184  0.0048144  -2.476     0.013487 *
X691.369995  -0.0128032  0.0045754  -2.798     0.005249 **
X701.549988   0.0135171  0.0045727   2.956     0.003199 **
X711.719971  -0.0090409  0.0039829  -2.270     0.023451 *
X721.900024   0.0104216  0.0038749   2.690     0.007290 **
X752.429993  -0.0046698  0.0025327  -1.844     0.065546 .
X772.780029  -0.0072958  0.0017501  -4.169 0.00003360736 ***
X864.349976   0.0029432  0.0020662   1.424     0.154664
X894.880005   0.0014172  0.0014275   0.993     0.321100
X1053.689941  0.0051946  0.0008781   5.916 0.00000000471 ***
X1235.270020 -0.0065666  0.0012336  -5.323 0.00000012922 ***
X1316.050049  0.0009883  0.0012109   0.816     0.414630
X1457.229980 -0.0004921  0.0004223  -1.165     0.244283
X2133.239990  0.0022167  0.0005756   3.851     0.000126 ***
---
Signif. codes:  0 ‘***’ 0.001 ‘**’ 0.01 ‘*’ 0.05 ‘.’ 0.1 ‘ ’ 1

Residual standard error: 2.507 on 889 degrees of freedom
Multiple R-squared:  0.2566,    Adjusted R-squared:  0.2365
F-statistic: 12.79 on 24 and 889 DF,  p-value: < 2.2e-16

> p=update(p,.~.-X589.619995)
> summary(p)

Call:
lm(formula = Class ~ X447.170013 + X477.690002 + X508.220001 +
    X528.570007 + X548.919983 + X559.090027 + X640.500000 + X660.849976 +
    X671.020020 + X681.200012 + X691.369995 + X701.549988 + X711.719971 +
```

```
   X721.900024 + X752.429993 + X772.780029 + X864.349976 + X894.880005 +
   X1053.689941 + X1235.270020 + X1316.050049 + X1457.229980 +
   X2133.239990, data = (g))

Residuals:
   Min     1Q  Median     3Q    Max
-6.1607 -1.6944 -0.0659  1.9394  6.7865

Coefficients:
             Estimate Std. Error t value      Pr(>|t|)
(Intercept)   2.7026100  1.1570152   2.336     0.019720 *
X447.170013  -0.0015457  0.0009908  -1.560     0.119088
X477.690002   0.0028506  0.0027958   1.020     0.308205
X508.220001  -0.0106426  0.0031355  -3.394     0.000719 ***
X528.570007  -0.0111108  0.0032393  -3.430     0.000631 ***
X548.919983   0.0075027  0.0039241   1.912     0.056203 .
X559.090027   0.0133172  0.0042520   3.132     0.001793 **
X640.500000   0.0047041  0.0041435   1.135     0.256558
X660.849976   0.0045738  0.0046761   0.978     0.328277
X671.020020   0.0060733  0.0049403   1.229     0.219269
X681.200012  -0.0118613  0.0048124  -2.465     0.013899 *
X691.369995  -0.0127633  0.0045738  -2.791     0.005375 **
X701.549988   0.0136071  0.0045698   2.978     0.002983 **
X711.719971  -0.0087231  0.0039573  -2.204     0.027757 *
X721.900024   0.0104645  0.0038734   2.702     0.007032 **
X752.429993  -0.0047136  0.0025313  -1.862     0.062911 .
X772.780029  -0.0073540  0.0017477  -4.208 0.00002840069 ***
X864.349976   0.0029573  0.0020655   1.432     0.152558
X894.880005   0.0014474  0.0014265   1.015     0.310544
X1053.689941  0.0052116  0.0008776   5.939 0.00000000412 ***
X1235.270020 -0.0066418  0.0012288  -5.405 0.00000008331 ***
X1316.050049  0.0010123  0.0012101   0.837     0.403078
X1457.229980 -0.0004715  0.0004213  -1.119     0.263284
```

```
X2133.239990  0.0022089  0.0005753   3.839      0.000132 ***
---
Signif. codes:  0 ‘***’ 0.001 ‘**’ 0.01 ‘*’ 0.05 ‘.’ 0.1 ‘ ’ 1

Residual standard error: 2.506 on 890 degrees of freedom
Multiple R-squared:  0.2562,    Adjusted R-squared:  0.2369
F-statistic: 13.33 on 23 and 890 DF,  p-value: < 2.2e-16

> p=update(p,.~.-X1316.050049)
> summary(p)

Call:
lm(formula = Class ~ X447.170013 + X477.690002 + X508.220001 +
   X528.570007 + X548.919983 + X559.090027 + X640.500000 + X660.849976 +
   X671.020020 + X681.200012 + X691.369995 + X701.549988 + X711.719971 +
   X721.900024 + X752.429993 + X772.780029 + X864.349976 + X894.880005 +
   X1053.689941 + X1235.270020 + X1457.229980 + X2133.239990,
   data = (g))

Residuals:
   Min     1Q  Median     3Q     Max
-6.1109 -1.6712 -0.0712  1.9696  6.8280

Coefficients:
             Estimate Std. Error t value Pr(>|t|)
(Intercept)   2.7971005  1.1512943   2.430 0.015315 *
X447.170013  -0.0016263  0.0009859  -1.650 0.099384 .
X477.690002   0.0027125  0.0027905   0.972 0.331289
X508.220001  -0.0105580  0.0031334  -3.370 0.000785 ***
X528.570007  -0.0111581  0.0032383  -3.446 0.000596 ***
X548.919983   0.0074326  0.0039225   1.895 0.058435 .
X559.090027   0.0131205  0.0042447   3.091 0.002057 **
X640.500000   0.0044337  0.0041302   1.073 0.283344
```

```
X660.849976   0.0045587  0.0046753   0.975 0.329794
X671.020020   0.0062246  0.0049361   1.261 0.207624
X681.200012  -0.0117984  0.0048110  -2.452 0.014383 *
X691.369995  -0.0125459  0.0045657  -2.748 0.006119 **
X701.549988   0.0138503  0.0045597   3.038 0.002455 **
X711.719971  -0.0089367  0.0039483  -2.263 0.023850 *
X721.900024   0.0108659  0.0038429   2.827 0.004797 **
X752.429993  -0.0047660  0.0025301  -1.884 0.059925 .
X772.780029  -0.0075975  0.0017230  -4.409 1.16e-05 ***
X864.349976   0.0029272  0.0020648   1.418 0.156646
X894.880005   0.0016066  0.0014136   1.137 0.256036
X1053.689941  0.0052369  0.0008769   5.972 3.38e-09 ***
X1235.270020 -0.0058891  0.0008369  -7.037 3.92e-12 ***
X1457.229980 -0.0004024  0.0004130  -0.974 0.330138
X2133.239990  0.0022314  0.0005746   3.883 0.000111 ***
---
Signif. codes:  0 '***' 0.001 '**' 0.01 '*' 0.05 '.' 0.1 ' ' 1

Residual standard error: 2.506 on 891 degrees of freedom
Multiple R-squared:  0.2556,    Adjusted R-squared:  0.2372
F-statistic:  13.9 on 22 and 891 DF,  p-value: < 2.2e-16

> p=update(p,.~.-X477.690002)
> summary(p)

Call:
lm(formula = Class ~ X447.170013 + X508.220001 + X528.570007 +
    X548.919983 + X559.090027 + X640.500000 + X660.849976 + X671.020020 +
    X681.200012 + X691.369995 + X701.549988 + X711.719971 + X721.900024 +
    X752.429993 + X772.780029 + X864.349976 + X894.880005 + X1053.689941 +
    X1235.270020 + X1457.229980 + X2133.239990, data = (g))

Residuals:
```

```
   Min     1Q  Median     3Q    Max
-6.0525 -1.7182 -0.0792  1.9857  6.8519

Coefficients:
             Estimate Std. Error t value Pr(>|t|)
(Intercept)   2.5049028  1.1113247   2.254 0.024439 *
X447.170013  -0.0015015  0.0009775  -1.536 0.124873
X508.220001  -0.0097915  0.0030324  -3.229 0.001288 **
X528.570007  -0.0110498  0.0032362  -3.414 0.000668 ***
X548.919983   0.0078746  0.0038960   2.021 0.043556 *
X559.090027   0.0135306  0.0042236   3.204 0.001405 **
X640.500000   0.0041464  0.0041195   1.007 0.314425
X660.849976   0.0048788  0.0046635   1.046 0.295771
X671.020020   0.0059731  0.0049292   1.212 0.225914
X681.200012  -0.0116410  0.0048081  -2.421 0.015672 *
X691.369995  -0.0118387  0.0045072  -2.627 0.008771 **
X701.549988   0.0134943  0.0045449   2.969 0.003066 **
X711.719971  -0.0092768  0.0039327  -2.359 0.018544 *
X721.900024   0.0109478  0.0038419   2.850 0.004479 **
X752.429993  -0.0045455  0.0025198  -1.804 0.071581 .
X772.780029  -0.0077121  0.0017189  -4.487 8.18e-06 ***
X864.349976   0.0028918  0.0020645   1.401 0.161635
X894.880005   0.0015613  0.0014127   1.105 0.269384
X1053.689941  0.0052733  0.0008761   6.019 2.56e-09 ***
X1235.270020 -0.0059346  0.0008356  -7.103 2.50e-12 ***
X1457.229980 -0.0003736  0.0004119  -0.907 0.364627
X2133.239990  0.0022518  0.0005742   3.922 9.47e-05 ***
---
Signif. codes:  0 ‘***’ 0.001 ‘**’ 0.01 ‘*’ 0.05 ‘.’ 0.1 ‘ ’ 1

Residual standard error: 2.506 on 892 degrees of freedom
Multiple R-squared:  0.2548,    Adjusted R-squared:  0.2372
F-statistic: 14.52 on 21 and 892 DF,  p-value: < 2.2e-16
```

```
> p=update(p,.~.-X1457.229980)
> summary(p)

Call:
lm(formula = Class ~ X447.170013 + X508.220001 + X528.570007 +
    X548.919983 + X559.090027 + X640.500000 + X660.849976 + X671.020020 +
    X681.200012 + X691.369995 + X701.549988 + X711.719971 + X721.900024 +
    X752.429993 + X772.780029 + X864.349976 + X894.880005 + X1053.689941 +
    X1235.270020 + X2133.239990, data = (g))

Residuals:
    Min      1Q  Median      3Q     Max
-6.0268 -1.6621 -0.0637  1.9798  6.8363

Coefficients:
             Estimate Std. Error t value Pr(>|t|)
(Intercept)   2.5267511  1.1109533   2.274 0.023178 *
X447.170013  -0.0014789  0.0009771  -1.514 0.130467
X508.220001  -0.0096972  0.0030303  -3.200 0.001423 **
X528.570007  -0.0110897  0.0032356  -3.427 0.000637 ***
X548.919983   0.0076334  0.0038865   1.964 0.049830 *
X559.090027   0.0136804  0.0042199   3.242 0.001232 **
X640.500000   0.0039927  0.0041156   0.970 0.332229
X660.849976   0.0046509  0.0046563   0.999 0.318138
X671.020020   0.0061279  0.0049257   1.244 0.213803
X681.200012  -0.0115220  0.0048059  -2.397 0.016713 *
X691.369995  -0.0117494  0.0045056  -2.608 0.009267 **
X701.549988   0.0132958  0.0045391   2.929 0.003485 **
X711.719971  -0.0090341  0.0039232  -2.303 0.021522 *
X721.900024   0.0107653  0.0038363   2.806 0.005122 **
X752.429993  -0.0042947  0.0025043  -1.715 0.086710 .
X772.780029  -0.0079463  0.0016992  -4.676 3.37e-06 ***
X864.349976   0.0029004  0.0020642   1.405 0.160348
```

```
X894.880005   0.0016447  0.0014096   1.167 0.243617
X1053.689941  0.0052472  0.0008755   5.993 2.98e-09 ***
X1235.270020 -0.0059750  0.0008343  -7.162 1.67e-12 ***
X2133.239990  0.0020043  0.0005052   3.968 7.84e-05 ***
---
Signif. codes:  0 '***' 0.001 '**' 0.01 '*' 0.05 '.' 0.1 ' ' 1

Residual standard error: 2.506 on 893 degrees of freedom
Multiple R-squared:  0.2541,    Adjusted R-squared:  0.2374
F-statistic: 15.21 on 20 and 893 DF,  p-value: < 2.2e-16

> p=update(p,.~.-X640.500000)
> summary(p)

Call:
lm(formula = Class ~ X447.170013 + X508.220001 + X528.570007 +
   X548.919983 + X559.090027 + X660.849976 + X671.020020 + X681.200012 +
   X691.369995 + X701.549988 + X711.719971 + X721.900024 + X752.429993 +
   X772.780029 + X864.349976 + X894.880005 + X1053.689941 +
   X1235.270020 + X2133.239990, data = (g))

Residuals:
   Min     1Q  Median     3Q    Max
-6.0252 -1.7065 -0.0426  2.0188  6.7819

Coefficients:
             Estimate Std. Error t value Pr(>|t|)
(Intercept)   2.0729779  1.0076601   2.057 0.039955 *
X447.170013  -0.0014054  0.0009741  -1.443 0.149434
X508.220001  -0.0097674  0.0030294  -3.224 0.001309 **
X528.570007  -0.0111923  0.0032338  -3.461 0.000564 ***
X548.919983   0.0081425  0.0038508   2.115 0.034747 *
X559.090027   0.0143583  0.0041615   3.450 0.000586 ***
```

```
X660.849976   0.0055307  0.0045670   1.211 0.226205
X671.020020   0.0064462  0.0049146   1.312 0.189982
X681.200012  -0.0108206  0.0047510  -2.278 0.022990 *
X691.369995  -0.0113762  0.0044890  -2.534 0.011440 *
X701.549988   0.0141307  0.0044567   3.171 0.001573 **
X711.719971  -0.0088191  0.0039168  -2.252 0.024589 *
X721.900024   0.0104818  0.0038250   2.740 0.006260 **
X752.429993  -0.0041504  0.0024998  -1.660 0.097211 .
X772.780029  -0.0079559  0.0016992  -4.682 3.28e-06 ***
X864.349976   0.0028208  0.0020625   1.368 0.171765
X894.880005   0.0016633  0.0014094   1.180 0.238279
X1053.689941  0.0052450  0.0008755   5.991 3.02e-09 ***
X1235.270020 -0.0060039  0.0008337  -7.201 1.27e-12 ***
X2133.239990  0.0019914  0.0005050   3.944 8.66e-05 ***
---
Signif. codes:  0 '***' 0.001 '**' 0.01 '*' 0.05 '.' 0.1 ' ' 1

Residual standard error: 2.506 on 894 degrees of freedom
Multiple R-squared:  0.2533,    Adjusted R-squared:  0.2374
F-statistic: 15.96 on 19 and 894 DF,  p-value: < 2.2e-16

> p=update(p,.~.-X894.880005)
> summary(p)

Call:
lm(formula = Class ~ X447.170013 + X508.220001 + X528.570007 +
    X548.919983 + X559.090027 + X660.849976 + X671.020020 + X681.200012 +
    X691.369995 + X701.549988 + X711.719971 + X721.900024 + X752.429993 +
    X772.780029 + X864.349976 + X1053.689941 + X1235.270020 +
    X2133.239990, data = (g))
```

```
Residuals:
    Min      1Q  Median      3Q     Max
-5.9657 -1.6531 -0.0563  1.9943  6.8855

Coefficients:
              Estimate Std. Error t value Pr(>|t|)
(Intercept)   2.3102095  0.9876204   2.339 0.019546 *
X447.170013  -0.0014029  0.0009743  -1.440 0.150247
X508.220001  -0.0100425  0.0030211  -3.324 0.000923 ***
X528.570007  -0.0111234  0.0032340  -3.440 0.000610 ***
X548.919983   0.0079295  0.0038474   2.061 0.039590 *
X559.090027   0.0142245  0.0041609   3.419 0.000658 ***
X660.849976   0.0056108  0.0045675   1.228 0.219607
X671.020020   0.0063735  0.0049153   1.297 0.195082
X681.200012  -0.0103303  0.0047339  -2.182 0.029353 *
X691.369995  -0.0115637  0.0044872  -2.577 0.010124 *
X701.549988   0.0141652  0.0044576   3.178 0.001535 **
X711.719971  -0.0089499  0.0039161  -2.285 0.022521 *
X721.900024   0.0106165  0.0038241   2.776 0.005615 **
X752.429993  -0.0030442  0.0023179  -1.313 0.189415
X772.780029  -0.0085398  0.0016259  -5.252 1.88e-07 ***
X864.349976   0.0038835  0.0018560   2.092 0.036678 *
X1053.689941  0.0053634  0.0008699   6.165 1.06e-09 ***
X1235.270020 -0.0059564  0.0008329  -7.151 1.79e-12 ***
X2133.239990  0.0019547  0.0005041   3.877 0.000113 ***
---
Signif. codes:  0 ‘***’ 0.001 ‘**’ 0.01 ‘*’ 0.05 ‘.’ 0.1 ‘ ’ 1

Residual standard error: 2.506 on 895 degrees of freedom
Multiple R-squared:  0.2522,    Adjusted R-squared:  0.2371
F-statistic: 16.76 on 18 and 895 DF,  p-value: < 2.2e-16
```

```
> p=update(p,.~.-X660.849976)
> summary(p)

Call:
lm(formula = Class ~ X447.170013 + X508.220001 + X528.570007 +
    X548.919983 + X559.090027 + X671.020020 + X681.200012 + X691.369995 +
    X701.549988 + X711.719971 + X721.900024 + X752.429993 + X772.780029 +
    X864.349976 + X1053.689941 + X1235.270020 + X2133.239990,
    data = (g))

Residuals:
   Min     1Q Median     3Q    Max
-5.930 -1.685 -0.041  1.940  6.892

Coefficients:
             Estimate Std. Error t value Pr(>|t|)
(Intercept)   2.3316334  0.9877468   2.361 0.018461 *
X447.170013  -0.0013937  0.0009745  -1.430 0.153031
X508.220001  -0.0099086  0.0030200  -3.281 0.001074 **
X528.570007  -0.0105984  0.0032065  -3.305 0.000987 ***
X548.919983   0.0080365  0.0038475   2.089 0.037011 *
X559.090027   0.0146063  0.0041505   3.519 0.000455 ***
X671.020020   0.0075816  0.0048173   1.574 0.115880
X681.200012  -0.0087207  0.0045502  -1.917 0.055612 .
X691.369995  -0.0105090  0.0044056  -2.385 0.017267 *
X701.549988   0.0152292  0.0043738   3.482 0.000522 ***
X711.719971  -0.0090310  0.0039166  -2.306 0.021349 *
X721.900024   0.0101673  0.0038077   2.670 0.007717 **
X752.429993  -0.0030756  0.0023184  -1.327 0.184985
X772.780029  -0.0084842  0.0016257  -5.219 2.24e-07 ***
X864.349976   0.0040334  0.0018525   2.177 0.029719 *
X1053.689941  0.0053083  0.0008690   6.109 1.50e-09 ***
X1235.270020 -0.0059186  0.0008326  -7.108 2.40e-12 ***
```

```
X2133.239990  0.0019105  0.0005030   3.798 0.000155 ***
---
Signif. codes:  0 ‘***’ 0.001 ‘**’ 0.01 ‘*’ 0.05 ‘.’ 0.1 ‘ ’ 1

Residual standard error: 2.507 on 896 degrees of freedom
Multiple R-squared:  0.2509,    Adjusted R-squared:  0.2367
F-statistic: 17.65 on 17 and 896 DF,  p-value: < 2.2e-16

> p=update(p,.~.-X721.900024)
> summary(p)

Call:
lm(formula = Class ~ X447.170013 + X508.220001 + X528.570007 +
    X548.919983 + X559.090027 + X671.020020 + X681.200012 + X691.369995 +
    X701.549988 + X711.719971 + X752.429993 + X772.780029 + X864.349976 +
    X1053.689941 + X1235.270020 + X2133.239990, data = (g))

Residuals:
    Min      1Q  Median      3Q     Max
-6.0706 -1.6978 -0.0836  2.0667  6.7476

Coefficients:
             Estimate Std. Error t value Pr(>|t|)
(Intercept)   2.4129497  0.9906450   2.436 0.015055 *
X447.170013  -0.0014275  0.0009778  -1.460 0.144659
X508.220001  -0.0101798  0.0030285  -3.361 0.000809 ***
X528.570007  -0.0107226  0.0032171  -3.333 0.000894 ***
X548.919983   0.0090489  0.0038418   2.355 0.018719 *
X559.090027   0.0153630  0.0041549   3.698 0.000231 ***
X671.020020   0.0057190  0.0047828   1.196 0.232110
X681.200012  -0.0102897  0.0045275  -2.273 0.023280 *
X691.369995  -0.0106855  0.0044201  -2.417 0.015827 *
X701.549988   0.0177594  0.0042845   4.145 3.72e-05 ***
```

```
X711.719971  -0.0010813  0.0025536  -0.423 0.672064
X752.429993  -0.0023103  0.0023085  -1.001 0.317198
X772.780029  -0.0070487  0.0015395  -4.579 5.34e-06 ***
X864.349976   0.0040865  0.0018587   2.199 0.028162 *
X1053.689941  0.0052375  0.0008716   6.009 2.71e-09 ***
X1235.270020 -0.0058860  0.0008354  -7.046 3.67e-12 ***
X2133.239990  0.0018907  0.0005046   3.747 0.000191 ***
---
Signif. codes:  0 '***' 0.001 '**' 0.01 '*' 0.05 '.' 0.1 ' ' 1

Residual standard error: 2.515 on 897 degrees of freedom
Multiple R-squared:  0.2449,    Adjusted R-squared:  0.2315
F-statistic: 18.19 on 16 and 897 DF,  p-value: < 2.2e-16

> p=update(p,.~.+X721.900024)
> summary(p)

Call:
lm(formula = Class ~ X447.170013 + X508.220001 + X528.570007 +
    X548.919983 + X559.090027 + X671.020020 + X681.200012 + X691.369995 +
    X701.549988 + X711.719971 + X752.429993 + X772.780029 + X864.349976 +
    X1053.689941 + X1235.270020 + X2133.239990 + X721.900024,
    data = (g))

Residuals:
   Min     1Q Median     3Q    Max
-5.930 -1.685 -0.041  1.940  6.892

Coefficients:
             Estimate Std. Error t value Pr(>|t|)
(Intercept)   2.3316334  0.9877468   2.361 0.018461 *
X447.170013  -0.0013937  0.0009745  -1.430 0.153031
X508.220001  -0.0099086  0.0030200  -3.281 0.001074 **
```

```
X528.570007  -0.0105984  0.0032065  -3.305 0.000987 ***
X548.919983   0.0080365  0.0038475   2.089 0.037011 *
X559.090027   0.0146063  0.0041505   3.519 0.000455 ***
X671.020020   0.0075816  0.0048173   1.574 0.115880
X681.200012  -0.0087207  0.0045502  -1.917 0.055612 .
X691.369995  -0.0105090  0.0044056  -2.385 0.017267 *
X701.549988   0.0152292  0.0043738   3.482 0.000522 ***
X711.719971  -0.0090310  0.0039166  -2.306 0.021349 *
X752.429993  -0.0030756  0.0023184  -1.327 0.184985
X772.780029  -0.0084842  0.0016257  -5.219 2.24e-07 ***
X864.349976   0.0040334  0.0018525   2.177 0.029719 *
X1053.689941  0.0053083  0.0008690   6.109 1.50e-09 ***
X1235.270020 -0.0059186  0.0008326  -7.108 2.40e-12 ***
X2133.239990  0.0019105  0.0005030   3.798 0.000155 ***
X721.900024   0.0101673  0.0038077   2.670 0.007717 **
---
Signif. codes:  0 '***' 0.001 '**' 0.01 '*' 0.05 '.' 0.1 ' ' 1

Residual standard error: 2.507 on 896 degrees of freedom
Multiple R-squared:  0.2509,    Adjusted R-squared:  0.2367
F-statistic: 17.65 on 17 and 896 DF,  p-value: < 2.2e-16

> p=update(p,.~.-X752.429993)
> summary(p)

Call:
lm(formula = Class ~ X447.170013 + X508.220001 + X528.570007 +
    X548.919983 + X559.090027 + X671.020020 + X681.200012 + X691.369995 +
    X701.549988 + X711.719971 + X772.780029 + X864.349976 + X1053.689941 +
    X1235.270020 + X2133.239990 + X721.900024, data = (g))

Residuals:
    Min      1Q  Median      3Q     Max
```

```
-5.8752 -1.6635 -0.0719  1.9723  6.9432

Coefficients:
             Estimate Std. Error t value Pr(>|t|)
(Intercept)   2.3850187  0.9873446   2.416 0.015909 *
X447.170013  -0.0014648  0.0009735  -1.505 0.132763
X508.220001  -0.0103574  0.0030022  -3.450 0.000587 ***
X528.570007  -0.0111742  0.0031783  -3.516 0.000460 ***
X548.919983   0.0076048  0.0038353   1.983 0.047692 *
X559.090027   0.0137157  0.0040975   3.347 0.000850 ***
X671.020020   0.0073907  0.0048172   1.534 0.125325
X681.200012  -0.0091697  0.0045395  -2.020 0.043683 *
X691.369995  -0.0110563  0.0043881  -2.520 0.011921 *
X701.549988   0.0184418  0.0036438   5.061 5.06e-07 ***
X711.719971  -0.0096084  0.0038940  -2.467 0.013792 *
X772.780029  -0.0093015  0.0015051  -6.180 9.72e-10 ***
X864.349976   0.0025776  0.0014931   1.726 0.084624 .
X1053.689941  0.0052184  0.0008667   6.021 2.53e-09 ***
X1235.270020 -0.0058220  0.0008298  -7.016 4.49e-12 ***
X2133.239990  0.0018641  0.0005020   3.714 0.000217 ***
X721.900024   0.0095429  0.0037801   2.525 0.011756 *
---
Signif. codes:  0 ‘***’ 0.001 ‘**’ 0.01 ‘*’ 0.05 ‘.’ 0.1 ‘ ’ 1

Residual standard error: 2.508 on 897 degrees of freedom
Multiple R-squared:  0.2494,    Adjusted R-squared:  0.236
F-statistic: 18.63 on 16 and 897 DF,  p-value: < 2.2e-16

> p=update(p,.~.-X447.170013)
> summary(p)

Call:
lm(formula = Class ~ X508.220001 + X528.570007 + X548.919983 +
```

```
   X559.090027 + X671.020020 + X681.200012 + X691.369995 + X701.549988 +
   X711.719971 + X772.780029 + X864.349976 + X1053.689941 +
   X1235.270020 + X2133.239990 + X721.900024, data = (g))

Residuals:
   Min     1Q  Median     3Q    Max
-5.9489 -1.6687 -0.0991  1.9512  6.8270

Coefficients:
             Estimate Std. Error t value Pr(>|t|)
(Intercept)   3.3004101  0.7781940   4.241 2.45e-05 ***
X508.220001  -0.0108390  0.0029872  -3.628 0.000301 ***
X528.570007  -0.0116537  0.0031645  -3.683 0.000245 ***
X548.919983   0.0073448  0.0038341   1.916 0.055727 .
X559.090027   0.0131405  0.0040825   3.219 0.001334 **
X671.020020   0.0073453  0.0048205   1.524 0.127917
X681.200012  -0.0092529  0.0045424  -2.037 0.041941 *
X691.369995  -0.0114585  0.0043830  -2.614 0.009091 **
X701.549988   0.0189408  0.0036312   5.216 2.27e-07 ***
X711.719971  -0.0092446  0.0038892  -2.377 0.017664 *
X772.780029  -0.0093658  0.0015055  -6.221 7.57e-10 ***
X864.349976   0.0026024  0.0014940   1.742 0.081872 .
X1053.689941  0.0052592  0.0008669   6.067 1.92e-09 ***
X1235.270020 -0.0059134  0.0008281  -7.141 1.92e-12 ***
X2133.239990  0.0019012  0.0005017   3.789 0.000161 ***
X721.900024   0.0095785  0.0037827   2.532 0.011504 *
---
Signif. codes:  0 ‘***’ 0.001 ‘**’ 0.01 ‘*’ 0.05 ‘.’ 0.1 ‘ ’ 1

Residual standard error: 2.51 on 898 degrees of freedom
Multiple R-squared:  0.2475,    Adjusted R-squared:  0.235
F-statistic: 19.69 on 15 and 898 DF,  p-value: < 2.2e-16
```

```
> p=update(p,.~.-X671.020020)
> summary(p)

Call:
lm(formula = Class ~ X508.220001 + X528.570007 + X548.919983 +
    X559.090027 + X681.200012 + X691.369995 + X701.549988 + X711.719971 +
    X772.780029 + X864.349976 + X1053.689941 + X1235.270020 +
    X2133.239990 + X721.900024, data = (g))

Residuals:
    Min      1Q  Median      3Q     Max
-5.8279 -1.6674 -0.1436  1.9978  6.9281

Coefficients:
             Estimate Std. Error t value Pr(>|t|)
(Intercept)   3.2174322  0.7768569   4.142 3.77e-05 ***
X508.220001  -0.0107043  0.0029881  -3.582 0.000359 ***
X528.570007  -0.0116551  0.0031669  -3.680 0.000247 ***
X548.919983   0.0076787  0.0038307   2.005 0.045313 *
X559.090027   0.0131362  0.0040855   3.215 0.001350 **
X681.200012  -0.0061575  0.0040658  -1.514 0.130261
X691.369995  -0.0090412  0.0040888  -2.211 0.027273 *
X701.549988   0.0204192  0.0035018   5.831 7.67e-09 ***
X711.719971  -0.0089407  0.0038870  -2.300 0.021667 *
X772.780029  -0.0093780  0.0015066  -6.224 7.40e-10 ***
X864.349976   0.0028246  0.0014880   1.898 0.057982 .
X1053.689941  0.0052642  0.0008675   6.068 1.91e-09 ***
X1235.270020 -0.0059988  0.0008268  -7.255 8.67e-13 ***
X2133.239990  0.0019419  0.0005014   3.873 0.000115 ***
X721.900024   0.0087582  0.0037469   2.337 0.019634 *
---
Signif. codes:  0 ‘***’ 0.001 ‘**’ 0.01 ‘*’ 0.05 ‘.’ 0.1 ‘ ’ 1
```

```
Residual standard error: 2.512 on 899 degrees of freedom
Multiple R-squared:  0.2456,    Adjusted R-squared:  0.2338
F-statistic:  20.9 on 14 and 899 DF,  p-value: < 2.2e-16

> p=update(p,.~.-X681.200012)
> summary(p)

Call:
lm(formula = Class ~ X508.220001 + X528.570007 + X548.919983 +
    X559.090027 + X691.369995 + X701.549988 + X711.719971 + X772.780029 +
    X864.349976 + X1053.689941 + X1235.270020 + X2133.239990 +
    X721.900024, data = (g))

Residuals:
    Min      1Q  Median      3Q     Max
-5.9570 -1.6368 -0.1085  1.9796  6.8532

Coefficients:
             Estimate Std. Error t value Pr(>|t|)
(Intercept)   3.2628238  0.7768362   4.200 2.93e-05 ***
X508.220001  -0.0105699  0.0029889  -3.536 0.000426 ***
X528.570007  -0.0121954  0.0031490  -3.873 0.000115 ***
X548.919983   0.0077550  0.0038331   2.023 0.043351 *
X559.090027   0.0129624  0.0040868   3.172 0.001567 **
X691.369995  -0.0132908  0.0029762  -4.466 8.99e-06 ***
X701.549988   0.0183700  0.0032321   5.684 1.78e-08 ***
X711.719971  -0.0089147  0.0038897  -2.292 0.022145 *
X772.780029  -0.0094699  0.0015065  -6.286 5.07e-10 ***
X864.349976   0.0025549  0.0014783   1.728 0.084299 .
X1053.689941  0.0052949  0.0008679   6.101 1.57e-09 ***
X1235.270020 -0.0059965  0.0008274  -7.247 9.16e-13 ***
X2133.239990  0.0018631  0.0004990   3.733 0.000201 ***
X721.900024   0.0099435  0.0036669   2.712 0.006821 **
```

```
---
Signif. codes:  0 ‘***’ 0.001 ‘**’ 0.01 ‘*’ 0.05 ‘.’ 0.1 ‘ ’ 1

Residual standard error: 2.513 on 900 degrees of freedom
Multiple R-squared:  0.2437,    Adjusted R-squared:  0.2327
F-statistic:  22.3 on 13 and 900 DF,  p-value: < 2.2e-16

> p=update(p,.~.-X864.349976)
> summary(p)

Call:
lm(formula = Class ~ X508.220001 + X528.570007 + X548.919983 +
    X559.090027 + X691.369995 + X701.549988 + X711.719971 + X772.780029 +
    X1053.689941 + X1235.270020 + X2133.239990 + X721.900024,
    data = (g))

Residuals:
    Min      1Q  Median      3Q     Max
-5.9020 -1.6580 -0.1535  2.0211  6.6700

Coefficients:
             Estimate Std. Error t value Pr(>|t|)
(Intercept)   3.3746999  0.7749871   4.355 1.49e-05 ***
X508.220001  -0.0103831  0.0029903  -3.472 0.000541 ***
X528.570007  -0.0121276  0.0031522  -3.847 0.000128 ***
X548.919983   0.0074706  0.0038338   1.949 0.051649 .
X559.090027   0.0127855  0.0040901   3.126 0.001829 **
X691.369995  -0.0110255  0.0026749  -4.122 4.11e-05 ***
X701.549988   0.0156092  0.0028128   5.549 3.77e-08 ***
X711.719971  -0.0084318  0.0038840  -2.171 0.030197 *
X772.780029  -0.0074690  0.0009650  -7.740 2.66e-14 ***
X1053.689941  0.0057269  0.0008321   6.883 1.10e-11 ***
X1235.270020 -0.0057280  0.0008136  -7.040 3.81e-12 ***
```

```
X2133.239990  0.0017006  0.0004906   3.466 0.000553 ***
X721.900024   0.0103847  0.0036620   2.836 0.004674 **
---
Signif. codes:  0 ‘***’ 0.001 ‘**’ 0.01 ‘*’ 0.05 ‘.’ 0.1 ‘ ’ 1

Residual standard error: 2.516 on 901 degrees of freedom
Multiple R-squared:  0.2411,    Adjusted R-squared:  0.231
F-statistic: 23.86 on 12 and 901 DF,  p-value: < 2.2e-16

> p=update(p,.~.-X548.919983)
> summary(p)

Call:
lm(formula = Class ~ X508.220001 + X528.570007 + X559.090027 +
   X691.369995 + X701.549988 + X711.719971 + X772.780029 + X1053.689941 +
   X1235.270020 + X2133.239990 + X721.900024, data = (g))

Residuals:
   Min     1Q  Median     3Q     Max
-5.8186 -1.6484 -0.1064  2.0306  6.8634

Coefficients:
             Estimate Std. Error t value Pr(>|t|)
(Intercept)   3.8742100  0.7324989   5.289 1.54e-07 ***
X508.220001  -0.0094921  0.0029597  -3.207 0.001388 **
X528.570007  -0.0104868  0.0030423  -3.447 0.000593 ***
X559.090027   0.0170303  0.0034671   4.912 1.07e-06 ***
X691.369995  -0.0113095  0.0026751  -4.228 2.60e-05 ***
X701.549988   0.0156131  0.0028172   5.542 3.92e-08 ***
X711.719971  -0.0083360  0.0038897  -2.143 0.032371 *
X772.780029  -0.0076196  0.0009634  -7.909 7.54e-15 ***
X1053.689941  0.0057087  0.0008333   6.851 1.36e-11 ***
X1235.270020 -0.0058382  0.0008129  -7.182 1.44e-12 ***
```

```
X2133.239990  0.0017815  0.0004896   3.638 0.000290 ***
X721.900024   0.0111387  0.0036472   3.054 0.002324 **
---
Signif. codes:  0 ‘***’ 0.001 ‘**’ 0.01 ‘*’ 0.05 ‘.’ 0.1 ‘ ’ 1

Residual standard error: 2.52 on 902 degrees of freedom
Multiple R-squared:  0.2379,    Adjusted R-squared:  0.2287
F-statistic:  25.6 on 11 and 902 DF,  p-value: < 2.2e-16

> p=update(p,.~.-X711.719971)
> summary(p)

Call:
lm(formula = Class ~ X508.220001 + X528.570007 + X559.090027 +
   X691.369995 + X701.549988 + X772.780029 + X1053.689941 +
   X1235.270020 + X2133.239990 + X721.900024, data = (g))

Residuals:
   Min     1Q  Median     3Q     Max
-5.8918 -1.6051 -0.0938  2.0667  6.5852

Coefficients:
             Estimate Std. Error t value Pr(>|t|)
(Intercept)   4.3996329  0.6916235   6.361 3.17e-10 ***
X508.220001  -0.0091249  0.0029606  -3.082 0.002118 **
X528.570007  -0.0108336  0.0030441  -3.559 0.000392 ***
X559.090027   0.0160571  0.0034441   4.662 3.60e-06 ***
X691.369995  -0.0118461  0.0026686  -4.439 1.02e-05 ***
X701.549988   0.0137272  0.0026815   5.119 3.75e-07 ***
X772.780029  -0.0066461  0.0008512  -7.808 1.61e-14 ***
X1053.689941  0.0057055  0.0008349   6.833 1.52e-11 ***
X1235.270020 -0.0060668  0.0008075  -7.513 1.39e-13 ***
X2133.239990  0.0019337  0.0004854   3.984 7.34e-05 ***
```

```
X721.900024   0.0047121  0.0020800   2.265 0.023726 *
---
Signif. codes:  0 ‘***’ 0.001 ‘**’ 0.01 ‘*’ 0.05 ‘.’ 0.1 ‘ ’ 1

Residual standard error: 2.525 on 903 degrees of freedom
Multiple R-squared:  0.2341,    Adjusted R-squared:  0.2256
F-statistic:  27.6 on 10 and 903 DF,  p-value: < 2.2e-16

>
```

Appendix 6.6: Sample file of a Classification Accuracy assessment for the Random Extracted Spectra, 16 Optimal wavebands and 0.6 Radians spectra Angle of Separation

Confusion Matrix: D:\PhD\Thesis-Re-Examination\Re-Re-Re-Processing\9. Classification\FinalOct2022Classification\16 Bands\Mfabeni16_06

Overall Accuracy = (8444/17306) 48.7923%

Kappa Coefficient = 0.3953

	Ground Truth (Pixels)				
Class	MfabeniL1TMer	MfabeniL1TMer	MfabeniL1TMer	MfabeniL1TMer	MfabeniL1TMer
Unclassified	0	0	0	0	0
ExtractedClas	405	30	0	0	8
ExtractedClas	9	1295	55	47	48
ExtractedClas	2	1	914	606	266
ExtractedClas	6	3	200	215	206
ExtractedClas	41	27	98	119	514
ExtractedClas	5	105	113	69	61
ExtractedClas	79	115	0	0	11
ExtractedClas	127	24	0	2	4
ExtractedClas	18	531	29	39	30
ExtractedClas	24	1	0	0	9
Total	716	2132	1409	1097	1157

	Ground Truth (Pixels)				
Class	MfabeniL1TMer	MfabeniL1TMer	MfabeniL1TMer	MfabeniL1TMer	MfabeniL1TMer
Unclassified	20	0	0	0	0
ExtractedClas	66	160	51	57	0
ExtractedClas	621	41	0	1058	28
ExtractedClas	19	0	2	46	37
ExtractedClas	77	3	23	34	28

ExtractedClas	400	9	53	79	23
ExtractedClas	2581	144	17	840	10
ExtractedClas	227	374	27	283	2
ExtractedClas	38	79	191	86	0
ExtractedClas	860	51	4	1517	0
ExtractedClas	39	52	0	0	438
Total	4948	913	368	4000	566

Ground Truth (Pixels)

Class	Total
Unclassified	20
ExtractedClas	777
ExtractedClas	3202
ExtractedClas	1893
ExtractedClas	795
ExtractedClas	1363
ExtractedClas	3945
ExtractedClas	1118
ExtractedClas	551
ExtractedClas	3079
ExtractedClas	563
Total	17306

Ground Truth (Percent)

Class	MfabeniL1TMer	MfabeniL1TMer	MfabeniL1TMer	MfabeniL1TMer	MfabeniL1TMer
Unclassified	0.00	0.00	0.00	0.00	0.00
ExtractedClas	56.56	1.41	0.00	0.00	0.69
ExtractedClas	1.26	60.74	3.90	4.28	4.15
ExtractedClas	0.28	0.05	64.87	55.24	22.99
ExtractedClas	0.84	0.14	14.19	19.60	17.80
ExtractedClas	5.73	1.27	6.96	10.85	44.43

ExtractedClas	0.70	4.92	8.02	6.29	5.27
ExtractedClas	11.03	5.39	0.00	0.00	0.95
ExtractedClas	17.74	1.13	0.00	0.18	0.35
ExtractedClas	2.51	24.91	2.06	3.56	2.59
ExtractedClas	3.35	0.05	0.00	0.00	0.78
Total	100.00	100.00	100.00	100.00	100.00

Ground Truth (Percent)

Class	MfabeniL1TMer	MfabeniL1TMer	MfabeniL1TMer	MfabeniL1TMer	MfabeniL1TMer
Unclassified	0.40	0.00	0.00	0.00	0.00
ExtractedClas	1.33	17.52	13.86	1.43	0.00
ExtractedClas	12.55	4.49	0.00	26.45	4.95
ExtractedClas	0.38	0.00	0.54	1.15	6.54
ExtractedClas	1.56	0.33	6.25	0.85	4.95
ExtractedClas	8.08	0.99	14.40	1.98	4.06
ExtractedClas	52.16	15.77	4.62	21.00	1.77
ExtractedClas	4.59	40.96	7.34	7.08	0.35
ExtractedClas	0.77	8.65	51.90	2.15	0.00
ExtractedClas	17.38	5.59	1.09	37.92	0.00
ExtractedClas	0.79	5.70	0.00	0.00	77.39
Total	100.00	100.00	100.00	100.00	100.00

Ground Truth (Percent)

Class	Total
Unclassified	0.12
ExtractedClas	4.49
ExtractedClas	18.50
ExtractedClas	10.94
ExtractedClas	4.59
ExtractedClas	7.88
ExtractedClas	22.80

ExtractedClas	6.46
ExtractedClas	3.18
ExtractedClas	17.79
ExtractedClas	3.25
Total	100.00

Class	Commission (Percent)	Omission (Percent)	Commission (Pixels)	Omission (Pixels)
ExtractedClas	47.88	43.44	372/777	311/716
ExtractedClas	59.56	39.26	1907/3202	837/2132
ExtractedClas	51.72	35.13	979/1893	495/1409
ExtractedClas	72.96	80.40	580/795	882/1097
ExtractedClas	62.29	55.57	849/1363	643/1157
ExtractedClas	34.58	47.84	1364/3945	2367/4948
ExtractedClas	66.55	59.04	744/1118	539/913
ExtractedClas	65.34	48.10	360/551	177/368
ExtractedClas	50.73	62.08	1562/3079	2483/4000
ExtractedClas	22.20	22.61	125/563	128/566

Class	Prod. Acc. (Percent)	User Acc. (Percent)	Prod. Acc. (Pixels)	User Acc. (Pixels)
ExtractedClas	56.56	52.12	405/716	405/777
ExtractedClas	60.74	40.44	1295/2132	1295/3202
ExtractedClas	64.87	48.28	914/1409	914/1893
ExtractedClas	19.60	27.04	215/1097	215/795
ExtractedClas	44.43	37.71	514/1157	514/1363
ExtractedClas	52.16	65.42	2581/4948	2581/3945
ExtractedClas	40.96	33.45	374/913	374/1118
ExtractedClas	51.90	34.66	191/368	191/551
ExtractedClas	37.92	49.27	1517/4000	1517/3079
ExtractedClas	77.39	77.80	438/566	438/563

Appendix 6.7: DEM Generated Using Various Interpolation Techniques

DEM of Mfabeni Wetland Generated using NATURAL NEIGHBOUR

DEM of Mfabeni Wetland Generated using SPLINE

DEM of Mfabeni Wetland Generated using IDW

DEM of Mfabeni Wetland Generated using TREND LINEAR

DEM of Mfabeni Wetland Generated using TOPO-TO-RASTER

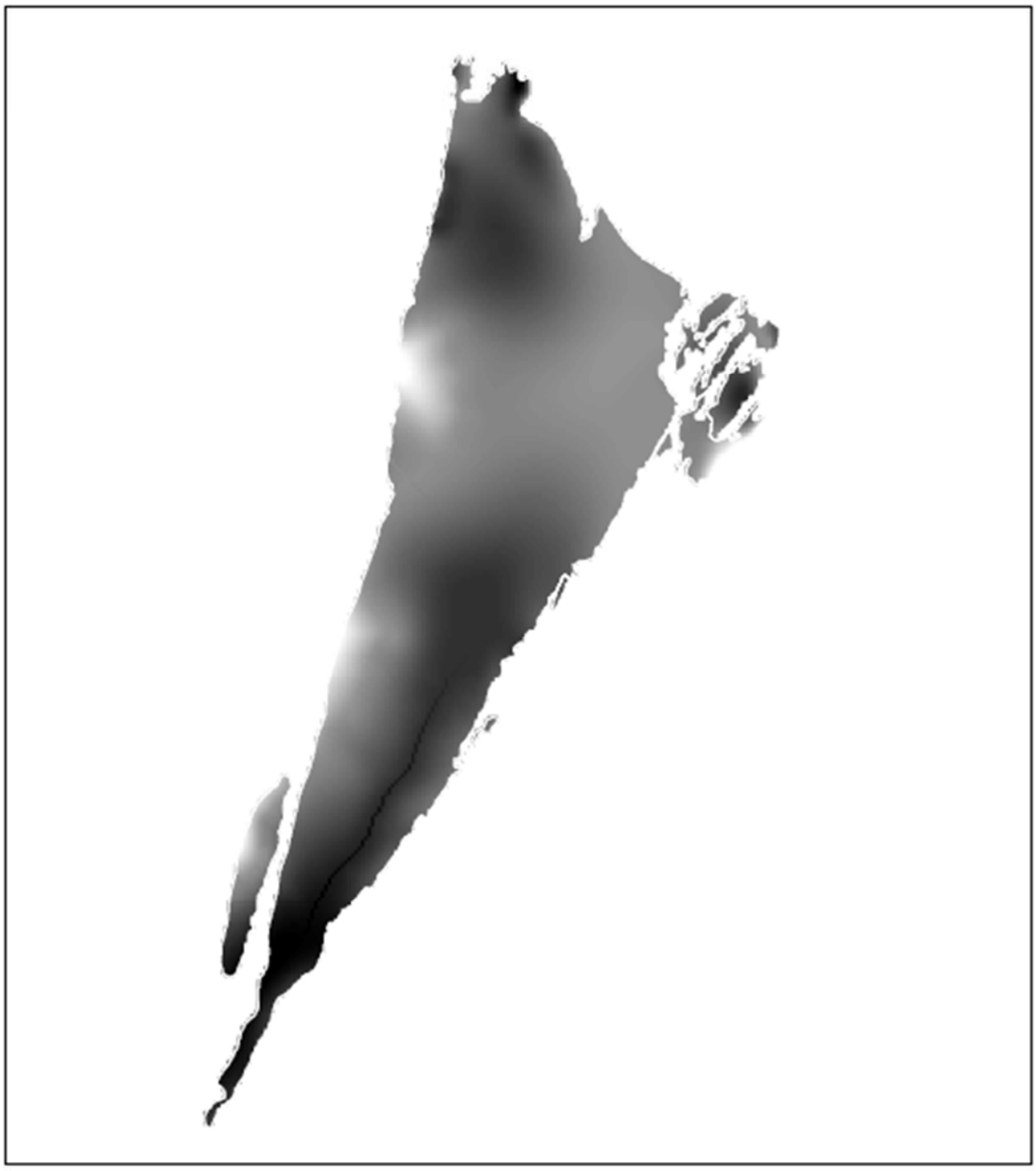

Appendix 6.8: More Transect profiles created across the Mfabeni Wetland to analyse the Distribution of the vegetation along an altitudinal gradient using different Orientations

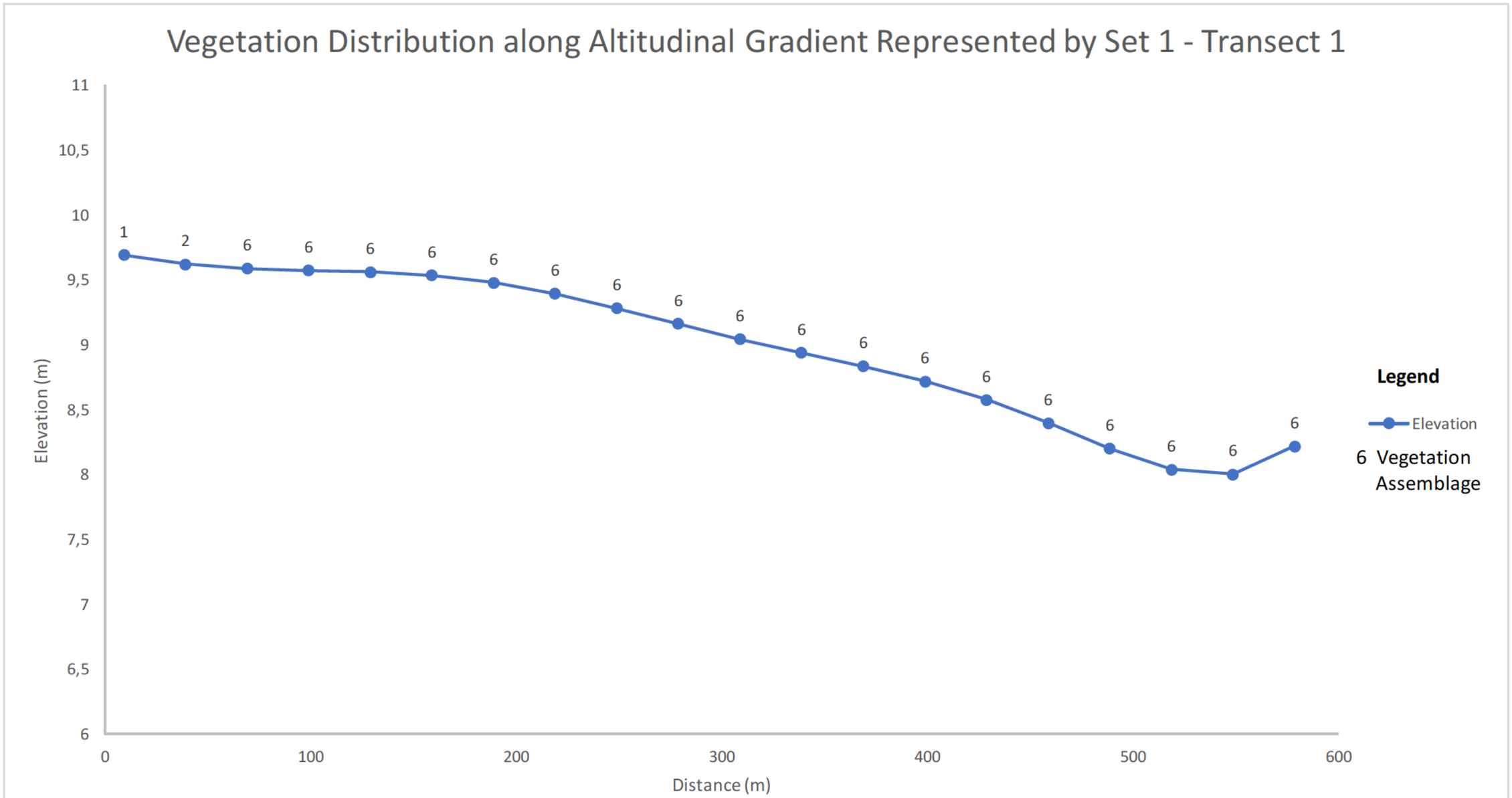

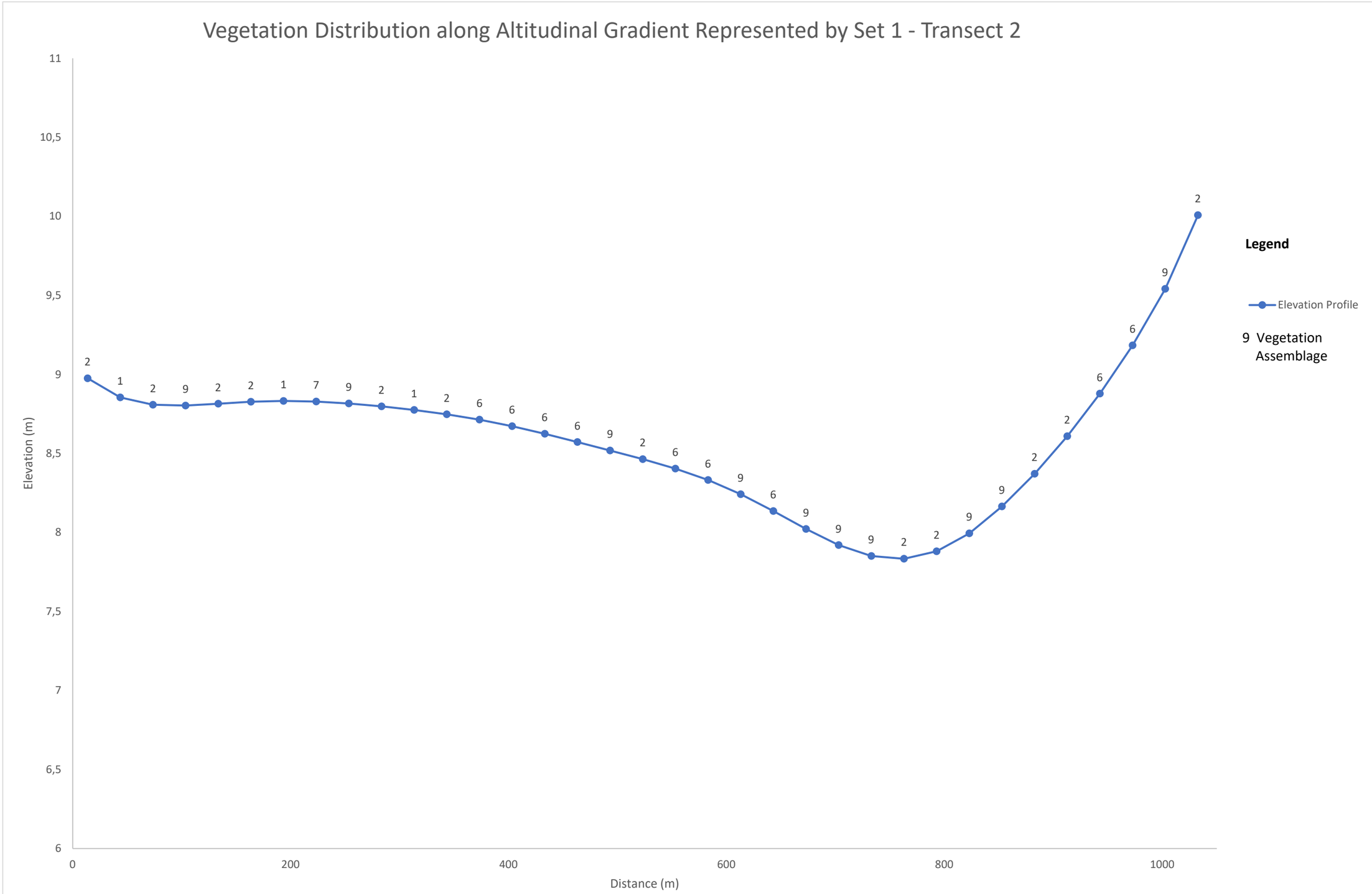
Vegetation Distribution along Altitudinal Gradient Represented by Set 1 - Transect 2
Elevation (m)
11
10,5
10
9,5
9
8,5
8
7,5
7
6,5
6
0
200
400
600
800
1000
Distance (m)
2 1 2 9 2 2 1 7 9 2 1 2 6 6 6 6 9 2 6 6 9 6 9 6 9 9 9 2 2 9 9 6 6 2
Legend
Elevation Profile
9 Vegetation Assemblage

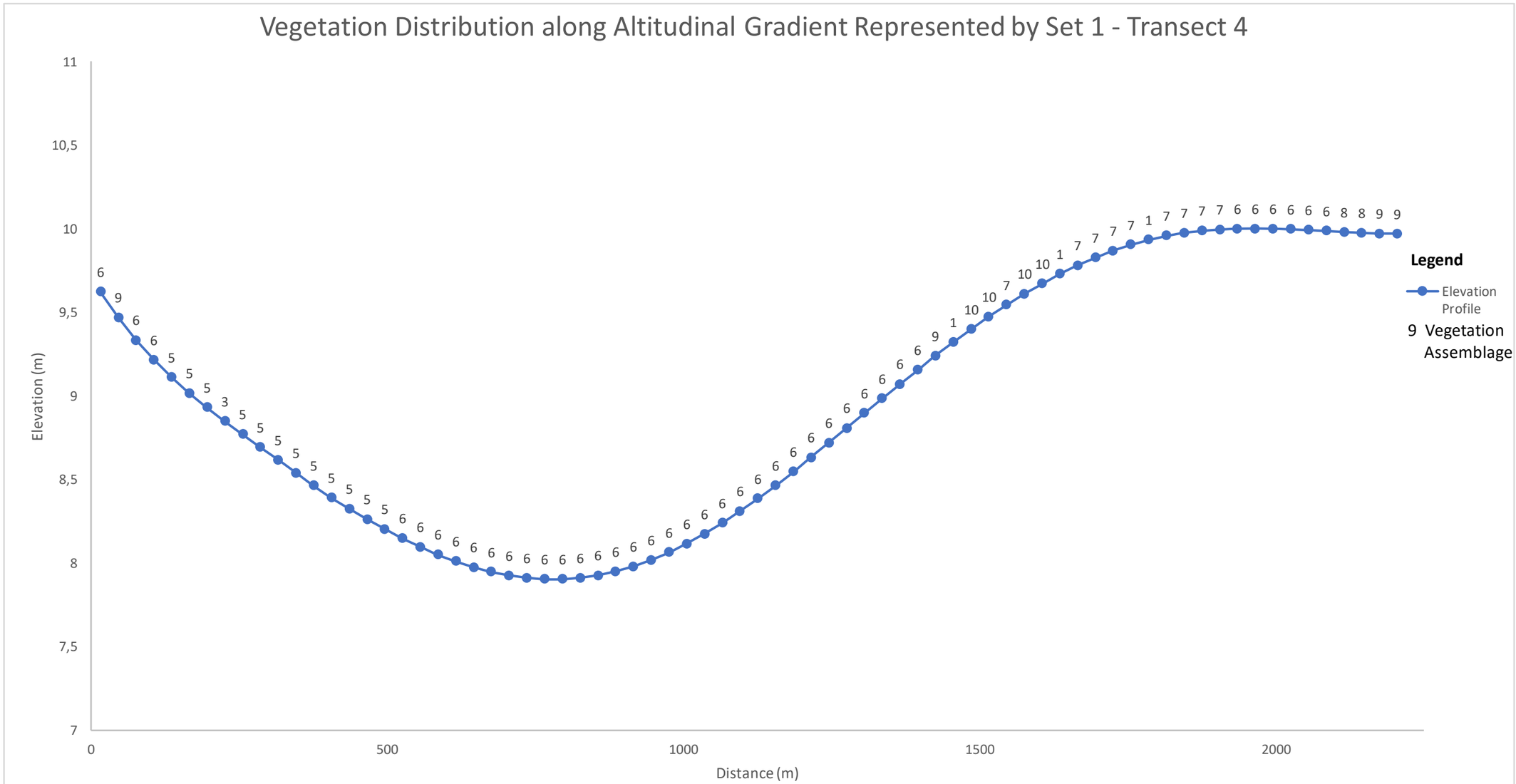
Vegetation Distribution along Altitudinal Gradient Represented by Set 1 - Transect 4
Elevation (m)
11
10,5
10
9,5
9
8,5
8
7,5
7
0
500
1000
1500
2000
Distance (m)
Legend
Elevation Profile
9 Vegetation Assemblage

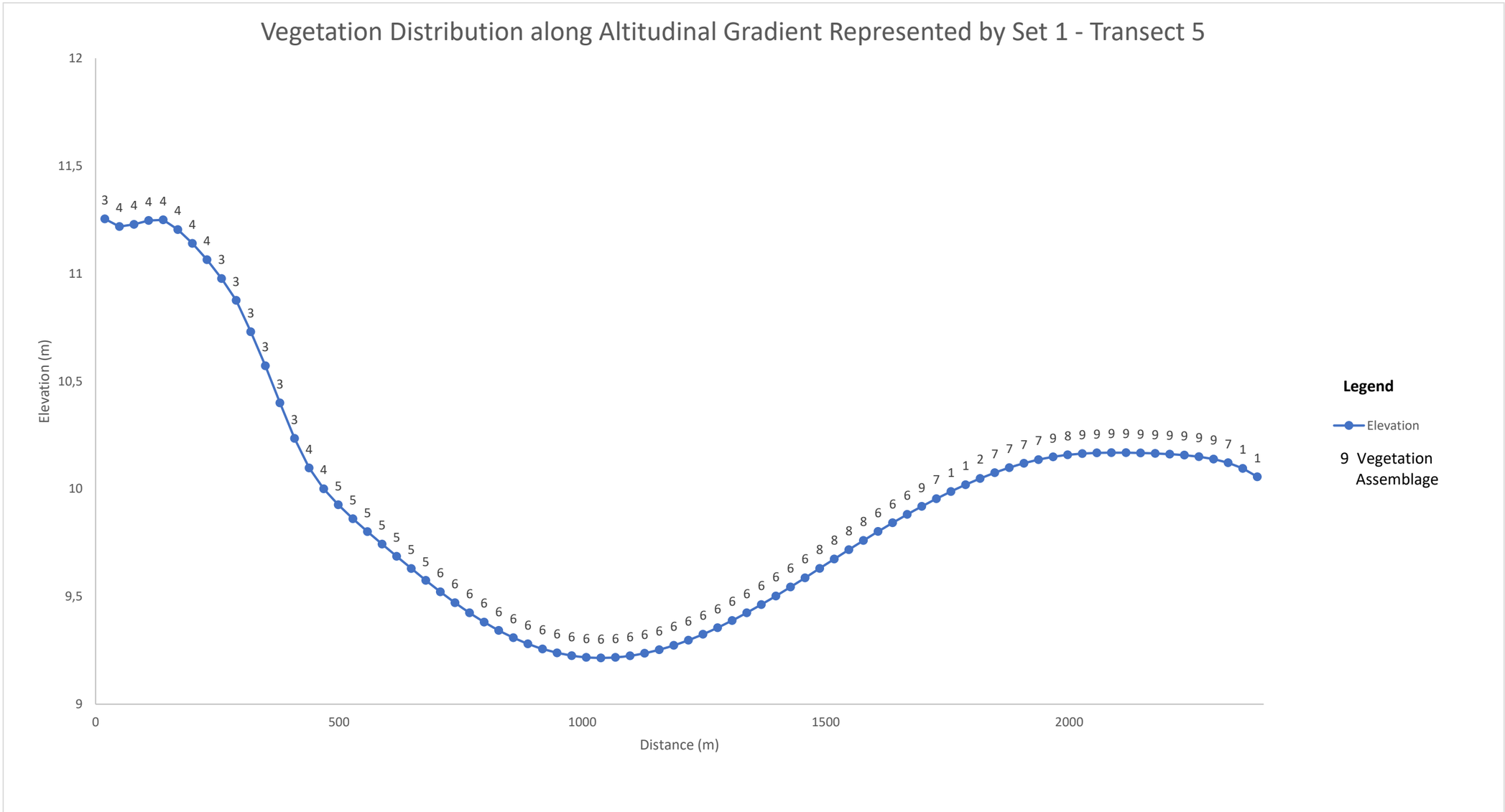
Vegetation Distribution along Altitudinal Gradient Represented by Set 1 - Transect 5
Elevation (m)
12
11,5
11
10,5
10
9,5
9
0
500
1000
1500
2000
Distance (m)
Legend
Elevation
9 Vegetation Assemblage

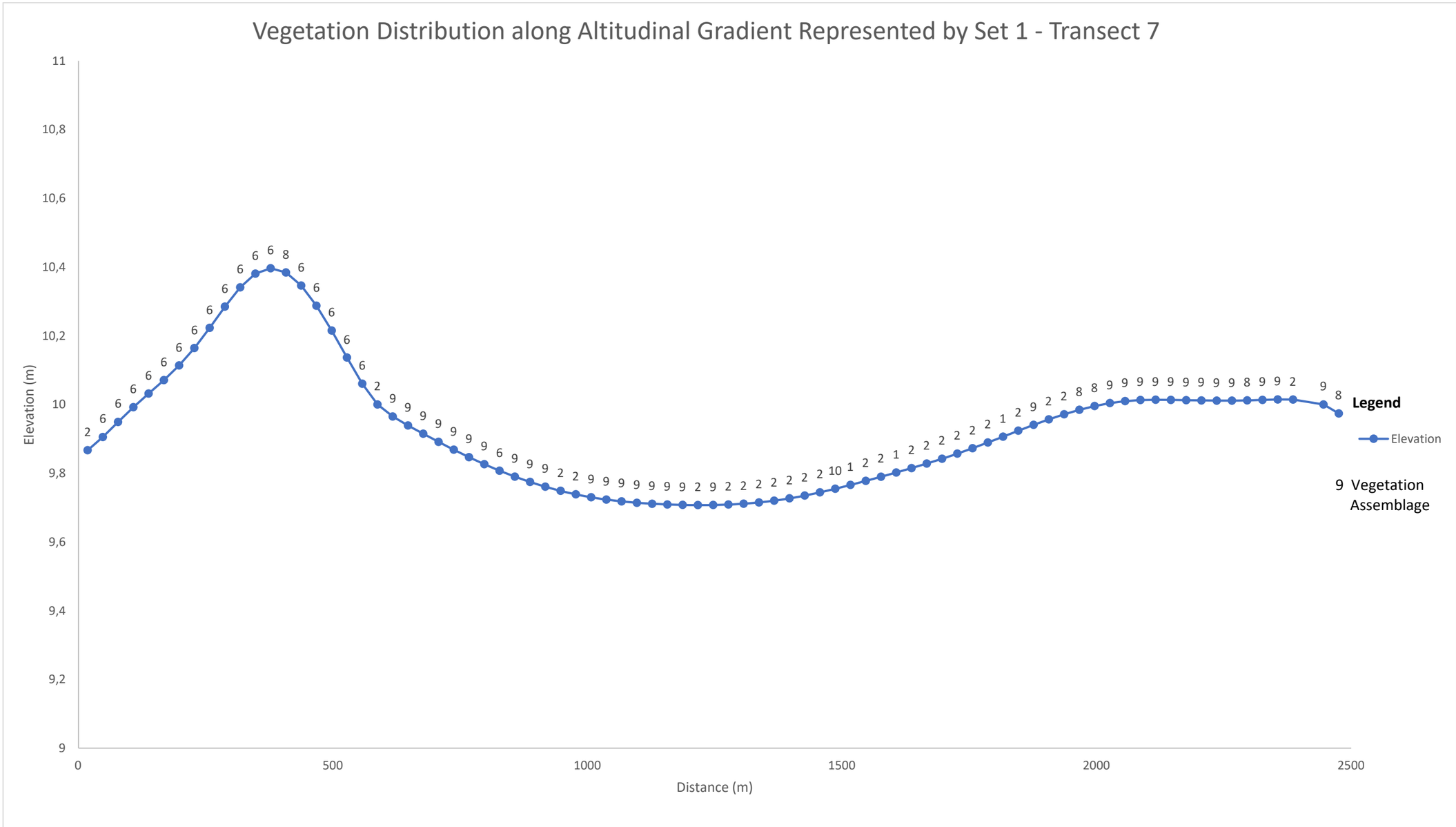
Vegetation Distribution along Altitudinal Gradient Represented by Set 1 - Transect 7
Elevation (m)
11
10,8
10,6
10,4
10,2
10
9,8
9,6
9,4
9,2
9
0
500
1000
1500
2000
2500
Distance (m)
Legend
Elevation
9 Vegetation Assemblage

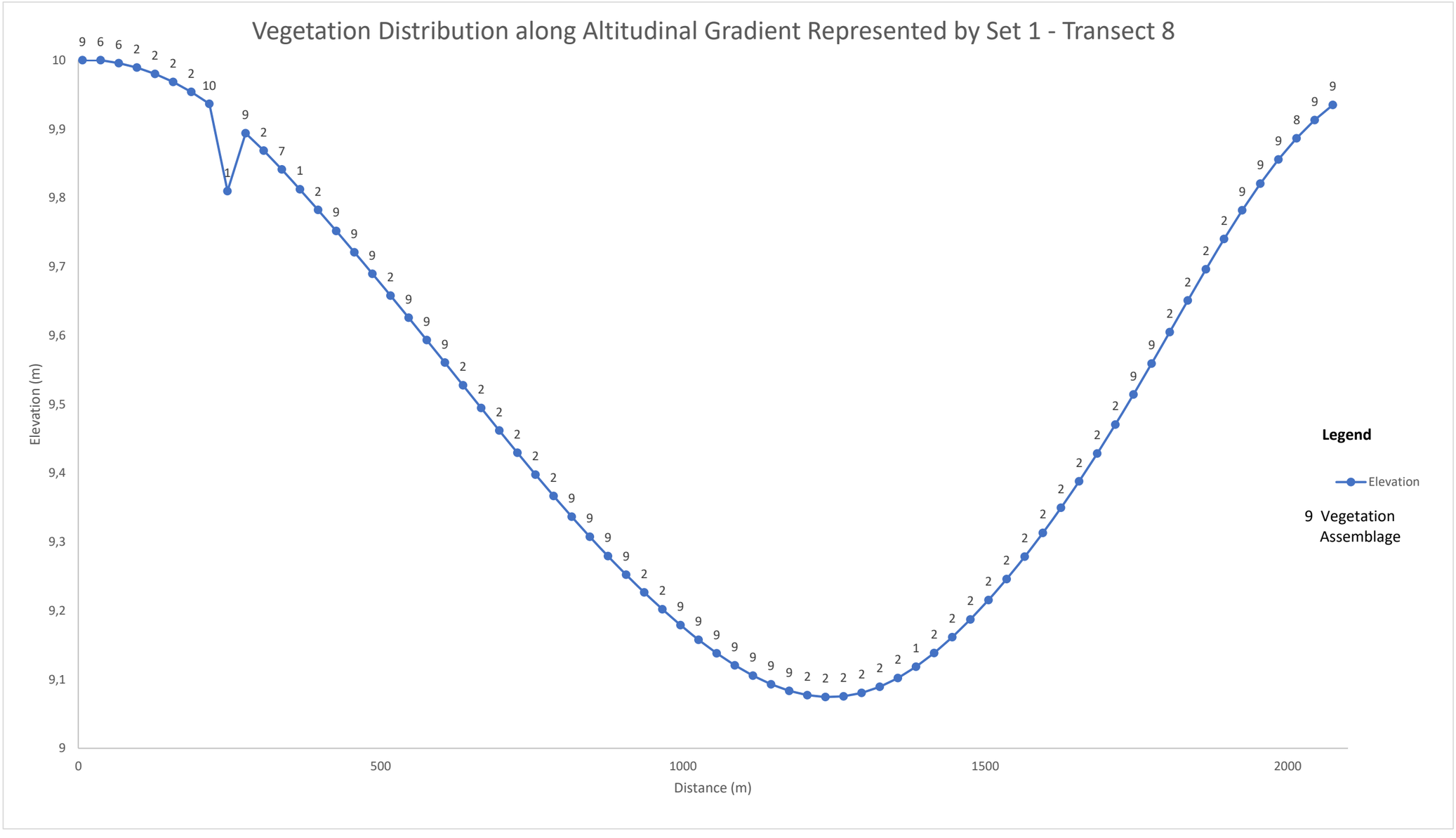
Vegetation Distribution along Altitudinal Gradient Represented by Set 1 - Transect 8
Elevation (m)
10
9,9
9,8
9,7
9,6
9,5
9,4
9,3
9,2
9,1
9
0
500
1000
1500
2000
Distance (m)
Legend
Elevation
9 Vegetation Assemblage

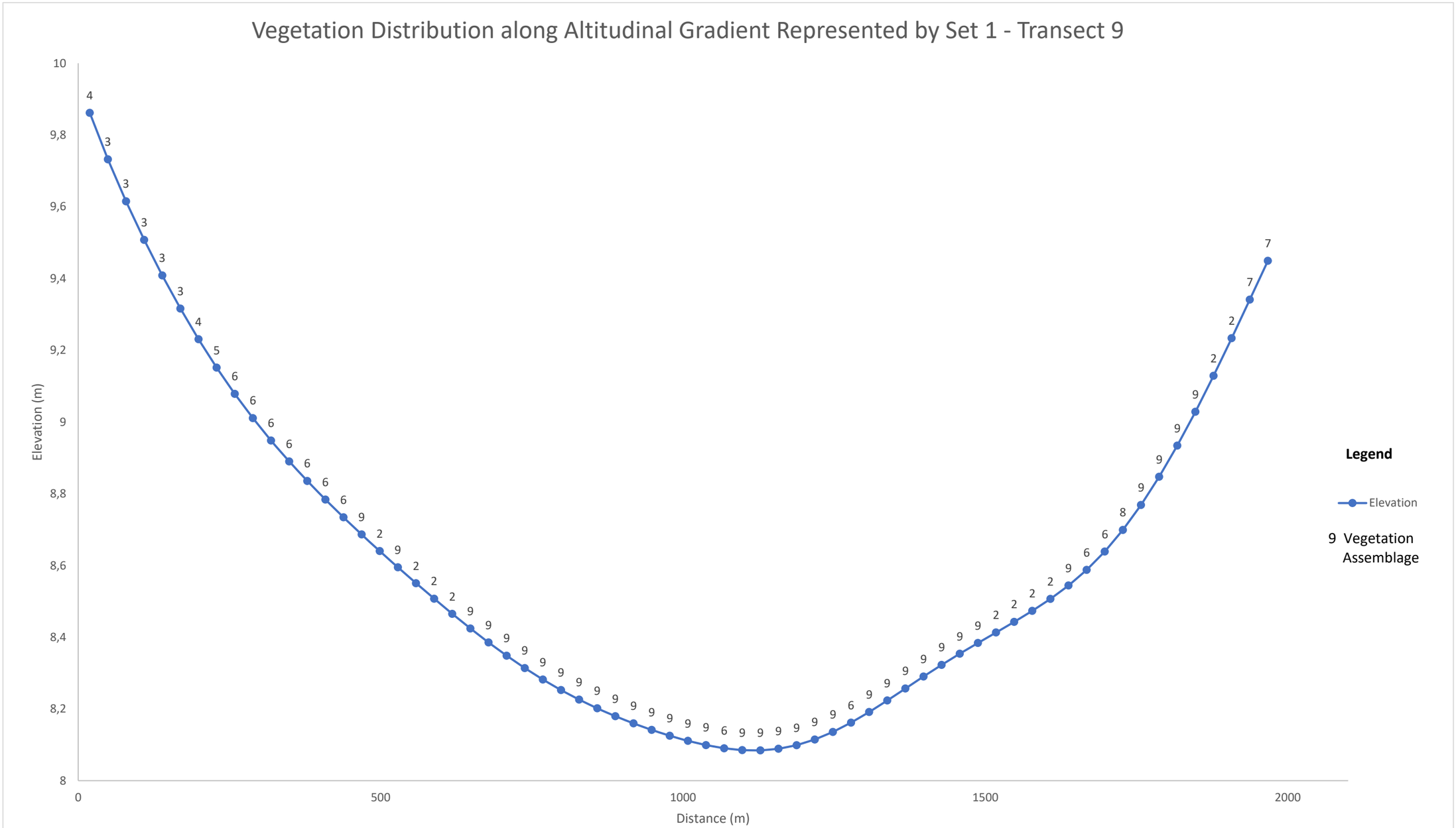
Vegetation Distribution along Altitudinal Gradient Represented by Set 1 - Transect 9
Elevation (m)
10
9,8
9,6
9,4
9,2
9
8,8
8,6
8,4
8,2
8
0
500
1000
1500
2000
Distance (m)
Legend
Elevation
9 Vegetation Assemblage

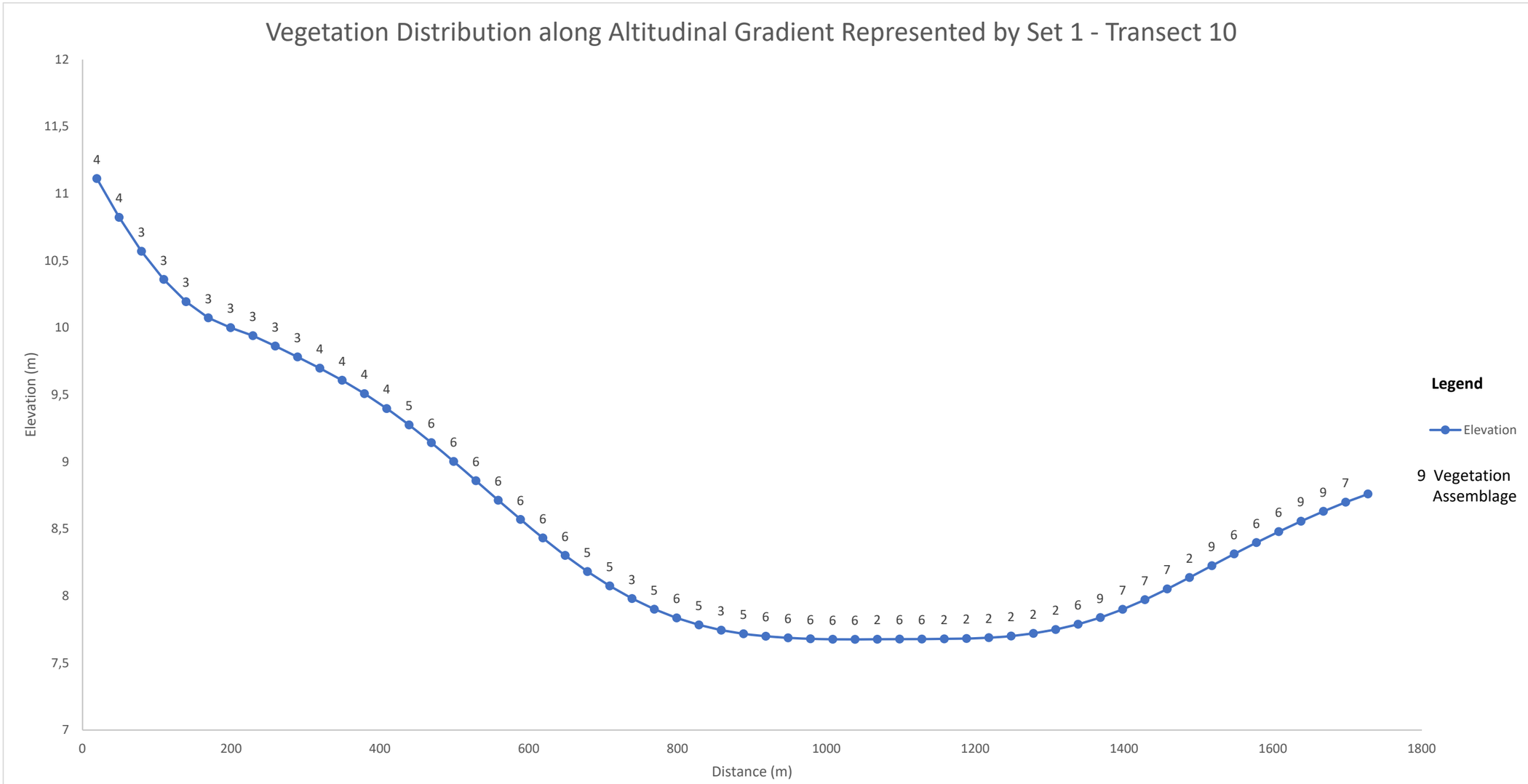
Vegetation Distribution along Altitudinal Gradient Represented by Set 1 - Transect 10
Elevation (m)
12
11,5
11
10,5
10
9,5
9
8,5
8
7,5
7
0
200
400
600
800
1000
1200
1400
1600
1800
Distance (m)
4 4 3 3 3 3 3 3 3 4 4 4 4 5 6 6 6 6 6 6 6 5 5 3 5 6 5 3 5 6 6 6 6 6 2 6 6 2 2 2 2 2 6 9 7 7 2 9 6 6 6 9 9 7
Legend
Elevation
9 Vegetation Assemblage

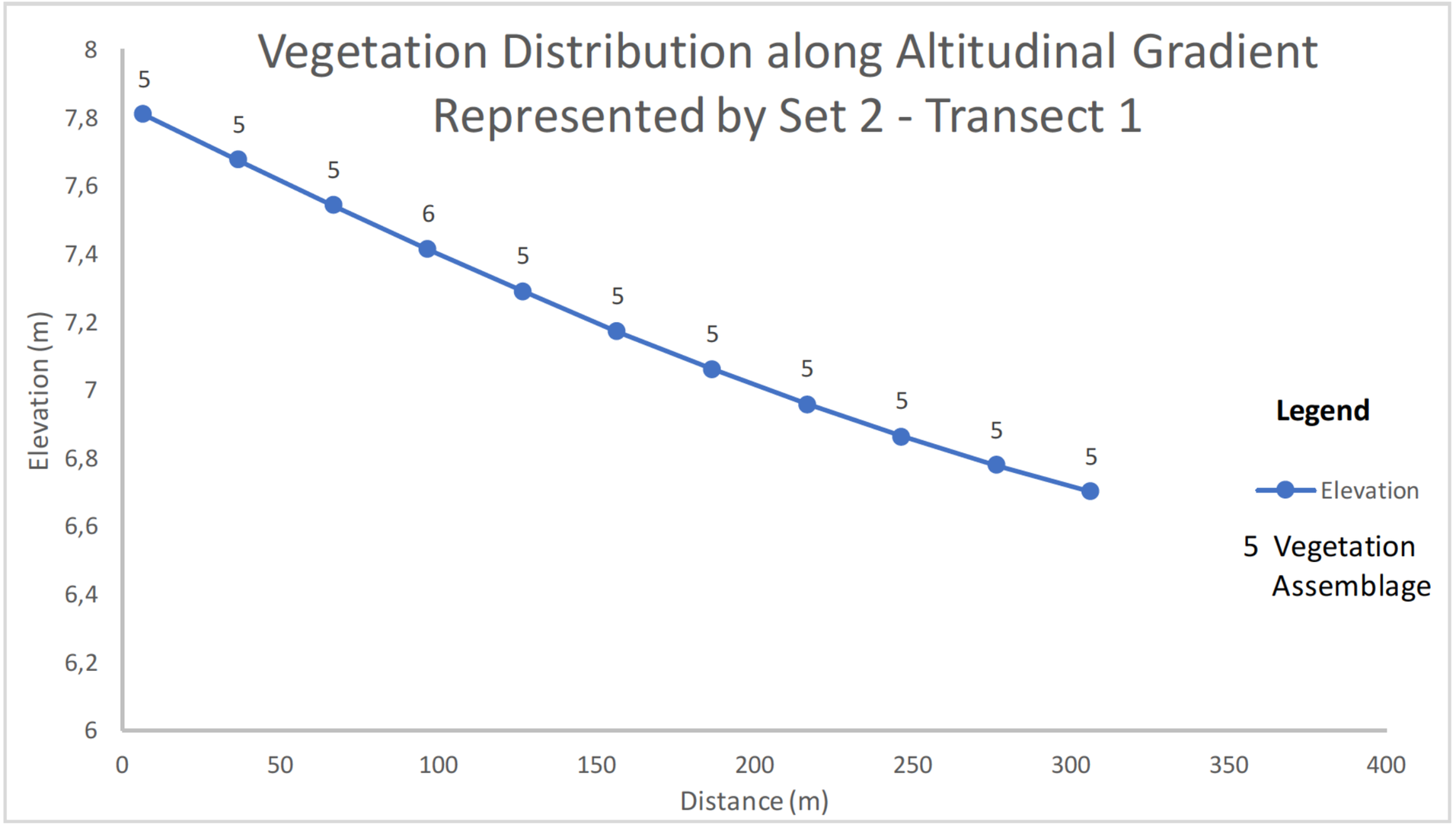
Vegetation Distribution along Altitudinal Gradient Represented by Set 2 - Transect 1
Elevation (m)
8
7,8
7,6
7,4
7,2
7
6,8
6,6
6,4
6,2
6
5
5
5
6
5
5
5
5
5
5
5
0
50
100
150
200
250
300
350
400
Distance (m)
Legend
Elevation
5 Vegetation Assemblage

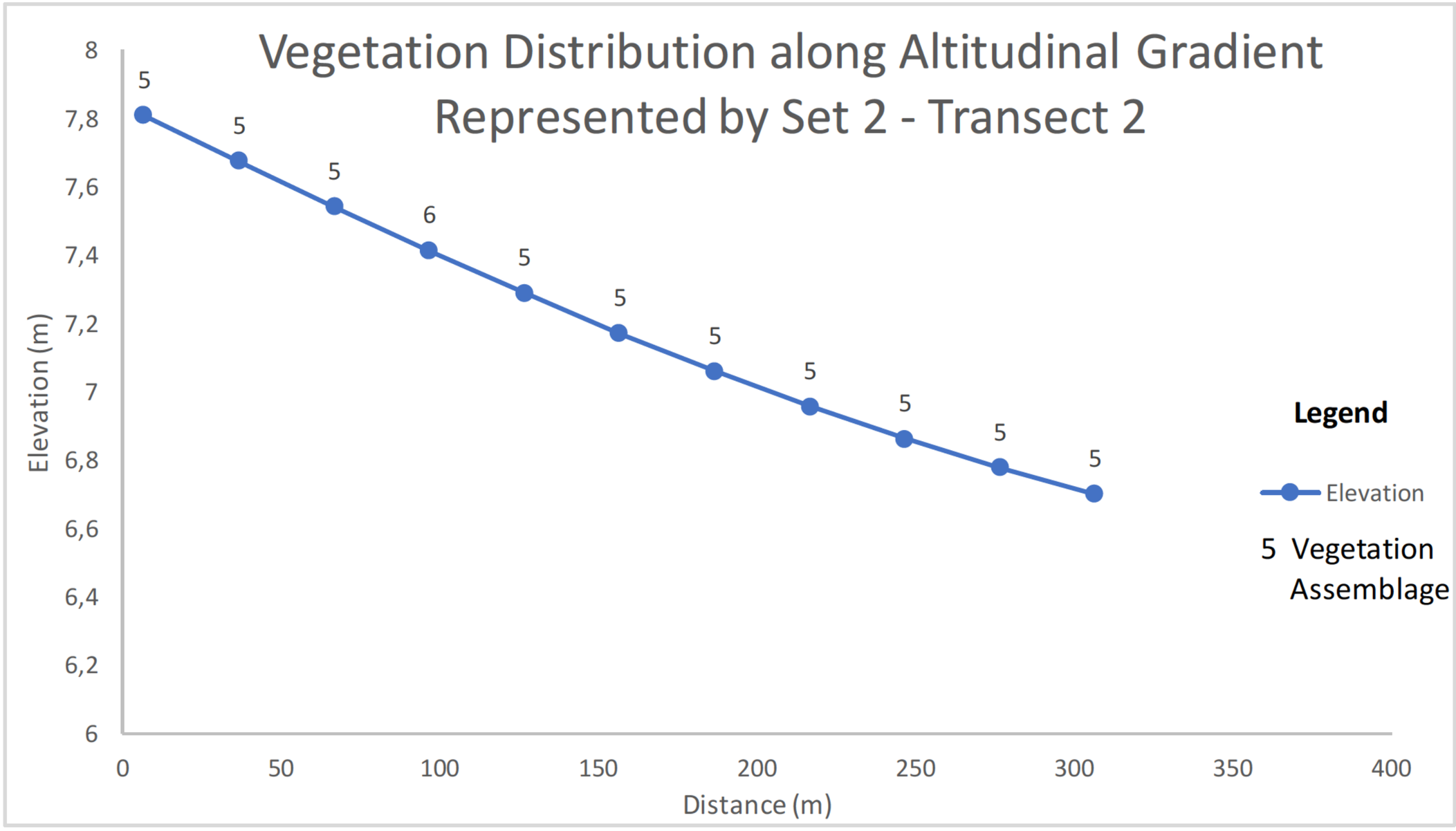
Vegetation Distribution along Altitudinal Gradient Represented by Set 2 - Transect 2
Elevation (m)
8
7,8
7,6
7,4
7,2
7
6,8
6,6
6,4
6,2
6
0
50
100
150
200
250
300
350
400
Distance (m)
5
5
5
6
5
5
5
5
5
5
5
Legend
Elevation
5 Vegetation Assemblage

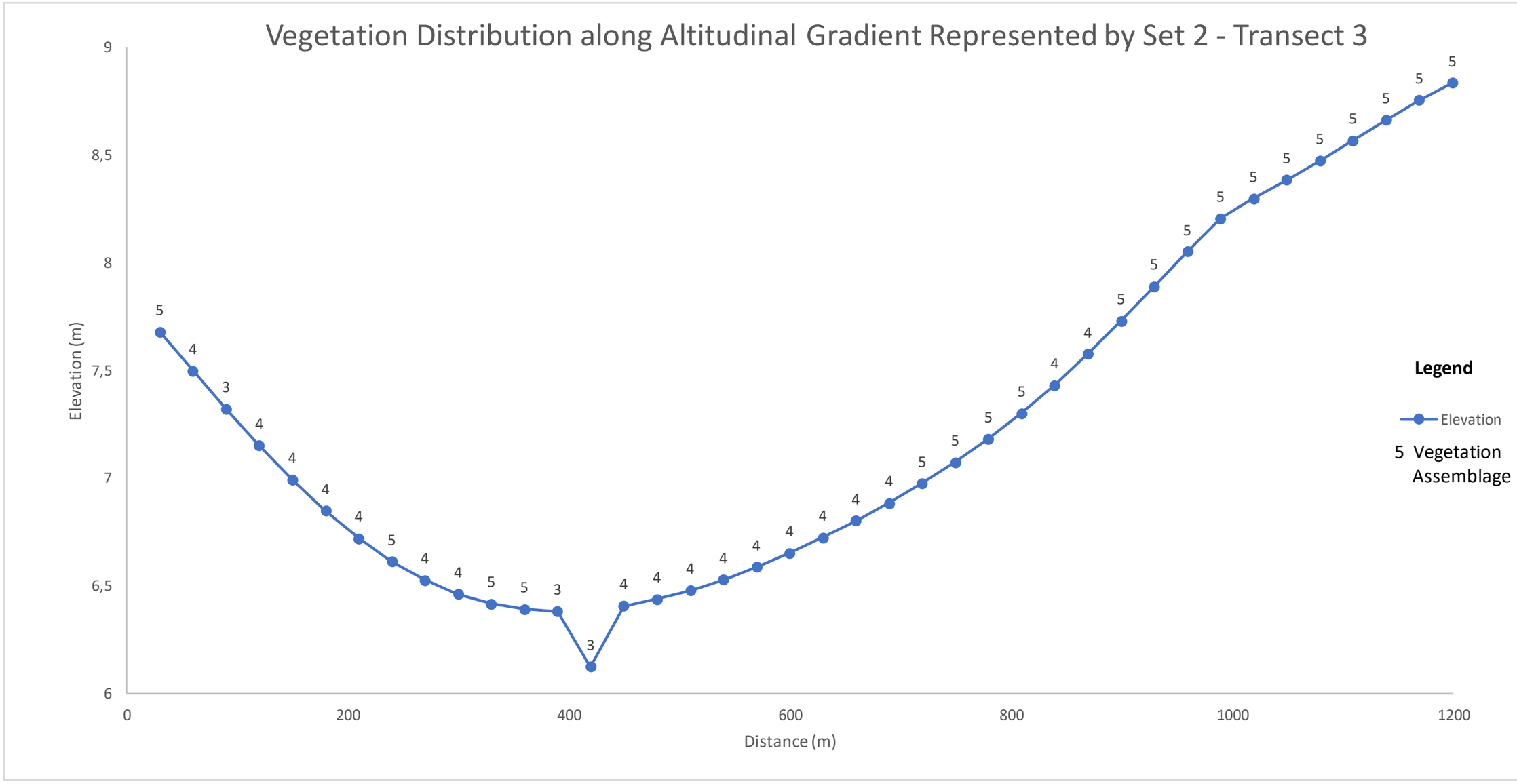
Vegetation Distribution along Altitudinal Gradient Represented by Set 2 - Transect 3
Elevation (m)
9
8,5
8
7,5
7
6,5
6
0
200
400
600
800
1000
1200
Distance (m)
5 4 3 4 4 4 4 5 4 4 5 5 3 4 4 4 4 4 4 4 4 5 5 5 5 5 5 5 5 5 5 5 5 5
Legend
Elevation
5 Vegetation Assemblage

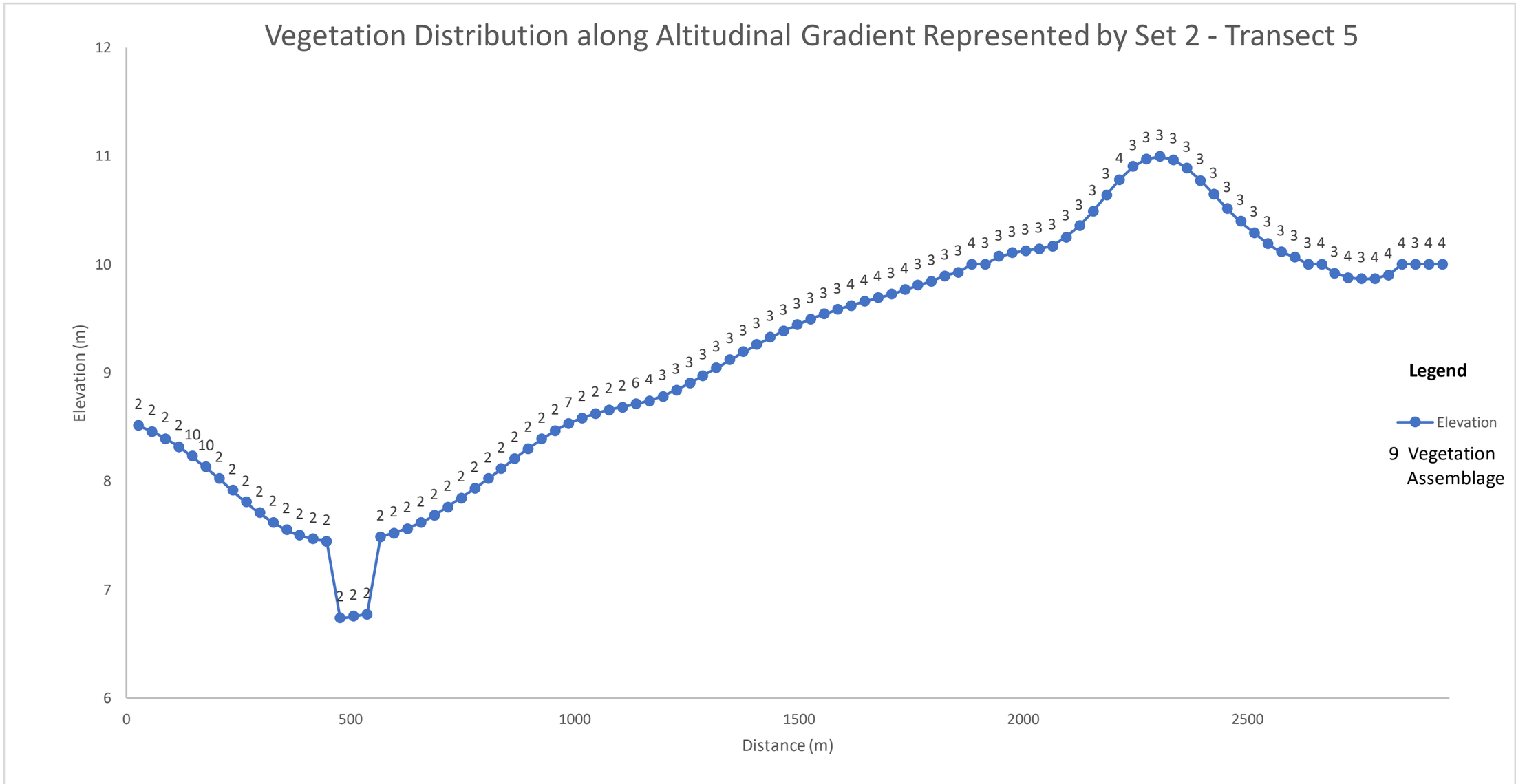
Vegetation Distribution along Altitudinal Gradient Represented by Set 2 - Transect 5
Elevation (m)
12
11
10
9
8
7
6
0
500
1000
1500
2000
2500
Distance (m)
Legend
Elevation
9 Vegetation Assemblage

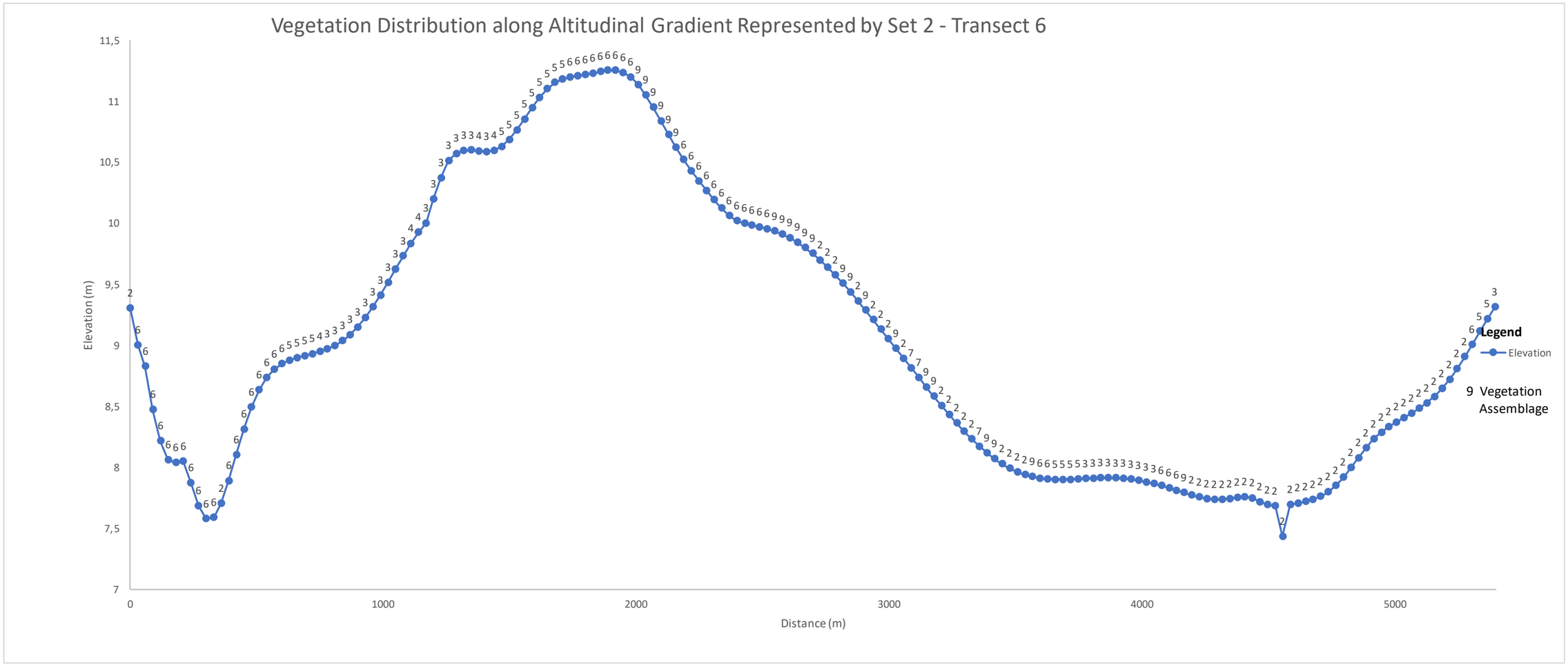
Vegetation Distribution along Altitudinal Gradient Represented by Set 2 - Transect 6
Elevation (m)
11,5
11
10,5
10
9,5
9
8,5
8
7,5
7
0
1000
2000
3000
4000
5000
Distance (m)
Legend
Elevation
9 Vegetation Assemblage

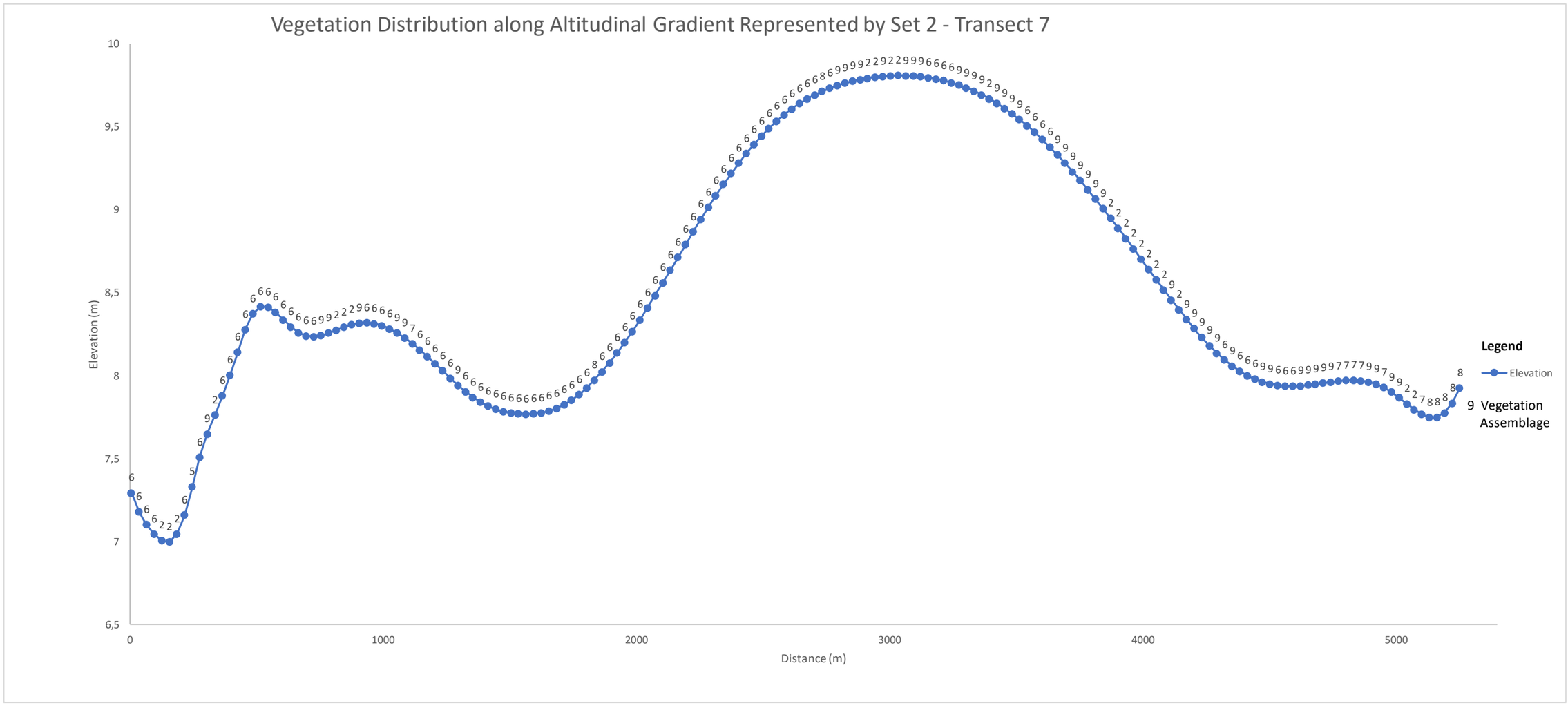
Vegetation Distribution along Altitudinal Gradient Represented by Set 2 - Transect 7
Elevation (m)
10
9,5
9
8,5
8
7,5
7
6,5
0
1000
2000
3000
4000
5000
Distance (m)
Legend
Elevation
Vegetation Assemblage

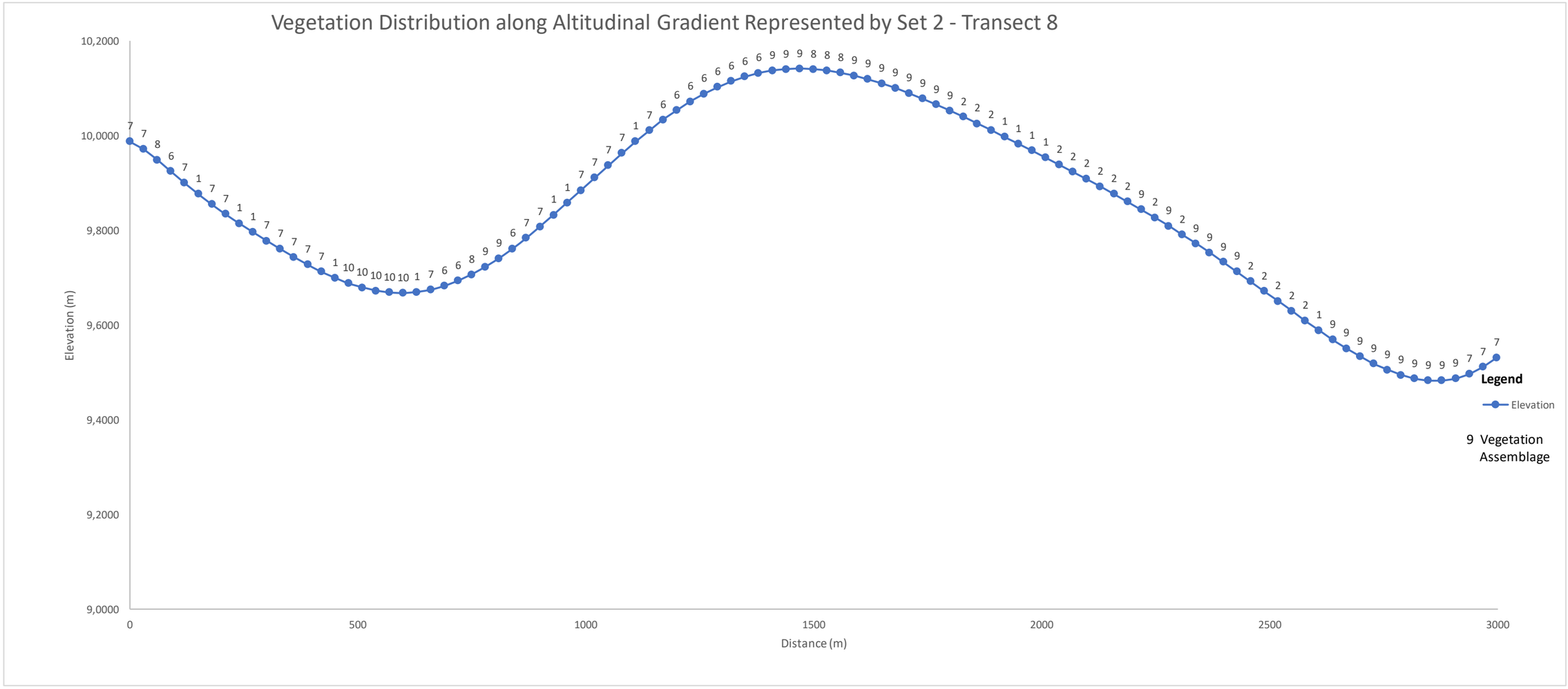
Vegetation Distribution along Altitudinal Gradient Represented by Set 2 - Transect 8
Elevation (m)
10,2000
10,0000
9,8000
9,6000
9,4000
9,2000
9,0000
0
500
1000
1500
2000
2500
3000
Distance (m)
Legend
Elevation
9 Vegetation Assemblage

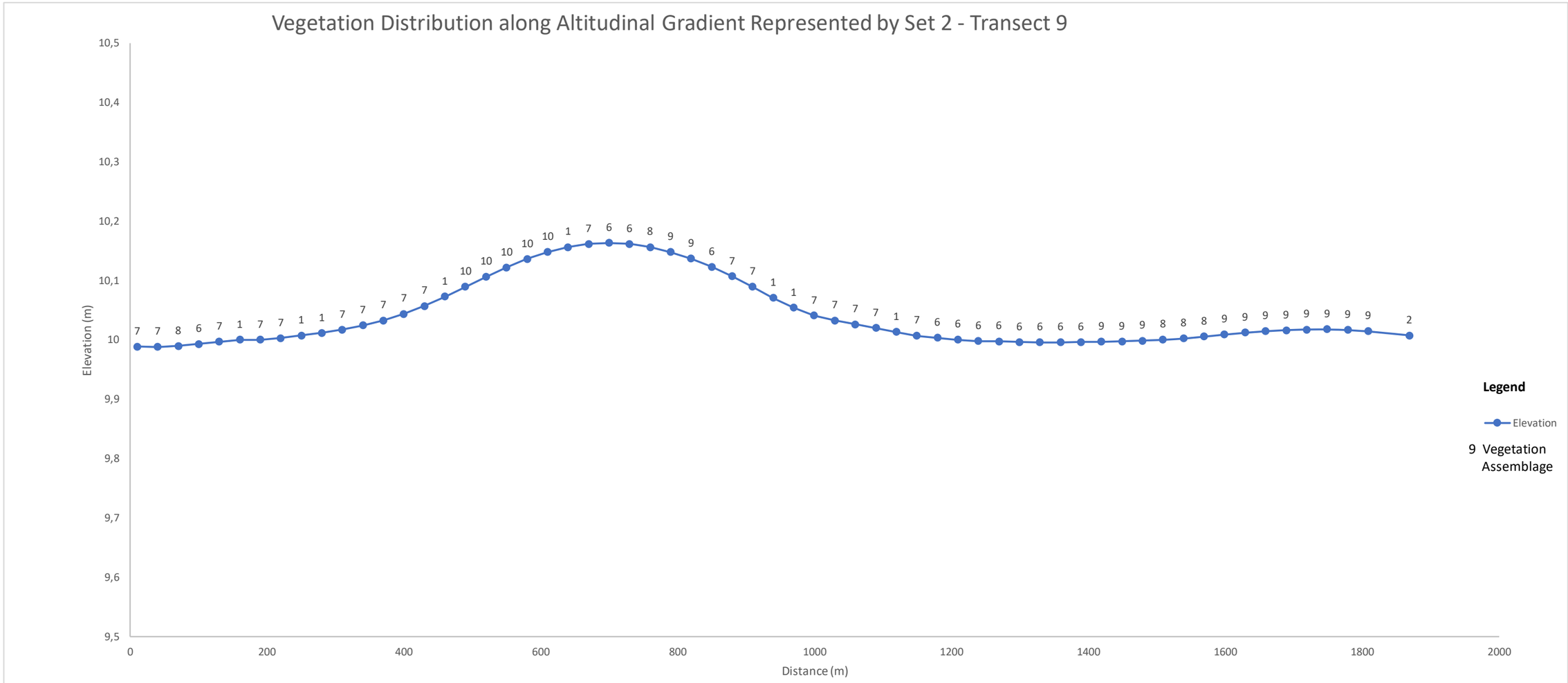
Vegetation Distribution along Altitudinal Gradient Represented by Set 2 - Transect 9
Elevation (m)
10,5
10,4
10,3
10,2
10,1
10
9,9
9,8
9,7
9,6
9,5
0
200
400
600
800
1000
1200
1400
1600
1800
2000
Distance (m)
7 7 8 6 7 1 7 7 1 1 7 7 7 7 7 1 10 10 10 10 10 1 7 6 6 8 9 9 6 7 7 1 1 7 7 7 7 1 7 6 6 6 6 6 6 6 6 9 9 9 8 8 8 9 9 9 9 9 9 9 9 2
Legend
Elevation
9 Vegetation Assemblage

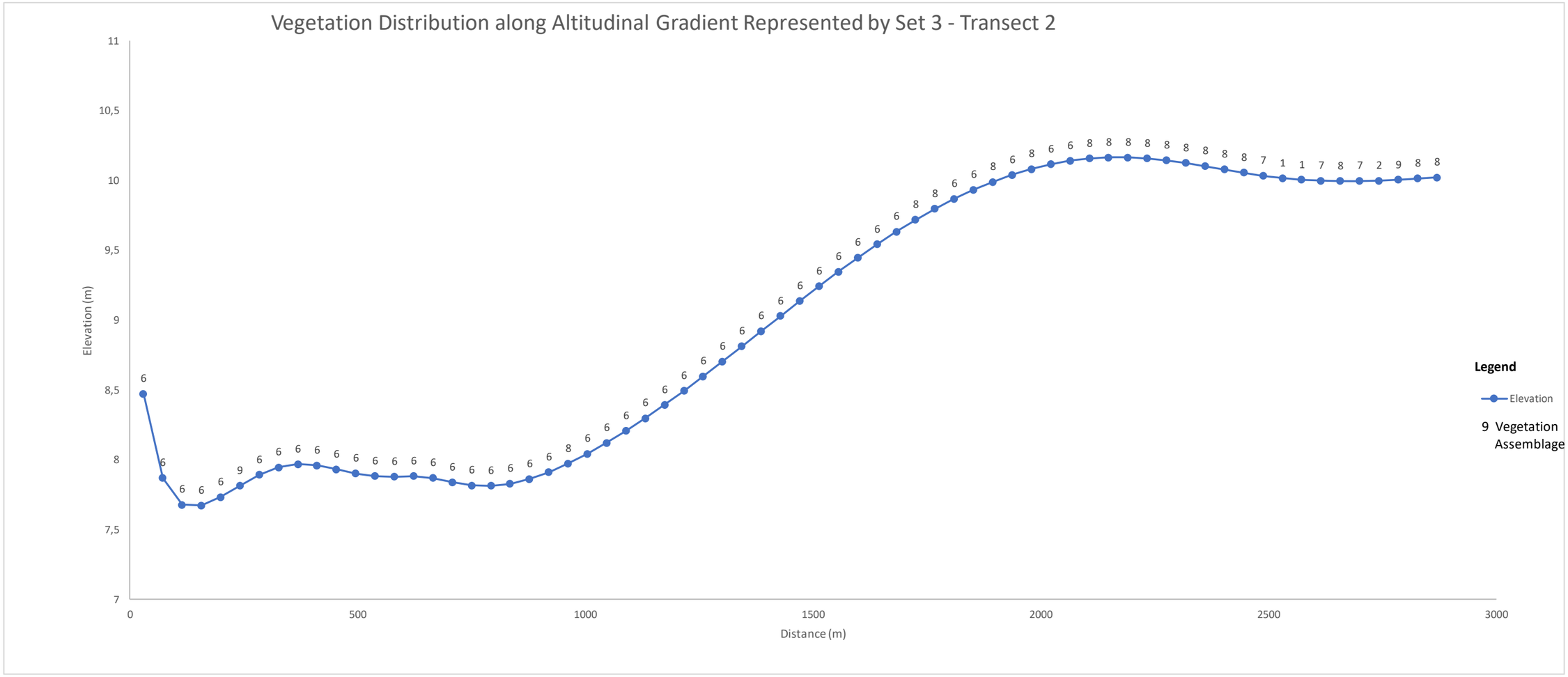
Vegetation Distribution along Altitudinal Gradient Represented by Set 3 - Transect 2
Elevation (m)
11
10,5
10
9,5
9
8,5
8
7,5
7
0
500
1000
1500
2000
2500
3000
Distance (m)
Legend
Elevation
9 Vegetation Assemblage

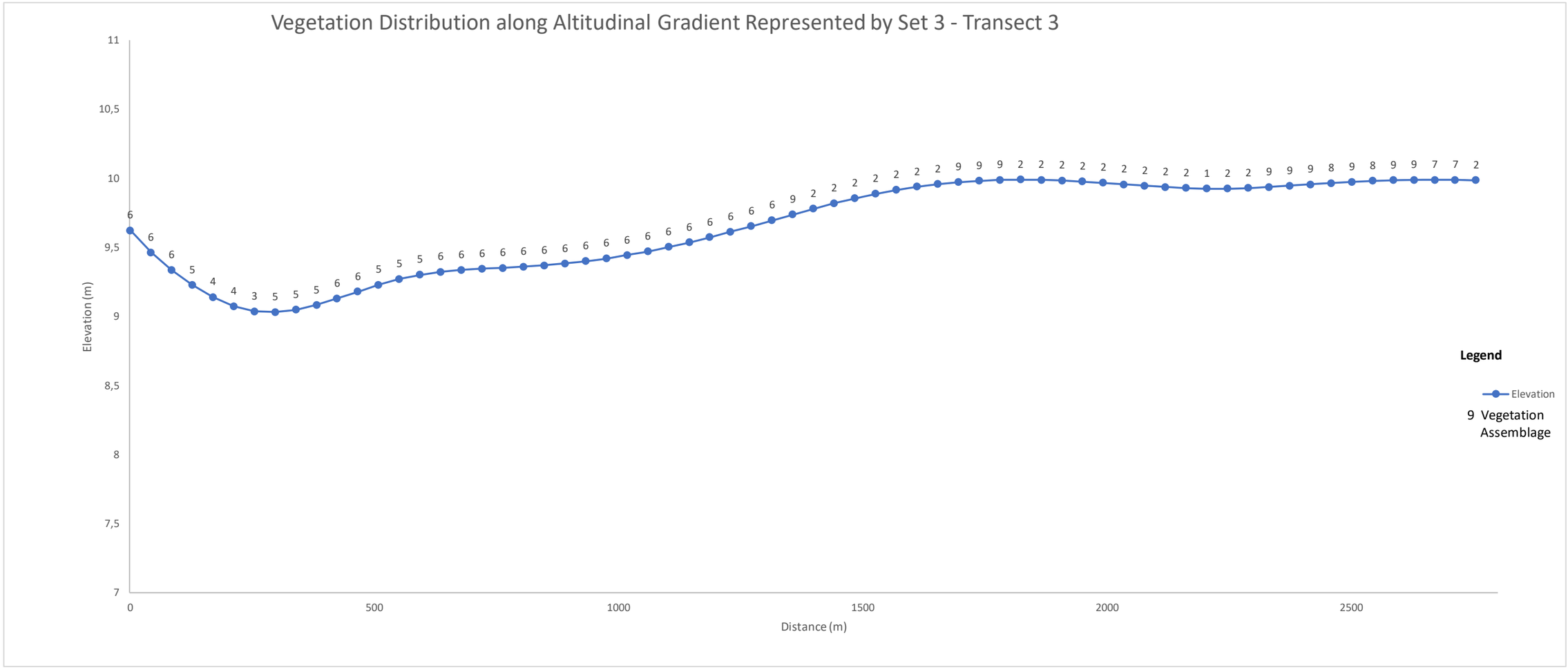
Vegetation Distribution along Altitudinal Gradient Represented by Set 3 - Transect 3
Elevation (m)
11
10,5
10
9,5
9
8,5
8
7,5
7
0
500
1000
1500
2000
2500
Distance (m)
6 6 6 5 4 4 3 5 5 5 6 6 5 5 5 6 6 6 6 6 6 6 6 6 6 6 6 6 6 6 6 6 9 2 2 2 2 2 2 2 9 9 9 2 2 2 2 2 2 2 2 2 2 1 2 2 9 9 9 8 9 8 9 9 7 7 2
Legend
Elevation
9 Vegetation Assemblage

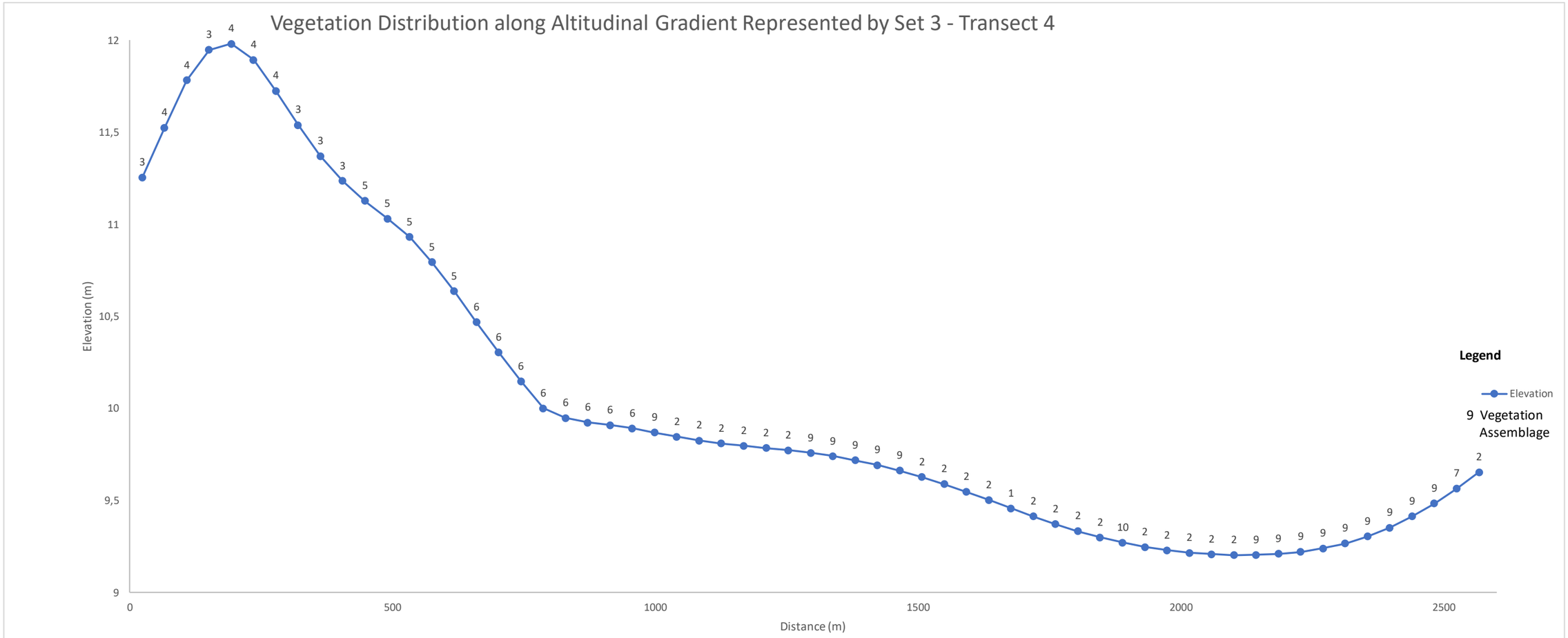
Vegetation Distribution along Altitudinal Gradient Represented by Set 3 - Transect 4
Elevation (m)
12
11,5
11
10,5
10
9,5
9
0
500
1000
1500
2000
2500
Distance (m)
Legend
Elevation
9 Vegetation Assemblage

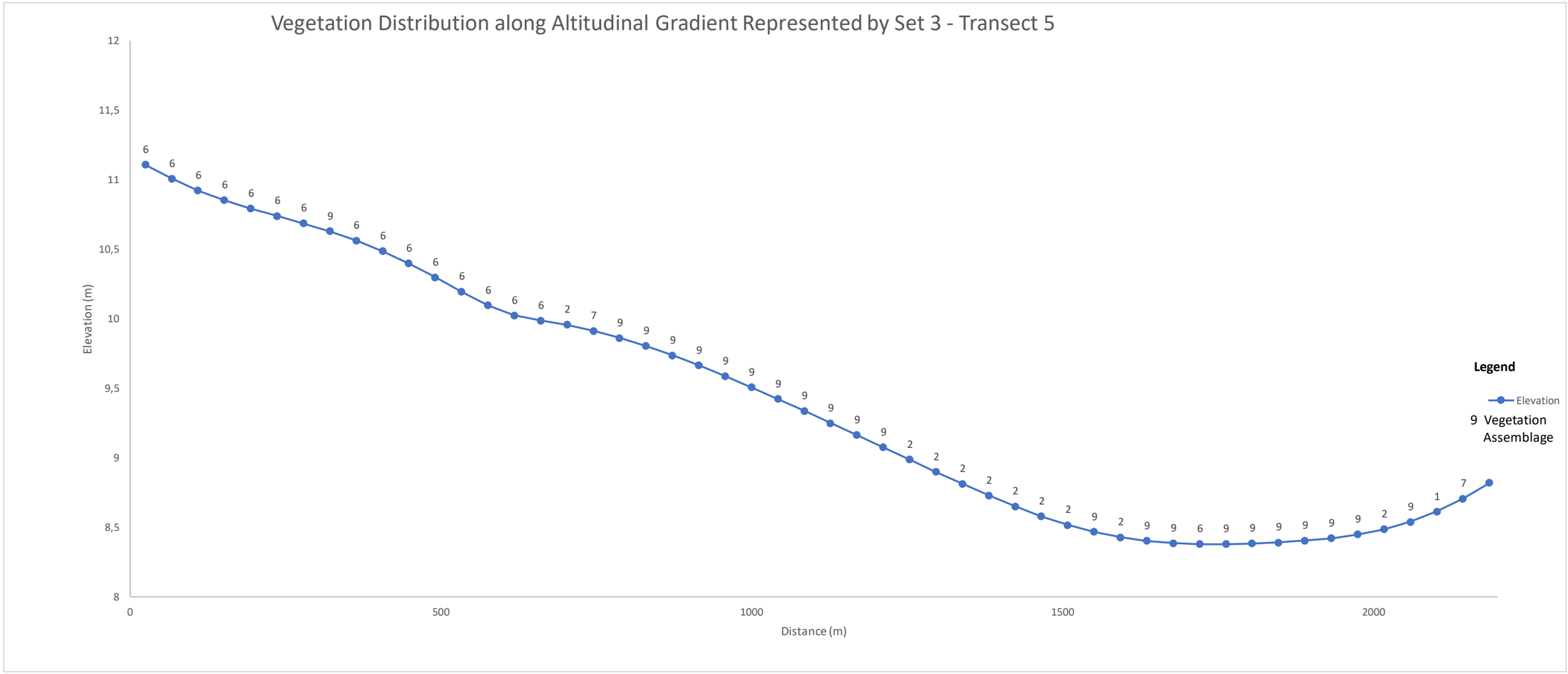
Vegetation Distribution along Altitudinal Gradient Represented by Set 3 - Transect 5
Elevation (m)
12
11,5
11
10,5
10
9,5
9
8,5
8
0
500
1000
1500
2000
Distance (m)
Legend
Elevation
9 Vegetation Assemblage

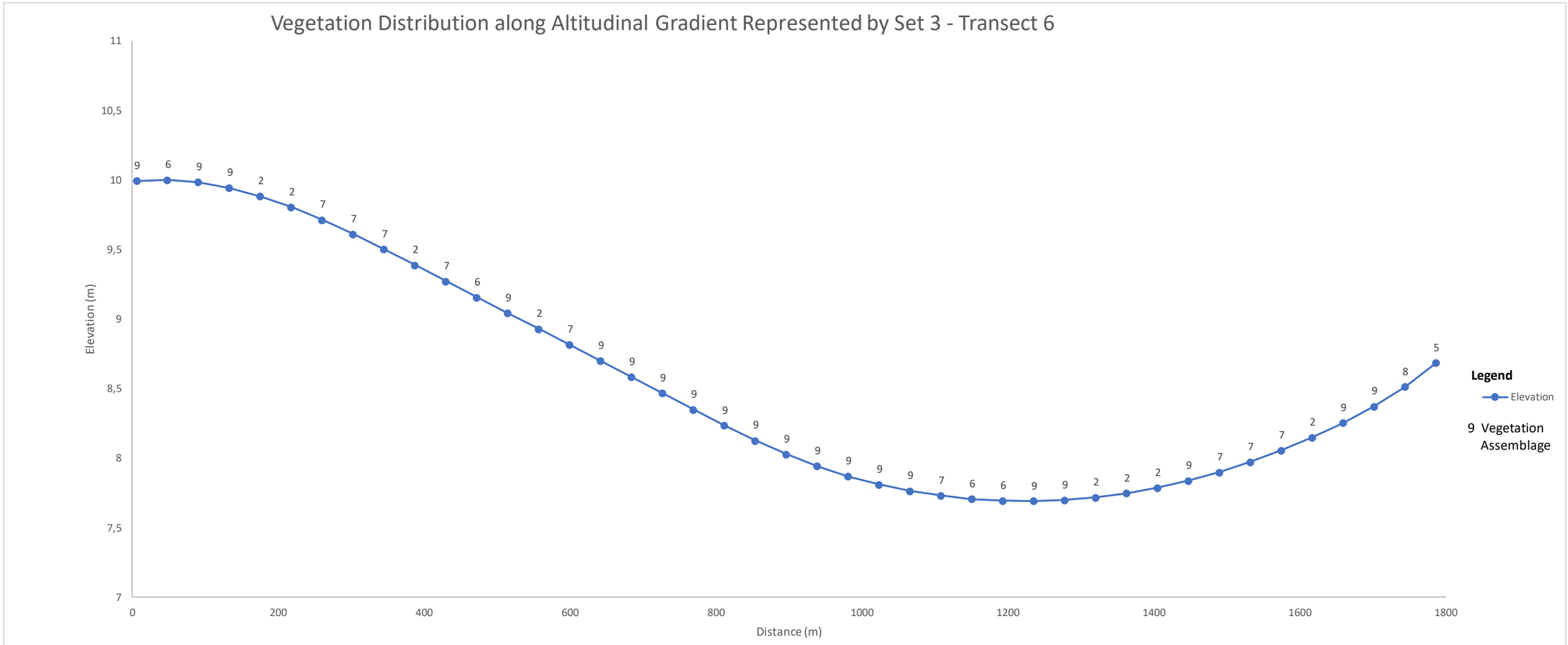
Vegetation Distribution along Altitudinal Gradient Represented by Set 3 - Transect 6
Elevation (m)
11
10,5
10
9,5
9
8,5
8
7,5
7
0
200
400
600
800
1000
1200
1400
1600
1800
Distance (m)
9 6 9 9 2 2 7 7 7 2 7 6 9 2 7 9 9 9 9 9 9 9 9 9 9 9 7 6 6 9 9 2 2 2 9 7 7 7 2 9 9 8 5
Legend
Elevation
9 Vegetation Assemblage

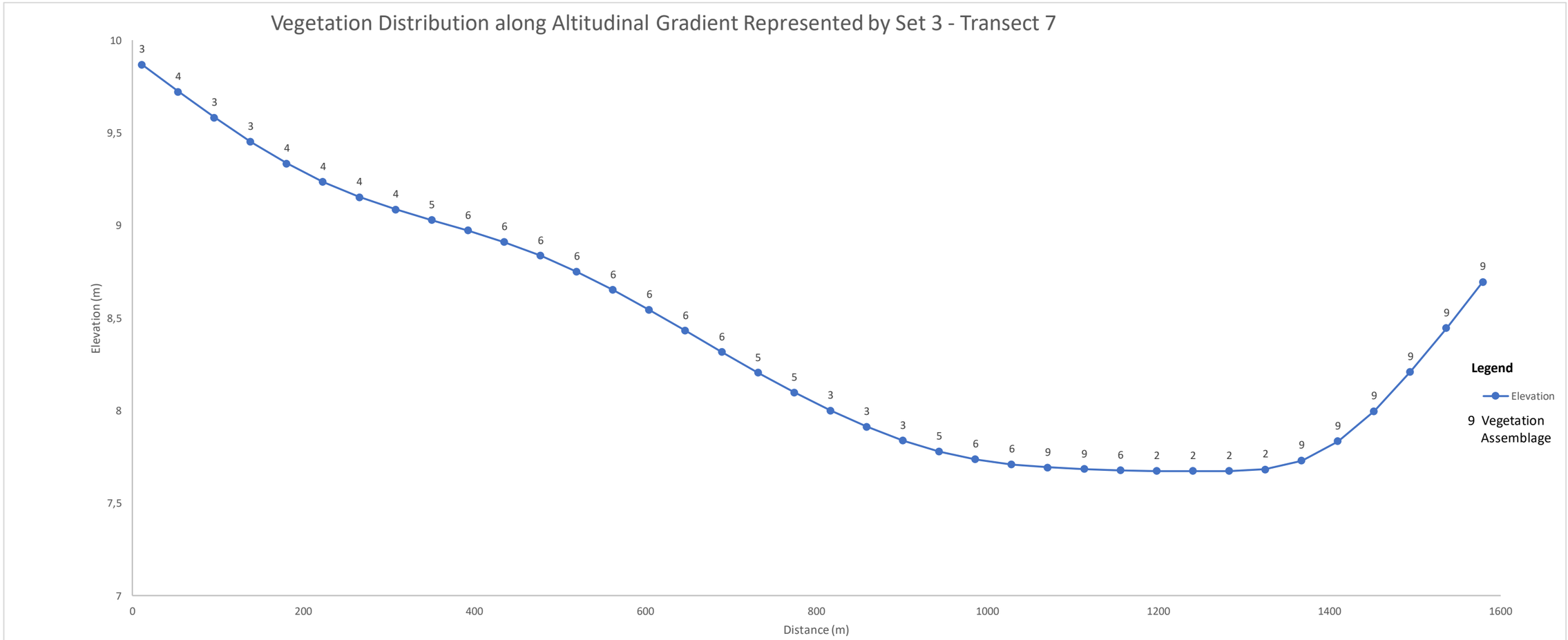
Vegetation Distribution along Altitudinal Gradient Represented by Set 3 - Transect 7
Elevation (m)
10
9,5
9
8,5
8
7,5
7
0
200
400
600
800
1000
1200
1400
1600
Distance (m)
3 4 3 3 4 4 4 4 5 6 6 6 6 6 6 6 6 5 5 3 3 3 5 6 6 9 9 6 2 2 2 2 9 9 9 9 9 9
Legend
Elevation
9 Vegetation Assemblage

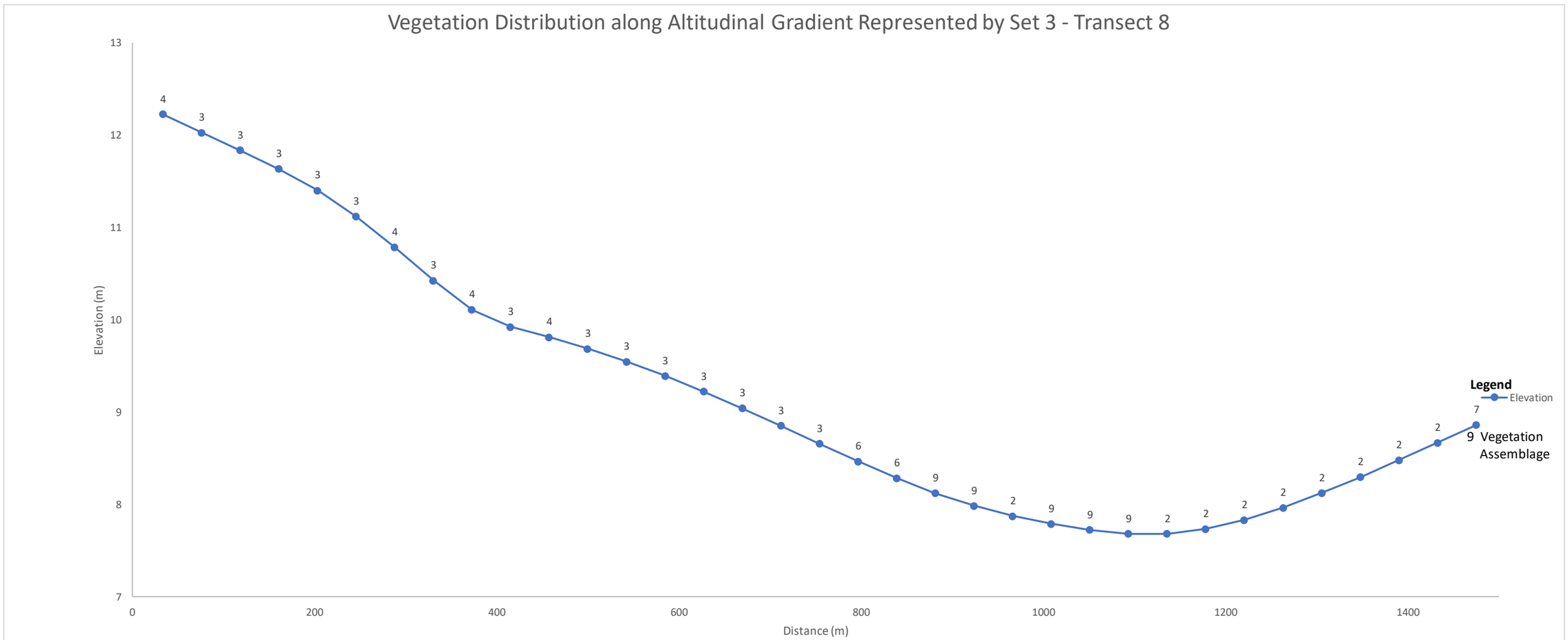
Vegetation Distribution along Altitudinal Gradient Represented by Set 3 - Transect 8
Elevation (m)
13
12
11
10
9
8
7
0
200
400
600
800
1000
1200
1400
Distance (m)
4 3 3 3 3 3 4 3 4 3 4 3 3 3 3 3 3 3 3 6 6 9 9 6 9 9 2 9 9 9 2 2 2 2 2 2 2 2 9
Legend
Elevation
Vegetation Assemblage

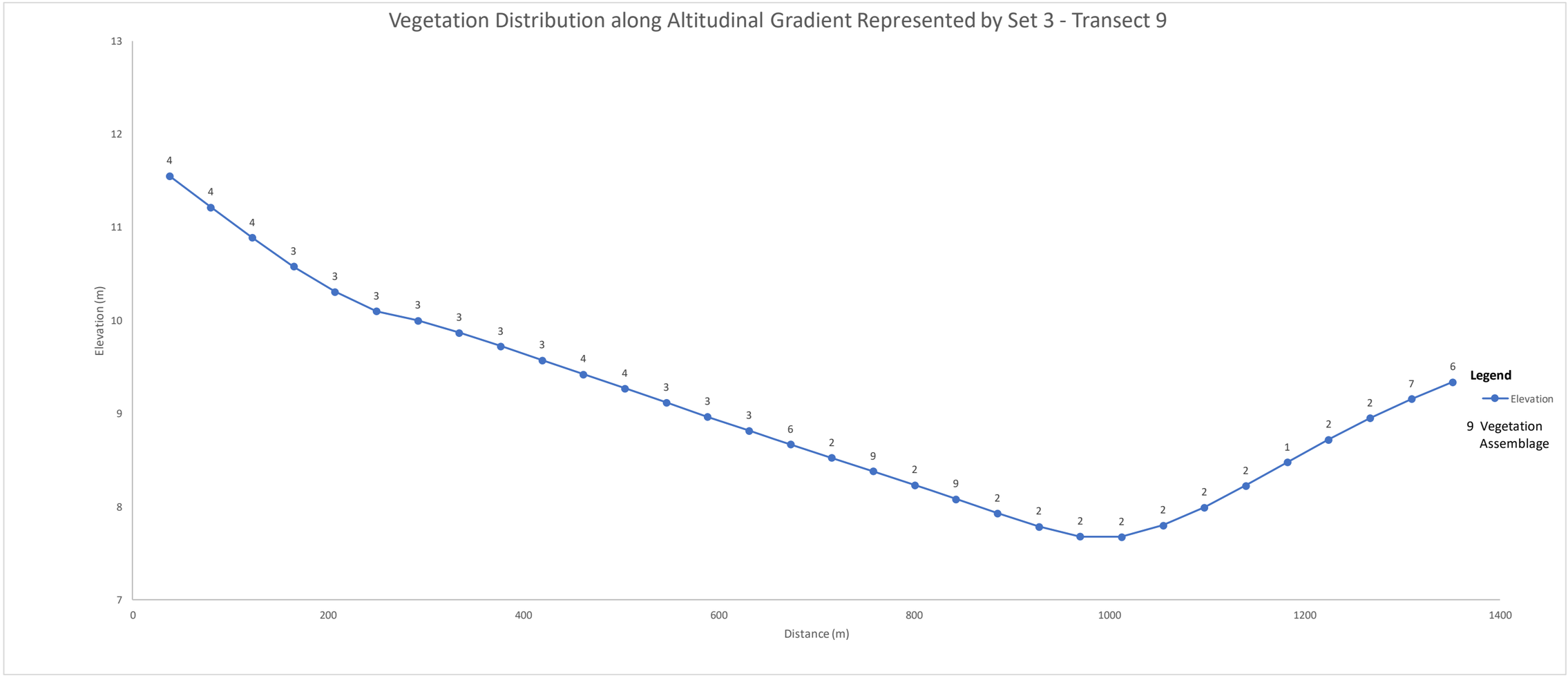
Vegetation Distribution along Altitudinal Gradient Represented by Set 3 - Transect 9
Elevation (m)
13
12
11
10
9
8
7
0
200
400
600
800
1000
1200
1400
Distance (m)
4 4 4 3 3 3 3 3 3 3 4 4 3 3 3 6 2 9 2 9 2 2 2 2 2 2 2 6 7 2 1 2 2 9
Legend
Elevation
9 Vegetation Assemblage

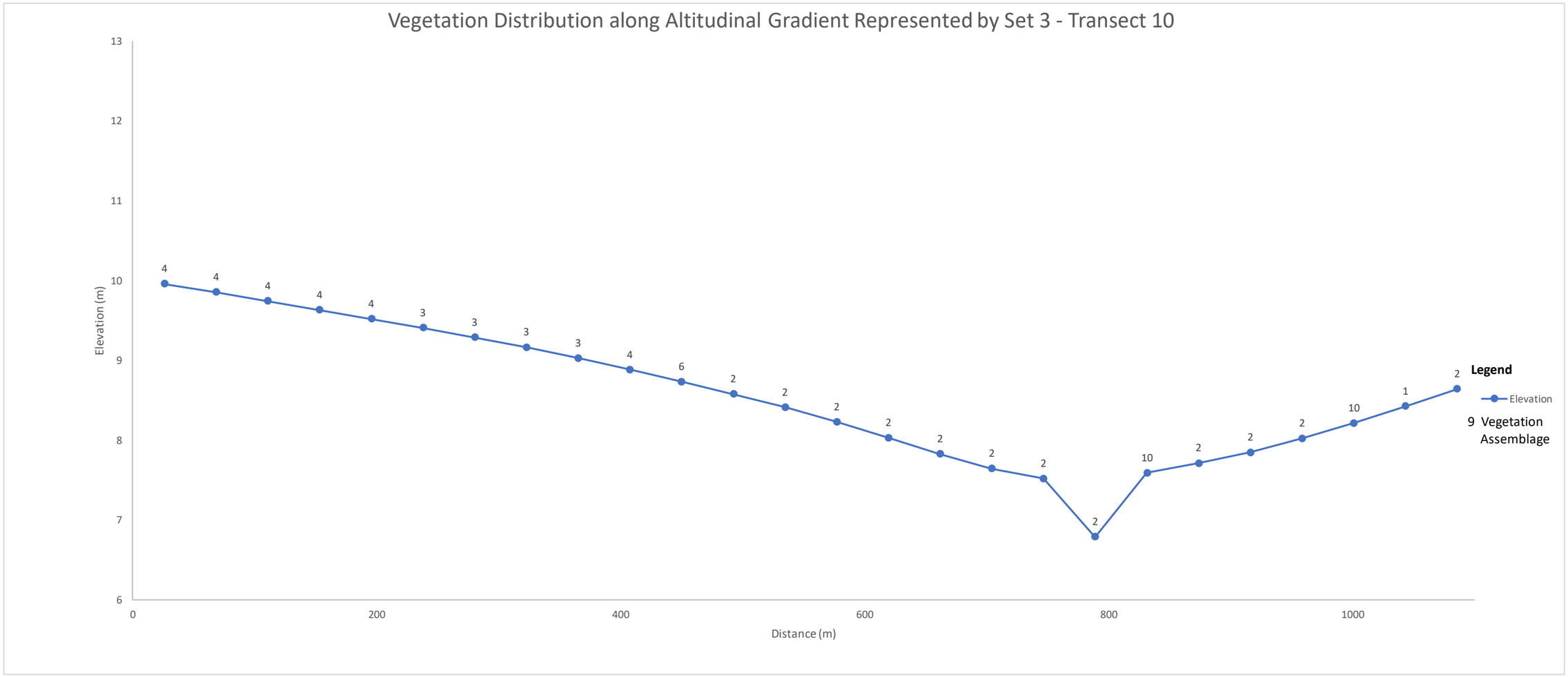
Vegetation Distribution along Altitudinal Gradient Represented by Set 3 - Transect 10
Elevation (m)
13
12
11
10
9
8
7
6
0
200
400
600
800
1000
Distance (m)
4 4 4 4 4 3 3 3 3 4 6 2 2 2 2 2 2 2 2 10 2 2 2 10 1 2
Legend
Elevation
9 Vegetation Assemblage

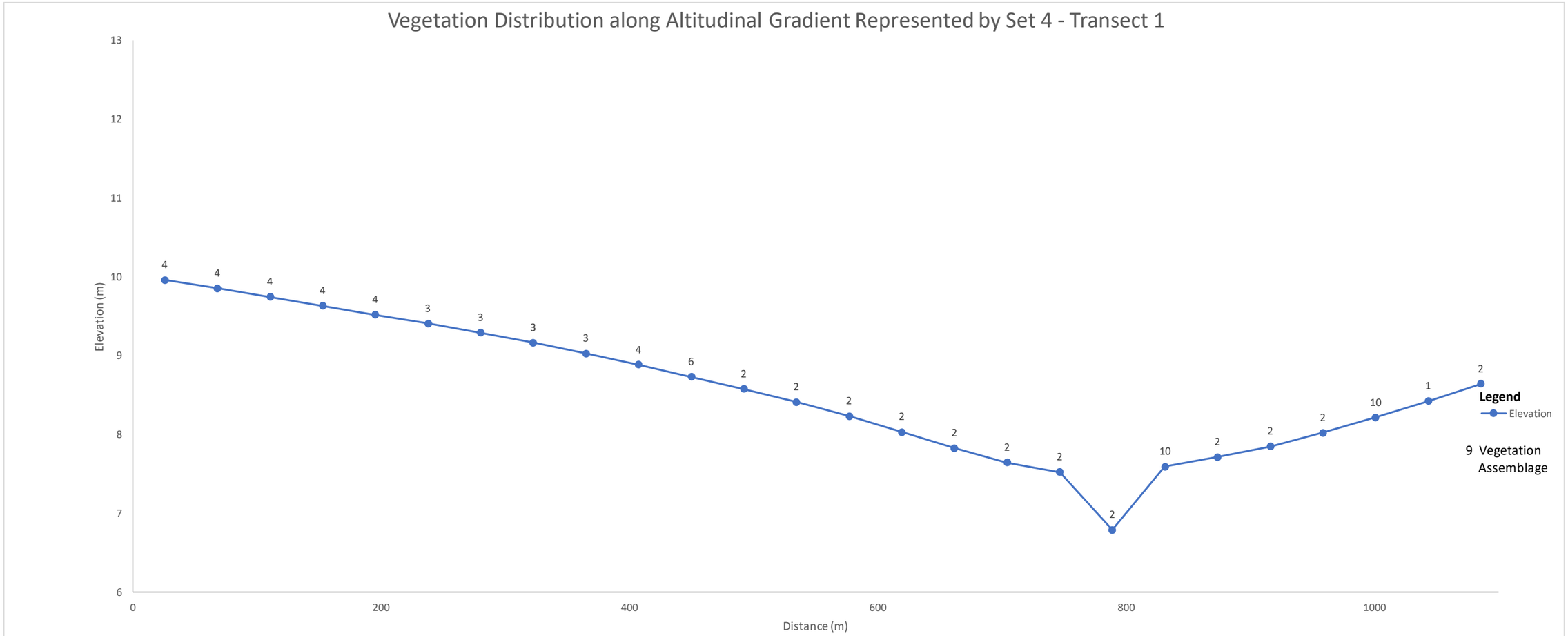
Vegetation Distribution along Altitudinal Gradient Represented by Set 4 - Transect 1
Elevation (m)
13
12
11
10
9
8
7
6
0
200
400
600
800
1000
Distance (m)
4 4 4 4 4 3 3 3 3 4 6 2 2 2 2 2 2 2 10 2 2 2 10 1 2
Legend
Elevation
9 Vegetation Assemblage

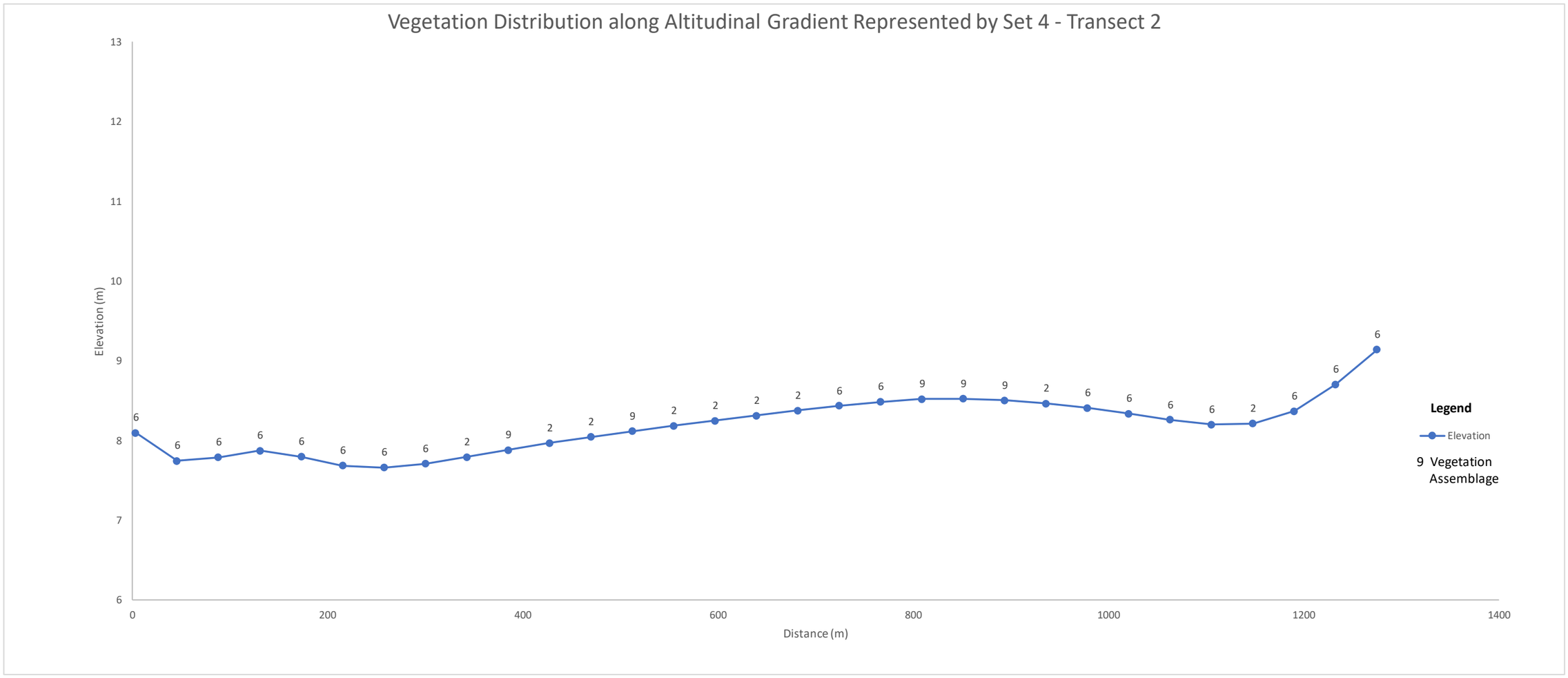
Vegetation Distribution along Altitudinal Gradient Represented by Set 4 - Transect 2
Elevation (m)
13
12
11
10
9
8
7
6
0
200
400
600
800
1000
1200
1400
Distance (m)
6 6 6 6 6 6 6 6 2 9 2 2 9 2 2 2 2 6 6 9 9 9 2 6 6 6 6 2 6 6 6
Legend
Elevation
9 Vegetation Assemblage

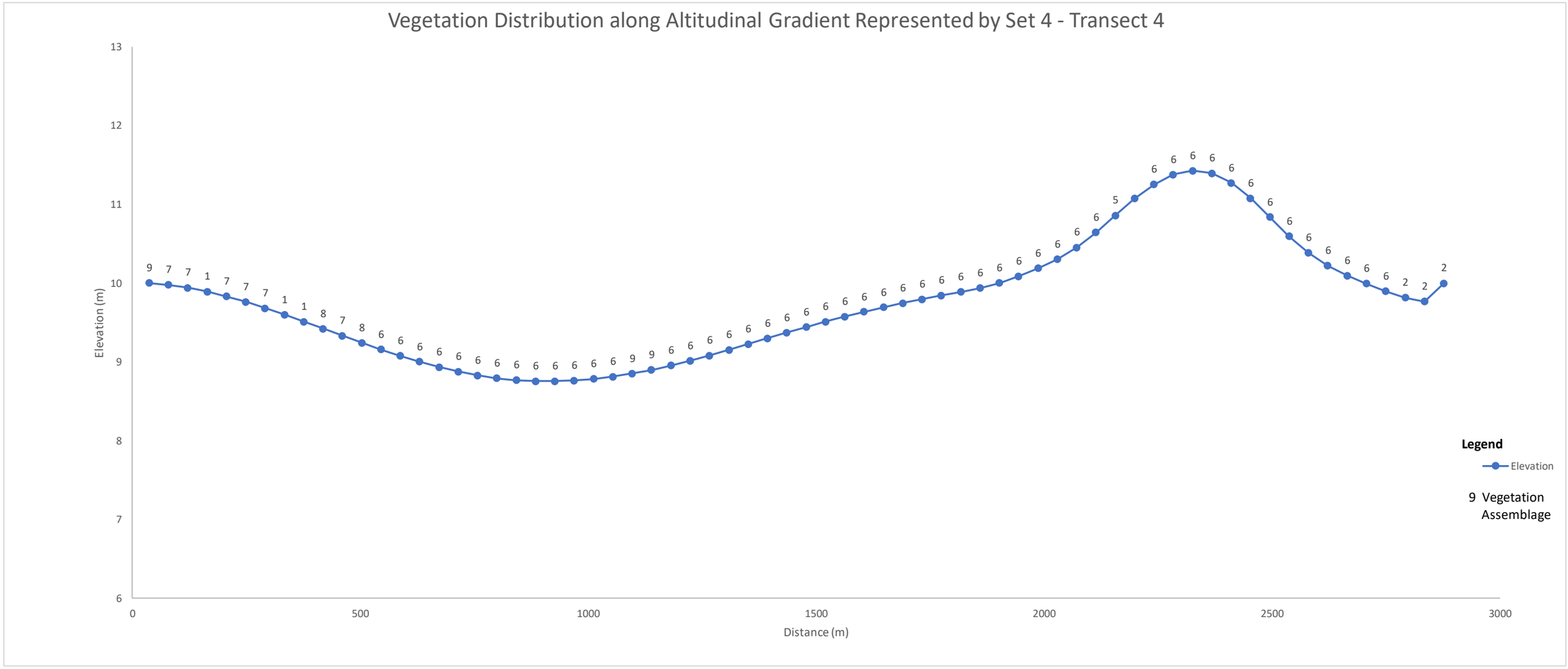
Vegetation Distribution along Altitudinal Gradient Represented by Set 4 - Transect 4
Elevation (m)
13
12
11
10
9
8
7
6
0
500
1000
1500
2000
2500
3000
Distance (m)
9 7 7 1 7 7 7 1 1 8 7 8 6 6 6 6 6 6 6 6 6 6 6 9 9 6 6 6 6 6 6 6 6 6 6 6 6 6 6 6 6 6 6 6 6 5 6 6 6 6 6 6 6 6 6 6 6 6 6 2 2 2
Legend
Elevation
9 Vegetation Assemblage

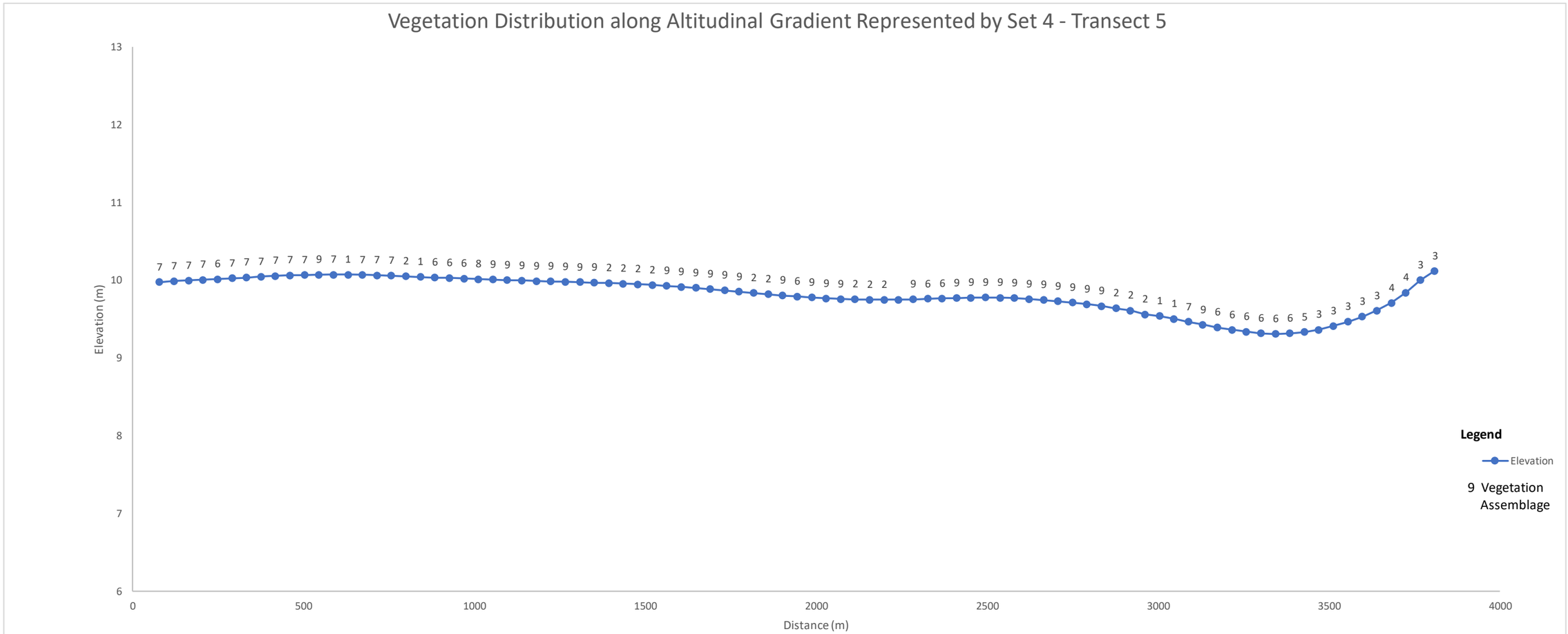
Vegetation Distribution along Altitudinal Gradient Represented by Set 4 - Transect 5
Elevation (m)
13
12
11
10
9
8
7
6
7 7 7 7 6 7 7 7 7 7 7 9 7 1 7 7 7 2 1 6 6 6 8 9 9 9 9 9 9 9 9 2 2 2 2 2 9 9 9 9 9 9 2 2 9 6 9 9 9 2 2 2 9 6 6 9 9 9 9 9 9 9 9 9 9 9 2 2 2 1 1 7 9 6 6 6 6 6 5 3 3 3 3 3 4 4 3 3
Legend
Elevation
9 Vegetation Assemblage
0
500
1000
1500
2000
2500
3000
3500
4000
Distance (m)

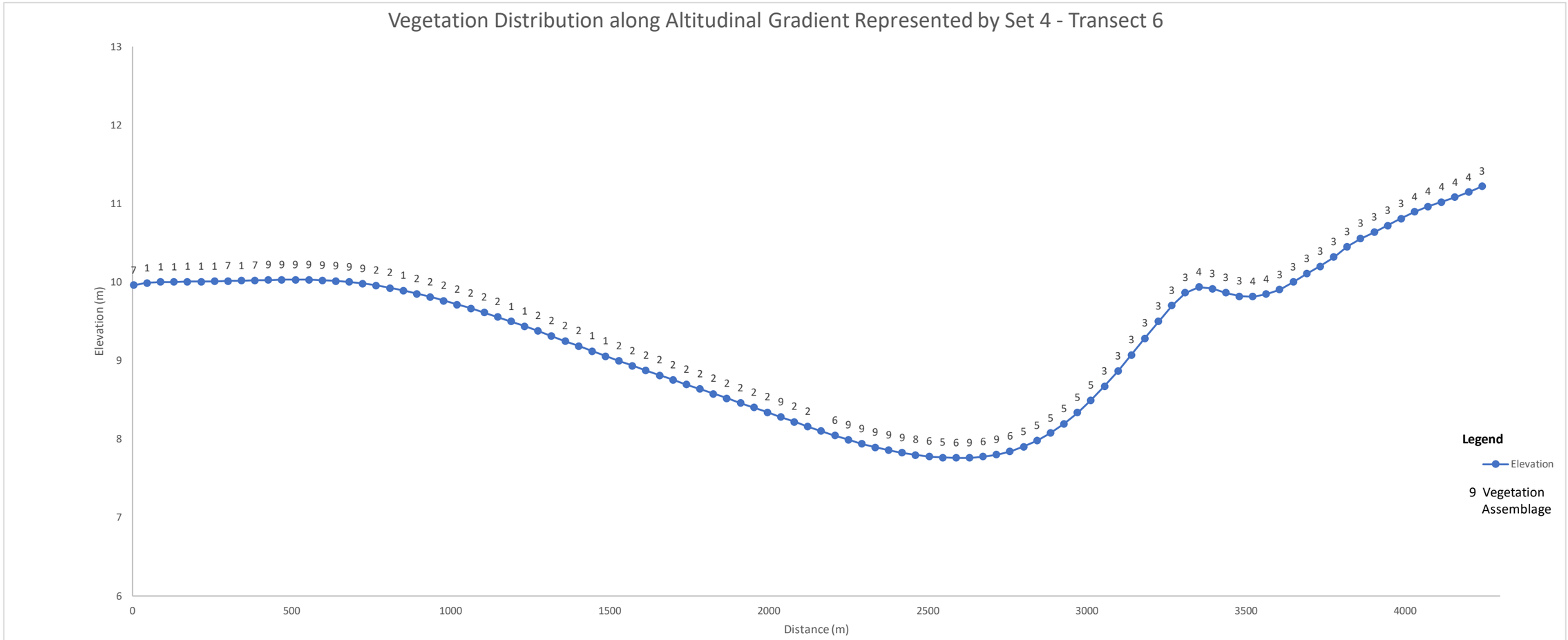
Vegetation Distribution along Altitudinal Gradient Represented by Set 4 - Transect 6
Elevation (m)
13
12
11
10
9
8
7
6
0
500
1000
1500
2000
2500
3000
3500
4000
Distance (m)
7 1 1 1 1 1 1 7 1 7 9 9 9 9 9 9 9 9 2 2 1 2 2 2 2 2 2 2 1 1 2 2 2 1 1 2 2 2 2 2 2 2 2 2 2 2 2 2 2 2 2 2 9 2 2 6 9 9 9 9 9 8 6 5 6 9 6 9 6 5 5 5 5 5 5 3 3 3 3 3 3 4 3 3 4 4 3 3 3 3 3 3 3 3 3 4 4 4 4 4 3
Legend
Elevation
9 Vegetation Assemblage

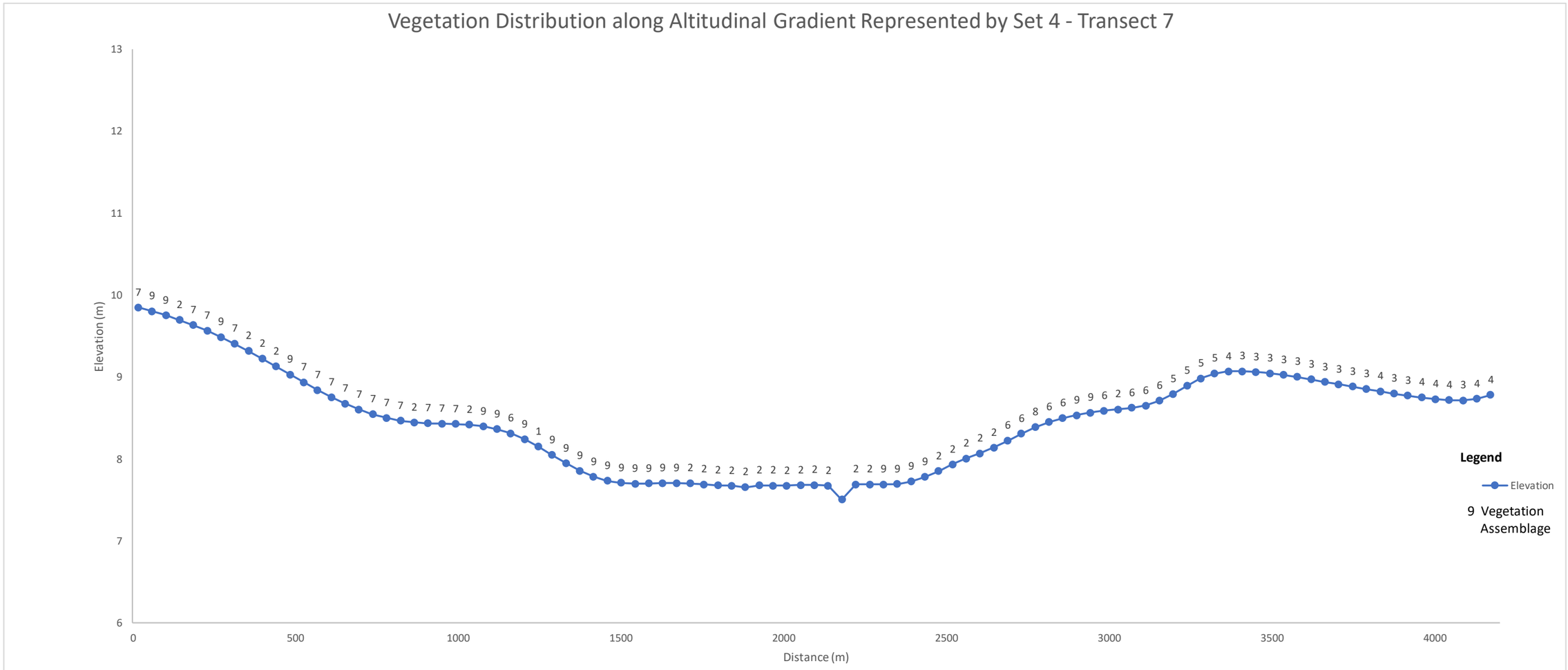
Vegetation Distribution along Altitudinal Gradient Represented by Set 4 - Transect 7
Elevation (m)
13
12
11
10
9
8
7
6
0
500
1000
1500
2000
2500
3000
3500
4000
Distance (m)
7 9 9 2 7 7 9 7 2 2 2 9 7 7 7 7 7 7 7 2 7 7 7 2 9 9 6 9 1 9 9 9 9 9 9 9 9 9 2 2 2 2 2 2 2 2 2 2 2 2 2 2 2 9 9 9 2 2 2 6 6 8 6 6 9 9 6 2 6 6 6 5 5 5 5 4 3 3 3 3 3 3 3 3 3 3 4 3 3 4 4 4 3 4 4
Legend
Elevation
9 Vegetation Assemblage

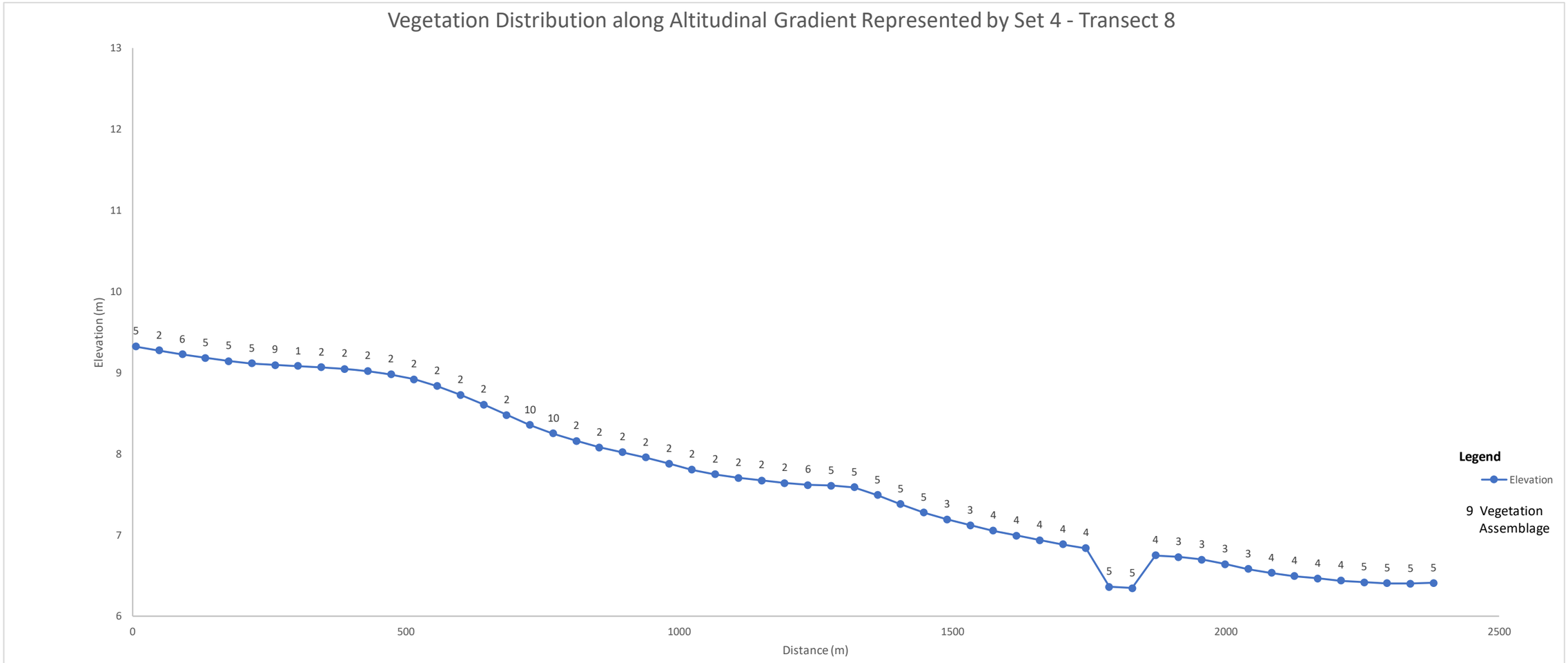
Vegetation Distribution along Altitudinal Gradient Represented by Set 4 - Transect 8
Elevation (m)
13
12
11
10
9
8
7
6
0
500
1000
1500
2000
2500
Distance (m)
5 2 6 5 5 5 9 1 2 2 2 2 2 2 2 2 2 10 10 2 2 2 2 2 2 2 2 2 2 6 5 5 5 5 5 3 3 4 4 4 4 4 4 5 5 4 3 3 3 3 4 4 4 4 5 5 5 5
Legend
Elevation
9 Vegetation Assemblage

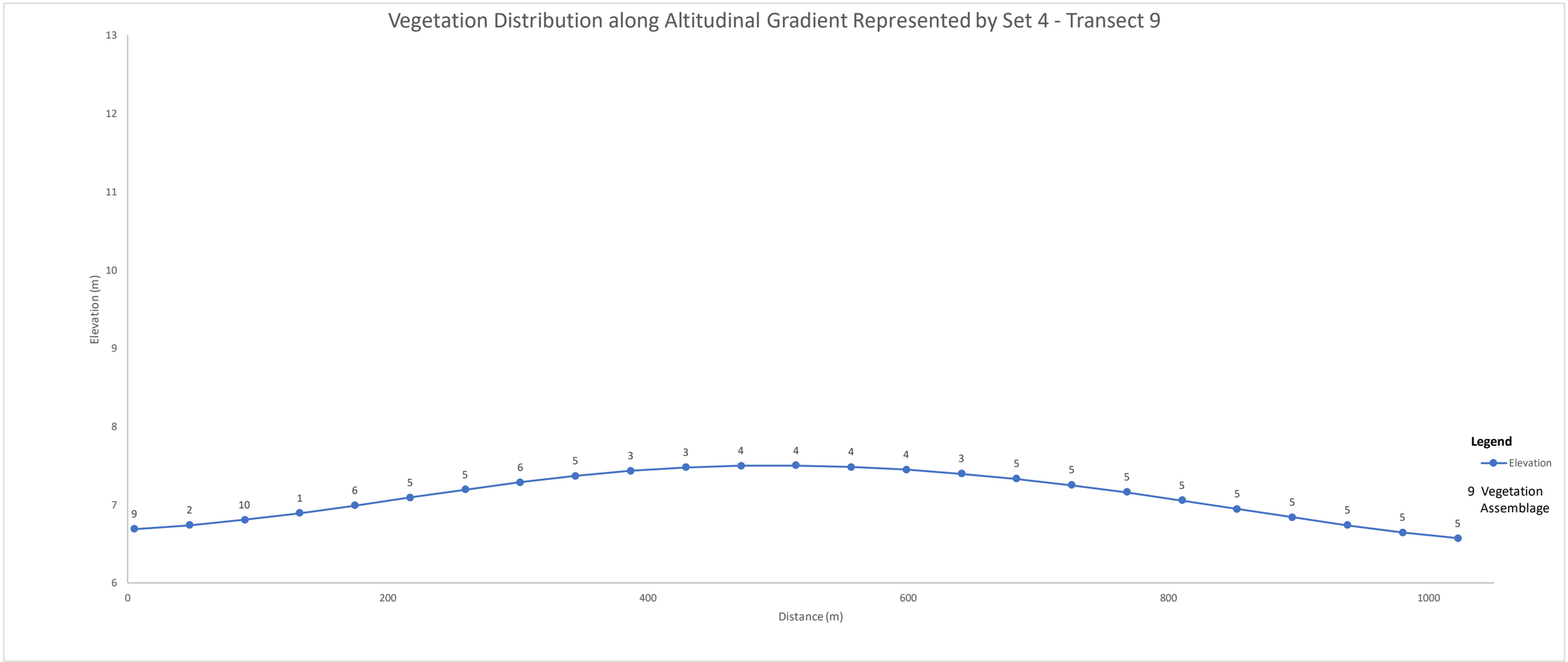
Vegetation Distribution along Altitudinal Gradient Represented by Set 4 - Transect 9
Elevation (m)
13
12
11
10
9
8
7
6
0
200
400
600
800
1000
Distance (m)
9
2
10
1
6
5
5
6
5
3
3
4
4
4
4
3
5
5
5
5
5
5
5
5
Legend
Elevation
9 Vegetation Assemblage

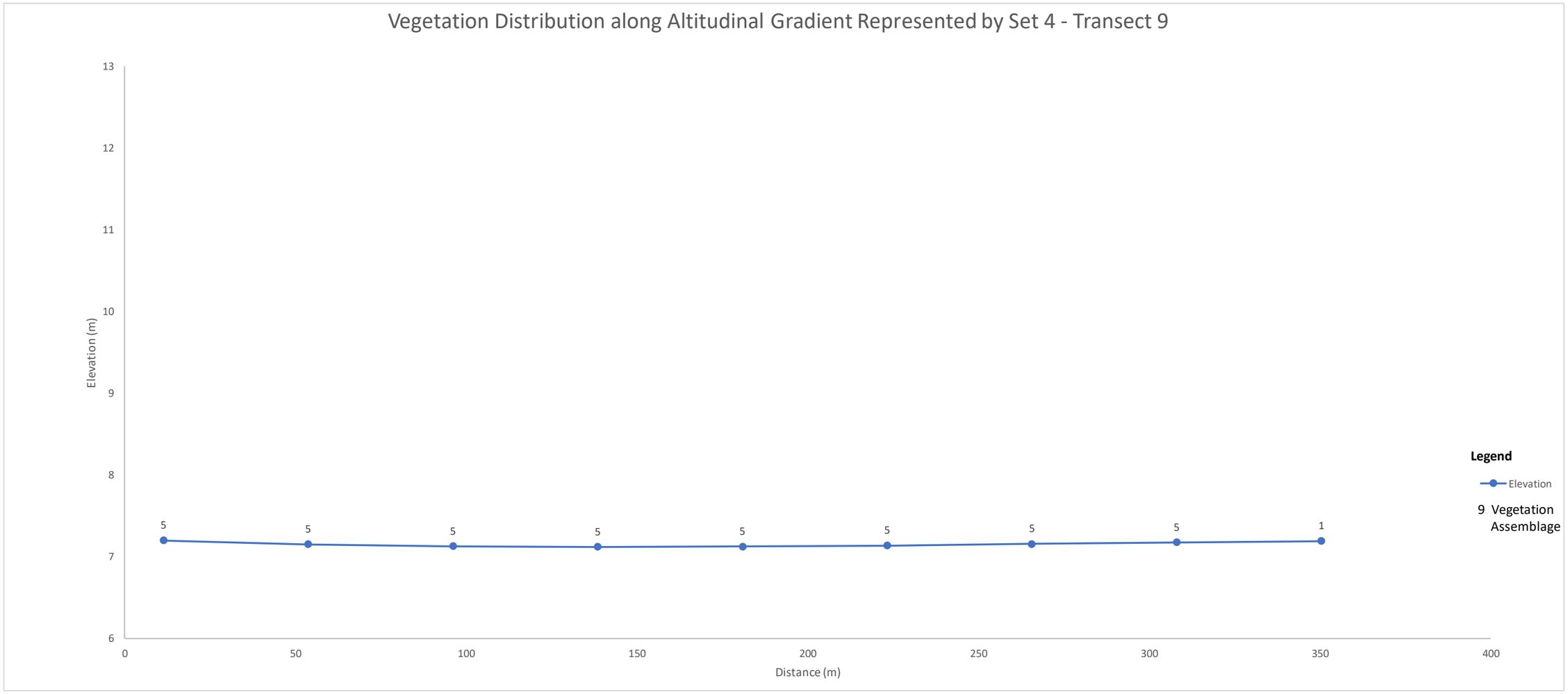
Vegetation Distribution along Altitudinal Gradient Represented by Set 4 - Transect 9
Elevation (m)
13
12
11
10
9
8
7
6
0
50
100
150
200
250
300
350
400
Distance (m)
5
5
5
5
5
5
5
5
1
Legend
Elevation
9 Vegetation Assemblage